THE APPLICATION OF A CALCITE TWINNING PALAEOPIEZOMETER TO THE CANTABRIAN OF N.W. SPAIN

by

KELVIN JAMES ROWE B.Sc.

A THESIS SUBMITTED FOR THE DEGREES OF DOCTOR OF PHILOSOPHY (UNIVERSITY OF LONDON) AND THE DIPLOMA OF IMPERIAL COLLEGE, UNIVERSITY OF LONDON

DEPARTMENT OF GEOLOGY,
IMPERIAL COLLEGE OF SCIENCE AND TECHNOLOGY (UNIVERSITY OF LONDON),
PRINCE CONSORT ROAD,
SOUTH KENSINGTON,
LONDON SW7 2BP.

Dedicated to my parents, Ida and Ken Rowe.

ABSTRACT

This thesis reports the results of an experimental investigation of twinning activity as a function of differential stress and grain size, leading to the full calibration of a calcite twinning palaeopiezometric technique. The experimental models formulated have been applied to two major thrust fault nappe complexes in the external Cantabrian zone of the Northern Spanish Hercynides.

A series of axisymmetric compressional experiments using a Nimonic testing apparatus has been performed on several calcitic rocks displaying a range of grain sizes. The textural data obtained from these experiments have been used to locate the position of the twinning field boundary (defined as the limit of the field where twinning becomes of significant volumetric importance). The twinning field boundary was shown to be a function of differential stress and grain size, and insensitive to temperature and strain rate. Experiments have been performed upon Carrara Marble (160μm grain size), and these have shown that the twinning field boundary lies at approximately 105MPa, while experiments on Taiwanese Marble (380μm grain size) have shown that the same boundary is located at approximately 10MPa. Previous experimental work on Solenhofen Limestone (5μm grain size) was also examined, and this showed that the twinning field boundary for this material lies at approximately 400MPa.

Two of the principal nappe complexes of the Cantabrian zone have been chosen for detailed study. These are 1) the Esla Nappe, and 2) the Somiedo Nappe, from the south-east and west of the zone, respectively. Specimens collected from a number of traverses from these complexes were studied using standard optical (including universal stage) techniques, and SEM analysis. The stress levels obtained from these textural analyses are typically in excess of 200MPa, although twinning activity shows fairly complex behaviour in near proximity to the thrust faults.

This thesis concludes with a discussion of some of the geological implications indicated by the formulation of the experimental models presented, and their application to a major natural system.

CONTENTS

ABSTRACT 1

CONTENTS 2

LIST OF FIGURES 8

LIST OF PLATES 16

LIST OF TABLES 18

LIST OF APPENDICES 19

LIST OF ABBREVIATIONS 20

ACHKNOWLEDGEMENTS 21

CHAPTER 1 : INTRODUCTION, TECHNIQUES USED AND STRUCTURE OF THESIS 22
1.1 SCOPE AND AIMS OF THESIS 22
1.2 TECHNIQUES AND APPARATUS USED IN STUDY 23
1.2.1 LABORATORY BASED TECHNIQUES 23
1.2.1.1 EXPERIMENTAL TECHNIQUES 24
1.2.1.1.1 EXPERIMENTAL ROCK DEFORMATION APPARATUS 24
1.2.1.1.2 THE NIMONIC APPARATUS 25
1.2.1.1.3 SPECIMEN-PISTON ASSEMBLY 25
1.2.1.1.4 END CLOSURE AND SEALS 25
1.2.1.1.5 LOADING PISTON/FORCE GAUGE ASSEMBLY 27
1.2.1.1.6 LOAD APPLICATION 27
1.2.1.1.7 FURNACES 31
1.2.1.1.8 PRESSURE SYSTEM 31
1.2.1.1.9 DATA MEASUREMENT 32
1.2.1.1.10 DATA RECORDING 32
1.2.1.1.11 SAMPLE DAMAGE INTRODUCED BY THE APPARATUS 32
1.2.1.1.12 SAMPLE PREPARATION 33
1.2.1.1.13 EXPERIMENTAL PROCEDURE 33
1.2.1.1.14 PREPARATION OF OPTICAL THIN SECTIONS 34
1.2.1.2 MICROSTRUCTURAL TECHNIQUES 35
1.2.1.2.1 OPTICAL MICROSCOPY 35
1.2.1.2.2 UNIVERSAL STAGE 35
1.2.1.2.3 DATA ACQUISITION AND HANDLING 36

1.2.1.2.4 SCANNING ELECTRON MICROSCOPY 37
1.2.1.2.5 MICROCHEMICAL ANALYSIS 37
1.2.2 FIELD TECHNIQUES 38
1.3 STRUCTURE OF THESIS 38

CHAPTER 2 : LITERATURE REVIEW 39
2.1 INTRODUCTION 39
2.2 STABILITY FIELDS OF CALCITE 39
2.3 STRUCTURE AND CRYSTALLOGRAPHY 41
2.4 OPTICAL AND PHYSICAL PROPERTIES 44
2.4.1 OPTICAL PROPERTIES 44
2.4.2 THERMAL PROPERTIES 44
2.4.3 PHYSICAL PROPERTIES 44
2.4.4 ELASTIC PROPERTIES 44
2.4.5 DIFFUSIONAL PROPERTIES 45
2.4.6 DEFORMATIONAL PROPERTIES 45
2.5 EXPERIMENTAL DEFORMATION OF CALCITIC ROCKS 48
2.5.1 MODES FO ROCK FAILURE 48
2.5.2 PRESSURE SENSITIVE DEFORMATION 50
2.5.3 PLASTIC DEFORMATION 53
2.5.3.1 HIGH DIFFERENTIAL STRESS FLOW BEHAVIOUR 54
2.5.3.1.1 GRAIN BOUNDARY EFFECTS 55
2.5.3.1.2 MICROSTRUCTURE 57
2.5.3.1.3 RATE CONTROLLONG STEP 58
2.5.3.1.4 TWINNING 59
2.5.3.1.4.1 BEHAVIOUR OF TWINS AT HIGH TEMPERATURE 59
2.5.3.1.4.2 THE TWINNING FIELD BOUNDARY 60
2.5.3.1.4.3 STRAIN ESTIMATION 60
2.5.3.2 INTERMEADIATE DIFFERENTIAL STRESS FLOW BEHAVIOUR 61
2.5.3.2.1 MICROSTRUCTURE 62
2.5.3.2.2 HIGH STRESS EXPONENTIAL, POWER FLOW LAW 63
2.5.3.2.2.1 MICROSTRUCTURE 63
2.5.3.2.3 LOW STRESS EXPONENTIAL, POWER FLOW LAW 63
2.5.3.2.3.1 MICROSTRUCTURE 64
2.5.3.2.4 RATE CONTROLLING STEP 64
2.5.3.3 LOW DIFFERENTIAL STRESS FLOW BEHAVIOUR 66
2.5.3.3.1 PRESSURE SOLUTION 66
2.5.3.3.2 SOLID STATE DIFFUSIONAL CREEP 67
2.5.3.3.3 GRAIN BOUNDARY SLIDING ACCOMMODATED CREEP 67
2.5.3.3.4 MICROSTRUCTURE 68
2.5.3.3.5 RATE CONTROLLING STEP 68

CHAPTER 3 : PALAEOPIEZOMETRIC TECHNIQUES 74
3.1 INTRODUCTION 74
3.2 DYNAMICALLY RECRYSTALLIZED AND SUBGRAIN GRAIN SIZE 74
3.2.1 LIMITATIONS 77
3.3 FREE DISLOCATION DENSITY 77
3.3.1 LIMITATIONS 78
3.4 TWINNING 78
3.5 LIMITATIONS OF THE TECHNIQUES 79

CHAPTER 4 : THE CALIBRATION OF TWINNING ACTIVITY AS A FUNCTION OF DIFFERENTIAL STRESS AND GRAIN SIZE 81
4.1 INTRODUCTION 81
4.2 STARTING MATERIALS 81
4.2.1 SOLENHOFEN LIMESTONE 81
4.2.2 CARRARA MARBLE 83
4.2.3 TAIWANESE MARBLE 83
4.3 CHOICE OF EXPERIMENTAL PARAMETERS 83
4.4 METHOD USED TO QUANTIFY TWINNING ACTIVITY 87
4.5 THE TWINNING FIELD BOUNDARY FOR SOLENHOFEN LIMESTONE 88
4.5.1 CONCLUSIONS 98
4.6 THE LOCATION OF THE TWINNING FIELD BOUNDARY FOR CARRARA MARBLE 98
4.6.1 INTRODUCTION 98
4.6.2 EXPERIMENTS 99
4.6.2.1 THE 500°C SERIES 101
4.6.2.2 THE 550°C SERIES 104
4.6.2.3 THE 400°C SERIES 107
4.6.2.4 THE 300°C SERIES 110
4.6.2.5 THE 200°C SERIES 110
4.6.2.6 THE 600°C SERIES 113
4.6.2.7 PREVIOUSLY REPOERTED DATA 113
4.6.2.8 CONCLUSIONS 117
4.7 THE LOCATION OF THE TWINNING FIELD BOUNDARY FOR TAIWANESE MARBLE 118
4.7.1 INTRODUCTION 118
4.7.2 SAMPLE PREPARATION 118
4.7.3 EXPERIMENTAL AND TEXTURAL ANALYSIS 118
4.7.3.1 THE 700°C SERIES 120
4.7.3.2 THE 600°C SERIES 123
4.7.3.3 THE 800°C SERIES 124
4.7.3.4 THE 500°C SERIES 127
4.7.3.5 THE 400°C SERIES 132
4.7.3.6 CONCLUSIONS 132

4.8 DISCUSSION AND CONCLUSIONS 135

CHAPTER 5 : INTRODUCTION TO THE FIELD AREA 192
5.1 PRELIMINARY STATEMENTS 192
5.2 INTRODUCTION TO THE FIELD AREA 192
5.3 THE CANTABRIAN ZONE 195
5.3.1 STRATIGRAPHY 198
5.3.2 GENERAL GEOLOGICAL STRUCTURE AND EVOLUTION 200
5.3.3 SELECTION OF THE FIELD AREA 202

CHAPTER 6 : FIELD AREA 1 : THE ESLA NAPPE 204
6.1 INTRODUCTION 204
6.2 LOCATION 204
6.3 FAULT ROCK CLASSIFICATION AND TERMINOLOGY 204
6.3.1 GLOSSARY OF FAULT ROCK TERMINOLOGY USED 205
6.4 ORIENTATION OF THE PETROFABRICS 206
6.5 GENERAL GEOLOGICAL SETTING 206
6.6 SAMPLE LOCALITIES 208
6.7 THE HANGING WALL 208
6.8 THE FAULT ROCKS 212
6.8.1 THE TRANSITIONAL UNIT 212
6.8.2 BRECCIAS 215
6.8.3 THE CATACLASTIC SERIES 215
6.8.4 CARBONIFEROUS GIROTTE 220
6.8.5 INTERPRETATION AND DISCUSSION 220
6.9 FOOTWALL ROCKS 225
6.9.1 INTRODUCTION 225
6.9.2 SAMPLING PROGRAM AND ORIENTATION OF THE THIN SECTIONS 225
6.9.3 METHOD OF ANALYSIS AND DATA PRESENTATION 226
6.9.4 THE RELATIONSHIP BETWEEN TWINNING ACTIVITY AND GRAIN SIZE 226
6.9.4.1 INTRODUCTION 226
6.9.4.2 TWINNING ACTIVITY AS A FUNCTION OF GRAIN SIZE 233
6.9.4.3 INTERPRETATION 233
6.9.4.3.1 GRAIN SIZE LIMITATIONS UPON TWINNING INCIDENCE AND PERCENTAGE VOLUME TWIN DOMAIN 233
6.9.4.3.2 TWINNING CUT-OFF 235
6.9.4.3.3 THE RELATIONSHIP BETWEEN THE TWINNING INCIDENCE, NUMBER OF TWINS AND PERCENTAGE VOLUME TWINNED DOMAIN 236
6.9.4.3.4 PALAEOSTRESS DETERMINATION 237
6.9.5 TWINNING ACTIVITY ASSOCIATED WITH THRUSTING 237

6.9.5.1 INTRODUCTION AND DATA PRESENTATION 237
6.9.5.2 INTERPRETATION AND DISCUSSION 237
6.9.5.3 CONCLUSIONS 243
6.9.6 PETROFABRICS 244
6.9.6.1 INTRODUCTION 244
6.9.6.2 DATA PRESENTATION 244
6.9.6.3 INTERPRETATION 244
6.9.6.3.1 THE EFFECT OF A PRE-DEFORMATIONAL FABRIC 244
6.9.6.3.2 DYNAMIC ANALYSIS TECHNIQUE 246
6.9.6.3.3 THE EFFECT OF A HETEROGENEOUS STRESS FIELD 248
6.9.6.4 CONCLUSIONS 250

CHAPTER 7 : FIELD AREA 2 : THE SOMIEDO NAPPE 251
7.1 INTRODUCTION 251
7.2 TECHNIQUES USED AND GENERAL AIMS OF THE STUDY 251
7.3 LOCATION AND PHYSIOGEOGRAPHIC FEATURES 251
7.4 GENERAL GEOLOGICAL SETTING 253
7.5 STRUCTURE OF THE SOMIEDO NAPPE 254
7.5.1 THE BASAL THRUST 254
7.5.2 GEOMETERY OF THE THRUST SHEET 257
7.5.2.1 MAJOR INTERNAL THRUST SYSTEMS 257
7.5.2.2 IMBRICATE THRUSTS 259
7.5.2.3 TECTONIC WEDGES 262
7.5.2.4 REVERSE THRUSTS 262
7.5.2.5 OBLIQUE RAMPS 262
7.5.3 DEVELOPMENT OF FOLDING 263
7.5.4 FACTORS WHICH DETERMINE THE ORIGINAL EMPLACEMENT OF THE NAPPE 263
7.5.5 TEXTURAL ANALYSIS 265
7.5.5.1 INTRODUCTION 265
7.5.5.2 SAMPLING PROGRAM AND ORIENTATION OF THE SPECIMENS 266
7.5.5.3 METHOD OF ANALYSIS AND DATA PRESENTATION 266
7.5.5.4 THE SANTA LUCIA TECTONIC WEDGE, EAST OF TORRESTIO 267
7.5.5.4.1 INTRODUCTION 267
7.5.5.4.2 TWINNING ACTIVITY AS A FUNCTION OF GRAIN SIZE 267
7.5.5.4.3 TWINNING CUT-OFF 268
7.5.5.4.4 THE RELATIONSHIP BETWEEN TWINNING INCIDENCE, NUMBER OF TWINS AND PERCENTAGE VOLUME TWIN DOMAIN 268
7.5.5.4.5 PALAESTRESS DETERMINATION 276
7.5.5.4.6 STRESS LEVELS ASSOCIATED WITH THRUSTING 278
7.5.5.4.7 PETROFABRICS 278

7.5.5.5 THE PORTILLA TECTONIC WEDGE, EAST OF LA CUETA 280
7.5.5.5.1 INTRODUCTION 280
7.5.5.5.2 TWINNING ACTIVITY AS A FUNCTION OF GRAIN SIZE 280
7.5.5.5.3 TWINNING CUT-OFF 280
7.5.5.5.4 THE RELATIONSHIP BETWEEN TWINNING INCIDENCE, NUMBER OF TWINS AND PERCENTAGE VOLUME TWIN DOMAIN 288
7.5.5.5.5 PALAEOSTRESS DETERMINATION 288
7.5.5.5.6 STRESS LEVELS ASSOCIATED WITH THRUSTING 290
7.5.5.5.7 PETROFABRICS 290
7.5.6 CONCLUSIONS 292

CHAPTER 8 : CONCLUSIONS, GENERAL DISCUSSION AND SUGGESTIONS FOR FURTHER RESEARCH 294
8.1 INTRODUCTION 294
8.2 CONCLUSIONS AND GENERAL DISCUSSION 294
8.2.1 EXPERIMENTAL WORK 294
8.2.2 FIELD WORK 296
8.3 SUGGESTIONS FOR FURTHER RESEARCH 298
8.4 CONCLUDING STATEMENT 302

APPENDICES 303

REFERENCES 321

LIST OF FIGURES

CHAPTER 1

FIGURE 1.1 Diagram of the Nimonic Apparatus (after Peach et al., 1981). 26

FIGURE 1.2 Diagram showing the detail of the Top Closure Assembly of the Nimonic Apparatus (after Shaw 1980). 28

FIGURE 1.3 Diagram showing the detail of the Lower Closure Assembly of the Nimonic Apparatus (after Shaw 1980). 29

FIGURE 1.4 Diagram showing the detail of the Loading Piston/Force Gauge Assembly of the Nimonic Apparatus (after Shaw 1980). 30

CHAPTER 2

FIGURE 2.1 Phase diagram for calcium carbonate. 40

FIGURE 2.2 The $CaO-CO_2-H_2O$ System at 1 kilobar. 40

FIGURE 2.3 Crystal structure of calcite. 42

FIGURE 2.4 Crystallographic planes in calcite. 42

FIGURE 2.5 Twinning in calcite. 49

FIGURE 2.6 Stress/strain curve for calcite single crystal. 49

FIGURE 2.7 Stress/strain curves for calcite deformed at 20°C, showing the importance of crystallographic orientation upon deformation path. 51

FIGURE 2.8 Cataclastic flow of quartzite around a deformation rig piston. 51

FIGURE 2.9 Stress/strain curves for Solenhofen Limestone, showing the effect of confining pressure apon rock strength (after Rutter 1974). 52

FIGURE 2.10 Grain boundary sliding model of Ashby and Verrall (1973). 70

FIGURE 2.11 Deformation mechanism chart for 100μm calcite (after Rutter 1976). 70

CHAPTER 3

FIGURE 3.1 Normalized plot of dynamically recrystallised grain size as a function of stress (after Schmid et al., 1980). 76

FIGURE 3.2 The Dynamic Analysis Technique (after Turner, 1954). 76

CHAPTER 4

FIGURE 4.1 Inverse Pole Figure for the Solenhofen Limestone starting material. 84

FIGURE 4.2 Stereographic projection for the c-axis of Carrara Marble starting material. 84

FIGURE 4.3 It contour map in Temperature/Strain rate space for the series of experiments performed upon Solenhofen Limestone. 91

FIGURE 4.4 It contour map in Differential Stress/Strain Rate space for the Solenhofen Limestone series of experiments, with the temperature of the experiments superimposed. 91

FIGURE 4.5 Iso-strain rate sections through Fig. 4.3. 92

FIGURE 4.6 Iso-temperature sections through Fig. 4.3. 92

FIGURE 4.7 Series of photomicrographs illustrating the increase in the importance of twinning with increasing strain rate for Solenhofen Limestone. 93

FIGURE 4.8 Series of photomicrographs illustrating the increase in the importance of twinning with decreasing temperature for Solenhofen Limestone. 96

FIGURE 4.9 Differential stress/strain curves for the 500°C series of experiments performed upon Carrara Marble. 137

FIGURE 4.10 Twinning activity/grain size diagrams for the 500°C series of experiments performed upon Carrara Marble. 138

FIGURE 4.11 Histograms showing the number of data points within each grain size interval for Fig. 4.10. 140

FIGURE 4.12 Differential stress/strain curves for the 550°C series of experiments performed upon Carrara Marble. 142

FIGURE 4.13 Twinning activity/grain size diagrams for the 550°C series of experiments performed upon Carrara Marble. 143

FIGURE 4.14 Histograms showing the number of data points within each grain size interval for Fig. 4.13. 145

FIGURE 4.15 Differential stress/strain curves for the 400°C series of experiments performed upon Carrara Marble. 146

FIGURE 4.16 Twinning activity/grain size diagrams for the 400°C series of experiments performed upon Carrara Marble. 147

FIGURE 4.17 Histograms showing the number of data points within each grain size interval for Fig. 4.16. 150

FIGURE 4.18 Differential stress/strain curves for the 300°C series of experiments performed upon Carrara Marble. 152

FIGURE 4.19 Twinning activity/grain size diagrams for the 300°C series of experiments performed upon Carrara Marble. 153

FIGURE 4.20 Histograms showing the number of data points within each grain size interval for Fig. 4.19. 155

FIGURE 4.21 Composite figure showing the rheological data, textural data and the number of data points within each grain size interval for the textural data. 156

FIGURE 4.22 Differential stress/strain curves for the 600°C series of experiments performed upon Carrara Marble. 157

FIGURE 4.23 Twinning activity/grain size diagrams for the 600°C

series of experiments performed upon Carrara Marble. 158

FIGURE 4.24 Histograms showing the number of data points within each grain size interval for Fig. 4.23. 160

FIGURE 4.25 It contour map in Temperature/Strain Rate space for the series of experiments performed upon Carrara Marble. 161

FIGURE 4.26 It contour map in Differential Stress/Strain Rate space for the Carrara Marble series of experiments, with the temperature of the experiments superimposed. 161

FIGURE 4.27 Iso-strain rate sections through Fig. 4.25. 162

FIGURE 4.28 Iso-temperature sections through Fig. 4.25. 162

FIGURE 4.29 It contour diagram for the Carrara Marble series of experiments plotted in Differential Stress/Grain Size. 163

FIGURE 4.30 Differential stress/strain curves for the 700°C series of experiments performed upon Taiwanese Marble. 164

FIGURE 4.31 Twinning activity/grain size diagrams for the 700°C series of experiments performed upon Taiwanese Marble. 165

FIGURE 4.32 Histograms showing the number of data points within each grain size interval for Fig. 4.31. 167

FIGURE 4.33 Differential stress/strain curves for the 600°C series of experiments performed upon Taiwanese Marble. 168

FIGURE 4.34 Twinning activity/grain size diagrams for the 600°C series of experiments performed upon Taiwanese Marble. 169

FIGURE 4.35 Histograms showing the number of data points within each grain size interval for Fig. 4.34. 172

FIGURE 4.36 Differential stress/strain curves for the 800°C series of experiments performed upon Taiwanese Marble. 174

FIGURE 4.37 Twinning activity/grain size diagrams for the 800°C

series of experiments performed upon Taiwanese Marble. 175

FIGURE 4.38 Histograms showing the number of data points within each grain size interval for Fig. 4.37. 177

FIGURE 4.39 Differential stress/strain curves for the 500°C series of experiments performed upon Taiwanese Marble. 178

FIGURE 4.40 Twinning activity/grain size diagrams for the 500°C series of experiments performed upon Taiwanese Marble. 179

FIGURE 4.41 Histograms showing the number of data points within each grain size interval for Fig. 4.40. 181

FIGURE 4.42 Differential stress/strain curves for the 400°C series of experiments performed upon Taiwanese Marble. 183

FIGURE 4.43 Twinning activity/grain size diagrams for the 400°C series of experiments performed upon Taiwanese Marble. 184

FIGURE 4.44 Histograms showing the number of data points within each grain size interval for Fig. 4.43. 186

FIGURE 4.45 It contour map in Temperature/Strain rate space for the series of experiments performed upon Taiwanese Marble. 188

FIGURE 4.46 It contour map in Differential Stress/Strain Rate space for the Taiwanese Marble series of experiments, with the temperature of the experiments superimposed. 188

FIGURE 4.47 Iso-strain rate sections through Fig. 4.45. 189

FIGURE 4.48 Iso-temperature sections through Fig. 4.45. 189

FIGURE 4.49 It contour diagram for the Taiwanese Marble series of experiments plotted in Differential Stress/Grain Size. 190

FIGURE 4.50 Diagram showing the temperature dependence of the number/percentage volume ratio for the Carrara and Taiwanese Marble series of experiments. 191

FIGURE 4.51 It contour diagram plotted in Differential Stress/log Grain Size space for the experimental data discussed in Chapter 4. 191

CHAPTER 5

FIGURE 5.1 Geological map of Spain 194

FIGURE 5.2 Geological map of the Cantabrian Zone. 196

FIGURE 5.3 General sedimentary sequence developed in the Cantabrian Zone. 199

FIGURE 5.4 Palinspastically restored structural section through the Cantabrian Zone. 201

CHAPTER 6

FIGURE 6.1 Figure showing the preparation and orientation of orientated thin sections and petrofabrics from orientated field specimens. 207

FIGURE 6.2 Map showing the Esla Nappe thrust trace and the locations of the sections studied with diagramatic sections showing the juxtaposition of the principal rock units. 209

FIGURE 6.3 Diagramatic model for breccia development at the base of the Esla Nappe. 224

FIGURE 6.4 Twinning activity data plotted as a function of grain size for the specimens collected from Portilla Limestone from the Cremenes-Corniero section. 227

FIGURE 6.5 Histograms showing the number of data points in each of grain size intervals of Fig. 6.4. 231

FIGURE 6.6 Schematic diagram showing the predicted relationships between twinning activity and grain size. 234

FIGURE 6.7 Percentage volume twin domain values for the Portilla Limestone plotted against distance below the thrust plane. 238

FIGURE 6.8 Selected petrofabrics showing the intensification of the fabric as the thrust is approached. 245

FIGURE 6.9 Selected Compression/Tension axes diagrams for the Portilla Limestone from the section studied. 247

FIGURE 6.10 Compression/Tension axes for those grains with more than ten twin lamellae. 247

FIGURE 6.11 Stress field configuration around a Type II crack tip. 249

CHAPTER 7

FIGURE 7.1 Structural map of the Somiedo Nappe showing the positions of the two sections studied. 252

FIGURE 7.2 The initiation of folds resulting from different thrust ramp/flat configurations. 258

FIGURE 7.3 Twinning activity data plotted as a function of grain size for the Santa Lucia Limestone from the Tectonic Wedge to the west of Torrestio. 269

FIGURE 7.4 Histograms showing the number of data points in each of grain size intervals of Fig. 7.3. 272

FIGURE 7.5 Experimental data plotted in Differential Stress/log Grain Size space with the It data from Fig. 7.3 superimposed. 277

FIGURE 7.6 Figure showing the stress levels obtained from Fig. 7.5 and their spatial relationship with the thrust. 277

FIGURE 7.7 Selected Petrofabrics from the Santa Lucia Tectonic Wedge. 279

FIGURE 7.8 Compression/Tension axes for those grains with more than ten twin lamellae from the Santa Lucia Tectonic Wedge. 279

FIGURE 7.9 Twinning activity data plotted as a function of grain size for the Portilla Limestone from the Tectonic Wedge to the west of La Cueta. 281

FIGURE 7.10 Histograms showing the number of data points in each of grain size intervals of Fig. 7.10. 284

FIGURE 7.11 Experimental data plotted in Differential Stress/log Grain Size space with the It data from Fig. 7.10 superimposed. 289

FIGURE 7.12 Figure showing the stress levels obtained from Fig. 7.10 and their spatial relationship with the thrust. 289

FIGURE 7.13 Selected Petrofabrics from the Portilla Tectonic Wedge. 291

FIGURE 7.14 Compression/Tension axes for those grains with more than ten twin lamellae from the Portilla Tectonic Wedge. 291

FIGURE 7.15 Figure showing the relationship between It and number/% volume twin domain. 293

CHAPTER 8

FIGURE 8.1 Percentage volume twin domain plotted as a function of Schmid Factor (After Spiers, 1981). 299

FIGURE 8.2 Diagram showing the transitions between modes of failure for Carrara Marble and Solenhofen Limestone. 301

FIGURE 8.3 Diagram showing the theoretical PTt path of a rock. 301

LIST OF PLATES

CHAPTER 4

PLATE 4.1 Photomicrographs of the experimental starting materials, Carrara Marble and Taiwanese Marble. 86

PLATE 4.2 Representative photomicrographs of the 500°C Series of Experiments performed upon Carrara Marble. 103

PLATE 4.3 Representative photomicrographs of the 550°C Series of Experiments performed upon Carrara Marble. 106

PLATE 4.4 Representative photomicrographs of the 400°C Series of Experiments performed upon Carrara Marble. 109

PLATE 4.5 Representative photomicrographs of the 300°C and 200°C Series of Experiments performed upon Carrara Marble. 112

PLATE 4.6 Representative photomicrographs of the 600°C Series of Experiments performed upon Carrara Marble. 115

PLATE 4.7 Representative photomicrographs of the 700°C Series of Experiments performed upon Taiwanese Marble. 122

PLATE 4.8 Representative photomicrographs of the 600°C Series of Experiments performed upon Taiwanese Marble. 126

PLATE 4.9 Representative photomicrographs of the 800°C Series of Experiments performed upon Taiwanese Marble. 129

PLATE 4.10 Representative photomicrographs of the 500°C Series of Experiments performed upon Taiwanese Marble. 131

PLATE 4.11 Representative photomicrographs of the 400°C Series of Experiments performed upon Taiwanese Marble. 134

CHAPTER 6

PLATE 6.1 A series of field photographs and photomicrographs from the hanging wall Lancara Limestone, Transitional Unit and Breccia Unit. 211

PLATE 6.2 Representative photomicrographs of the Transitional Unit. 214

PLATE 6.3 Representative photomicrographs and SEM photographs of the Breccia Unit. 217

PLATE 6.4 Representative photomicrographs and SEM photographs from the Cataclastic Unit. 219

PLATE 6.5 Representative photomicrographs from the Footwall Units of the Esla Nappe. 222

PLATE 6.6 Representative photomicrographs of the Portilla Limestone from the Cremenes-Corniero section. 240

PLATE 6.7 Representative photomicrographs of the Portilla Limestone from the Cremenes-Corniero section. 242

CHAPTER 7

PLATE 7.1 Field photographs showing the development of cataclasis and cleavage from the Somiedo Nappe. 256

PLATE 7.2 Field photographs showing some of the characteristic structural features of the Somiedo Nappe. 261

PLATE 7.3 Representative photomicrographs from the Santa Lucia Tectonic Wedge, west of Torrestio. 275

PLATE 7.4 Representative photomicrographs from the Portilla Tectonic Wedge, east of La Cueta. 288

LIST OF TABLES

CHAPTER 2

TABLE 2.1 Calcite Unit Cells. 43

TABLE 2.2 Thermal and Elastic Properties. 43

TABLE 2.3 Plastic Properties and Diffusion Data for Calcite. 46

TABLE 2.4 Twinning and Slip Systems for Calcite. 46

TABLE 2.5 Data Summary. 71

CHAPTER 4

TABLE 4.1 Table listing the physical properties of the experimental materials used in this Thesis. 82

TABLE 4.2 List of experiments used in the location of the twinning field boundary for Solenhofen Limestone (Spiers, 1981). 90

TABLE 4.3 List of the experiments performed to locate the position of the twinning field boundary for Carrara Marble. 100

TABLE 4.4 List of the experiments used to locate the approximate position of the twinning field boundary for Carrara Marble (after Spiers, 1981). 116

TABLE 4.5 List of the experiments performed to locate the position of the twinning field boundary for Taiwanese Marble. 119

LIST OF APPENDICES

APPENDIX 1 : EXPERIMENTAL DATA RECORDING AND PROCESSING 303
LISTING 1 : THE COMPUTER PROGRAM "PREM2" 306
LISTING 2 : THE COMPUTER PROGRAM "CRFILES" 309
LISTING 3 : THE COMPUTER PROGRAM "DATRED7" 311

APPENDIX 2 : COMPUTER PROGRAM USED TO DRAW X-Y GRAPHS 312
LISTING 4 : THE COMPUTER PROGRAM "MULPLOT" 313

APPENDIX 3 : COMPUTER PROGRAM USED TO DRAW HISTOGRAMS 314
LISTING 5 : THE COMPUTER PROGRAM "HISTO" 315

APPENDIX 4 : COMPUTER PROGRAM USED TO RECORD AND MANIPULATE TEXTURAL DATA 316
LISTING 6 : THE COMPUTER PROGRAM "D.BASE" 317

APPENDIX 5 : COMPUTER PROGRAM USED TO DRAW FIG. 6.11 318
LISTING 7 : THE COMPUTER PROGRAM "STRESS" 318

APPENDIX 6 : ACID-ETCH TECHNIQUE USED TO PRODUCE ULTRA THIN SECTION 319

NOTE The author realises that the quality of the reproduction of the Listings is not perfect, however in order that the length of the Thesis be optimised they were reduced to the magnification presented. Copies of these programs are available from the Department of Geology, Imperial College of Science and Technology.

LIST OF ABBREVIATIONS

The following is a list of some of the key abbreviations used in this Thesis, and is not a definitive list.

Å - Angström
BSI - Back Scattered Imagery
CPO - Crystallographic preferred orientation
CRSS - Critical Resolved Shear Stress
°C - degrees Celsius
Cr-Al - Chromium-Aluminum
cm - centimetre
DAT - Dynamic Analysis Technique
e - strain rate
Fig. - Figure
gbs - grain boundary sliding
gbm - grain boundarey migration
IPF - Inverse Pole Figure
km - kilometre
kW - kilowatt
LVDT - Linear Variable Displacment Transducer
mm - milimetre
MPa - Mega Pascal
mv - milivolt
% - percentage
psi - pounds per square inch
sec - second
SEI - Secondary Electron Imagery
SEM - Scanning Electron Microscopy
$\sigma 1$, $\sigma 2$, $\sigma 3$ - sigma 1, 2 and 3, principal stress axes, $\sigma 1 \geq \sigma 2 \geq \sigma 3$
μm - micron

Note that the spelling of Solenhofen Limestone used in this Thesis is the English spelling.

ACKNOWLEDGEMENTS

Over the three years of my Ph.D. there are many people to whom I am indebted both for advice (often critical) and friendship both in and out of the public houses that are dotted around Imperial College. To thank all in the space of this page would be impossible, but to you all a big thanks. the following are some of the people to whom I am especially grateful.

Firstly I would like to thank my supervisor Dr. Ernie Rutter for his encouragement, suggestions and general giudance for the duration of the research, and for his critical reading of the majority of the text. Additionally I would like to thank Dr. Stanley White who also gave of his time to read several Chapters, and for his general comments over the three years.

The staff and students of Oviedo University have provided essential logistical and technical assistence, without which the fieldwork presented in this Thesis would have impossible. In particular I am grateful to Drs. Andres Perez-Estaun, Juan Luis Allonso, Nemesio Herredia and Floro Garcia.

Robert Holloway has been invaluable both for maintaining the rock deformation apparatus and who with, Drs. Robert Maddock and Ernie Rutter, taught me how to use the machines whose potential for destruction will long be remembered. Dick Giddens provided expert tuition for operation of the Jeol 733 SEM and introduced the opportunity for the odd afternoon playing cricket. Alan Jones and the staff of the Rock Cutting Lab. both for providing excellent thin sections, instruction which enabled me to make my own thin sections and not a little encouragement. The staff of the Photographic Department have given freely of their time to try and instruct me as to the subtleties of photography, and I think that my various unsuccessful attempts to become the D. Bailey of the geological world have at least given them some humorous moments. I am extremely grateful to Mr. Nick Morton in particular who produced the excellent Plates presented in this Thesis.

My fellow postgraduate students have provided many informative, stimulating and amusing discussions, many thanks to Mohammed Amen, Peter Bretan, Saranne Cessford, Andy Hyett, Robert Maddock, Howard Obee, Bill Shea, Jeremy Young, Jill Walker and last but not least Yi Wang. Good luck in all that you do for the future.

Finally I thank my parents, Ida and Ken, for their consistent support, including financial assistance on several occasions, and to Nicky for checking the spelling, constant encouragement and for making it all worthwhile, espicially during the hectic period of the writing up.

Many thanks to you all.

CHAPTER 1 : INTRODUCTION

1.1 SCOPE AND AIMS OF THESIS

The level of differential stress acting on and transmitted by rocks, and the extent to which it can be inferred from their microstructures is of great significance to all earth scientists, and to structural geologists in particular. It has practical implications, e.g. the mechanisms of earthquake generation and prediction, and the interpretation of in-situ stress data for engineering applications. A number of methods relating observed plastic strain microstructures to differential stress have been published. These are based upon theoretical considerations, observations of naturally deformed materials, and/or their calibration with experimentally deformed specimens.

The principal palaeo-stress indicating microstructures are :

1. Dynamically recrystallised and subgrain grain size, e.g. Twiss (1977) and Ross et al. (1980).

2. Free dislocation density, e.g. Goetz and Kohlstedt (1977), Schmid et al. (1977), Schmid et al. (1980) and Briegel and Goetze (1975).

3.Twinning, e.g. Jamison and Spang (1976), Tullis (1980), Spiers (1981), and Spiers and Rutter (1984).

These techniques and their limitations are discussed fully in Chapter 3. It will suffice to say for the moment that twinning is probably the most reliable.

Calcite is one of the most common of upper crustal minerals. When calcite is subjected to an applied stress under the low temperatures typical of upper crustal deformation it responds by some combination of twinning and intracrystalline glide. Cataclasis may also be significant if effective confining pressure is low.

Several workers, e.g. Spiers (1981), Schmid (1982a) have noted that for calcite the amount of twinning varies with :

1. Differential stress.

2. Grain size.

In this study therefore, a series of experiments have been carried out on different grain size calcitic materials, in which temperature, confining pressure and strain rate were varied for each test to give different differential stress levels. This has led to the full calibration of a calcite twinning palaeopiezometer.

The second aim of this project is to investigate the application of the experimental models to the Northern Spanish Hercynian fold and thrust belt, the Cantabrian zone. The Cantabrians represent the external part of the orogenic belt, and are characterised by a well layered shelf sedimentary sequence. The region displays Rocky Mountain style "thin skinned" fold and thrust tectonics. The entire zone has subsequently suffered oroclinal bending so that transport directions of the nappes now appear to be directed towards the centre of the Cantabrian Arc.

Dolomitic and quartzitic rocks at high crustal levels deform predominantly by cataclastic processes as a result of their inablity to accommodate strain by intracrystalline processes at low temperatures. This is in direct contrast to the behaviour typical of calcitic rocks, where a significant amount of intracrystalline plasticity by twinning occurs under these conditions. These relationships are well displayed in the Cantabrian zone, and the study of the contrasting styles of behaviour has formed a significant part of this study.

The aims of this project have been to formulate models using the techniques of experimental rock deformation. These models have led to the quantification of a method by which differential stress can be inferred from natural rocks, and it is hoped that this will lead to an understanding of the state of stress associated with the formation of orogenic belts.

1.2 TECHNIQUES AND APPARATUS USED IN STUDY

This section reviews the techniques and describes the apparatus used in this study.

1.2.1 LABORATORY BASED TECHNIQUES

The laboratory based techniques can be subdivided into ;

1. Experimental rock deformation techniques.

2. Microstructural study techniques.

1.2.1.1 EXPERIMENTAL TECHNIQUES.

The experimental rock deformation apparatus and the sample preparation techniques are described in this section. For a description of the experimental starting materials and the selection of the deformational parameters employed the reader is referred to Chapter 4. Note that the general procedures for sample preparation are reported here, any departure from this will be described where appropriate in Chapter 4.

1.2.1.1.1 EXPERIMENTAL ROCK DEFORMATION APPARATUS

The Experimental Rock Deformation Laboratory is located in room LG 12, in the basement of the Royal School of Mines Building at Imperial College. There are installed two types of triaxial, externally heated, fluid medium rock deformation apparatus. These are :

(1) Heard type apparatus - built by Rutter (1970) and based on an original design of Heard (1963).

(2) Nimonic apparatus - the prototype was designed and built at Imperial College by Rutter, Holloway and Shaw in 1979, and is described in Peach et al., 1981. During the period of my research a second Nimonic apparatus became operational. This was of a similar design to the prototype machine but incorporated several improvements which improved reliability and performance.

The Heard rig's pressure vessel is made from a hot-work pressure die-casting steel which, owing to the extremely corrosive nature of water at elavated temperature, uses silicone oil as a confining medium. Hence an upper limit of a little over 400°C is imposed upon these machines. Above this temperature the silicone oil begins to polymerise. The pressure vessel of the Nimonic apparatus is made from Nimonic 105 Superalloy (Henry Wiggins & Co.) which is highly resistant to water at elevated temperatures. Hence water is used as the confining medium. The alloy begins to age at around 850°C, which is therefore regarded as an upper working temperature. The machine can be operated to 400MPa confining pressure at 600°C, 250MPa at 700°C and 150MPa at 800°C.

The majority of the experiments reported in this thesis required temperatures in the range of 400°C to 700°C, therefore the Nimonic apparatus only was used. Furthermore, the majority of the experiments were performed on the prototype machine. This particular machine is described below, and is

referred to throughout this thesis as "the Nimonic apparatus". Where the newer Nimonic apparatus was used this machine is referred to as "Nimonic II".

1.2.1.1.2 THE NIMONIC APPARATUS

This apparatus is described in the laboratory manual written by Shaw (1980), and the reader is referred to this document for a full treatment of the selection process of the materials used in the construction, and their physical, chemical, material and thermomechanical properties. Only an outline of the key points is given below.

1.2.1.1.3 SPECIMEN - PISTON ASSEMBLY

The pressure vessel and pistons of the Nimonic apparatus were fabricated from forged "Nimonic 105", which is a nickel-cobalt-chronium alloy. This material is strong and highly resistant to creep at temperatures up to 800-900°C, above which rapid weakening occurs.

The vertical pressure vessel is mounted above a gearbox driven ballscrew assembly, via which axial load is applied. The axial force gauge assembly is carried in the lower moving piston, so that specimen insertion and retrieval can be carried out without the pressure vessel/furnace assembly having to be dismantled.

The apparatus is figured in cross section in Fig. 1.1. The specimen is encapsulated in a 0.25mm wall thickness tubular copper jacket which had been previousely annealed by heating to redness followed by quenching in water, and cleaned by immersion in 50:50 nitric acid. The copper jacket is sealed onto the tapered ends of the pistons with internally tapered nimonic swaging rings.

The upper piston has a 1.5mm diameter hole down its complete length via which pore fluid pressure, if required, is introduced. It also allows insertion of an internal sheathed thermocouple onto the top of the specimen. The specimen-piston assembly is introduced and retrieved from the vertical pressure vessel via the top closure assembly, and is inserted until the lower piston rests on the loading-piston/force gauge assembly (see later).

1.2.1.1.4 END CLOSURES AND SEALS

These have three functions :

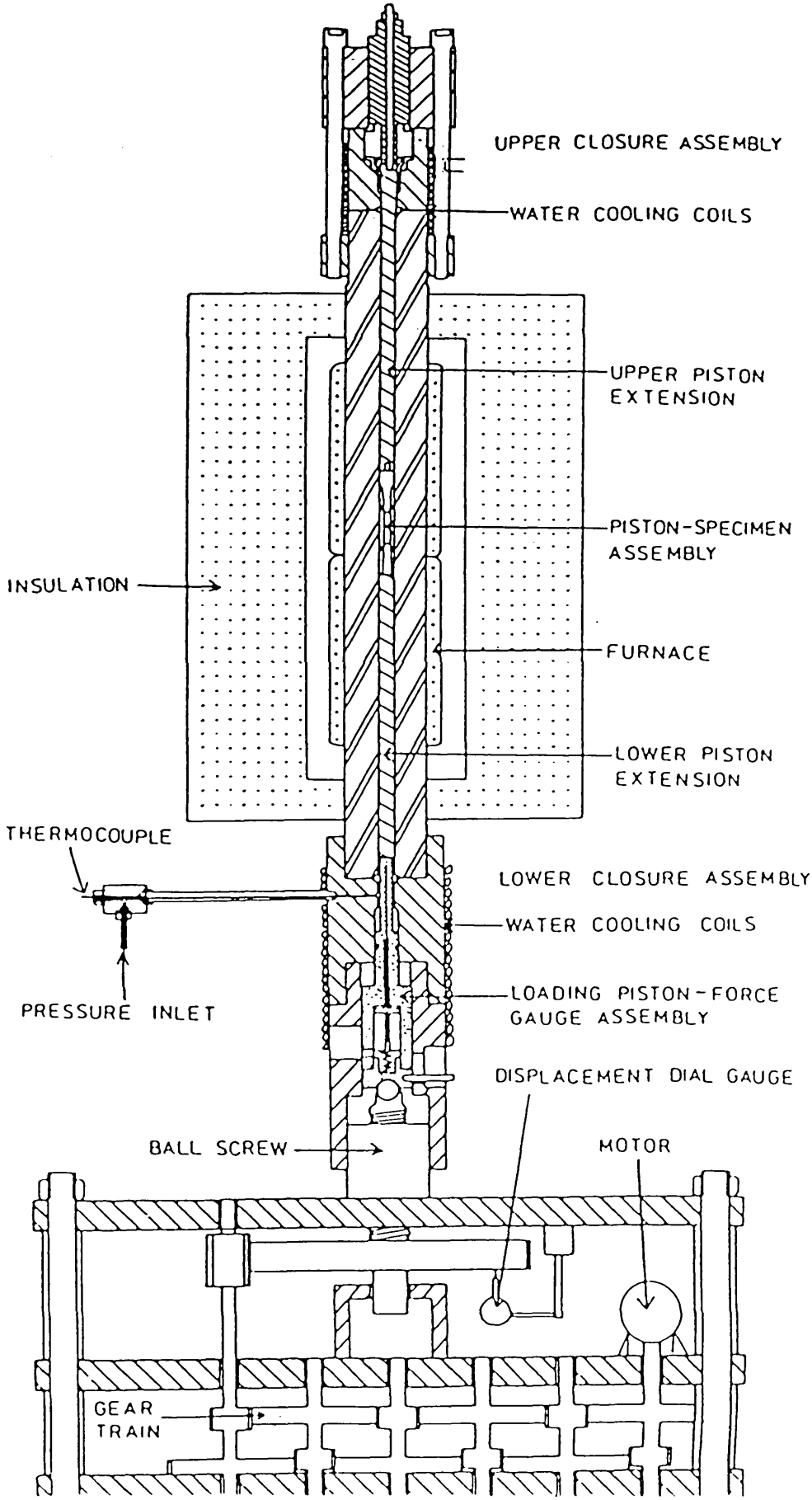


FIGURE 11 Diagram of the Nimonic Apparatus (after Shaw, 1980).

(1) To render the vessel pressure-tight.

(2) To enable specimen insertion and retrieval.

(3) Permit application and measurement of axial load.

The top closure assembly (Fig. 1.2) allows specimen insertion and retrieval, and forms the static end block during deformation. The closure itself is a hybrid. A bolted flange/face abutment closure connects the nimonic pressure vessel to the steel end-closure components via a copper delta-ring seal. A screwed end cap closure assembly using a rubber "o" ring seals the steel end closure assembly to the piston, and supports the axial load and the force due to the confining pressure.

The lower closure assembly (Fig. 1.3) allows the application of axial load, and consists of two parts. The lower simply links the ball screw assembly to the pressure vessel and houses the loading piston/force gauge assembly (see later), while the upper is an extension of the pressure vessel. The seals are of the same types as for the top closure assembly.

Both closures are surrounded by water cooling jackets which lowers the temperature of the seals during operation below 80°C, and maintains a uniform thermal profile along the length of the pressure vessel. Thermal gradients in the sample area do not exceed 3°C/cm during operation (Shaw ,1980) even at the highest operating temperatures. The recirculating water pump and refrigeration system employed is described by Rutter (1970).

1.2.1.1.5 LOADING PISTON/FORCE GAUGE ASSEMBLY

The loading piston/force gauge assembly (Fig. 1.4) is an integral part of the lower closure assembly, and consists essentially of a hollow thrust block, housing the force gauge transducer body. The elastic distortion of the hollow steel column above the transducer body is transmitted by a central unstressed rod to the movable core of the transducer (a DC type linear variable differential transformer - LVDT). The displacement of the core of the LVDT provides a measure of the axial load applied to the specimen.

1.2.1.1.6 LOAD APPLICATION

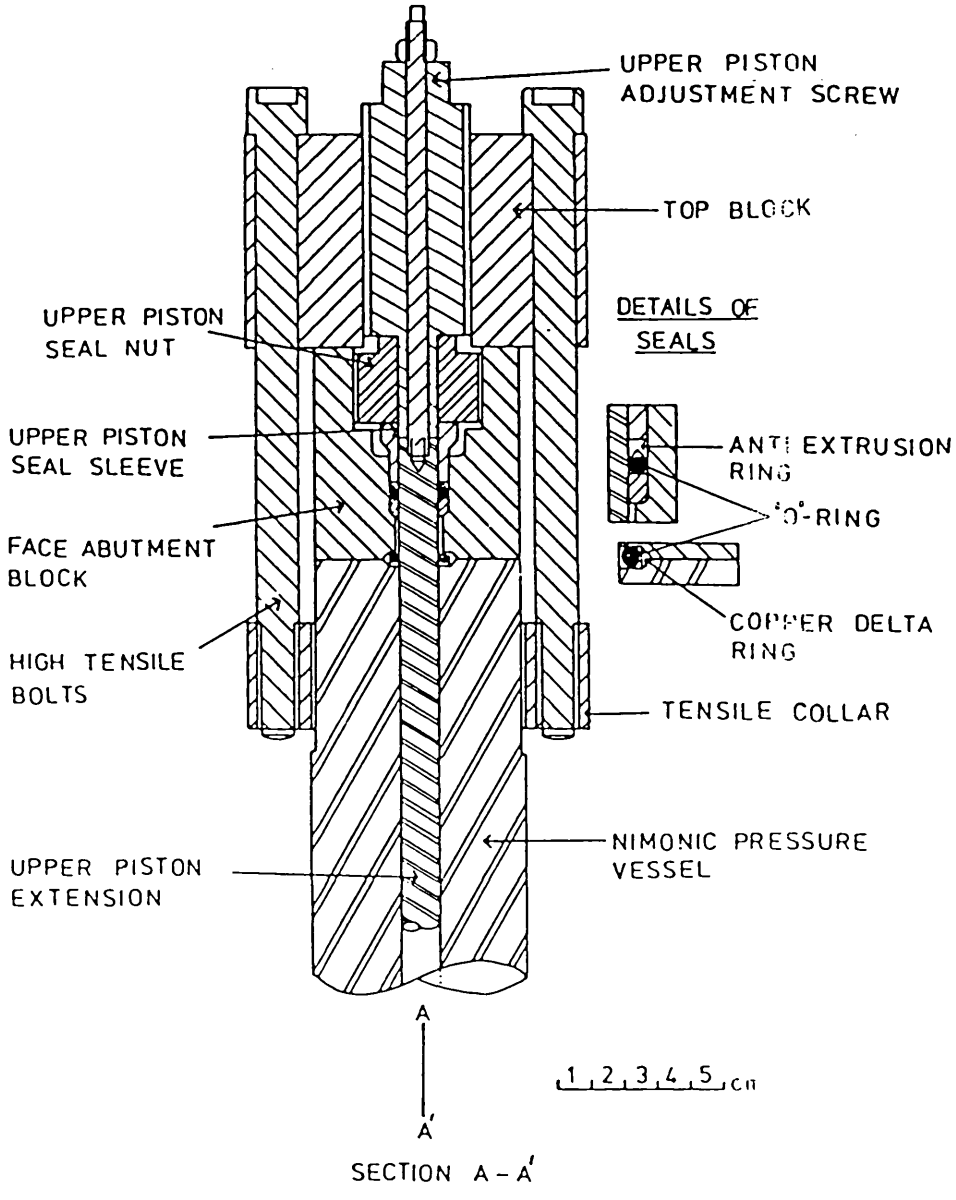


FIGURE 1.2 Cross sectional diagram of the Top Closure Assembly of the Nimonic Apparatus, shown in Fig. 1.1 (after Shaw, 1980).

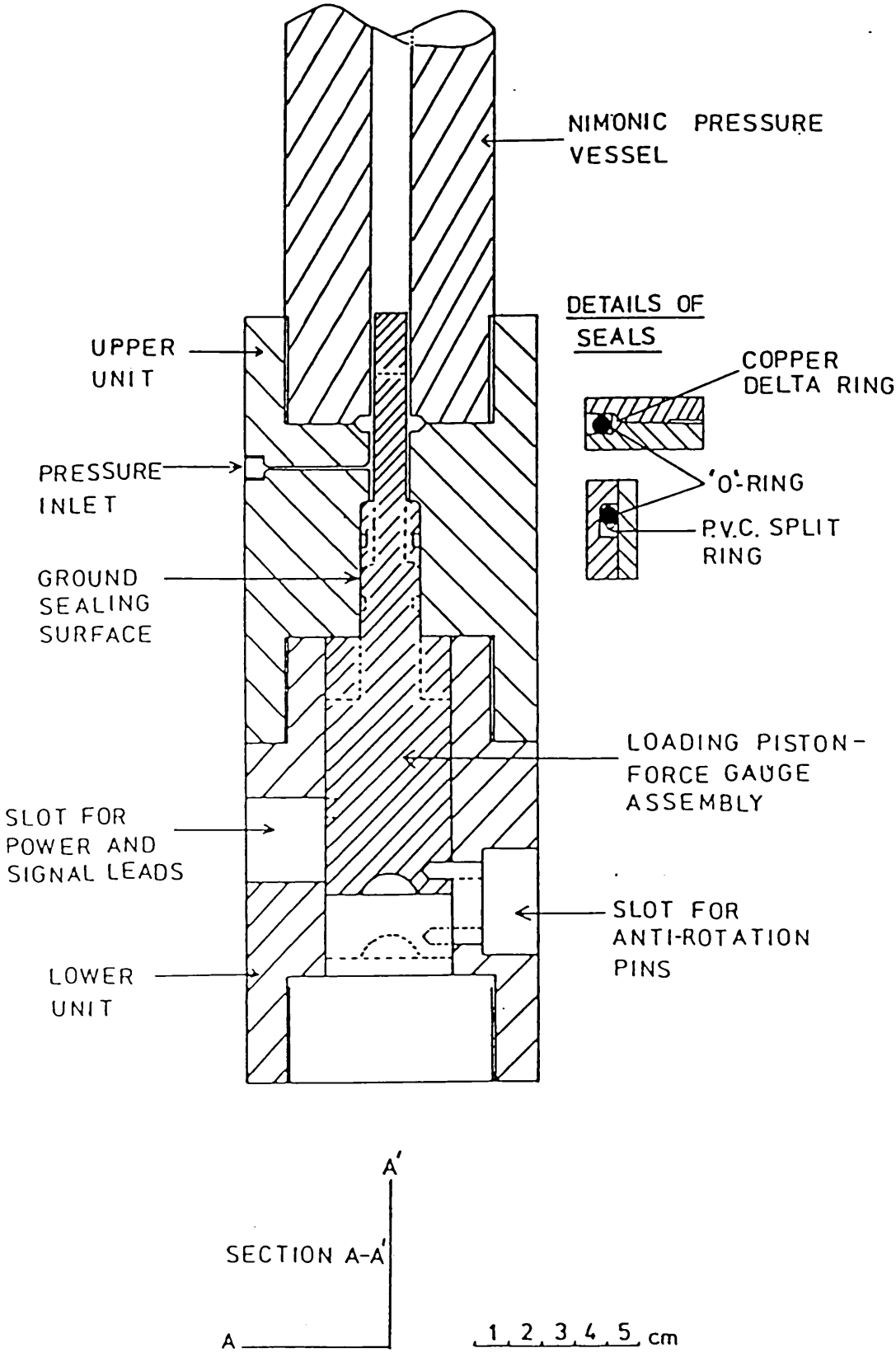


FIGURE 1.3 Cross sectional diagram of the Bottom Closure Assembly of the Nimonic Apparatus, shown in Fig. 1.1 (after Shaw, 1980).

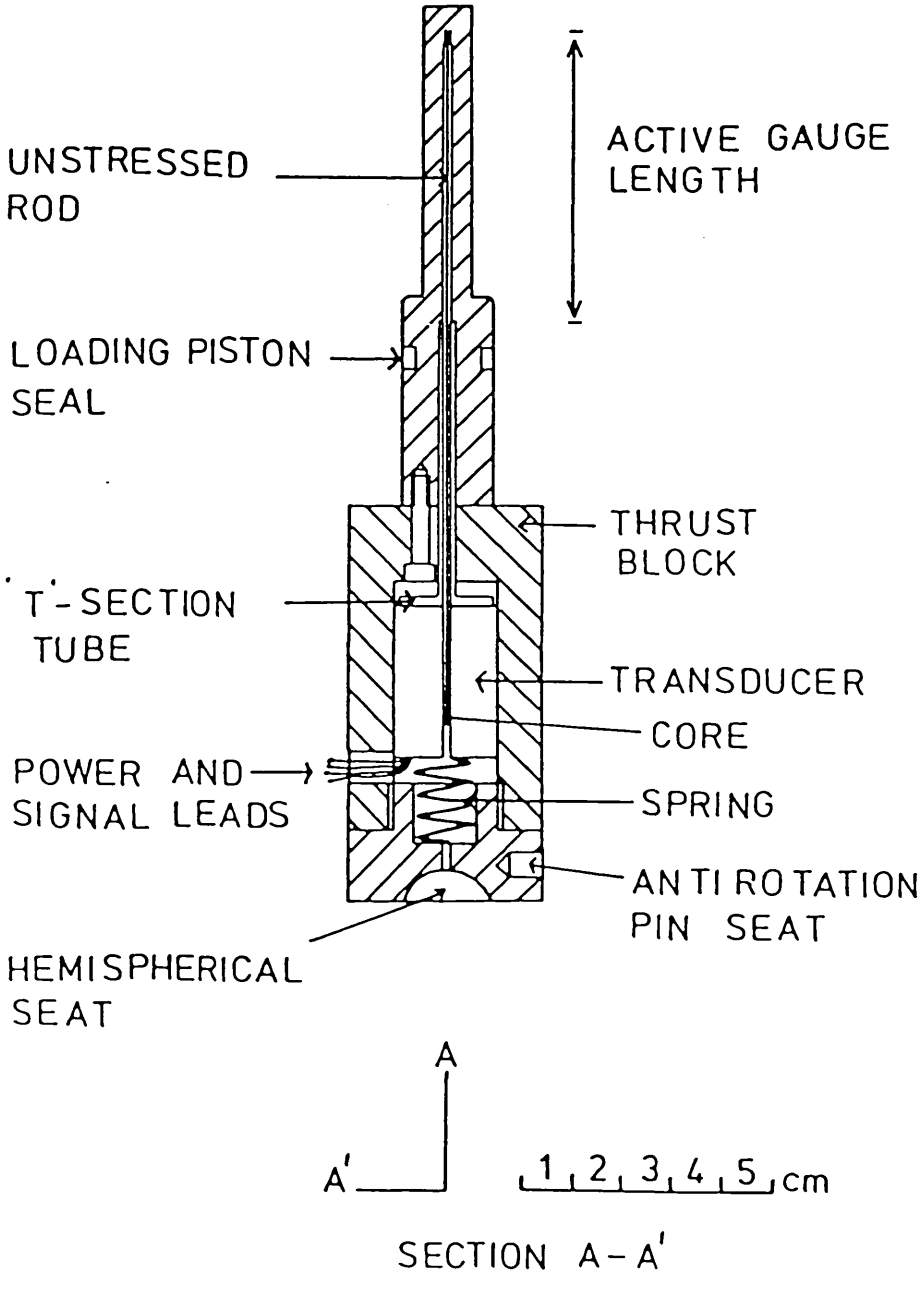


FIGURE 1.4 Cross sectional diagram of the Loading Piston/Force Gauge Assembly of the Nimonic Apparatus, shown in Fig. 1.1 (after Shaw, 1980)

The lower unit of the lower closure assembly connects the pressure vessel to the loading frame, whilst in the upper piston assembly, load is transmitted to the pressure vessel via the upper closure, Shaw (1980).

Axial load is applied by advancing the loading piston into the pressure vessel. The loading piston is pushed by a non rotating thrust block which is coupled by a 1.5cm diameter steel ball to the loading ballscrew. The ballscrew is driven by a reversable, constant speed induction motor, via a series of 10:1 reduction gears, and this allows strain rates ranging between 10^{-3} and $10^{-6}/sec^{-1}$ to be achieved. The motor/gear assembly is situated at the bottom of the apparatus. Limit switches restrict the up-down motion of the loading piston to the design limits by cutting power to the drive motor.

A trolley-mounted steel frame supports the loading frame, and is used to mount pressure gauges, valves, power connections and four protective steel screens.

1.2.1.1.7 FURNACES

The apparatus is heated by two symmetrically mounted 1kW cylindrical resistance furnaces, mounted on the outside of the pressure vessel. Surrounding the furnaces are two stainless steel half cylinders which are packed with Triton Kaowool, which acts as thermal insulation.

The furnaces are controlled by a Eurotherm controller driving a pair of thyristors by fast-cycle switching. This regulates power to the furnaces once a set target temperature has been reached. Thermal overshoot is limited by setting maximum furnace power on two variable transformers which feed the controller. The temperature measurement for the controller is made by a Cr-Al thermocouple, which rests on the outside of the pressure vessel, between the two furnaces. A temperature sensor on the water cooling jacket at one end of the vessel trips a safety cut-out if the cooling water recirculation system should fail.

1.2.1.1.8 PRESSURE SYSTEM

As stated above, water is the confining medium employed. The pressure is generated by a mobile, single stage compressed air driven pump which can supply up to 300MPa, and is connected to the apparatus via stainless steel pressure tubing. The confining pressure inlet is located in the lower closure assembly (see Fig. 1.3).

Pore pressure is generated by the same pump system, and the pore pressure inlet in centrally placed in the upper piston (see above).

1.2.1.1.9 DATA MEASUREMENT

Temperature, axial force, axial piston displacement, confining and pore pressure are all measured in terms of the millivolt (mV) output from their respective calibrated transducers.

Specimen temperature is measured using a Cr-Al thermocouple which is positioned on the top of the specimen via the pore pressure inlet. Cold junction temperature is maintained at 30°C in a temperature regulated enclosure. Axial load is measured in terms of the output from the internal force gauge and axial displacement is measured by a dial gauge and LVDT which are mounted on the main drive shaft. Two conventional Bourdon tube pressure gauges are bolted onto the portable steel frame and these measure confining pressure and pore pressure. Electrical pressure sensing is made via two 300MPa Intersonde pressure transducers.

1.2.1.1.10 DATA RECORDING

During operation the mV analogues of the various test parameters are recorded on a "JJ" flat bed recorder. Any two of the test parameters can be recorded at any one time, the others are written on manually. In general the writer chose to record force gauge and displacement as a function of time, because these are the dynamic test variables.

A second data recording system has recently been commissioned by Dr. E.H. Rutter, this now permits the on-line logging of all the mV output analogues using a precision digital voltmeter coupled to a BBC microcomputer via an IEEE interface. The interface, its calibration and the software were developed by Dr. Rutter, the latter are described and listed in Appendix 1, together with the data reduction procedures. The microcomputer is now the primary data handling system and the "JJ" recorder is used as a backup system.

1.2.1.1.11 SAMPLE DAMAGE INTRODUCED BY THE APPARATUS

Spiers (1981) states that there are a number of "disadvantageous characteristics of the Nimonic apparatus regarding sample damaging and slow quench annealing". Below temperatures of 350°C this is generally restricted to

minor annealing features. However at greater temperatures the microstructural corruption problems may become more pronounced because of :

(1) The greater thermal expansion/contraction coefficients of both the specimen and the apparatus.

(2) The increased time for annealing effects.

(3) The liquid/vapour phase change of the confining medium, the critical temperature is 374°C, which causes a sudden pressure drop which may damage the specimen.

However these effects are minor if present, and the author has no evidence to suggest that there has been any microstructural corruption of the experimental data reported in this thesis.

1.2.1.1.12 **SAMPLE PREPARATION**

Conventional cylindrical samples measuring 6mm in diameter by 12-15mm in length were prepared. These were fabricated from blocks of the starting materials using a water lubricated diamond coring tool attached to a drilling machine. The end of the specimens were sawn and ground so that their ends were flat and parallel to within 0.02mm. Specimen diameter was measured at six points and the greatest and least lengths were measured and recorded.

The cores fabricated from Carrara Marble were drilled in an arbitary but constant direction, whilst the cores fabricated from Taiwanese Marble were drilled parallel to the slight shape fabric in the starting material. For a description of the starting materials, see Chapter 4.

Both the drill and the grinder used in sample preparation are located in room LG 8 of the Royal School of Mines Building at Imperial College.

1.2.1.1.13 **EXPERIMENTAL PROCEDURE**

A strict procedure was followed for every experiment reported in this thesis. The specimen was inserted into the middle of the previously annealed copper jacket, and the lower piston of the Specimen-Piston Assembly is pushed into the copper jacket until it makes contact with the specimen. This process was repeated for the top piston of the Specimen-Piston Assembly. The copper

jacket was sealed onto the ends of the pistons with nimonic swaging rings (see section 1.2.1.1.3).

After the Specimen-Piston Assembly was inserted into the pressure vessel and the top closure seals are tightened, the pressure vessel was pressurised. The variacs controlling power to the furnaces were turned on and subsequently the desired temperature was reached. This typically required 1½ hours for a temperature of 700°C. After making adjustments to the confining pressure and temperature the load is ready to be applied.

The gear ratio selected was engaged, and after the test parameters have been entered into the computer and written onto the "JJ" recorder, the motor was turned on and the test run. The test was usually terminated after a period of steady state flow of the specimen had been recorded, and the motor was reversed to its starting position.

The reverse order of operations was carried out for the post deformational procedure, and the specimen was removed from the pistons prior to sectioning.

1.2.1.1.14 PREPARATION OF OPTICAL THIN SECTIONS

After the post deformational procedures, outlined above, the experimentally deformed material was examined using standard flat stage and detailed universal stage transmission optical techniques. Thin sections of all the experimental cores and most of the field specimens were prepared by the author.

Thin sections were cut from the experimental cores such that the long axis of the specimen, and therefore $\sigma 1$ during deformation, was along the long axis of the thin section (see the section "Field Techniques" for the orientation of the field specimens). Standard thickness (i.e. 30μm) thin sections were prepared using the excellent facilities of the Rock Cutting Section at Imperial College. As the specimens were not required to be remounted, i.e. for Transmission Electron Microscopy, they were mounted in epoxy resin as this gave a much improved finish and made section preparation much easier.

The extreme birefringence of calcite means that standard thickness thin sections are often too thick (depending upon the grain size). Therefore to facilitate microstructural observations and texture determination the standard thin sections were further thinned, by a specially developed acid-etch technique (described in Appendix 6), to between 10 and 20μm for the experimental

specimens and between 2 and 20μm for the field specimens. These thicknesses were found to be the optimum for universal stage work.

1.2.1.2 MICROSTRUCTURAL TECHNIQUES

These were used to determine crystallographic orientation data and textural characteristics.

1.2.1.2.1 OPTICAL MICROSCOPY

The orientated thin sections were given a preliminary examination using standard optical techniques. Because the general grain size was greater than 20μm optical microscopy gave adequate resolution. Optical microscopy was used as a means of determining which areas would be most fruitful for study using the universal-stage, and for the naturally deformed specimens it provided a means of selecting the best specimens for electron microscopy.

1.2.1.2.2 UNIVERSAL STAGE

Throughout this thesis the crystal nomenclature used is that given by Turner et al. (1954).

All of the microstructural, crystallographic and textural data reported in this thesis were determined on a grain by grain basis using standard universal stage (u-stage) techniques (Turner and Weiss, 1963). The complete crystallographic orientation of each grain was determined as a means of checking that the planar features observed were e-twins. The angle c^e for calcite is 26°, although in practise measured angles would range between 22° and 30°.

Two types of u-stage were used :

(1) Zeiss Ultraphot II microscope and accompanying Zeiss u-stage.

(2) A microscope/u-stage set manufactured by Cooke, Troughton and Simms, i.e. Vickers.

As the primary aim of this thesis is the determination of a calcite twinning palaeopiezometer as a function of differential stress and grain size, the textural data obtained was not transformed into Inverse Pole Figure diagrams. For a full treatment of the deformational textures which develop in calcitic rocks the reader is referred to Spiers (1981). The discussion of the

textural data in Chapter 2, and the discussion of the starting materials in Chapter 4, involves the description and reproduction of some Inverse Pole Figure diagrams. The notation for these diagrams is given in Spiers (1981) pp 28,31.

1.2.1.2.3 DATA ACQUISITION AND HANDLING

Each thin section to be analysed was photographed under varying magnifications, typically *10 for Carrara Marble and between *5 and *7 for Taiwanese Marble, depending upon the grain size in the specimen. This built up a mosaic of the thin section. The photography was carried out using a Zeiss camera and macro apparatus in the Photography Section in the Geology Department at Imperial College.

Using the u-stage a traverse was made parallel to $\sigma 1$ along the thin section, and as each grain was analysed it was ticked off and its outline drawn on a tracing overlay on the photomicrograph. For each grain the c-axis and e-twin orientations were recorded in the form suggested by Turner and Weiss (1963, p 237). For each twin set in each grain the number of twins was measured. The volume percent of twin per grain was measured by a process of drawing the grain and dividing it up by means of an arbitarily dimensioned grid. Hence the number of squares being occupied by the twinned domain can be calculated as percentage of the total grain.

After the textural characteristics had been recorded the grain dimensions were estimated in the form of orthogonal X (parallel to the specimen width) and Y (parallel to the length of the specimen) coordinates. The same coordinates are later measured from the tracing overlay and these are incorporated into the computer program D.BASE, which calculates the grain geometries from the known magnification of the photographic print. These calculated values are then compared with the same values estimated visually from the u-stage to check for any error. The verified grain geometries are entered with the twin information into the program D.BASE, which stores the information in the form of a sequential disc file. A full description and listing of D.BASE is given in Appendix 4.

The major limitation upon the investigation of twin activity as a function of differential stress and grain size has been the difficulty of finding a suitable range of grain size marbles and limestones. This problem has been alleviated to some extent by using the natural variation in grain size in the starting materials. This was accomplished by using the excellent search menu in the program D.BASE, which narrowed the data set down on the basis of mean

grain size. The values thus obtained were used to fill in the gaps in the differential stress/grain size maps, and in the calculation of the linear regression plots and histograms presented in Chapter 4. The regression and histogram diagrams were drawn using the programs MULPLOT AND HISTO which are described and listed in Appendices 2 and 3.

The full process from preparing a specimen for experimentation to plotting the linear regression diagrams takes at least 8 (*12 hour) working days for a 200 grain data set.

1.2.1.2.4 SCANNING ELECTRON MICROSCOPY

The JEOL 733 JXA SEM Superprobe equipped with an x-ray energy dispersive (EDS) spectrometer was used to examine selected specimens to high resolution. The instrument affords several modes of operation, the principal ones being :

(1) Secondary Electron Emission (SEI mode)

(2) Backscattered Electron Emission (BSE mode)

These two modes of electron imagery are reviewed by White et al. (1984) and Lloyd (1985).

The SEI mode was used on several orientated, lightly polished and etched experimental specimens in an attempt to image the twin activity (the twin planes being preferentially etched relative to the surface). This technique was unsuccessful owing to the difficulty of relating orientation data from the u-stage to the SEM, and the variable nature of the etching technique, which meant that variations in twinning activity and grain size could not be resolved.

The BSE mode is an atomic number contrast image and hence was of no use for single phase specimens, e.g. the experimental and most of the field specimens. However BSE imagery was of great use for the natural cataclastic fault rocks discussed in Chapter 6.

1.2.1.2.5 MICROCHEMICAL ANALYSIS

Owing to the relatively simple chemical compositions of the phases involved in the cataclastic zones analysed in Chapter 6, chemical analysis was restricted to fingerprinting. Where further information was required a Link

Spectra System utilising a ZAF4 routine was used on the JEOL 733 Superprobe described above. This allowed chemical characterisation of individual phases.

1.2.2 FIELD TECHNIQUES

The extrapolation of the experimental models to the Cantabrian fold and thrust belt required a comprehensive sampling program. This was carried out in two field seasons, the first between April and June, 1984, and the second in September of the same year. Large scale sampling/geological maps were prepared of the sampling localities. In addition to this a third field season was spent making a smaller scale geological map of a large part of the Somiedo thrust sheet between June and September, 1985.

Because of the large extent of the region studied, several areas for detailed study were selected with the help of the excellent geological maps prepared by the staff and students of Oviedo University. All the specimens collected were carefully orientated in the field.

1.3 STRUCTURE OF THESIS

Although the structure of this thesis is outlined in the contents page, this section explains the contents in a little more detail to aid presentation. Chapter 2 reviews the previous work performed on calcitic materials and opens with a number of introductory sections on calcite in general. Chapter 3 details the principal palaeopiezometric techniques that have been used and, more importantly, critically reviews their limitations. Chapter 4 reports on the results of experiments performed by the author and the calibration of a calcite twinning palaeopiezometer. The beginning of Chapter 4 reports previous work on twinning activity for Solenhofen Limestone.

Chapter 5 introduces the field area in general and goes on to describe the two principal areas that the author studied for this thesis. In Chapter six and seven the data from the two field areas are compared with the experimental models previously formulated in Chapter 4. Chapter 8 discusses the conclusions and examines some of the implications of this work. This thesis closes with some suggestions for further research.

CHAPTER 2 : LITERATURE REVIEW

2.1 INTRODUCTION

Calcite is the major rock forming carbonate mineral, and is an important constituent in sedimentary environments, varying from chemical precipitates in saline lakes, to shelf sequences and calcareous pelagic oozes. It occurs in metamorphic and igneous rocks, and as a common hydrothermal and replacement vein mineral. Together with silica rocks, calcitic rocks are amongst the most important constituents of Upper Crustal levels in the Earth, the latter being essentially restricted to the uppermost levels. Hence the study of these materials is of great significance for structural geologists seeking to understand the behaviour of crustal rocks.

Generally for any material the set of operative glide systems determining rheology depends upon the imposed set of deformational parameters. Hence any crystallographic preferred orientations developed in a plastically deformed rock mass are indicators, at least potentially, of these parameters, such as temperature, stress and deformational path.

The previous work in this field, reviewed in this chapter, has revealed for calcitic rocks that the microstructure developed depends upon a range of experimental parameters such as temperature, stress, effective confining pressure, strain and strain rate. See Wenk *et al.*, 1973; Schmid *et al.*, 1977; and Casey *et al.*, 1978. However it has been possible to correlate specific types of rheological behaviour to the operative crystallographic glide systems (Spiers, 1981). The experimental investigation of the development of microstructures and textures has great significance in the interpretation of natural systems.

2.2 : STABILITY FIELDS OF CALCITE

Calcite is the most commonly occurring polymorph of $CaCO_3$, although there are several stable forms, depending upon temperature/pressure conditions (Fig. 2.1). There are five types of calcite, other than the aragonite polymorph; all are distinct on basis of their physical properties resulting from anion disordering.

Although Wenk *et al.* (1973) worked on metastable I and II, and Schmid *et al.* (1977, 1980) deformed calcite of types I, IV and V, most experimental work has been carried out on calcite I (Spiers, 1981).

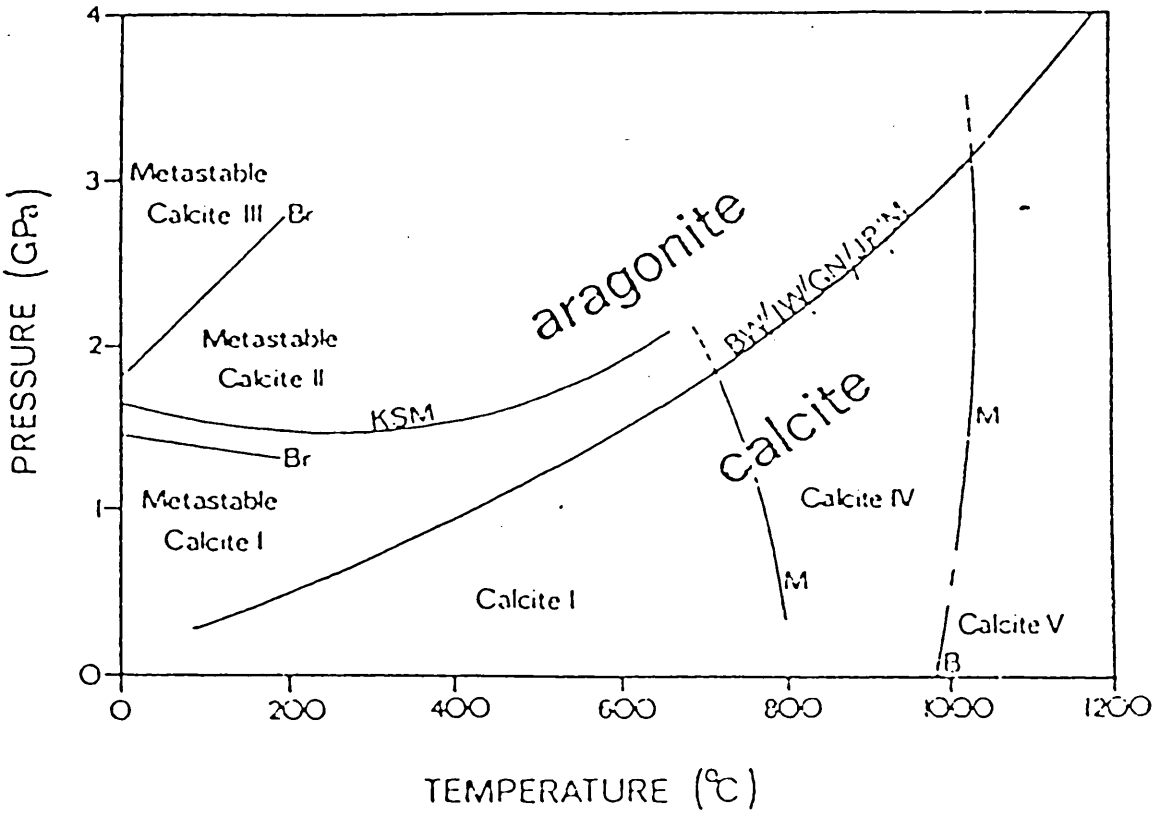


FIGURE 2.1 Phase diagram for calcium carbonate. KEY : B - Boeke (1912), Br - Bridgman (1939), BW - Boettcher and Wyllie (1968), IW - Irving and Wyllie (1968), GN - Goldsmith and Newton (1969), JP - Johannes and Puhan (1971), KSM - Kondo, Suito and Matsushima (1972 and M - Mirwald (1976).
After Spiers (1981).

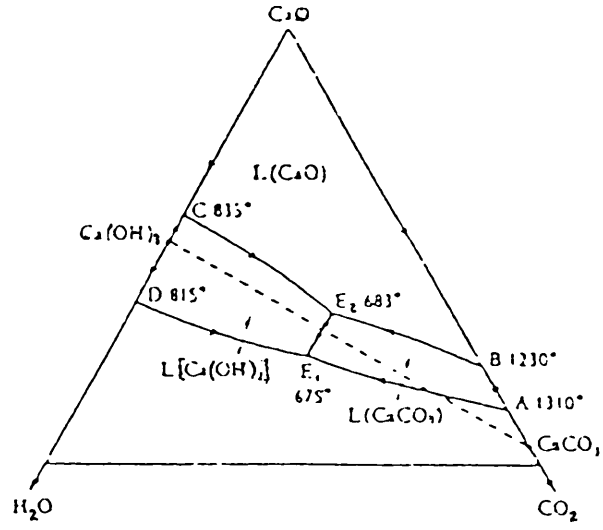


FIGURE 2.2 Enlarged and distorted view of the liquidus field boundaries in the system $CaO-CO_2-H_2O$ at 1000 bars. "L" signifies the position of the liquidus boundaries of the primary crystalline phases. After Wyllie and Tuttle (1960).

The calcite-aragonite polymorphism results from the radius of the calcium ion being very close to the limiting value for the transition from rhombohedral structural type (calcite) to orthorhombic structural type (aragonite). This transition can be bought about by grinding at room temperature for a few hours, and is the subject of current experimental work by Gillot at Rennes University, France.

Calcite has a thermal dissociation temperature at one atmosphere, of 894.4°C, and at 100 and 500 lb/ins CO_2 pressure it is 985°C and 1100°C, respectively. Experimental data has shown that calcite melts incongruently to liquid and vapour at 1310°C ± 10°C for one Kbar confining pressure, Deer et al. (1963, while the presence of water at one Kbar pressure has been noted by Wyllie and Tuttle (1960) to produce small amounts of melt at 740°C. See Fig. 2.2 for more details of the $CaO-CO_2-H_2O$ system, and the position of the liquidus boundaries.

2.3 : STRUCTURE AND CRYSTALLOGRAPHY

Calcite has trigonal symmetry and the structure is that of a four molecule face centred rhombohedral cell, with arh = 6.42Å, and a = 101° 55', and whose axes (100), (010) and (001) are that of the perfect cleavage rhomb. This cell contains four $CaCO_3$ groups, and is a pseudo cell since successive CO^{3} triangles along the rhomb edge point in opposite directions. Thus a true face centred rhombohedral, or morphological, cell would have arh = 12.84Å and contain 32 $CaCO_3$ groups. For Miller indexing the rhombohedron with a = 101° 55' is usually (100), or (1011) for Miller-Bravais indexing.

The lattice can be described as a rhombohedral two molecule primitive unit cell, with arh = 6.37Å and a = 46° 05', containing two $CaCO_3$, which is twice as long as the morphological cell in their common (111) direction, (Deer et al., 1963), Fig. 2.3. If the faces of the unit cell are taken as (100), then the cleavage rhombs faces become (211), or (1014) using Miller-Bravais. See Table 2.1 for further information on unit cell dimensions.

Each plane can be labelled with three Miller indices, (HKL), or four Miller-Bravais indices, (hkil); these are given on Fig. 2.4 together with the corresponding lower case notation.

In addition to the rhombohedral axial system, the hexagonal axial system has also been used for calcite, and the corresponding primitive and

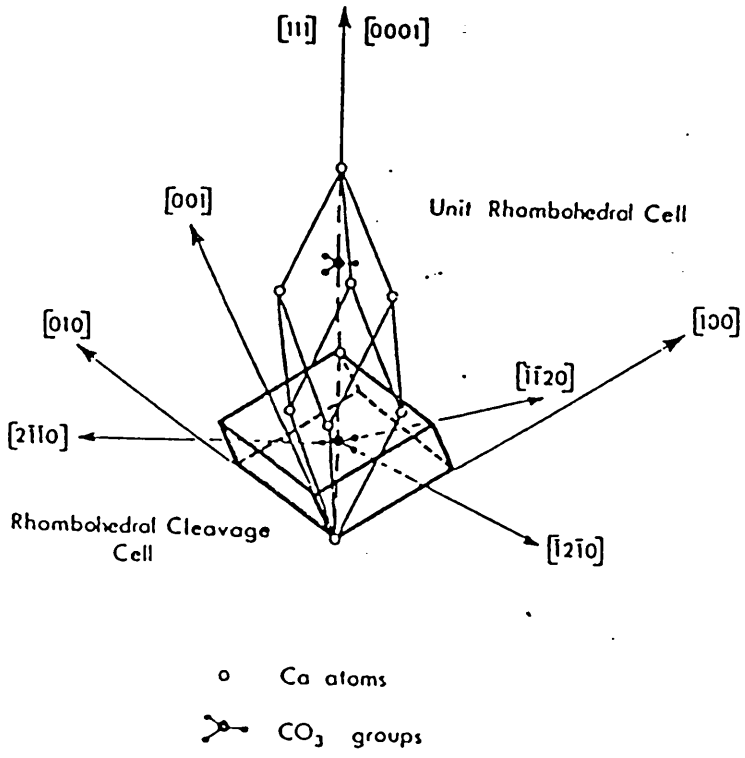


FIGURE 2.3 Crystal structure of calcite. Diagram showing the relationships between the rhombohedral cleavage cell and the unit cell. After Nicolas and Poirier (1976).

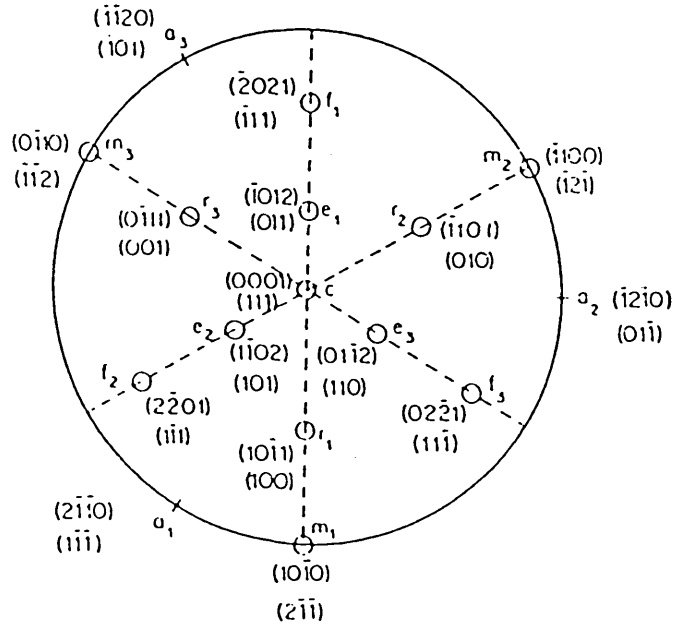


FIGURE 2.4 Diagram showing the crystallographic planes in calcite. For each plane Miller indices (HKL) and Miller-Bravais indices are given relative to the cleavage cell.

TABLE 2.1 : CALCITE UNIT CELLS

		X-ray smallest cell	Cleavage rhomb pseudo-cell	Cleavage rhomb true-cell
Rhombohedral axes	a_{rh} (Å)	6.37	6.42	12.85
	α_{rh}	46°05′	101°55′	101°55′
	Z_{rh}	2	4	32
	Cleavage rhomb indices	{211}	{100}	{100}
Hexagonal axes	a_{hex} (Å)	≃5	≃10	≃20
	c_{hex} (Å)	≃17	≃8.5	≃17
	Z_{hex}	6	12	96
	Cleavage rhomb indeces	{1014}	{1011}	{1011}

TABLE 2.2 : THERMAL AND ELASTIC PROPERTIES

Thermal Properties		Units	Reference
SC Thermal Conductivity	4.98(c), 3.18 (c)	$Jm^{-1}s^{-1}k^{-1}$	Nye (1976)
SC Thermal Expansion Coefficient	25.0 (c),-5.6 (c)	$*10^{-6}K^{-1}$	Nye (1976)
PC Thermal Expansion Coefficient	8 (L), 7 (M)	$*10^{-6}K^{-1}$	Clark (1966)
PC Specific Heat	900	$J.Kg^{-1}\ K^{-1}$	Clark (1966)

Elastic Properties : (298°K)

SC Compressibility		8.2(c), 2.71(c)	$*10^{12}Pa^{-1}$	After Spiers(1981)
PC Young's Modulus	(Calculated)	0.95(V), 0.71(R)	$*10^{11}Pa^{-1}$	After Spiers (1981)
E	(Measured)	0.63(L), 0.70(M)	$*10^{11}Pa^{-1}$	Clark (1966)
PC Shear Modulus	(Calculated)	0.37(V), 0.27(R)	$*10^{11}Pa^{-1}$	After Spiers (1981)
μ	(Measured)	0.24(L), 0.26(M)	$*10^{11}Pa^{-1}$	Clark (1966)
PC Poisson's Ratio	(Calculated)	0.29(V), 0.34(R)		After Spiers (1981)
V	(Measured)	0.33(L), 0.34(M)		Clark (1966)
PC Temperature Coefficient		$\frac{1}{\mu}.d\mu$	$-0.32*10^{-3}K^{-1}$	After Spiers(1981)

Where :

SC = Single Crystal, PC = Polycrystal, L = Limestone, M = Marble, V = Voight and R = Reuss.

morphological cells contain six and 96 molecules, respectively. The lattice parameters are given in Table 2.1. Throughout this review the commom lower case notation will be used.

The carbon-oxygen bonds are mainly covalent, while the calcium-oxygen bonds are an equal mixture of covalent and ionic bonding. Many divalent cations can partially replace calcium, e.g. Mg, Mn and Fe form isostructural carbonates and may be present as a result of substitution and solid solution, although most calcite is relatively free from other ions and is very close to pure $CaCO_3$.

2.4 : OPTICAL AND PHYSICAL PROPERTIES

2.4.1 OPTICAL PROPERTIES

Calcite is uniaxial of negative sign and displays extreme birefringence, this being attributed to the configuration of the CO_3 groups (Deer et al., 1963). Many specimens exhibit luminescence and/or fluorescence, depending upon trace element content.

2.4.2 THERMAL PROPERTIES

Calcite exhibits both positive and negative coefficients of thermal expansion, positive parallel to the c-axis and vice versa for negative. Graf and Lamar (1955) attribute this to the carbonate rotating out of their crystallographic plane, hence reducing the projected C-O distance on the basal plane.

2.4.3 PHYSICAL PROPERTIES

The specific gravity of calcite averages 2.9. Other physical properties exhibit strong anisotropy, depending upon orientation parallel or perpendicular to (1000), the basal plane. This is typified by hardness, which is 2.5 for the former and 3.25 for the latter.

2.4.4 ELASTIC PROPERTIES

The anisotropy which is characteristic of some of the physical properties also typifies the elastic properties. This results in an elastically compliant direction parallel to the c-axis where maximum compressibility occurs. This is distinct from plastic behaviour, where this direction is the anti-twinning vector, and would be, presumably, "plastically hard" at low temperatures which

are slip system initiation prohibitive. See later. Conversely, elastic stiffness occurs in the direction normal to the c-axis (Patterson, 1963; Dandekar, 1968). The temperature/pressure dependence of these elastic parameters have been shown, by the ratio of linear compressibility, parallel and normal to the c-axis, to have the opposing affects upon anisotropy. i.e. temperature-induced reduction offsets pressure-induced anisotropy.

Spiers (1981) reports that the elastic constants for uniformly orientated polycrystals varies with the method of calculation. When compared to natural specimens there is a reduced Youngs and Shear Modulus, and Poissons ratio, which is possibly related to porosity in natural specimens, crystallographic preferred orientation and grain size variations, and/or a combination of these effects.

2.4.5 DIFFUSIONAL PROPERTIES

The diffusion properties of calcite have great significance with regard to intracrystalline creep, e.g. Nabarro-Herring and Coble creep, and may be rate determining, at least in part. Anderson (1969) has studied isotopic exchange between calcite and CO_2. He found that below 550°C structure sensitive extrinsic diffusion of C_{14} was observed, while between 550°C and 850°C intrinsic diffusion of C_{14}, C_{13} and O_{18} occurred.

When CO_2 pressure exceeds the equilibrium partial pressure, enhanced O_{18} diffusity occurs, an order of magnitude higher diffusity at CO_2 pressure of 100 bars compared to CO_2 pressure of 1 bar. This may be due to defect growth during the diffusion, with a concomitant effect on concentration gradients.

The formation and migration of carbonate ion point defects should affect both oxygen and carbon diffusivities equally, and hence the observed discrepancy may result from a more fundamental mechanism for anion diffusity in calcite which has not yet been determined. At present no data are available for calcium diffusity in calcite. See Table 2.2 and 2.3 for data summarising diffusivity, elasticity and thermal properties.

2.4.6 DEFORMATIONAL PROPERTIES

When deformed, calcite responds plastically by twinning and/or translation glide or slip, depending upon the imposed deformational parameters (Table 2.3), although e-twinning, r and f slip are by far the most common.

TABLE 2.3 : PLASTIC PROPERTIES AND DIFFUSION DATA FOR CALCITE

Plastic Properties

Main Twin System :	e {0112}<0111>	+ve sense	Turner et al. (1954)
	CRSS yield ≃ 5.0MPa (25-800°C)		Spiers (1981)
Main Slip System :	r {1011}<1102>	-ve sense	Turner et al. (1954)
	CRSS yield ≃ 150-185MPa (25°C)		Spiers (1981)
	≃ 10MPa (400°C)		
	≃ 5MPa (800°C)		
	f {0221}<1102>	-ve sense	Turner et al. (1954)
	CRSS yield ≃ 240MPa (25°C)		Spiers (1981)
	≃ 50MPa (500°C)		
	≃ 15MPa (800°C)		
Average Burgers Vector	b	= 6.3 * 10^{-10}m	Goetze & Kohlstedt (1977)

Where : CRSS = Critical Resolved Shear Stress.

Diffusion Data

550°-850°C	D_1 (Carbon) = $1.3*10^{3}$ exp(-88,000/RT)cm^2/sec	Anderson (1969)
<550°C	D_1 (Carbon) = $4.6*10^{16}$ exp(-17,000/RT)cm^2/sec	

$$D_1 = d_o \exp\left(\frac{-H}{RT}\right)$$

Units : H(Kcals/mole), D_o cm^2/sec

TABLE 2.4 : TWINNING AND SLIP SYSTEMS FOR CALCITE

The directions in the hexagonal cell are given as the intersections of the planes. Sense refers to the trigonal axis [0001] orientated vertically, and +ve shear indicates displacement of the upper portion of the crystal upwards relative to the lower.

Twinning plane	Twinning direction	Sense	Number of systems	Comments
e_1	$[e_1:e_2]$	+	3	Very common
(1012)	[(1012):(1210)			Large srain
(011)	[100]			
r1	$[r_1:f_2]$	+	3	Uncommon at
(1011)	[(1011):(2201)]			>300°C
(100)	[011]			Strain is low
f_1	$[f_1:a_2]$	-	3	Rare
(2021)	[(2021):(1210)]			Strain is low
(111)	[211]			

Slip plane	Slip direction	Sense	Number of systems	Comments
r_1	$[r^1:f^2]$	-	3	Common
(1011)	[(1011):(2201)]			Strain may be
(100)	[011]			large
f_1	$[r_2:f_2]$,$[r_2:f_1]$	-	6	Uncommon
(2021)	(1101):(0221)],[(0111):(2021)]			
(111)	[101],[011]			
a_2	$[r_1:f_2]$	Neutral	3	Very rare
(1210)	[(1011):(2201)]			
(011)	[011]			

The complex effects of elastic anisotropy upon imaging contrast in transmission electron microscopy have meant that the relationships between dislocations and their Burgers vectors in the operative slip systems are as yet unsatisfactorily resolved.

The idea of a unique critical resolved shear stress (CRSS) for twinning is misleading as CRSS varies with strain and this can be highly heterogeneous. Twinning is a rapid deformational mode and is distinct from slip system operation which is a progressive shear. Initiation of twinning requires nucleation, after which the twin lamellae can grow rapidly by concentrating stress at the tip. The nucleation of a twin requires stress concentration and/or enhancement, and as a result there is no unique CRSS value as there is for slip systems.

There is a drastic and significant difference in CRSS between e-twinning (average values) and r and/or f slip, see Table 2.3. At low temperatures the CRSS for twin activation is much lower than that for r or f slip. However with increasing temperature the CRSS for the two deformational processes converge, i.e. the CRSS for slip decreases, until at high temperatures r and f slip are easier than e-twinning (Griggs et al., 1960; Spiers, 1981).

Braillon et al. (1972) has shown for calcite single crystals that CRSS for r slip is related to temperature by the formula:

$$\sigma \ (Kg/mm^2) = \sigma 0 - 2.8 \ (\text{sqr. rt. temperature}) \qquad (2.1)$$

, between 100°C and 375°C, and decreases from 22 kg/mm^2 at 25°C to 0.75 kg/mm^2 at 600°C. Spiers also reports that strain rate reduction results in lower strengths, while confining pressure has little effect on CRSS. The conditions under which these systems operate experimentally are discussed later.

E-twinning is induced easily at room temperature by compression normal to (0001), the cleavage planes remain parallel to each other during twinning, and the shear has a high value:

$$S = 2 \tan 19^\circ 9' \qquad (2.2)$$

$$= 0.694$$

This corresponds to a maximum of 29% strain for twinning resulting from compression normal to (0001) and 41% for compression parallel to (0001). The

c-axis rotates through 52.5° during the process (Handin and Griggs, 1951), Fig. 2.5.

Slip systems in calcite have been extensively studied: r slip is the most common at relatively low temperatures, relative to f slip (Turner et al., 1954; Griggs et al., 1960; and Keith and Gilman, 1960), although for single crystals the later authors showed f slip to be dominant over r slip in the temperature range 20°C to 600°C.

The importance of the original crystallographic configuration of calcite as regards the subsequent microstructural development has been shown by Braillon et al., 1972. They compressed single crystals of calcite parallel to (0001),anti-twinning, i.e. -ve sense of shear, and found that temperature was important for activation of slip, c.f. Spiers (1981). At temperatures lower than 100°C the crystals respond by brittle fracture. Between 100°C and 600°C plasticity in the form of r slip was observed, no f slip being recorded. Note that confining pressure was zero for these tests, and it is probable that r slip would be operative at lower temperatures at confining pressures sufficient to inhibit cataclasis, c.f. section 2.5.2.

The importance of strain accumulation is also indicated. Above 200°C the stress/strain curves show three distinct stages as strain accumulates, Fig. 2.6.

For palaeostress estimates in particular and rheological investigation in general it can be seen from the above that a uniform starting fabric is of great importance. Turner et al., 1954; Heard and Raleigh, 1972, and Fig. 2.7 show the extrapolating experimental data for comparison with natural specimens, i.e. a uniform starting fabric must be assumed, unless we are to include other factors in our observations.

2.5 EXPERIMENTAL DEFORMATION OF CALCITIC ROCKS

The remainder of this chapter is divided into three sections. The first is a general introduction on modes of rock failure, the second discusses the regime of pressure sensitive, dilatant cataclastic deformation, the faulting to flow transition and the mechanical transition to plasticity. Plasticity is discussed in the third section.

2.5.1 MODES OF ROCK FAILURE

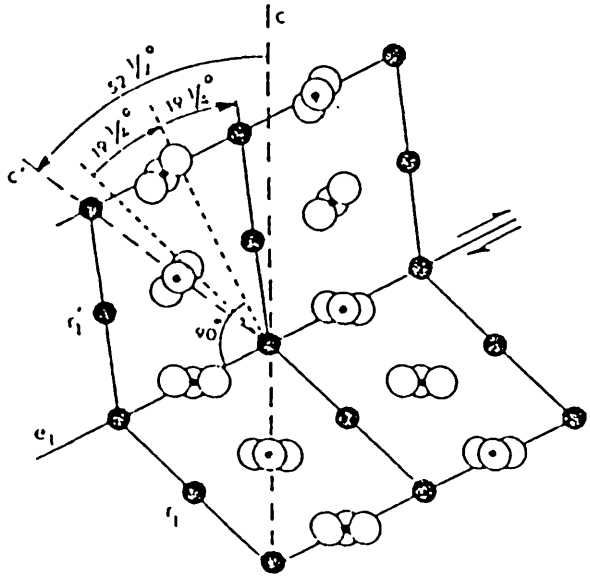


FIGURE 2.5 The operation of the e-twinning system in calcite. Arrows show the sense of shear. Closed circles represent calcium ions.

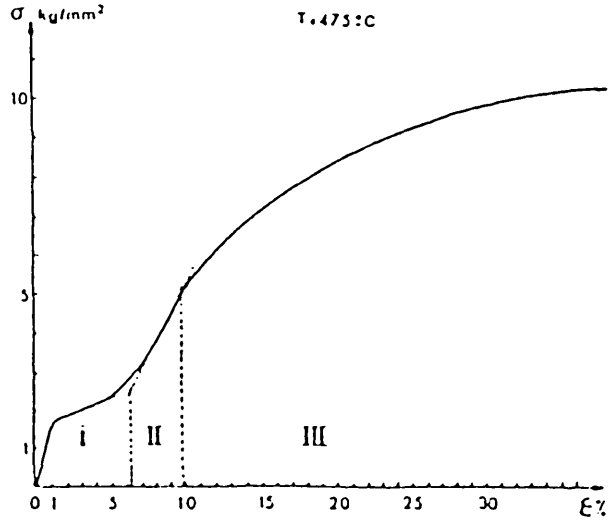


FIGURE 2.6 Differential Stress/Strain curve for single crystal calcite, compressed along the c-axis at 475°C. Note the three strain rate behavioural responses. After Braillon et al., 1972.

It is relevant to discuss briefly the brittle/ductile, or the faulting to flow, transition as it emphasises the importance of scale. Ductility is the ability of a rock body to accommodate strain by flow, and does not imply any specific deformation mechanism. Hence a more accurate term is plasticity. For example, in calcite e-twinning is an essentially brittle event in that the lattice shears in a response to a build up of CRSS along the e-crystallographic plane. This lattice reorganisation has enabled strain to be accommodated within the grain, i.e. it enables ductility.

In rocks at upper crustal levels deformation is often restricted to discrete localised zones. When viewed at a larger scale the rock has displayed plasticity, but the mechanism has been cataclastic. Hence scale must be included in any discussion of the faulting/flow transition and associated relationships and processes.

2.5.2 PRESSURE SENSITIVE DEFORMATION

From room temperature up to approximately 400°C, the strength of calcitic rocks and correspondingly the faulting/flow transition for an experimental "run", and a given rock specimen, is dependent upon the effective confining pressure (Rutter, 1972). Effective confining pressure is defined as the difference between the pressure exerted by the internal pore fluids in a specimen and the external confining pressure.

The influence of effective confining pressure results from the fact that cataclastic deformation normally involves volume change. Mechanically, frictional forces between cohesionless surfaces partially control the materials strength. Cracks nucleate from the pore spaces between the particles and propagate along grain contacts as these are obvious zones of weakness within a specimen, as any inhomogeneity acts as a stress concentrator. These microcracks are by definition dilatational, although there is usually a component of shear present, and enable the material to flow ductily. This form of ductility is known as cataclastic flow, (Fig. 2.8).

Obviously when effective confining pressure is increased, friction is increased, and the nucleation and propagation of these microcracks is prohibited. As a result the materials strength is increased, i.e. greater differential stress is required to initiate cataclastic flow at higher levels of effective confining pressure. Fig. 2.9. Rock strength in this region is insensitive to all but effective confining pressure.

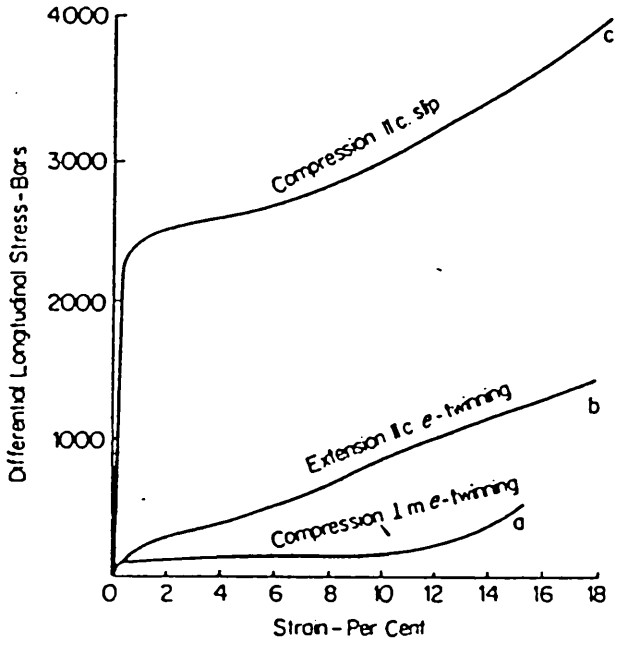


FIGURE 2.7 Differential Stress/Strain curves for calcite deformed at 20°C, showing the importance of crystallographic orientation upon deformation path : (a) and (b) : e-twinning possible. (c) : e-twinning impossible.
After Turner et al., 1954.



FIGURE 2.8 Cataclastic flow of quartzite around pistons of the Nimonic Apparatus deformation rig. After Hadizdeh and Rutter 1984.

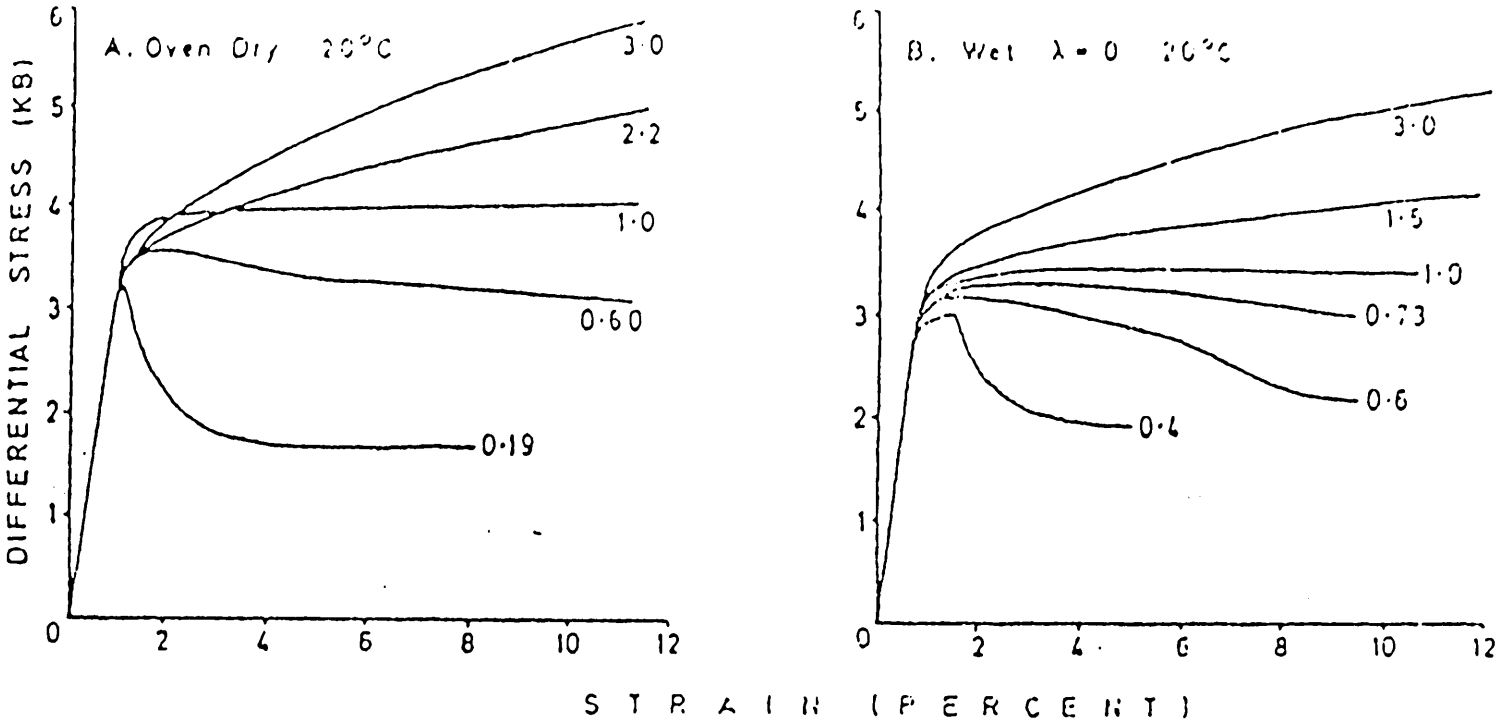


FIGURE 2.9 Differential stress/strain curves for the series of experiments performed by Rutter (1972) upon Solenhofen Limestone at room temperature. These curves show the effect of confining pressure upon the strength of a rock.

Cataclastic flow may be thought of as frictionally controlled grain boundary sliding (g.b.s.), (Schmid, 1982a), but this must not be confused with g.b.s. sensus stricto. See later.

Microcracks, especially at higher flow stresses, often propagate in the form of "long cracks", which are not restricted to grain boundaries, but may develop from a series of microcracks of differing character. This long crack cataclasis is common as a strain accommodating mechanism in the upper crust, although it is difficult to produce experimentally, because experimental materials are perfect and natural materials are not. Additionally the small size of the specimens used means larger scale features are difficult to reproduce experimentally, (Hadizdeh and Rutter, 1984).

At progressively higher levels of effective confining pressure (σ3eff), the progressive inhibition of cataclastic flow means that an increasing percentage of the strain accumulating in a specimen has to be taken up by intracrystalline processes, and for calcitic rocks, at these experimental conditions, twinning on the e-crystallographic plane is initiated. There is no sharp change from one deformation mechanism to another; instead there is a gradual change in response to the changing experimental conditions.

Hence we may see two separate deformation mechanisms operating in one specimen. As in the brief discussion on modes of rock failure, this also demonstrates the importance of scale, as within a specimen undergoing cataclastic flow, some grains may be deforming by e-twinning.

Above 400°C both σ3eff. and pore pressure cease to be important factors controlling the rheological properties of calcitic rocks, and for 10% strain between 400°C and 500°C both Carrara Marble and Solenhofen Limestone's stress/strain curves show the beginnings of steady state flow, Rutter (1974). This is the result of the flow behaviour becomimg temperature dependent, i.e. thermally activated deformation occurs. Resultingly the strength of a rock becomes strain rate sensitive, i.e. at low strain rates e.g. $10^{(-6)}/sec^{(-1)}$ for experimental runs there will be a lower flow stress than for faster strain rates. See Chapter 4.

2.5.3 PLASTIC DEFORMATION

In the high temperature/high pressure regime there is no dilatancy, i.e. all deformation is plastic and/or diffusive. The plastic regime can be sub-

divided into three regimes represented by different flow laws, this is determined largely by stress level.

2.5.3.1 HIGH DIFFERENTIAL STRESS FLOW BEHAVIOUR

Above 0.3 Tm, where Tm is the temperature of melting, diffusional processes become important, and as a result dislocations can climb one interatomic distance, by adding or removing a line of atoms along the edge of the half plane concerned.

At intermediate temperature (0.5 Tm) and high strain rates the high stress field is characterised by an exponential flow law, which has the form :

$$e = A1 \exp\left(\frac{-H}{RT}\right) \exp\left(\frac{\sigma}{\sigma 0}\right) \qquad (2.3)$$

After Rutter (1974).

Where σ = differential stress at that temperature/pressure.

H = apparent activation energy for flow.

R = gas constant.

A1 and $\sigma 0$ are empirical material constants.

This is derived from the equation of state of Dorn (1957). This relationship assumes that strain rate is controlled by the resistance of a rock to glide and is known as dislocation glide, or Ashby and Verrall's (1978) low temperature plasticity.

Exponential flow occurs after an initial period of work hardening before the yield point, and is a quasi-steady state flow of the rock. For any given constant strain rate experiment the slope of the plastic strain behaviour may be positive or negative, work hardening and softening, respectively, see Chapter 4.

Work hardening is a generality, as the rheological behaviour of a specimen results from an interplay between work hardening and work softening, or recovery processes. The two later terms are here taken as being equivalent.

The former upon which there is no significant wetting effect (Rutter, 1974, c f. Fig. 2.9 a and b) increases the internal energy state of a grain by a build up of the dislocation density inside a grain, due to a resistance to slip. The converse is true of recovery. A full discussion of the recovery processes is not

warranted here (see Nicolas and Poirier, 1976, pp 129, 136), although a brief summary is given below of the main recovery processes :

1. Dislocation annihilation, opposing burgers vectors.

2. Coarsening of the dislocation mechanism.

3. Dislocation climb past barriers.

4. Dislocations climbing into dislocation walls, defining misorientated subgrains.

5. Cross slip of screw dislocations.

Recrystallisation is the most effective way of reducing the internal energy state of a crystal, resulting in a lower internal strain energy under conditions of dynamic recrystallisation, or zero if there is static recrystallisation, through a change in grain size.

Generally the recovery rate increases with temperature and decreases with increasing pressure, i.e. work hardening will dominate at lower temperatures and higher pressures.

When a dislocation, defined as a crystal lattice defect, moves through a crystal lattice it may be blocked by any barrier, e.g. air bubbles, impurities, opposing dislocations, grain boundaries etc. These obstacles can be overcome by increasing the internal energy state of the crystal, this being temperature sensitive.

2.5.3.1.1 GRAIN BOUNDARY EFFECTS

Grain boundaries are an obvious and effective obstacle to slip, i.e. the presence of grain boundaries increases the stress required to deform a given specimen at a given strain. This is known as grain boundary hardening.

Grain boundary hardening predominates at lower strains, because at progressively higher strains the dislocations have progressively greater difficulty in crossing the dislocation tangles inside a give grain. When a dislocation on a slip or twinning plane encounters an obstacle, e.g. a grain boundary, if that boundary is of sufficient energy that a dislocation can not

progress, under the applied stress conditions, then the result is a pile up of dislocations on that slip plane :

$$\sigma^* = n\,\sigma \qquad (2.4)$$

Where σ^* is the shear stress at the head of the pile up.
n is the number of dislocations.
σ is the stress applied.

That is, a stress concentration is the result of the pile up. This stress build up may be sufficient to initiate and nucleate slip in adjacent grains, facilitating multiple slip in the grain boundaries, resulting in strain compatibilty. The complex grain boundary morphology of Solenhofen limestone (see Spiers, 1981, and Table 4.1) may correspondingly cause the regions of intracrystalline slip to dominate deformation at conditions for which coarser material, e.g. Carrara marble, which has a simpler grain boundary morphology, would deform by e-twinning.

If the resistance of the boundary to shear is gb then dislocations will pile up until :

$$\sigma\ gb = n\,\sigma \qquad (2.5)$$

Hirth and Lothe (1967) have shown that :

$$n \propto L^{(1/2)} \qquad (2.6)$$

Where L is the length of the dislocations pile up.

The stress necessary to transect the grain boundary, assuming that L is proportional to the grain diameter, d, (this is the critical assumption) is :

$$\sigma = \sigma\ \frac{gb}{n} \propto \sigma\ gb\ L^{(1/2)} \propto \sigma\ gb\ d^{(1/2)} \qquad (2.7)$$

$$\text{Or } \sigma y = \sigma + kd^{(1/2)} \qquad (2.8)$$

Where σ and k are constants.
d is the grain size.
(Nicolas and Poirier, 1976).

It has been increasingly realised over the last ten years that grain size is an important factor in the deformation of calcitic rocks in particular, and other rocks, potentially, at least in general. Up to 500°C the rheology and strength of calcitic rocks is grain size dependent. At constant temperature and strain rate a small grain size leads to a higher flow stress.

This is known in metallurgy as the Hall-Petch law, and has been investigated by Olsson (1974) for the temperature range 20 to 300°C, see Nicolas and Poirier (1976). Its significance is that a fine grained material is harder to deform than a coarser one.

2.5.3.1.2 MICROSTRUCTURE

The optical microscopic features typically developed are undulose extinction, grain flattening and at higher strains a crystallographic preferred orientation, which all indicate that lattice bending develops. However, for a given stress level, the grain size controls the microstructural response that occurs, as discussed previously.

Spiers (1981) has shown by detailed crystallographic analysis using the universal stage that Solenhofen Limestone (grain size 3-5μm) deforms by glide on r and f slip systems at temperatures above 600°C. No change in grain boundary morphology, or the development of e-twins was reported.

Carrara marble (grain size averaging 200μm), (Rutter (1974), Spiers (1981) and Schmid (1982a)), and Yule marble (grain size 300 μm), (Heard and Raleigh (1972)), exhibit distinctly heterogeneous deformation on the grain scale. The internal strain features that develop depend upon the orientation of the grain with respect to the principal stress axis, i.e. for those grains favourably orientated strain tends to be accommodated by e-twinning, while less favourably orientated grains develop heterogeneous internal strain features and kink bands. The grains orientated with highest CRSS on their twin planes will deform preferentially; thus there may be considerable variation in the amount of twinning in a given specimen, assuming no initial preferred orientation. High strain gradients can therefore develop across grain boundaries.

Early formed twins are often bent and rotated, the grains exhibiting undulose extinction, see Chapter 4. In addition early formed twins can be offset by later ones, (Schmid et al., 1980).

For Yule Marble, Heard and Raleigh (1972) have reported that in addition to e-twinning there is activity on r, f and a slip systems. Spiers (1981) has found that the main glide system for Carrara marble was r slip. As temperature increases, for constant grain size, at or above 800°C, e-twinning decreases in importence and intracrystalline glide on r and f slip systems becomes dominant. At temperatures lower than 500°C and strains below 10%, Rutter (1974) has noted the lack of dislocation climb, i.e. dislocations being confined to their slip planes, in accordance with the climb velocity being proportional to :

$$\frac{Dsd}{L} * \frac{\sigma}{kT} \qquad (2.9)$$

Where Dsd is the self diffusion coefficient.

L is the average distance from the dislocation at which the vacancy concentration is in equilibrium (this is independent of differential stress).

σ is the compressive stress working for the absorption and against the creation of a vacancy.

k is a constant.

T is temperature.

2.5.3.1.3 RATE CONTROLLING STEP

For a dislocation to climb one interatomic distance, atoms have to be brought in or removed by diffusion (this is distinct from the movement of dislocations on a slip plane), which is obviously stress and temperature dependent because diffusion is the rate controlling step.

From microstructural studies dislocation glide is thought to be the main strain accommodating mechanism for high stress (exponential law) flow. This corresponds to the thermally activated micromechanical model for dislocation glide of Ashby and Verrall (1978). Resistance to flow results from the inherent properties of the grain itself, i.e. the lattice forces (known as Peierls forces) and impurities within the lattice, e.g. inclusions, defects etc. Any of these will cause impediments to the passage of dislocations through a crystal. The recovery processes active are unknown, although Nicolas and Poirier (1976) suggest thermally activated cross slip resulting in annihilation of dislocations as being dominant.

Shaw (1982) has suggested a correlation of apparent activation energies with the presence of various types of impurities, and has noted the impure

Solenhofen Limestone has a lower apparent activation energy than pure Carrara Marble. However the finer grain size of the former, together with the higher energy boundaries (c f. Table 4.1) would promote grain boundary diffusion. Rutter (1974) has suggested that an extrinsic diffusion mechanism may be the relevant diffusion rate controlling factor. Note that the grain boundary hardening effect, discussed earlier, will work against this.

The result may be a combination of the above processes for any one specimen.

2.5.3.1.4 TWINNING

The twinning dislocation propagates in the direction of shear, defining a burgers circuit around a ledge in the twin boundary. The shear does not correspond to a lattice period and the twinning dislocation is thus imperfect, occurring when the dislocation sweeps across the boundary.

For the twinning field a fine grained limestone's strength will be largely dependent upon resistance to movement around the twin tip, i.e. yield strength increases near the boundaries, (Schmid, 1982a). Constriction of twins at grain boundaries implies that twinning can only accommodate strain in the grain interiors, the boundaries deforming by slip, plus at higher temperatures grain boundary sliding, (Turner et al., 1954). For a coarser marble, stress concentrations in the grain boundaries will have a small effect on the bulk strength of the aggregate. This mechanical effect is distinct from that of the Hall-Petch law discussed in section (2.5.3.1.1).

Twins typical of lower temperatures are thin, planar and numerous, (Chapter 6, 7 and Plate 4.1b); correspondingly there is little evidence of twin boundary migration. The two distinct types of twin may be termed plastic and elastic, high and low temperature, respectively.

2.5.3.1.4.1 BEHAVIOUR OF TWINS AT HIGH TEMPERATURE

The high temperature twins, typical of experiments, e.g. Chapter 4, are indicative of twin boundary migration, i.e. the twin grows laterally as the next lattice plane in the crystal shears, (C. Willaime, pers. com.).

The twin lamellae boundaries are pinned by the "hard" nature of the grain boundary and the crystallographic orientation of adjacent grains, assuming a uniform texture. This accounts for typical, thick, lozenge shaped high

temperature twins with irrational boundaries, some even terminating inside grains.

Twin boundary migration as a mechanism of twin growth results in irrational twins and represents the rapid displacement of the twin boundary perpendicular to the plane of the twin, resulting in rapid thickening of the twinned domain, this being distinct from grain boundary migration where climb of grain boundary dislocations occurs. With twinning we have glide of the dislocations in the boundary, (Nicolas and Poirier, 1976).

2.5.3.1.4.2 THE TWINNING FIELD BOUNDARY

Rutter (1970) first noted that there is a twinning cut-off value, which for Solenhofen Limestone is above 300°C at moderate strain rates, whereas for Carrara Marble, (Rutter, 1974, Schmid et al., 1980 and Spiers, 1981), and Yule Marble, (Heard and Raleigh, 1972), the twinning field cut-off is approximately at 1 Kbar, at 700°C.

The amount of twinning varies with :

1. Differential stress.

2. Grain size.

Spiers (1981), and Chapter 4, have shown that the twinning field boundary, as a function of stress is independent of strain rate. It transects isotherms and Rutter (1974) has shown that the effect of pore fluid is minimal.

By calibrating the twinning field boundary against the controlling variables Spiers (1981) has suggested that the possiblity of a reliable calcite twinning paleopiezometer arises. The series of experiments leading to the full calibration of a calcite twinning palaeopiezometer is presented in Chapter 4.

5.3.1.4.3 STRAIN ESTIMATION

There are two methods for small bulk strain estimation as afunction of twinning activity: both use standard optical techniques and a large data set. Shear strain is estimated from the ratio of twinned domains width for each host grain.

The methods are :

1. Conel (1962) (After Spiers, 1981) :

This technique transforms the shear strain for each twin set to the sample reference axes X, Y and Z, and obtains the bulk strain tensor. The data is then averaged after normalising for the effect of grain size to give the average bulk strain tensor.

2. Groshong (1972) :

This uses a least squares routine to solve strain equations to give the bulk strain tensor based on using the twin sets as shear strain gauges.

Both methods are accurate indicators of principal strain directions, but only give upper limit order of magnitude estimates for the amount of shear strain. Spiers (1981) has shown the heterogeneity of strain on the grain scale as a result of grains being orientated preferentially for twinning, therefore favourably orientated grains display "excessive twinning activity". Spiers (1981) suggested that the Conel method can give reasonable estimates of the maximum possible strain if the amount of twinning per grain is accurately measured.

Hence the relationship between strain and twinning activity is complex and probably indeterminable in practice as this can only be assumed.

2.5.3.2 INTERMEDIATE DIFFERENTIAL STRESS FLOW BEHAVIOUR

While it must be noted that any divisions between stress fields will be artificial, there is a change in the rheological behaviour of calcitic rocks in the intermediate stress field, represented by a change in the flow law. In the intermediate stress field, stress and strain are found experimentally to be related by a power flow law which has the form :

$$e = A2 \exp\left(\frac{-H}{RT}\right) \sigma^{n} \qquad (2.10)$$

Where σ is the differential stress at constant strain rate and temperature.

H is the apparent activation flow energy.

R is the gas constant.

A2 is an empirical material constant.

n is the empirical material constant stress exponential, or stress dependence.

After Shaw, 1980.

Experimental data indicates that after a few percent strain under a work hardening regime steady state flow occurs with a constant flow stress. The change from exponential to power flow occurs when strain rate is reduced, and/or temperature is increased.

Schmid et al., (1980) state that the grain size dependence of flow stress becomes less pronounced in this field, and in the low stress field (section 2.5.3.3) smaller grain size leads to a lower flow stress. Grain size is of less importance where diffusion related processes are operative.

Although the strain rate is probably by dislocation climb out of the glide plane, dislocation glide still accommodates most of the bulk strain, as is the case for high stress flow. Grain boundaries are not expected to be important where dislocation climb is operative. Diffusion is stress and temperature dependent, this being consistent with Kirby and Raleigh's (1973) micromechanical models. The only difference in this field is that stress can now be accommodated by dislocation climb.

2.5.3.2.1 MICROSTRUCTURE

Climb of dislocation allows their aggregation into subgrain walls. The subgrains form, in this case, by the progressive misorientation of the lattice until they form a separate mosaic of equiaxed grains in equilibrium with the new stress fields configuration and magnitude. Hobbs (1968) suggested this as a method of dynamic recrystallisation. The migration of dislocations into dislocation, or subgrain, walls, complementary with dynamic recrystallisation, leads to a steady state situation by maintaining a free dislocation density within the subgrain. This is stress dependent, and various authors have proved that dislocation density can be used as a palaeostress indicator e.g. Twiss (1977), see Chapter 3.

Schmid et al., (1977) by detailed crystallographic analysis of Solenhofen Limestone have shown that dislocation glide on r and f slip systems is dominant, resulting in the development of preferred crystallographic orientation and a grain shape fabric. The same authors noted that another strain accumulating mechanism was operative, that of diffusion or plastically accommodated grain boundary sliding. This involves the displacement of grains relative to one another by movement along their boundaries, (see section 2.5.3.3, superplasticity), this accommodates less than 20% of bulk strain in this stress regime.

Electron microscopy revealed subgrain development, sometimes equiaxed (1μm), but more commonly elongate (1μm * 2μm) in the direction of overall fabric development. These subgrains have uniform, high dislocation densities, in the form of dislocation loops or dipoles (locking pairs of opposite edge dislocations on parallel slip planes, Nicolas and Poirier, 1976), all indicative of recovery by dislocation climb.

2.5.3.2.2 HIGH STRESS EXPONENTIAL, POWER FLOW LAW

Yule and Carrara Marble's rheological properties suggest a further division of the power flow law based on the magnitude of the stress exponent in equation (2.8). From Table 2.5, both Yule and Carrara Marble in the stress regime 20 to 100 MPa have a high value of n, being in the range 7.6 to 8.3. This is termed high stress exponent, power flow law.

2.5.3.2.2.1 MICROSTRUCTURE

The observed microstructure, (Schmid *et al.*, 1980), involves development of a core and mantle structure. Where, in the core of the old grains generally elongate subgrains and kink bands are developed, Nicolas and Poirier (1976) have suggested that this elongation results from preferential slip on single or a limited number of slip systems, while the mantle, or grain boundary, is characterised by equant, equiaxed subgrains, produced by progressive misorientation, eventually resulting in recrystallisation.

Twinning is rare in this stress regime, but when present there is usually evidence for twin boundary migration. Also there is evidence for grain boundary migration. The later is stress induced and causes recrystallisation of those grains with highest internal energy. As in Solenhofen Limestone, grain boundary sliding was of minor importance, i.e. accommodating less than 20% of bulk strain.

2.5.3.2.3 LOW STRESS EXPONENTIAL, POWER FLOW LAW

The second form of the power flow law is that of the low stress exponent, n in equation (2.8) being of the order of 4.2 for experimental conditions in excess of 900°C and differential stress lower than 20MPa.

2.5.3.2.3.1 MICROSTRUCTURE

Schmid et al., (1980) describe the associated microstructure as one of homogeneous, equiaxed subgrains, with grain boundary sliding accommodating between 20 and 50% of bulk strain (an important, but variable contribution). The equiaxed nature of the subgrains probably results from homogeneous, simultaneous slip activity on several systems, as the CRSS for the different systems have converged at the higher temperatures. See Table 2.3.

The developments of subgrains and recrystallised grains are the response of the rock to the new deformational parameters imposed upon it, in an attempt to produce a new equilibrium microstructure. Given time the whole rock would be replaced by the new grain size. An important consequence of total dynamic recrystallisation is that the tectonic reduction of grain size can conceivably lead to a change in the dominant flow process to grain boundary sliding with diffusional accommodation, with concomitant weakening.

Schmid et al., (1980), in experiments above 1000°C, noted another recrystallisation mechanism, thermally activated, in which large (grain size averages 1000μm), irregular grains are developed by the high mobility of grain boundaries. This occurs simultaneously with subgrain rotation.

2.5.3.2.4 RATE CONTROLLING STEP

The rate controlling step in the power law regime is not known with certainty. Anderson (1969) determined experimentally the activation energies for diffusion of carbon and oxygen species in calcite. The activation energies in this field are very close to the 88 kcal/mole$^{(-1)}$ calculated for intrinsic self diffusion (Schmid et al., 1980). This model is consistent with dislocation climb being activated and hence is likely to be the rate controlling process for deformation. This is consistent with Weertmans 1968 model (where subgrains form at the beginning, and then remain constant through the subsequent deformation), and Kirby and Raleigh (1973) have found a correspondence in many other materials between activation energies.

From the observed temperature dependence of the shear modulus, Evans and Langdon (1976) showed that in high temperature experiments there was a discrepancy between calculated activation energy for flow and real, or observed, flow energy. The magnitude of this discrepancy, known as the modulus compensation effect, Shaw (1983), may be 5 - 20 kcal/mole, using Danaekar's

(1968) elastic constants. The temperature coefficient of the shear modulus for calcite polycrystals is :

$$\frac{1}{\mu_o} * \frac{du}{dT} \qquad (2.11)$$

$$= -0.32 * 10^{(-3)} K^{(-1)}$$

Where μ is the proportionality coefficient, between the shear modulus and the shear strains.

For Carrara Marble the apparent activation energy for power flow is approximately 100 kcal/mole, but taking into account the modulus compensatory effect, this figure is very close to the diffusion energies of calcium and oxygen in calcite of 88 kcal/mole. Hence it is probable that the intrinsic diffusion energies are rate controlling for dislocation glide.

However the lower activation energies for diffusion of Yule Marble and Solenhofen Limestone (Heard and Raleigh, 1972; Schmid et al., 1980) indicate that other processes are involved. Extrinsic diffusion, e.g. of impurities, is favoured by high pressure, due to their lower activation volume, (Ashby and Verrall, 1978), these have lower activation energies than lattice, or internal, diffusion. The latter is also true for grain boundary diffusion.

Heard and Raleigh (1972) and Schmid et al., (1977, 1980) have suggested that the models of Weertman (1968, "Weertman Creep") are applicable for their experiments. Strain is accumulated by glide on r and f slip systems, and the rate controlling factor is diffusion controlled dislocation climb, see earlier. "n" in equation (2.8) is observed as being 4.7, and the model prediction is 4.5, which is a close correlation.

For Carrara Marble, and presumably for Yule Marble and other similar grain size marbles the occurrence of the high and low stress exponent, power flow law requires explanation. Schmid et al., (1980) proposed that heterogeneous strain, involving exponential flow in the grain cores and power flow in the mantles, giving the low stress exponent, power flow law, overall. Additionally, in the low stress exponent, power flow law, there is an increase in the contribution of grain boundary sliding to the bulk strain. Grain boundary sliding has a stress exponent value of 1 - 2. Therefore the overall stress exponent value observed may average approximately 4.

To conclude, the intermediate stress regime is a composite deformational regime, with several discrete deformational mechanisms operative. Correspondingly, the form of the flow law varies within the overall field, although, broadly that of power flow law applies.

2.5.3.3 LOW DIFFERENTIAL STRESS FLOW BEHAVIOUR

In the low stress field the dominant deformational mechanisms involve creep by diffusional processes. Schmid (1982a) states that three separate deformational mechanisms can be operative; these are :

1. Pressure solution.

2. Creep by solid state diffusion, essentially Coble and Nabarro-Herring creep.

3. Creep by grain boundary sliding (g.b.s.), leading to superplasticity.

2.5.3.3.1 PRESSURE SOLUTION

The conditions of pressure solution are difficult to reproduce experimentally because it operates at very low strain rates, i.e. low temperatures and stresses, and hence is applicable to a wide range of upper crustal rocks. By increasing temperature at low stresses in order to obtain measurable strain rate the activation threshold for other mechanisms, e.g. g.b.s. and solid state diffusion will be crossed.

Flow stresses at a given strain rate are nearly temperature insensitive in the pressure solution field (Rutter, 1976), this results from :

1. Decreased solubility of calcite with increased temperature.

2. Increased pressure sensitivity of calcite solubility with increased temperature.

Additionally diffusivity with the grain boundary fluid film (if present) is not expected to be overly temperature sensitive (Schmid, 1982a).

2.5.3.3.2 SOLID STATE DIFFUSIONAL CREEP

Solid state diffusional mass transfer has not yet been observed experimentally in rocks. At moderate temperatures and in the presence of fluids, pressure solution leads to a higher strain rate, i.e. it is more effective and efficient.

5.3.3.3 GRAIN BOUNDARY SLIDING ACCOMMODATED CREEP

Edington et al. (1976), and most other authors regard g.b.s. as the main strain producing mechanism of superplasticity. Superplasticity is defined as extreme ductility in extension of materials. This is essentially a metallurgical definition and can be further qualified for rocks as : having a low value of power in the flow law, i.e. low stress :

$$\text{strain rate} \propto \sigma^{(n)} \qquad (2.12)$$

Where n is between one and three for stress relaxation experiments, and 1.7 in constant stress tests. C.f. the low stress exponential, power flow law previously discussed, which may be transitionary between power flow law and superplasticity.

At high temperatures and low stresses for Solenhofen Limestone, Schmid et al. (1977), we have increased strain rate sensitivity, i.e. superplasticity, or grain size dependent creep :

$$\text{strain rate} = A3\, d^{(-b)} \exp\left(\frac{-H}{RT}\right) \sigma^{(n)} \qquad (2.13)$$

Where σ is differential stress at that strain rate and absoulute temperature, T.

H is the apparent activation energy for flow.

R is the gas constant.

A3 is an empirical material constant.

d is grain size.

b is the grain size exponent.

n is the stress exponent.

This is, essentially, a power flow law with a grain size variable, and with g.b.s. as the main deformation mechanism. Superplasticity was found to be dominant at low stresses, below 400 bars at 900°C and below 1000 bars at 600°C. No Coble Creep was observed.

2.5.3.3.4 **MICROSTRUCTURE**

In the experiments of Schmid et al. (1977), the microstructure of Solenhofen Limestone became equiaxed, polygonal and the grain boundaries developed a low energy state. Grain boundary migration represents a large distortion of the original material. Even at high strains grain flattening accumulated less than 30% of the bulk strain. The variable b in formula (2.11) varied between 2 and 3, this being determined from different grain sizes, resulting from high temperature grain growth. Electron microscopy revealed minor subgrain formation, and a highly variable dislocation density.

From detailed crystallographic analysis, Casey et al., (1978) have noted for the low stress field that little or no crystallographic preferred orientation was developed, and that the texture resembled that of the original. This is distinct from exponential and power flow behaviour where a crystallographic preferred orientation develops, depending on which crystallographic vector is operative.

2.5.3.3.5 **RATE CONTROLLING STEP**

In contrast to the high stress field the grain size sensitivity is such that a finer grain size results in a lower flow stress. This is the result of decreased diffusional paths and increased number of grain boundaries for diffusional reactions.

Microdynamic models for superplasticity assume, usually, that strain rate at any given temperature and stress is not controlled by friction and viscous resistance to sliding at grain boundaries, but by the slowest event during the process of g.b.s. and neighbour swapping, i.e. the minor change in shape that grains have to undergo in order to move past each other.

There are two models for neighbour swapping :

1. Ball and Hutchinson (1969) :

In this model dislocations pile up at unfavourable grain boundaries (this stress concentration may give rise to minor local diffusion if fluid is present) and these escape by climb into the grain boundary.

2. Ashby and Verrall (1973) :

In this model local diffusional mass transfer is dominant, obviously this is enhanced if fluid is present. Fig. 2.10.

There will be be almost certainly a combination of the two models outlined above in any one specimen.

Evans and Langdon's (1976) micromechanical models for g.b.s. predict $d^{(-b)}$ and n values, depending on the sliding accommodating mechanism :

a. Diffusional flow : n = 1, and b = 3.

b. Dislocation processes : n = 2, and b = 2.

Rutter (1976) has included the processes of solid state diffusion and pressure solution in a deformation mechanism chart (Fig. 2.11). The very nature of low stress field deformational mechanisms means that time is of great importance, and their experimental duplication is difficult.

Schmid (1982a) has superimposed the theoretical predictions of Rutter (1976) for diffusional creep on those of experimentally derived flow laws and found for superplasticity that close corelation exists between the two data sets.

Further experimental work is required on natural specimens to enable further understanding on what are extremely important processes in nature.

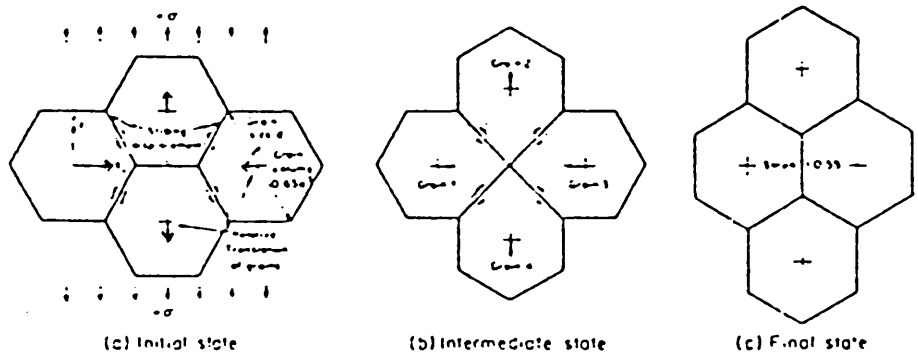


FIGURE 2.10 The grain boundary sliding model of Ashby and Verrall (1973). In this model a total of 53% strain is accommodated by the process of neighbour swapping, the intermediate step takes place by diffusion to enable strain compatability to be maintained in the grain boundary regions.

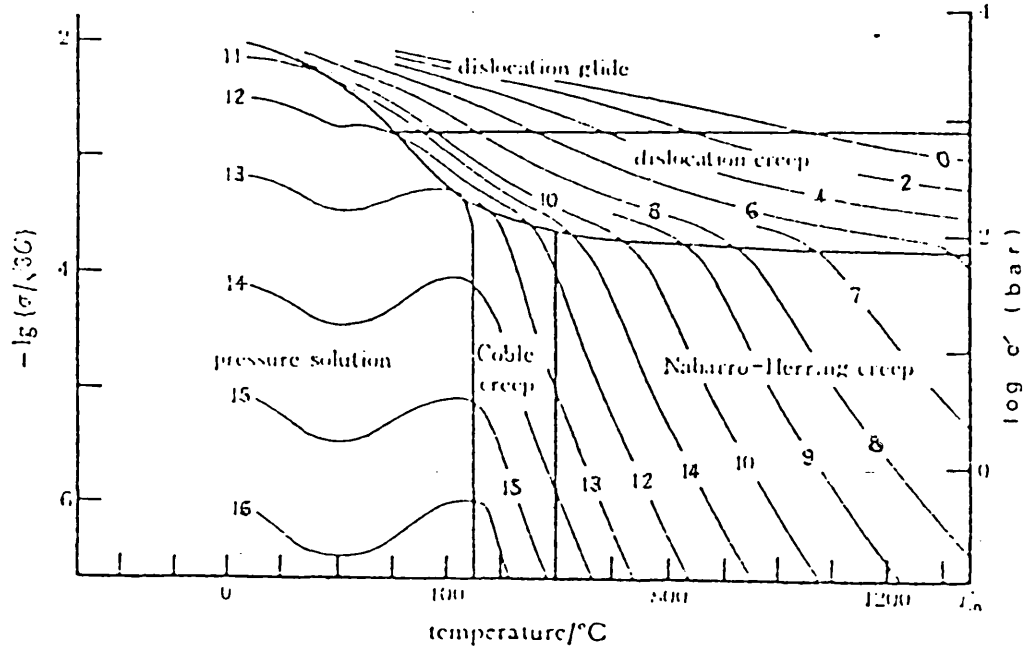


FIGURE 2.11 Deformation mechanism chart for 100μm grain size calcite. The strain rate contours in the pressure solution field are subhorizontal, reflecting that this process is temperature insensitive in this model. After Rutter, 1976.

TABLE 2.5 : DATA SUMMARY

A. SOLENHOFEN LIMESTONE

	EXPERIMEMNTAL CONDITIONS	RHEOLOGICAL PARAMETERS	MICROSTRUCTURE	COMMENTS	
1. EXPONENTIAL FLOW $e = A1\exp(\frac{-H}{RT})\exp(\frac{\sigma}{\sigma 0})$	T = 400-500°C σ_{diff} = 220MPa+ σ_3 = 150MPa	log A1(sec^{-1})=-0.12 H(Kcal/mole)= 47.1 σ0(MPa) = 16.04	e-twinning	Regime I Low T plasticity Constant e exp.	*1
	T = 600-900°C σ_{diff} = 190MPa+ σ_3 = 300MPa	As above	Intracrystalline glide on r and f slip systems	In the low T range the rate control. step is diff. assisted.	*2
2. POWER FLOW LAW $e = A2\exp(\frac{-H}{RT})\sigma$	T = 600-900°C σ_{diff}=100-190MPa σ_3 = 35MPa+	logA2($s^{-1}MPa^{-1}$)=-2.33 H(Kcal/mole) = 71.1 n = 4.7	Dislocation creep of r and f slip systems	Regime II High T plasticity g.b.s.= 20% strain	*2
3. SUPERPLASTICITY $e = A3d\exp(\frac{-H}{RT})\sigma$	T = 600-900°C σ_{diff}=100MPa(600°C) σ_{diff}=35MPa(900°C) σ_3 = 300MPa	lgA3($s^{-1}MPa^{-1}\mu m^{-1}$)=3.98 H = 50.9 n = 1.66 b = 3 d(μm) = 5	Diffusion creep	Regime III g.b.s= 60% strain	*2

All symbols as for text.

REFERENCES :

*1 - Rutter (1974), *2 - Schmid et al. (1977).

*3 - Schmid et al. (1980), *4 - Heard and Raleigh (1972).

B. CARRARA MARBLE

	EXPERIMENTAL CONDITIONS	RHEOLOGICAL PARAMETERS	MICROSTRUCTURE	COMMENTS
1. EXPONENTIAL FLOW Formulae as for Carrara Marble	T = 400-500°C σ_{diff} = 120MPa σ_3 = 150MPa	logA1(sec^{-1})=5.77 H(Kcal/mole)=62.1 σ0(MPa)=11.41	e-twinning	As for Table *1 2.5A
	T = 600-700°C σ_{diff} = 100MPa σ_3 = 300MPa		Intracrystalline glide	*3
2. POWER FLOW σ_{diff}=100MPa(600°C	T = 600-900°C H(Kcal/mole)=100.1 σ_{diff}=20MPa(900°C) σ_3 = 300MPa	logA2($s^{-1}MPa^{-1}$)=-5.5 Intracrys. glide & n = 7.63	e-twinning at low T. High stress exponent, g.b.s. Core & mantle subgrain struct.	g.b.s.=10% strain *3 power flow law.
	T = 900-1050°C σ_{diff} = 20MPa σ_3 = 300MPa	logA2($s^{-1}MPa^{-1}$)=2.93 H(Kcal/mole) = 102.1 n = 4.23	Extensive recrys. & g.b. migration. Equiaxed subgrain structure	g.b.s.=20-50% *3 strain. Low stress exponent, power flow law

3. SUPERPLASTICITY No data.

C. YULE MARBLE

	EXPERIMENTAL CONDITIONS	RHEOLOGICAL PARAMETERS	MICROSTRUCTURE	COMMENTS
1. EXPONENTIAL FLOW Formulae as for Carrara Marble	T = 400-500°C σ_{diff} = 80MPa σ_3 = 500MPa	Foliation logA1(sec^{-1})= 7.3 8.28 H(Kcal/mole)=56.8 61.6 σ0(MPa) =13.5 9.50	e-twinning	g.b.s.= 10% *4
2. POWER FLOW	T = 500-800°C σ_{diff} = 80MPa σ_3 = 500MPa	Foliation logA2($s^{-1}MPa^{-1}$)=-12.3 13.2 H(Kcal/mole) = 60.7 62.0 n = 7.54 8.3	e-twinning at low T., g.b.s.= 10% *4 & intracrys. plast. at moderate to high temperatures	

2. SUPERPLASTICITY No data.

CHAPTER 3 : PALAEOPIEZOMETERY

3.1 INTRODUCTION

A number of methods relating observed microstructures to differential stress, essentially in the plastic field, have been published. These are based upon theoretical considerations, observations of naturally deformed materials, and/or their calibration with experimentally deformed specimens.

The following are the main palaeo-stress indicating microstructures :

1. Dynamically recrystallised and subgrain grain size.

2. Free dislocation density.

3.Twinning.

3.2 DYNAMICALLY RECRYSTALLISED AND SUBGRAIN GRAIN SIZE

When a mineral is deformed, the original grain size will probably be in disequilibrium with the new environmental parameters imposed, and hence grain size will try to re-equilibrate in response. Hence an equilibrium grain size may be expected to exist.

For Solenhofen Limestone grain growth occurred when the limestone was deformed (Schmid et al., 1977),while for Yule Marble (Heard and Raleigh, 1972), the coarse grained matrix of the oolitic marble (Schmid and Paterson, 1977), and Carrara Marble (author), grain size reduction occurred under similar experimental conditions, thus backing up theoretical observations.

Subgrain formation and rotation is an important method of recrystallisation, and is related to stress by :

$$\text{stress (diff.)} = k1\ u\ \underline{b}\ Dsg^{(v)} \qquad (3.1)$$

, while recrystallised grain size is related to stress by :

$$\text{stress (diff.)} = k2\ Drg^{(w)} \qquad (3.2)$$

Where k1, k2,v and w are constants.

$\underline{b}$ is the average burgers vector.

u is the rigidity modulus of the material.

Dsg is subgrain size.

Drg is recrystallised grain size.

The theoretical basis for these relationships is given by Kohlstedt (1980) and Edwards et al., (1982).

Twiss (1977), based on proved metallurgical relationships and principles, and empirical data from ceramics, metals, quartz and olivine, derived an approximate theoretical palaeopiezometric relationships which is applicable for deformation by dislocation creep :

$$\frac{\text{stress (diff.)}}{\Gamma} = K \left(\frac{d}{b}\right)^{-p} \qquad (7.3)$$

Where d is subgrain or recrystallised grain size.

Γ is the elastic constant.

b is the average burgers vector.

K and p are constants.

This differs from (7.1) and(7.2) in that (7.3) is normalised by Γ and b to a dimensionless form, while K and p vary for subgrain and recrystallised grain size.

Schmid et al., (1980) for Carrara Marble, deformed between 600°C and 1050°C and at strain rates between $10^{(-2)}$ and $10^{(-6)}$/$sec^{(-1)}$, noted two separate mechanisms of recrystallisation, as reported in Chapter 2 :

1. Subgrain rotation.

2. Grain boundary migration.

The latter was observed only above 1000°C, and hence in a narrow stress range. Both the recrystallised and subgrain size were equivalent, recrystallised grains being 38 $\pm$ 10μm (each representing a group of 50 specimens), and both are in turn inversely proportional to flow stress at time of formation.

When the log. ratios of stress and grain size are plotted, the slope, p, was 1.01 $\pm$ 0.05. This agrees well with Twiss's (1977) empirical relationships for the subgrain rotation method of recrystallisation (Fig. 3.1) for grain size between 5 and 43 μm, and 1000 to 100 bars, respectively. But Twiss's model for dynamic recrystallisation was found not to be applicable in Schmid et al.,

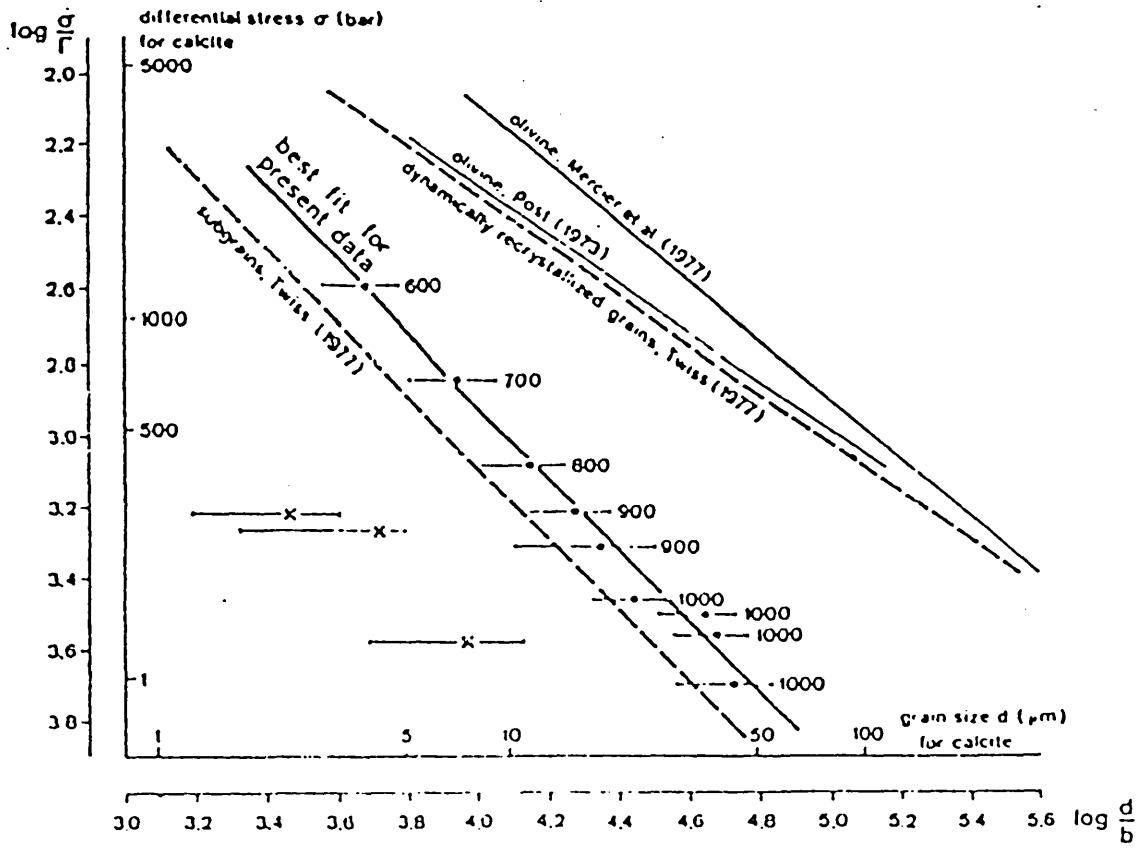


FIGURE 3.1 Normalized plot of dynamically recrystallised grain size as a function of Differential Stress. Subgrains (crosses) are plotted for comparison. After Schmid et al., 1980.

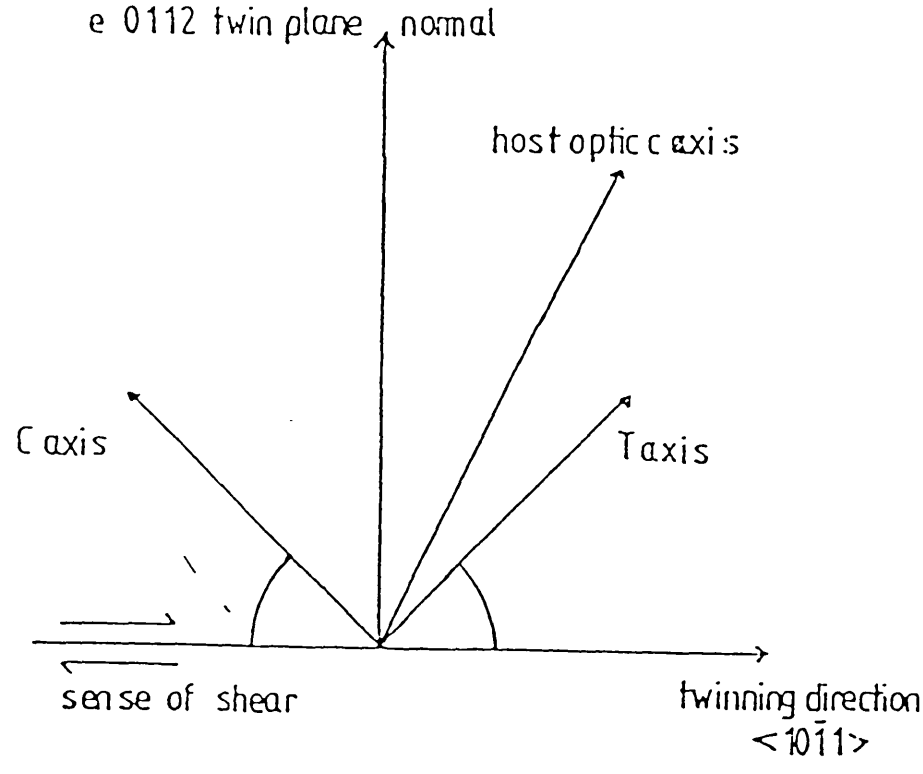


FIGURE 3.2 Dynamic Analysis Technique (DAT), showing the relationships between the Compression (C) and Tensional (T) axes, and the crystallographic directions.

(1980) experiments on Carrara Marble, the conditions of which are outlined above. The effect of temperature variation upon grain size has not been determined, especially with respect to the subgrain rotation mechanism, but the stress relationship of grain size appears to correlate well between 10 and 100 MPa.

Electron microscope scale subgrains (Schmid et al., 1980) showed a wide variablity in shape and size, and no clear relationship was observed. However, by plotting the smallest grains on Fig. 3.1, they define a similar slope, but at an order of magnitude smaller size to the other grains.

3.2.1 LIMITATIONS

Obviously a problem with natural specimens is the resetting, or modification of the microstructure by a subsequent tectonic event.

Subgrain sizes requilibrate quickly in response to increasing stress, as seen in experiments, but are more sluggish in response to decreasing stress (Pontikis and Poirier, 1975, and Ross et al., 1980) and therefore subgrain size does record the highest stress level the rock has been subjected to. To rework grain size probably requires relatively high values of temperature and stress, as is evidenced by the presence of relict grains in ancient mylonite belts.

To conclude this section, further experiments are required to extend the calibrated range of differential stresses, and especially further work is required on the grain bounday migration method of recrystallisation.

3.3 FREE DISLOCATION DENSITY

The density of free dislocation (pf) is related to stress by the following relationship :

$$\text{stress (diff.)} = k1 \; u \; b\sqrt{pf} \qquad (3.4)$$

Key to terms as in (7.2), where k1 is a material constant, usually between 0.5 and 5.

This relationship (Nicolas and Poirier, 1976) has been calibrated experimentally for Yule Marble (Goetze and Kohlstedt, 1977), Carrara Marble (Schmid et al., 1980) and Solenhofen Limestone (Schmid et al., 1977, and Briegel and Goetze 1975). The marbles show a close correlation between theory and the

experimental observations for stress in excess of 60 MPa (k1 = 2), while below 60 MPa there was no significant difference between starting and finishing dislocation density, although there was a large variation on the grain scale.

Reduction of pf below that of the starting material has been observed by Goetze and Kohlstedt (1977) and Schmid et al., (1980). The former was characterised by slow kinetics - deformation annealing ?, while the later can be explained by predeformational annealing, resulting from heating of the specimen prior to application of differential stress.

Conversely, a high pf was observed by Schmid et al., (1980) for low flow stresses, and was interpreted as the result of post experimental cooling and depressuration, an experimental compliance ?

For Solenhofen Limestone at low to intermediate stresses, Schmid et al., (1977) found that in the regime of superplasticity there was a wide scatter of pf values. This was largely the result of the presence of two types of grain, one virtually devoid of dislocations, while for the other the converse is true with pf = 7 * $10^{(9)}/cm^2$, (possibly there is an element of machine compliance here also). In the dislocation creep regime (power flow law) for Solenhofen Limestone there was increased correlation between pf and stress.

At high stress (exponential flow law) for Solenhofen Limestone there was a close correlation with that of the Yule Marble data of Goetze and Kohlstedt (1977), and Briegel and Goetze (1975). Hence for differential stress in excess of 60 MPa there is confidence in the values of pf from experiments.

3.3.1 LIMITATIONS

However, dislocation densities require very little strain to be completely reset (White 1979a), where recovery is negligible, so prohibiting development of subgrains and recrystallised grains. They will record the most recent event, particularly that of uplift.

3.4 TWINNING

The shearing of a crystal lattice in resonse to applied stress is a commonly observed phenomenon, especially in calcitic rocks. To operate the shear requires a build up resolved shear stress on that plane in a unique shearing sense relative to the crystallographic axis, until failure occurs; then if stress continues to increase the next most favourably orientated plane will

shear (or the twin will widen), and so on until the stress is removed. Hence the volume of twinned domain represents a unique value of differential stress.

The stress required for twinning is independent of strain rate (see Chapter 4) and temperature, while pore fluid pressure has an insignificant effect, but is strongly dependent upon grain size, see section (2.5.3.1.4.2, and Chapter 4). The full experimental calibration of a calcite twinning palaeopiezometer technique is presented in this thesis, and was first proposed by Spiers (1981).

Calcite twinning has been used for many years by structural geologists. In 1953, Turner proposed the Dynamic Analysis Technique, whereby the orientation of C (compression) and T (tensional) axes can be obtained from a large number of grains, the preferred concentration defining the principal stress axis, Fig. 3.2

Another palaeopiezometric technique has been proposed by Jamieson and Spang (1976) based on calcite twinning. This method assumes axisymmetric compression, homogeneous strain and a uniform starting texture. Hence assigning a given CRSS for those grains with one, two or three twin sets, the development of one, two or three twin sets is a function of applied differential stress. Spiers (1981) has pointed out that the state of stress can be highly heterogeneous from grain to grain and is only poorly characterised by single crystals. Hence the selection of the appropriate CRSS will vary for different twin sets, although order of magnitude estimates are possible. Tullis (1980) points out that for metals imperfections may give rise to a range of CRSS for twin initiation.

3.5 LIMITATIONS OF THE METHODS

The application of palaeopiezometric techniques to natural systems can be seen to be fraught with difficulties as a result of thefact that we are making important decisions regarding the environmental parameters operative. These will govern the microstructures that develop. Nicolas and Poirier, 1976, Twiss, 1977, and White, 1979a, have reviewed the theoretical basis for the relationships discussed in this chapter, and have discussed their problems of application.

Commonly, stress levels calculated by these methods, even for single samples, often show a wide variation of the stress parameter. Norton and White (in press) state that the paucity of data means that the inconsistences in the

results outlined above can not be tested. We need to now if the said inconsistences are due to their being reset in response to different stress levels (and by implication, time dependent microstructural responses to stress variations), or as a result of data errors.

Further experimental work is required in order to increase our knowledge of the principal methods outlined above, and their application to nature, particularily the effects of resetting, or modification of these parameters.

CHAPTER 4 : THE CALIBRATION OF TWINNING ACTIVITY AS A FUNCTION OF DIFFERENTIAL STRESS AND GRAIN SIZE

4.1 INTRODUCTION

This chapter reports the detailed experimental investigation of calcite twinning activity as a function of differential stress and grain size.

In the preliminary sections there are descriptions of the starting materials, choice of general experimental deformation parameters, and the various methods used to measure twinning activity. The author then examines the twinning activity of Solenhofen Limestone, as reported by Spiers (1981). This is followed by the authors own series of experiments upon Carrara Marble and Taiwanese Marble.

The nature of the experimental and textural data presented in this chapter necessarily requires the use of a large number of graphs, see later.

4.2 STARTING MATERIALS

The following are the materials used for the investigation of twinning activity as a function of differential stress and grain size. Table 4.1 lists the principal properties of the starting materials described in this chapter.

4.2.1 SOLENHOFEN LIMESTONE : (Upper Jurassic, Bavaria)

This is a fine grained (5μm, but ranging from 3 to 26μm), well lithified calcite mudstone, which is 95% pure (the impurities being quartz and clay minerals, Wenk et al. (1973), Schmid et al. (1977)), and has a porosity of approx. 5%, Rutter (1972).

Examination by Spiers (1981) of ultra thin sections have shown that the grain boundaries and grain morphologies are highly irregular. Apart from fine scale bedding laminations and stylolites the rock is homogeneous. Extensive textural analysis of Solenhofen Limestone by Siemes (1966), Wenk et al. (1973) and Casey et al. (1978) have shown that a weak c axis concentration normal to bedding exists, Fig. 4.1. The material is free from twins.

	SOLNHOFEN LST.	CARRARA MARBLE	TAIWANESE MARBLE
Average grain size	4-5μm Rutter, 1974	150μm Rutter, 1974	380μm Author
Grain shape	Prismatic	Equiaxed, polygonal	Slight elongation
Grain boundary morphology	Embayed and lobate Schmid et al., 1977	Mixed : curved and sutured Schmid et al., 1980	Mixed : curved and sutured
Initial porosity	1.5-3.0% Rutter, 1974	≈ 0.2% Rutter, 1974	Visual estimate; < 1%
Composition and impurities	$CaCO_3$ = 96% $MgCO_3$ = 1.2% R_2O_3 = 0.3% Insoluble = 1.5%	$CaCO_3$ = 98% $MgCO_3$ = 1.8% R_2O_3 = 0.1% Insoluble = 0.1%	$CaCO_3$ > 99%
Crystallographic preferred orientation	Weak, c-axis parallel to bedding Kern, 1977	Isotropic	Weak grain shape fabric

TABLE 4.1 Initial physical properties of the experimental materials studied in Chapter 4

4.2.2 CARRARA MARBLE : (Carrara, Italy)

This is a pure (99%+) white granoblastic marble, whose average grain size varies between 150 and 200μm. Quartz is the only contaminant phase and forms between 0 and 1% modal percent.

The experiments presented here were made on specimens taken from the same block as used by Owens and Rutter (1978) and Spiers (1981). The former authors have shown Carrara Marble to be 97%+ pure with a porosity of less than 1%.

In thin section this material is almost free from twinning and any other optically visible strain effects. This fact, together with its extremely uniform initial starting crystallite orientation distribution, (Ramez and Murrell, 1964; Owens and Rutter, 1978) makes it an ideal starting material for experimental work. Figure 4.2 shows the uniform initial texture of Carrara Marble, and Plate 4.1a shows a micrograph of undeformed Carrara Marble..

4.2.3 TAIWANESE MARBLE : (Taiwan)

This is a pure white/clear marble, which shows a range of grain sizes from 100 to 1000μm. No contaminant phases were observed by the author. In thin section the grain boundaries are regular and there are numerous thin, planar, low temperature twins, which appear to have given the material a very weak grain shape fabric.

The material was purchased from Heal's of London in the form of a polished slab 6mm thick. Specimens were prepared so that the lineation defined by the shape fabric was parallel to the specimen's long axis.

4.3 CHOICE OF DEFORMATION PARAMETERS

This section describes in general terms the environmental experimental conditions selected for the experiments performed. For the specific conditions employed for a given test the reader is referred to the description of the experiments themselves later in this chapter.

The deformational parameters were selected on the basis of existing data (see Spiers, 1981), to favour the development of e-twinning when the specimen was undergoing post-yield flow. The following general experimental parameters were used :

1. Temperature : in the range 400 to 700°C.

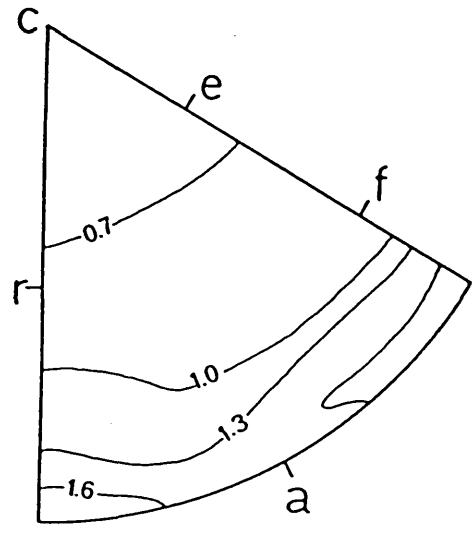


FIGURE 4.1 Initial texture of Solenhofen Limestone determined by Casey et al. (1978) and represented in the IPF plotted for the pole to bedding.

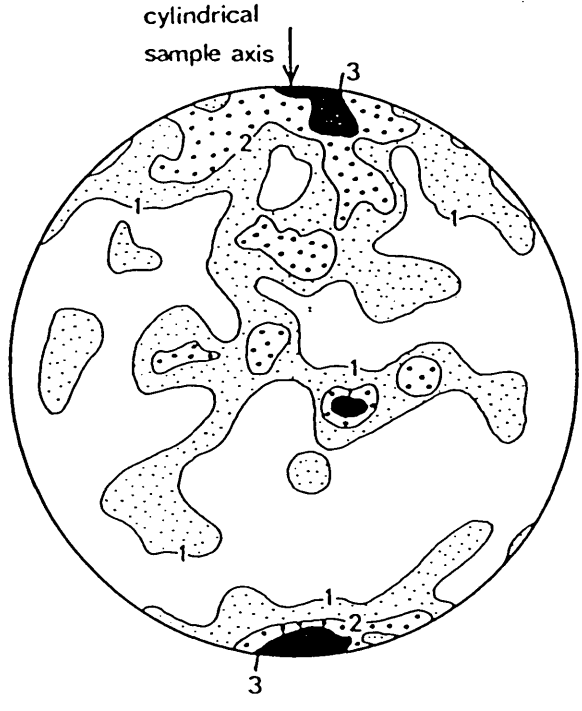


FIGURE 4.2 Initial c axis texture of Carrara Marble, after Spiers (1981) based on the u-stage measurements of 200 grains.

PLATE 4.1 Initial starting materials used for the experiments presented in this thesis.

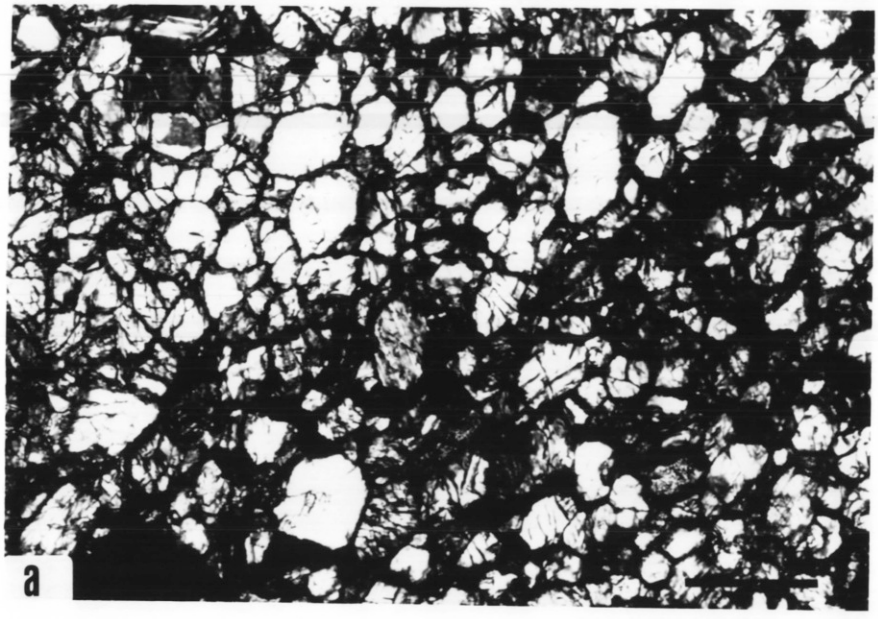
(a) Carrara Marble :
This photomicrograph shows an undeformed sample of Carrara Marble. The general absence of twins, simple, low energy grain boundaries and the variation in grain size are all clearly shown.

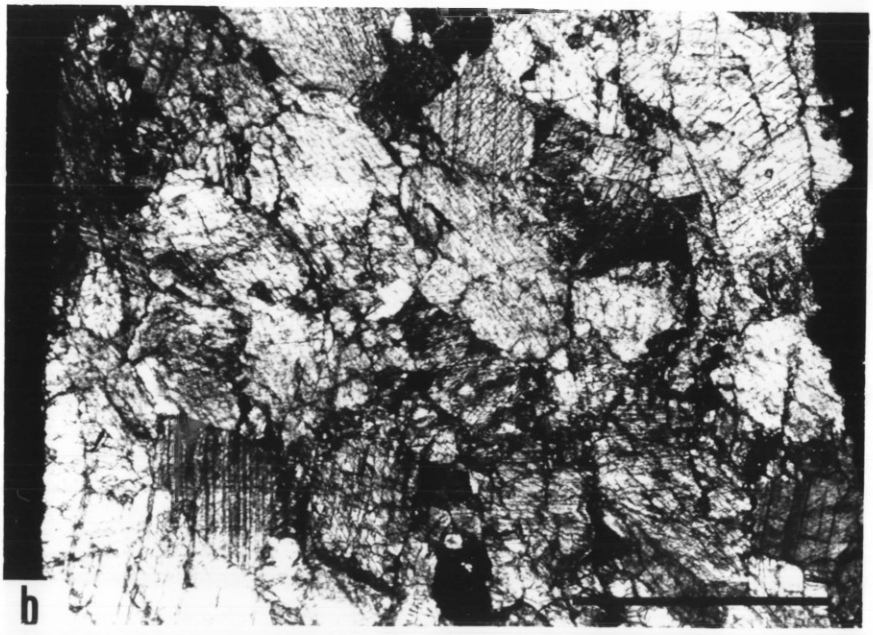
The scale bar is 200μm.

(b) Taiwanese Marble :
This photomicrograph shows an undeformed sample of Taiwanese Marble. The profusion of low temperature, natural twins are clearly visible, c f. the high temperature twins developed in the following photomicrographs in this chapter. The grain boundary morphology is variable, but generally a low energy morphology is developed. The considerable grain size variation is clearly shown.

The scale bar is 1000μm.

PLATE 4.1





2. Confining pressure : typically 15,000psi (105MPa).
3. Pore pressure : zero.
4. Strain rate : varying from $4.4*10^{-4}/sec^{-1}$ to $5.7*10^{-7}/sec^{-1}$.
5. Strain : varying from 10 to 25%.

Differential stress is obtained from the raw force gauge output and time data for a specific test, and applying a series of corrections for :

a. The effects of temperature and pressure on the stiffness of the force gauge.
b. The change in cross specimen area during deformation.
c. The load supported by the copper jacket.
d. Machine stiffness.

In practise the differential stress/strain data was calculated by the computer program DATRED7, and the corrections were applied following a series of calibrations for the specific apparatus used. See Appendix 1 for the full listing and data reduction procedures.

4.4 METHOD USED TO QUANTIFY TWINNING ACTIVITY

In the section "Microstructural Techniques" in Chapter 1, the technique devised to determine the percentage volume twinned domain and the grain size for a particular grain were explained. The author realises that grain size measurements obtained from a two dimensional cut is not necessarily representative of the true grain size of a specimen. However the various techniques published in the literature all involve the use of a large data set (typically >200), which are then used to predict the principal grain size for that specimen. The textural data presented in this thesis involve the reduction of the data set on the basis of grain size, and therefore the data sets involved are much smaller than those for which the published corrections are accurate. This fact together with the range of grain sizes in the specimens analysed by the author and their logical relationship with twinning activity mean that no correction for a two dimensional cut can be applied, and it is suggested that the grain size measurements obtained in this thesis are as accurate as possible using the standard techniques available to the author.

The grain size and twinning activity data outlined above were recorded together with the number of twins and the thickness per twin for each host grain and twin set. This parameter was calculated as :

$$\mu m/twin = MGA/Nt \qquad (4.1)$$

Where MDA is the mean grain diameter and Nt is the number of twins in the twin set.

This value was then stored in a database by the program D.BASE (see Appendix 4.

In addition to the above data, twinning activity for a data set can be quantified by calculating the twinning incidence parameter, It (Spiers, 1981). This is defined as :

$$It = (n/N)*100 \qquad (4.2)$$

Where N is the total number of grains in the data set and n is the number of twinned grains in that data set.

It is a measure of the probability of encountering a twinned grain in a sample batch, and together with the percentage volume twin domain (%Vt) parameter gives a good indication of the importence of twinning in a data set. The It parameter has the advantage that it can be calculated easily, and that it is insensitive to strain, Spiers (1981).

The It parameter can be used to define the twinning field boundary, which is the boundary of the environmental regime wherein twinning is of significant volumetric importance. This is discussed in full below with reference to the specific experimental materials.

4.5 THE TWINNING FIELD BOUNDARY FOR SOLENHOFEN LIMESTONE

Spiers (1981) investigated the e to e/ah texture transition in Solenhofen Limestone. He observed that this texture transition coincided with the disappearence of twinning in experiments above 400°C, and quantified this using the It parameter. Therefore the It values reported by Spiers define the twinning field boundary for Solenhofen Limestone.

The rock samples used in the above textural studies were obtained from experiments performed at Imperial College by Rutter (1974) as part of his investigation into the rheology of Solenhofen Limestone. They were deformed using the Heard apparatus (see Spiers pp 74,78), at conditions of 150 MPa confining pressure and temperatures ranging from 20°C to 500°C, producing 10-15% strain normal to bedding.

Table 4.2 lists the experimental parameters for these tests together with their corresponding It values. These are plotted in temperature/strain rate space in Fig. 4.2, superimposed upon which are the corresponding It values for each experiment which have been contoured. The twinning field boundary has been selected as being represented by the 10% It contour, which reflects the fact that twinned grains do persist outside of the twinning field. However these are of negligible volumetric importance, and many such twins may have been introduced during cooling and depressurization. These twins are typically of two types :

1. Thin, planar twins.
2. Broad, lensoid twins.

Both of these persist to the highest temperatures and lowest strain rates examined. The former are typical offloading, cooling and depressurisation twins, while the latter are syndeformational and indicate that twinning does persist at least to temperatures of 500°C at laboratory strain rates.

The lack of twin boundary migration in these experiments indicates that the disappearance of twinning is the result of a weakening of slip on the r and f slip systems relative to twinning. This is associated with an increase in the homogeneity of deformation (Spiers, 1981).

The twinning field boundary is described in temperature/strain rate space by :

$$T = 33 * \log_{10}(e) + k \qquad (4.3)$$

Where T is the temperature at which the boundary is located for a specific strain rate (e), and k is a constant equal to 565. Spiers (1981).

With reference to Figs. 4.3, 4.5 and 4.6, and Fig. 4.7 and 4.8, the amount of twinning decreases with increasing temperature and decreasing strain rate, see below. This is accompanied by a tendency for the twins to become broader, and in some cases irregular, with increasing temperature and slower strain rates. This is the result of higher temperature and time allowing the twin boundary to overcome lateral constraints, and limited twin boundary migration occurs. Figures 4.7 and 4.8 show a series of micrographs taken from the specimens plotted in Fig. 4.3 showing the two trends described above in more detail.

SAMPLE No.	T°(C)	e(sec)$^{-1}$	P(MPa)	σ(MPa)	It(%)
128	20	$3.0 * 10^{-4}$	150	538.5	76.7
123	20	$4.3 * 10^{-5}$	150	519.0	62.5
315	20	$5.9 * 10^{-7}$	150	504.1	42.7
115	200	$2.7 * 10^{-4}$	150	472.1	71.3
246	200	$3.1 * 10^{-5}$	150	446.9	58.0
124	200	$3.0 * 10^{-7}$	150	437.7	37.7
26	200	$3.0 * 10^{-8}$	150	446.9	22.6
316	300	$3.2 * 10^{-4}$	150	469.8	61.7
34	300	$2.1 * 10^{-5}$	150	442.3	39.3
318	300	$3.0 * 10^{-6}$	150	446.9	23.6
329	300	$5.9 * 10^{-8}$	150	423.9	17.3
117	400	$3.1 * 10^{-4}$	150	413.6	31.1
122	400	$3.1 * 10^{-6}$	150	393.0	8.9
126	500	$3.1 * 10^{-4}$	150	364.4	5.5
230	500	$1.6 * 10^{-5}$	150	347.2	5.2
231	500	$4.2 * 10^{-7}$	150	297.9	5.9
159	500	$1.0 * 10^{-7}$	150	268.1	5.9

TABLE 4.2 Table listing the specimens examined to locate the position of the twinning field boundary for Solenhofen Limestone. T(°C) is temperature, e(sec)$^{-1}$ is the strain rate, P(MPa) is the confining pressure, σ(MPa) is the differential stress at 10% strain, and It(%) is the corresponding twinning incidence parameter. See text for discussion. Data after Rutter (1974).

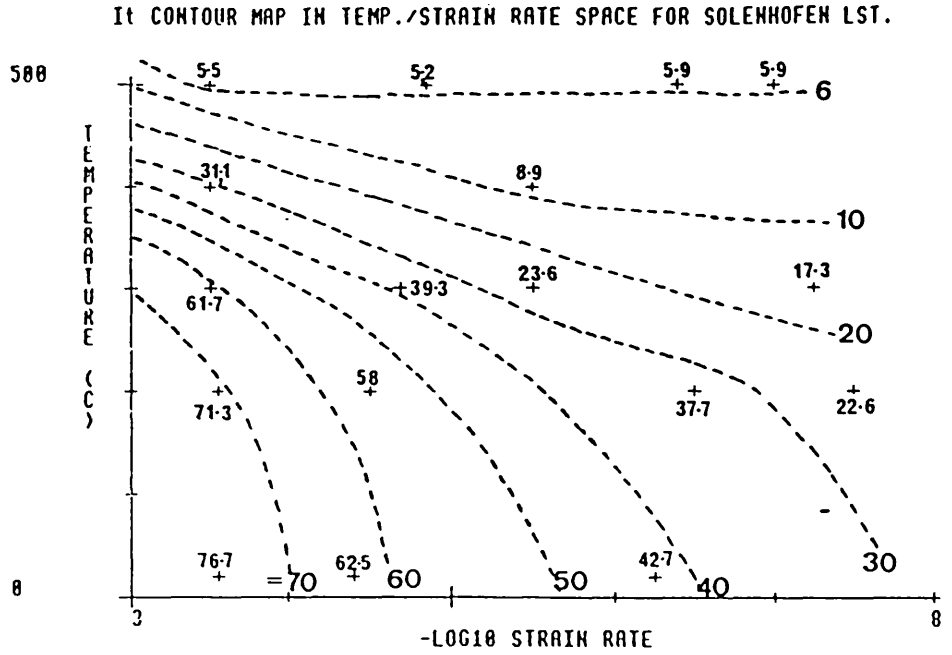


FIGURE 4.3 It contour map in Temperature/Strain Rate space for the series of experiments performed upon Solenhofen Limestone, see Table 4.2 and Spiers (1981). The 10% It contour defines the Twinning Field Boundary.

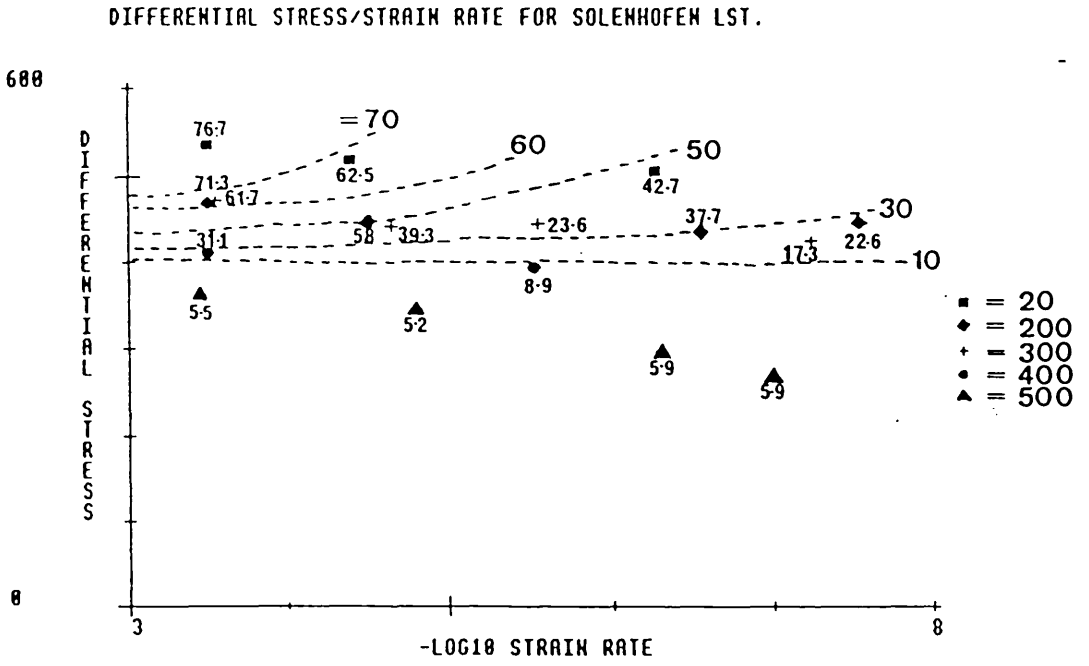


FIGURE 4.4 It contour map in Differential Stress/Strain Rate space for the series of experiments performed upon Solenhofen Lst., with the temperature of the experiments superimposed.

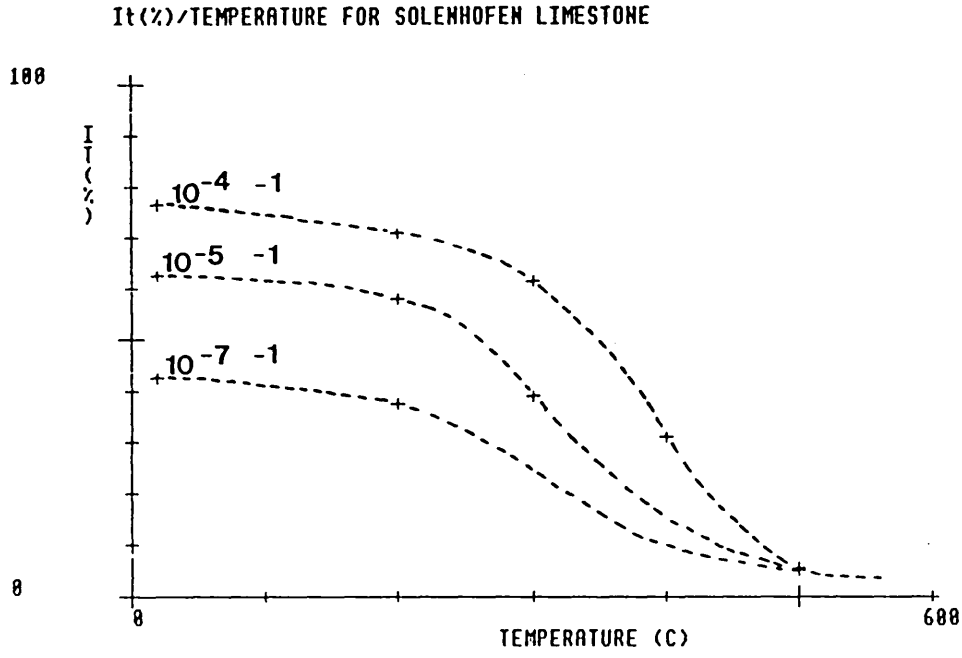


FIGURE 4.5 Iso-Strain Rate sections through Fig. 4.3, demonstrating the decrease in twinning activity as represented by the It parameter with increasing temperature at various Strain Rates. See Table 4.2 for the experimental and textural parameters which correspond to the crosses in this Figure.

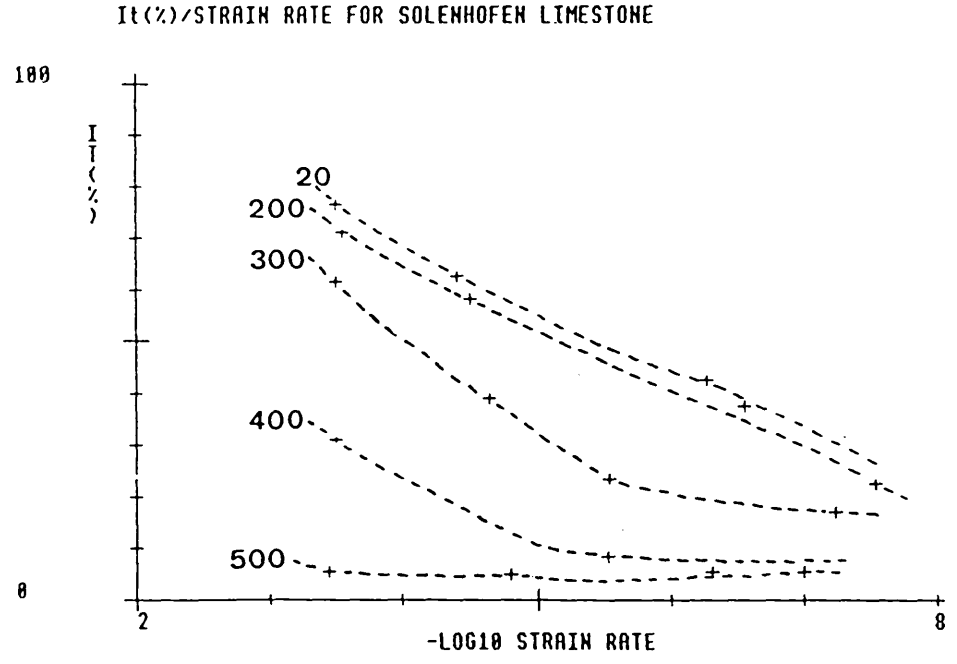


FIGURE 4.6 Iso-Temperature sections through Fig. 4.3, demonstrating the decrease in twinning activity as represented by the It parameter with decreasing strain rate at various Temperatures. See Table 4.2 for the corresponding experimental and textural parameters represented by the crosses.

FIGURE 4.7 Series of photomicrographs of Solenhofen Limestone showing the increase in twinning activity with decreasing temperature.

KEY : (a) - 126, (b) - 117, (c) - 316, (d) - 115 and (e) - 128

The deformational parameters selected for these experiments are given in Table 4.2, and the compression direction is vertical.

(a) In this sample twinning is virtually absent, and a slight grain shape fabric is developed.

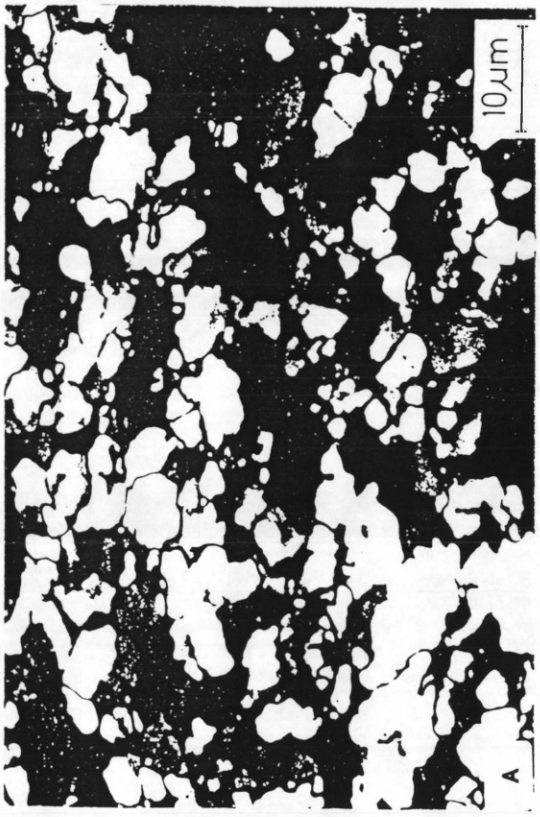
(b) Twinning is more common than in (a) but less so than in the following photomicrographs. The twins that are present are high temperature in character, see text.

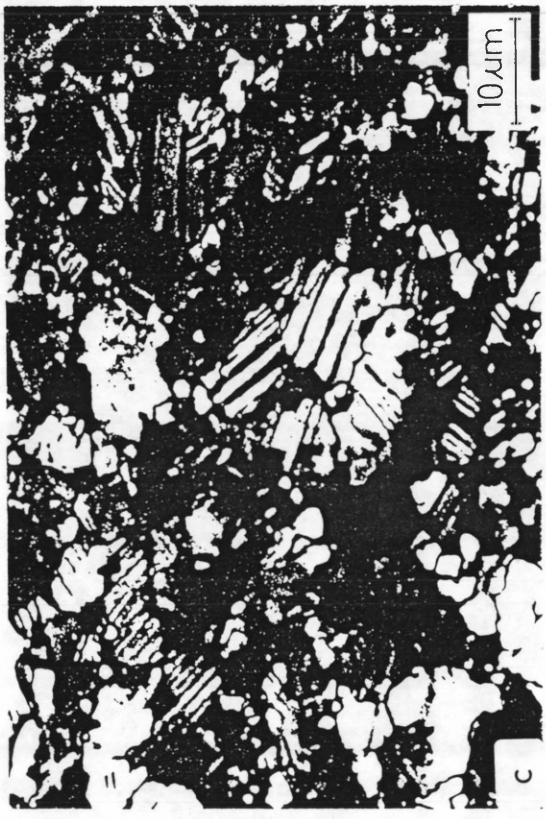
(c) Twinning is more common than in (a) or (b), and the twins are thinner because of the lower temperature of experimentation.

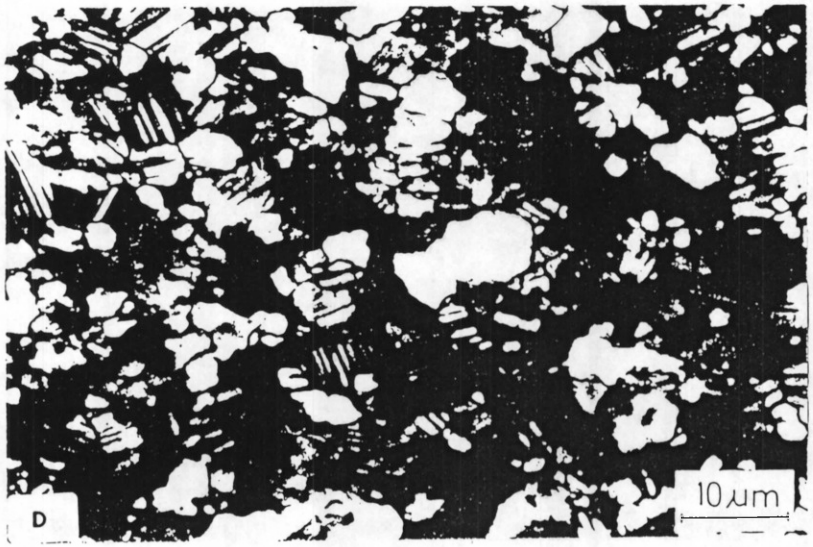
(d) Low temperature twins are the dominant microstructural characteristic.

(e) Twins are thin and parallel sided, and a slight grain flattening fabric is developed.


10 μm
B


10 μm
A


10 μm
C


D
10 µm

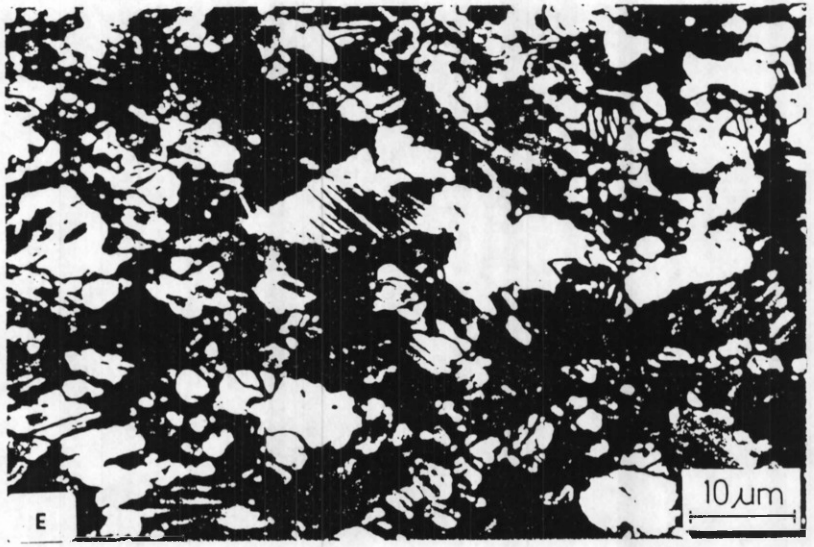

E
10 µm

FIGURE 4.8 Series of photomicrographs of Solenhofen Limestone showing the increase in twinning activity with increasing strain rate.

KEY : (a) - 329, (b) - 318, (c) - 34 and (d) - 316

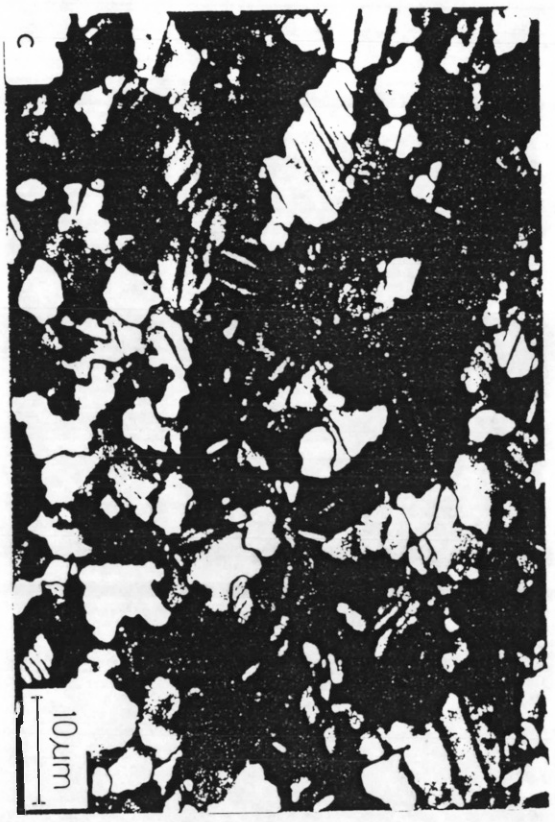
The deformational parameters selected for these experiments are given in Table 4.2, and the compression direction is vertical.

(a) In this sample twinning is virtually absent.

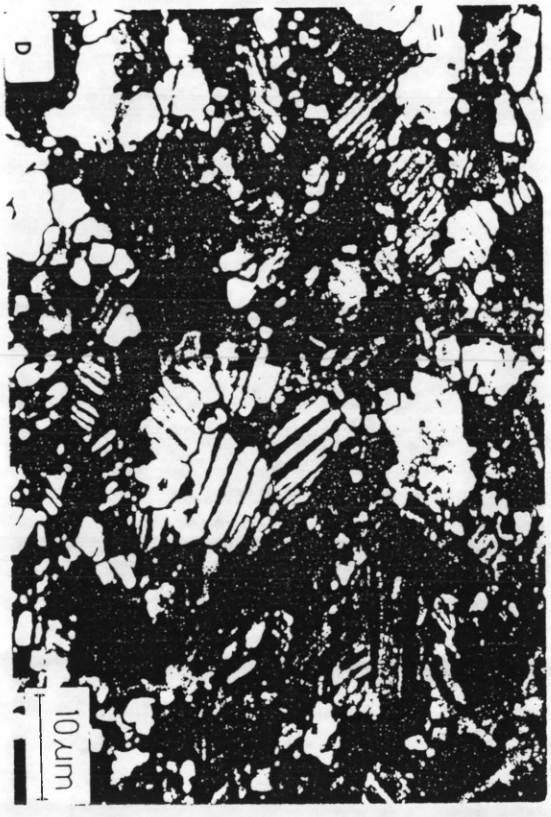
(b) Twinning is more common than in (a) but less so than in the following photomicrographs.

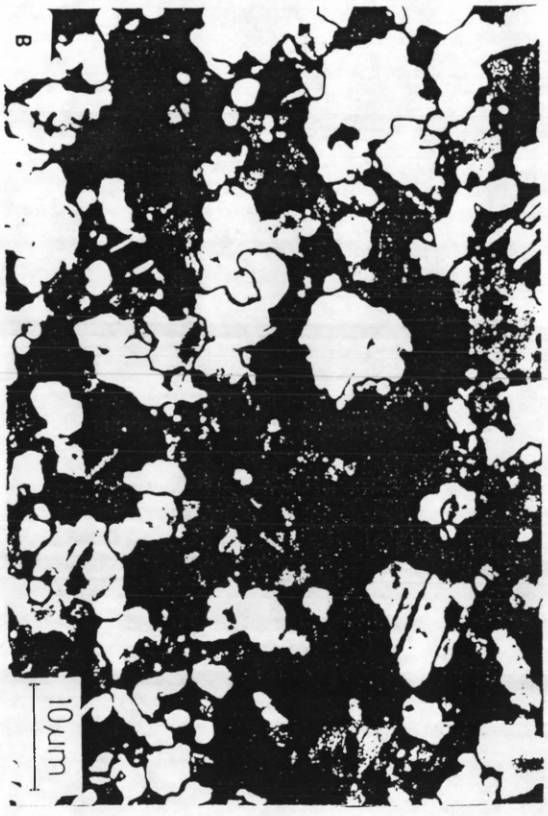
(c) Twinning is fairly common, but perceptibly less important than at faster strain rates, i.e. (d).

(d) In this sample twins are very common, and are generally thin and parallel sided.


C
10μm


A
10μm


D
10μm


B
10μm

Figures 4.5 and 4.6 are constant strain rate and temperature sections, respectively, through Figure 4.3 and demonstrate that the It values decrease with increasing temperature and decreasing strain rate as stated above.

However when these It values are plotted as a function of differential stress it is clear that It is dependent upon the differential stress level. This is shown in Fig. 4.4, in which the same Solenhofen Limestone data are plotted in differential stress/strain rate space. It is clear from this diagram that the It parameter is insensitive to strain rate. Moreover, when the temperatures of the experiments are superimposed upon Fig. 4.4 it is obvious that the It values are also insensitive to temperature.

Therefore twinning incidence is independent of temperature and strain rate, but depends on stress, which leads to the idea that twinning incidence may form the basis of a useful palaeopiezometer.

These characteristics are of obvious significance when extrapolating experimental models to natural ones, which are typically characterised by relatively low temperature and low strain rate.

4.5.1 CONCLUSION

To conclude this section, the twinning field boundary, as defined by an It of approx. 10%, for Solenhofen Limestone (5μm grain size) lies approx. at 400 MPa differential stress. Above this stress level the importance of twinning increases, until at 500 MPa, It values of approx. 50% were observed for strain rates of $3.1 * 10^{-4}/sec^{-1}$.

The It contour map of Fig. 4.4 shows that at lower strain rates twinning activity is characterised by slightly higher stress levels, so that palaeostress levels inferred from It values are likely to be conservative estimates.

4.6 THE LOCATION OF THE TWINNING FIELD BOUNDARY FOR CARRARA MARBLE

4.6.1 INTRODUCTION

It was shown in the preceding section that the twinning field boundary, as defined by an It(%) value of 10%, for Solenhofen Limestone lies at approx. 400MPa. Therefore, because we know that for the exponential flow regime a coarser grain size leads to a lower flow stress (see Chapter 2), the twinning field boundary for Carrara Marble was predicted to lie between 100 and 200MPa.

Hence the experimental conditions were chosen in the first instance on the basis of data previously obtained by Rutter and Rusbridge (1977); Owens and Rutter (1978); Casey et al., (1978) and Spiers (1981), in their investigations into the development of the e-texture in marbles.

The ultimate aim of this study was to accumulate as many data points as possible in temperature/strain rate space, given the constraints of time and experimental limitations. Therefore a confining pressure of 15,000psi (approx. 104MPa) was selected for the bulk of the experiments. A series of experiments were performed over a range of strain rates but each at a constant temperature. When the series the tests at a specific temperature had been completed, the next temperature was selected and the process repeated. It is emphazied that the post deformation procedure involved sectioning the experimental samples as soon as possible after each test, and the preliminary textural observations were used as a basis for the selection of the next set of experimental parameters.

4.6.2 EXPERIMENTS

Table 4.3 lists the experiments performed on Carrara Marble with their corresponding It values and corresponding mean grain sizes. As stated in Chapter 1, a major problem in locating the twinning field boundary in differential stress/grain size space has been the lack of natural rocks of appropriate grain sizes. In an attempt to provide a solution to this problem a method by which the textural data set for each experiment is subdivided on the basis of mean grain size has been used. In practise this was accomplished using the computer program D.BASE, see Appendix 6. The results of this data reduction are presented for each specimen below.

For each thin section 300 hundred grains were analysed, and for the first hundred of these the percentage volume twin domain parameter was also calculated. The experiments are described in the order that they were performed, i.e. all tests run at the same temperature are described together. For the exact experimental conditions employed for each test see Table 4.3. As stated in the introduction of this chapter, the textural and experimental data obtained requires the presentation of a large number of graphs. It was decided in order to preserve continuity in the text that the corresponding graphs are presented at the end of the section detailing the series of experiments performed upon Carrara Marble. The Plates corresponding to the experiments are included in the text.

SAMPLE No.	T(°C)	e(sec)$^{-1}$	P(MPa)	σ(MPa)	e(%)	It(%)	d(μm)
KCM-10	500.0	$4.4 * 10^{-4}$	106.7	269.3	18.3	97.67	126.5
KCM-11	500.9	$8.3 * 10^{-5}$	103.8	243.2	30.1	79.33	144.75
KCM-12	500.5	$1.8 * 10^{-5}$	103.7	183.0	13.2	41.0	151.25
KCM-13	548.0	$4.7 * 10^{-4}$	106.5	234.1	22.1	74.0	147.25
KCM-14	499.9	$4.5 * 10^{-6}$	105.0	175.0	14.2	36.0	155.0
KCM-15	549.7	$8.5 * 10^{-5}$	104.0	185.0	18.0	48.0	140.5
KCM-16	400.8	$4.2 * 10^{-4}$	101.3	279.6	14.4	99.0	151.5
KCM-17	400.5	$8.4 * 10^{-5}$	104.3	263.0	15.0	93.87	128.0
KCM-18	400.4	$3.7 * 10^{-4}$	103.4	273.1	7.1	97.67	182.25
KCM-19	400.3	$1.8 * 10^{-5}$	138.9	214.4	20.3	62.0	186.0
KCM-20	400.0	$5.0 * 10^{-6}$	136.3	190.1	10.1	42.33	159.0
KCM-21	300.1	$2.3 * 10^{-5}$	170.9	203.4	20.4	46.33	165.25
KCM-22	300.3	$5.6 * 10^{-6}$	171.3	191.0	23.1	42.33	164.75
KCM-23	201.0	$5.7 * 10^{-7}$	203.5	91.3	14.8	3.33	154.0
KCM-24	600.3	$5.8 * 10^{-4}$	105.4	151.8	19.5	21.33	152.0
KCM-25	600.5	$8.4 * 10^{-5}$	104.4	125.5	9.1	14.0	155.5
KCM-26	600.1	$2.1 * 10^{-5}$	103.8	99.8	21.8	8.33	147.5
KCM-27	550.2	$1.2 * 10^{-5}$	102.6	170.1	13.4	35.67	158.25

TABLE 4.3 Table listing the experiments performed in the investigation of the twinning field boundary and twinning activity in Carrara Marble. T(°C) is the temperature, e(sec)$^{-1}$ is the strain rate, P(MPa) is the confining pressure, σ(MPa) is the differential stress, e(%) is the strain, It(%) is the twinning incidence parameter and d(μm) is the corresponding mean grain size. See text for discussion.

4.6.2.1 THE 500°C SERIES : KCM-10, 11, 12 and 14

The reduced differential stress/strain data for these experiments are presented in Fig. 4.9. The corresponding It values (see Table 4.3) indicate that these experiments plot well into the twinning field, although the decrease in twinning activity with decresing strain rate is clearly shown by the series of micrographs presented in Plate 4.2. However the average grain size to which these It values correspond shows a considerable variation, and this must be accounted for in any discussion of twinning activity. See below.

Figure 4.10 shows the reduction of the textural data on the basis of grain size. For each specimen, referred to as a, b, c and d, there are three diagrams, referred to as 1, 2 and 3. This notation will be used in every section from here onwards. All plot mean grain size on the horizontal scale and It(%), number of twins, and percentage volume twin domain, repectively, on the vertical axis. The linear regression lines shown in these diagrams are intended to show the trend of the values. The values used to draw the contour maps in Fig. 4.27 and 4.28 are based on the actual values listed in Table 4.3. Additionally the actual data points resulting from the reduction of the data set on the basis of grain size presented in the It/mean grain size diagrams in this and the following sections are used to construct the contour diagrams presented in Fig. 4.31.

The It/mean grain size diagrams in Fig. 4.10 show a consistent trend, with the It values increasing rapidly with increasing grain size. Note that It = 100% indicates that all of the grains observed are twinned. However the relationship is not linear, showing a rapid increase of It throughout the low and mid grain size ranges, and a levelling off of It at the larger grain size intervals. The more complex relationship displayed by KCM-12 can be interpreted as being the result of relatively high activity on the second twin set, which accommodates strain, presumably as a result of more favourably orientated second twin planes in this specimen. The second twin set generally shows more variable development than the first twin set.

The number of twins (diagrams 2) exhibit a consistent trend and the actual values are remarkably similar for all the 500°C experiments, particularly between the last two. The percentage volume twin domain diagrams (diagrams 3) reflect the trends shown in diagrams 1 and 2, and the ratio of number of twins/percentage volume twin domain is approximately 1:1.2. The second twin set reflect the trends of the primary set.

PLATE 4.2 Representative photomicrographs of the 500°C Series of experiments performed upon Carrara Marble.

KEY : (a) - KCM-10, (b) - KCM-11, (c) - KCM-12 and (d) - KCM-14

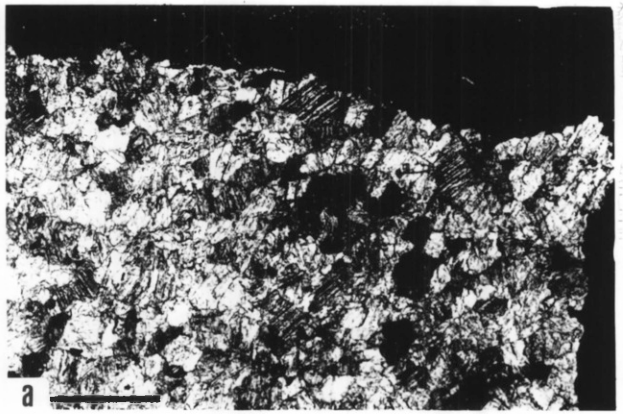
The deformational parameters selected for these experiments are given in Table 4.3.

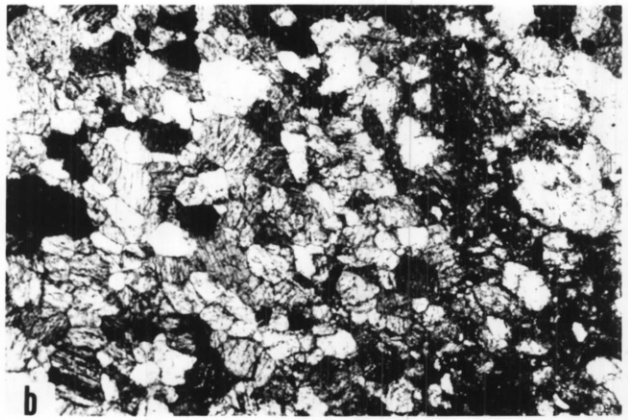
This series of photomicrographs shows the decrease in twinning activity with decreasing strain rate, note also the variation in grain size, both within and between specimens. High temperature character twins are clearly seen in (a) and (b)

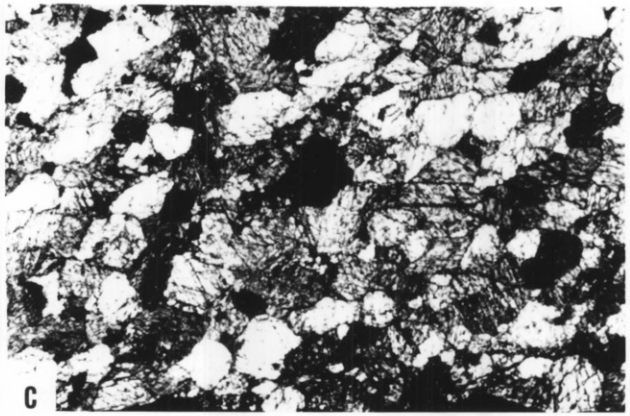
The fault developed in (b) is the result of offloading of the experiment and was excluded from the textural analysis.

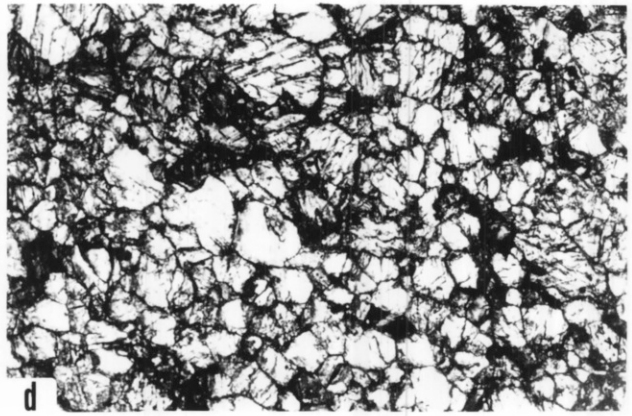
The scale bar for all these photomicrographs is as shown in (a) and represents 200μm.

PLATE 4.2









These diagrams indicate that there is the possibility of using the number, and the percentage volume parameters in the same way that It is being used to indicate the relationship between differential stress and grain size.

Histograms representing the number of data points in each grain size interval used in the previous figures are shown in Fig. 4.11. There are two histograms per specimen, the first represents those grains for which percentage volume twin domain values have been calculated (indicated by the suffix "%" in the heading of these histograms) and the second represents the whole data set, including those for which the volume twin domain have been calculated. For Carrara Marble there are 100 points in the former and 300 in the latter. A weighting of points on the grain size axis of the diagrams presented in Fig. 4.10 according to the number of data points represented by each grain size interval may hide important variations in the data set. Additionally as the data set as a whole displays consistent trends, both for a single sample and when compared with other samples, the degree of confidence in the data is high.

4.6.2.2 THE 550°C SERIES : KCM-13, 15 and 27

The reduced stress/strain data for these experiments are presented in Fig. 4.12. As for the previous series of tests, the It values indicate that we are in the twinning field (see Table 4.3 and Figs. 4.25 to 4.29).

Twinning activity decreases as strain rate decreases, this is clearly shown in the micrographs represented in Plate 4.3, and decreases with increasing temperature (c.f. the It values for the 500°C series). However, the twins characterising the micrographs of Plate 4.3 are clearly broader than those in Plate 4.2. These broader twins are characteristic of high temperature deformation, which permits a degree of twin boundary migration which need not be the result of high strain levels in the same way as at low temperatures. This feature is reflected in the volume of twin domain represented in Fig. 4.13, although it is more marked in KCM-13. The ratio of number/volume of twins is 1:1.5, c f. the same ratio for the 500°C series which was 1:1.2.

The It parameter for KCM-13 shows the same characteristic trend as noticed in the preceding section except that the It parameter increases much more rapidly. This may be a manifestation of "excessive twin activity", see Chapter 2, where the larger grain sizes preferentially exhibit excessive twinning. These trends are reflected by the second twin set.

PLATE 4.3 Representative photomicrographs of the 550°C Series of experiments performed upon Carrara Marble.

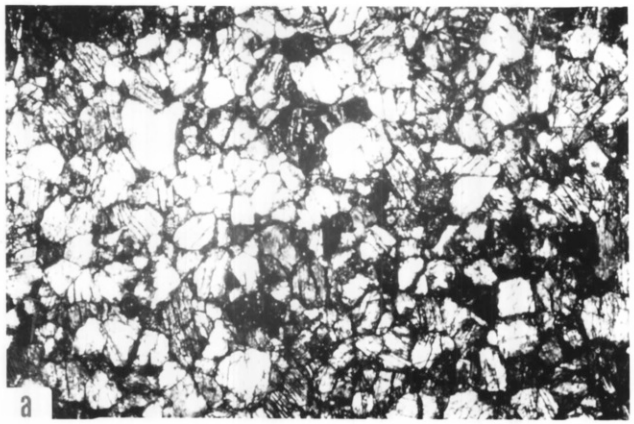
KEY : (a) - KCM-13, (b) - KCM-15 and (c) - KCM-27

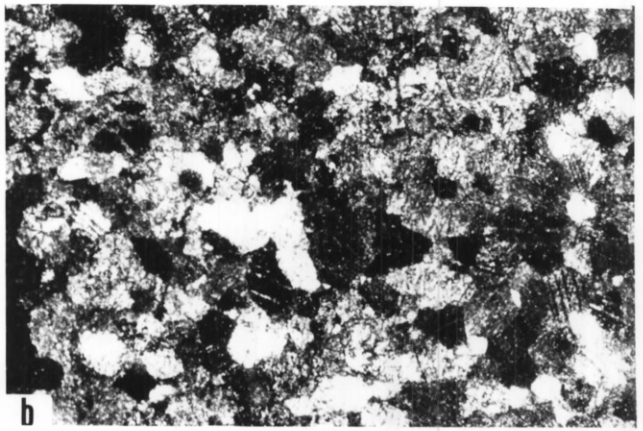
The deformational parameters selected for these experiments are given in Table 4.3.

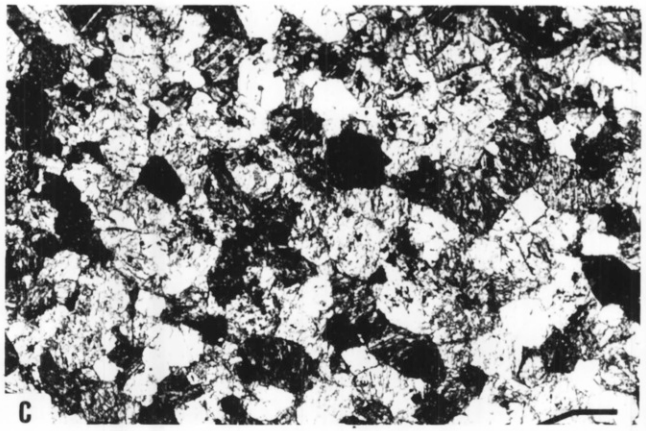
This series of photomicrographs again shows the decrease in twinning activity with decreasing strain rate. The high temperature twins are broader than those shown in Plate 4.2, which demonstrates the temperature control upon the percentage volume twin domain parameter. See text.

The scale bar for all these photomicrographs is as shown in (c) and represents 200μm.

PLATE 4.3







The number of data points in each grain size interval shown in Fig. 4.13 is represented in Fig. 4.14. Although the range of grain sizes for this interval appear to be Gaussian in their distribution, it was found that the data set could not be replotted with smaller grain size intervals.

4.6.2.3 THE 400°C SERIES : KCM-16, 18, 19 and 20

The reduced stress/strain data for these experiments is presented in Fig. 4.15, and the corresponding deformational parameters and It values are shown in Table 4.3. As a result of the lower temperatures relative to the experiments previousely described, the differential stress and the corresponding It parameters are high, e.g. KCM-16 where the It parameter is 99%.

Plate 4.4 shows four micrographs from these experiments, illustrating the dominance of twinning. As in Plates 4.2 and 4.3 the decrease in twinning activity with decreasing strain rate can be seen. A duplicate experiment, KCM-18, was performed on Nimonic II (see Chapter 1) at identical conditions to KCM-16, for purposes of comparison. KCM-18 was terminated as soon as steady state flow was recorded, at a lower percentage strain relative to KCM-16 (see Table 4.3). As a result the differential stress was slightly lower(273.1 as compared to 179.6), as was It (97.67 as compared to 99). This is an extremely good correlation between the two types of machine and suggests there is no obvious machine dependent effect upon the data. A micrograph of KCM-18 is included in Plate 4.4.

When the It values in the reduced data sets are compared there is a close correlation, the slightly depressed values in the smaller grain size intervals in KCM-16 can be explained by the higher activity on the second twin set. Both the number of twins and the percentage of twinned domain show very close correlation between the two specimens (Fig. 4.16).

Figure 4.16 shows the characteristic trend of the It parameter as a function of grain size in the low to medium grain size intervals. The ratio of the twinning number/volume is approx. 1:1 at the higher strain rates, but this ratio increases to 1:1.6, and is even higher for KCM-20. This may be a manifestation of increased confining pressure for the lower strain rate experiments (see Table 4.3), which affects the sample and inhibits any lateral migration on the grain scale, or because the lower strain rates allow some highly stressed twins to grow laterally, or a combination of the two. By comparing the micrographs in Plate 4.4 for KCM-16 and KCM-20 the twins in the latter display a slightly lozenge shape compared to those of the former. In

PLATE 4.4 Representative photomicrographs of the 400°C Series of experiments performed upon Carrara Marble.

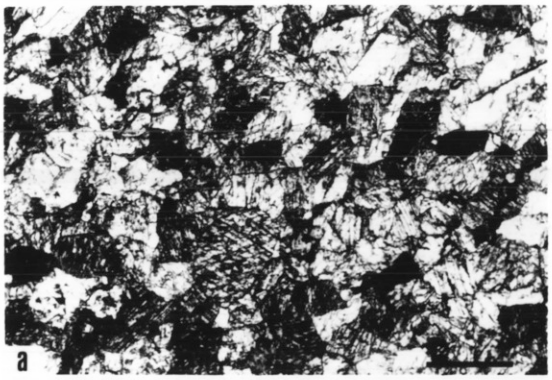
KEY : (a) - KCM-16, (b) - KCM-18, (c) - KCM-17, (d) - KCM-19 and (e) - KCM-20

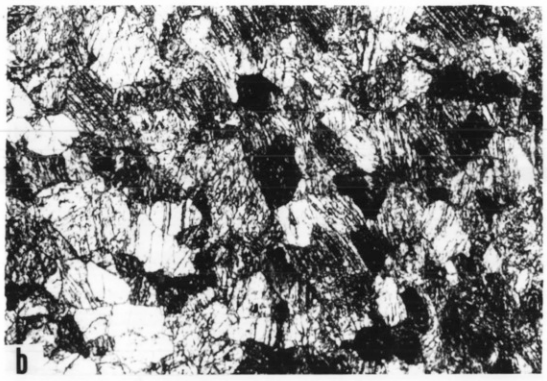
The deformational parameters selected for these experiments are given in Table 4.3.

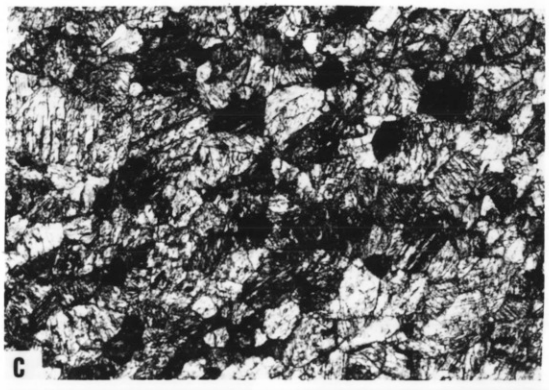
This series of photomicrographs again shows the decrease in twinning activity with decreasing strain rate. Print (b) is the experiment performed on the Nimonic II Apparatus under identical environmental conditions to (a), the textures of (a) and (b) are clearly identical. See text.

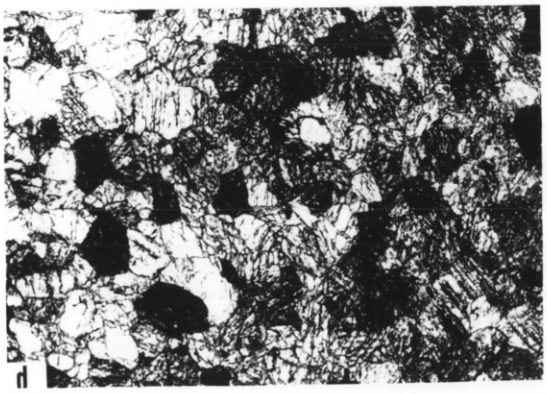
The scale bar for all these photomicrographs is as shown in (a) and represents 200μm.

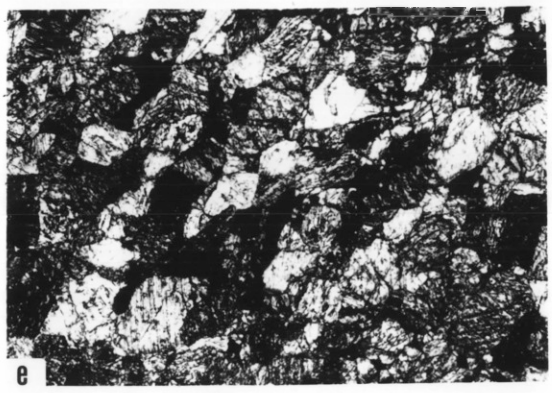
PI ATE 4.4











general these twins are expected to be typically thin, planar features because the temperature at which they were deformed is relatively low and hence twin boundary migration is difficult relative to experiments performed at higher temperatures, see before.

Histograms showing the number of data points used in the construction of the diagrams in Fig. 16 are presented in Fig. 4.17.

4.6.2.4 THE 300°C SERIES : KCM-21 and 22

For these experiments confining pressure was increased to approx. 170MPa in order that higher stress levels may be obtained at lower strain rates, this results in the corresponding It values for these experiments being above 10%, and hence affording more information on twinning activity at low strain rates. See Table 4.3 for the full experimental parameters. The reduced stress/strain data is presented in Fig. 4.18.

The photomicrographs for these samples are presented in Plate 4.5a and b, and it is obvious that their It values are very similar. Note that these twins are typical low temperature twins (c.f. section 4.6.2.3).

With reference to Fig 4.19, the higher grain size intervals of KCM-21 exhibit higher It values. This is interpreted as being due to the excessive twinning activity being preferentially developed in the larger grains of the material when deformed at the higher flow stresses accessible at 300°C. The ratio of twin number/volume also reflects this, being 1:1.8 for KCM-21, while the same ratio is 1:1 for KCM-22.

Histograms showing the number of data points in each grain size interval are presented in Fig. 4.20. The relatively pronounced monomodal distribution in KCM-22 may be a contributary factor explaining the high percentage volume twin domain in this specimen.

4.6.2.5 THE 200°C SERIES : KCM-23

A single experiment was performed at this low temperature at a high confining pressure and low strain rate in order to obtain some information about the nature of the twinning field boundary at strain rates less than 10^{-6}/sec^{-1}. The reduced stress/strain data is presented in Fig. 4.21c, the corresponding photomicrograph is shown in Plate 4.5c and the twinning activity data as a function of grain size is shown in Fig. 4.21a.

PLATE 4.5 Representative photomicrographs of the 300°C and 200°C Series of experiments performed upon Carrara Marble.

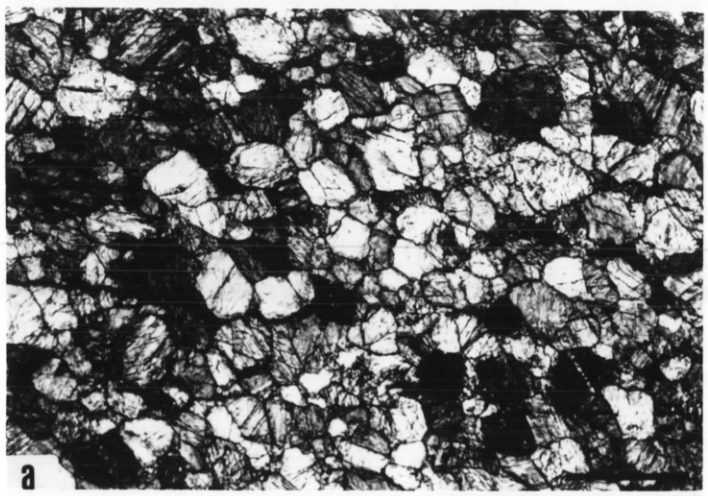
KEY : (a) - KCM-21, (b) - KCM-22 and (c) - KCM-23

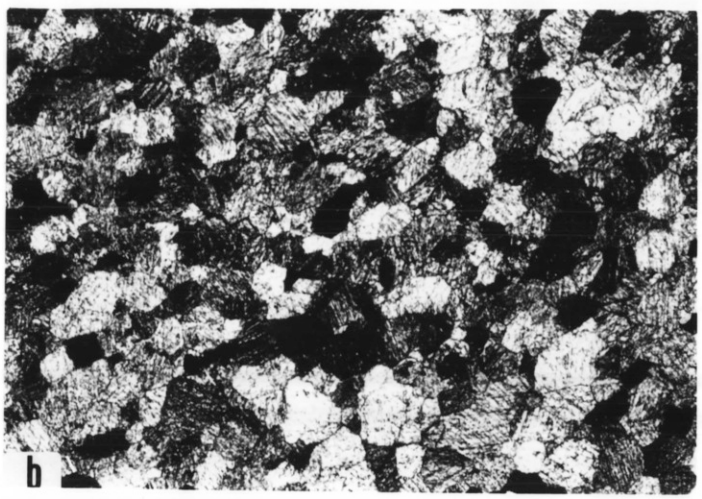
The deformational parameters selected for these experiments are given in Table 4.3.

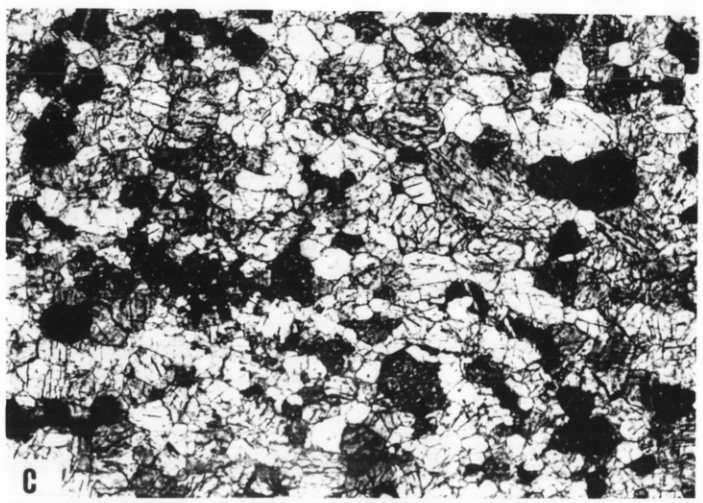
Prints (a) and (b) have been deformed at 300°C, while (c) was deformed at 200°C. The low temperatures of experimentation of these tests is reflected in the character of the twins which are typically low temperature, i.e. thin and planar. See text.

The scale bar for all these photomicrographs is as shown in (a) and represents 200μm.

PLATE 4.5







KCM-23 has a It value of 3.33% and so twinning is of negligible importance. However for grains with a mean diameter in excess of 250μm, It values greater than 20% are recorded, thus considerable information can be gained from specimens with a low bulk It.

Grain size histograms are presented in Fig. 4.21b.

4.6.2.6 THE 600°C SERIES : KCM-24, 25 and 26

This series of experiments was performed in order to gain information from the 90 to 170MPa range of differential stresses, the reduced stress/strain data is presented in Fig. 4.22. Photomicrographs are presented in Plate 4.6. The low It values corresponding to the observed stress levels and the high temperature character of the twins may be clearly seen.

The reduced data set is presented in Fig. 4.23, and the dependence of It upon grain size is graphically illustrated again. The It values in these high temperature experiments show an almost linear relationship with grain size, possibly as a consequence of the more homogeneous deformation on the grain scale which is characteristic of high temperature deformation. Higher temperatures leads to a convergence of the levels of shear stresses required for intracrystalline slip and twinning (Spiers, 1981).

The lozenge shaped, high temperature twins with irrational boundaries are reflected in the ratio of twin number/volume, which is relatively high for these experiments, although this parameter is highly variable. Fig. 4.24 shows the histograms of the number of data points for each grain size interval shown in Fig. 4.23.

4.6.2.7 PREVIOUSLY REPORTED DATA

A preliminary investigation of the location of the twinning field boundary in temperature/strain rate space was carried out by Spiers (1981) on previously deformed samples of Carrara Marble. The experimental parameters are listed in Table 4.4. Although no It values were obtained by Spiers, these specimens have been re-examined by the present author and the results are included in Fig. 4.50.

PLATE 4.6 Representative photomicrographs of the 600°C Series of experiments performed upon Carrara Marble.

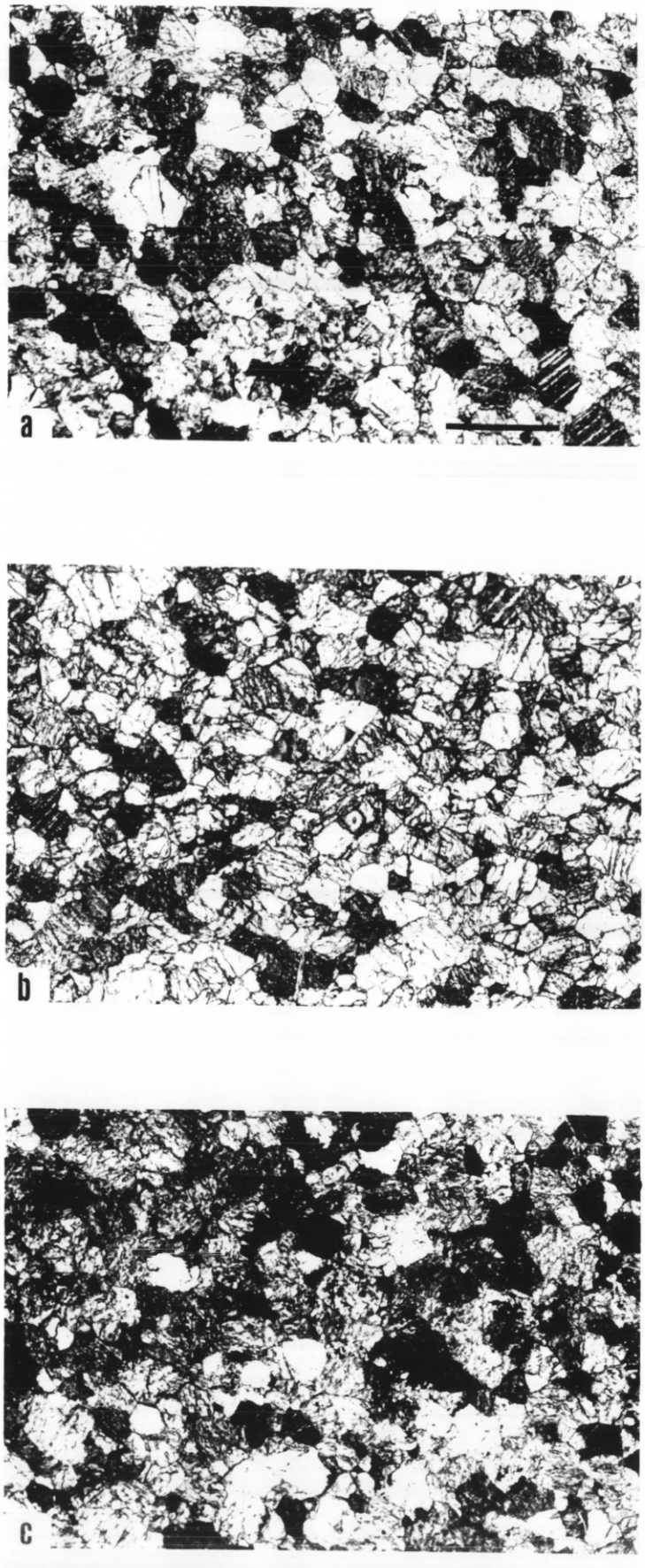
KEY : (a) - KCM-24, (b) - KCM-25 and (c) - KCM-26

The deformational parameters selected for these experiments are given in Table 4.3.

The low It values clearly shown by these experiments correspond to the observed stress levels and the high temperature nature of the twins developed in the larger grains is also clearly illustrated.

The scale bar for all these photomicrographs is as shown in (a) and represents 200μm.

PLATE 4.6



SAMPLE No.	T(°C)	e(sec)$^{-1}$	σ(MPa)	P(MPa)	e(%)	APPARATUS	EXPERIMENTALIST
CH3	750	$5.5 * 10^{-5}$	107.1	100	21	Nimonic	Spiers
NC16	700	$6.0 * 10^{-7}$	55.6	140	25	Nimonic	Shaw
NC12	600	$5.2 * 10^{-5}$	163.9	150	25	Nimonic	Shaw
NC14	600	$5.0 * 10^{-6}$	142.0	150	20	Nimonic	Shaw
NC15	600	$6.5 * 10^{-7}$	123.1	150	25	Nimonic	Shaw
CM141	500	$1.2 * 10^{-7}$	137.5	150	8	Heard	Rutter
CM504 [1]	400	$3.2 * 10^{-5}$	401.0	200	34	Heard	Rutter
CS8	400	$2.9 * 10^{-7}$	248.4	150	47	Heard	Shaw

TABLE 4.4 Table listing the experiments used to locate the approximate position of the twinning field boundary for Carrara Marble. T(°C) is the temperature, e(sec)$^{-1}$ is the strain rate, σ(MPa) is the differential stress, P(MPa) is the confining pressure and e(%) is the strain.
[1] This specimen is reported in Owens and Rutter (1978).
This table is taken from Spiers (1981).

4.6.2.8 CONCLUSIONS

It is clear from Fig. 4.26 that the decrease in twinning activity with increasing temperature and decreasing strain rate is the direct result of the decreasing level of differential stress (see following section). The twinning field boundary is described in temperature/strain rate space by the relation :

$$T = 33.\log_{10}(e) + 832 \qquad (4.3)$$

Where T is the temperature (°C) at which the boundary occurs for a strain rate $e(sec)^{-1}$ (Spiers (1981). This is consistent with the new data of the present author.

To conclude this section the It paramaters shown in the Table 4.3 and which correspond to the experiments performed in this section are shown in temperature/strain rate space in Fig. 4.25. The It data has been contoured and the twinning field boundary which is represented by the 10% It contour. Fig. 4.25 demonstrates that twinning activity decreases with increasing temperature and decreasing strain rate. Figs 4.27 and 4.28 show constant strain rate and temperature sections (respectively) through Fig. 4.25, and demonstrate the decrease in It with decreasing strain rate and increasing temperature.

However, as demonstrated for Solenhofen Limestone, the cause of the temperature and strain rate effects upon twinning activity is the concomitant effect that temperature and strain rate have upon the level of differential stress. Figure 4.26 shows the It parameters in differential stress/strain rate space, with the superposition of the temperature of the experiments, and demonstrates the strain rate and temperature insensitivity of the It parameter, which is even more marked than was observed for Solenhofen Limestone.

The treatment of the textural data, discussed in the preceding text, on the basis of division into classes of different grain size, is presented in Fig. 4.29. This graphically illustrates the effect of grain size upon twinning activity in a way never previously demonstrated. The twin/μm parameter was calculated for the grains in the experiments reported above. It was found that the general trend was of a reduction of the values, i.e. an increase in the probability of encountering a twin in a given grain, for It values between 0% and approx. 20%. For It values above 20% the twins/μm parameter inconsistently averaged between 15 and 25μm.

The It data will be combined with other twinning activity data from the other series of experiments, and fully discussed at the end of this chapter.

4.7 THE LOCATION OF THE TWINNING FIELD BOUNDARY FOR TAIWANESE MARBLE

4.7.1 INTRODUCTION

It has been shown in the preceding sections that the twinning field boundary for Solenhofen Limestone (5μm grain size) lies at approximately 400MPa, and that the same boundary for Carrara Marble (160μm average grain size) lies at approximately 110MPa. Based on these considerations it was predicted that the twinning field boundary for Taiwanese Marble (380μm average grain size) would lie between 0 and 50MPa. Higher experimental temperatures were therefore required, relative to the previous experiments on finer grained rocks. Table 4.5 contains details of the experimental parameters used for each experiment, together with its It value and the corresponding grain size.

The experimental procedure was the same as for Carrara Marble. Once again immediate post deformation sectioning and preliminary textural investigation of the specimens provided the basis for the selection of the experimental parameters for the subsequent tests.

4.7.2 SAMPLE PREPARATION

The specimens were fabricated by coring a 6mm thick polished slab (see section 4.2.3). Specimens were assembled by placing two of these cylinders end to end to obtain an aspect ratio similar to that used in the Carrara Marble experiments discussed in the previous section, prior to insertion in the copper jacket. This type of specimen assembly behaves like a normal single cylinder specimen. A photomicrograph of undeformed Taiwanese Marble is shown in Plate 4.1b.

Obviously, any grain which was truncated at this mid section join was not included in the textural anaysis because the original grain size could not be determined. Plate 4.7b shows an example of the mid section join from KTM-2.

4.7.3 EXPERIMENTS AND TEXTURAL ANALYSIS

Table 4.5 lists all the experiments performed on this material. Grains of Taiwanese Marble have many pre-existing natural twins (see section 4.2.3). However the experimental twins are of the broad, high temperature, type, and it

SAMPLE No.	T(°C)	e(sec)$^{-1}$	P(MPa)	σ(MPa)	e(%)	It(%)	d(μm)
KTM-1	700.2	3.5 * 10^{-4}	104.4	106.4	14.7	51.0	356.75
KTM-2	700.5	5.9 * 10^{-5}	103.7	72.3	7.9	43.0	378.75
KTM-3	702.0	1.8 * 10^{-5}	104.6	52.4	16.8	38.0	377.5
KTM-4	600.1	3.3 * 10^{-4}	103.6	149.2	14.8	62.5	394.5
KTM-5	599.9	6.1 * 10^{-5}	104.3	108.0	13.1	51.0	279.0
KTM-6	600.1	1.6 * 10^{-5}	105.7	80.0	11.6	43.0	375.5
KTM-7	600.0	2.5 * 10^{-6}	102.9	59.0	10.9	39.5	391.0
KTM-8	799.7	6.6 * 10^{-5}	104.4	41.9	9.8	32.0	353.5
KTM-9	800.0	3.4 * 10^{-4}	103.9	74.1	11.5	37.0	302.0
KTM-10	500.5	6.8 * 10^{-5}	103.6	161.4	14.2	62.5	354.75
KTM-11	499.8	2.9 * 10^{-4}	102.7	191.3	9.8	71.0	418.25
KTM-12	499.2	3.4 * 10^{-5}	107.1	120.3	13.1	53.5	396.75
KTM-13	398.0	2.8 * 10^{-4}	104.0	214.2	9.8	72.0	322.75
KTM-14	500.2	3.0 * 10-6	104.4	96.7	11.9	46.0	365.25
KTM-15	599.7	2.8 * 10^{-4}	104.1	140.2	12.8	61.0	409.5
KTM-16	401.6	7.1 * 10^{-5}	104.8	209.1	15.2	72.5	354.5
KTM-17	402.2	1.1 * 10^{-5}	104.6	156.8	9.8	61.5	358.0
KTM-18	400.8	2.8 * 10^{-6}	105.4	121.7	16.2	59.0	455.0

TABLE 4.5 Table listing the experiments performed in the investigation of the twinning field boundary and twinning activity in Taiwanese Marble. T(°C) is the temperature, e(sec)$^{-1}$ is the strain rate, P(MPa) is the confining pressure, σ(MPa) is the differential stress, e(%) is the strain, It(%) is the twinning incidence parameter and d(μm) is the corresponding mean grain size. See text for discussion.

was in practise very easy to distinguish between the two types. The textural data presented in this section is concerned with the experimentally induced twins only. The twinning field boundary is therefore taken at the same It value as for the previous sections, i.e. 10%.

For each thin section 200 grains were analysed and it is for the first hundred of these that the percentage volume twin domain was also calculated. There are two histograms showing the number of data points for each grain size interval for each experiment, one for the twin volume (indicated by the suffix "%" in the heading) and the second for the whole data set. The number of grains analysed is one hundred fewer than for Carrara Marble because the larger grain size for Taiwanese Marble meant that for data sets in excess of this figure a departure from the grain by grain analysis technique used throughout this work would be required. The textural data set was then grouped on the basis of grain size as before.

The experiments are described in the order that they were performed.

4.7.3.1 THE 700°C SERIES : KTM-1, 2 and 3

The reduced differential stress/strain data for these experiments are presented in Fig. 4.30. The corresponding It values in Table 4.5 show that these experiments plot in the twinning field. The effect of decreasing strain rate upon differential stress, and therefore on It, may also be clearly seen. The It parameter is plotted as a function of differential stress/strain rate in Fig. 4.46, and differential stress/grain size in Fig. 4.49.

Plate 4.7 shows a series of photomicrographs, one from each of these experiments, which illustrates the effect of decreasing strain rate upon twinning activity. This figure also demonstrates the effect of grain size, with the larger grains being preferentially twinned, and the broad high temperature twins being restricted to the grain interiors. The photomicrograph of specimen KTM-3 (Plate 4.7c) shows the effect of piston damage to the end of the specimen, which causes localized twin bending and recrystallization. These regions were not included in the textural analysis.

The re-grouping of the textural data set on the basis of grain size is presented in Fig. 4.31 and graphically illustrates the dependence of twinning activity upon grain size. Note that the grain size intervals chosen are arbitrary and constant, i.e. every 100μm for Taiwanese Marble. The upper limit chosen depends upon the number of data points falling within that interval,

PLATE 4.7 Representative photomicrographs of the 700°C Series of experiments performed upon Taiwanese Marble.

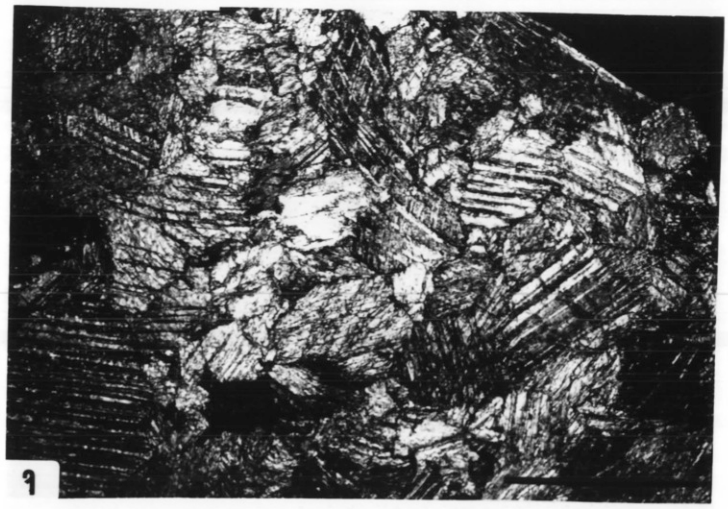
KEY : (a) - KTM-1, (b) - KTM-2 and (c) - KTM-3

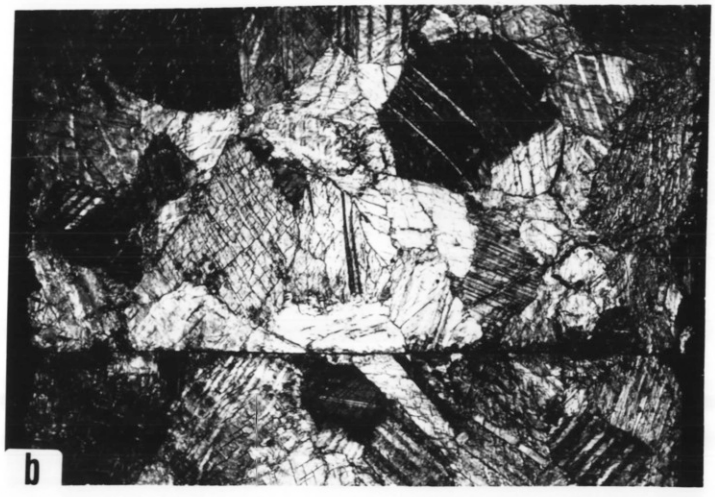
The deformational parameters selected for these experiments are given in Table 4.5.

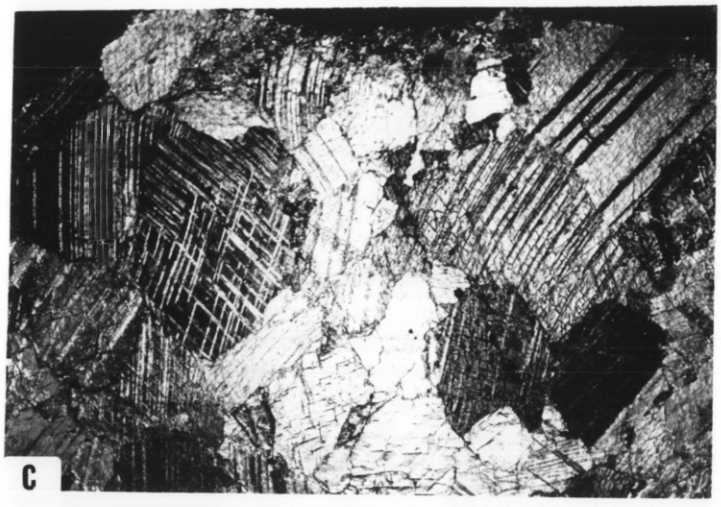
The decrease in twinning activity with decreasing strain rate is clearly shown, as is the difference between the high temperature twins (broad with irrational twin boundaries) and the low temperature twins (thin and planar). Constriction of the high temperature twins by the grain boundaries is visible in (c).

The scale bar for all these photomicrographs is as shown in (a) and represents 1000μm.

PLATE 4.7







and the requirement for a reasonable number of data points from within the upper range of grain sizes. Typically if the number of data points (i.e grains) within a grain size interval was below ten, then this subset was combined with adjacent grain size interval subsets. Generally, for Taiwanese Marble, all the data points above 700μm were summed, as one class. There remains a general lack of data points for the 700-900μm range.

The It diagrams (diagrams 1 of Fig. 4.31) show a near linear relationship, although the characteristic trend of rapidly increasing It values in the low to mid grain size intervals, with a levelling off of the It parameter for the larger grain sizes as observed for Carrara Marble was also observed. Twinning activity for the second twin set shows a less marked increase with grain size, however for those specimens deformed at the higher stress levels, i.e KTM-1, the two twin sets become similar in their activity. This is represented on Fig. 4.31 by the linear regression lines becoming sub parallel. Thus when It values for the first twin set approach 100%, the second twin set becomes increasingly active, with the higher grain size intervals exhibiting excessive twin activity. As a result the second twin set becomes able to accommodate strain in a manner identical to the first twin set.

The ratio of twin number/volume is markedly different from that observed for Carrara Marble, with ratios of 1:3 for KTM-2 and KTM-3, and 1:2.5 for KTM-1. This is a reflection of the higher temperature of these experiments favouring lateral twin boundary migration.

Histograms showing the number of data points for each of the grain size intervals in each of the experiments described above are presented in Fig. 4.32. This material shows an essentually even spread of grain sizes, which makes it of great use for the aims of this thesis.

4.7.3.2 THE 600°C SERIES : KTM-4, 5, 6, 7 and 15

The reduced differential stress/strain data for this series of experiments is shown in Fig. 4.33, and the corresponding deformational parameters and It parameters are shown in Table 4.5. These experiments were performed at lower temperatures, relative to the previous experiments, and hence the differential stress and the corresponding It values are higher than for the 700°C series described in the previous section. Note that the It data for KTM-5 are lower than that for KTM-2. This is explained by the lower mean grain size in the former (279μm) relative to the latter (378.75μm). This clearly demonstrates the effect of grain size upon twinning activity.

Plate 4.8 shows a representative micrograph from each of these experiments, and demonstrates the decrease in twinning activity associated with decreasing strain rate. In addition to the series of experiments performed on the Nimonic I apparatus, a duplicate experiment, KTM-15, was performed on the Nimonic II apparatus (see Chapter 1) at identical experimental conditions to KTM-4. In order to obtain an additional data point in differential stress/grain size space, KTM-15 was terminated at the onset of steady state flow. Therefore a lower percentage strain (12.8 relative to 14.8) and a marginally lower differential stress (140.2 relative to 149.2) results. The corresponding It values reflect this variation in differential stress (61.0 relative to 62.5). This represents an excellent correlation between the two machines, and as stated in section 4.6.2.3, suggests that there is no obvious machine dependence in the data. A micrograph of KTM-15 is included in Plate 4.8 for comparison with KTM-4.

Figure 4.34 presents the textural data for these experiments, plotted as a function of grain size. Note that the data from KTM-4 and KTM-15 is practically identical (see above discussion). The It values, number of twins and percentage volume twin domain for this series of tests shows a consistent reduction in the twinning activity with decreasing strain rate. The characteristic trend in the It values observed in the previous experimental data sets is also observed in all of the experiments presented in this section. The ratio of twin number/volume is typically between 1:2 for the higher strain rates and 1:1.3 for the lower strain rates. This reflects the development of thinner twins relative to those formed in the previous, higher temperature experimental series.

The number of data points represented in each grain size interval for the above discussion is shown in the histograms presented in Fig. 4.35. The range of grain sizes is almost identical to those of the preceding section.

4.7.3.3 THE 800°C SERIES : KTM-8 and 9

Two experiments were performed at 800°C in order to obtain information for differential stress in the range 30 to 80MPa. Figure 4.36 shows the differential stress/strain data for these experiments. The It values, see Table 4.5, show that despite the relatively low stress levels these experiments plot within the twinning field.

The high temperature twins are clearly shown, preferentially developed in the larger grains in the photomicrographs from these experiments presented

PLATE 4.8 Representative photomicrographs of the 600°C Series of experiments performed upon Taiwanese Marble.

KEY : (a) - KTM-4, (b) - KTM-15, (c) - KTM-5, (d) - KTM-6 and (e) - KTM-7

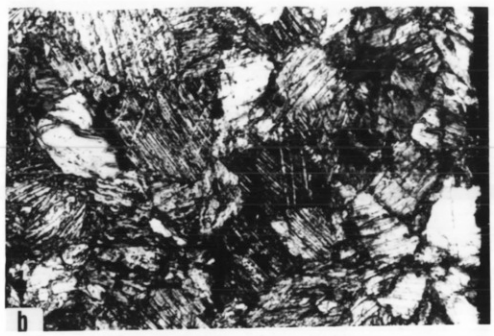
The deformational parameters selected for these experiments are given in Table 4.5.

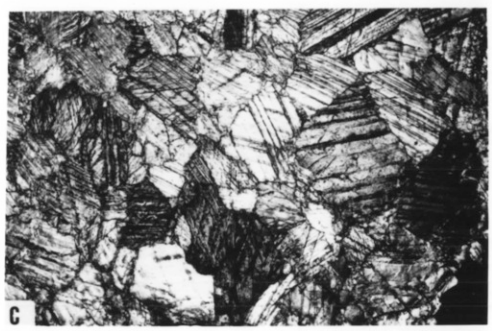
Print (b) is a duplicate experiment performed on Nimonic II under identical experimental conditions to (a). The decrease in twinning activity with decreasing strain rate and the high temperature character of the twins is clearly shown.

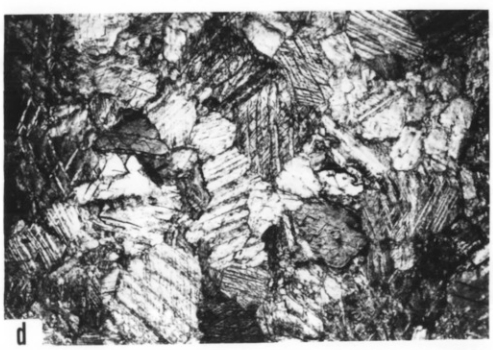
The scale bar for all these photomicrographs is as shown in (a) and represents 1000μm.

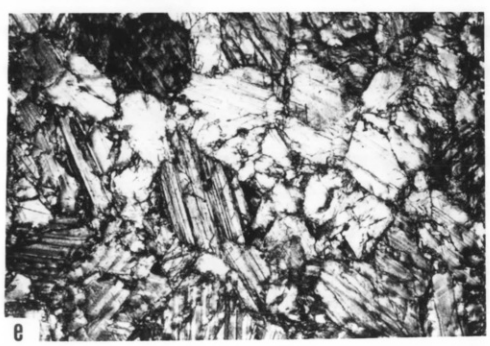
PLATE 4.8


a


b


c


d


e

in Plate 4.9. The presence of high temperature twins is emphazied by the twin number/volume ratio, which is greater than 1:1.6, see Fig. 4.37. Twinning activity as represented by the It parameter shows the same consistent trends as a function of grain size as reported for the previous experiments. The second twin set is poorly developed, and occurs in the larger grain sizes only.

Histograms showing the number of data points for each grain size interval used in plotting the above diagrams are presented in Fig. 4.38. These show that the data set for KTM-8 has a bias towards the lower grain size intervals, but this does not have an important effect upon the mean grain size (see Table 4.5). The considerable variation in the grain size distribution for this material can be seen by comparing KTM-8 and KTM-9 in Fig. 4.38.

4.7.3.4 THE 500°C SERIES : KTM-10, 11, 12 and 14

The reduced differential stress/strain data for this series of experiments are shown in Fig. 4.39, and the detailed experimental parameters, It parameters and mean grain size are shown in Table 4.5. These data show that these experiments plot well into the twinning field with It values greater than 45%, c.f. Fig. 4.40(1) with 4.37(1). Representative photomicrographs are presented in Plate 4.10, and these graphically illustrate the decrease in twinning activity associated with decreasing strain rate.

Figure 4.40 shows the textural data reduced on the basis of grain size from these experiments. A feature of these diagrams is the increased prominence of the second twin set with increased differential stress levels. Usually the second twin set is first recorded at It values of approx. 40%, beyond which it shows poor development and defines a shallow slope. As the It values for the first twin set approach 100% the second twin set shows increased prominence, until it defines a slope typical of that of the first twin set. This is interpreted in terms of the preferential occurrence of excessive twin activity in the larger grain sizes for the second twin set, which becomes more prominent when twinning on the first twin set has been initiated for the majority of grains, i.e. It approaches 100%.

The ratio of twin number/volume is in excess of 1:1.5 for all of the experiments reported in this section, although there is variability between individual specimens. Histograms showing the number of data points in the grain size intervals for the diagrams discussed above are presented in Fig. 4.41.

PLATE 4.9 Representative photomicrographs of the 800°C Series of experiments performed upon Taiwanese Marble.

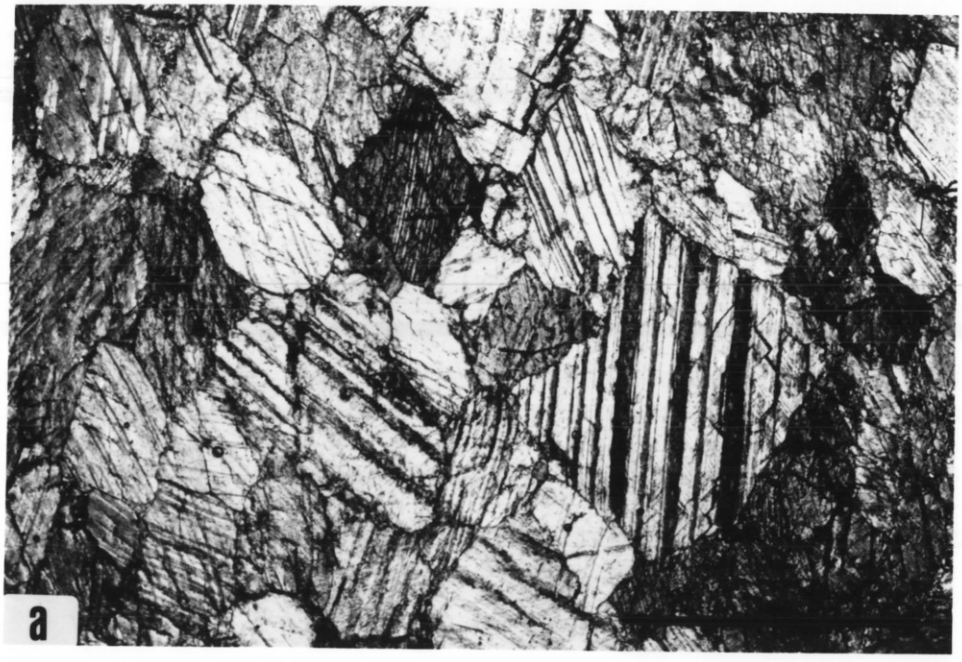
KEY : (a) - KTM-9 and (b) - KTM-8

The deformational parameters selected for these experiments are given in Table 4.5.

These photomicrographs demonstrate the high temperature character of the twins that have developed under these relatively high experimental temperatures. The twins are preferentially developed in the larger grains, and the decrease in twinning activity with decreasing strain rate is again shown.

The scale bar for all these photomicrographs is as shown in (a) and represents 1000μm.

PLATE 4.9



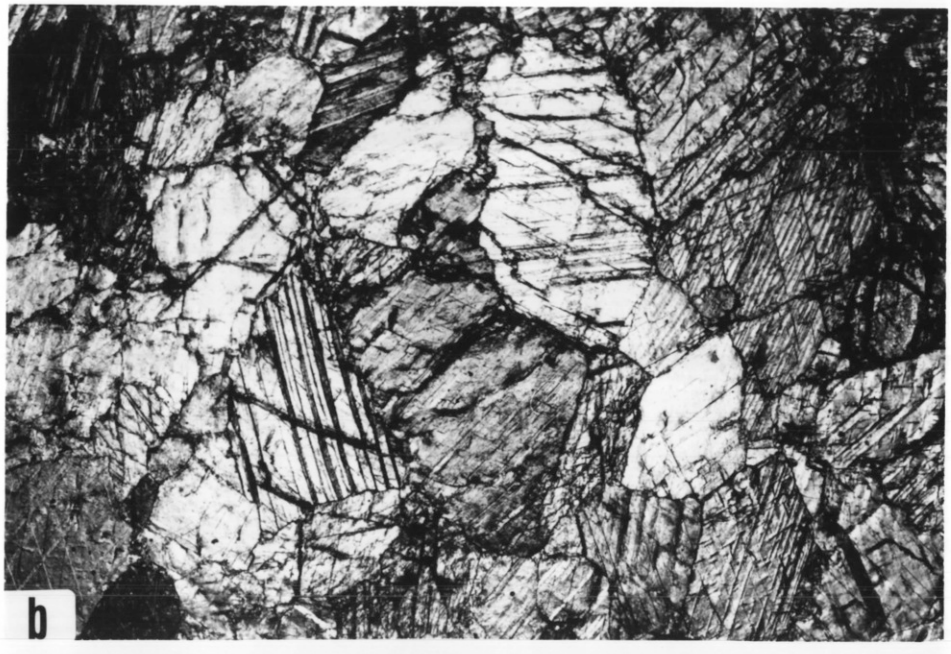


PLATE 4.10 Representative photomicrographs of the 500°C Series of experiments performed upon Taiwanese Marble.

KEY : (a) - KTM-10, (b) - KTM-11, (c) - KTM-12 and (d) - KTM-14

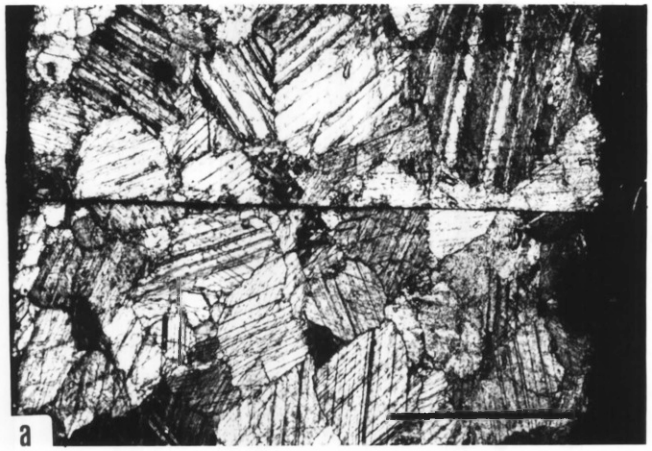
The deformational parameters selected for these experiments are given in Table 4.5.

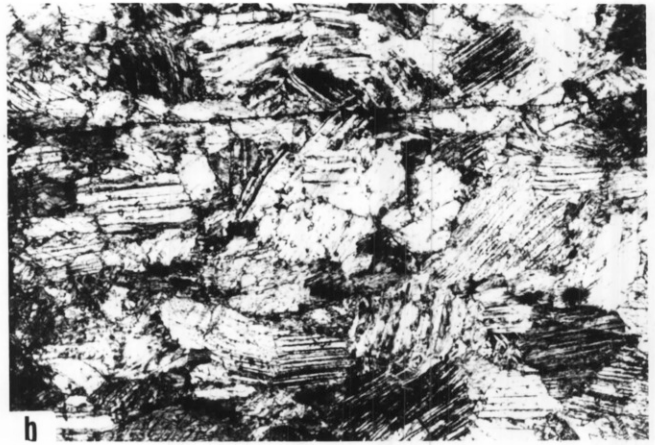
These photomicrographs exhibit higher twinning incidence values than those of the previous plates for Taiwanese Marble which results from the lower temperature of experimentation for the 500°C samples. This is reflected also in the relatively low temperature character of the twins developed in these tests.

The twins are preferentially developed in the larger grains, and the decrease in twinning activity with decreasing strain rate is clearly shown.

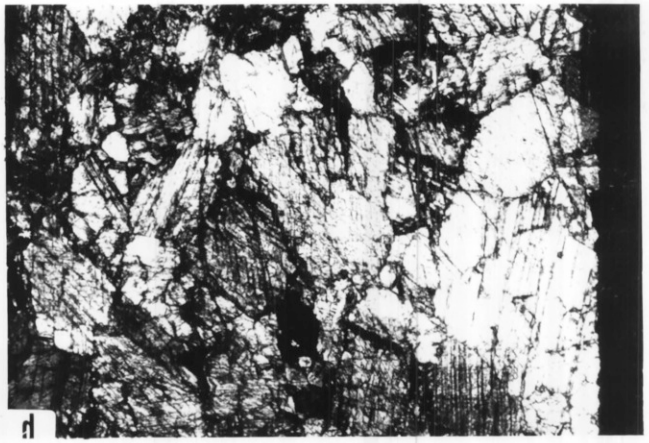
The scale bar for all these photomicrographs is as shown in (a) and represents 1000μm.

PLATE 4.10









4.7.3.5 THE 400°C SERIES : KTM-13, 16, 17 and 18

The differential stress/strain data for these experiments is presented in Fig. 4.42, and details of the experimental parameters and textural data are given in Table 4.5. These samples all lie above the 55% It contour in the twinning field, see Fig. 4.45.

Plate 4.11 presents four photomicrographs representing the experiments performed in this series. These illustrate the dependence of twinning activity upon differential stress level, as produced by varying strain rate. The textural data presented in Fig. 4.43 shows the variation in twinning activity indicated by the photomicrographs in the previous figure, and also demonstrates the effect of grain size on the twinning activity within a single sample. As discussed in the preceding section, the second twin set shows increasing prominence with increased levels of differential stress. The ratio of twin number/volume is consistently high, although these ratios do decrease with decreasing strain rate. This is in accordance with the decrease in twinning activity associated with relatively low experimental temperatures.

Histograms showing the number of grains analysed in each of the grain size intervals for the diagrams presented in Fig. 4.43 are shown in Fig. 4.44.

4.7.3.6 CONCLUSIONS

To conclude this section the It values obtained from the textural analysis of the Taiwanese Marble as presented in the preceding sections are plotted together in temperature/strain rate space in Fig. 4.45. The crosses are centred on their exact coordinates of the experiments, see Table 4.5, and the corresponding It values are contoured to show the position of the twinning field boundary, which is taken as the 10% It contour. As was discussed for Solenhofen Limestone and Carrara Marble in the preceding sections, twinning activity decreases with increasing temperature and decreasing strain rate. This is demonstrated by Figs. 4.47 and 4.48, which represent constant strain rate and temperature sections, respectively, through Fig. 4.45.

Figure 4.46 shows a plot of all the Taiwanese Marble experiments in differential stress/strain rate space, and clearly demonstrates that the effects of temperature and strain rate upon twinning activity result from the concommitant effect that these parameters have upon the level of differential stress. As discussed for the previous data, the It contours in Fig. 4.46 show

PLATE 4.11 Representative photomicrographs of the 400°C Series of experiments performed upon Taiwanese Marble.

KEY : (a) - KTM-13, (b) - KTM-16, (c) - KTM-17 and (d) - KTM-18

The deformational parameters selected for these experiments are given in Table 4.5.

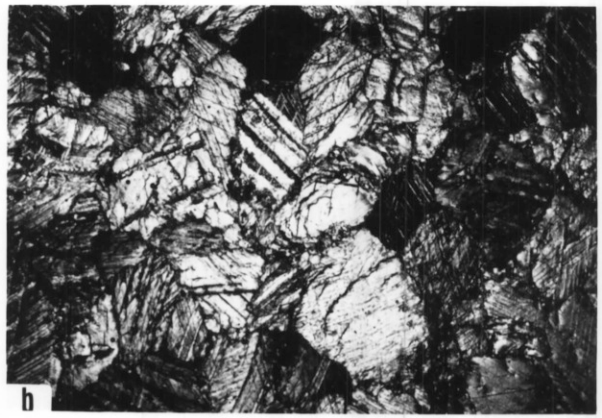
Both the decrease in twinning activity with decreasing strain rate and the relatively low temperature twins are illustrated. C f. the previous plates in this chapter and those of Chapters 6 and 7.

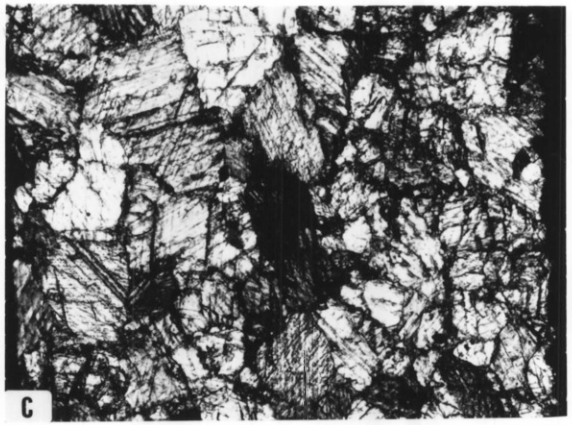
The twinning activity characteristic of the larger grains sizes in these photomicrographs is higher than that of the smaller grain size intervals.

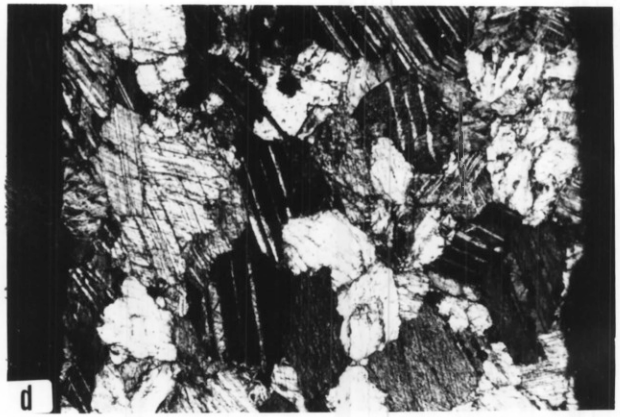
The scale bar for all these photomicrographs is as shown in (a) and represents 1000μm.

PLATE 4.11









that twinning activity is a function of differential stress, and is insensitive to strain rate and temperature.

The reduction of the textural data for Taiwanese Marble discussed in the above text is presented in Fig. 4.49, and illustrates the effect of grain size upon twinning activity. As was briefly discussed in the previous section the twins/μm parameter shows a wide variation in values when It values exceed the 20% It interval. The exact position of the twinning field boundary for the mean grain size was obtained by extrapolating this data to the the mean grain size on Fig. 4.49. Thus the twinning field boundary for a grain size of 380μm represents a differential stress level of approx. 10MPa.

4.8 DISCUSSION AND CONCLUSIONS

The rheology of Carrara Marble and Taiwanese Marble as shown by their differential stress/strain curves, modes of deformation and microstructures are comparable with that of other workers for calcitic materials for similar experimental conditions.

The twins/μm was found to be unsuitable for all but a very general indication of the position of the twinning field boundary. This results from the complex relation between the two competing values used in these calculations, i.e. the twinning data used in this calculation , and the grain diameter. However the other twinning activity data show a consistent trend for individual specimens, with an increase in the twinning activity with increasing grain size, and it is suggested that the reduction of the full data set on the basis of grain size is an extremely useful tool in order to provide a check on the data. In addition to which both the number of twins and the percentage volume twin domain can be used to indicate the approximate position of the twinning field boundary. However the development of twin boundary migration as a result of high experimental temperatures means that the ratio of number of twins/volume of twin ratio is dependent upon temperature, Fig. 4.50. The field data presented in Chapters 6 and 7 show that the ratio of number of twins/volume of twin domain is consistently 1:1 for low temperature, natural twins, and that these parameters are logically related to the It parameter in the manner shown on Fig. 7.9.

It has been shown in the preceding sections that twinning activity is a function of differential stress and grain size. The twinning field boundary, as defined by the 10% It contour interval, lies at 400MPa for Solenhofen Limestone (5μm grain size), 110MPa for Carrara Marble (160μm grain size), and 10Mpa for

Taiwanese Marble (380μm grain size). In addition to this data, twinning persists in Yule Marble (400μm grain size) to experimental temperatures of 800°C for labratory strain rates (Griggs et al., 1960; and Heard and Raleigh, 1972, see Chapter 2). This agrees well with the data presented in section 4.7 for Taiwanese Marble. Furthermore, the limited experimental data available for Courrendlin Limestone (1-2μm grain size) shows that twinning is absent at 300°C, i.e. twinning disappears at higher differential stress levels than for Solenhofen Limestone. Schmid (1982a) reported that twinning in experimentally deformed oolitic limestone showed that twinning is more difficult for the finer grain size fraction of the matrix. To conclude, all data from previously deformed experimental data agrees extremely well with the data presented here.

The insensitivity of the twinning activity to both temperature and strain rate is of great significance when extrapolating the twinning field boundary to geologically realistic temperatures and strain rates. The temperature and strain rate insensitivity of the twinning activity data is very similar for the three rock types studied. The data for Taiwanese Marble does not show the sharp intercept on the respective temperature and strain rate axis as occurs for the other materials examined. This is a result of the twinning activity for Taiwanese Marble being above the twinning field boundary because of the relatively large grain size of this material.

Figure 4.51 shows the It data obtained from the experiments discussed in this chapter, plotted in differential stress/-log grain size space. The crosses represent the actual It values presented in the previous sections, and the reader is refered to the It(%)/grain size diagrams for these values. The It values have been contoured, and this diagram shows the differential stress and grain size dependence of twinning activity. Therefore it is proposed that this diagram forms the basis of a reliable palaeopiezometric technique, whereby the It parameter can be calculated for a data set, and knowing the grain size the stress level represented by this level of twinning activity can be obtained.

The calcite twinning palaeopiezometric technique formulated in this chapter has been used to obtain differential stress levels from two of the principal thrust/nappe complexes from the north-western Spanish Cantabrian zone. The results of this extrapolation and application of the experimental models are presented in Chapters six and seven.

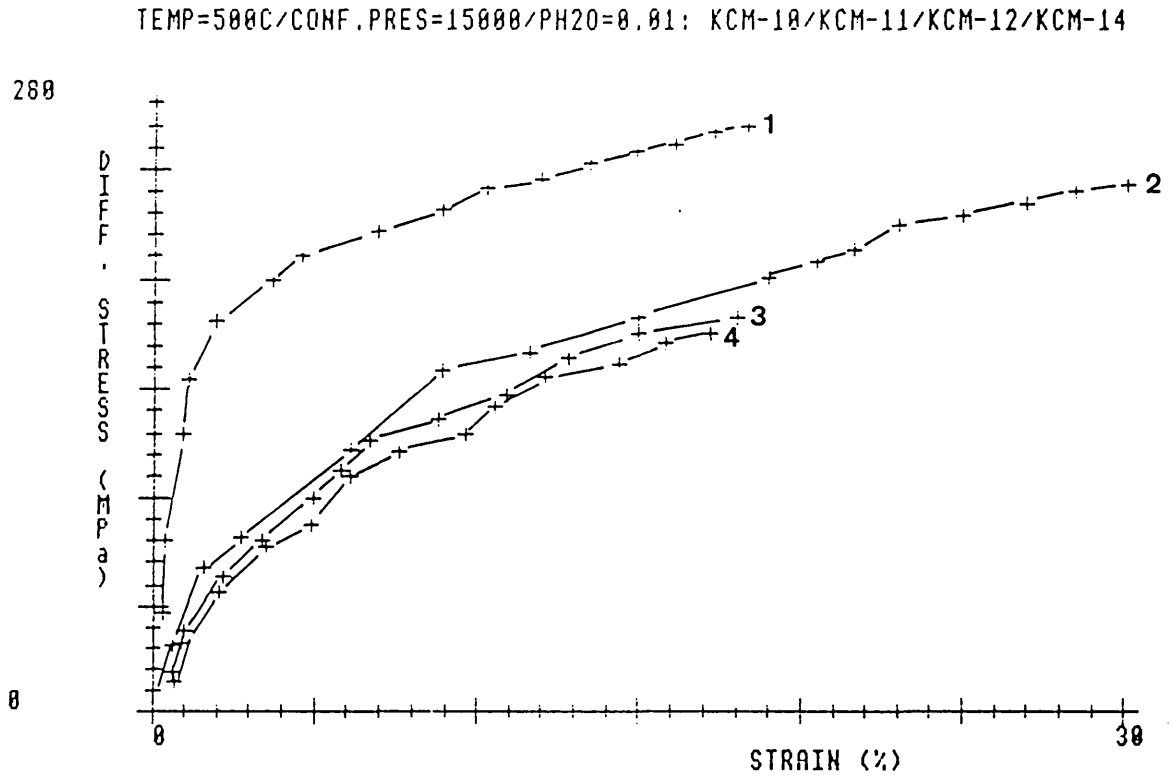


FIGURE 4.9 Stress/strain curves for the 500°C series of experiments performed upon Carrara Marble, see section 4.6.2.1. 1 = KCM-10, 2 = KCM-11, 3 = KCM-12 and 4 = KCM-14.

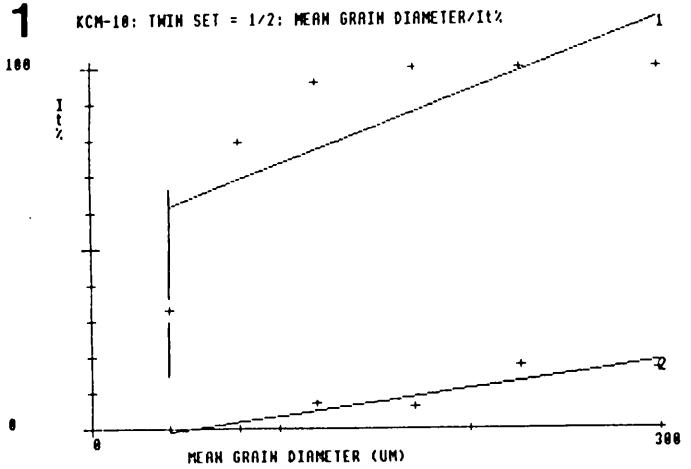
FIGURE 4.10 Textural data for Carrara Marble deformed at 500°C.

This series of diagrams present the twinning activity data determined for this series of experiments plotted as a function of grain size. There are three diagrams, plotting It, number of twins, and percentage volume twin domain (1, 2 and 3 respectively) for each each of the four experiments (a, ,b, c and d) performed at this temperature on this material.

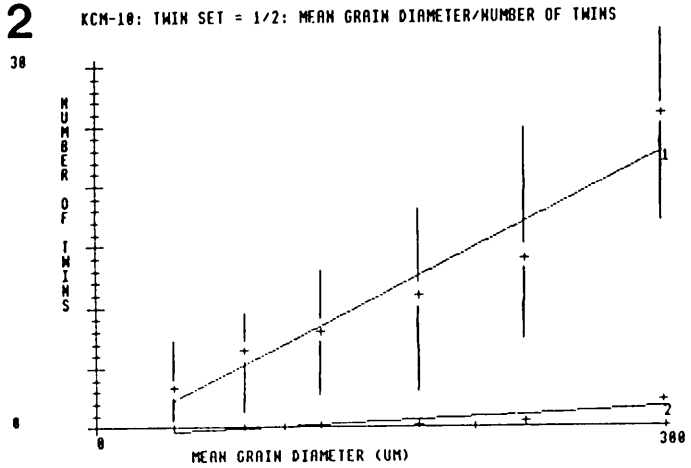
For each sample two twin sets have been analysed, the primary, or principal, twin set and the secondary twin set (1 and 2 respectively). The range bars shown for the relevant groups represent the full range of the values determined for each grain size interval. The individual experiments are identified by their respective headings.

See text for discussion.

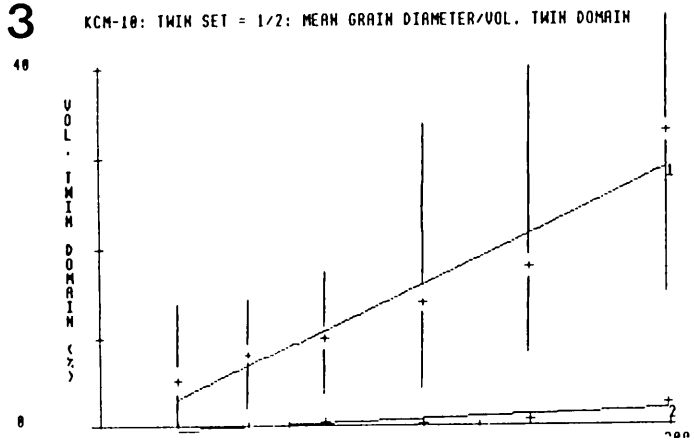
a 1


KCM-10: TWIN SET = 1/2: MEAN GRAIN DIAMETER/It%
100
0
It%
0
300
MEAN GRAIN DIAMETER (UM)
1
2

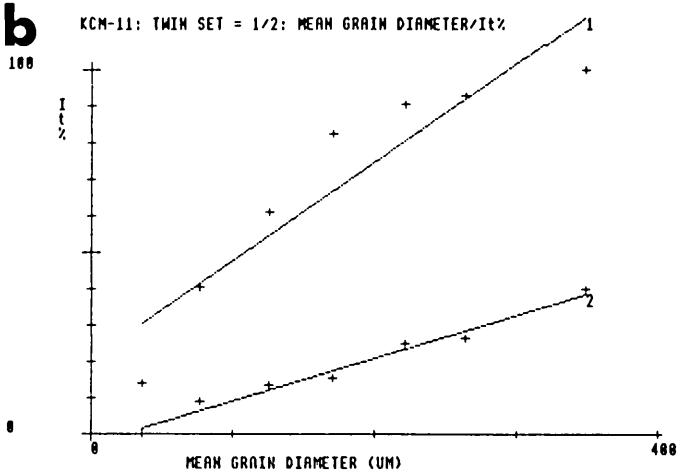
2

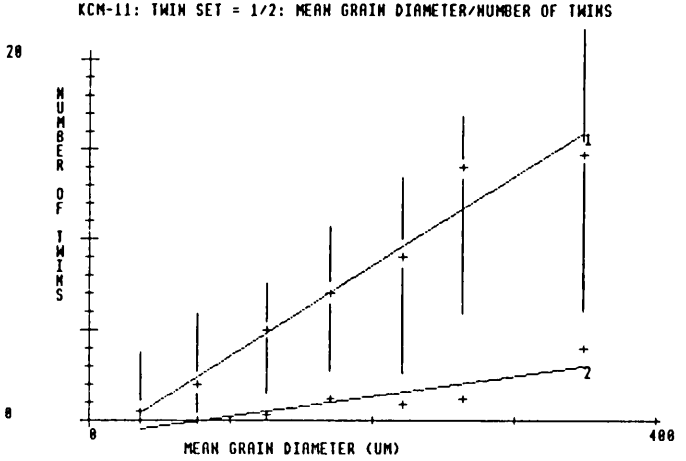

KCM-10: TWIN SET = 1/2: MEAN GRAIN DIAMETER/NUMBER OF TWINS
30
0
NUMBER OF TWINS
0
300
MEAN GRAIN DIAMETER (UM)
1
2

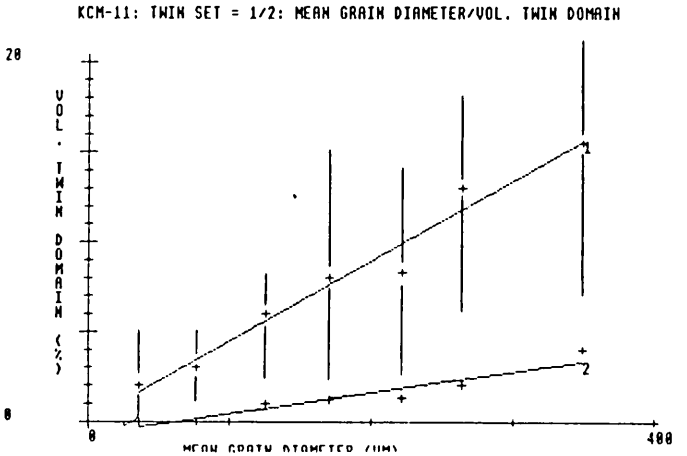
3


KCM-10: TWIN SET = 1/2: MEAN GRAIN DIAMETER/VOL. TWIN DOMAIN
40
0
VOL. TWIN DOMAIN (%)
1
2

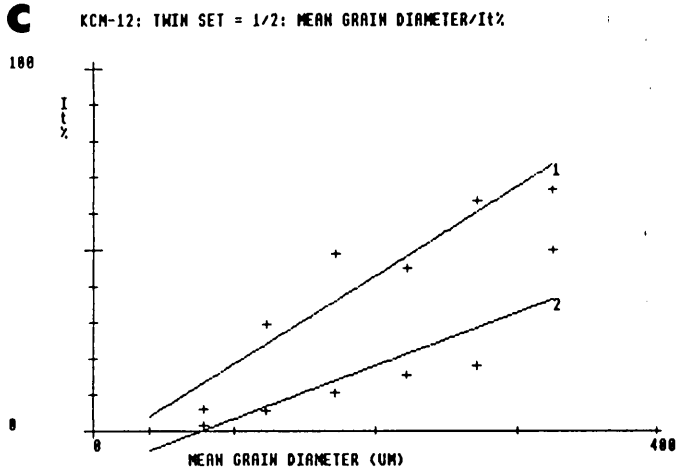
b

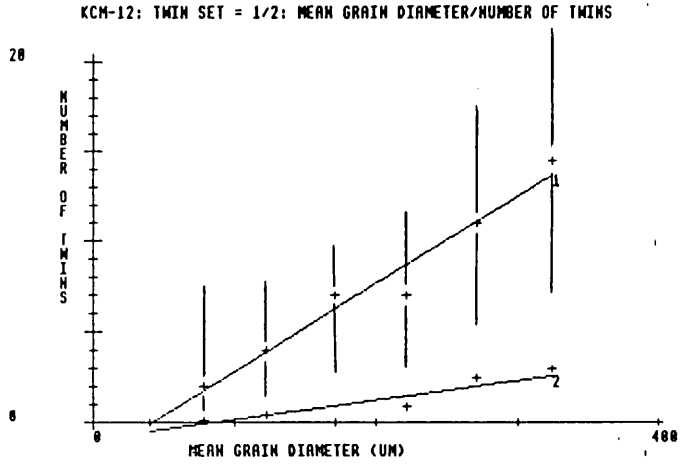

KCM-11: TWIN SET = 1/2: MEAN GRAIN DIAMETER/It%
100
0
It%
0
400
MEAN GRAIN DIAMETER (UM)
1
2

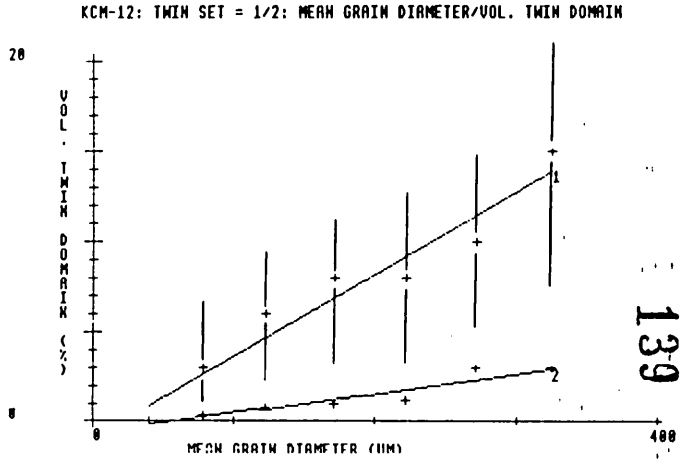

KCM-11: TWIN SET = 1/2: MEAN GRAIN DIAMETER/NUMBER OF TWINS
20
0
NUMBER OF TWINS
0
400
MEAN GRAIN DIAMETER (UM)
1
2


KCM-11: TWIN SET = 1/2: MEAN GRAIN DIAMETER/VOL. TWIN DOMAIN
20
0
VOL. TWIN DOMAIN (%)
0
400
1
2

c


KCM-12: TWIN SET = 1/2: MEAN GRAIN DIAMETER/It%
100
0
It%
0
400
MEAN GRAIN DIAMETER (UM)
1
2


KCM-12: TWIN SET = 1/2: MEAN GRAIN DIAMETER/NUMBER OF TWINS
20
0
NUMBER OF TWINS
0
400
MEAN GRAIN DIAMETER (UM)
1
2


KCM-12: TWIN SET = 1/2: MEAN GRAIN DIAMETER/VOL. TWIN DOMAIN
20
0
VOL. TWIN DOMAIN (%)
0
400
1
2

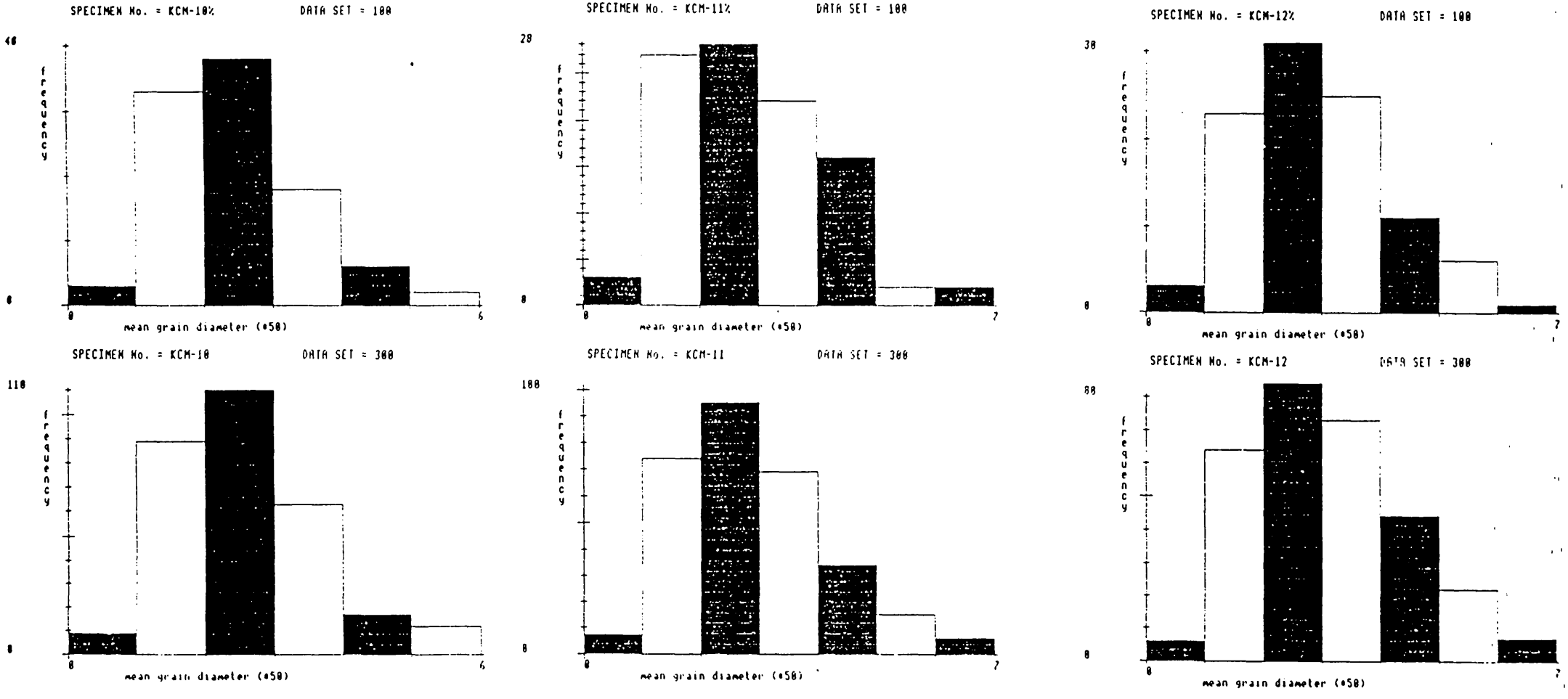
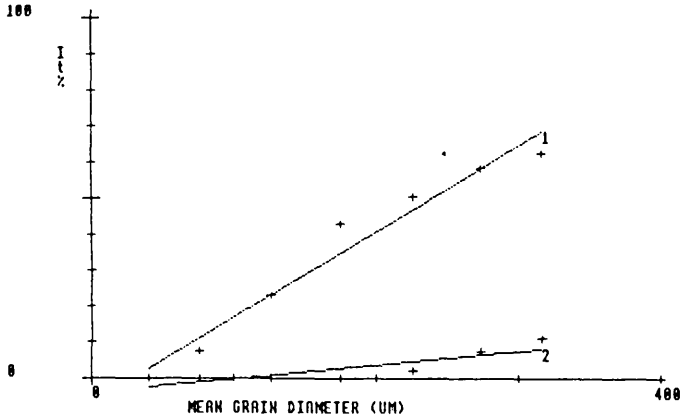
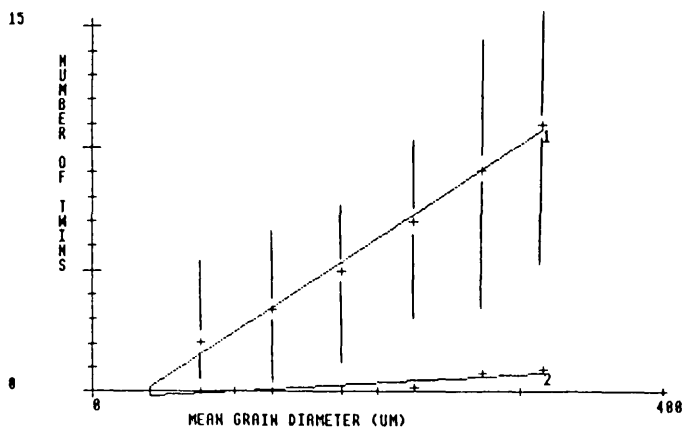


FIGURE 4.11 Histograms showing the number of data points (grains) in each of the grain size intervals for the diagrams of Fig. 4.10, the 500°C series of experiments upon Carrara Marble see section 4.6.2.1. Note that Fig. 4.11d is shown with Fig. 4.10d. The suffix "%" in the sample heading identifies those grains for which the volume twin fraction has been calculated. See text.

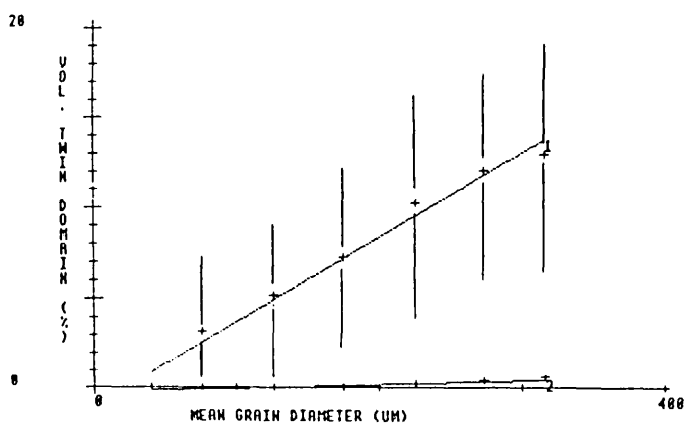
d 1 KCM-14: TWIN SET = 1/2: MEAN GRAIN DIAMETER/It%

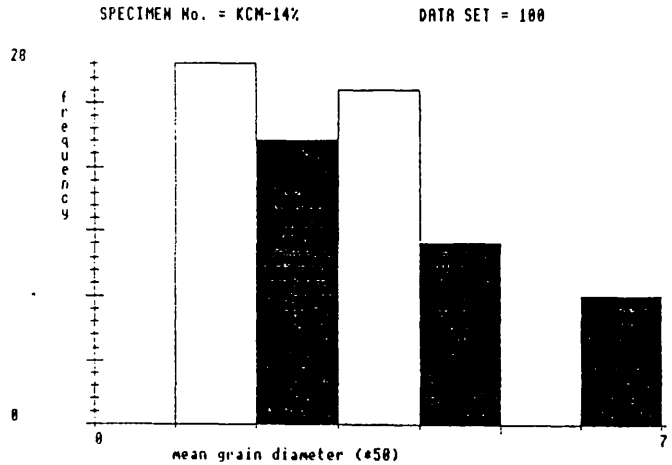


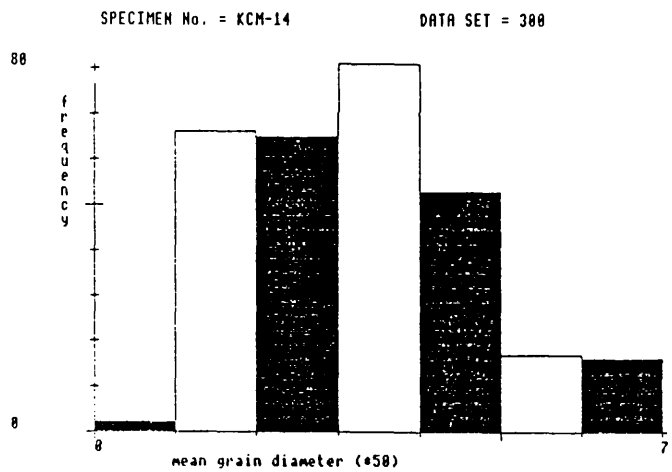
2 KCM-14: TWIN SET = 1/2: MEAN GRAIN DIAMETER/NUMBER OF TWINS



3 KCM-14: TWIN SET = 1/2: MEAN GRAIN DIAMETER/VOL. TWIN DOMAIN







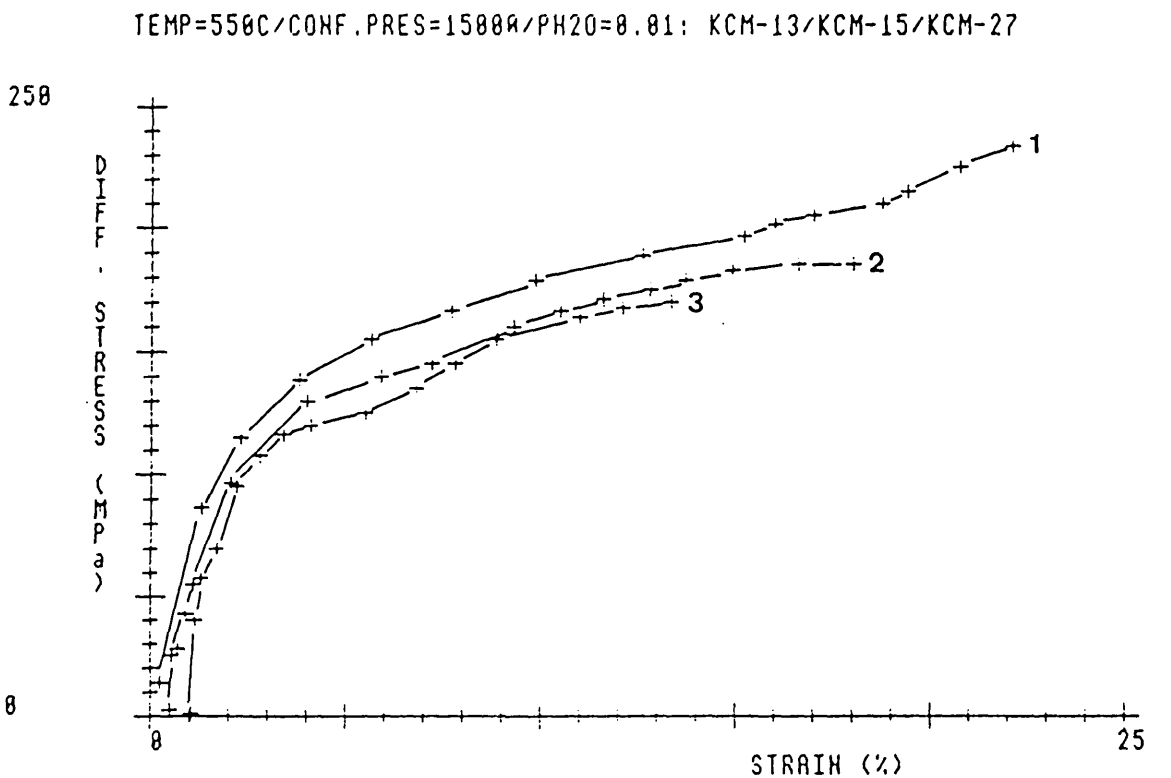


FIGURE 4.12 Stress/strain curves obtained for the 550°C Series of experiments performed upon Carrara Marble, see section 4.6.2.2. 1 = KCM-13, 2 = KCM-15 and 3 = KCM-27.

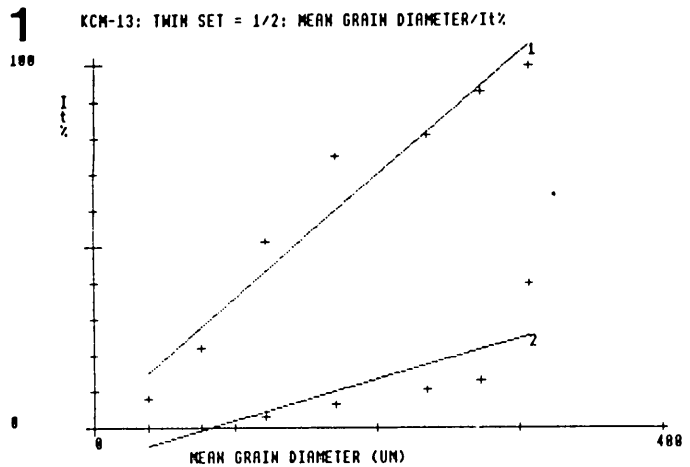
FIGURE 4.13 Textural data for Carrara Marble deformed at 550°C.

This series of diagrams present the twinning activity data determined for this series of experiments plotted as a function of grain size. There are three diagrams, plotting It, number of twins, and percentage volume twin domain (1, 2 and 3 respectively) for each each of the four experiments (a, ,b and c) performed at this temperature on this material.

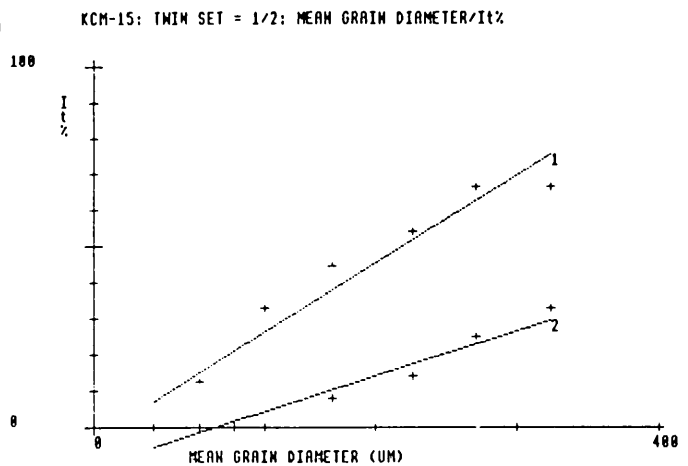
For each sample two twin sets have been analysed, the primary, or principal, twin set and the secondary twin set (1 and 2 respectively). The range bars shown for the relevant groups represent the full range of the values determined for each grain size interval. The individual experiments are identified by their respective headings.

See text for discussion.

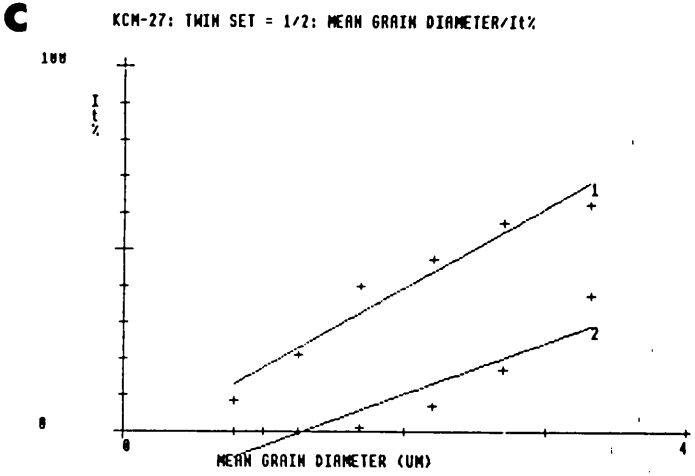
a 1


KCM-13: TWIN SET = 1/2: MEAN GRAIN DIAMETER/It%
100
0
It%
0
400
MEAN GRAIN DIAMETER (UM)
1
2

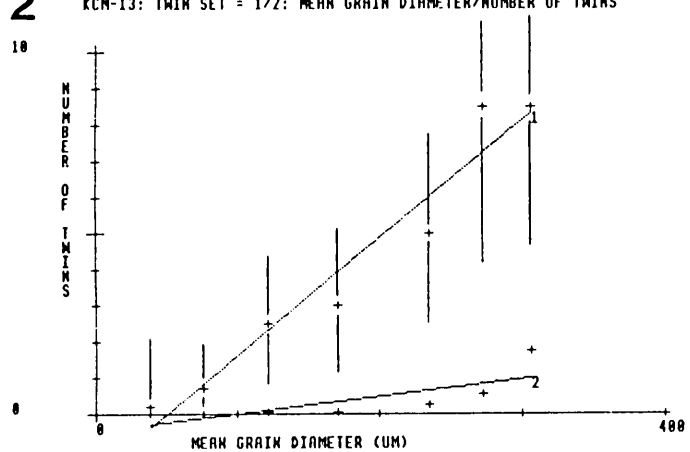
b

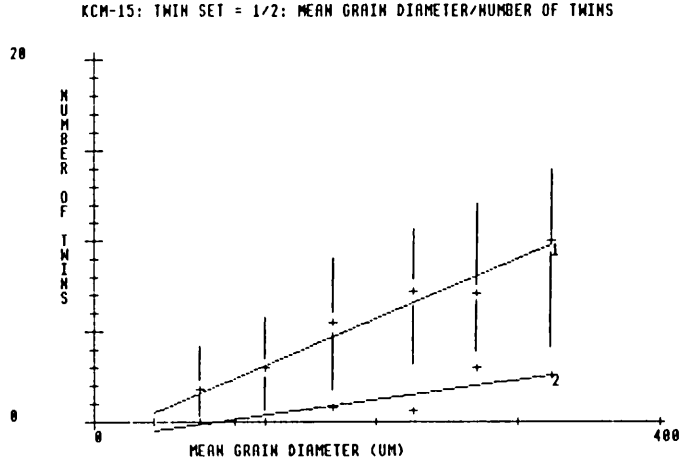

KCM-15: TWIN SET = 1/2: MEAN GRAIN DIAMETER/It%
100
0
It%
0
400
MEAN GRAIN DIAMETER (UM)
1
2

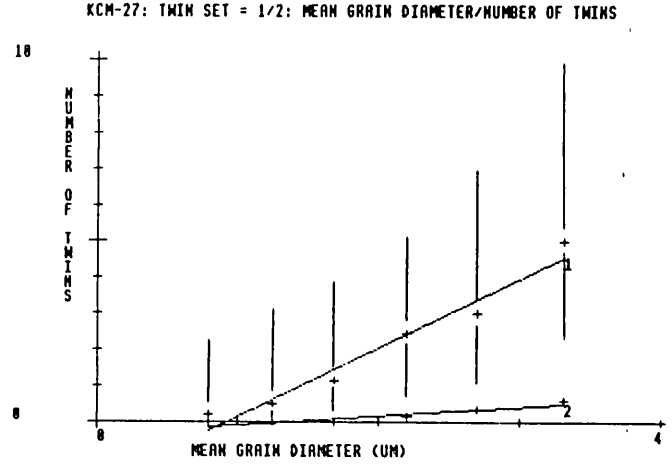
c


KCM-27: TWIN SET = 1/2: MEAN GRAIN DIAMETER/It%
100
0
It%
0
MEAN GRAIN DIAMETER (UM)
1
2

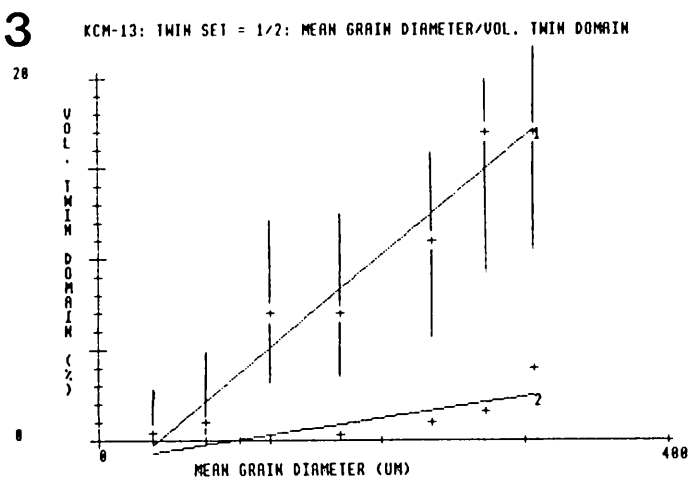
2

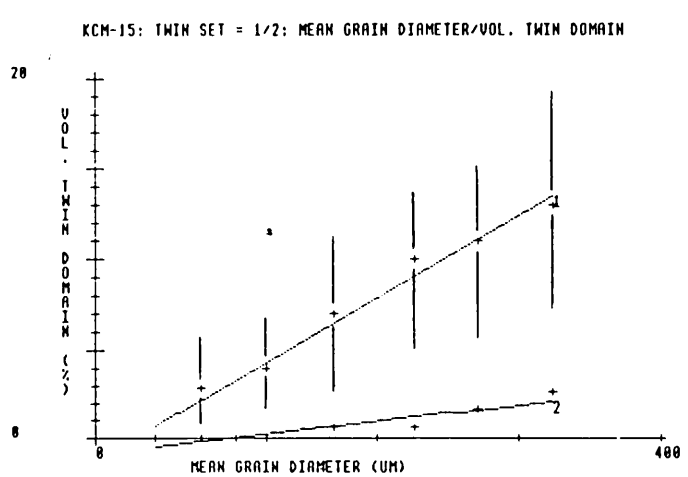

KCM-13: TWIN SET = 1/2: MEAN GRAIN DIAMETER/NUMBER OF TWINS
10
0
NUMBER OF TWINS
0
400
MEAN GRAIN DIAMETER (UM)
1
2

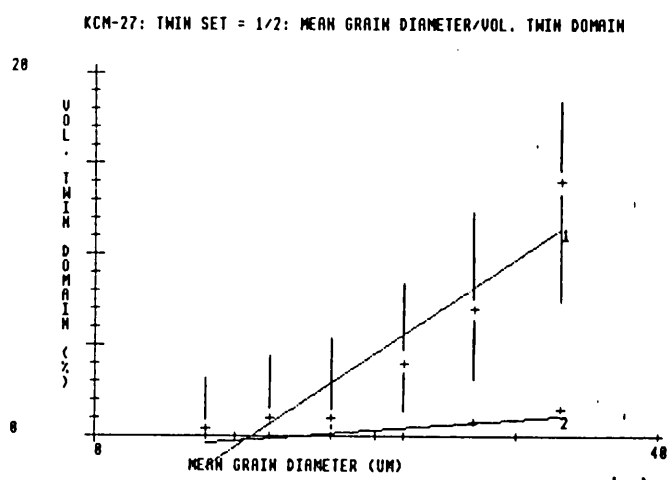

KCM-15: TWIN SET = 1/2: MEAN GRAIN DIAMETER/NUMBER OF TWINS
20
0
NUMBER OF TWINS
0
400
MEAN GRAIN DIAMETER (UM)
1
2


KCM-27: TWIN SET = 1/2: MEAN GRAIN DIAMETER/NUMBER OF TWINS
10
0
NUMBER OF TWINS
0
MEAN GRAIN DIAMETER (UM)
1
2

3


KCM-13: TWIN SET = 1/2: MEAN GRAIN DIAMETER/VOL. TWIN DOMAIN
20
0
VOL. TWIN DOMAIN (%)
0
400
MEAN GRAIN DIAMETER (UM)
1
2


KCM-15: TWIN SET = 1/2: MEAN GRAIN DIAMETER/VOL. TWIN DOMAIN
20
0
VOL. TWIN DOMAIN (%)
0
400
MEAN GRAIN DIAMETER (UM)
1
2


KCM-27: TWIN SET = 1/2: MEAN GRAIN DIAMETER/VOL. TWIN DOMAIN
20
0
VOL. TWIN DOMAIN (%)
0
MEAN GRAIN DIAMETER (UM)
1
2

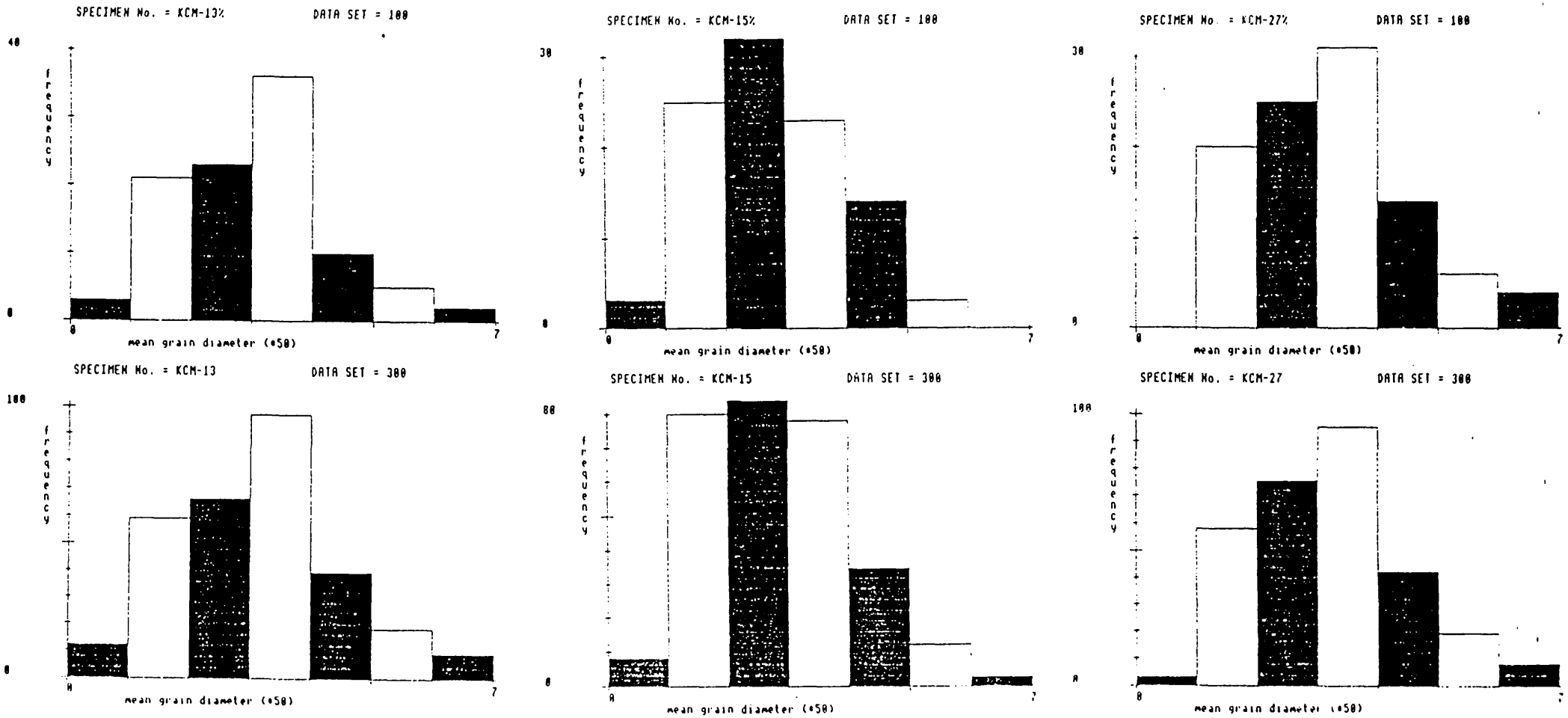


FIGURE 4.14 Histograms showing the number of data points (grains) in each of the grain size intervals for the diagrams of Fig. 4.13, the 550°C series of experiments upon Carrara Marble see section 4.6.2.3. The individual samples are identified by their headings as for Fig. 4.11.

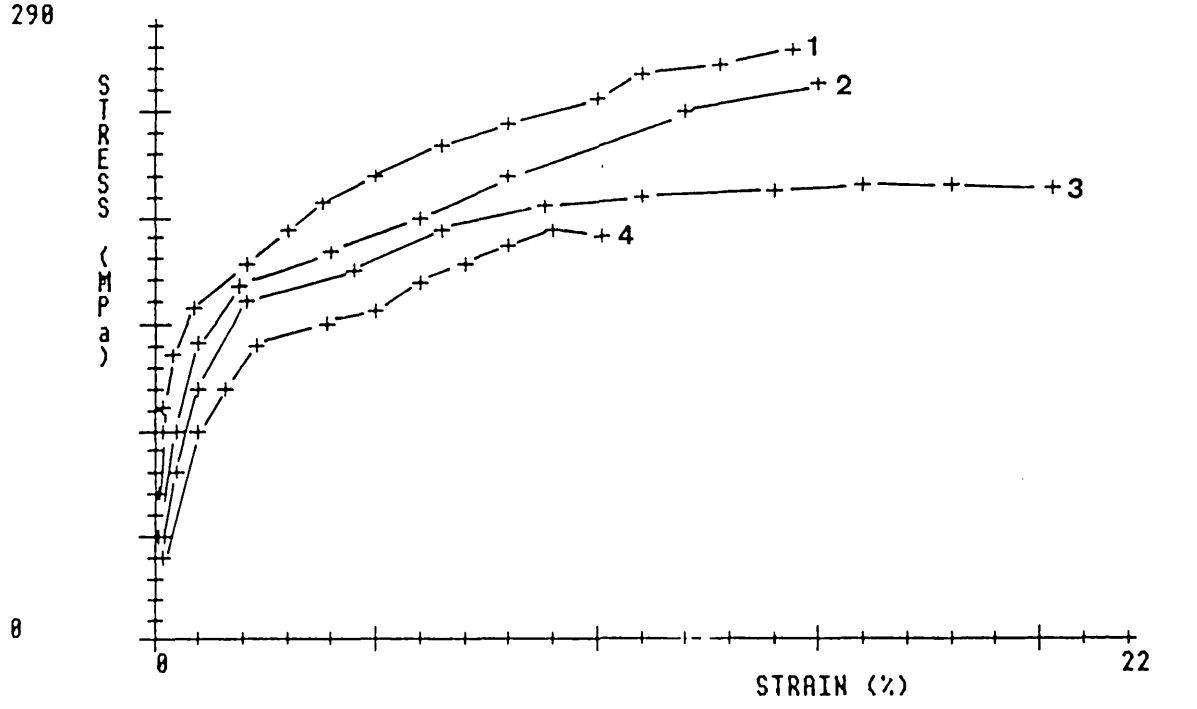


FIGURE 4.15 Stress/strain curves obtained for the 400°C series of experiments performed upon Carrara Marble, see section 4.6.2.3. 1 = KCM-16, 2 = KCM-17, 3 = KCM-19 and 4 = KCM-20. Note that the duplicate experiment, KCM-18, has a stress/strain curve identical to that of KCM-16.

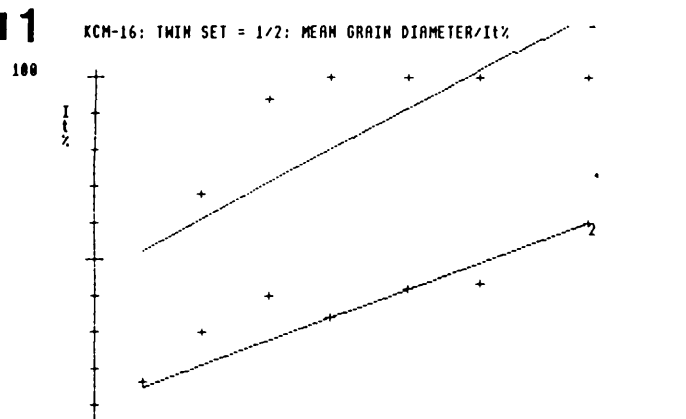
FIGURE 4.16 Textural data for Carrara Marble deformed at 400°C.

This series of diagrams (cont. on next page) present the twinning activity data determined for this series of experiments plotted as a function of grain size. There are three diagrams, plotting It, number of twins, and percentage volume twin domain (1, 2 and 3 respectively) for each each of the four experiments (a, b, c, d and e) performed at this temperature on this material.

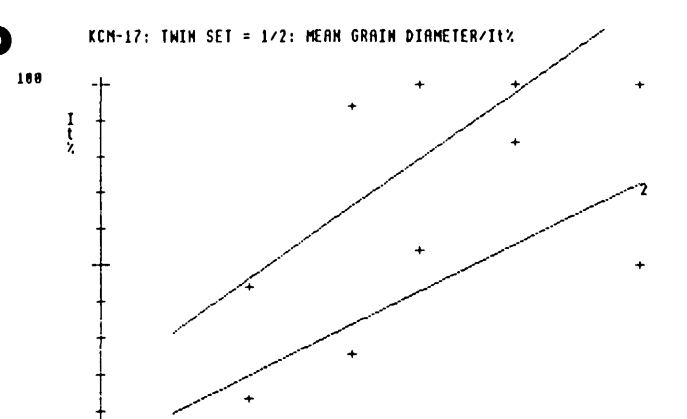
For each sample two twin sets have been analysed, the primary, or principal, twin set and the secondary twin set (1 and 2 respectively). The range bars shown for the relevant groups represent the full range of the values determined for each grain size interval. The individual experiments are identified by their respective headings.

Note that the apparent higher It values for sample KCM-18 are a manifestation of the predominance of larger grains in this specimen. The linear regressed lines are shown in order to illustrate the respective trends of the data sets. See text for discussion.

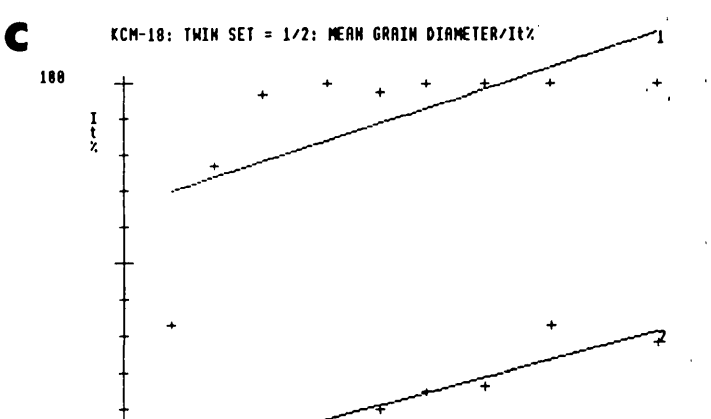
a 1


KCM-16: TWIN SET = 1/2: MEAN GRAIN DIAMETER/It%
100
0
It%
0
400
MEAN GRAIN DIAMETER (UM)
1
2

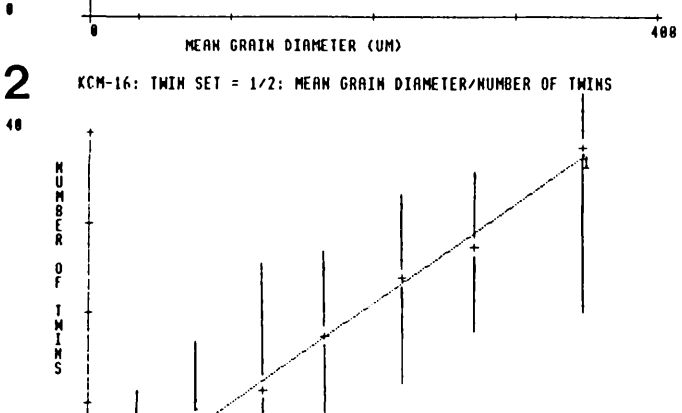
b

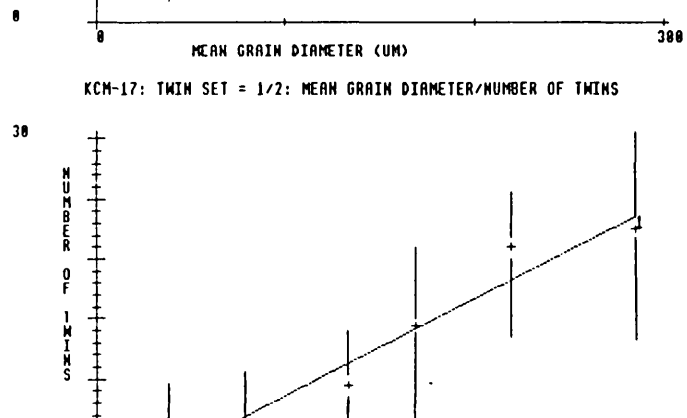

KCM-17: TWIN SET = 1/2: MEAN GRAIN DIAMETER/It%
100
0
It%
0
300
MEAN GRAIN DIAMETER (UM)
1
2

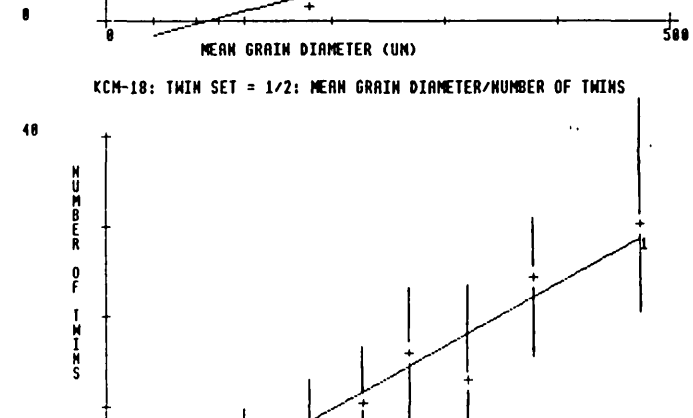
c


KCM-18: TWIN SET = 1/2: MEAN GRAIN DIAMETER/It%
100
0
It%
0
500
MEAN GRAIN DIAMETER (UM)
1
2

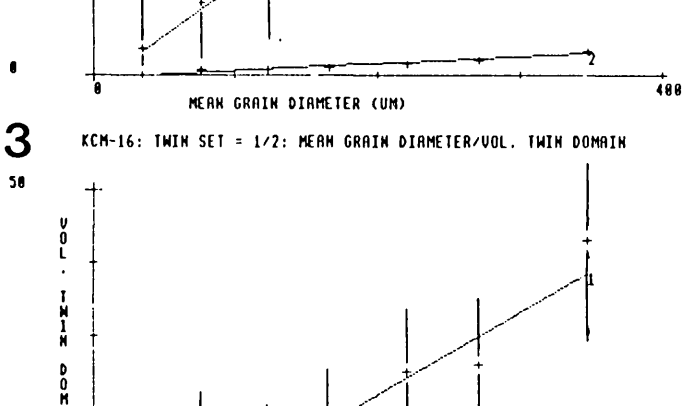
2

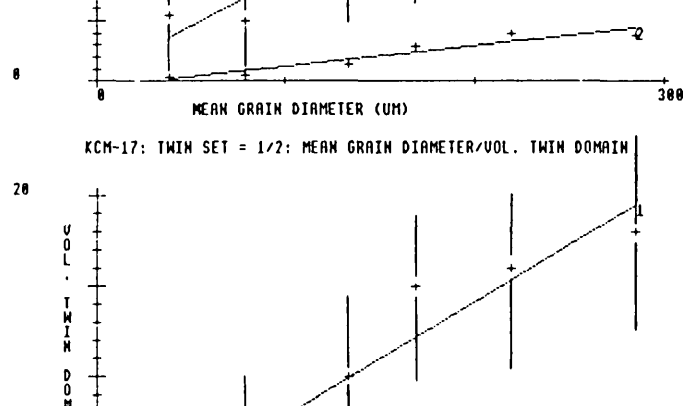

KCM-16: TWIN SET = 1/2: MEAN GRAIN DIAMETER/NUMBER OF TWINS
40
0
NUMBER OF TWINS
0
400
MEAN GRAIN DIAMETER (UM)
1
2

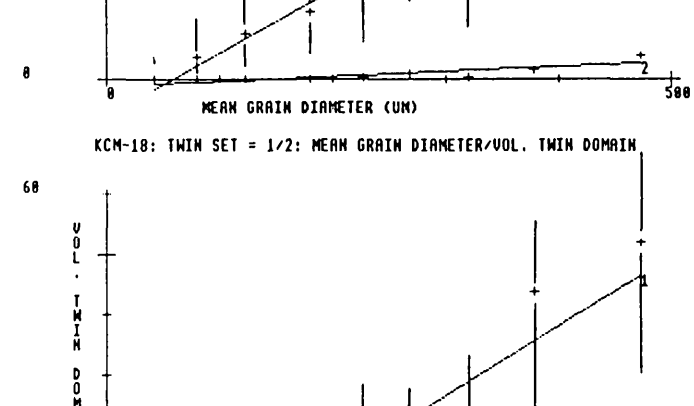

KCM-17: TWIN SET = 1/2: MEAN GRAIN DIAMETER/NUMBER OF TWINS
30
0
NUMBER OF TWINS
0
300
MEAN GRAIN DIAMETER (UM)
1
2


KCM-18: TWIN SET = 1/2: MEAN GRAIN DIAMETER/NUMBER OF TWINS
40
0
NUMBER OF TWINS
0
500
MEAN GRAIN DIAMETER (UM)
1
2

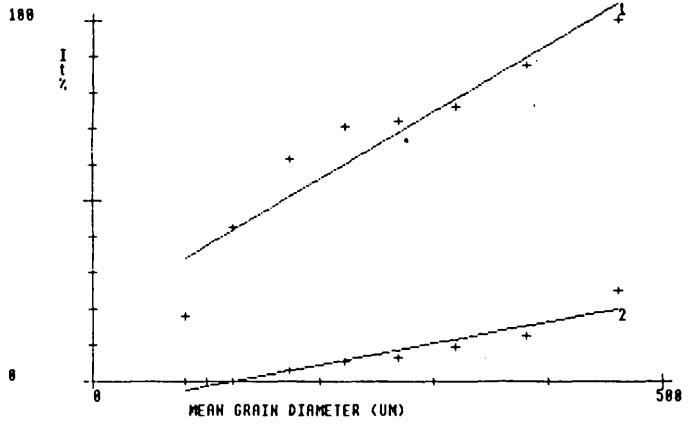
3


KCM-16: TWIN SET = 1/2: MEAN GRAIN DIAMETER/VOL. TWIN DOMAIN
50
0
VOL. TWIN DOMAIN (%)
0
400
1
2

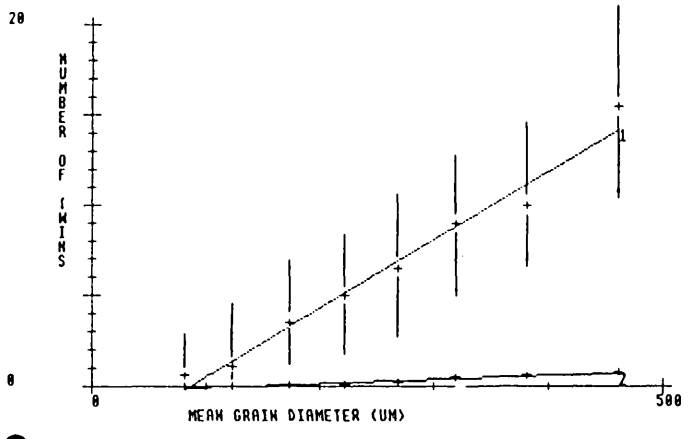

KCM-17: TWIN SET = 1/2: MEAN GRAIN DIAMETER/VOL. TWIN DOMAIN
20
0
VOL. TWIN DOMAIN (%)
0
300
1
2


KCM-18: TWIN SET = 1/2: MEAN GRAIN DIAMETER/VOL. TWIN DOMAIN
60
0
VOL. TWIN DOMAIN (%)
0
500
1
2

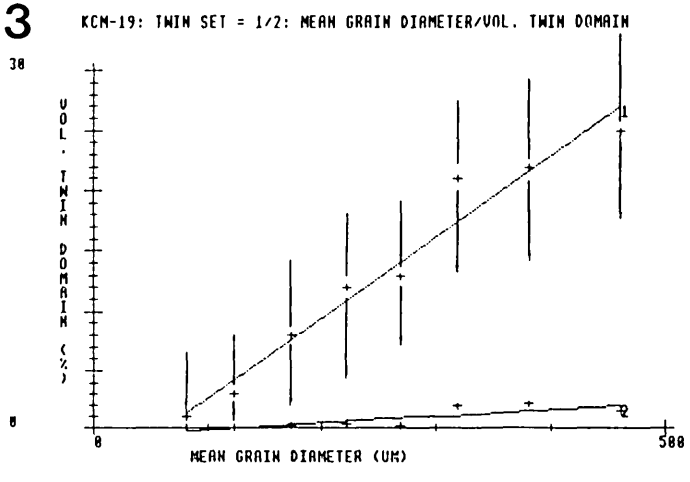
d 1


KCM-19: TWIN SET = 1/2: MEAN GRAIN DIAMETER/It%
100
It%
0
0
500
MEAN GRAIN DIAMETER (UM)
1
2

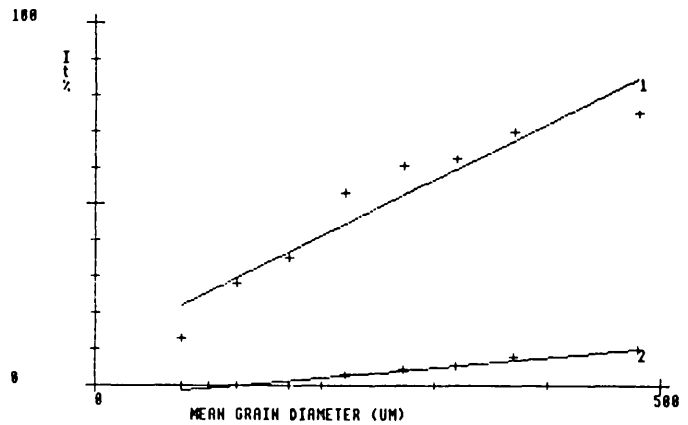
2

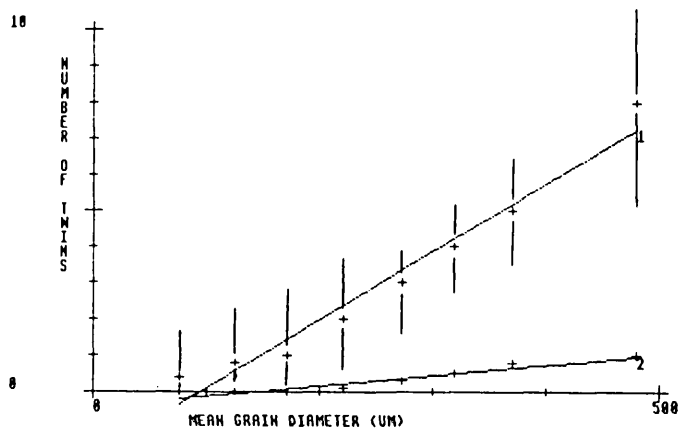

KCM-19: TWIN SET = 1/2: MEAN GRAIN DIAMETER/NUMBER OF TWINS
20
NUMBER OF TWINS
0
0
500
MEAN GRAIN DIAMETER (UM)
1
2

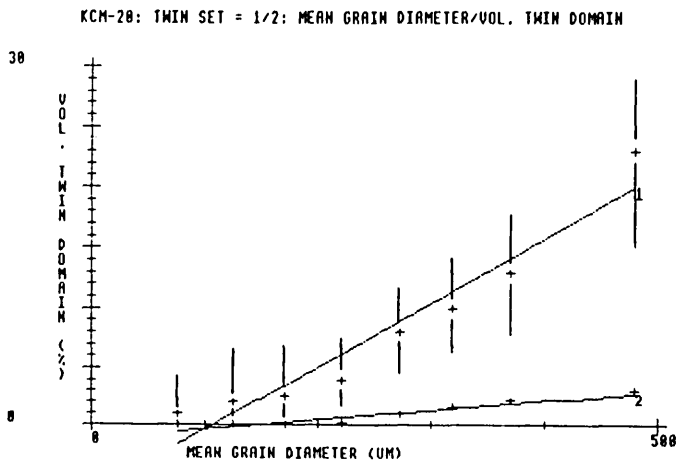
3


KCM-19: TWIN SET = 1/2: MEAN GRAIN DIAMETER/VOL. TWIN DOMAIN
30
VOL. TWIN DOMAIN (%)
0
0
500
MEAN GRAIN DIAMETER (UM)
1
2

e


KCM-20: TWIN SET = 1/2: MEAN GRAIN DIAMETER/It%
100
It%
0
0
500
MEAN GRAIN DIAMETER (UM)
1
2


KCM-20: TWIN SET = 1/2: MEAN GRAIN DIAMETER/NUMBER OF TWINS
10
NUMBER OF TWINS
0
0
500
MEAN GRAIN DIAMETER (UM)
1
2


KCM-20: TWIN SET = 1/2: MEAN GRAIN DIAMETER/VOL. TWIN DOMAIN
30
VOL. TWIN DOMAIN (%)
0
0
500
MEAN GRAIN DIAMETER (UM)
1
2

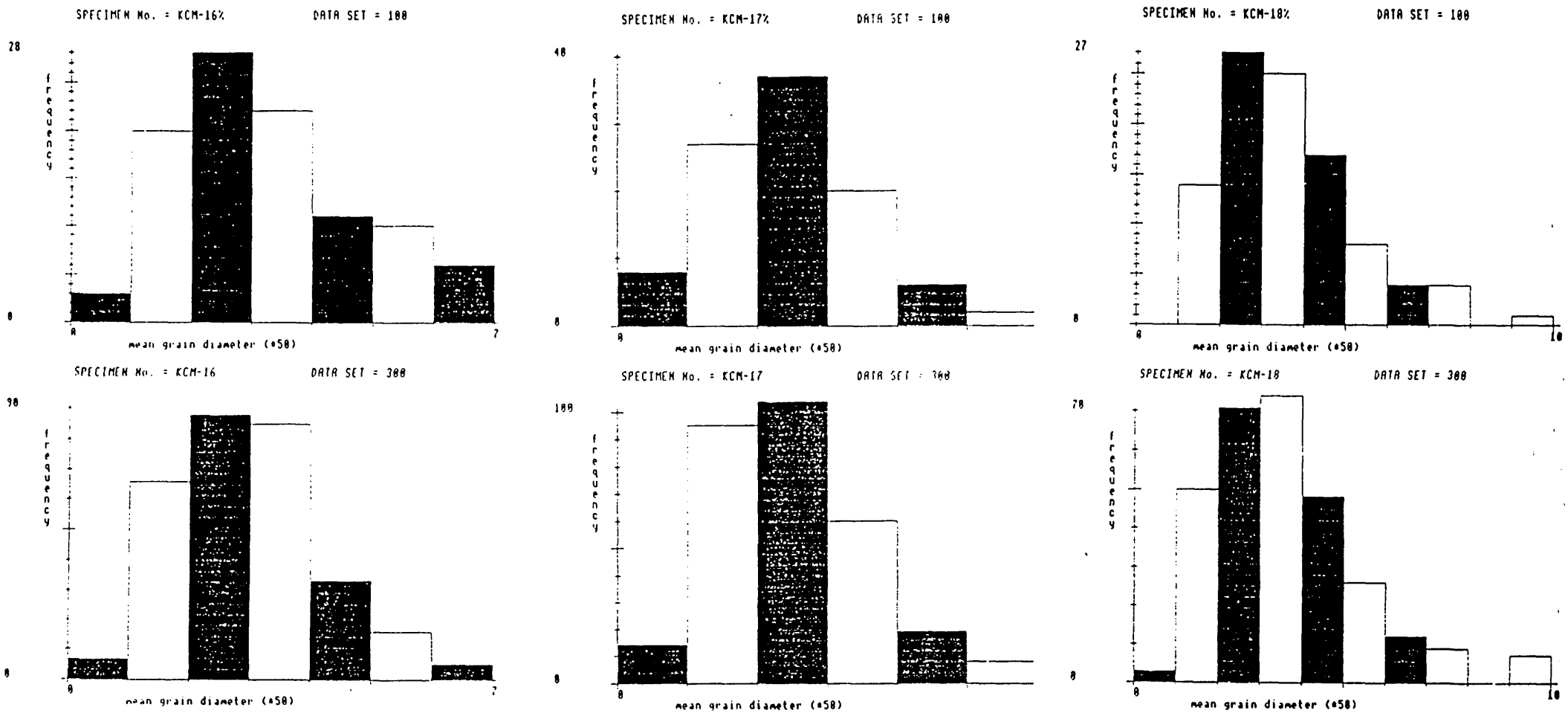
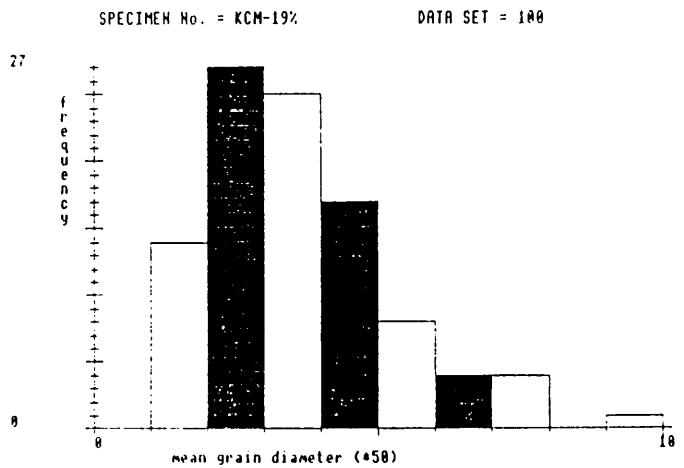
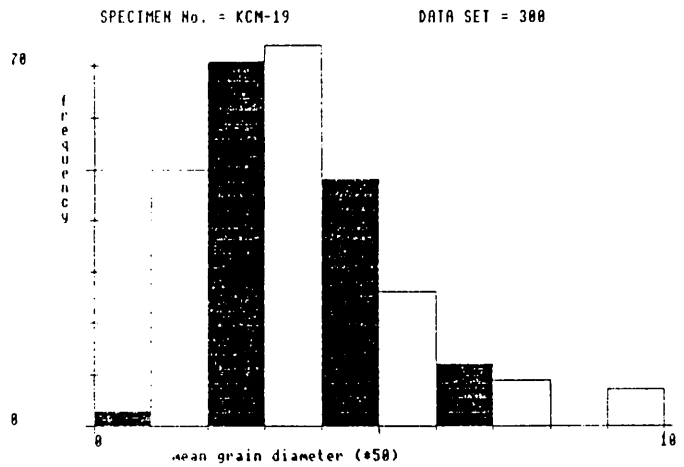
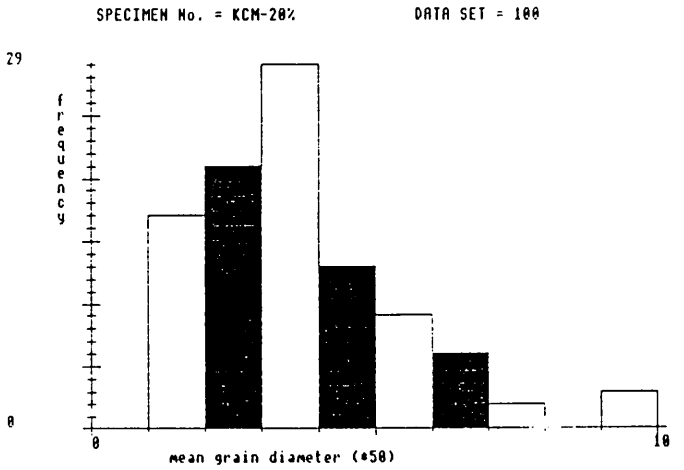
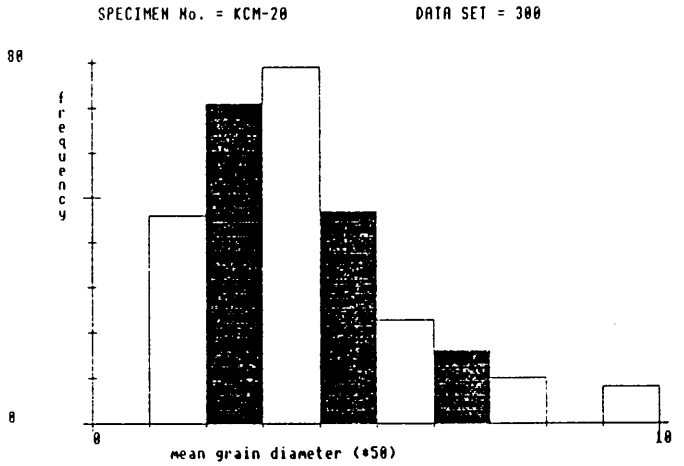


FIGURE 4.17 (Cont. over) Histograms showing the number of data points (grains) in each of the grain size intervals for the diagrams of Fig. 4.16, the 400°C series of experiments upon Carrara Marble see section 4.6.2.3. The individual samples are identified by their headings as for Fig. 4.11.


SPECIMEN No. = KCM-19%
DATA SET = 100
27
0
frequency
0
10
mean grain diameter (*50)


SPECIMEN No. = KCM-19
DATA SET = 300
70
0
frequency
0
10
mean grain diameter (*50)


SPECIMEN No. = KCM-20%
DATA SET = 100
29
0
frequency
0
10
mean grain diameter (*50)


SPECIMEN No. = KCM-20
DATA SET = 300
80
0
frequency
0
10
mean grain diameter (*50)

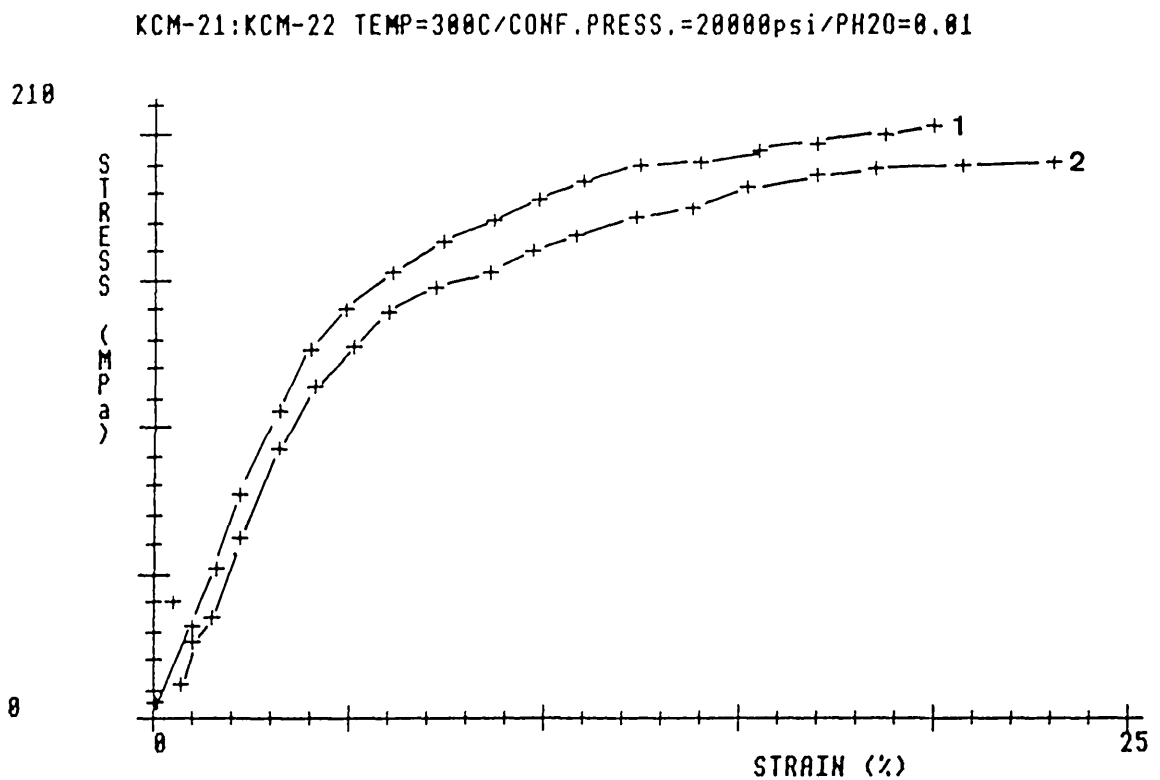


FIGURE 4.18 Stress/strain curves obtained for the 300°C series of experiments performed upon Carrara Marble, see section 4.6.2.4. 1 = KCM-21 and 2 = KCM-22

FIGURE 4.19 Textural data for Carrara Marble deformed at 300°C.

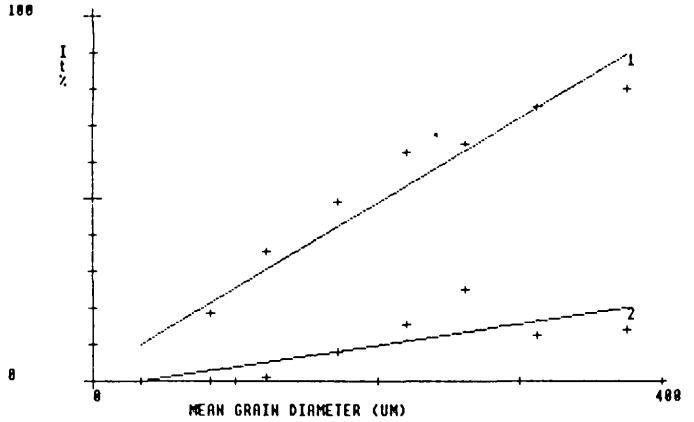
This series of diagrams present the twinning activity data determined for the two experiments (a and b respectively) deformed at this temperature, plotted as a function of grain size. There are three diagrams, plotting It, number of twins, and percentage volume twin domain (1, 2 and 3 respectively).

For each sample two twin sets have been analysed, the primary, or principal, twin set and the secondary twin set (1 and 2 respectively). The range bars shown for the relevant groups represent the full range of the values determined for each grain size interval. The individual experiments are identified by their respective headings.

See text for discussion.

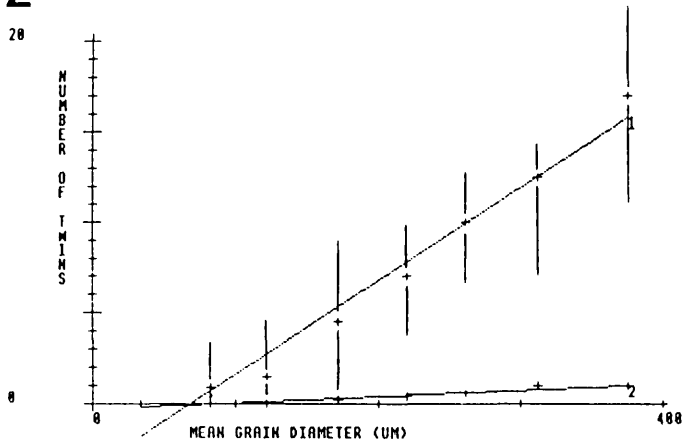
a 1

KCM-21: TWIN SET = 1/2: MEAN GRAIN DIAMETER/It%



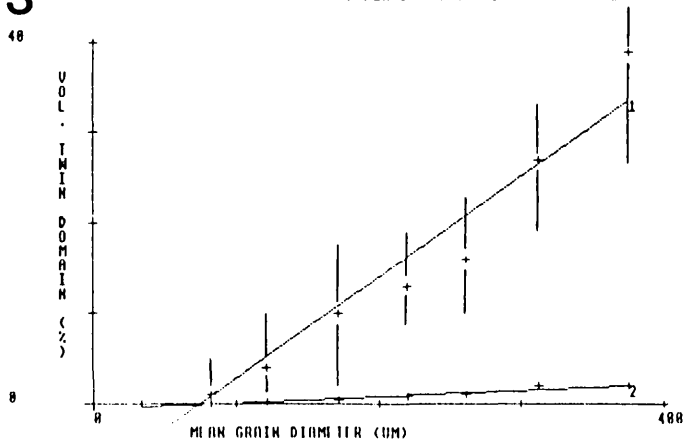
2

KCM-21: TWIN SET = 1/2: MEAN GRAIN DIAMETER/NUMBER OF TWINS



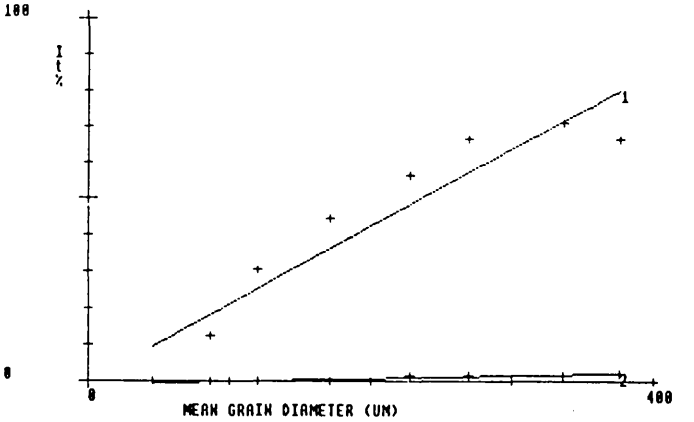
3

KCM-21: TWIN SET = 1/2: MEAN GRAIN DIAMETER/VOL. TWIN DOMAIN

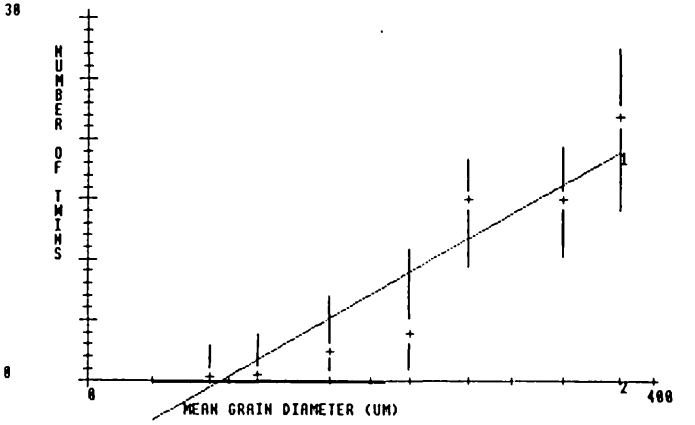


b

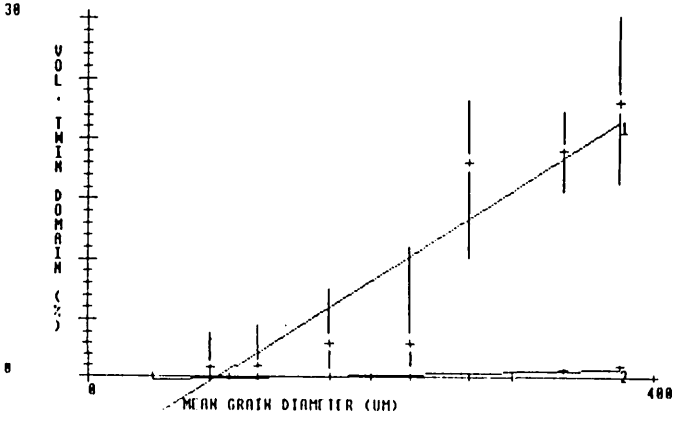
KCM-22: TWIN SET = 1/2: MEAN GRAIN DIAMETER/It%



KCM-22: TWIN SET = 1/2: MEAN GRAIN DIAMETER/NUMBER OF TWINS



KCM-22: TWIN SET = 1/2: MEAN GRAIN DIAMETER/VOL. TWIN DOMAIN



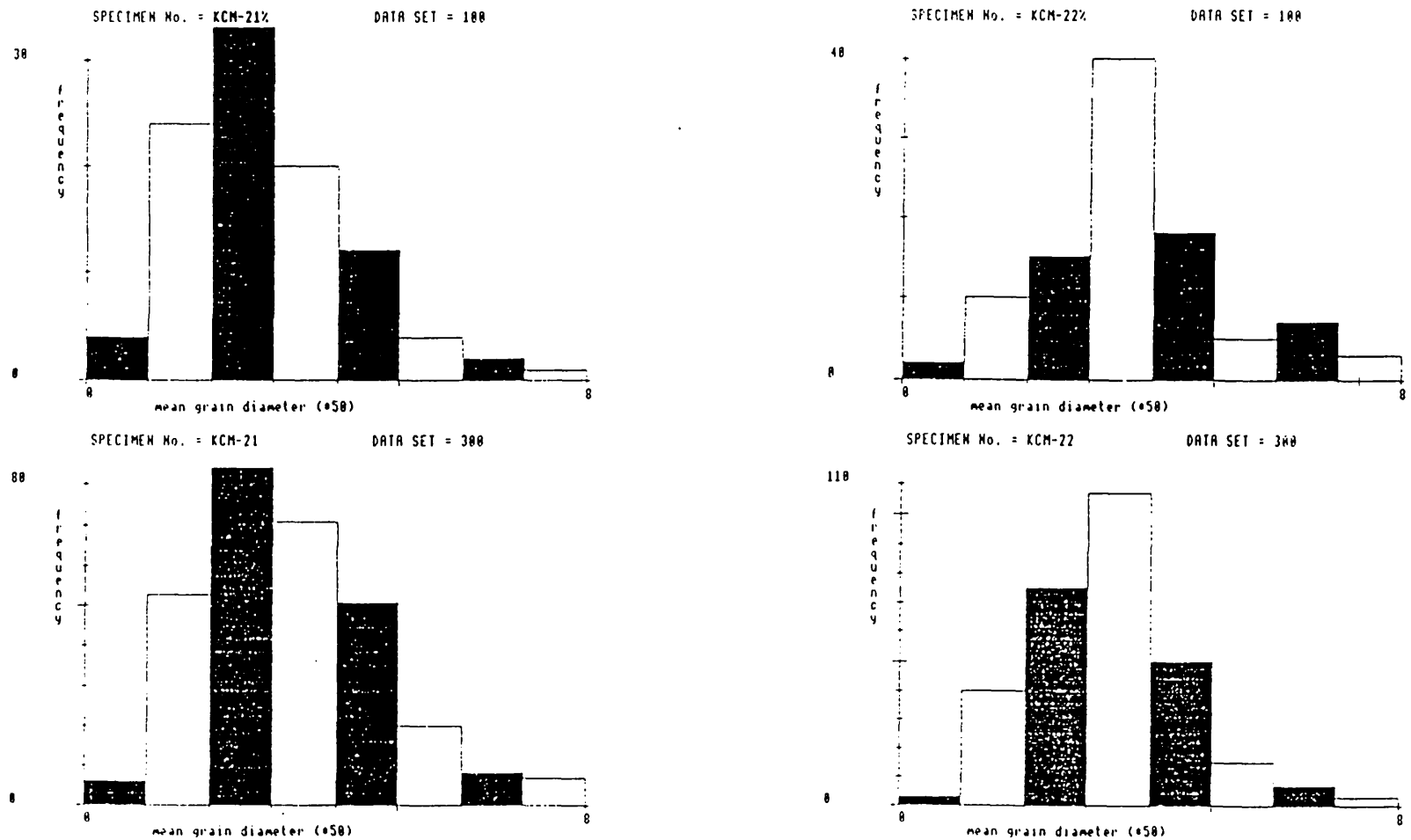


FIGURE 4.20 Histograms showing the number of data points (grains) in each of the grain size intervals for the diagrams of Fig. 4.19, the 300°C series of experiments upon Carrara Marble see section 4.6.2.4. The individual samples are identified by their headings as for Fig. 4.11.

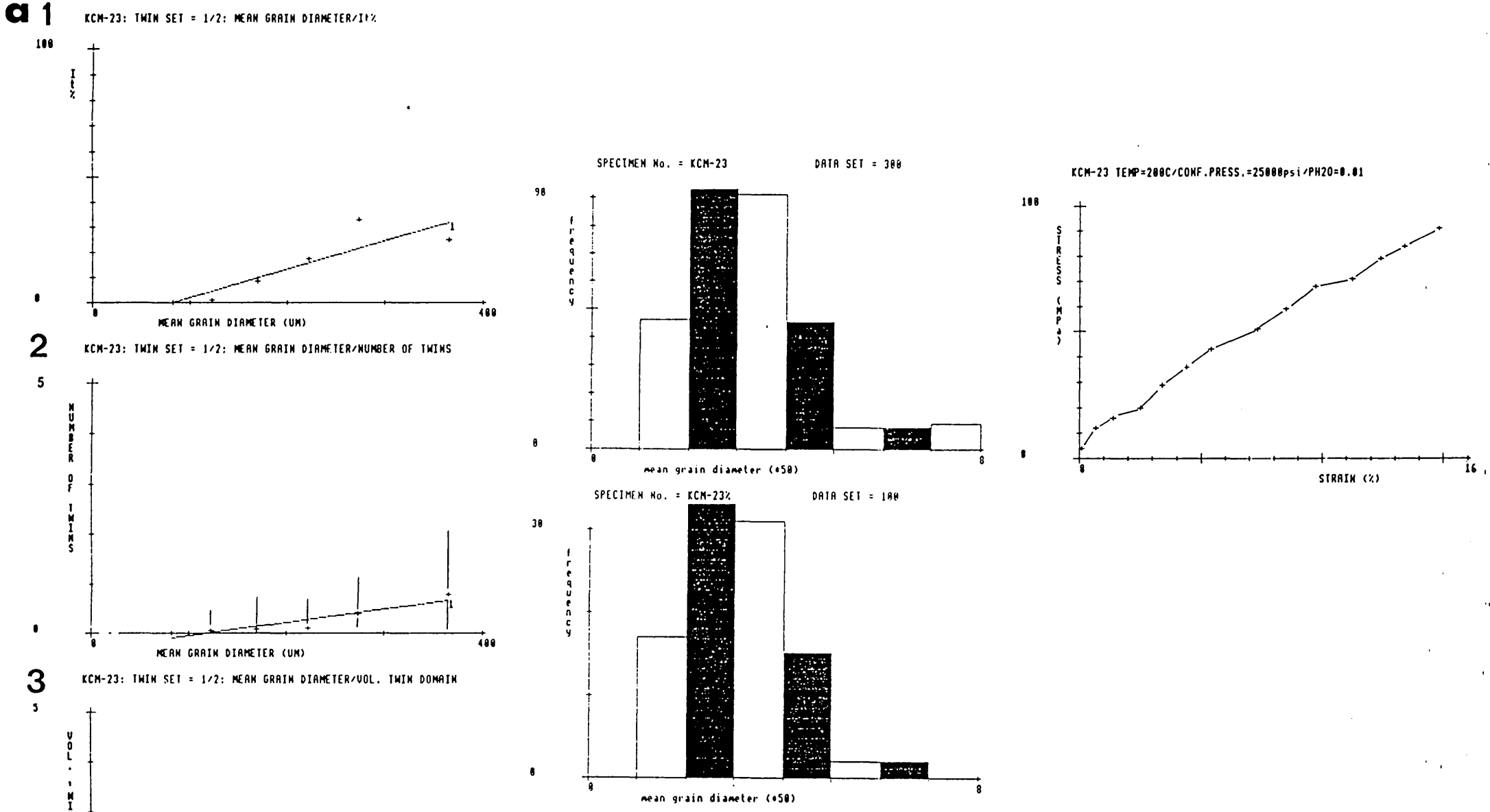


FIGURE 4.21 Composite figure showing the data obtained from the experimental and subsequent textural analysis of the single 200°C experiment, KCM-23. Fig. 4.21a shows the twinning activity data as a function of grain size, Fig. 4.21b shows the number of data points (grains) for each of the grain size intervals of Fig.4.21a, and Fig. 4.21c shows the stress/strain curve for this experiment.

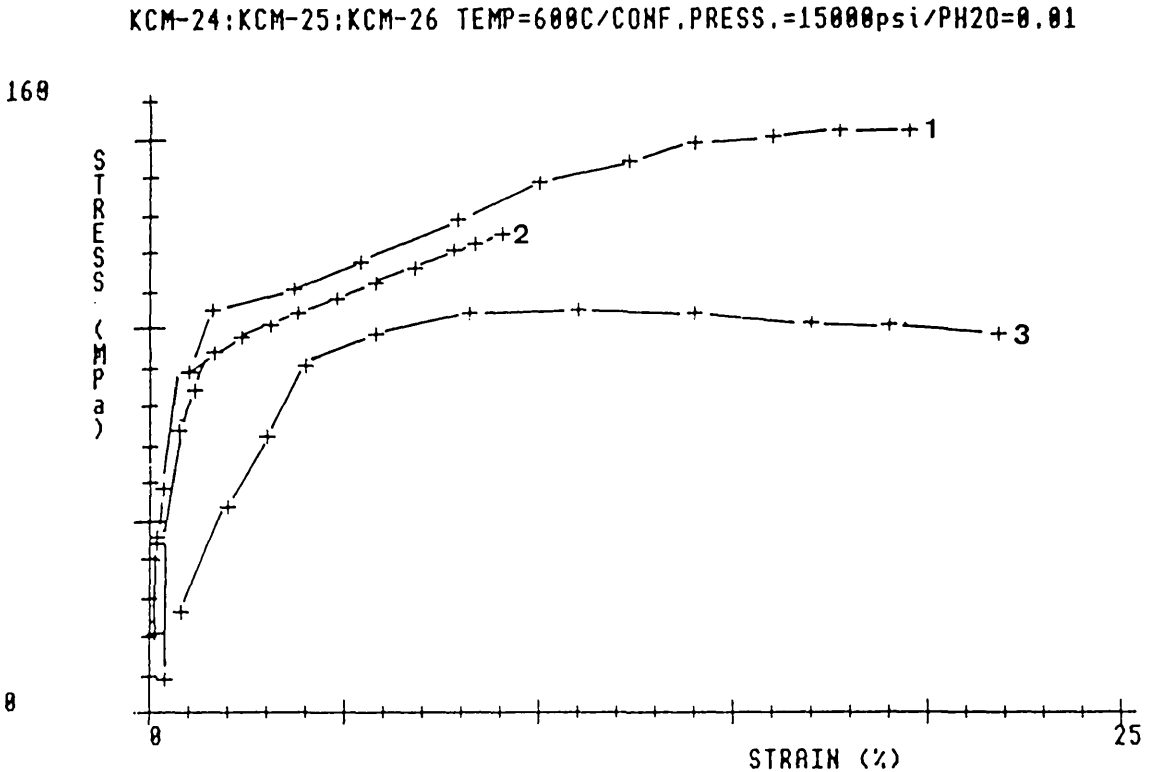


FIGURE 4.22 Stress/strain curves for the 600°C series of experiments performed upon Carrara Marble, see section 4.6.2.6. 1 = KCM-24, 2 = KCM-25 and 3 = KCM-26.

FIGURE 4.23 Textural data for Carrara Marble deformed at 600°C.

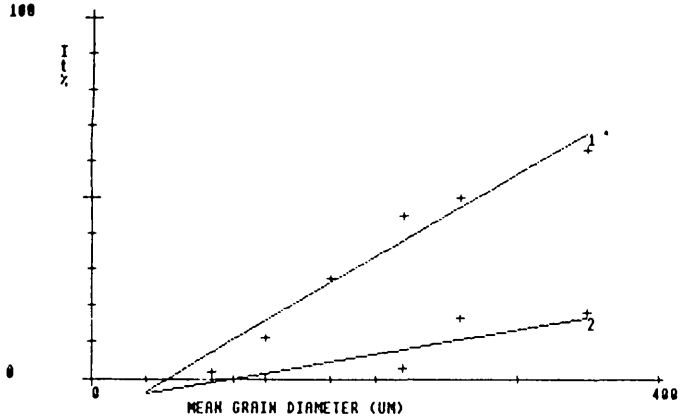
This series of diagrams present the twinning activity data determined for the three experiments (a, b and c respectively) deformed at this temperature, plotted as a function of grain size. There are three diagrams, plotting It, number of twins, and percentage volume twin domain (1, 2 and 3 respectively).

For each sample two twin sets have been analysed, the primary, or principal, twin set and the secondary twin set (1 and 2 respectively). The range bars shown for the relevant groups represent the full range of the values determined for each grain size interval. The individual experiments are identified by their respective headings.

See text for discussion.

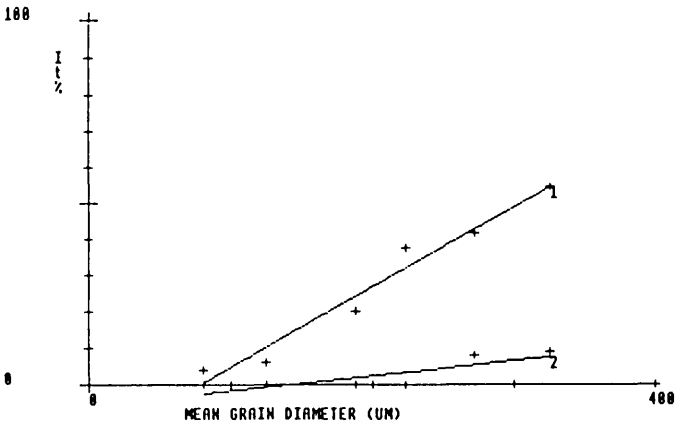
a 1

KCM-24: TWIN SET = 1/2: MEAN GRAIN DIAMETER/It%



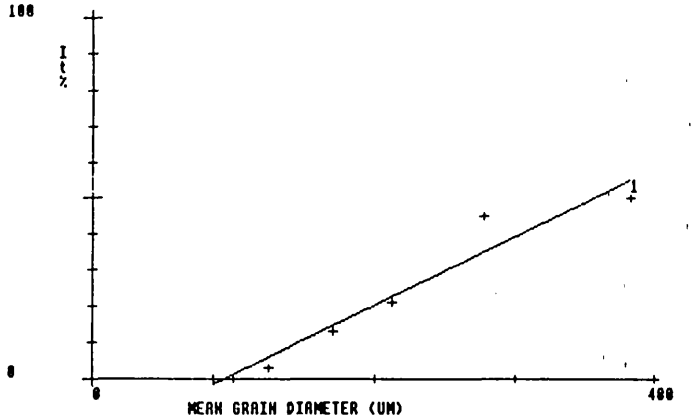
b

KCM-25: TWIN SET = 1/2: MEAN GRAIN DIAMETER/It%



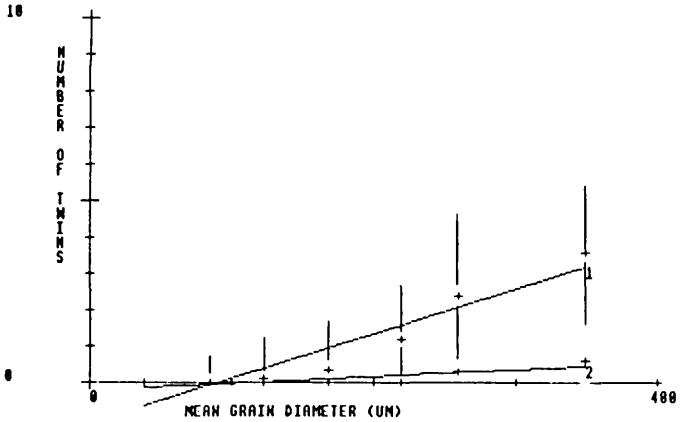
c

KCM-26: TWIN SET = 1/2: MEAN GRAIN DIAMETER/It%

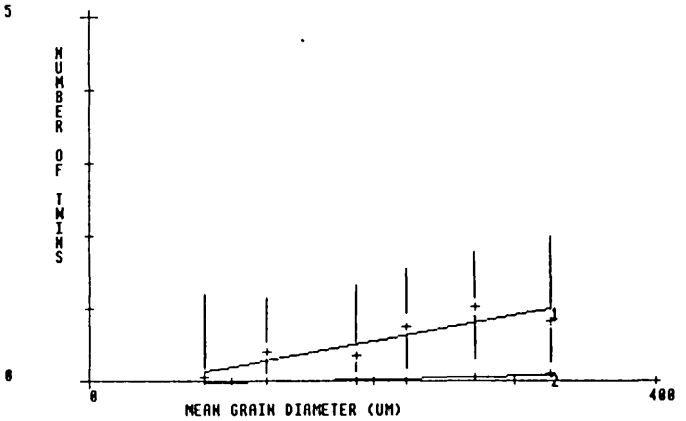


2

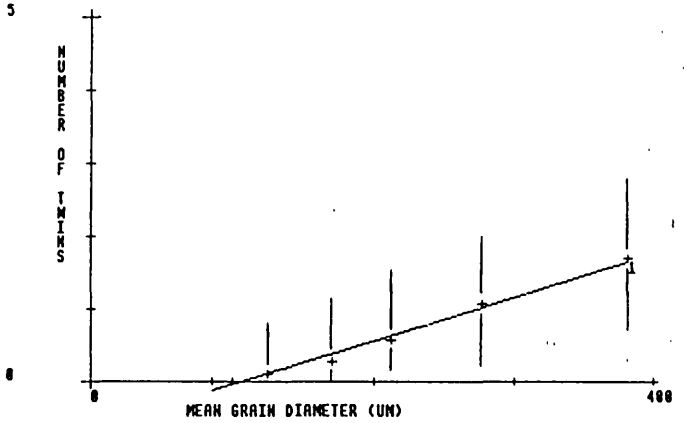
KCM-24: TWIN SET = 1/2: MEAN GRAIN DIAMETER/NUMBER OF TWINS



KCM-25: TWIN SET = 1/2: MEAN GRAIN DIAMETER/NUMBER OF TWINS

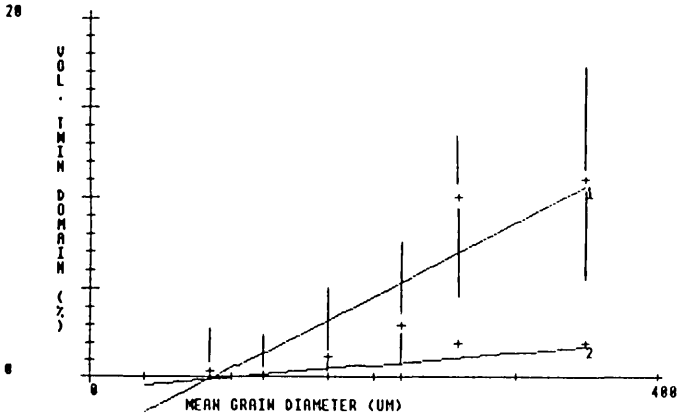


KCM-26: TWIN SET = 1/2: MEAN GRAIN DIAMETER/NUMBER OF TWINS

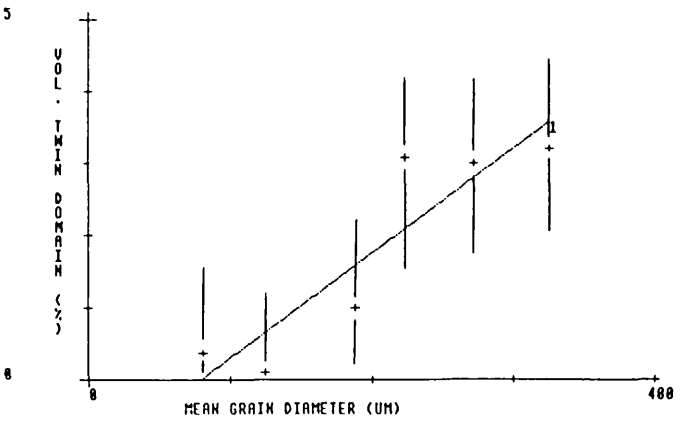


3

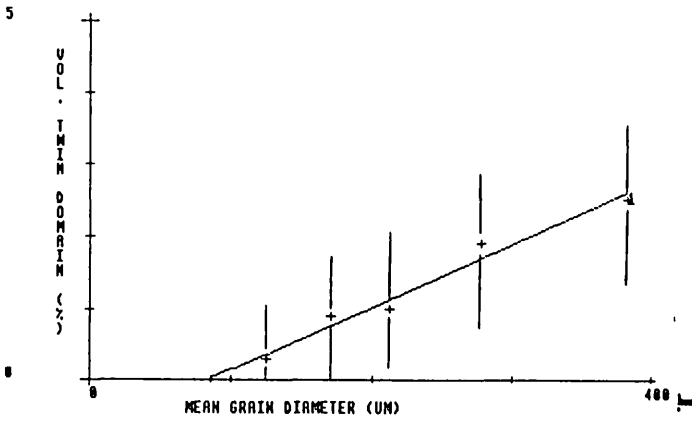
KCM-24: TWIN SET = 1/2: MEAN GRAIN DIAMETER/VOL. TWIN DOMAIN



KCM-25: TWIN SET = 1/2: MEAN GRAIN DIAMETER/VOL. TWIN DOMAIN



KCM-26: TWIN SET = 1/2: MEAN GRAIN DIAMETER/VOL. TWIN DOMAIN



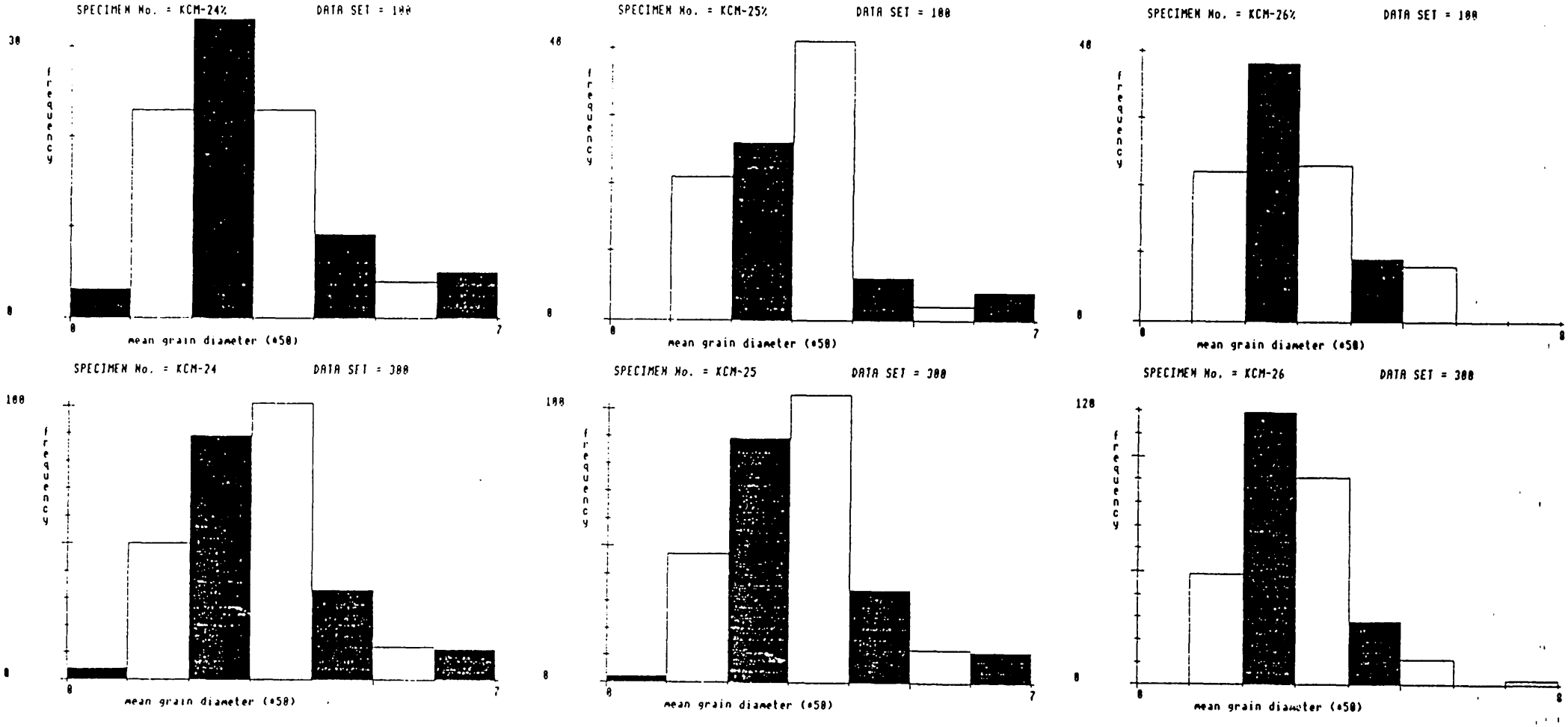


FIGURE 4.24 Histograms showing the number of data points (grains) in each of the grain size intervals for the diagrams of Fig. 4.23, the 600°C series of experiments upon Carrara Marble see section 4.6.2.6. The individual samples are identified by their headings as for Fig. 4.11.

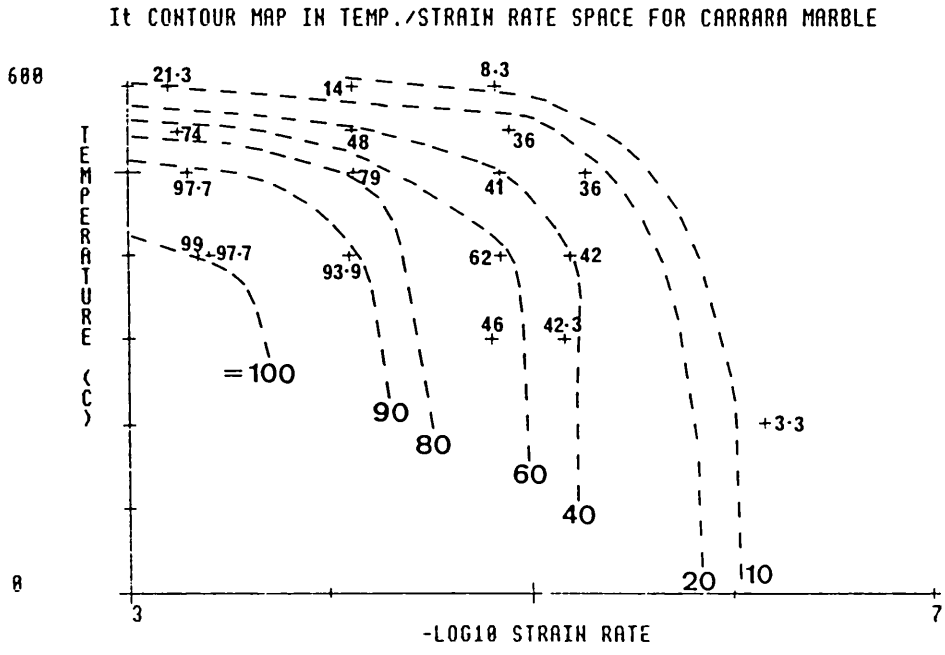


FIGURE 4.25 It contour map in Temperature/Strain Rate space for the series of experiments performed upon Carrara Marble. The 10% It contour defines the Twinning Field Boundary. See Table 4.3 for the corresponding experimental and textural parameters.

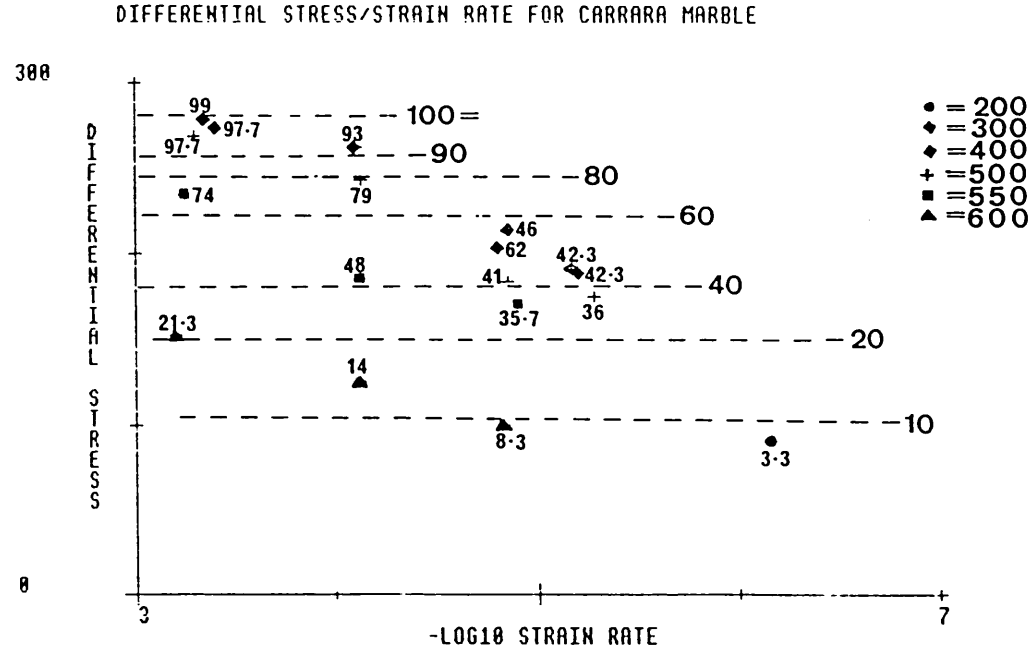


FIGURE 4.26 It contour map in Differential Stress/Strain Rate space for Carrara Marble series of experiments, with the temperature of the experiments superimposed.

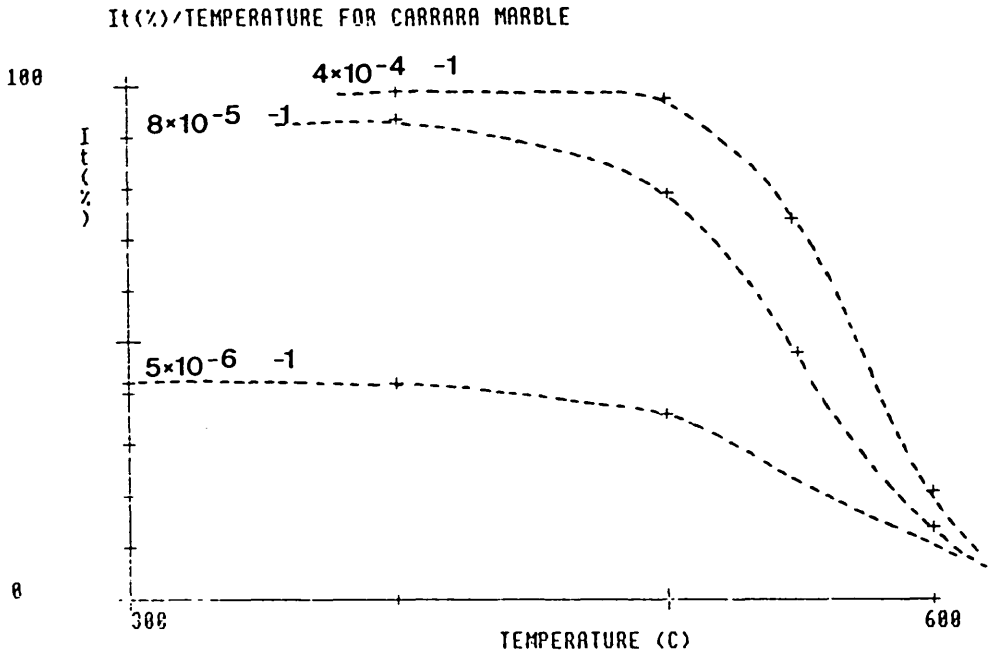


FIGURE 4.27 Iso-Strain Rate sections through Fig. 4.25, demonstrating the decrease in twinning activity as represented by the It parameter with increasing temperature at various Strain Rates. See Table 4.3 for the experimental and textural parameters which correspond to the crosses in this Figure.

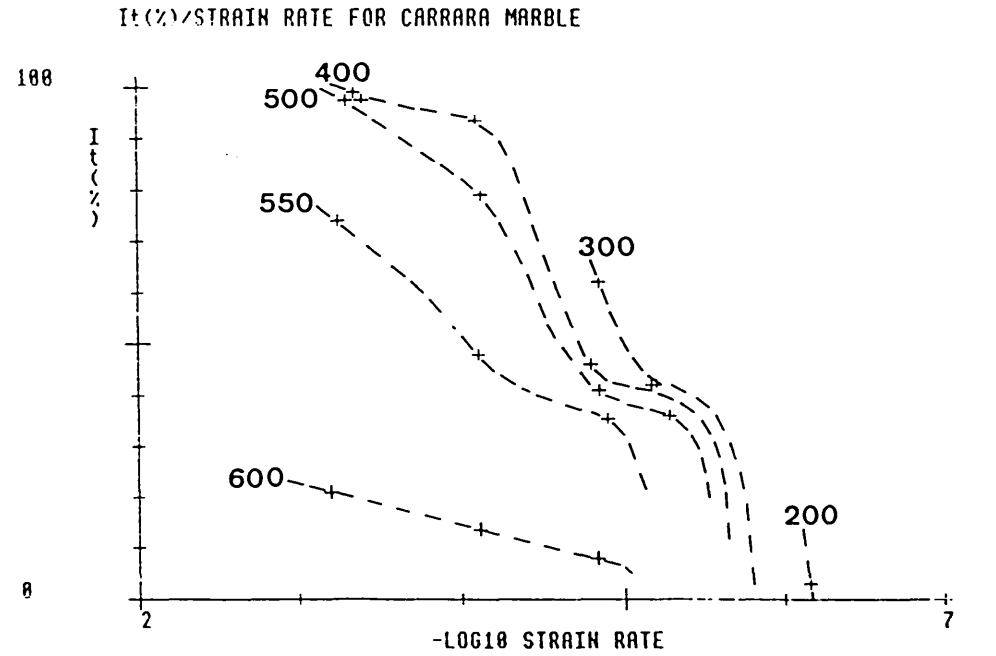


FIGURE 4.28 Iso-Temperature sections through Fig. 4.25, demonstrating the decrease in twinning activity as represented by the It parameter with decreasing Strain Rate at various temperatures. See Table 4.3 for the experimental and textural parameters which correspond to the crosses in this Figure.

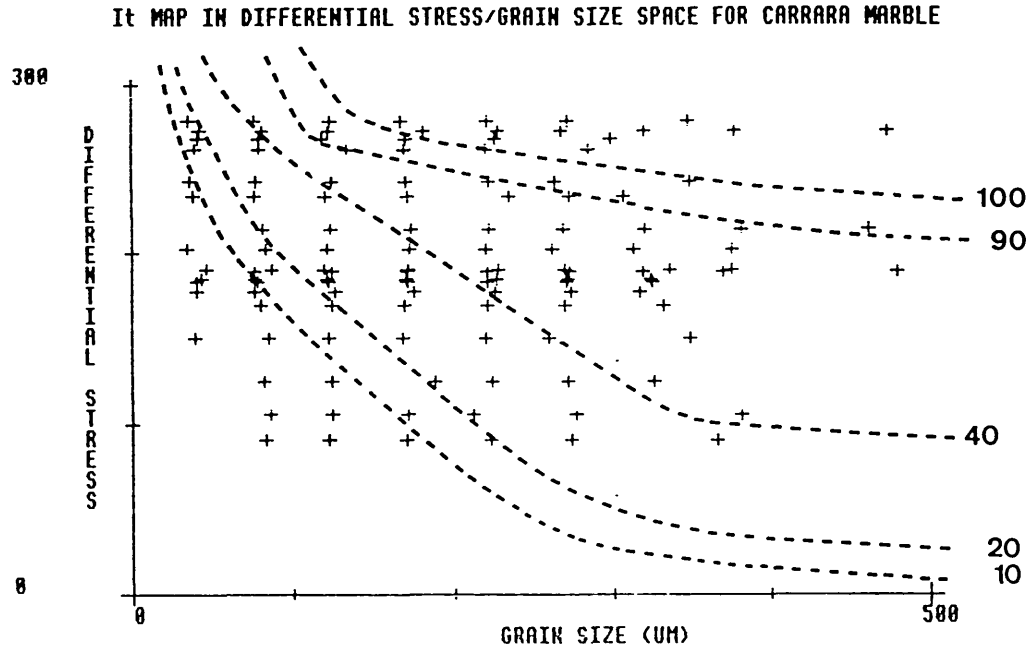


FIGURE 4.29 It contour map for the Carrara Marble series of experiments plotted in Differential Stress/Grain Size space. In order to enable clarity the principal contours only are shown. The 10% It contour defines the Twinning Field Boundary. As discussed in the text, in order to obtain as many data points as possible from a given experimental material, the textural data determined was divided on the basis of mean grain size. Therefore for each sample a series of It data points over a range of grain sizes, but at a unique level of Differential Stress are obtained. Thus the data manifests itself in a series of data points forming an horizontal

line when plotted in the manner shown in this diagram. The reader is referred to Table 4.3 for the overall It/mean grain size parameters of the sample as a whole.

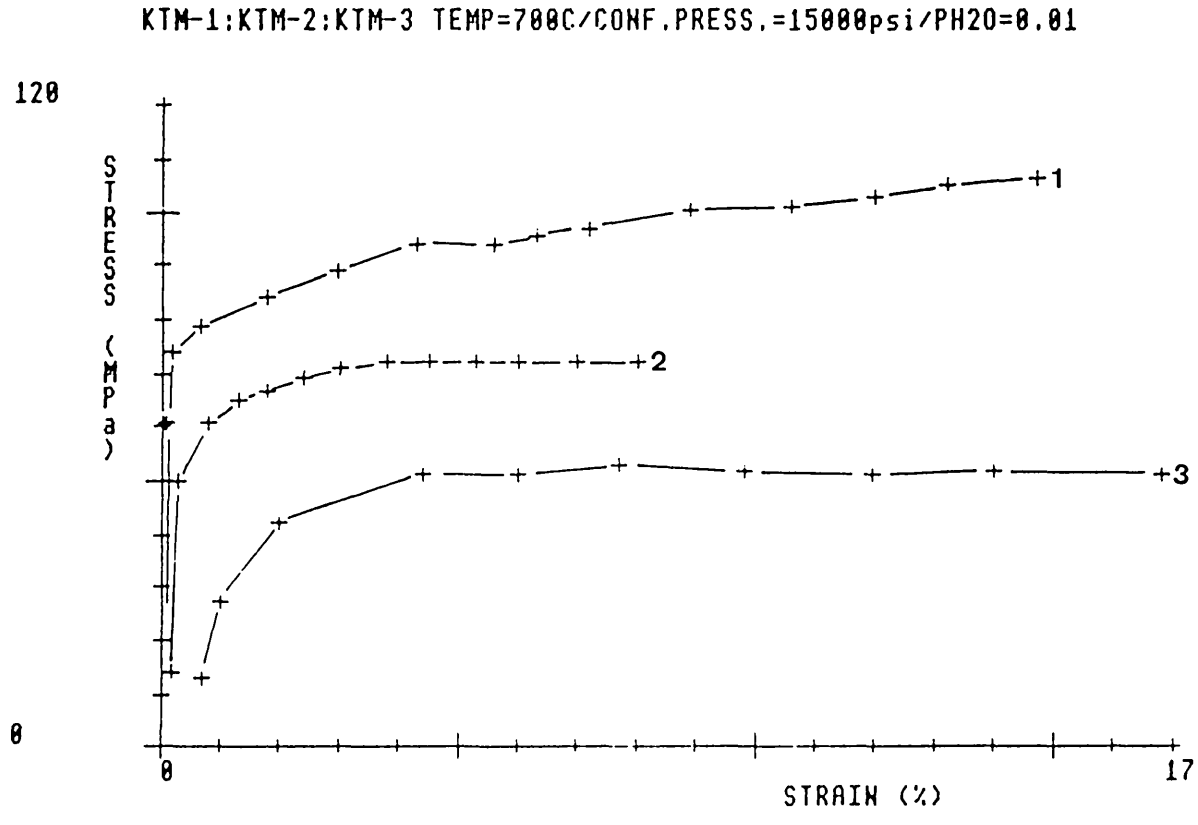


FIGURE 4.30 Stress/strain curves obtained for the 700°C series of experiments performed upon Taiwanese Marble, see section 4.7.3.1. 1 = KTM-1, 2 = KTM-2 and 3 = KTM-3

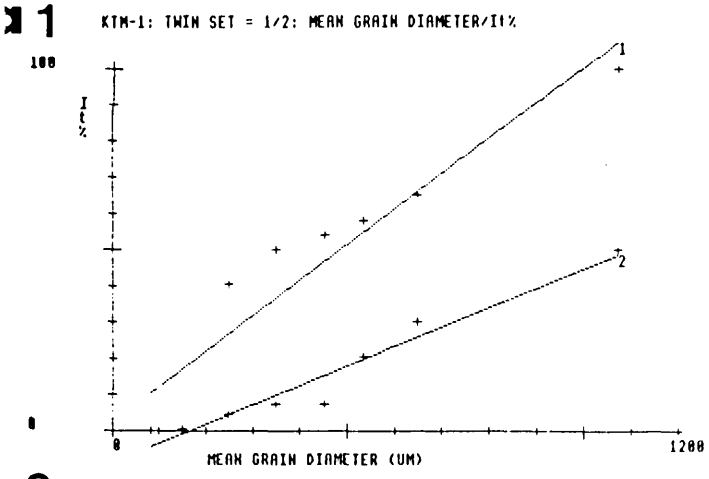
FIGURE 4.31 Textural data for Taiwanese Marble deformed at 700°C.

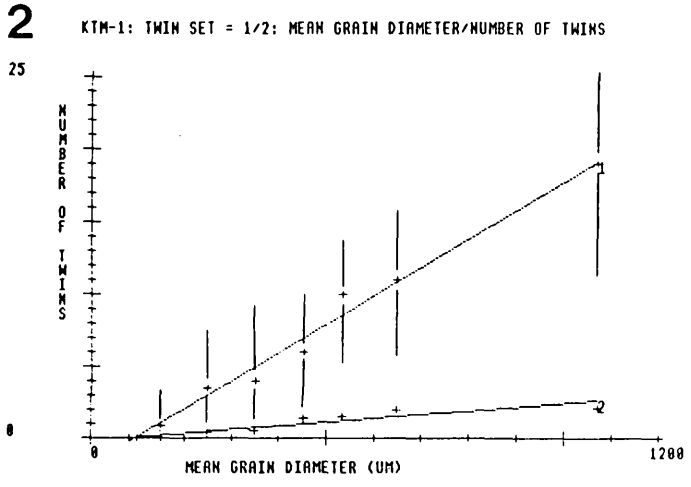
This series of diagrams present the twinning activity data determined for the three experiments (a, b and c respectively) deformed at this temperature, plotted as a function of grain size. There are three diagrams, plotting It, number of twins, and percentage volume twin domain (1, 2 and 3 respectively).

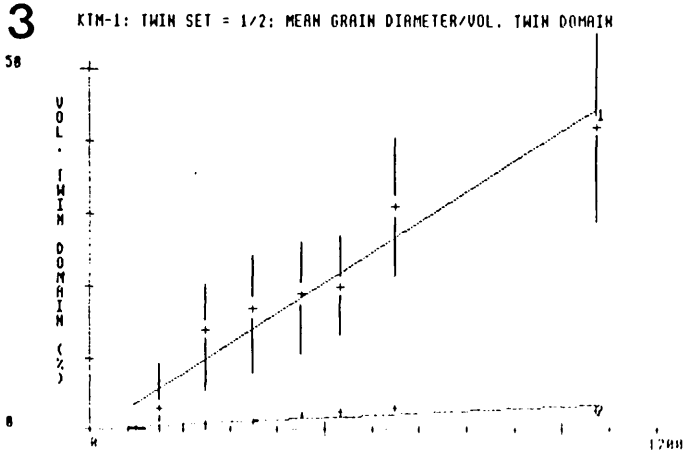
For each sample two twin sets have been analysed, the primary, or principal, twin set and the secondary twin set (1 and 2 respectively). The range bars shown for the relevant groups represent the full range of the values determined for each grain size interval. The individual experiments are identified by their respective headings.

See text for discussion.

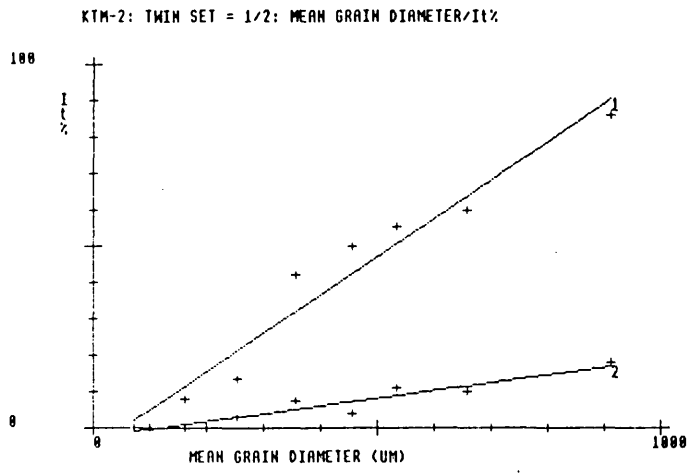
a

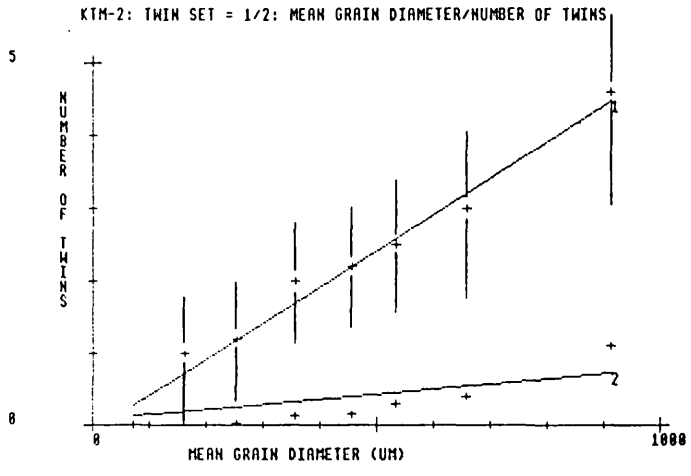

KTM-1: TWIN SET = 1/2: MEAN GRAIN DIAMETER/It%
100
It%
0
0
1200
MEAN GRAIN DIAMETER (UM)

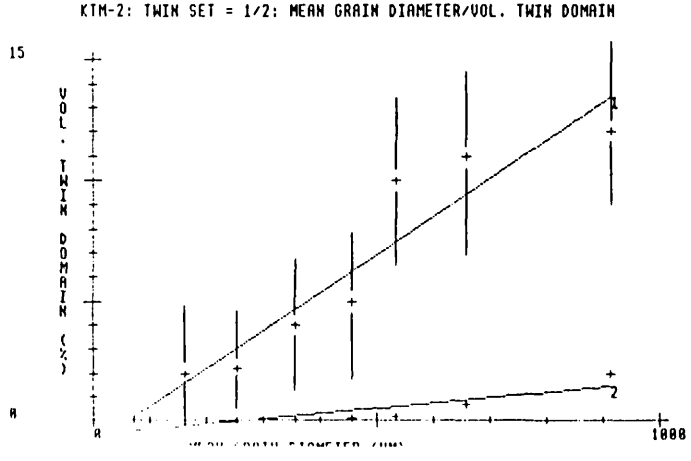

KTM-1: TWIN SET = 1/2: MEAN GRAIN DIAMETER/NUMBER OF TWINS
25
NUMBER OF TWINS
0
0
1200
MEAN GRAIN DIAMETER (UM)


KTM-1: TWIN SET = 1/2: MEAN GRAIN DIAMETER/VOL. TWIN DOMAIN
50
VOL. TWIN DOMAIN (%)
0
0
1200

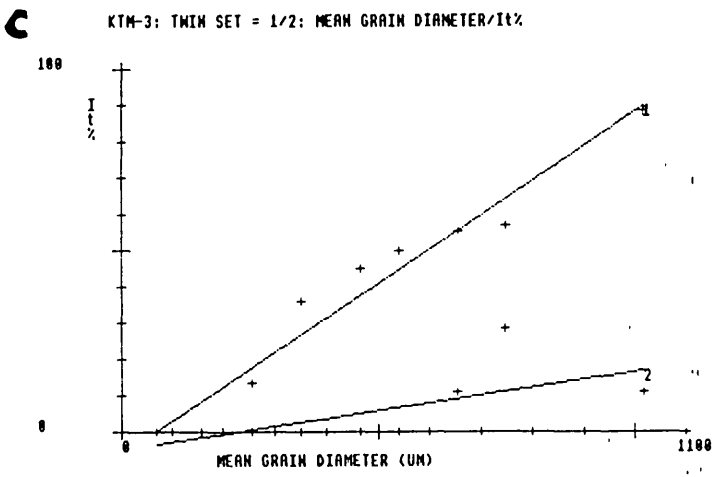
b

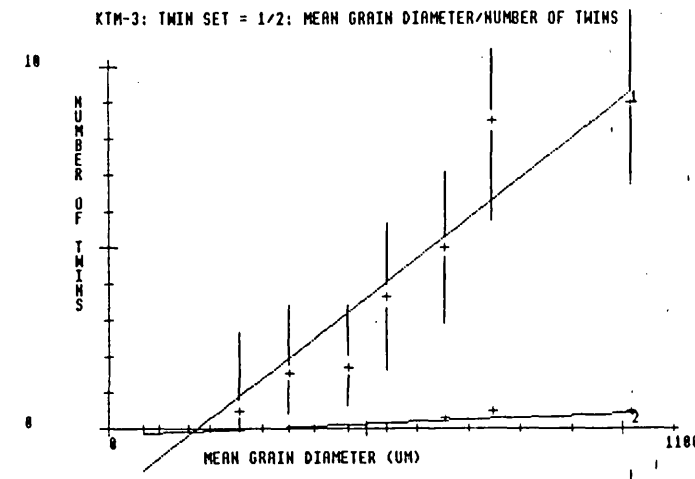

KTM-2: TWIN SET = 1/2: MEAN GRAIN DIAMETER/It%
100
It%
0
0
1000
MEAN GRAIN DIAMETER (UM)

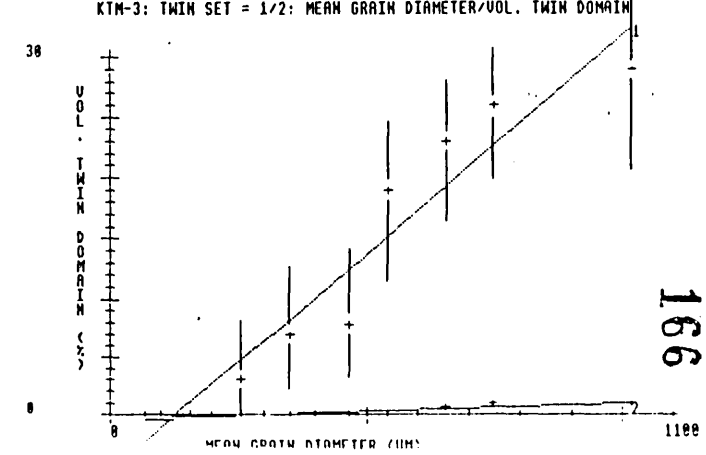

KTM-2: TWIN SET = 1/2: MEAN GRAIN DIAMETER/NUMBER OF TWINS
5
NUMBER OF TWINS
0
0
1000
MEAN GRAIN DIAMETER (UM)


KTM-2: TWIN SET = 1/2: MEAN GRAIN DIAMETER/VOL. TWIN DOMAIN
15
VOL. TWIN DOMAIN (%)
0
0
1000

c


KTM-3: TWIN SET = 1/2: MEAN GRAIN DIAMETER/It%
100
It%
0
0
1100
MEAN GRAIN DIAMETER (UM)


KTM-3: TWIN SET = 1/2: MEAN GRAIN DIAMETER/NUMBER OF TWINS
10
NUMBER OF TWINS
0
0
1100
MEAN GRAIN DIAMETER (UM)


KTM-3: TWIN SET = 1/2: MEAN GRAIN DIAMETER/VOL. TWIN DOMAIN
30
VOL. TWIN DOMAIN (%)
0
0
1100

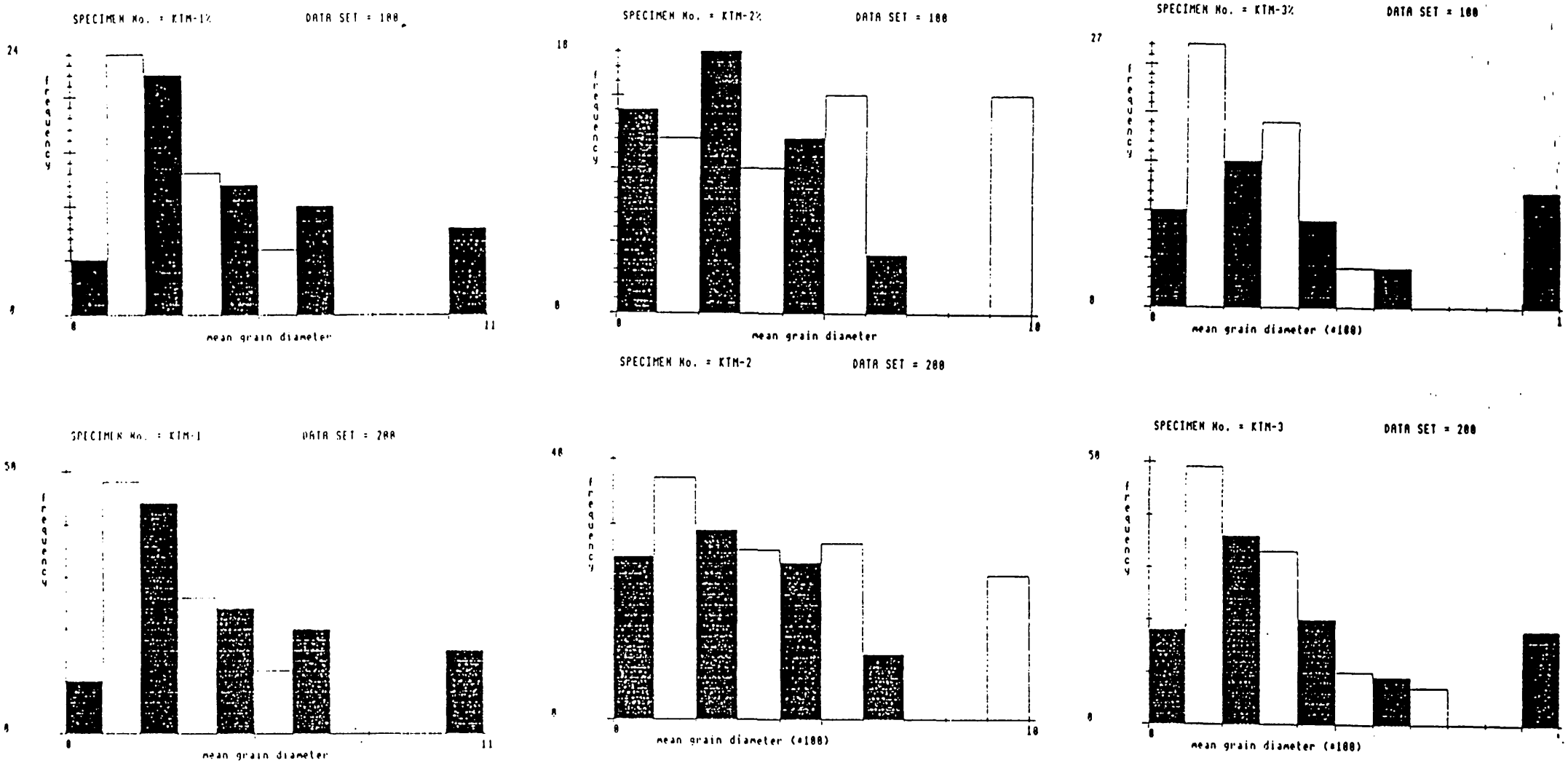


FIGURE 4.32 Histograms showing the number of data points (grains) in each of the grain size intervals for the diagrams of Fig. 4.31, the 700°C series of experiments upon Taiwanese Marble, see section 4.7.3.1. The individual samples are identified by their headings as for Fig. 4.11.

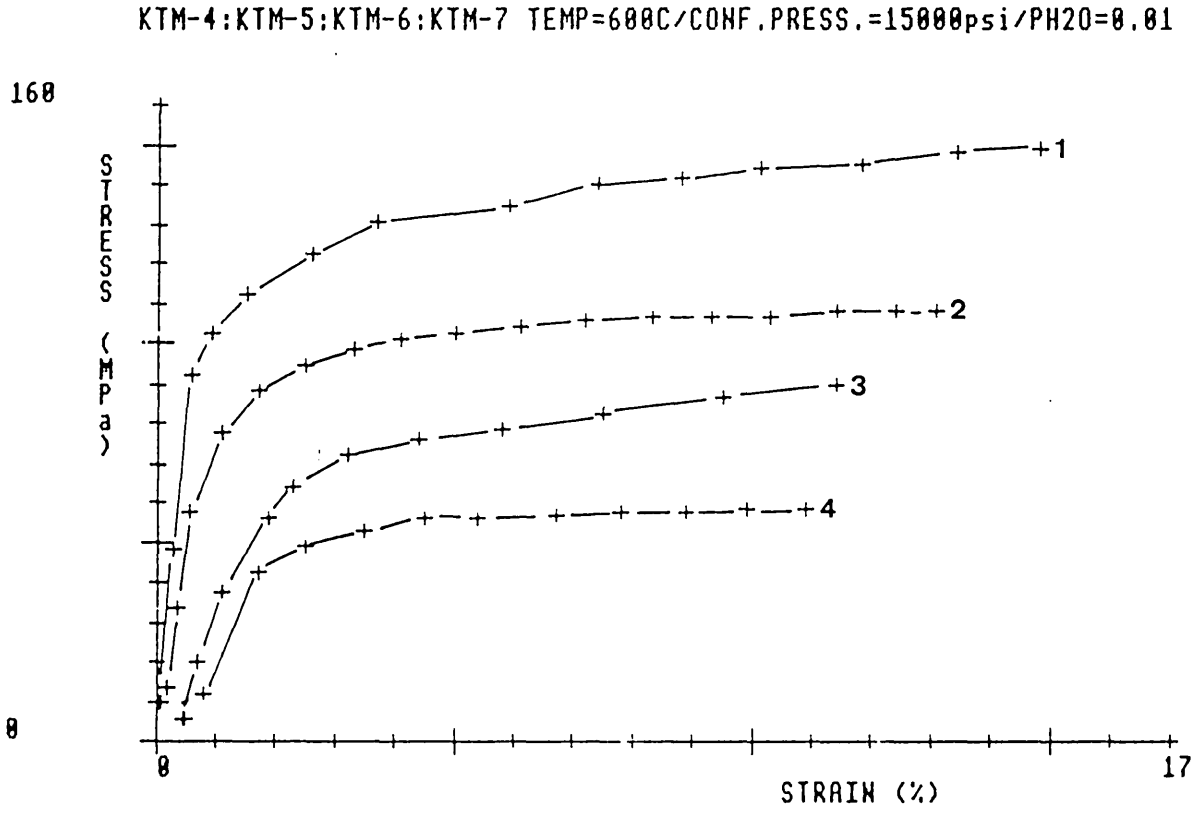


FIGURE 4.33 Stress/strain curves for the 600°C series of experiments performed upon Taiwanese Marble, see section 4.7.3.1. 1 = KTM-4, 2 = KTM-5, 3 = KTM-6 and 4 = KTM-7. Note that the duplicate experiment, KTM-15, has a stress/strain curve identical to that of KTM-4.

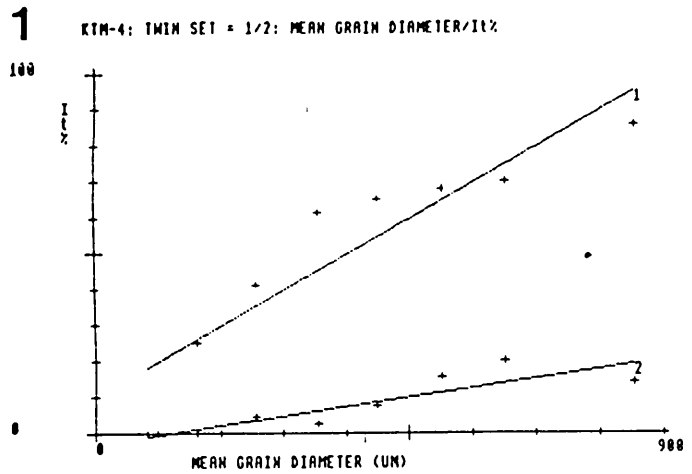
FIGURE 4.34 Textural data for Taiwanese Marble deformed at 600°C.

This series of diagrams present the twinning activity data determined for this series of experiments (a, b, c, d and e respectively) deformed at this temperature, plotted as a function of grain size. There are three diagrams, plotting It, number of twins, and percentage volume twin domain (1, 2 and 3 respectively).

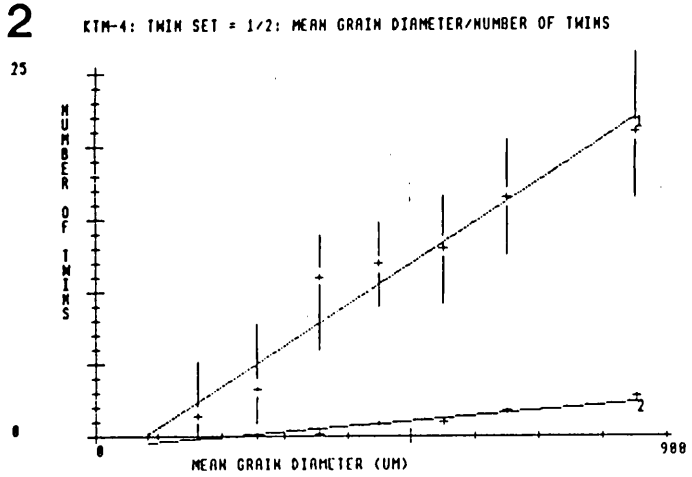
For each sample two twin sets have been analysed, the primary, or principal, twin set and the secondary twin set (1 and 2 respectively). The range bars shown for the relevant groups represent the full range of the values determined for each grain size interval. The individual experiments are identified by their respective headings.

See text for discussion.

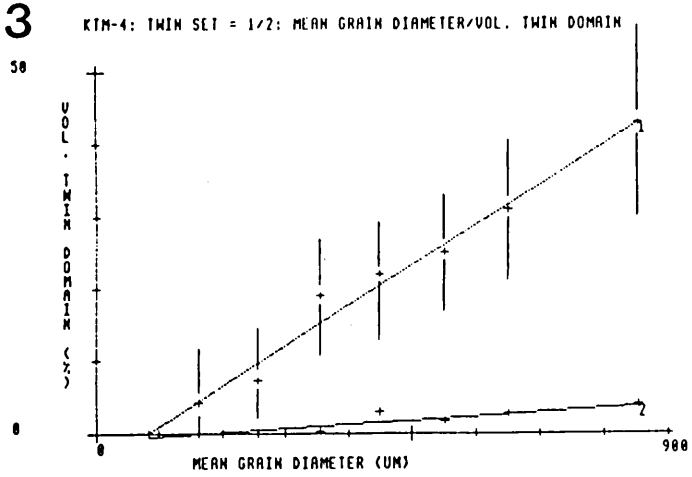
a 1


KTM-4: TWIN SET = 1/2: MEAN GRAIN DIAMETER/It%
100
0
It%
1
2
0
900
MEAN GRAIN DIAMETER (UM)

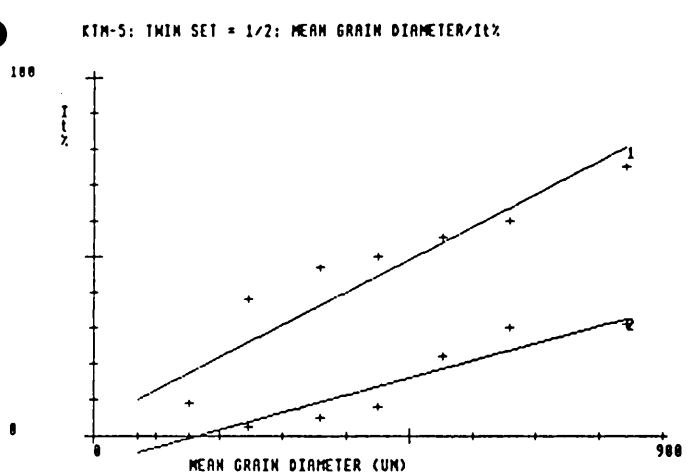
2

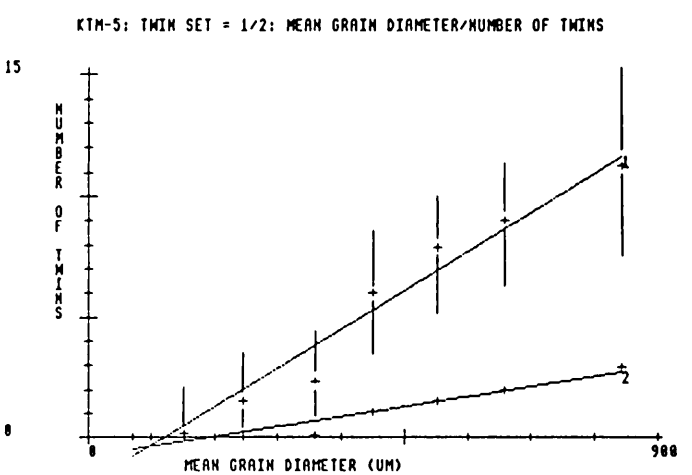

KTM-4: TWIN SET = 1/2: MEAN GRAIN DIAMETER/NUMBER OF TWINS
25
0
NUMBER OF TWINS
1
2
0
900
MEAN GRAIN DIAMETER (UM)

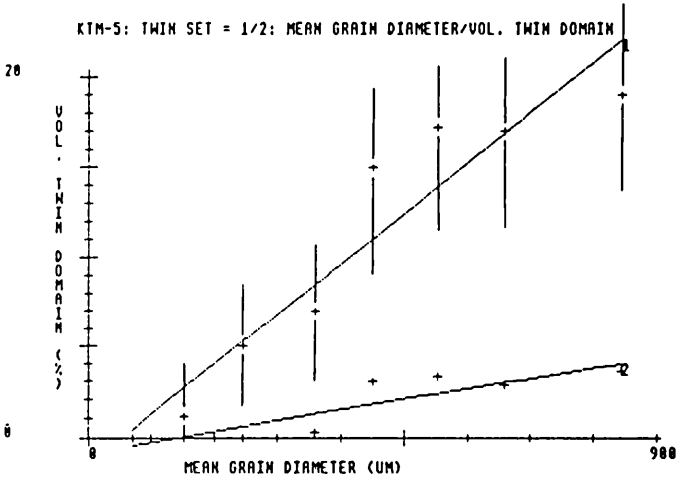
3


KTM-4: TWIN SET = 1/2: MEAN GRAIN DIAMETER/VOL. TWIN DOMAIN
50
0
VOL. TWIN DOMAIN (%)
1
2
0
900
MEAN GRAIN DIAMETER (UM)

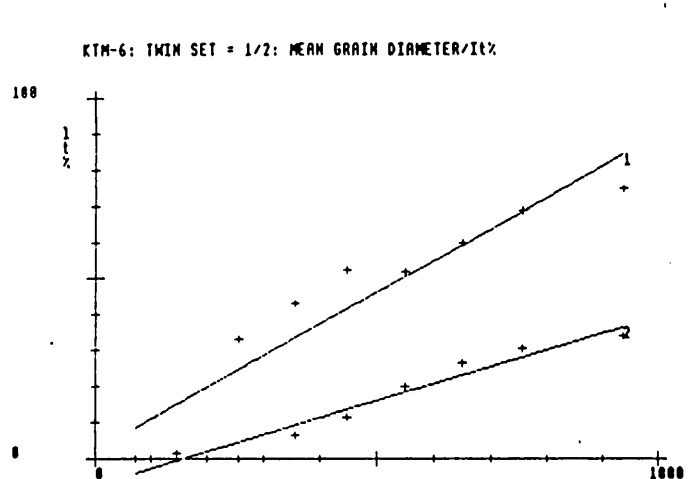
b

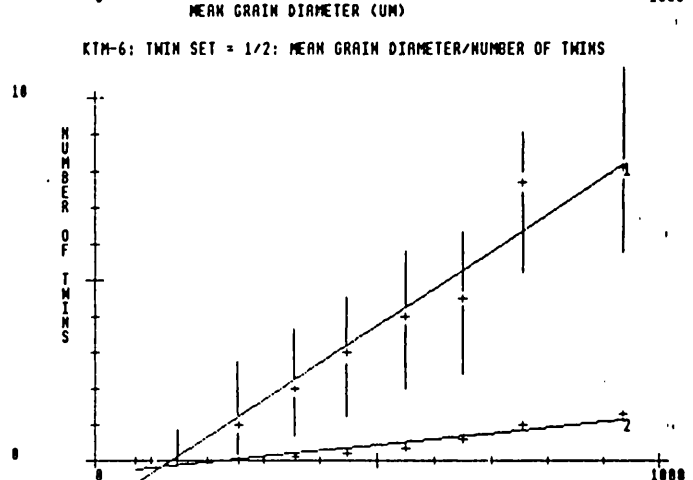

KTM-5: TWIN SET = 1/2: MEAN GRAIN DIAMETER/It%
100
0
It%
1
2
0
900
MEAN GRAIN DIAMETER (UM)

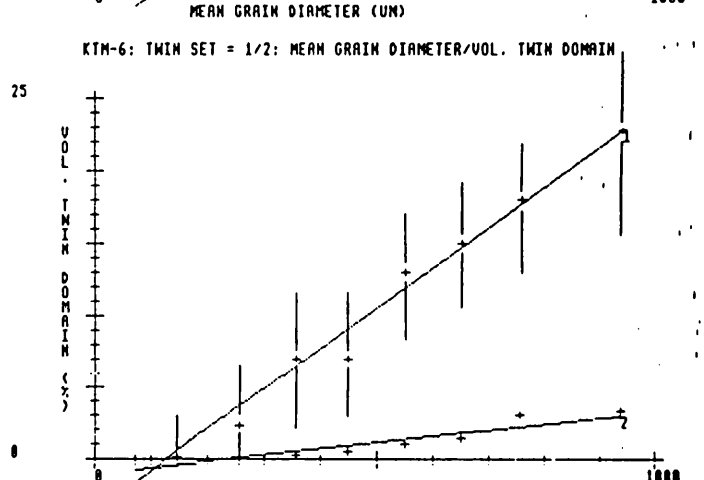

KTM-5: TWIN SET = 1/2: MEAN GRAIN DIAMETER/NUMBER OF TWINS
15
0
NUMBER OF TWINS
1
2
0
900
MEAN GRAIN DIAMETER (UM)


KTM-5: TWIN SET = 1/2: MEAN GRAIN DIAMETER/VOL. TWIN DOMAIN
20
0
VOL. TWIN DOMAIN (%)
1
2
0
900
MEAN GRAIN DIAMETER (UM)

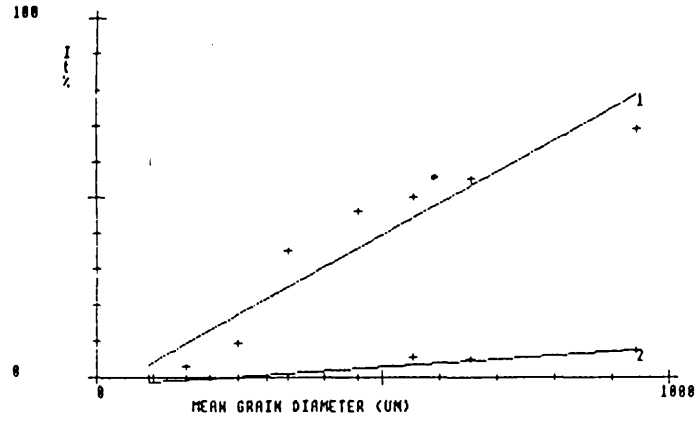
c


KTM-6: TWIN SET = 1/2: MEAN GRAIN DIAMETER/It%
100
0
It%
1
2
0
1000
MEAN GRAIN DIAMETER (UM)

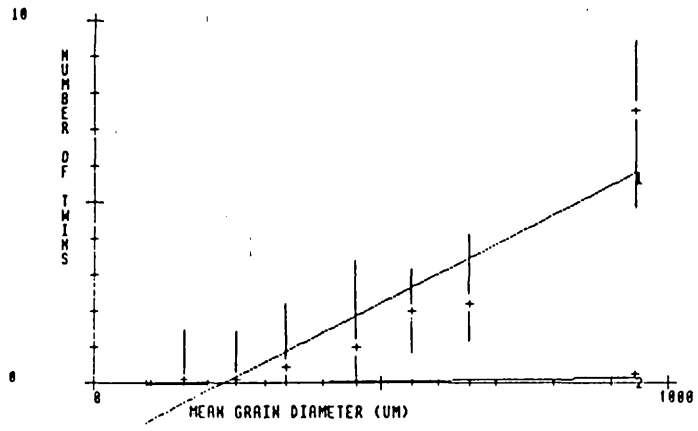

KTM-6: TWIN SET = 1/2: MEAN GRAIN DIAMETER/NUMBER OF TWINS
10
0
NUMBER OF TWINS
1
2
0
1000
MEAN GRAIN DIAMETER (UM)


KTM-6: TWIN SET = 1/2: MEAN GRAIN DIAMETER/VOL. TWIN DOMAIN
25
0
VOL. TWIN DOMAIN (%)
1
2
0
1000
MEAN GRAIN DIAMETER (UM)

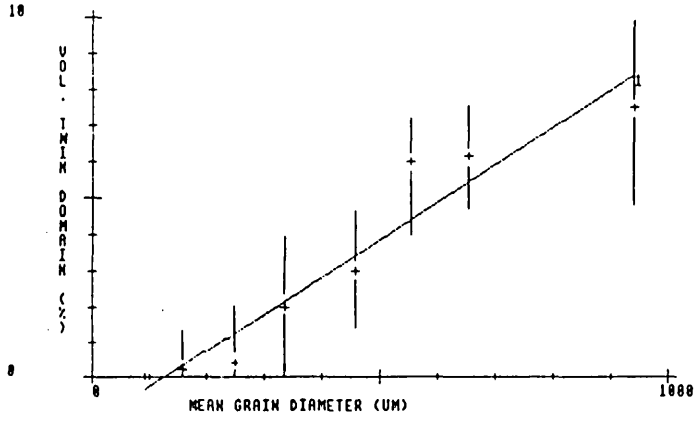
d1


KTM-7: TWIN SET = 1/2: MEAN GRAIN DIAMETER/It%
100
0
It%
1
2
0
1000
MEAN GRAIN DIAMETER (UM)

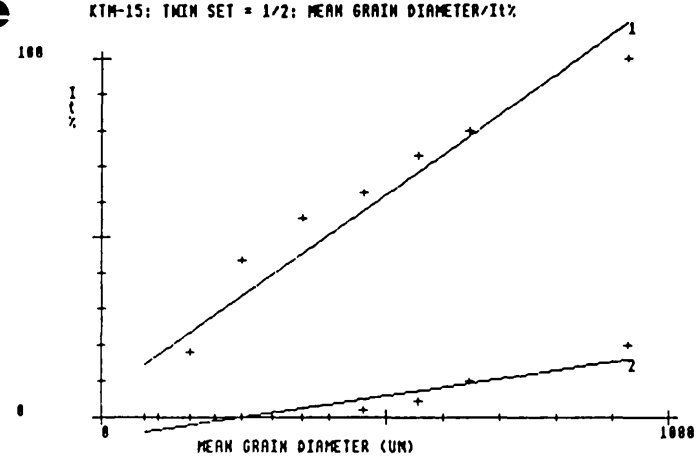
2

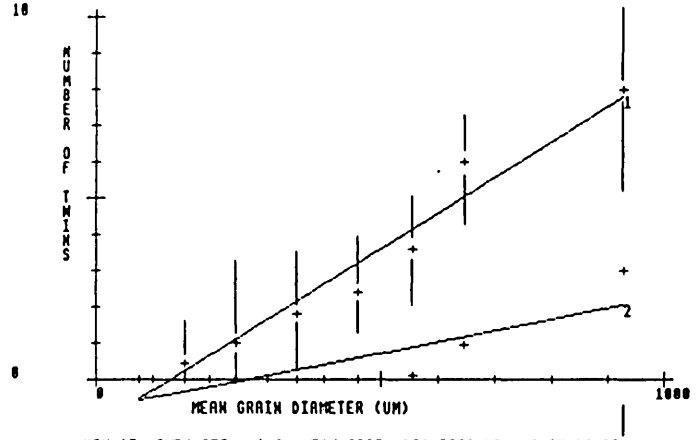

KTM-7: TWIN SET = 1/2: MEAN GRAIN DIAMETER/NUMBER OF TWINS
10
0
NUMBER OF TWINS
1
2
0
1000
MEAN GRAIN DIAMETER (UM)

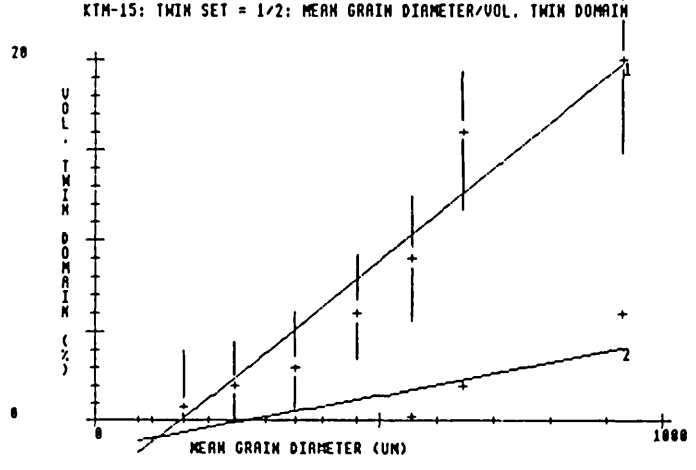
3


KTM-7: TWIN SET = 1/2: MEAN GRAIN DIAMETER/VOL. TWIN DOMAIN
10
0
VOL. TWIN DOMAIN (%)
1
0
1000
MEAN GRAIN DIAMETER (UM)

e


KTM-15: TWIN SET = 1/2: MEAN GRAIN DIAMETER/It%
100
0
It%
1
2
0
1000
MEAN GRAIN DIAMETER (UM)


KTM-15: TWIN SET = 1/2: MEAN GRAIN DIAMETER/NUMBER OF TWINS
10
0
NUMBER OF TWINS
1
2
0
1000
MEAN GRAIN DIAMETER (UM)


KTM-15: TWIN SET = 1/2: MEAN GRAIN DIAMETER/VOL. TWIN DOMAIN
20
0
VOL. TWIN DOMAIN (%)
1
2
0
1000
MEAN GRAIN DIAMETER (UM)

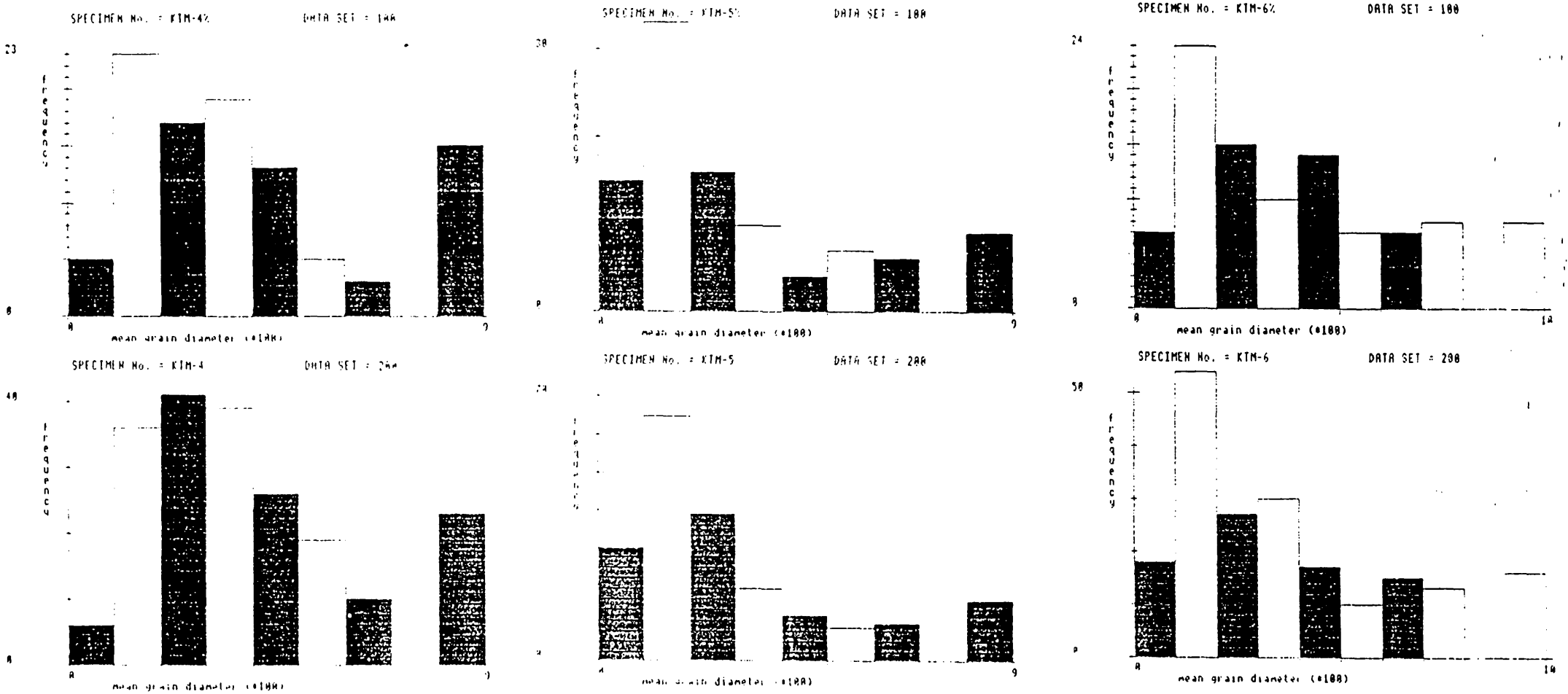
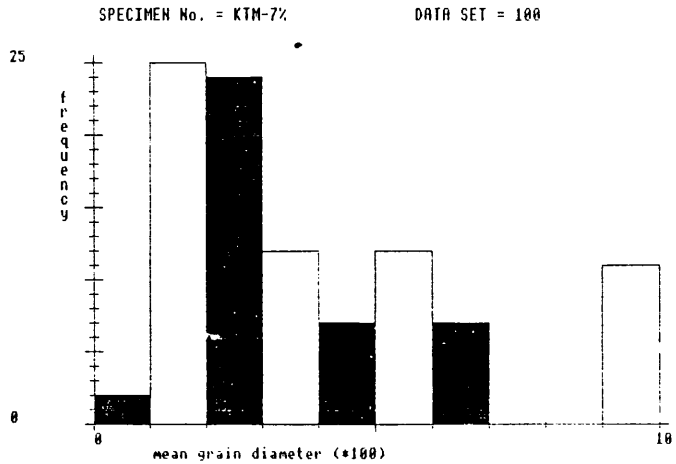
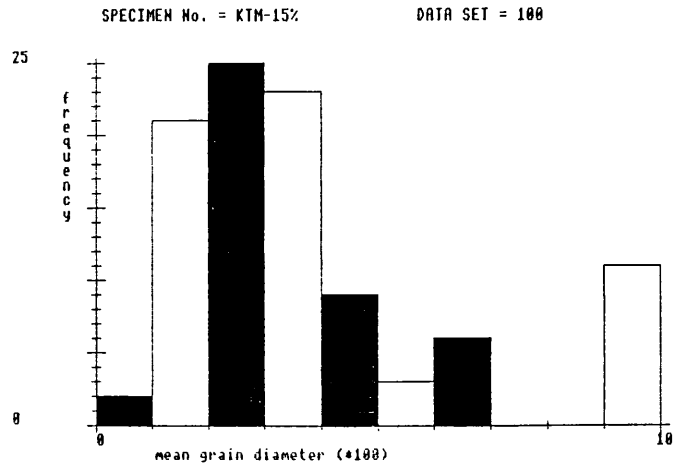
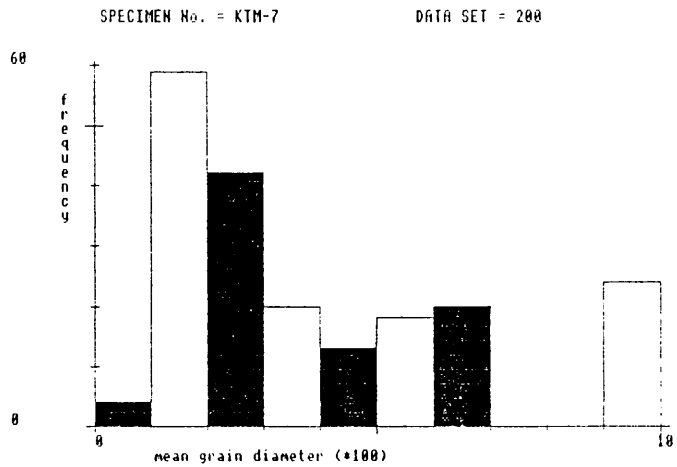
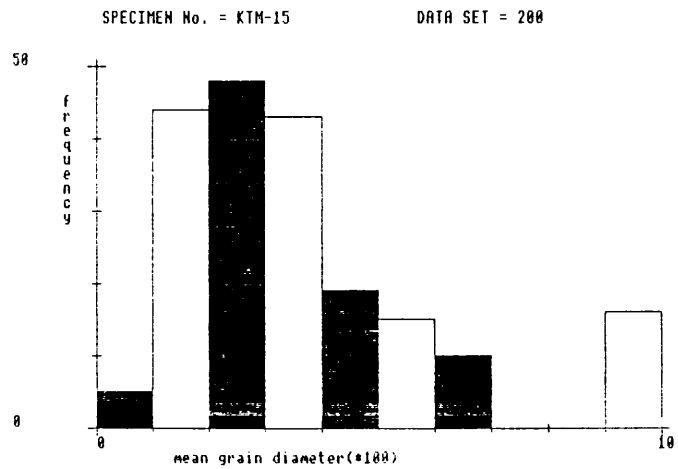


FIGURE 4.35 (Cont. over) Histograms showing the number of data points (grains) in each of the grain size intervals for the diagrams of Fig. 4.34, the 600°C series of experiments upon Taiwanese Marble, see section 4.7.3.2. The individual samples are identified by their headings as for Fig. 4.11.


SPECIMEN No. = KTM-7%
DATA SET = 100
25
0
frequency
0
10
mean grain diameter (*100)


SPECIMEN No. = KTM-15%
DATA SET = 100
25
0
frequency
0
10
mean grain diameter (*100)


SPECIMEN No. = KTM-7
DATA SET = 200
60
0
frequency
0
10
mean grain diameter (*100)


SPECIMEN No. = KTM-15
DATA SET = 200
50
0
frequency
0
10
mean grain diameter(*100)

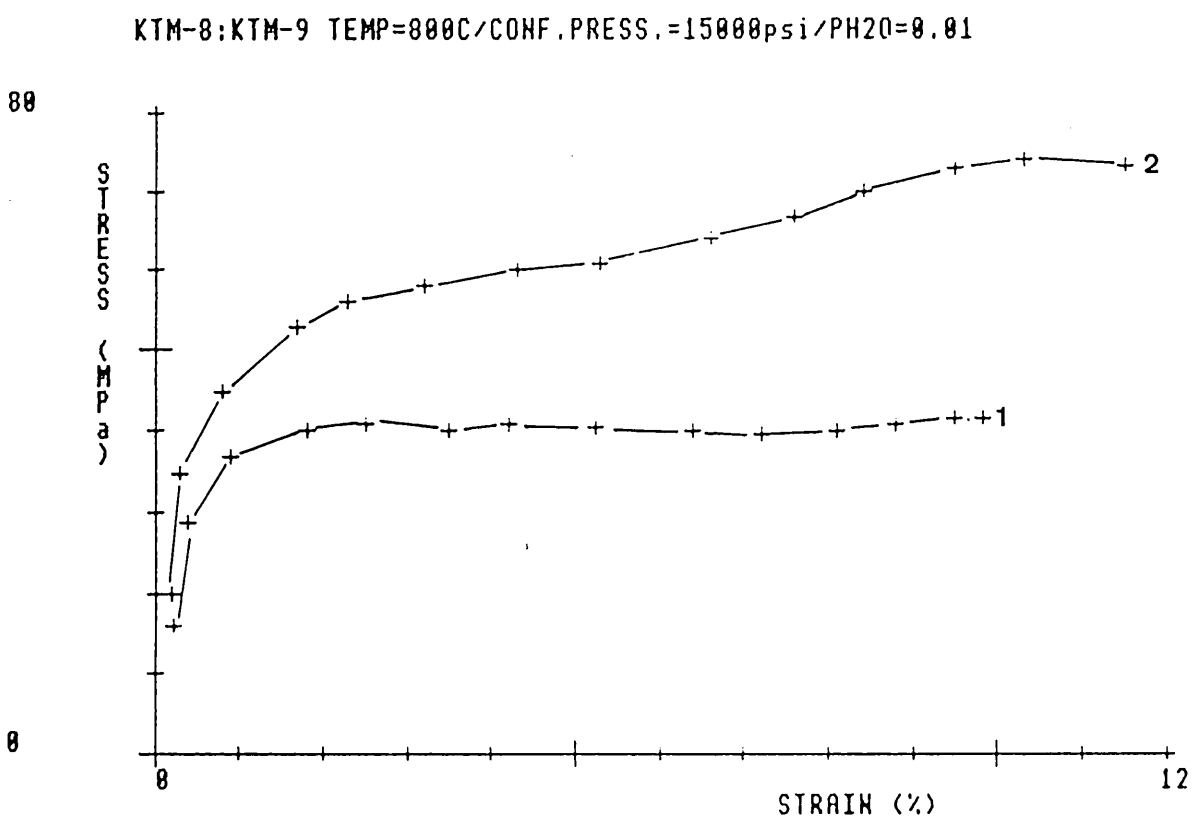


FIGURE 4.36 Stress/strain curves obtained for the 800°C series of experiments performed upon Taiwanese Marble, see section 4.7.3.3. 1 = KTM-8 and 2 = KTM-9.

FIGURE 4.37 Textural data for Taiwanese Marble deformed at 800°C.

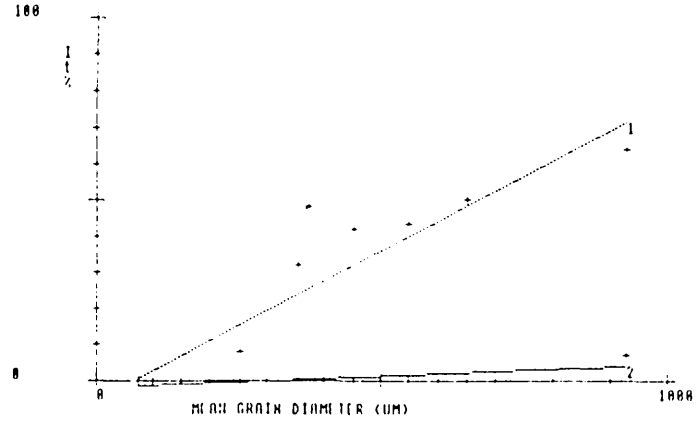
This series of diagrams present the twinning activity data determined for these two experiments (a and b respectively) deformed at this temperature, plotted as a function of grain size. There are three diagrams, plotting It, number of twins, and percentage volume twin domain (1, 2 and 3 respectively).

For each sample two twin sets have been analysed, the primary, or principal, twin set and the secondary twin set (1 and 2 respectively). The range bars shown for the relevant groups represent the full range of the values determined for each grain size interval. The individual experiments are identified by their respective headings.

See text for discussion.

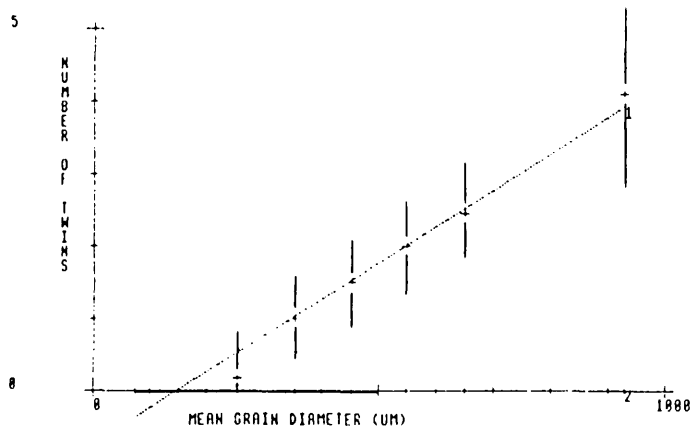
a 1

KTM-8: TWIN SET = 1/2: MEAN GRAIN DIAMETER/It%



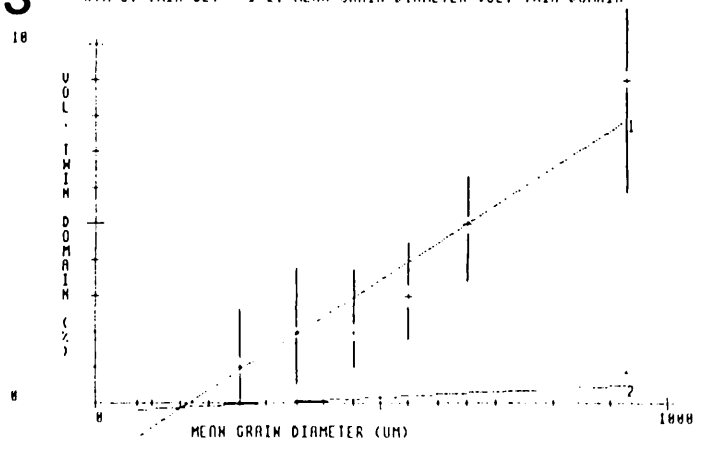
2

KTM-8: TWIN SET = 1/2: MEAN GRAIN DIAMETER/NUMBER OF TWINS



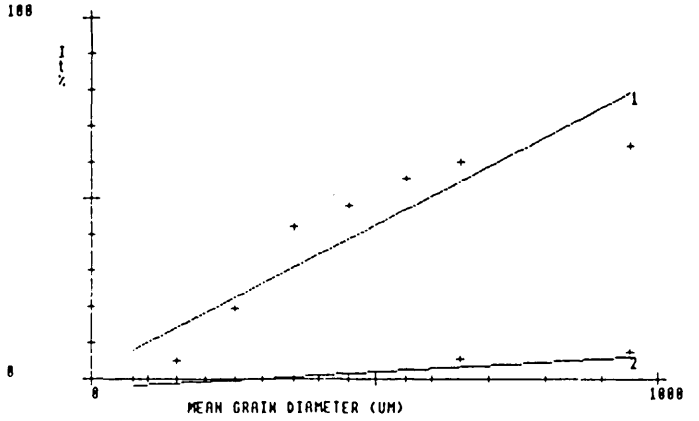
3

KTM-8: TWIN SET = 1/2: MEAN GRAIN DIAMETER/VOL. TWIN DOMAIN

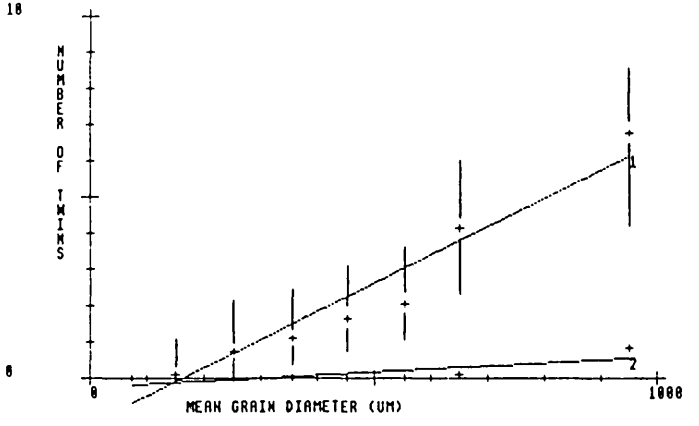


b

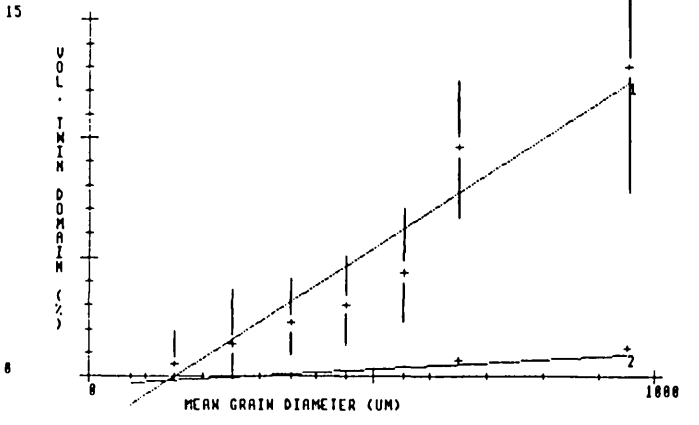
KTM-9: TWIN SET = 1/2: MEAN GRAIN DIAMETER/It%



KTM-9: TWIN SET = 1/2: MEAN GRAIN DIAMETER/NUMBER OF TWINS



KTM-9: TWIN SET = 1/2: MEAN GRAIN DIAMETER/VOL. TWIN DOMAIN



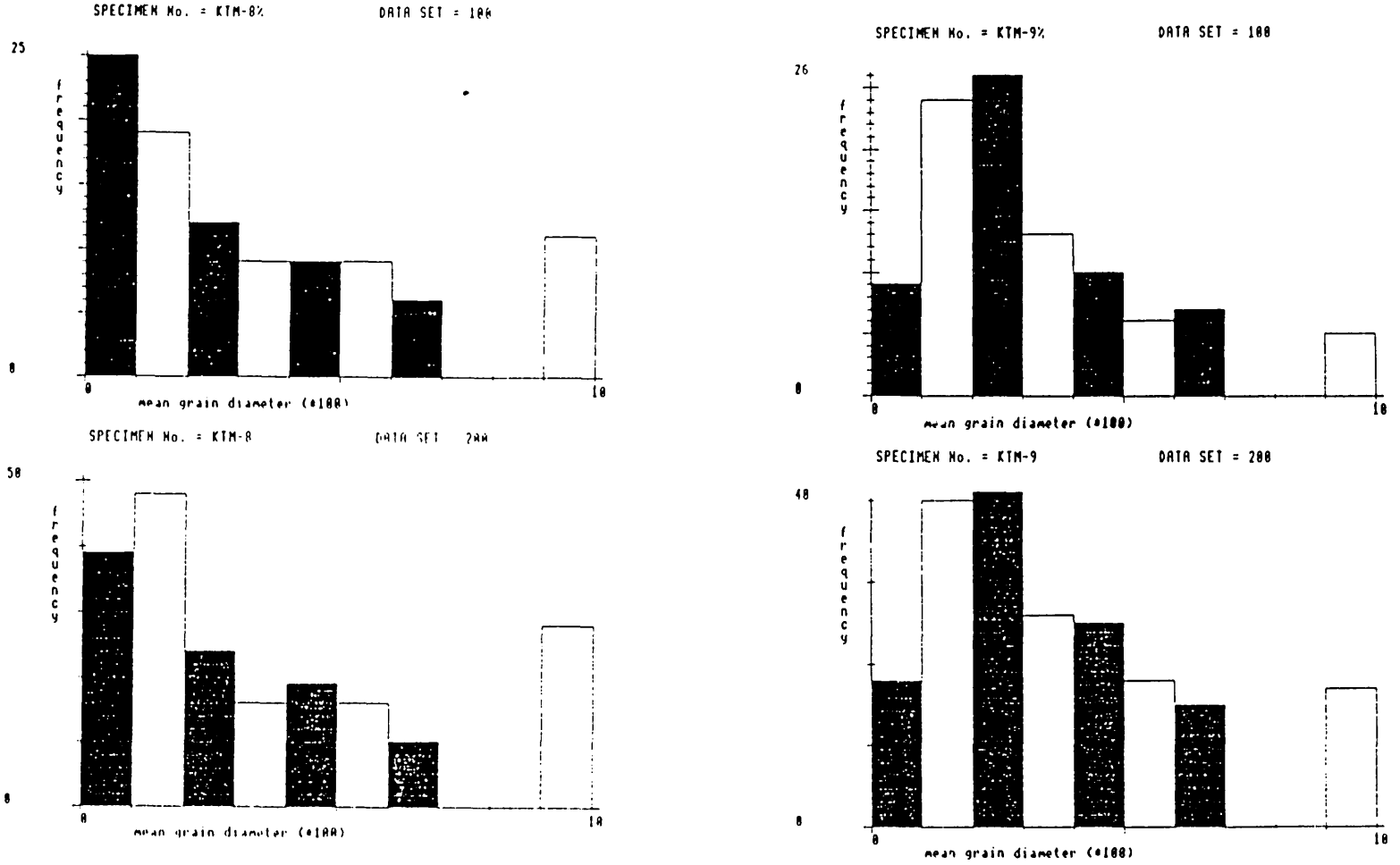


FIGURE 4.38 Histograms showing the number of data points (grains) in each of the grain size intervals for the diagrams of Fig. 4.37, the 800°C series of experiments upon Taiwanese Marble, see section 4.7.3.3. The individual samples are identified by their headings as for Fig. 4.11.

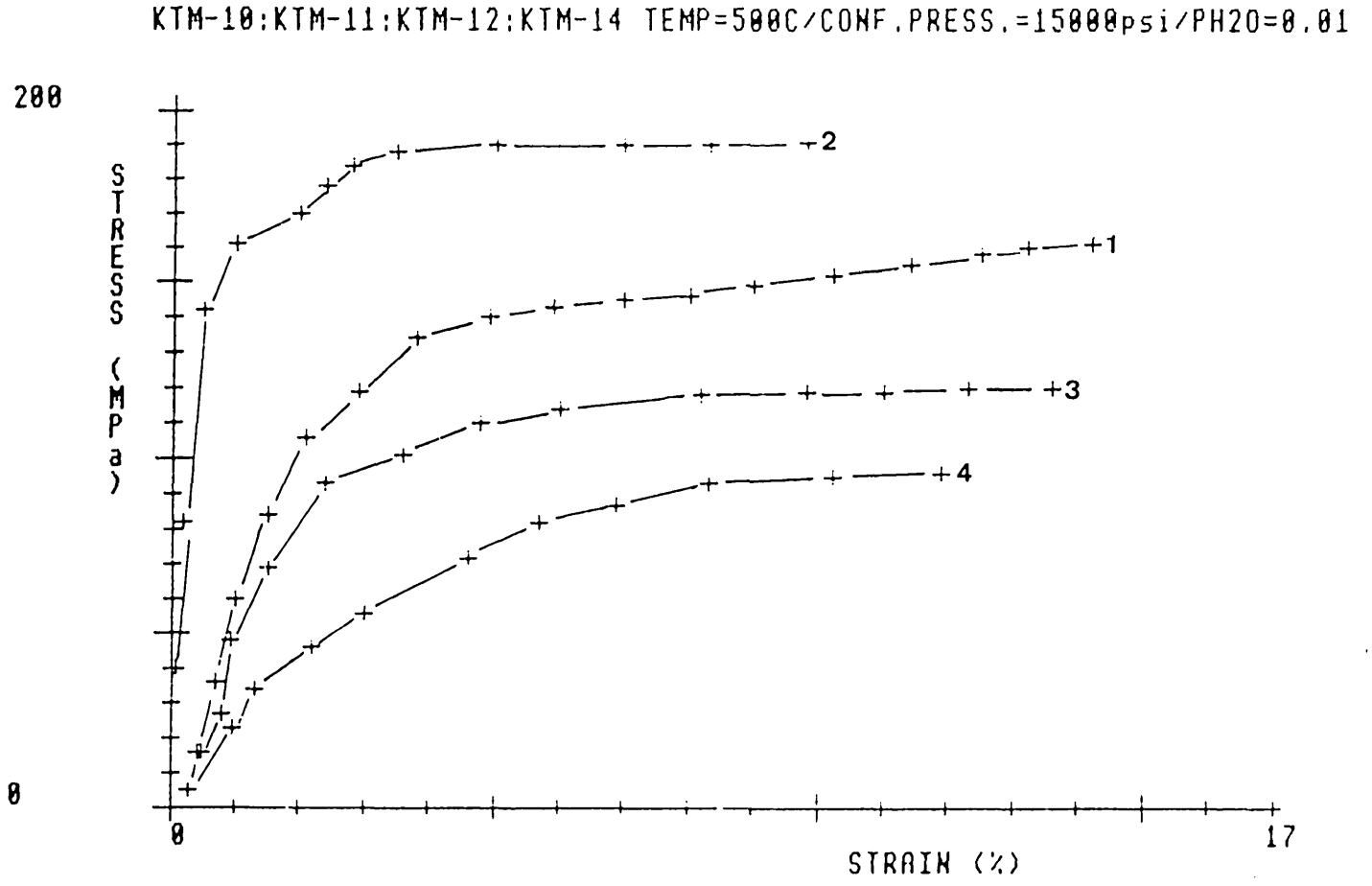


FIGURE 4.39 Stress/strain curves obtained for the 500°C series of experiments performed upon Taiwanese Marble, see section 4.7.3.4. 1 = KTM-10, 2 = KTM-11, 3 = KTM-12 and 4 = KTM-14

FIGURE 4.40 Textural data for Taiwanese Marble deformed at 500°C.

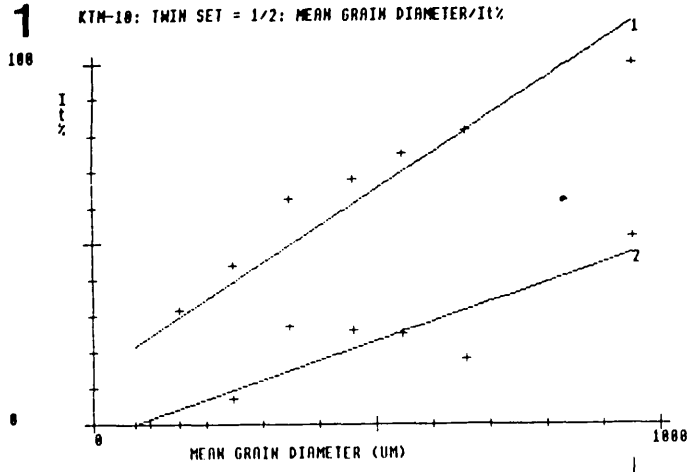
This series of diagrams present the twinning activity data determined for the series of experiments (a, b, c and d respectively) deformed at this temperature, plotted as a function of grain size. There are three diagrams, plotting It, number of twins, and percentage volume twin domain (1, 2 and 3 respectively).

For each sample two twin sets have been analysed, the primary, or principal, twin set and the secondary twin set (1 and 2 respectively). The range bars shown for the relevant groups represent the full range of the values determined for each grain size interval. The individual experiments are identified by their respective headings.

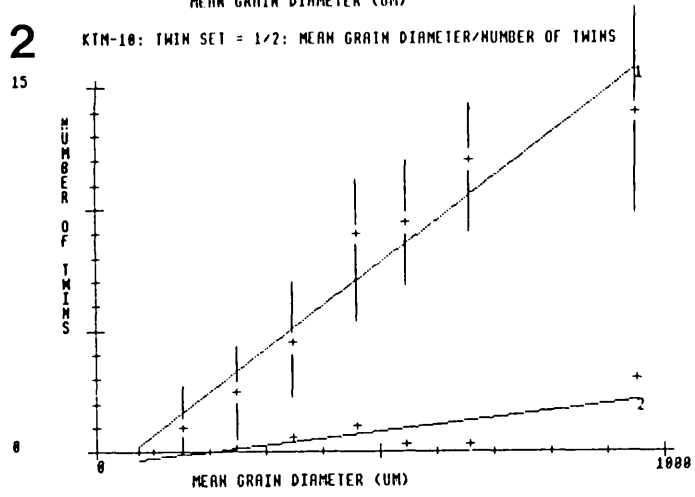
See text for discussion.

a

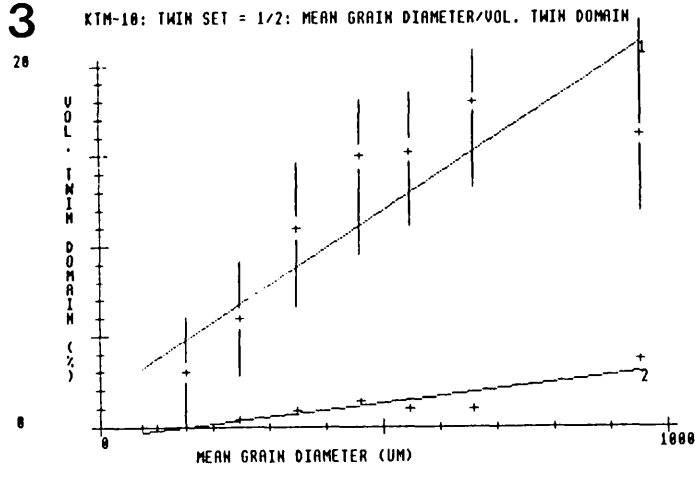
1


KTM-10: TWIN SET = 1/2: MEAN GRAIN DIAMETER/It%
100
0
It%
0
1000
MEAN GRAIN DIAMETER (UM)
1
2

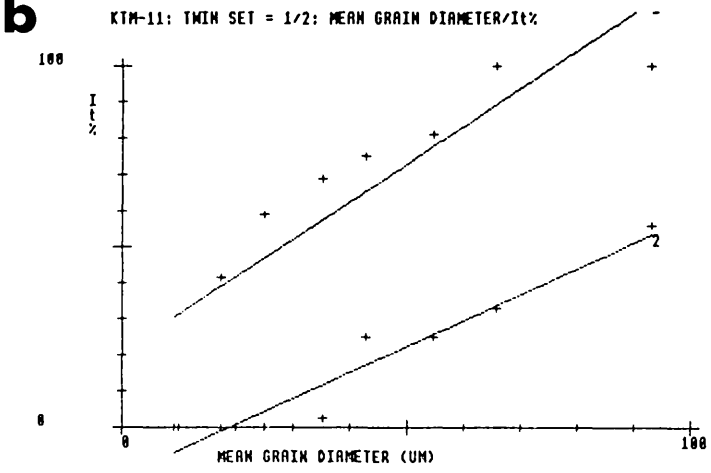
2

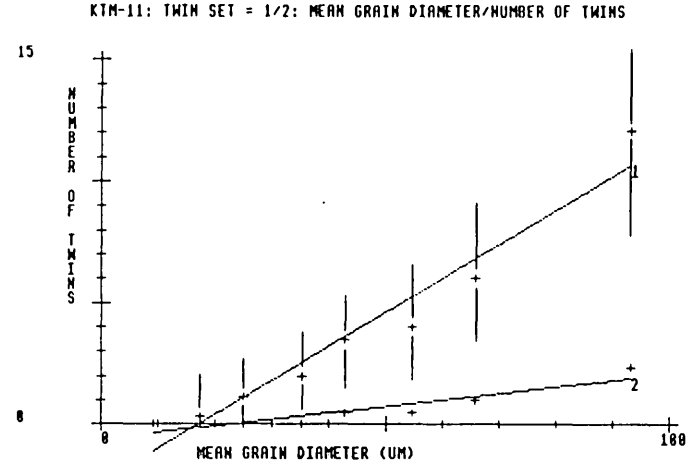

KTM-10: TWIN SET = 1/2: MEAN GRAIN DIAMETER/NUMBER OF TWINS
15
0
NUMBER OF TWINS
0
1000
MEAN GRAIN DIAMETER (UM)
1
2

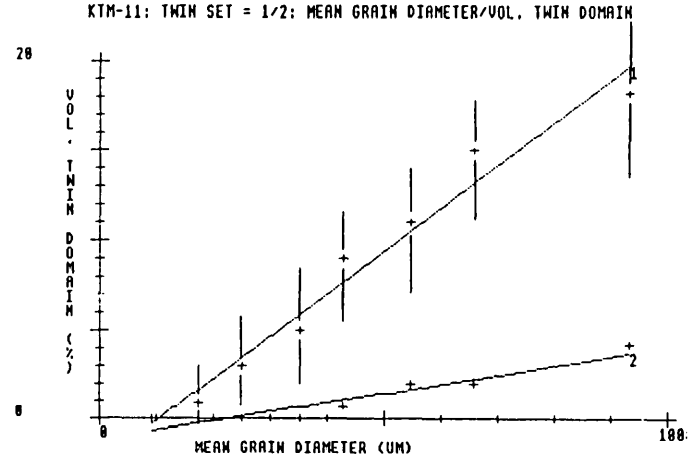
3


KTM-10: TWIN SET = 1/2: MEAN GRAIN DIAMETER/VOL. TWIN DOMAIN
20
0
VOL. TWIN DOMAIN (%)
0
1000
MEAN GRAIN DIAMETER (UM)
1
2

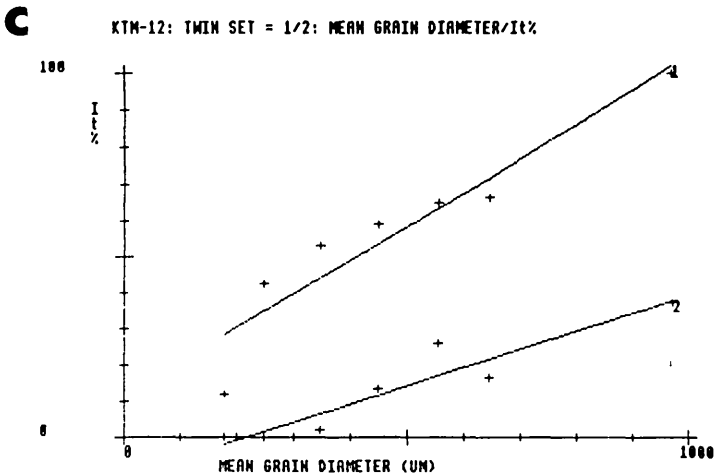
b

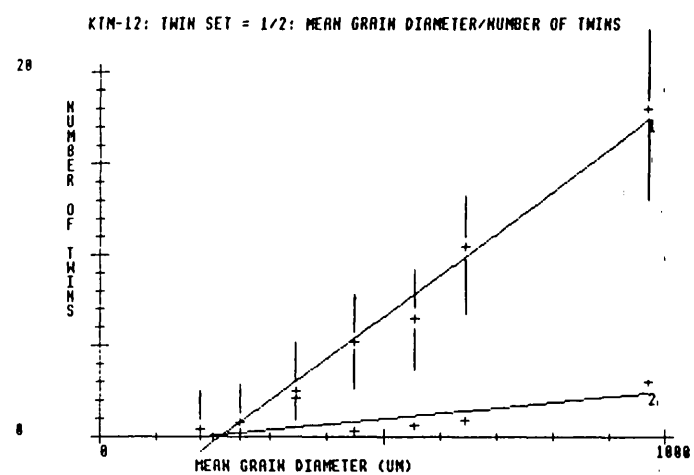

KTM-11: TWIN SET = 1/2: MEAN GRAIN DIAMETER/It%
100
0
It%
0
100
MEAN GRAIN DIAMETER (UM)
1
2

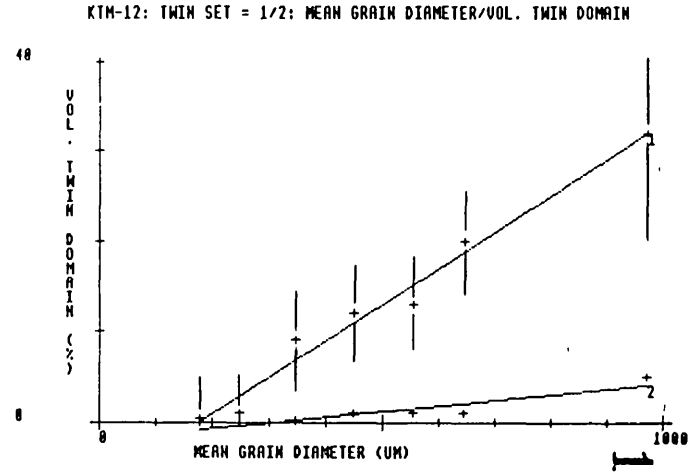

KTM-11: TWIN SET = 1/2: MEAN GRAIN DIAMETER/NUMBER OF TWINS
15
0
NUMBER OF TWINS
0
100
MEAN GRAIN DIAMETER (UM)
1
2


KTM-11: TWIN SET = 1/2: MEAN GRAIN DIAMETER/VOL. TWIN DOMAIN
20
0
VOL. TWIN DOMAIN (%)
0
100
MEAN GRAIN DIAMETER (UM)
1
2

c


KTM-12: TWIN SET = 1/2: MEAN GRAIN DIAMETER/It%
100
0
It%
0
1000
MEAN GRAIN DIAMETER (UM)
1
2


KTM-12: TWIN SET = 1/2: MEAN GRAIN DIAMETER/NUMBER OF TWINS
20
0
NUMBER OF TWINS
0
1000
MEAN GRAIN DIAMETER (UM)
1
2


KTM-12: TWIN SET = 1/2: MEAN GRAIN DIAMETER/VOL. TWIN DOMAIN
40
0
VOL. TWIN DOMAIN (%)
0
1000
MEAN GRAIN DIAMETER (UM)
1
2

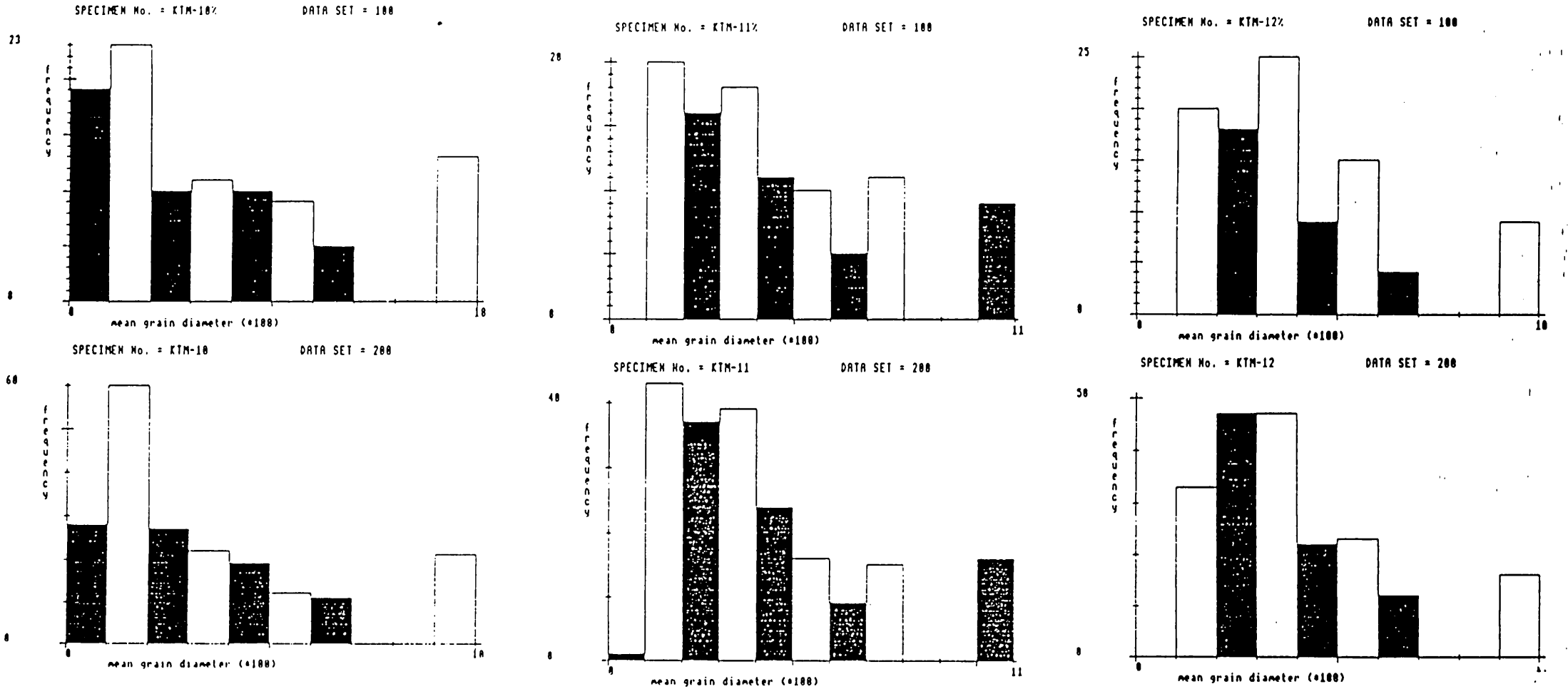
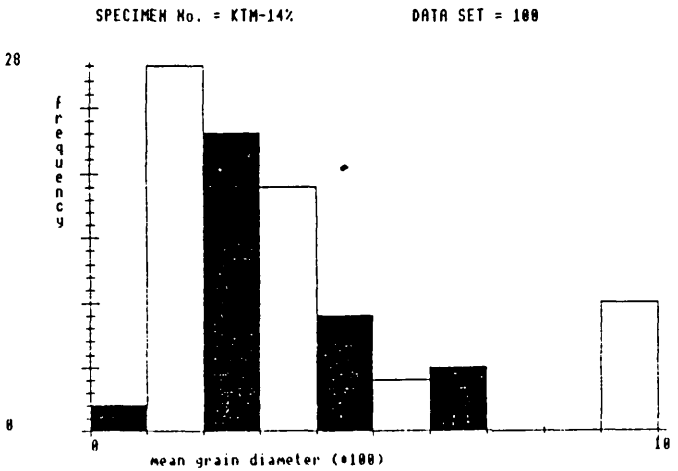
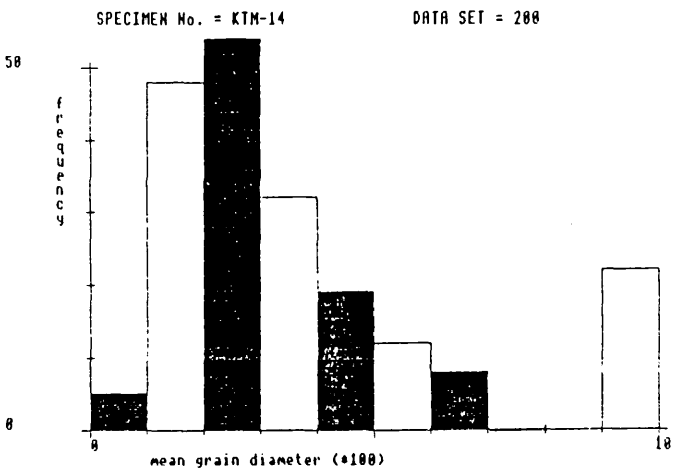
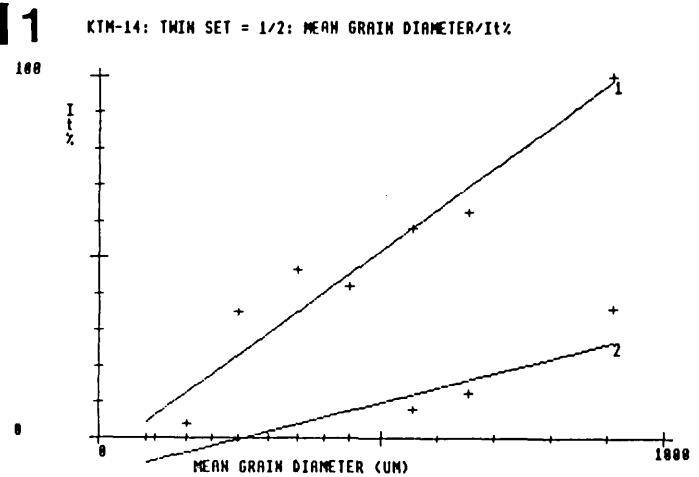


FIGURE 4.41 Histograms showing the number of data points (grains) in each of the grain size intervals for the diagrams of Fig. 4.40, the 500°C series of experiments upon Taiwanese Marble, see section 4.7.3.4. Note that Fig. 4.41d is shown with Fig. 4.40d. The individual samples are identified by their headings as for Fig. 4.11.

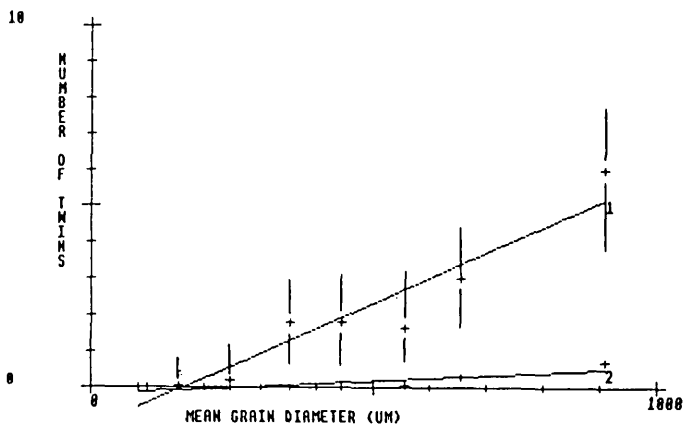

SPECIMEN No. = KTM-14%
DATA SET = 100
20
0
frequency
0
10
mean grain diameter (*100)


SPECIMEN No. = KTM-14
DATA SET = 200
50
0
frequency
0
10
mean grain diameter (*100)

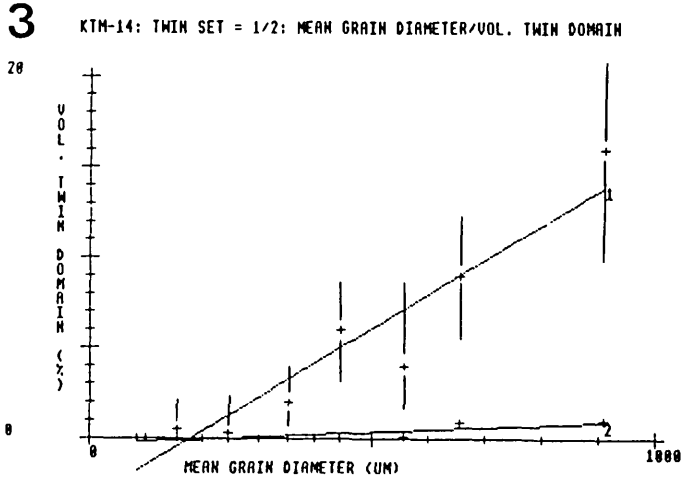
d1


KTM-14: TWIN SET = 1/2: MEAN GRAIN DIAMETER/It%
100
0
It%
1
2
0
1000
MEAN GRAIN DIAMETER (UM)

2


KTM-14: TWIN SET = 1/2: MEAN GRAIN DIAMETER/NUMBER OF TWINS
10
0
NUMBER OF TWINS
1
2
0
1000
MEAN GRAIN DIAMETER (UM)

3


KTM-14: TWIN SET = 1/2: MEAN GRAIN DIAMETER/VOL. TWIN DOMAIN
20
0
VOL. TWIN DOMAIN (%)
1
2
0
1000
MEAN GRAIN DIAMETER (UM)

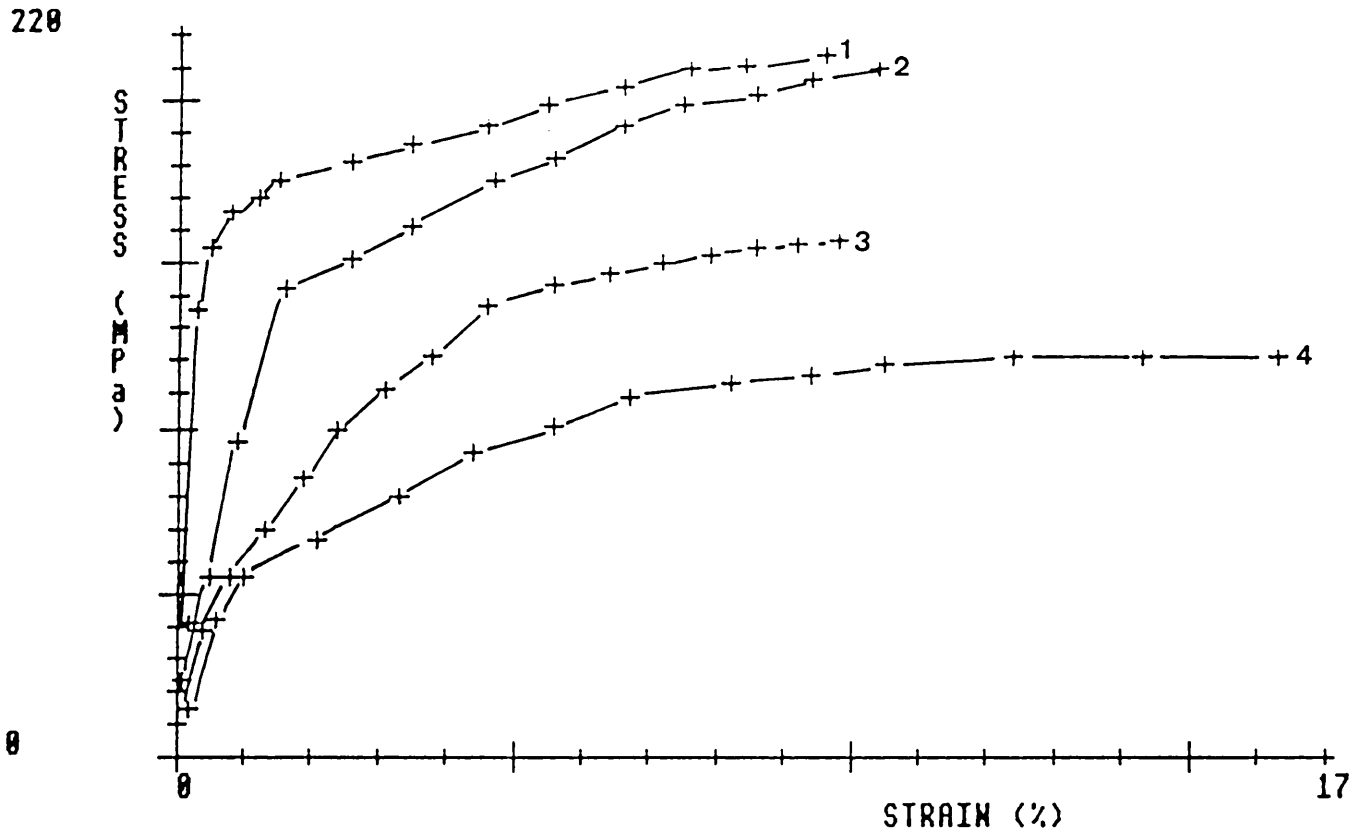


FIGURE 4.42 Stress/strain curves obtained for the 400°C series of experiments performed upon Taiwanese Marble, see section 4.7.3.5. 1 = KTM-13, 2 = KTM-16, 3 = KTM-17 and 4 = KTM-18.

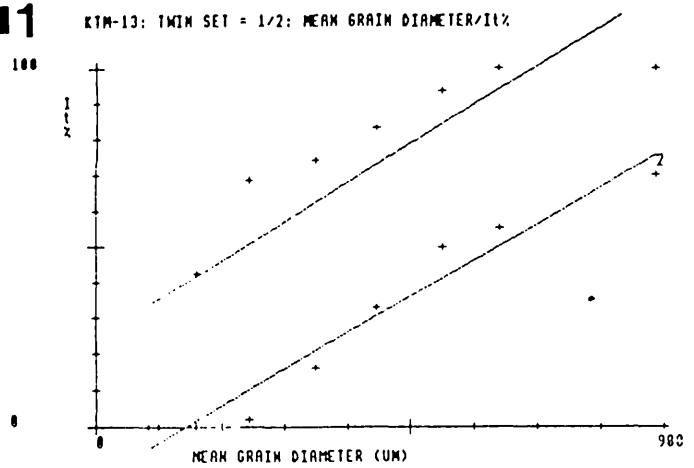
FIGURE 4.43 Textural data for Taiwanese Marble deformed at 400°C.

This series of diagrams present the twinning activity data determined for the series of experiments (a, b, c and d respectively) deformed at this temperature, plotted as a function of grain size. There are three diagrams, plotting It, number of twins, and percentage volume twin domain (1, 2 and 3 respectively).

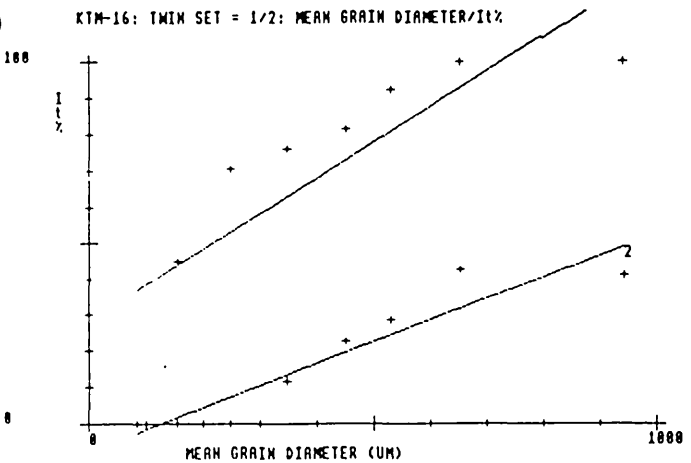
For each sample two twin sets have been analysed, the primary, or principal, twin set and the secondary twin set (1 and 2 respectively). The range bars shown for the relevant groups represent the full range of the values determined for each grain size interval. The individual experiments are identified by their respective headings.

See text for discussion.

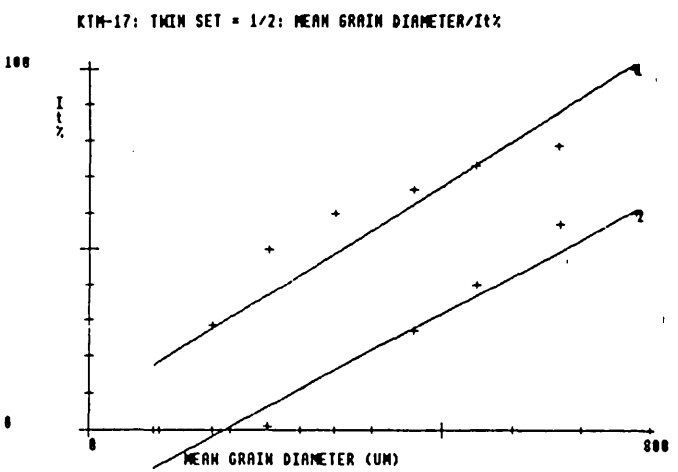
a1


KTM-13: TWIN SET = 1/2: MEAN GRAIN DIAMETER/It%
100
It%
0
0
MEAN GRAIN DIAMETER (UM)
900
1
2

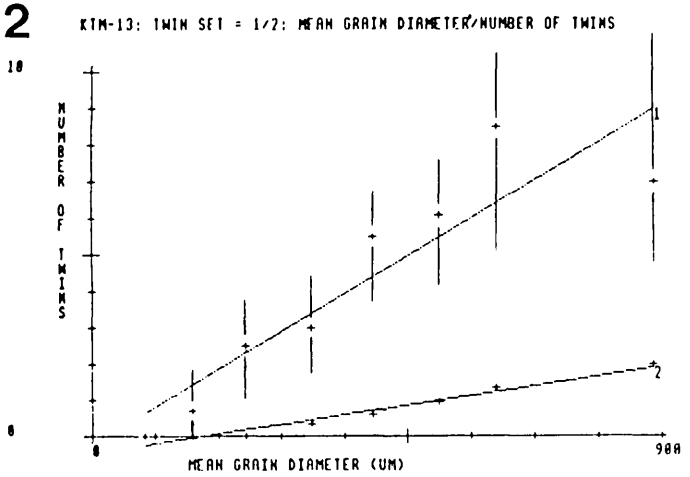
b

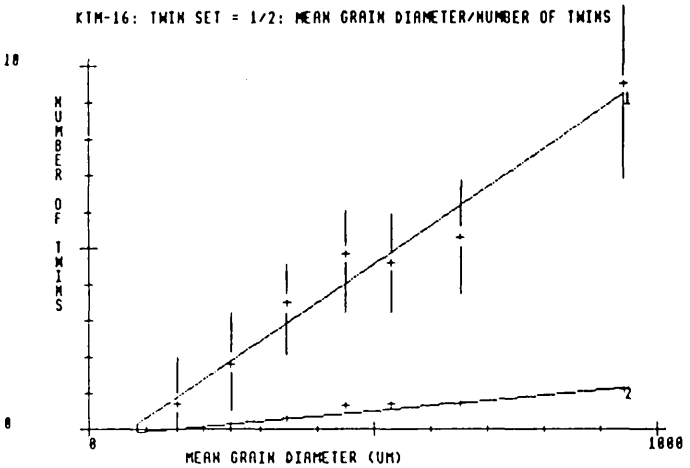

KTM-16: TWIN SET = 1/2: MEAN GRAIN DIAMETER/It%
100
It%
0
0
MEAN GRAIN DIAMETER (UM)
1000
1
2

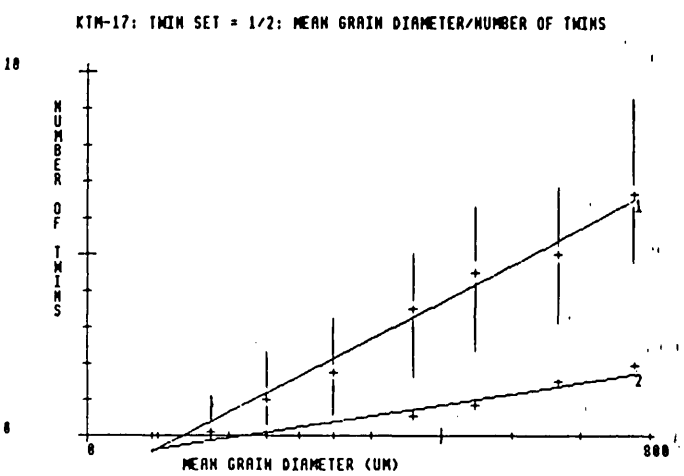
c


KTM-17: TWIN SET = 1/2: MEAN GRAIN DIAMETER/It%
100
It%
0
0
MEAN GRAIN DIAMETER (UM)
800
1
2

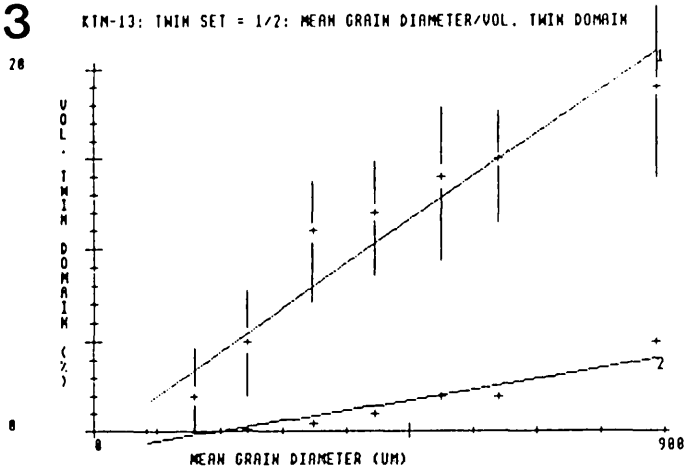
2

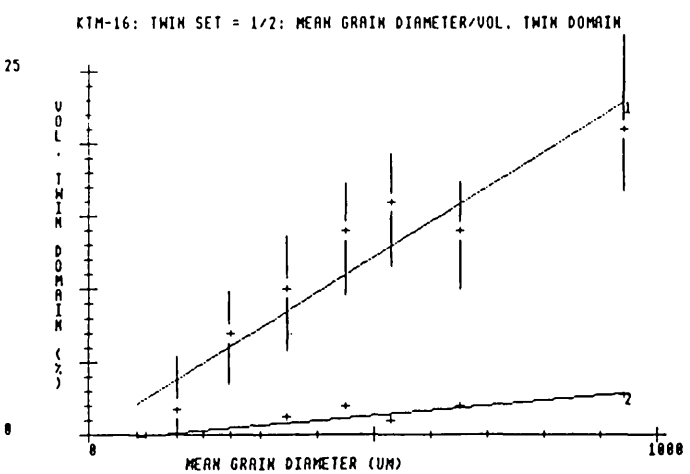

KTM-13: TWIN SET = 1/2: MEAN GRAIN DIAMETER/NUMBER OF TWINS
10
NUMBER OF TWINS
0
0
MEAN GRAIN DIAMETER (UM)
900
1
2

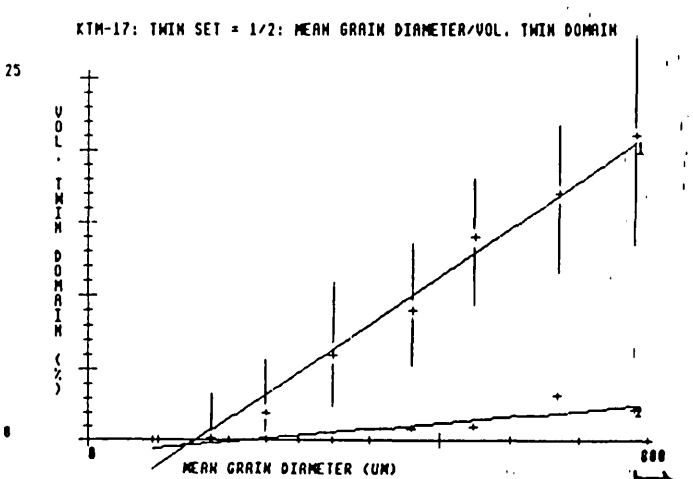

KTM-16: TWIN SET = 1/2: MEAN GRAIN DIAMETER/NUMBER OF TWINS
10
NUMBER OF TWINS
0
0
MEAN GRAIN DIAMETER (UM)
1000
1
2


KTM-17: TWIN SET = 1/2: MEAN GRAIN DIAMETER/NUMBER OF TWINS
10
NUMBER OF TWINS
0
0
MEAN GRAIN DIAMETER (UM)
800
1
2

3


KTM-13: TWIN SET = 1/2: MEAN GRAIN DIAMETER/VOL. TWIN DOMAIN
20
VOL. TWIN DOMAIN (%)
0
0
MEAN GRAIN DIAMETER (UM)
900
1
2


KTM-16: TWIN SET = 1/2: MEAN GRAIN DIAMETER/VOL. TWIN DOMAIN
25
VOL. TWIN DOMAIN (%)
0
0
MEAN GRAIN DIAMETER (UM)
1000
1
2


KTM-17: TWIN SET = 1/2: MEAN GRAIN DIAMETER/VOL. TWIN DOMAIN
25
VOL. TWIN DOMAIN (%)
0
0
MEAN GRAIN DIAMETER (UM)
800
1
2

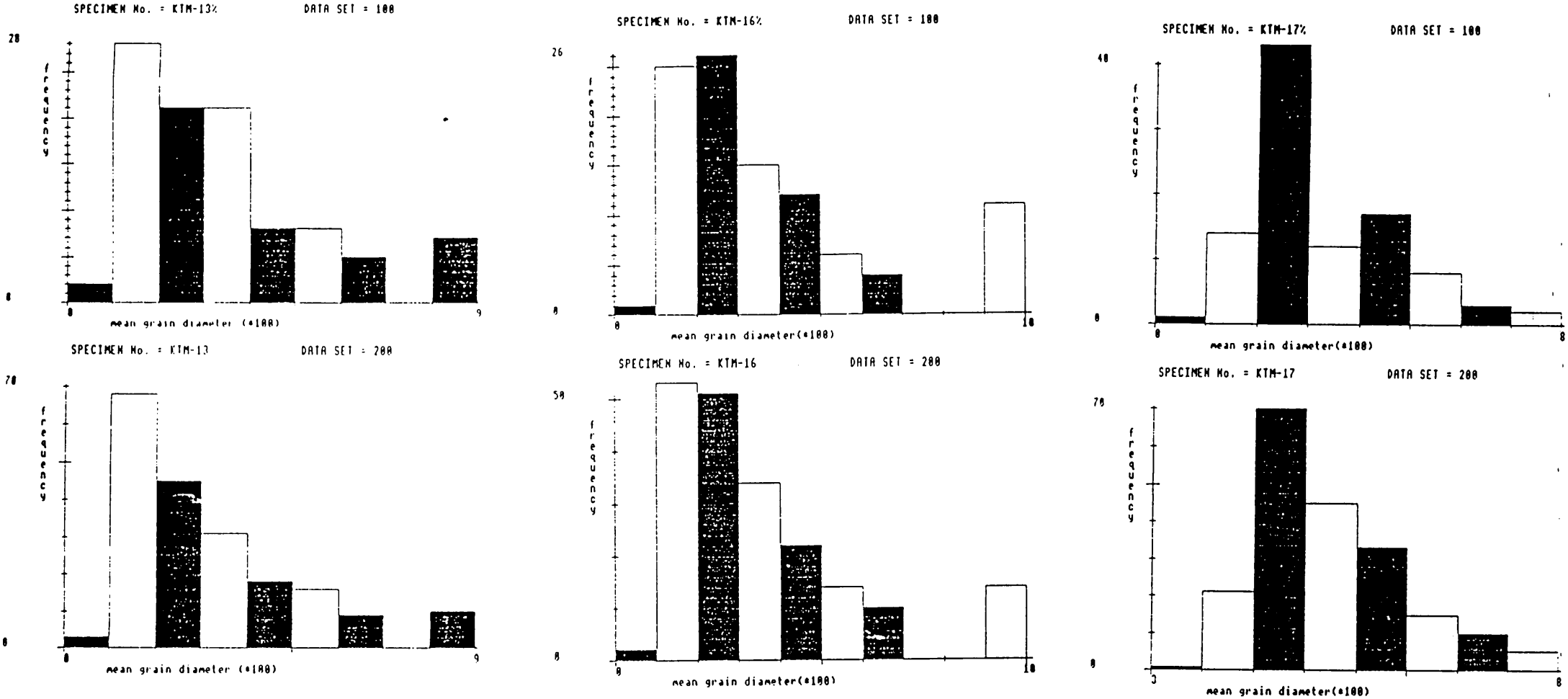
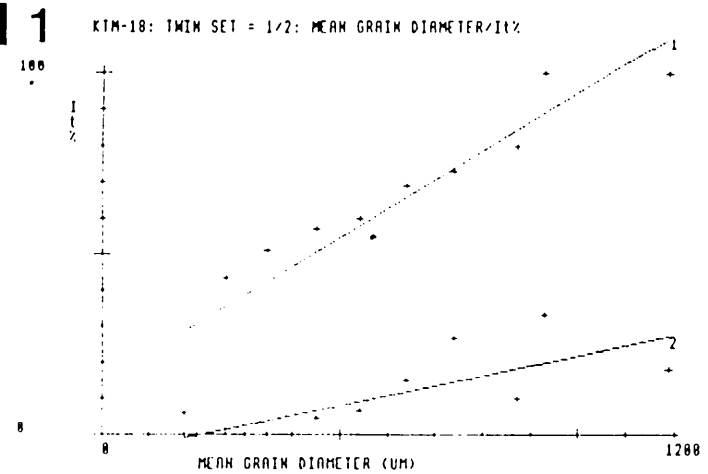
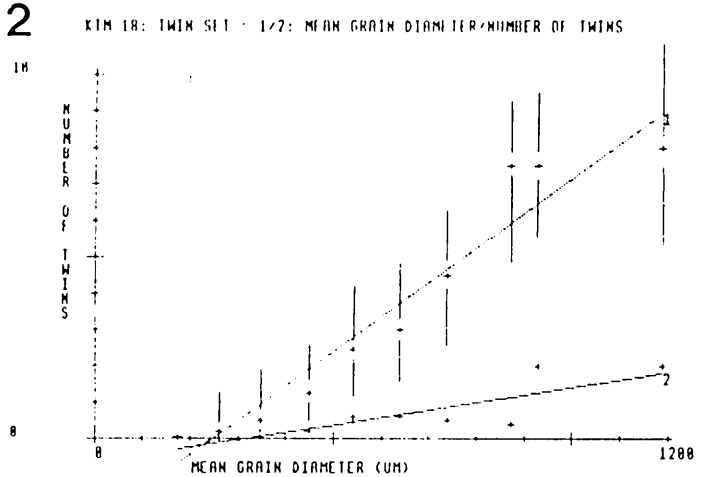


FIGURE 4.44 Histograms showing the number of data points (grains) in each of the grain size intervals for the diagrams of Fig. 4.43, the 400°C series of experiments upon Taiwanese Marble, see section 4.7.3.5. Note that Fig. 4.44d is shown with Fig. 4.43d. The individual samples are identified by their headings as for Fig. 4.11.

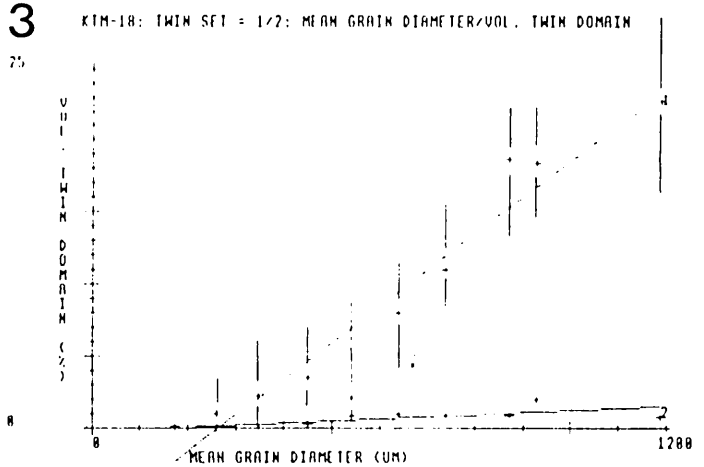
d 1

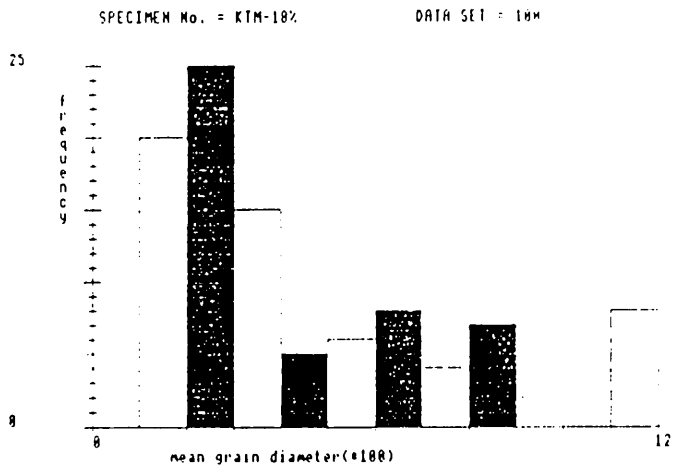

KIM-18: TWIN SET = 1/2: MEAN GRAIN DIAMETER/I1%
100
I1%
0
0
1200
MEAN GRAIN DIAMETER (UM)
1
2

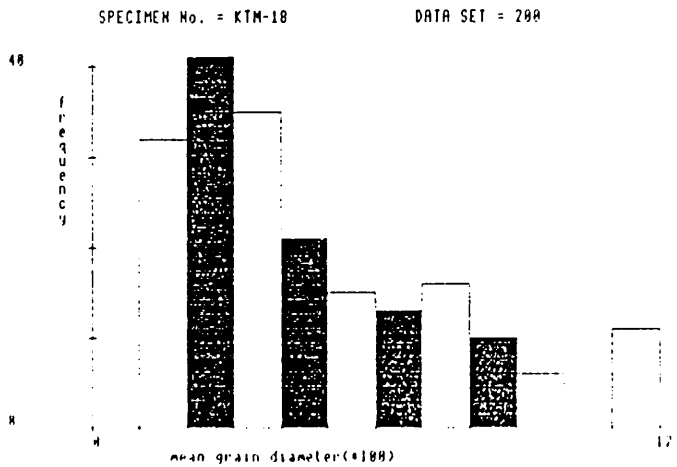
2


KIM 18: TWIN SET = 1/2: MEAN GRAIN DIAMETER/NUMBER OF TWINS
1M
NUMBER OF TWINS
0
0
1200
MEAN GRAIN DIAMETER (UM)
1
2

3


KIM-18: TWIN SET = 1/2: MEAN GRAIN DIAMETER/VOL. TWIN DOMAIN
25
VOL. TWIN DOMAIN (%)
0
0
1200
MEAN GRAIN DIAMETER (UM)
1
2


SPECIMEN No. = KIM-18%
DATA SET = 100
25
frequency
0
0
12
mean grain diameter(*100)


SPECIMEN No. = KIM-18
DATA SET = 200
40
frequency
0
0
12
mean grain diameter(*100)

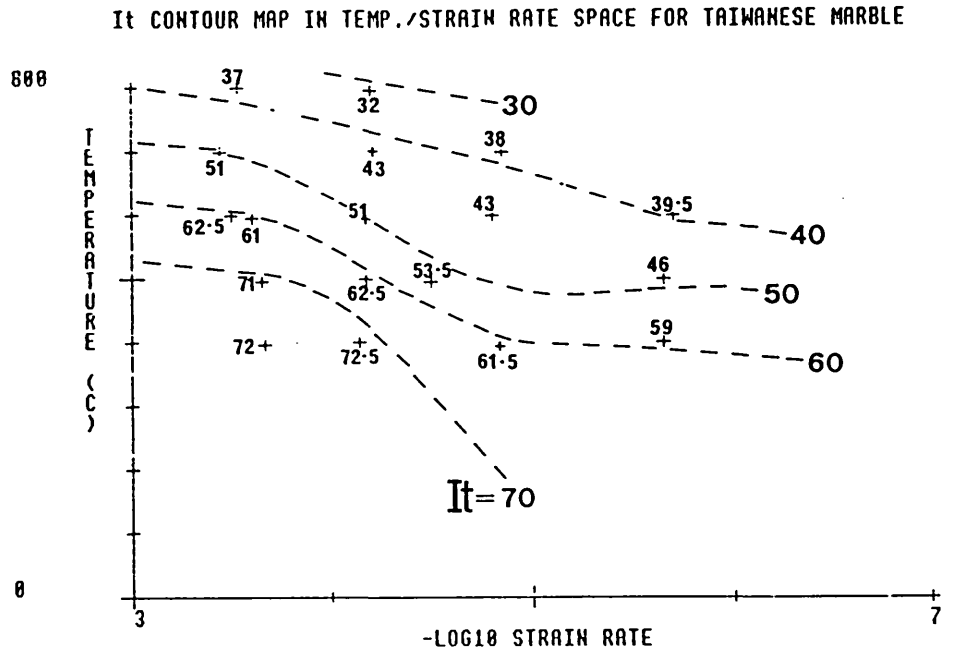


FIGURE 4.45 It contour map in Temperature/Strain Rate space for the series of experiments performed upon Taiwanese Marble. The 10% It contour defines the Twinning Field Boundary. See Table 4.5 for the corresponding experimental and textural parameters.

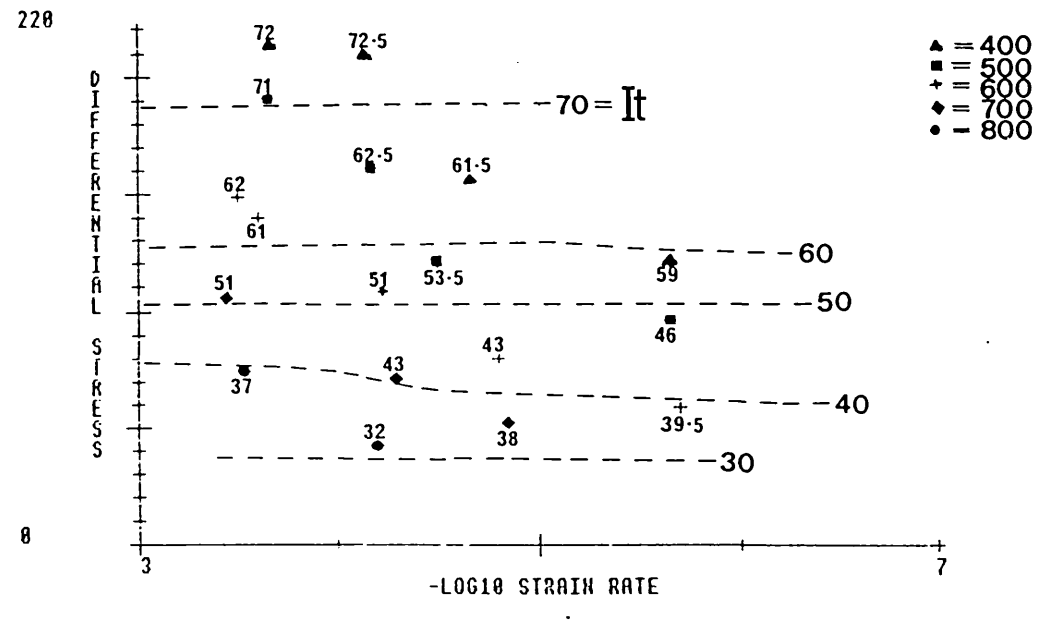


FIGURE 4.46 It contour map in Differential Stress/Strain Rate space for Taiwanese Marble series of experiments, with the temperature of the experiments superimposed.

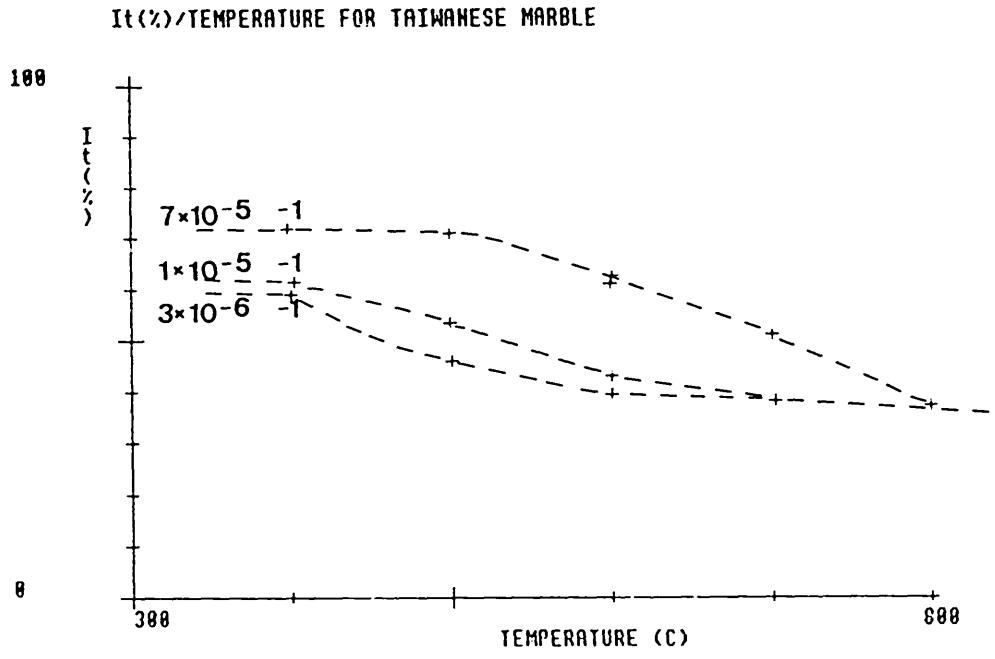


FIGURE 4.47 Iso-Strain Rate sections through Fig. 4.45, demonstrating the decrease in twinning activity as represented by the It parameter with increasing temperature at various Strain Rates. See Table 4.5 for the experimental and textural parameters which correspond to the crosses in this Figure.

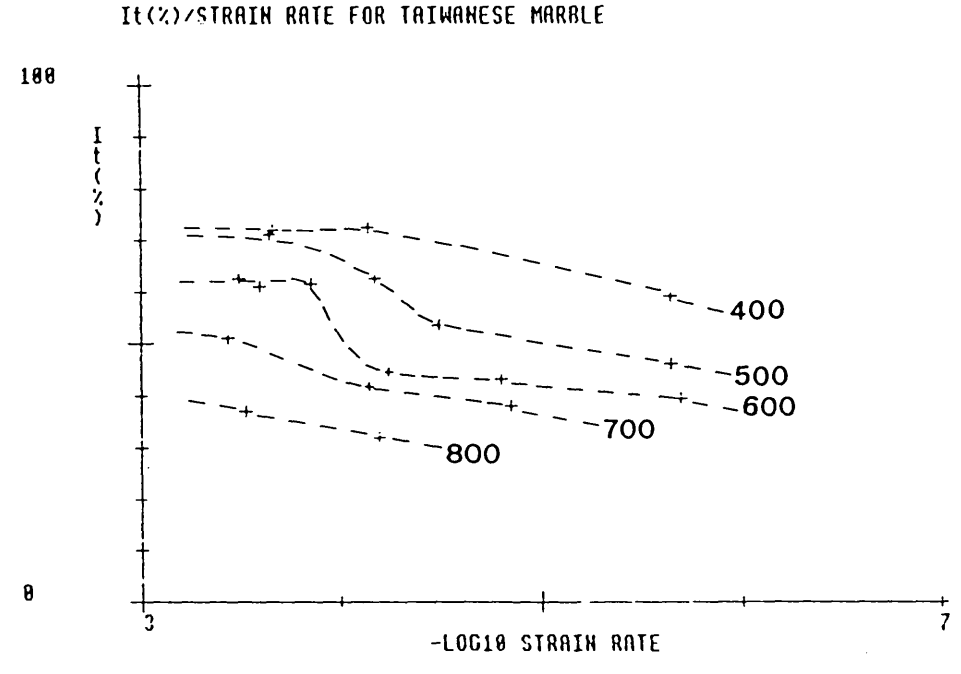


FIGURE 4.48 Iso-Temperature sections through Fig. 4.45, demonstrating the decrease in twinning activity as represented by the It parameter with decreasing Strain Rate at various temperatures. See Table 4.5 for the experimental and textural parameters which correspond to the crosses in this Figure.

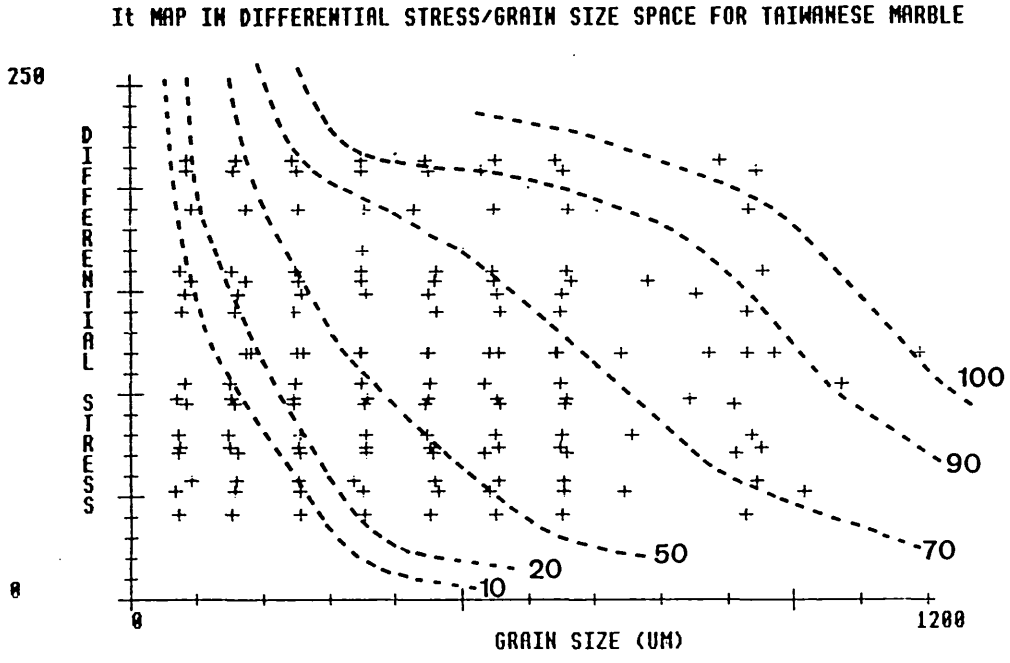


FIGURE 4.49 It contour map for the Taiwanese Marble series of experiments plotted in Differential Stress/Grain Size space. In order to enable clarity the principal contours only are shown. The 10% It contour defines the Twinning Field Boundary. As discussed in the text, in order to obtain as many data points as possible from a given experimental material, the textural data determined was divided on the basis of mean grain size. Therefore for each sample a series of It data points over a range of grain sizes, but at a unique level of Differential Stress are obtained. Thus the data manifests itself in a series of data points forming an horizontal line for each sample when plotted in the manner shown in this diagram. The reader is referred to Table 4.5 for the overall It/mean grain size parameters of the samples as a whole.

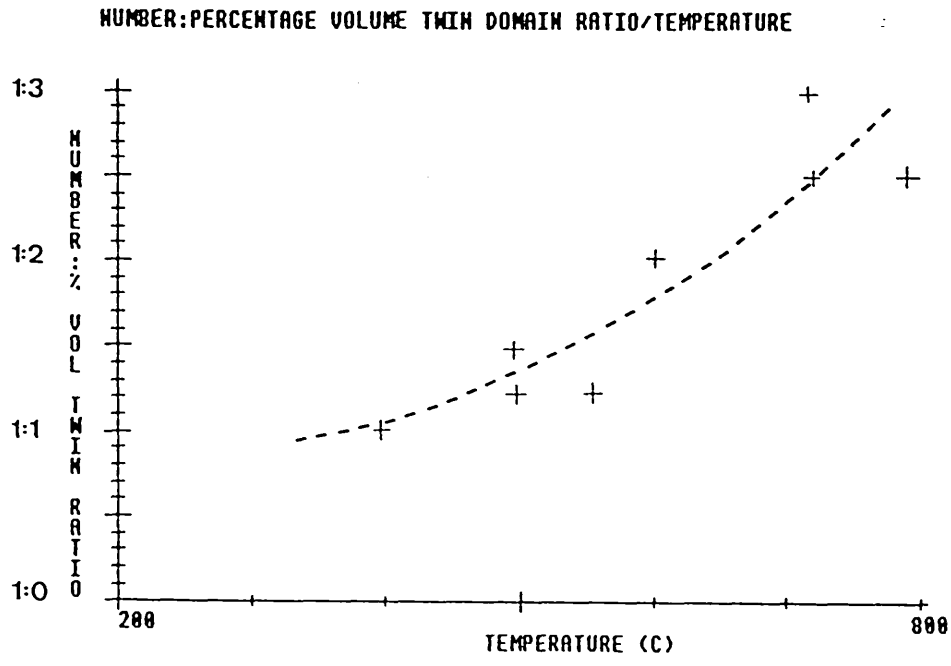


FIGURE 4.50 Diagram showing the increase in percentage volume twin domain with increasing temperature of deformation. Crosses represent real as opposed to interpolated data. See text for discussion.

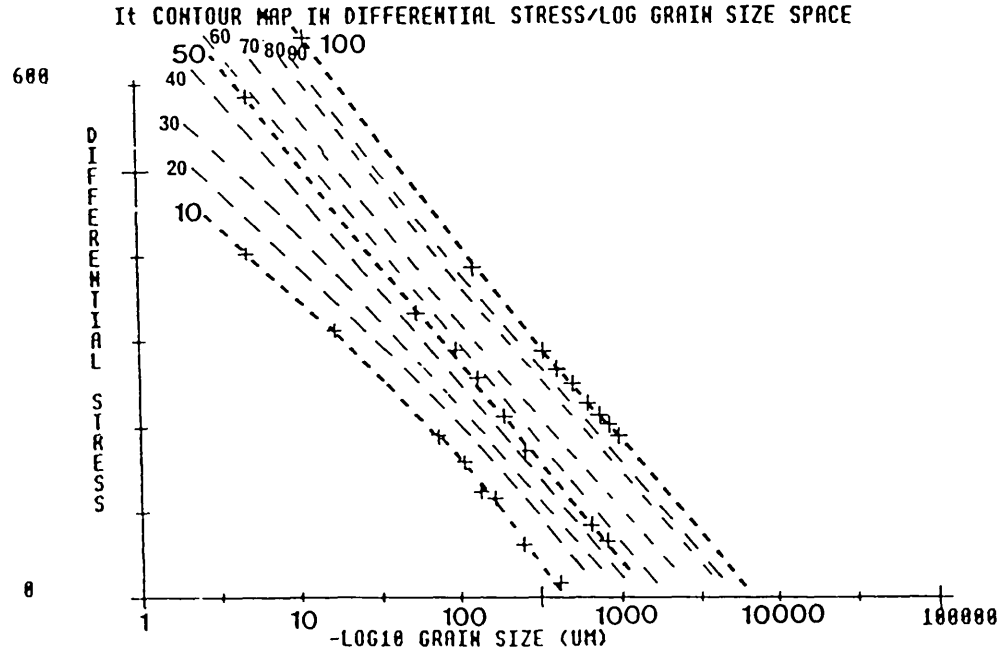


FIGURE 4.51 Twinning incidence parameters for the whole of the data presented in this chapter plotted as a function of Differential Stress and Grain Size. Crosses represent real as opposed to interpolated data points.

CHAPTER 5 : INTRODUCTION TO THE FIELD AREA

5.1 PRELIMINARY STATEMENTS

The second major aim of this thesis is to extrapolate the experimental models formulated in Chapter 4 to a major natural system. Intuitively, one of the major problems associated with the application of experimental data to a natural system is that the former are relatively simple, and the variables well constrained and controlled relative to the latter. Therefore the primary qualification regarding the choice of the natural system to be studied was its simplicity. The more complicated the system the greater the departure from labratory conditions and hence other factors will have to be included in the extrapolation of the experimental models.

The Hercynian Cantabrian zone of Northern Spain was chosen because it fulfilled the above considerations. In addition to its relative simplicity the Cantabrians have the following advantages :

1. The general geological structure, sedimentology and geological history is well known. This includes recent interpretations, e.g. the construction of palinspastically restored sections, produced by the staff and students of Oviedo University, N. Spain, who provided essential background and logistical assistance.

2. The major decollement horizon and many other important structural contacts occur in calcitic horizons.

3. The general level of exposure is good.

This chapter gives a detailed general introduction to the Cantabrian zone, its sedimentology, structure and geological evolution, and explains the selection of the two principal field areas within the Cantabrian zone. These two field areas form the contents of Chapters six and seven.

5.2 INTRODUCTION TO THE FIELD AREA

The northern coastal ranges and their hinterland to the west of the Pyrenean chain display the most complete section through a Variscan orogenic belt preserved in Europe. In addition it is thought to represent a section in the Earth's crust. The Cantabrian mountains of northern Spain and the coastal ranges extending from the provinces of Asturias in the east through to Galicia

in the west provide a near complete view of the stratigraphy, structure and metamorphism of this orogenic belt.

The most prominent feature of this belt is its arcurate form, which gives rise to the Asturian, or Ibero-Armorican Arc. The major structural divisions of the zone were first proposed by Lotze (1945), and these have been used by all subsequent workers. For a full review the orogenic belt the reader is referred to Julivert (1981). The principal lithotectonic units are shown in Figure 5.1, and a broad description is given below :

1. The Cantabrian Zone

This zone is described in detail in the next section. The Cantabrians are the most external unit of the Ibero-Armorican Arc recognised, but are now preserved in the geometric core of the arc, see Fig. 5.1. The Cantabrian zone is bounded to the east by uncomformably lain Permian mollasic deposits, and to the south by flat lying Mesozoic sediments. The western boundary is the cleavage front marked by the upwelling of the mass of Precambrian material which forms the Narcea Antiform.

The stratigraphy across the whole of the orogenic belt shows a general thinning of the sequence towards the east and shows it was formed on a relatively stable continental platform. Hence the Cantabrians display an incomplete and relatively thin Cambrian to Silurian sedimentary sequence, with locally developed Devonian successions, and a well developed Carboniferous sequence. Precambrian rocks are found in the extreme south and west of the zone only, see above.

Metamorphism and plutonism are absent and the Cantabrians are essentially cleavage free. Cleavage is developed locally where deformation is intense, and also in the far west of the zone adjacent to the contact with the Narcea Antiform.

As this zone formed the open water basin to the west was also developing, and this is described in the next section.

2. The West-Asturian-Leonese Zone

This zone extends from the Cantabrian Zone in the east to the Galician-Castilian Zone to the west and south-west, see Fig. 5.1. Pre-Cambrian rocks are present in the cores of the major antiformal structures, e.g. the Narcea and Mondonedo Antiforms, but the zone is characterised by a thick Cambrian to

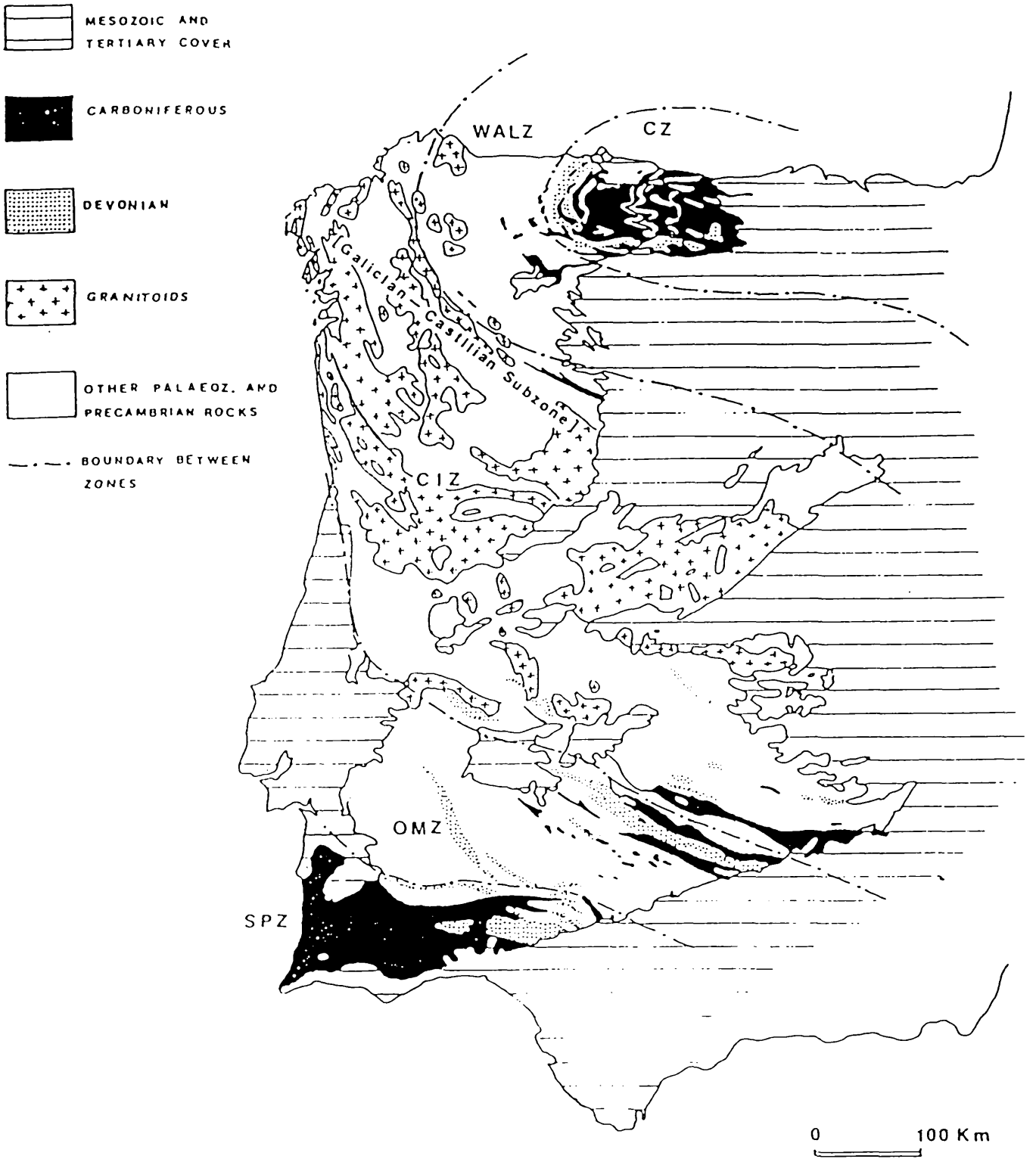


FIGURE 5.1 Geological map of the Iberian Peninsular, showing the principal geological regions. CZ - The Cantabrian Zone. WALZ - The West Asturian-Leonese Zone.

Silurian sedimentary sequence, with a poorly developed early Devonian to Stephanian sequence locally present.

The West-Asturian-Leonese Zone is distinct from the Cantabrian Zone in that in the former a penetrative cleavage is developed in the pelitic rocks. Metamorphism and plutonism are present across the whole zone, increasing in intensity towards the west, and the more internal zones.

Granitic rocks found in the west of this zone are the post-tectonic, biotite (alkaline) bearing granites and granodiorites, Capdevila and Floor (1970).

3. The Galician-Castilian Zone

This is the internal zone of the orogenic belt. Here metamorphism reaches amphibolite facies, with a fully developed penetrative cleavage and schistosity, and granitic plutonic complexes form approximately 50% of the surface exposure. These granitoids are calc-alkaline and are older than the alkaline types developed in the West-Asturian-Leonese Zone. However it is possible to recognise the alkaline granites in the east of this zone, and younger batholitic granodiorites which cut older granites in the Mondonedo Nappe.

There are a number of catazonal complexes present in this zone which contain basic and ultrabasic rocks, and eclogitic materials, e.g. the Cabo Ortegal Complex. The current hypothesis is that these represent a series of thrust bound ocean floor slices, thrust onto the rocks of the internal zone.

5.3 THE CANTABRIAN ZONE

The position of the Cantabrian Zone and its relationship to the other zones of the Ibero-Armorican Arc are outlined in the previous section, and is shown in Fig. 5.1. Figure 5.2 shows a general geological map of the Cantabrians, which also shows the main physio-geographic features of the region after Julivert (1971). These are :

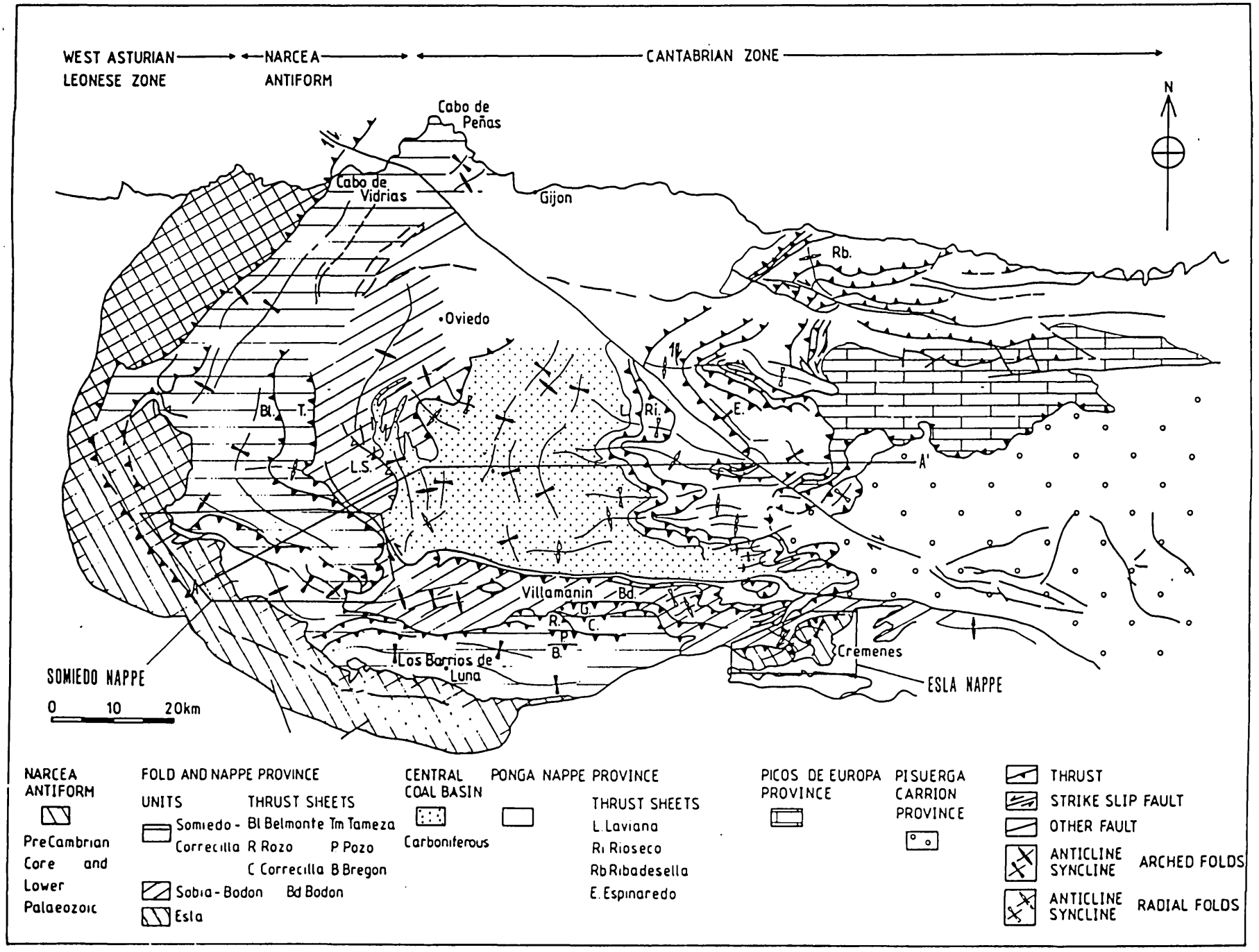
1. The fold and nappe province.
2. The Ponga Nappe province.
3. The Picos de Europa province.
4. The Central Coal Basin.
5. The Pisuerga-Carrion province.

The evolution of these provinces is discussed in the following sections.

FIGURE 5.2 Structural Geological map of the Cantabrian Zone.

This map shows the principal structural units that comprise the Cantabrian Zone, the location of which is shown on Fig. 5.1.

A-A' marks the line of the structural section presented in Fig. 5.4, and the location of the two field areas studied in Chapters 6 and 7 are shown.


WEST ASTURIAN LEONESE ZONE
NARCEA ANTIFORM
CANTABRIAN ZONE
N
Cabo de Peñas
Cabo de Vidrias
Gijon
Rb.
•Oviedo
Bl.
T.
L.S.
L
Ri.
E.
A'
Villamanin
Bd.
G
R.
C.
P
B.
Los Barrios de Luna
Cremenes
SOMIEDO NAPPE
ESLA NAPPE
0 10 20km
NARCEA ANTIFORM
PreCambrian Core and Lower Palaeozoic
FOLD AND NAPPE PROVINCE
UNITS
Somiedo - Correcilla
Sobia - Bodon
Esla
THRUST SHEETS
Bl Belmonte Tm Tameza
R Rozo P Pozo
C Correcilla B Bregon
Bd Bodon
CENTRAL COAL BASIN
Carboniferous
PONGA NAPPE PROVINCE
THRUST SHEETS
L Laviana
Ri Rioseco
Rb Ribadesella
E Espinaredo
PICOS DE EUROPA PROVINCE
PISUERGA CARRION PROVINCE
THRUST
STRIKE SLIP FAULT
OTHER FAULT
ANTICLINE
SYNCLINE
ARCHED FOLDS
ANTICLINE
SYNCLINE
RADIAL FOLDS

5.3.1 STRATIGRAPHY

Marcos and Pulgar (1982) have divided the stratigraphy of the Cantabrians into a preorogenic sequence (Cambrian to Devonian), and a synorogenic sequence (Carboniferous). The general stratigraphic sequence is shown in Fig. 5.3.

The preorogenic sediments form a wedge of supracrustal clastic and carbonate sediments thinning towards the east. Sedimentation occurred in a stable, shallow shelf environment, upon a substratum of Precambrian conglomerates, sandstones and shales. The Cambrian/Precambrian boundary is an angular unconformity, and is exposed in the south-west of the region.

The thinning of the supracrustal wedge occurs as a result of the onlap of the sedimentary sequence onto the emerging continental shelf to the east, although pre-Famennian (Late Devonian) erosion would have contributed. The latter indicates that sedimentation in these times was becoming increasingly non marine. The provinence area was emergent, or semi-emergent in the east, with open sea conditions to the west (Mendez and Bedia, 1976; and Garcia-Ramos, 1978). The entire preorogenic sequence is of the order of 4000-6000 metres thick (Marcos and Pulgar, 1982). This sedimentary sequence displays a remarkable anisotropy, which is of great interest when styles of deformation and deformation mechanisms are studied, see following chapters.

Carboniferous sedimentation was mainly synorogenic and was accompanied by basin migration and subdivision, with many local facies and thickness variations and breaks in sedimentation. The conditions started in the late Devonian where sediments have many uncomformities, with a condensed sequence forming in the lower Carboniferous sequence, and which marks the pre-synorogenic transition. The sequence illustrates the progressive onset of the deformation from the west, causing uplift, and ultimately giving rise to the thick synorogenic sediments, see below.

A restricted platform existed during Namurian and Westphalian times and a thick carbonate unit known as the Caliza de Montana (Mountain Limestone) was deposited (Sanchez de la Torre and Lastra, 1978). This represents the last stable depositional environment across the whole of the zone before the onset of deformation. This relatively stable environment persisted for the whole of the upper Carboniferous in the east of the Cantabrian Zone, giving rise to the Picos de Europa Limestone (Maas, 1974).

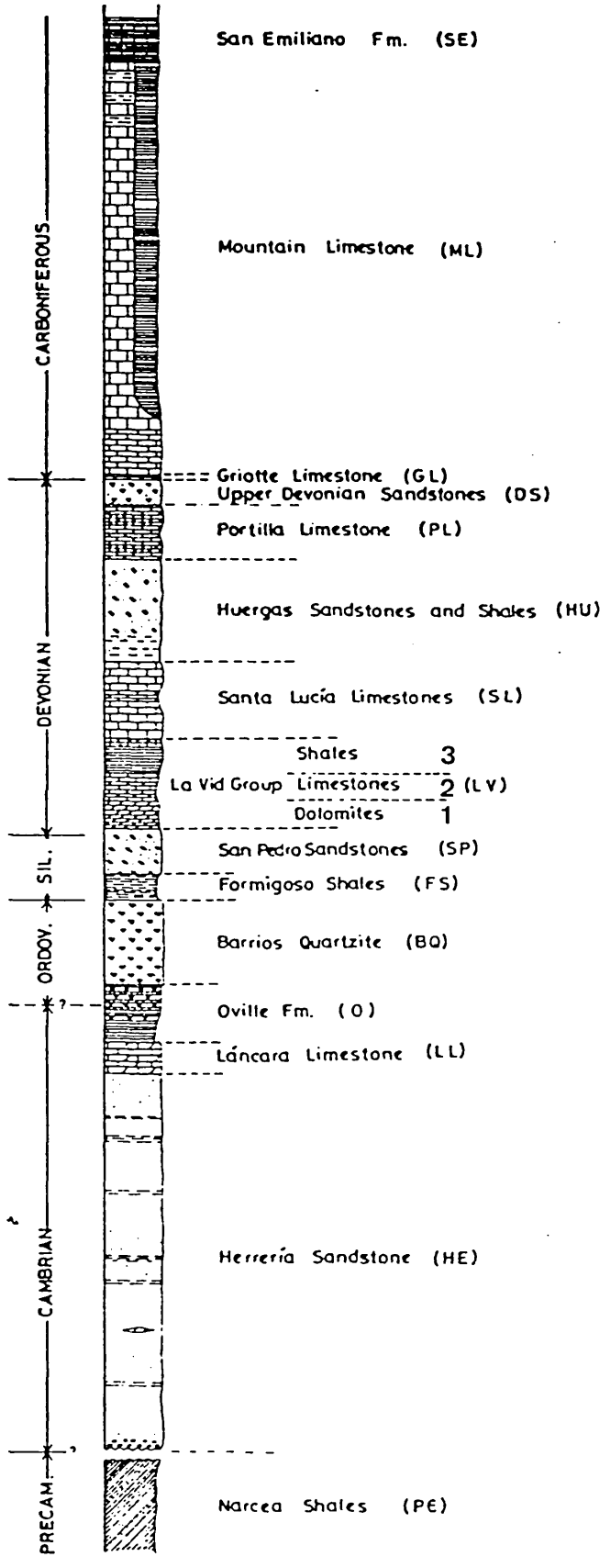


FIGURE 5.3 General Stratigraphic Sequence for the Cantabrian Zone (After Bastida et al., 1987). Note that this is the sequence from the west of the Cantabrian Zone.

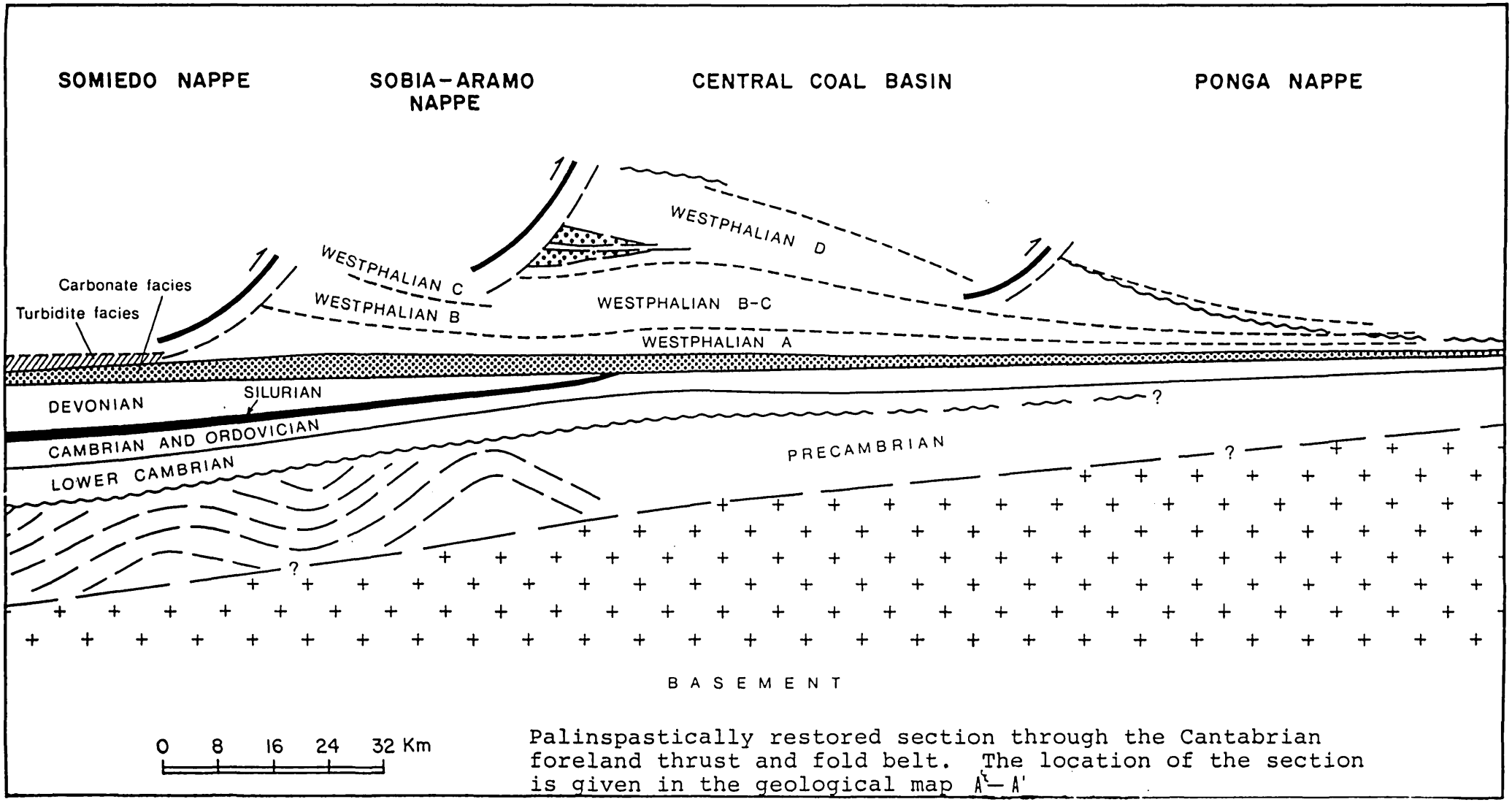
To the west, turbiditic sediments are developed above and below the Caliza de Montana. In the Central Coal Basin the Upper Carboniferous sequence is 6000 metres thick and is deposited in the form of a thick clastic wedge. This is comprised of paralic sediments, including marine limestones, sandstones, shales, conglomerates and coal horizons. The Pisuerga-Carrion Province is the flysch basin, and represents the eastern sector of the synorogenic clastic wedge.

As the deformation front migrated towards the east the basin foredeep formed as an isostatically induced peripheral depression due to lithospheric loading caused by the emplacement of the thrust sheets (Bally et al., 1966; Price, 1973). This basin is a very effective sedimentary trap. As suggested by Price (1973) the absence of uncomformities in a clastic wedge indicates that there has been continuous tectonic activity. Therefore the lack of any breaks in the sedimentation of the Westphalian indicates that there was intense deformation of the developing cordillera at this time. In the lower Stephanian the first uncomformities are present, indicating a decrease in the rate of sedimentation and a corresponding tectonic calm (Marcos and Pulgar, 1982). This tectonostratigraphic evolution is indicated on Fig. 5.4.

5.3.2 GENERAL GEOLOGICAL STRUCTURE AND EVOLUTION

The Cantabrian Zone displays typical thin skinned Appalachian style thrust tectonics, which developed during the Hercynian orogenic period. Deformation occurred at shallow crustal levels, hence the general lack of metamorphism in this zone. The thrust sheets were subsequently affected by two episodes of folding, the first probably developed concurrently with the emplacement of the nappes, and the second formed later as a result of the closure of the arc. These are referred to as the longitudinal and radial systems, respectively, as a result of their spatial relationship with the arc (Julivert and Pello, 1967; Julivert and Marcos, 1973), see Fig.5.2. The transport directions are now all directed towards the centre of the arc as a result of the oroclinal folding.

Marcos and Pulgar (1982) have palinspastically restored a section across the west and central sectors of the Cantabrian zone, Fig. 5.4. The approximate line of this section is indicated on Fig. 5.2. This diagram shows the general eastwards sedimentary thinning of the stratigraphy, and the relative positions of the major thrust sheets. Although no borehole or seismic data is available the assumption of "thin skinned" tectonics is validated by the existence of a general décollement level within the Cambrian Lancara Limestone. This is exposed in a number of localities across the zone.



Palinspastically restored section through the Cantabrian foreland thrust and fold belt. The location of the section is given in the geological map A'— A'

The stratigraphic evolution of the synorogenic sediments have been used to establish the movement periods of the thrust sheets. The most active period of tectonism occurred in the western sector of the zone in lower Westphalian times, and in upper Westphalian times in the eastern sector (Marcos and Pulgar, 1982). This agrees with the general model for the development of the external zone with the deformation front propagating from the west to the east during Westphalian times, achieving approximately 50% shortening in this direction.

The closure of the arc from a curvature of between 55°-70° in Permian times to 150°-165° by the end of the Westphalian is indicated by palaeomagnetic studies (Ries et al., 1980). Julivert and Arbolya (1984) have suggested that this closure can be resolved into a rotational nappe emplacement component (40°-60°) and a radial folds (40°-50°) component.

The last phase of deformation recognised in the Cantabrians is the development of strike slip faults, e.g. the Ventaniella Fault, as a consequence of Alpine tectonism in the Pyrenees. This has led to a number of thrust faults reactivating as strike slip faults in the Ponga Nappe Province, as this zone is at the centre of the zone and therefore has the greatest space problems due to the arc closure.

5.3.3 SELECTION OF THE AREAS OF STUDY

The ultimate aim of this study is the quantification of the state of stress associated with the emplacement of the nappes in the Cantabrian Zone. In order to achieve this aim an extensive sampling program was carried out across most of the major faults of the external zone. It was soon realised by the author that several regions warranted detailed study, but because of time limitations a detailed study was carried out of two of the principal nappe complexes exposed in the Cantabrians, namely :

1. The Esla Nappe : Situated in the south-east sector of the Cantabrians, and comprising a stacked nappe complex which has been subsequently been folded by both the longlitudinal and radial fold sets.

2. The Someido Nappe : Situated in the western sector of the Cantabrians, and comprising of a large thrust sheet which has a complicated internal structure and ordering. This complex has also been folded by both fold sets, but owing to its location on the periphery of the Cantabrians the shortening is less than that suffered by the Esla Nappe.

The location of these two complexes is shown on Fig. 5.2. Details of the research carried out and the results are presented in the following chapters.

CHAPTER 6 : FIELD AREA 1 : THE ESLA NAPPE

6.1 INTRODUCTION

This chapter details the results of the field work carried out on the Esla Nappe, which is the first of the two field areas studied. After the preliminary statements regarding location , relief, access, climate, drainage, the fault rock terminology used and the orientation of the specimens and thin sections, the chapter examines specimens from five localities where the principal thrust fault is well exposed with the aim of investigating the rheological properties of the materials associated with the emplacement of the nappe.

6.2 LOCATION

The Esla Nappe is situated in the south-eastern corner of the Cantabrians in the region known as the fold and nappe province (Juilvert, 1971). Geographically it is situated between the towns of Riano, Bonar and Cistierna, on the southern slope of the Cordillera. The exact location is shown on Fig. 5.2.

Relief across the Esla Nappe is variable, ranging from rolling hills (500 metres above sea level) to vertical limestone cliffs (1600 metres above sea level for the higher mountains in the area). The majority of the land is farmed, but the higher slopes are wooded. Climate is variable, however the location on the southern slope of the cordillera assures a continental climate for the summer months. The area is drained by one major river, the Rio Esla, and numerous smaller tributaries. Access was by one major road, with many smaller roads and farm tracks providing good access to the sections studied. Exposure across the nappe is good, although the shale horizons are heavily vegetated.

6.3 FAULT ROCK CLASSIFICATION AND TERMINOLOGY

The Cantabrian Zone is the external zone of the Hercynides in N. Spain, see Chapter 5, and are essentially cleavage and metamorphism free. Therefore the fault rocks exposed have formed at shallow levels in the Earth's Crust, typically the depth of formation is essentially the thickness of the thrust sheet itself. Hence the dominant deformation mechanism on the hand specimen scale is cataclastic, i.e. the rocks "deformation context" (Mawer, 1985) is characterised by brittle processes. A full discussion of the evolution of the

nomenclature currently in use, and its limitations is not warranted in this thesis (see Obee, 1985; and Maddock, 1986), although the terminology used is described below, and is based on Sibson, 1977.

6.3.1 GLOSSARY OF FAULT ROCK TERMINOLOGY USED

1. **Fault gouge**: A very fine grained rock formed predominantly of clay minerals, with very fine grained host rock particles. Visible rock fragments should form less than 30% of the rock (Sibson, 1977). A fault gouge can be cohesive or in-cohesive, and foliated or non-foliated depending upon its composition. The clay minerals are commonly aligned and rock fragments if present can show elongation as a result of cataclatic flow (Hall, 1983).

2. **Fault breccia**: A rock in which visible angular fragments of wallrock are set in a finer grained matrix of clay minerals and rock fragments (Obee, 1985). The angular fragments should form more than 30% of the rock (Sibson, 1977). Cementation of the rock may occur after faulting as a result of mineral precipatation through ground water or hydrothermal solution circulation (Obee, 1985). A fault breccia can be cohesive or in-cohesive, and foliated or non-foliated depending upon its composition and subsequent deformational history.

3. **Cataclasite**: A cohesive fault rock consisting of angular to sub-angular fragments set in a finer grained matrix and brought about through micro-cracking, rigid-body rotation and frictional sliding (Obee, 1985). Note that clasts can be rounded, depending upon their pre-deformational morphology. Although the term was first used by Grubenmann and Niggli (1924) to describe a "aphanitic structureless rock" the term has been extended and now encompasses foliated and non-foliated rocks (Obee, 1985). A foliated cataclasite (regarded by some authors as a mylonite, S.H. White pers. com.) forms as a result of increased fluid/rock interaction which encourages mineral growth, and/or by the preferred alignment of clasts. Cataclasites are sub-divided on the basis of the proportion of the matrix: protocataclasite (10-50%); cataclasite (50-90%); ultracataclasite (90-100%).

Modification of the fault rocks described above can occur as a result of the effects of pressure solution, which can transport material away from, and to, appropriate regions and may form a pressure solution cleavage in an otherwise unfoliated fault rock.

6.4 ORIENTATION OF THE PETROFABRICS

In the field, orientated specimens were collected from the fault zones chosen to be studied. This enabled the production of orientated thin sections in the laboratory, Fig. 6.1.

Based upon the field observations of the writer and utilising the excellent geological maps of the staff and students of Oviedo University (N. Spain) the geometry and general movement direction of the nappe is known. This enabled thin sections to be cut so that they contained the probable movement direction i.e. parallel to the lineation if present, but were perpendicular to the foliation of the fault rocks.

Each of the petrofabrics presented here have the movement direction indicated by the tick and are cut normal to the foliation (see Fig. 6.1), unless otherwise indicated.

6.5 GENERAL GEOLOGICAL SETTING

The nomenclature of the stratigraphic sequence is as illustrated in Fig. 5.3. The Esla Nappe is a typical Cantabrian nappe and consists of a thrust sheet of Cambrian to Devonian rocks (approximately 2km in thickness), which rests on Devonian and Carboniferious sediments. The movement direction has been determined by Marcos, pers. com. (using the Dynamic Analysis Technique of Turner 1954, see later), and Allonso, 1987 (using restored nappe geomet ries) to be towards the north-east. Folding by both longitudinal and radial fold sets has resulted in the sinuous thrust fault trace that we now observe, and results in the exposure of the autochton underneath the thrust sheet, Fig. 6.2.

The decollement surface is situated near the base of the Cambrian Lancara Limestone, and the thrust surface remains parallel to this horizon for the majority of the thrust sheet. Frontal hanging wall fold/ramp structures are visible in the section between the villages of Argovejo and Remolina (Julivert and Arboleya, 1984). This particular region of the nappe is unique in the Cantabrians in that the frontal region is preserved, and the relationships between olistostromic flysch style sedimentation and the emplacement of the nappe have been described (Arboleya, 1981; Alonso, 1982).

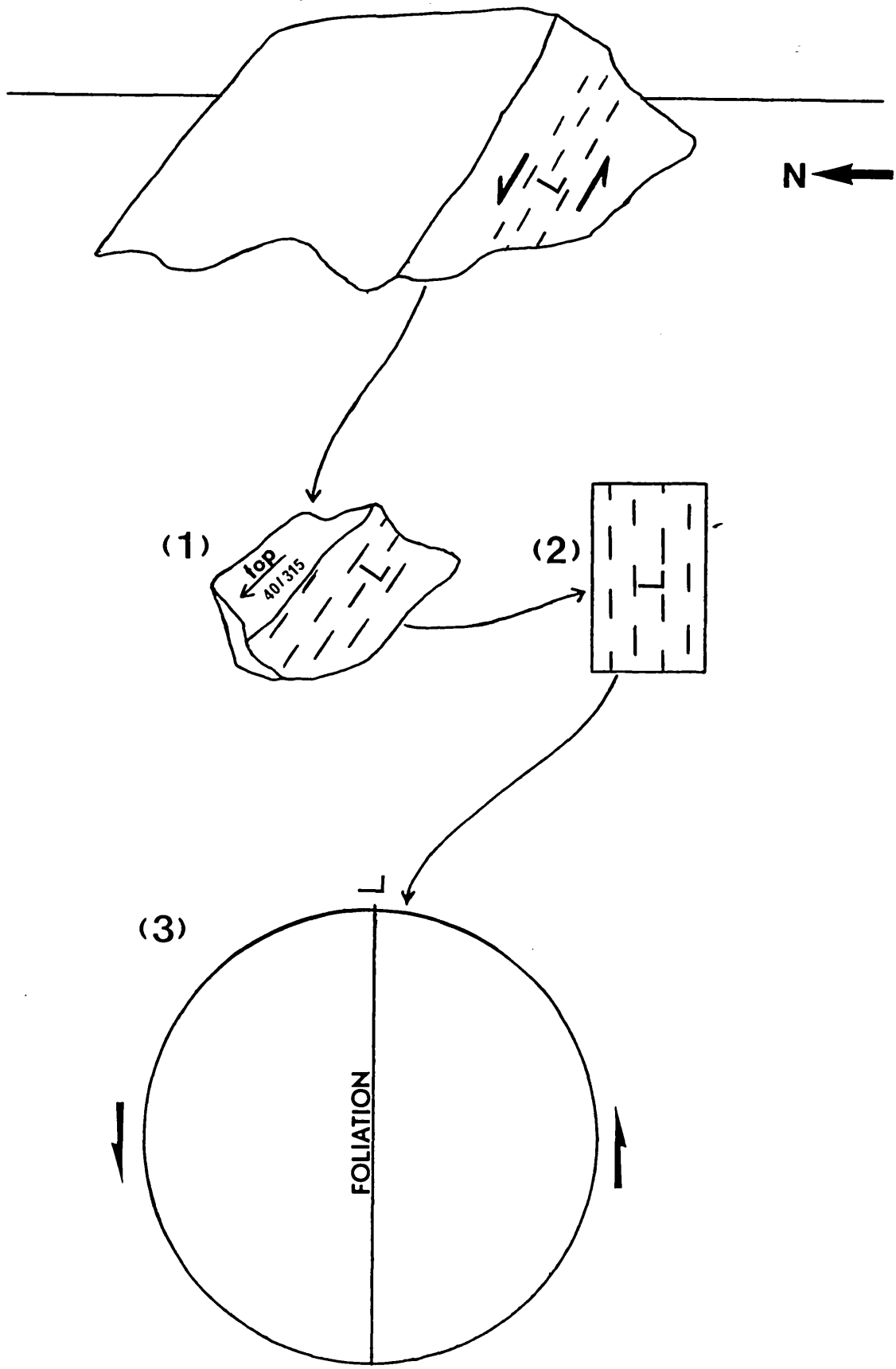


FIGURE 6.1 Diagram showing the steps used to prepare orientated fabric diagrams from orientated field samples. The sense of shear applies to all the petrofabrics presented in this thesis. (1) Orientated field specimen. (2) Orientated thin section. (3) Orientated petrofabric. L is the lineation, or movement direction.

6.6 SAMPLE LOCALITIES

Specimens were collected from five localities where the major thrust fault was well exposed, these are shown on Fig. 6.2. These are :

1. Road section north of Cremenes (Cremenes section).
2. Road section between Cremenes and Corniero (Cremenes-Corneiro section).
3. Section east of Velilla Valdore (Velilla Valdore section).
4. Section north of Valdore (Valdore section).
5. Section north-east of Verdiago (Verdiago section).

The results from the microscopic and petrofabric analysis are discussed in the format :

1. Hanging wall, i.e. the Lancara Limestone.
2. Fault rocks.
3. Footwall materials, i.e the Portilla Limestone and the Devonian Superior Sandstone, note that the Carboniferous Griotte although in the footwall, forms part of the fault rock and is described in that section.

Detailed petrofabric analysis of the Portilla Limestone forming the footwall rocks have been carried out for palaeo-stress estimates because they have remained essentially passive during the emplacement of the nappe. This is in contrast to the rocks which comprise the hanging wall which have been folded and unfolded as a result of their movement over ramps. Therefore the footwall has greater potential for palaeostress estimates. In addition to which the Lancara Limestone was found to be micritic in character and individual grains could not be resolved. Consequently not even a qualitative study could be undertaken.

6.7 THE HANGING WALL

The optical strain features are randomly orientated fractures and pressure solution stylolites, see Plate 6.1a, b and e. Both of these features increase in intensity with proximity to the thrust fault.

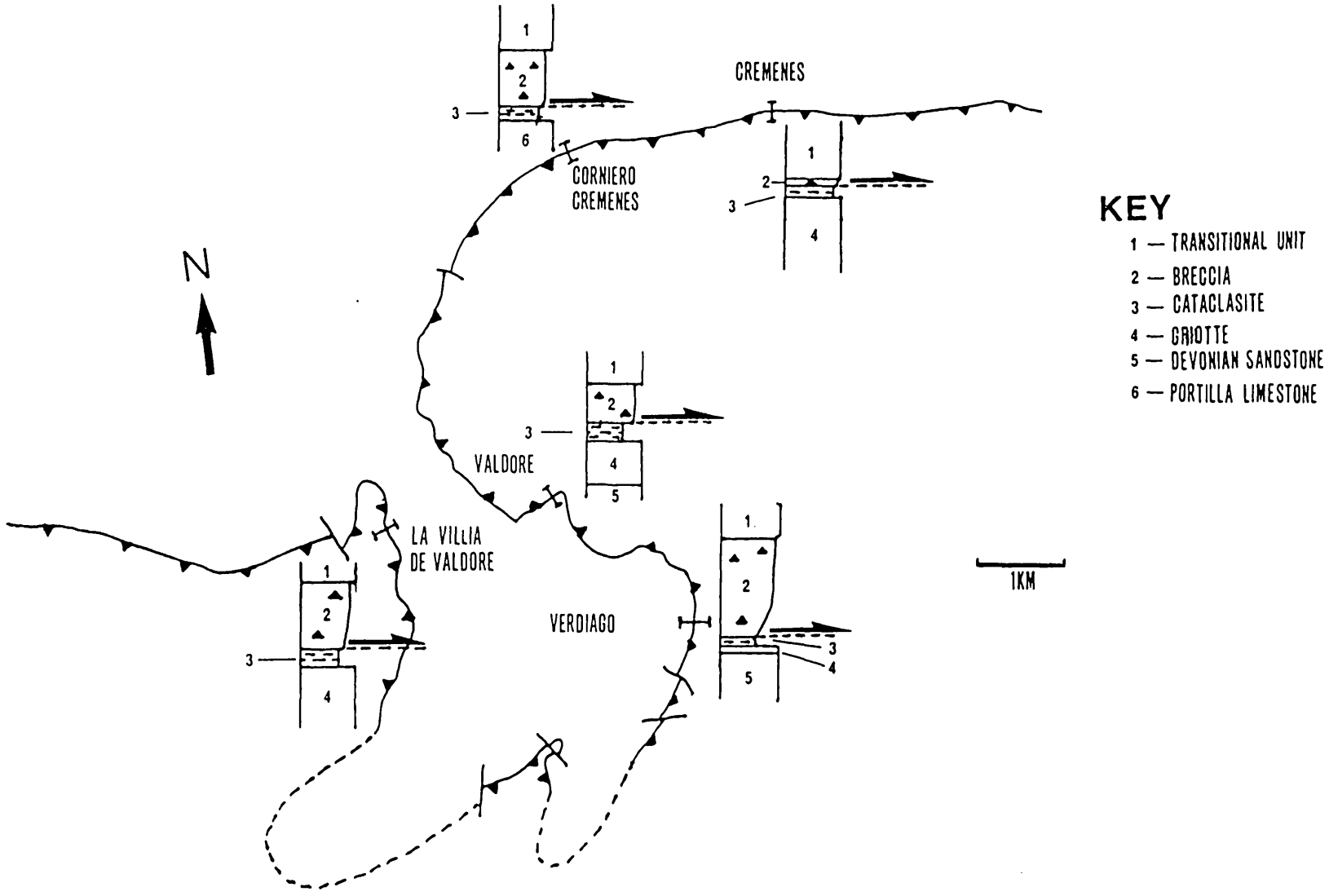


FIGURE 6.2 Specimen location map of the Esla Nappe, showing the fault trace (solid line is the exposed fault trace), with stratigraphic columns of the sections studied, see text. The vertical scale of these stratigraphic columns is 1cm = 1m true, while the variation in the width of the units is intended to graphically illustrate the individual units. The transport direction is from the south-west.

PLATE 6.1 The microstructures characteristic of the hanging wall Lancara Limestone in proximity to the thrust and the Transitional Unit, through to the Breccia Unit.

The orientation of all the field photographs presented in this Thesis is the same as that of the petrofabrics illustrated in Fig. 6.1, unless otherwise indicated in the caption, e.g. (e). The scale bar on all the photomicrographs is 1mm.

This Plate consists of a series of photographs showing the progressive increase in intensity of deformation with proximity to the thrust in the hanging wall and Transitional Unit through to the margins of the Breccia Unit, see text.

(a) and (b) are a field and its corresponding photomicrograph from the Lancara Formation, approximately 0.8m above the contact with the Transitional Unit. The fracture intensity is low and movement along the randomly orientated fracture planes appears to be very small. There is a limited amount of grain size reduction along these fractures.

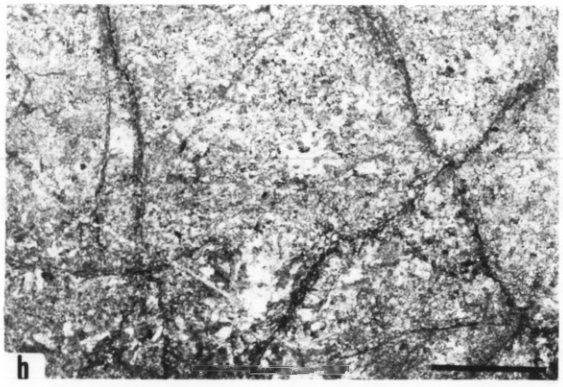
(c) and (d) are a field and its corresponding photomicrograph from the Transitional Unit. Relative to (a) and (b) the fracturing here is pervasive, although the character of the fracturing appears to be identical.

(e) This photomicrograph shows a styolite orientated sub-parallel to the thrust plane, and perpendicular to the calcite infilled fractures.

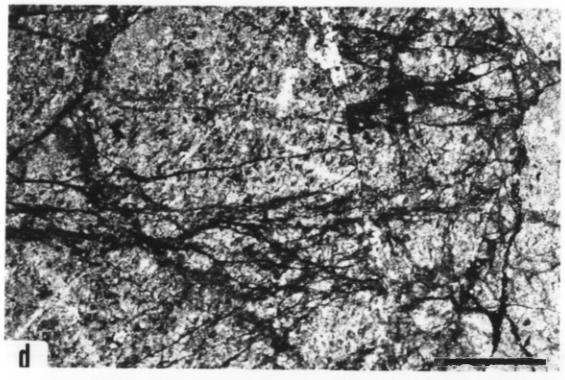
(f) This shows an outcrop of the Breccia Unit, with fragments of Lancara Limestone in a matrix of calcite and quartz grains, see following Plate.

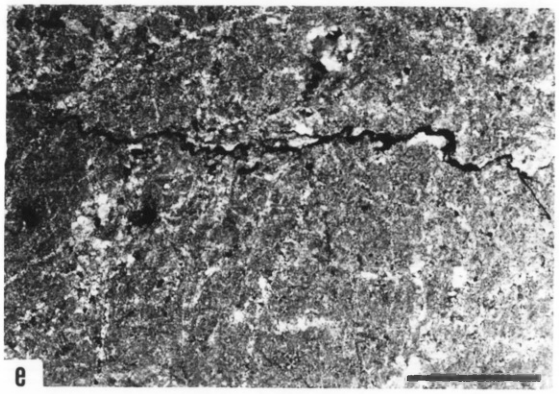
PLATE 6.1

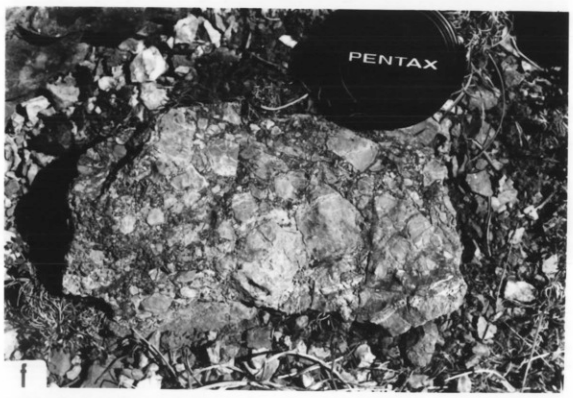












6.8 THE FAULT ROCKS

At the base of the hanging wall there is a distinct, narrow band of deformation, varying in width from 0.5- 4.5 metres, which can be recognised in all of the sections studied. There is a distinct sequence observed in the field which characterise all of the sections studied, this is :

1. A transitional unit between undeformed Lancara and the fault rocks.

2. Calcareous, or "crush" (Arboleya, 1980), breccia.

3. Cataclastic series.

4. Recrystallized Carboniferous griotte.

The base of the nappe is situated in the cataclasites. The location of the contact is shown in relation to the fault rocks of the sections studied in Fig. 6.2.

6.8.1 THE TRANSITIONAL UNIT

This unit is derived from the Lancara Limestone of the hanging wall, which becomes progressively fractured as we approach the fault plane, eventually forming the calcareous breccias of the next unit. Outcrop scale deformation is restricted to pervasive fracturing, Plate 6.1c and d.

In thin section the rock displays a number of stylolites which are parallel to the fault plane and are marked by the presence of insoluble residue. These appear to have been initiated at the contacts between small quartz grains and the limestone, Plate 6.2a, and become increasingly common as we approach the fault plane. The stylolites progressively concentrate the quartz grains, as is seen in the sequence of photomicrographs presented in Plate 6.2a-e. This process if taken to its extreme can isolate angular blocks of limestone, which are then incorporated into the breccia, Plate 6.2e.

The concentration of the quartz grains in the way suggested above requires the removal of a great deal of calcareous material in the form of solution. It is estimated that in excess of 60% of the rock would have to be removed to give the observed concentration of quartz grains, assuming the composition of the Lancara Formation is homogeneous. There is evidence that this material is deposited in the fractures and calcite veins that

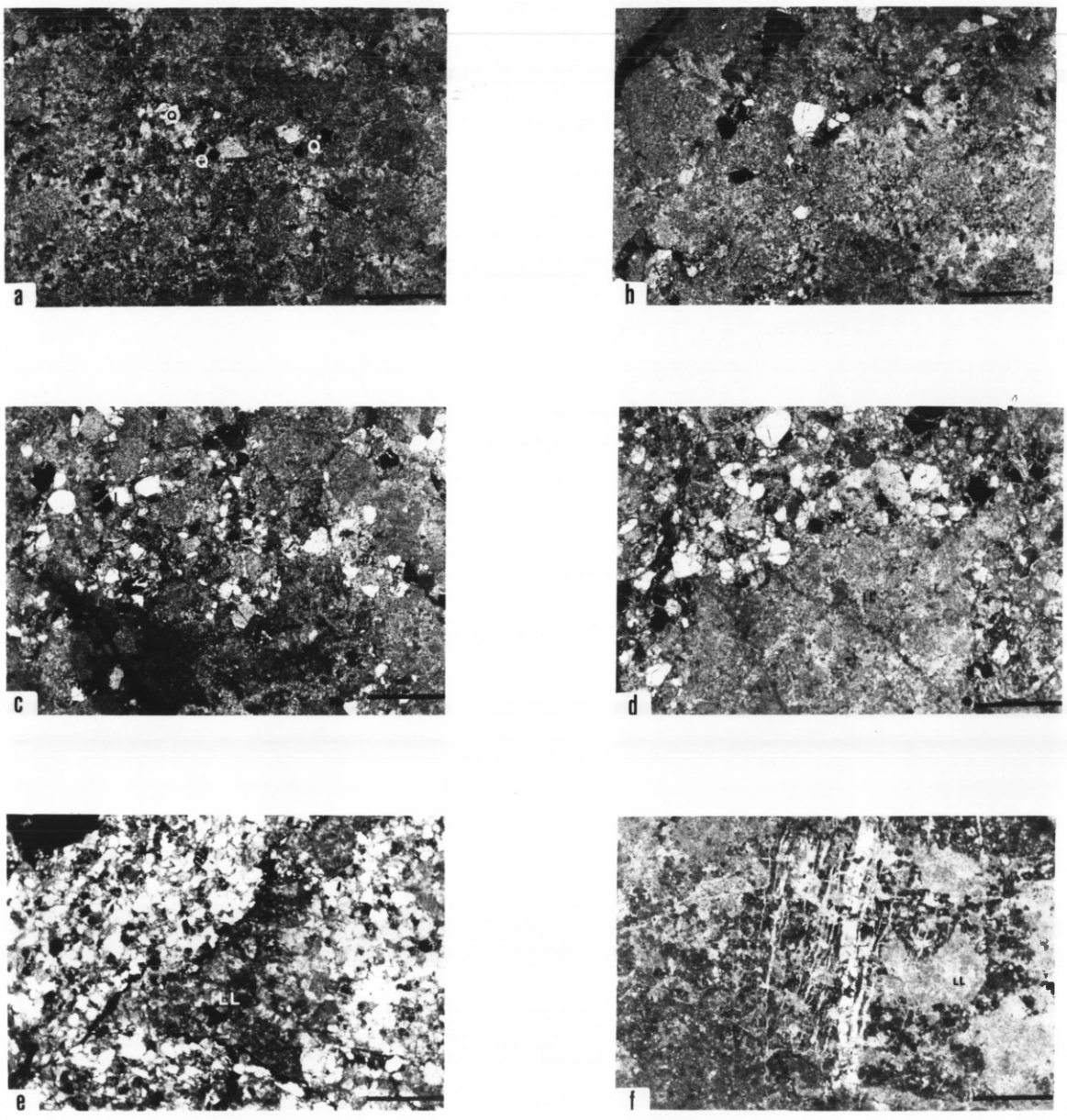
PLATE 6.2 The microstructures characteristic of the Transitional Unit.

This Plate shows the progressive concentration of quartz grains (Q) along pressure solution stylolites (PS) with proximity to the thrust in the Transitional Unit. A feature of the quartz grains are the impingement fractures (I), clearly shown in (c) and (d). The orientation of the fractures indicate that $\sigma 1$ was perpendicular to the thrust plane at the time of their formation, which is consistent with the orientation of the principal stress axes which formed the stylolites. The scale bar on all the photomicrographs is 1mm.

(a), (b) and (c) show the progressive concentration of quartz grains very clearly. This process continues until the rock unit consists principally of quartz grains with isolated blocks of Lancara Limestone (LL) as in (d). (e) clearly shows an angular block of Lancara Limestone, the margins of which are formed by styolites, surrounded by quartz grains.

(f) This shows a photomicrograph of Lancara Limestone from the Transitional Unit showing the pervasive nature of the calcite veining that is commonly developed. These veins are orientated perpendicular to the thrust plane.

PLATE 6.2



characterise the base of the Lancara in and above the transition zone, as these are dilatant regions. In some cases these calcite veins form >50% of the rock, Plate 6.2f.

6.8.2 BRECCIAS

Calcareous, or "crush" (Arboleya, 1980), breccia. This is derived from the Lancara by the process of progressive fracturing and stylolite concentration of quartz grains described above, and forms the base of the hanging wall. This unit varies in thickness from the Verdiago section, where 2.8 metres is developed to the Cremenes section where it is five cms thick. Fig. 6.2.

In the field the angular fragments of limestone up to 4cm's in length are clearly visible (Plate 6.1f),and have been identified as Lancara on the basis of sedimentary structures (Arboleya, 1980). The matrix consists of small quartz grains (65%) and clay minerals (35%).

The quartz grains in the breccia are free from optical strain features and fractures (with the exception of fractures associated with the formation of the stylolites, Plate 6.3), and appear to be undeformed. However some of the rock fragments have clearly been cemented and subsequently incorporated into the breccia as we see it now, suggesting that there has been some relative movement associated with the development of this rock unit, Plate 6.3a.

6.8.3 THE CATACLASTIC SERIES

This unit marks the position of the fault plane and contains all the features typical of cataclastic deformation. It is possible to recognise a progressive sequence from protocataclasite developed on the margins of the zone, through cataclasite to a thin band of ultracataclasite developed in the centre of the unit, Plate 6.4.

Fragments of limestone are common in the region of the protocataclasite, but are less common in the cataclasite and are not observed in the ultracataclasite. In the Valdore and Verdiago sections elongate, boudin type blocks of leached and highly twinned Carboniferous girotte are found. These are derived from the footwall underlying the cataclastic series. In addition to this at the latter of these two localities there are several blocks of Devonian Superior sandstone (Perez-Estaun, pers. com), which are easily identifiable because of the proliferation of

PLATE 6.3 The microstructures characteristic of the Breccia Unit.

This Plate shows a series of photomicrographs and Back Scattered SEM micrographs from the Breccia Unit. The scale bar in all of the photomicrographs is 1mm.

(a), (b) and (c) - These show the microstructures characteristic of the Breccia Unit. This unit consists of rounded quartz grains and fragments of Lancara Limestone in a fine grained matrix of calcite. (a) and (b) are orientated so that the long axis of the print is parallel to the thrust plane, and thus the slight shape fabric which is visible is consistent with the thrust movement direction. (a) Shows evidence of reworking of the clasts in the form of a previously cemented fragment of breccia (X).

(d), (e) and (f) - These are SEM micrographs of the breccia, and afford higher resolution study of this material. The dominant microstructural feature of these micrographs is the impingement cracks developed in the quartz grains (dark clasts). The lighter material is calcite. Micrograph (f) is from the breccia adjacent to the contact with the Cataclastic Unit, and shows the development of a cataclastic zone situated in the centre of the micrograph. This is consistent with the overall trend which is of intensification of deformation as we approach the thrust contact.

PLATE 6.3

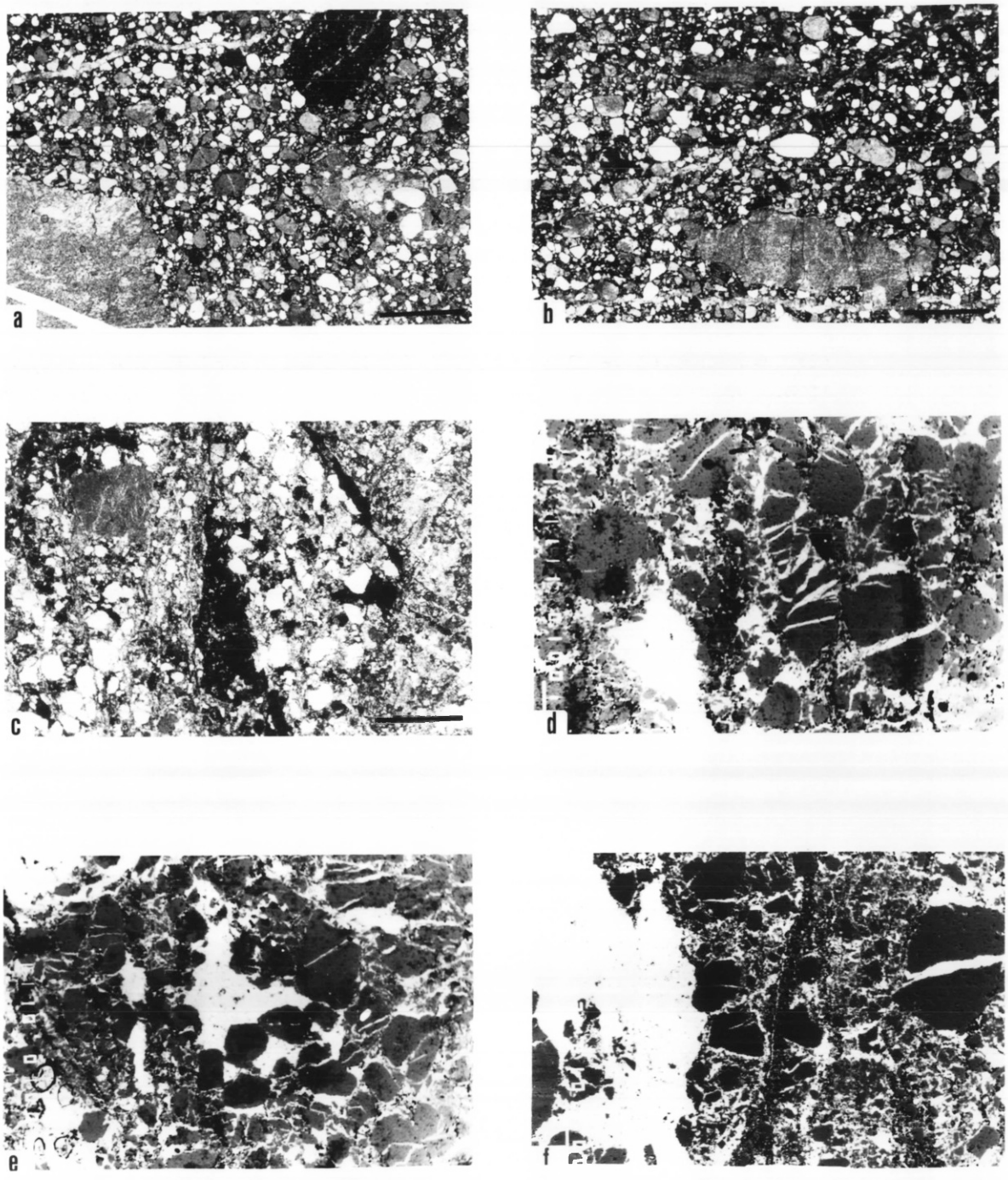


PLATE 6.4 The microstructures characteristic of the Cataclastic Unit.

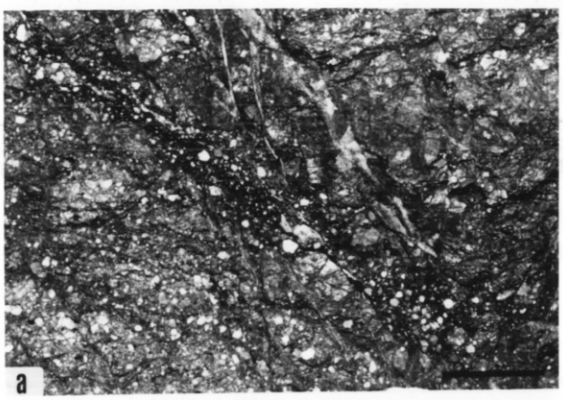
This Plate shows a series of photomicrographs and Back Scattered SEM micrographs from the Cataclastic Unit. The scale bar in all of the photomicrographs is 1mm.

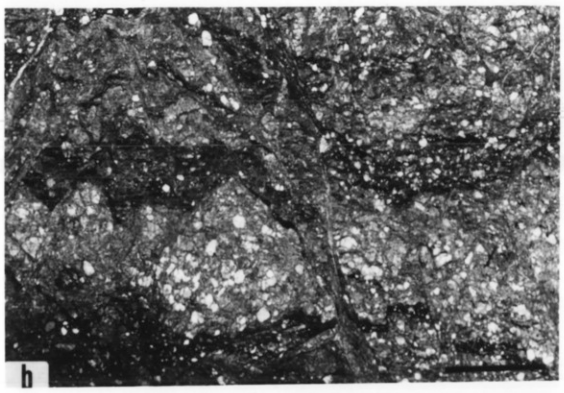
(a), (b) and (c) - These show the microstructures characteristic of the Cataclastic Series of rocks developed in this Unit. (a) and (b) are orientated so that the long axis of the print is parallel to the movement direction, and thus the shape fabric and foliation which is visible is consistent with the thrust movement direction. The rock is formed of quartz grains and Lancara Limestone rock fragments and the matrix is predominantly clay minerals.

(c) - Shows a fragment of the Carboniferous Griotte which has been incorporated into the fault zone from the footwall, and which has been strongly recrystallized.

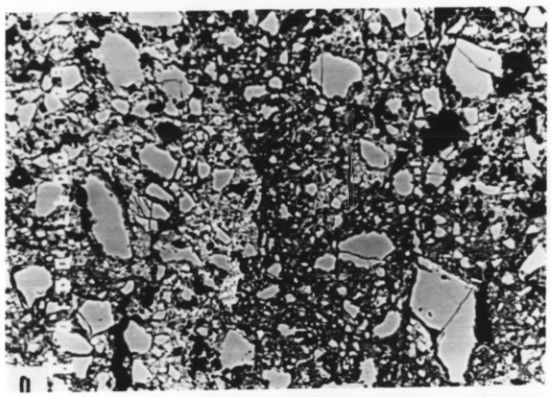
(d), (e) and (f) - These are SEM micrographs of the breccia, and afford higher resolution study of this material. The lighter clasts are quartz grains and the matrix is comprised of clay minerals. Considerable mechanical grain size reduction has occured, note the scale bar. There is an absence of chemical reaction/alteration of the quartz clasts.

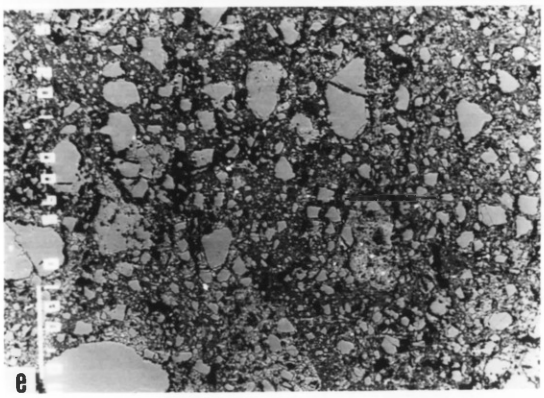
PLATE 6.4

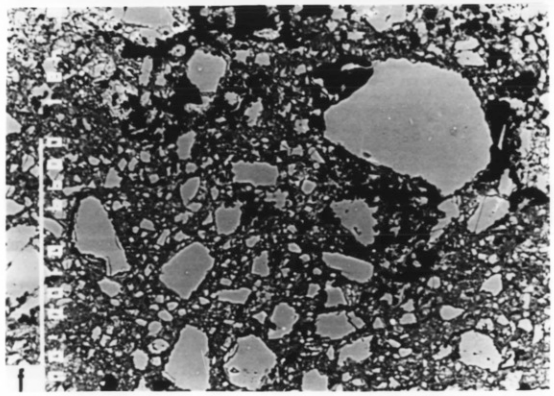












characteristic worm burrows. These blocks have been incorporated from the rock unit below the Carboniferous Griotte which forms the footwall in this locality. See following discussion.

6.8.4 CARBONIFEROUS GRIOTTE

This zone forms the footwall in all of the sections studied, although the degree to which it has been deformed varies between localities. This horizon loses its characteristic red colour below the fault contact (taken as the cataclastic zone), for a depth of up to a metre, instead the rock displays an distinctive white/pink coloration.

Optical microscopy reveals that the grains of calcite are recrystallized and have strongly serrated boundaries, which are often marked by the presence of quartz grains, Plate 6.5a and b. The average grain size was in excess of two milimetres, and as a result the grains are very highly twinned. The heavy twinning and the serrated grain boundaries (thus making difficult accurate grain size measurements) indicated that this rock unit would not be of use for palaeo-stress determination, see section 6.8.4.3.3.

6.8.5 INTERPRETATION AND DISCUSSION

The most striking feature of the fault rocks described above is the abundance of quartz grains. The origin of this material is problematical, since they occur in the matrix of the cataclasites and breccia, but not in the clasts (except where there is evidence to suggest reworking of the breccia after a period of cementation, Plate 6.2a).

It was shown in section 6.8.1 that disseminated quartz grains in the Lancara are progressively concentrated along pressure solution seams, prior to their incorporation into the fault rock. However the general purity of the Lancara (99% calcite) in all the specimens studied suggests that although some of the quartz may have been introduced into the fault zone by this method it is not a valid explanation for the observed abundance in these fault rocks. Additionally the orientation of the stylolites (parallel to the fault plane) and the orientation of the cracks in the quartz grains in the styolites indicates that they formed with $\sigma 1$ at 90° to the movement direction. Therefore it is proposed that pressure solution was dominant in those periods when the fault was relatively inactive and the orientation of $\sigma 1$ corresponded to the overburden of the thrust sheet. The C and T diagrams

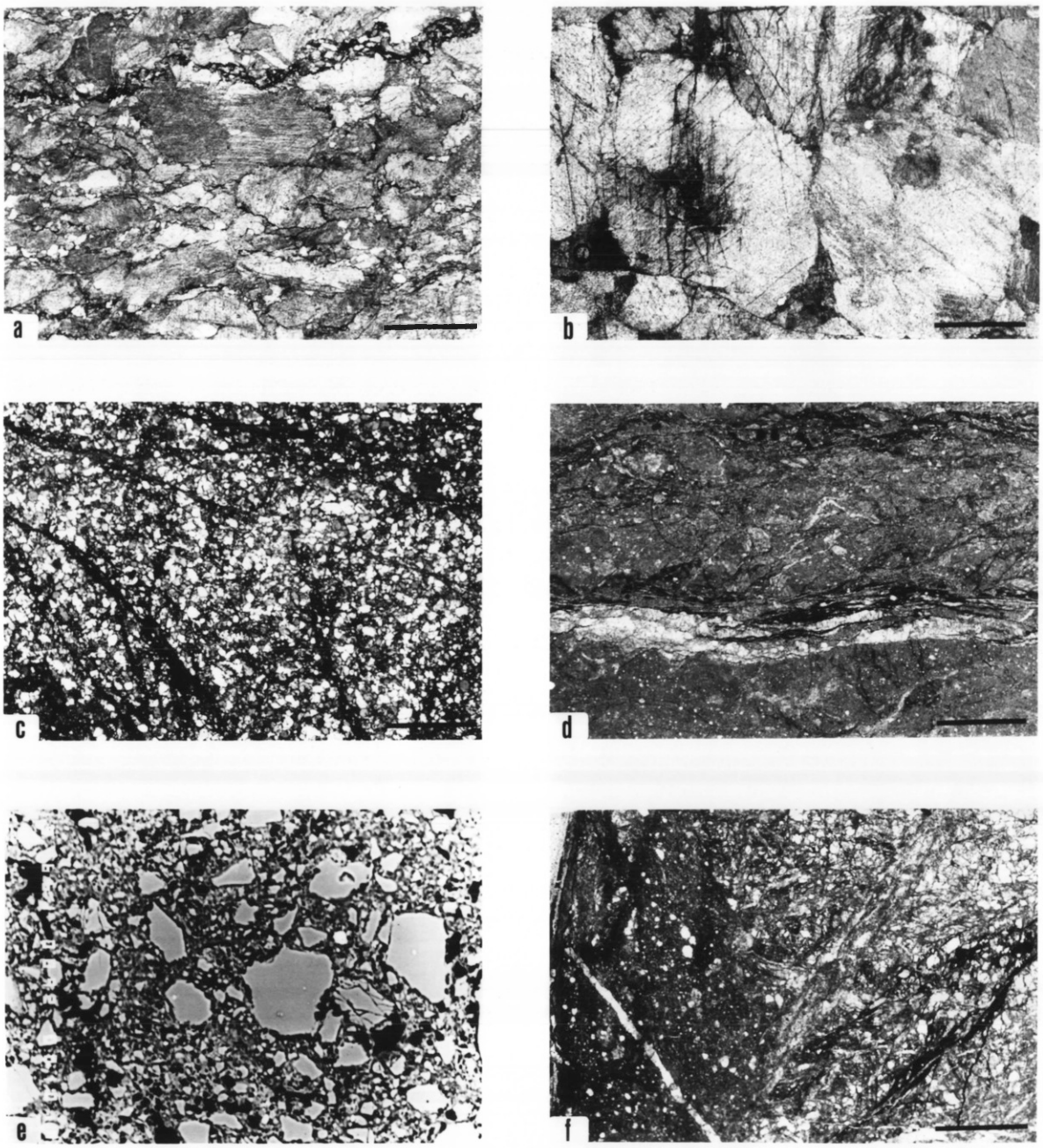
PLATE 6.5 The microstructures characteristic of the Footwall Rocks.

This Plate shows a series of photomicrographs and a single Back Scattered SEM micrograph from the materials which comprise the footwall of the Esla Nappe. The scale bar in all of the photomicrographs is 1mm.

(a) and (b) - Show the Carboniferous Griotte which has been strongly recrystallized. The large grains have been heavily twinned and many have serrated edges with small quartz grains along them as a result of pressure solution. (a) is marked by the presence of a cataclastic zone filled with quartz grains. This may be "channel" by which quartz grains have been incorporated from the Devonian Superior Sandstone through the Girotte into the Cataclastic Series at the base of the thrust.

(c), (d), (e) and (f) show the Devonian Superior Sandstone which is the unit below the Carboniferous Griotte. The contact between these two footwall units is marked by a zone of "fluidization", which has resulted in a thin layer of a gouge like material. This is shown in (d) and (e), the latter is a SEM micrograph and demonstrates the fine grained nature of this material with quartz grains in a matrix of clay minerals. (f) is from the contact between the Girotte and the Sandstone and clearly shows the latter injecting up into the former. (c) shows the Devonian Superior Sandstone below the gouge like layer and shows a series of cataclastic zones. These mark the onset of the deformation which results in the production of the gouge like layer.

PLATE 6.5



presented in Fig. 6.9 and 6.10 illustrate that the compression direction, although variable, indicates that σ1 was orientated at a high angle to the fault plane, for calcite twin lamellae from the Portilla Limestone comprising the footwall in the Corniero-Cremenes section.

Stratigraphically below the Carboniferous Griotte described in section 6.8.4 is the Devonian Superior sandstone, and the quartz grains in this unit appear to be identical to those observed in the fault rocks. It is proposed that elevated pore fluid pressure in accordance with the Hubbert and Rubey (1959) model for nappe emplacement occured in the footwall rocks exposed in the sections studied, i.e. the Carboniferous Girotte and the Devonian Superior sandstone.

The presence of fluid at the base of the nappe promoted leaching of the iron oxides, which gave the griotte its characteristic red colour, and produces the deformed pink/white girotte now observed in the footwall. The iron is now found in veins. Concomitant recrystallization of the girotte will reduce the pore spaces and locally increase the pore fluid pressure resulting in localised hydraulic fracture in the girotte. The presence of high intermittent fluid pressure at the top of the sandstone unit causes fluidization and cataclastic breakdown of the rock, Plate 6.5c-f. Examination of one specimen from the top of the sandstone unit shows that the rock is reduced to a fine grained gouge (Plate 6.5d and e), however there is no discernable displacement along this level. The quartz grains now inject up through the fractures developed in the girotte and onto the base of the nappe where they are incorporated into the cataclasites, Plate 6.4.

This is backed up by the presence of quartz grains marking the boundaries of the calcite grains which form the girotte, Plate 6.4a and b, and the presence of intact blocks of recrystallized Carboniferous Griotte and Devonian Superior sandstone in the cataclasitic zone.

The above model (represented diagramatically in Fig. 6.3) suggests that the fault rocks described in the preceding section are the result of the occurrence of a sandstone unit (i.e. the Devonian Superior sandstone unit) in close proximity to the thrust plane. If this is true then in those areas where the thrust fault has ramped up sequence to higher stratigraphic levels, and fluid pressure can not produce the hydraulic fracturing to "connect" with the Devonian Superior sandstone, we would not expect to see a thick zone of breccia and cataclasite. This is the case at the Cremenes

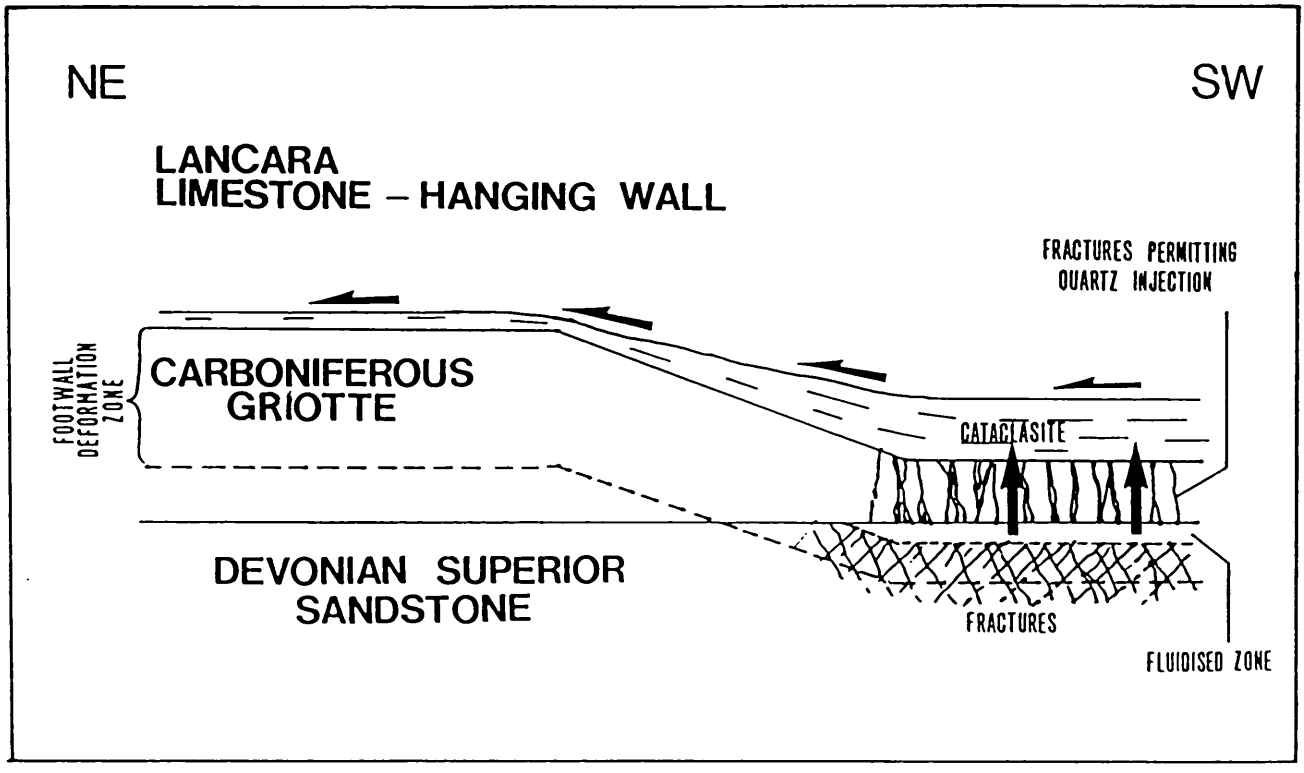


FIGURE 6.3 Diagramatic cross section illustrating the development of the breccia and cataclastic fault rocks by the incorporation of quartz grains from the footwall units.
See text for discussion.

section, Fig. 6.2, where the thrust overlies a four meter thick sequence of the Carboniferous Griotte. Here the breccia is five cm s thick and the cataclasite is 14 cm s thick.

Therefore the thick breccia/cataclasite series developed over most of the base of the Esla Nappe is a localised feature related to the juxtaposition of the Devonian Superior sandstone unit and the thrust fault. It is a structural paradox that the thickest development of the fault rock series corresponds to the deformation associated with a small fraction of its movement, and that the majority of the nappe emplacement history is represented by a much narrower band of deformation.

6.9 FOOTWALL ROCKS

6.9.1 INTRODUCTION

As stated in section 6.6 the footwall has greatest potential for palaeo-stress estimates, because of its passive role during the emplacement of the nappe. However, of the five sections studied only two have a limestone unit (the Portilla Limestone of Devonian age) preserved in the footwall. These are :

1. The Corniero-Cremenes section.
2. The Velilla de Valdore section.

When examined in detail the latter was found to be strongly dolomitised and was unsuitable for comparison with the experimental data presented in Chapter 4. Therefore the former only was examined, the resuts of this analysis are presented below.

6.9.2 SAMPLING PROGRAM AND ORIENTATION OF THE THIN SECTIONS

Orientated specimens were collected from the Portilla Limestone of Devonian age from the Corniero-Cremenes road section, see Fig. 6.2. The distance between specimens varies according to exposure, but the specimens were collected with a bias towards a lower sampling interval as the thrust contact is approached. The distance between the nine specimens analysed, and their spatial relationships to the fault are shown on Fig. 6.7. The orientation of the specimens and their fabric diagrams is shown in section 6.4 and Fig. 6.1.

6.9.3 METHOD OF ANALYSIS AND DATA PRESENTATION

For each thin section 100 grains were analysed using the Universal Stage. The twinning activity and grain size measurements were obtained by the techniques described in Chapter 1. The data set obtained was subdivided into groups according to mean grain size. The grain size interval each group represents is arbitrary, and was taken at 100μm intervals. However, as a result of the large data set in certain groups, it was felt that these could be further divided into 50μm subgroups. The breakdown of the twinning activity data for each thin section analysed is shown in the diagrams presented in Fig. 6.4, and the number of data points in each grain size division is shown in the histograms of Fig. 6.5.

Because twinning activity is a function of:
(a) differential stress, and
(b) grain size (see Chapter 2 and 4),
for each thin section (assuming homogeneous stress distribution throughout the thin section) the range of twinning activity values represent a unique stress level. This method of representing the data has a two-fold advantage:

1. It allows cross correlation and comparison of the twinning activity values as a function of grain size.

2. It allows normalisation of the twinning activity for the whole data set from a thin section to a "standard" grain size, and so enables a direct comparison with the experimental data presented in Chapter 4.

6.9.4 THE RELATIONSHIP BETWEEN TWINNING ACTIVITY AND GRAIN SIZE.

6.9.4.1 INTRODUCTION

As a result of there being few untwinned grains in the data sets analysed the It(%) values obtained were high, see diagrams (1)a-i in Fig. 6.4. This is the result of the mean grain size being above the critical mean grain size which contains the twinning cut-off value. The number of twins and the percentage volume twinned domain per grain were also calculated and it is hoped that these can be extrapolated to indicate the position of the twinning field boundary if there is a general lack of the critical grain size.

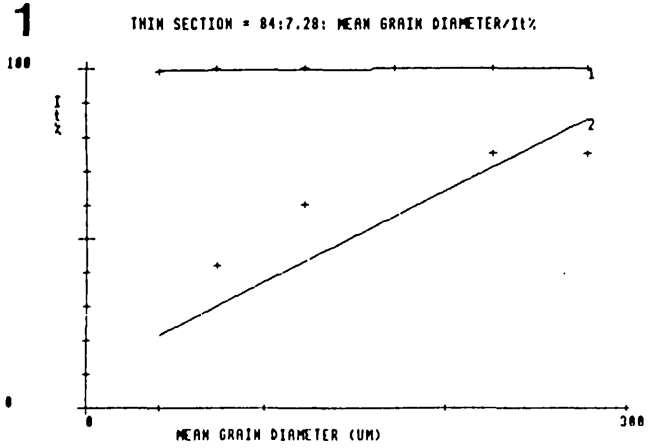
FIGURE 6.4 Textural data from the Cremenes-Corniero section of the Esla Nappe

The series of diagrams (cont. on the following pages) in this figure present the twinning activity data determined for the samples analysed from the Portilla Limestone (which forms the footwall of the Esla Nappe from the Cremenes-Corniero section), plotted as a function of grain size. There are three diagrams for each of the nine samples analysed from this locality, plotting It, number of twins, and percentage volume twin domain (1, 2 and 3 respectively).

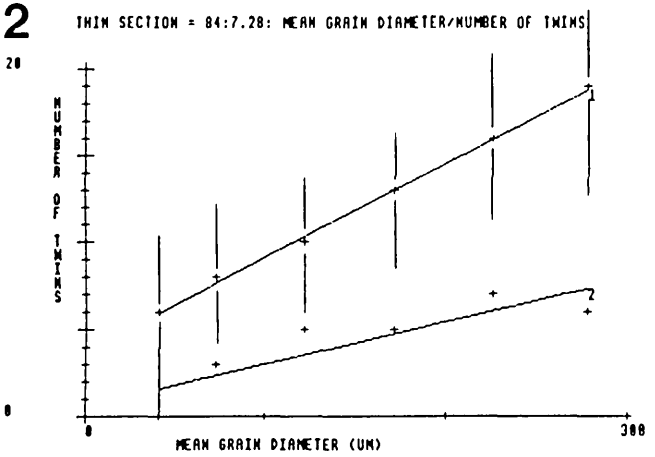
For each sample two twin sets have been analysed, the primary, or principal, twin set, and then second twin set (1 and 2 respectively). The range bars for the appropriate parameters represent the full range of the values determined for each grain size interval.

The individual samples are identified by their respective headings.

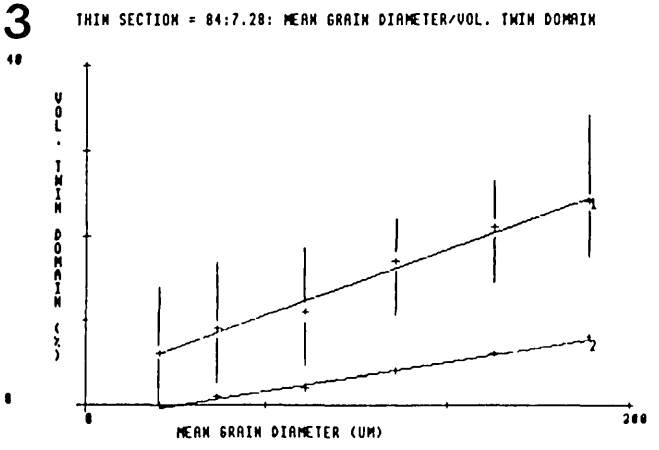
a **1**


THIN SECTION = 84:7.28: MEAN GRAIN DIAMETER/It%
100
It%
0
0
300
MEAN GRAIN DIAMETER (UM)

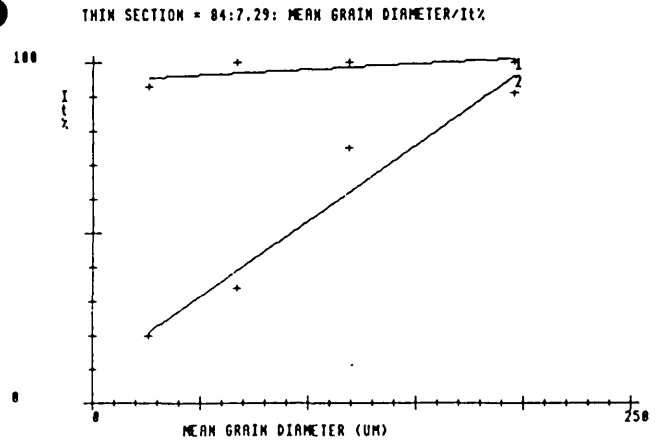
2

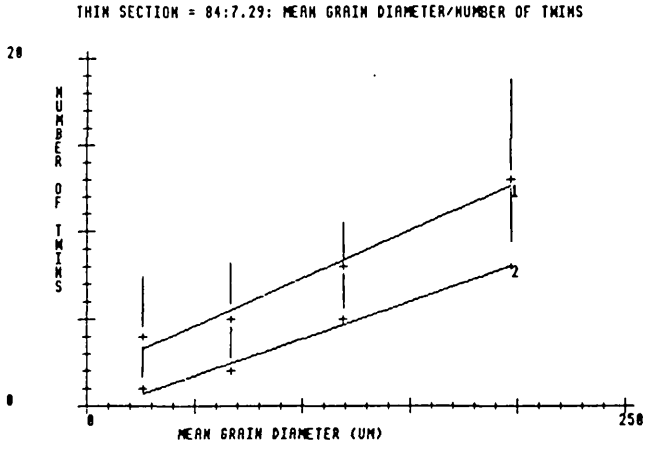

THIN SECTION = 84:7.28: MEAN GRAIN DIAMETER/NUMBER OF TWINS
20
NUMBER OF TWINS
0
0
300
MEAN GRAIN DIAMETER (UM)

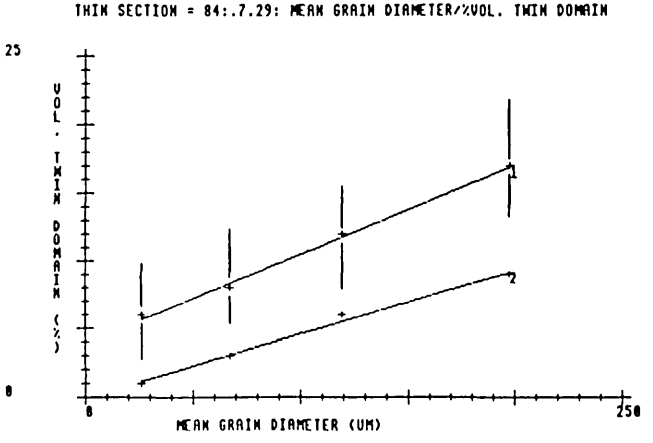
3


THIN SECTION = 84:7.28: MEAN GRAIN DIAMETER/VOL. TWIN DOMAIN
40
VOL. TWIN DOMAIN (%)
0
0
300
MEAN GRAIN DIAMETER (UM)

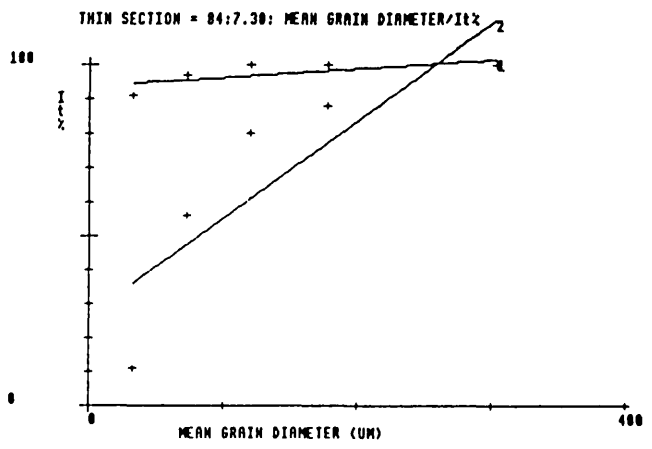
b

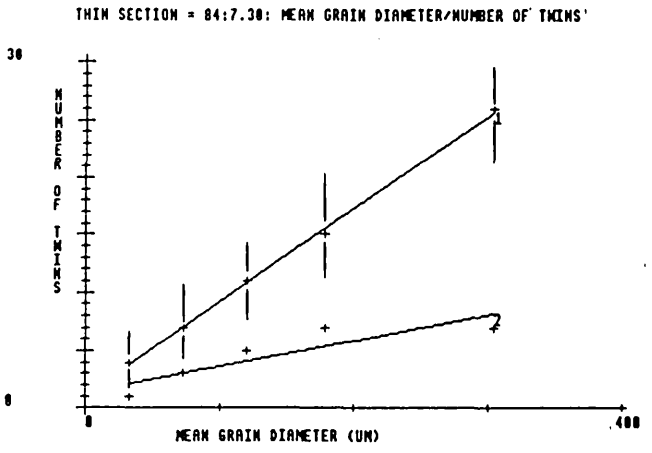

THIN SECTION = 84:7.29: MEAN GRAIN DIAMETER/It%
100
It%
0
0
250
MEAN GRAIN DIAMETER (UM)

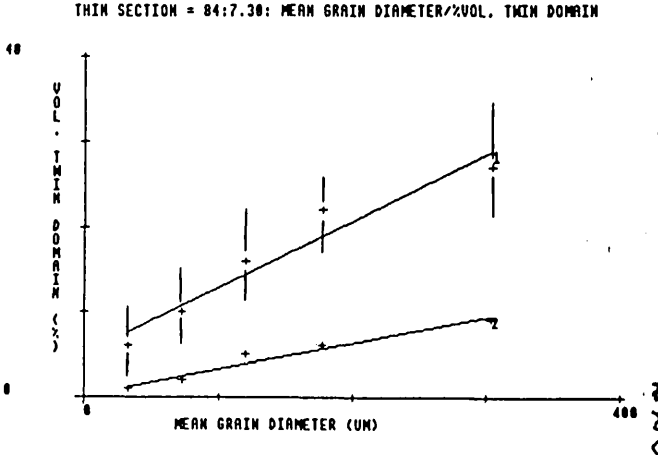

THIN SECTION = 84:7.29: MEAN GRAIN DIAMETER/NUMBER OF TWINS
20
NUMBER OF TWINS
0
0
250
MEAN GRAIN DIAMETER (UM)


THIN SECTION = 84:.7.29: MEAN GRAIN DIAMETER/%VOL. TWIN DOMAIN
25
VOL. TWIN DOMAIN (%)
0
0
250
MEAN GRAIN DIAMETER (UM)

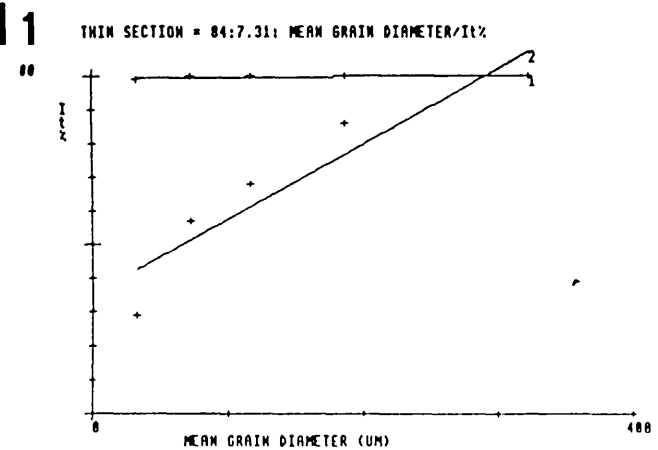
c


THIN SECTION = 84:7.30: MEAN GRAIN DIAMETER/It%
100
It%
0
0
400
MEAN GRAIN DIAMETER (UM)

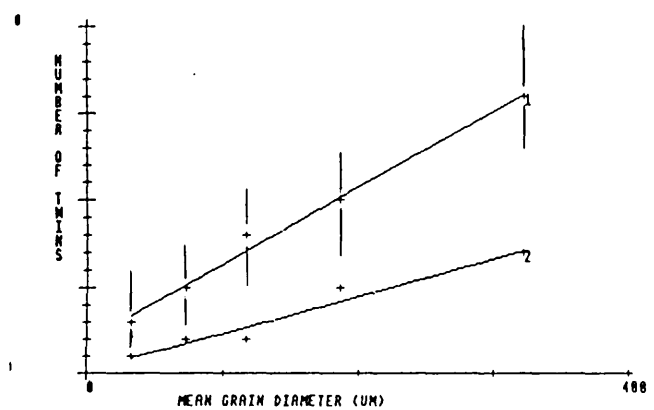

THIN SECTION = 84:7.30: MEAN GRAIN DIAMETER/NUMBER OF TWINS
30
NUMBER OF TWINS
0
0
400
MEAN GRAIN DIAMETER (UM)


THIN SECTION = 84:7.30: MEAN GRAIN DIAMETER/%VOL. TWIN DOMAIN
40
VOL. TWIN DOMAIN (%)
0
0
400
MEAN GRAIN DIAMETER (UM)

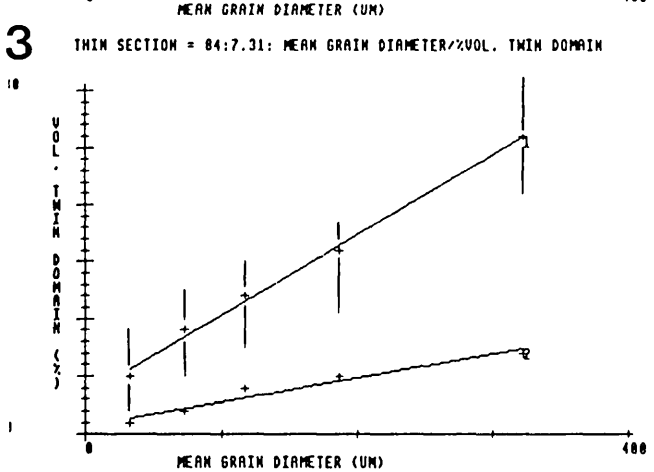
d **1**


THIN SECTION = 84:7.31: MEAN GRAIN DIAMETER/It%
100
It%
0
0
400
MEAN GRAIN DIAMETER (UM)

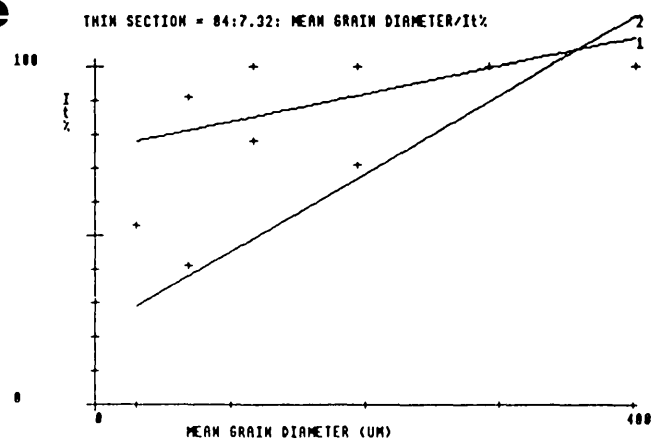
2

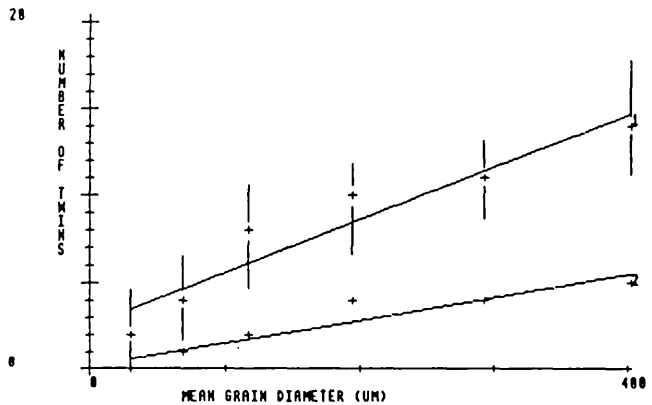

THIN SECTION = 84:7.31: MEAN GRAIN DIAMETER/NUMBER OF TWINS
NUMBER OF TWINS
0
0
400
MEAN GRAIN DIAMETER (UM)

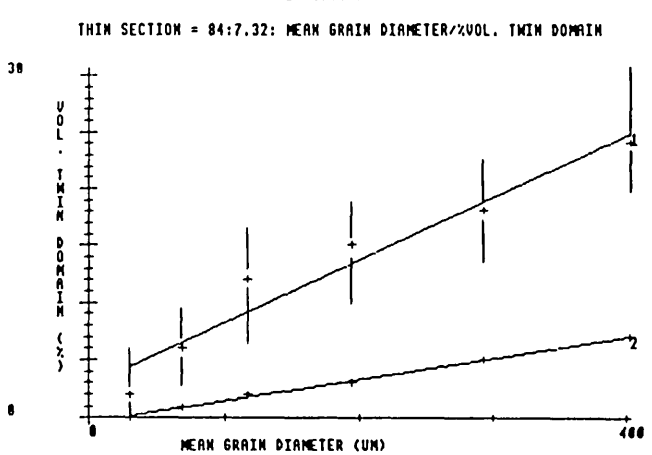
3


THIN SECTION = 84:7.31: MEAN GRAIN DIAMETER/%VOL. TWIN DOMAIN
VOL. TWIN DOMAIN (%)
0
400
MEAN GRAIN DIAMETER (UM)

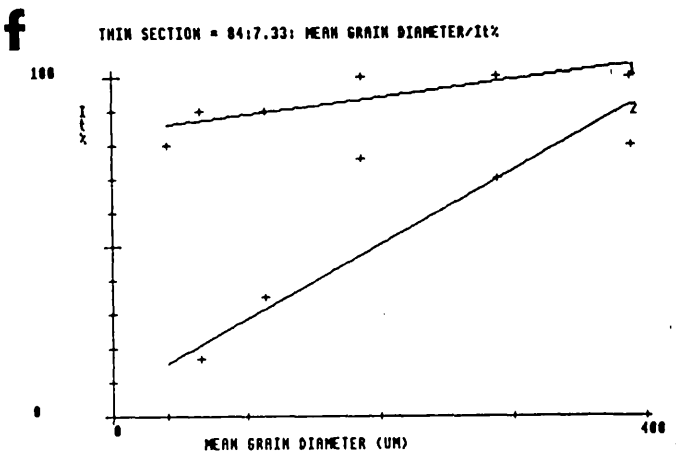
e

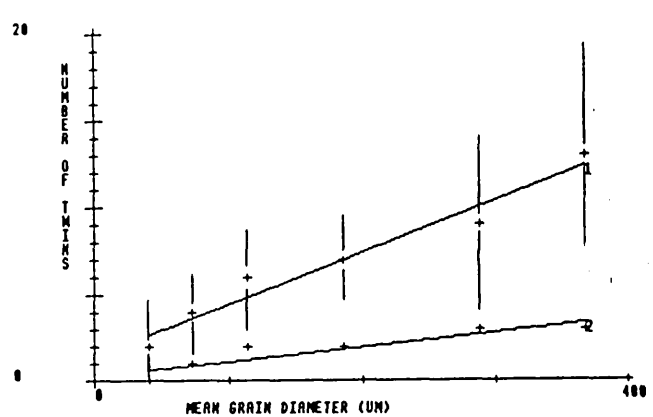

THIN SECTION = 84:7.32: MEAN GRAIN DIAMETER/It%
100
It%
0
0
400
MEAN GRAIN DIAMETER (UM)

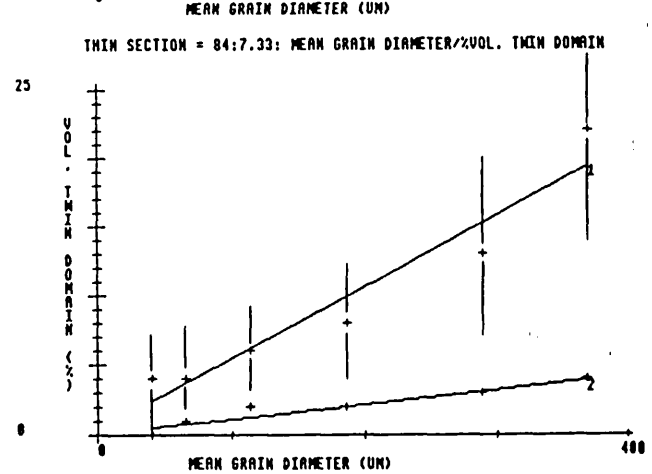

THIN SECTION = 84:7.32: MEAN GRAIN DIAMETER/NUMBER OF TWINS
NUMBER OF TWINS
0
0
400
MEAN GRAIN DIAMETER (UM)


THIN SECTION = 84:7.32: MEAN GRAIN DIAMETER/%VOL. TWIN DOMAIN
VOL. TWIN DOMAIN (%)
0
400
MEAN GRAIN DIAMETER (UM)

f

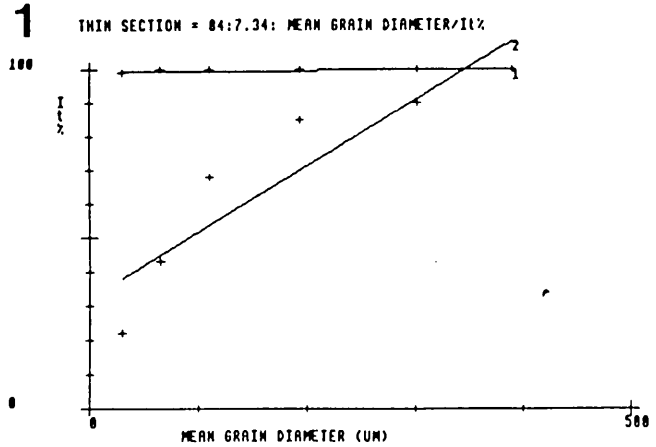

THIN SECTION = 84:7.33: MEAN GRAIN DIAMETER/It%
100
It%
0
0
400
MEAN GRAIN DIAMETER (UM)


THIN SECTION = 84:7.33: MEAN GRAIN DIAMETER/NUMBER OF TWINS
NUMBER OF TWINS
0
0
400
MEAN GRAIN DIAMETER (UM)

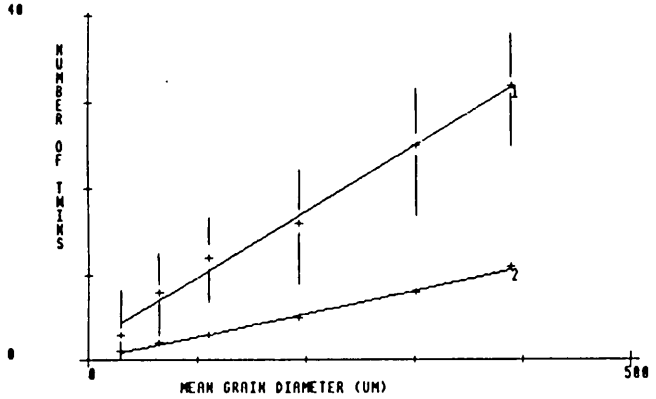

THIN SECTION = 84:7.33: MEAN GRAIN DIAMETER/%VOL. TWIN DOMAIN
VOL. TWIN DOMAIN (%)
0
400
MEAN GRAIN DIAMETER (UM)

g

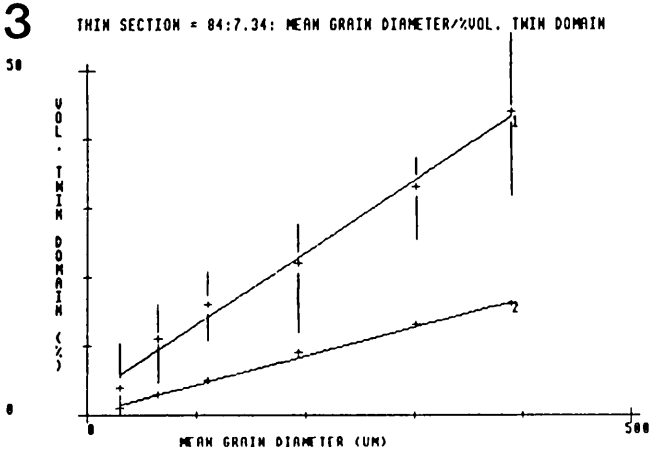
1


THIN SECTION = 84:7.34: MEAN GRAIN DIAMETER/It%
100
0
It%
0
500
MEAN GRAIN DIAMETER (UM)
1
2

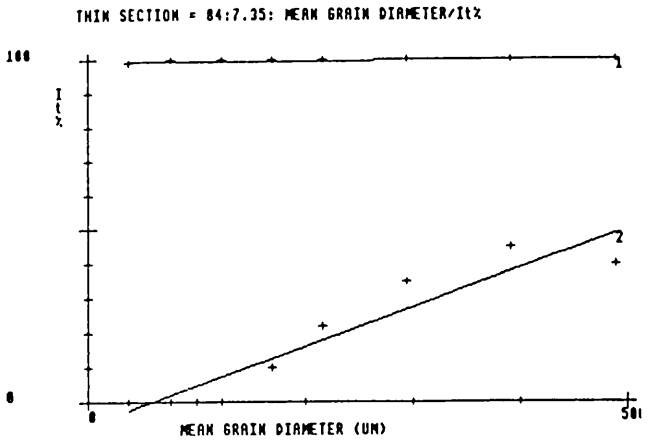
2

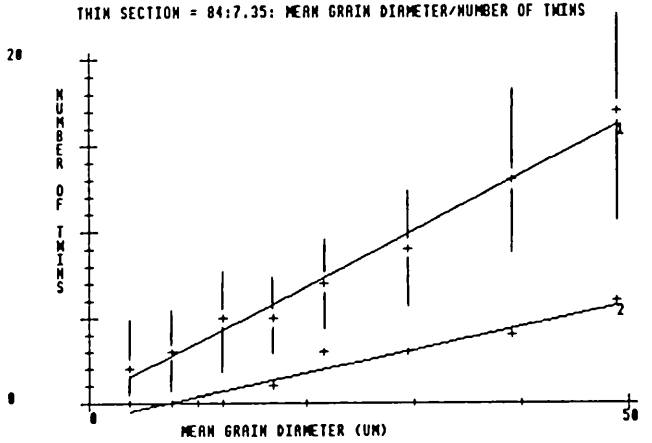

THIN SECTION = 84:7.34: MEAN GRAIN DIAMETER/NUMBER OF TWINS
40
0
NUMBER OF TWINS
0
500
MEAN GRAIN DIAMETER (UM)
1
2

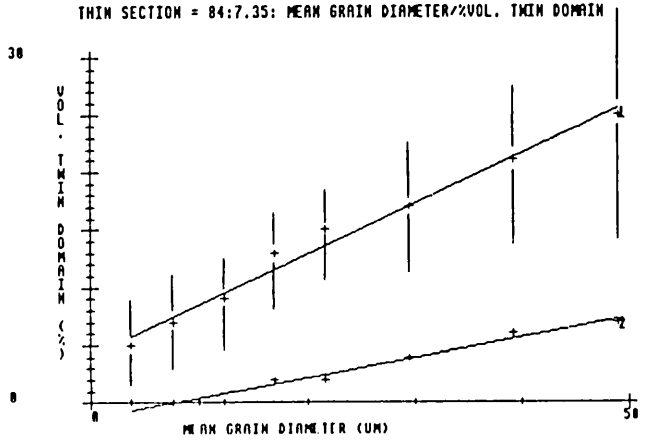
3


THIN SECTION = 84:7.34: MEAN GRAIN DIAMETER/%VOL. TWIN DOMAIN
50
0
VOL. TWIN DOMAIN (%)
0
500
MEAN GRAIN DIAMETER (UM)
1
2

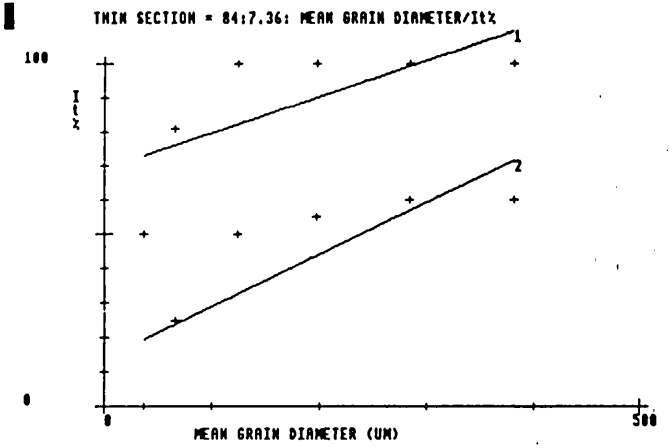
h

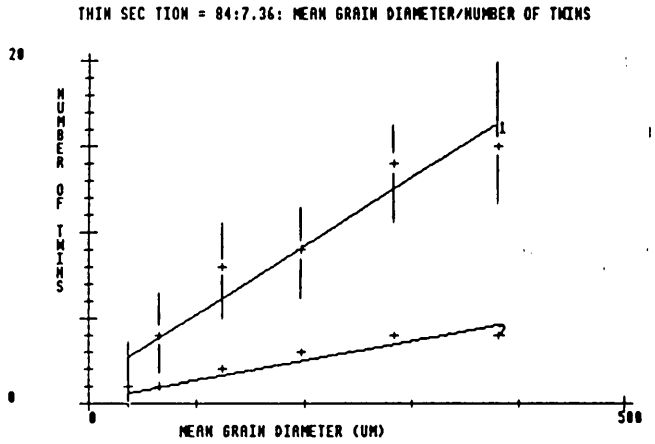

THIN SECTION = 84:7.35: MEAN GRAIN DIAMETER/It%
100
0
It%
0
500
MEAN GRAIN DIAMETER (UM)
1
2


THIN SECTION = 84:7.35: MEAN GRAIN DIAMETER/NUMBER OF TWINS
20
0
NUMBER OF TWINS
0
500
MEAN GRAIN DIAMETER (UM)
1
2


THIN SECTION = 84:7.35: MEAN GRAIN DIAMETER/%VOL. TWIN DOMAIN
30
0
VOL. TWIN DOMAIN (%)
0
500
MEAN GRAIN DIAMETER (UM)
1
2

i


THIN SECTION = 84:7.36: MEAN GRAIN DIAMETER/It%
100
0
It%
0
500
MEAN GRAIN DIAMETER (UM)
1
2


THIN SEC TION = 84:7.36: MEAN GRAIN DIAMETER/NUMBER OF TWINS
20
0
NUMBER OF TWINS
0
500
MEAN GRAIN DIAMETER (UM)
1
2

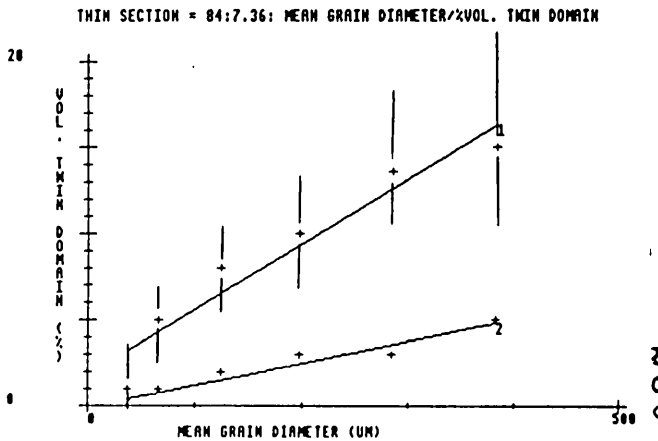
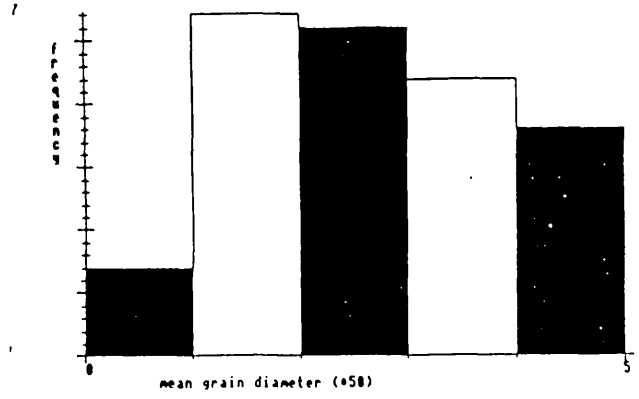
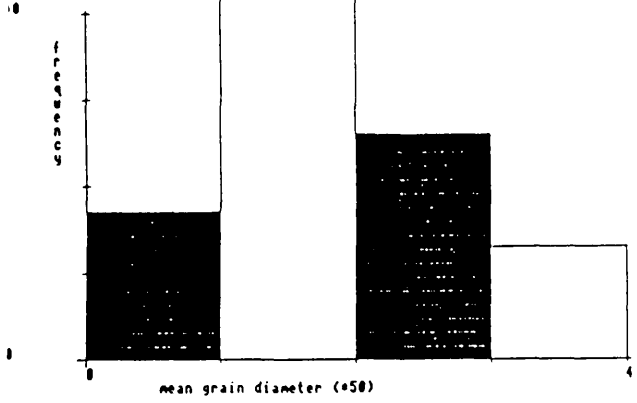

THIN SECTION = 84:7.36: MEAN GRAIN DIAMETER/%VOL. TWIN DOMAIN
20
0
VOL. TWIN DOMAIN (%)
0
500
MEAN GRAIN DIAMETER (UM)
1
2

FIGURE 6.5 Histograms showing the number of data points (grains) in each of the grain size intervals for the diagrams in Fig. 6.4. The individual samples are identified by their respective headings.

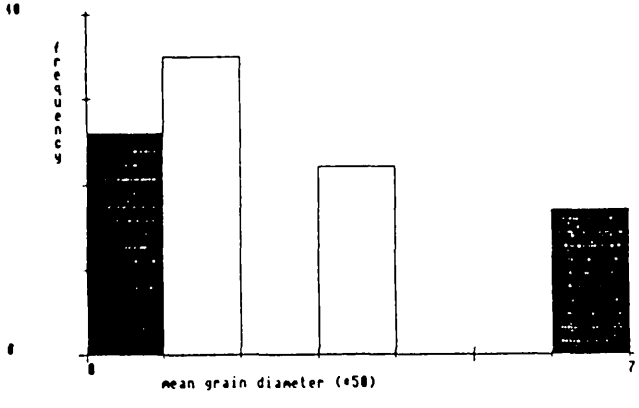
THIN SECTION = 84:7.28 DATA SET = 100



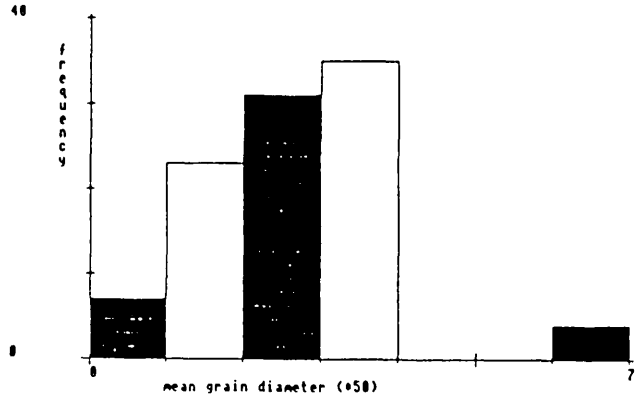
THIN SECTION = 84:7.29 DATA SET = 100



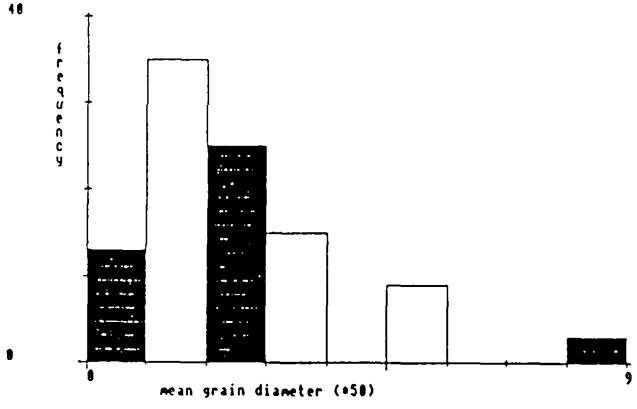
THIN SECTION = 84:7.30 DATA SET = 100



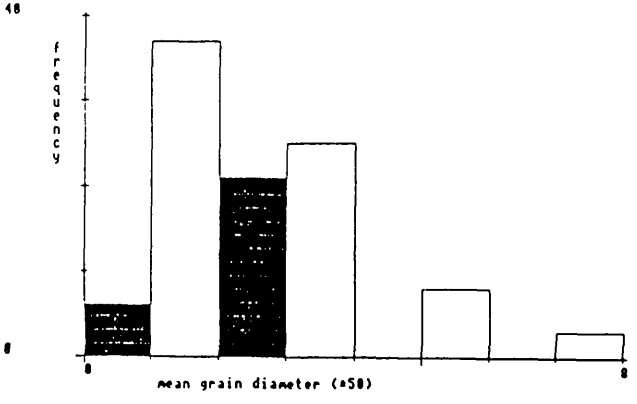
THIN SECTION = 84:7.31 DATA SET = 100



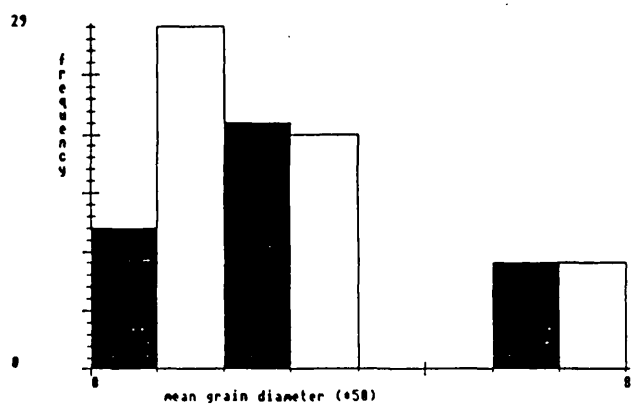
THIN SECTION = 84:7.32 DATA SET = 100



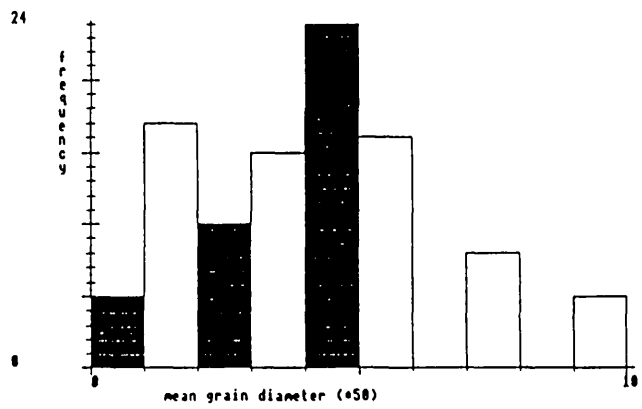
THIN SECTION = 84:7.33 DATA SET = 100



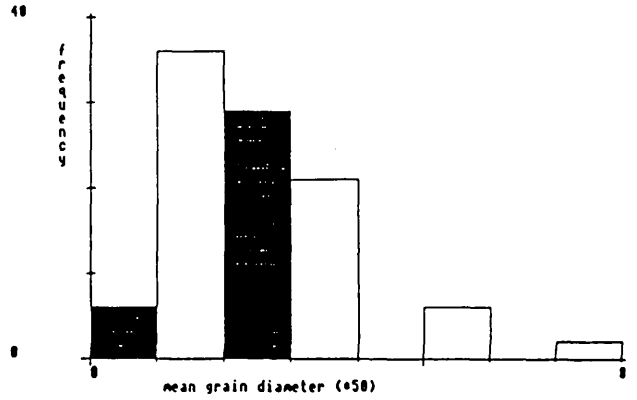
THIN SECTION = 84:7.34 DATA SET = 100



THIN SECTION = 84:7.35 DATA SET = 100



THIN SECTION = 84:7.36 DATA SET = 100



6.9.4.2 TWINNING ACTIVITY AS A FUNCTION OF GRAIN SIZE

Fig. 6.4 shows the twinning activity data plotted as a function of grain size for each of the nine thin sections analysed from the Portilla Limestone. The bars represent the full range of the values recorded. The linear regression lines shown in the diagrams presented in Fig. 6.4 have correlation coefficients in excess of 94%, several are above 99%, which is an excellent fit.

Close inspection of the diagrams in Fig. 6.4 reveals that the data set for any one thin section may be more complicated than the simple linear regression indicates. We can fit a line through any data set, and by so doing hide detailed complications within that data set, see later.

6.9.4.3 INTERPRETATION

6.9.4.3.1 GRAIN SIZE LIMITATIONS UPON TWINNING INCIDENCE AND PERCENTAGE VOLUME TWINNED DOMAIN

The twinning field boundary would be represented by a vertical line on, or an intercept of the linear regressed line with the grain size axis in Fig. 6.4, as shown in Fig. 6.6. As grain size is reduced, twinning activity progressively becomes of lesser volumetric importance (Spiers 1981, Schmid 1982); therefore the percentage volume twinned domain per grain falls to, or approximates to zero as grain size decreases to levels where the applied differential stress is insufficient to initiate twinning.

However, from Fig. 6.4 there is no such clear intercept on the grain size axis for any of the data sets. The absence of a twinning field boundary may indicate high levels of differential stress (for example the twinning field boundary for Solenhofen Limestone (5μm grain size) is approximately at 400MPa) or unforseen complication of twinning activity in this natural system.

There is no immediately obvious reason why we should expect to find a simple linear relationship between percentage volume twinned domain and grain size. It is indicated in Fig. 6.4 that the twinning activity increases with increasing apparent grain diameter with an approximately linear function. Assuming that the shape of the grains are spheres, then twinning activity would be expected to increase approximately as a cubed function of

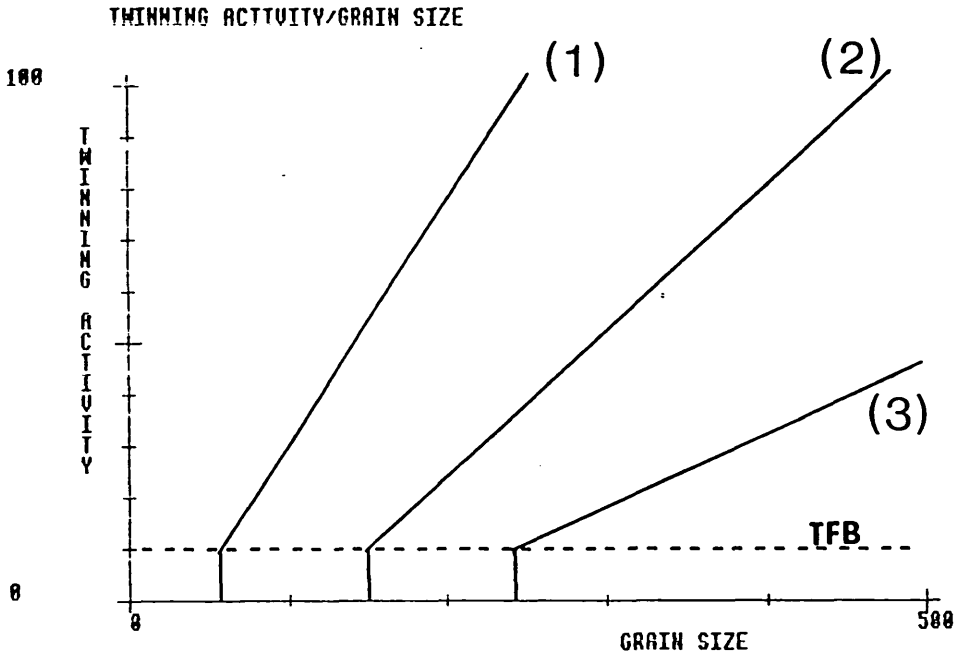


FIGURE 6.6 Diagram showing the theoretical relationships between twinning activity and grain size. TFB is the twinning field boundary, and the numbers represent the predicted twinning activity which results from higher stress levels with increased proximity to a thrust plane.

grain size, as the volume of the grain increases. This is not observed from the data reduction represented in Fig. 6.4.

This relationship may be further complicated by "excessive twin activity" in calcite observed by Spiers (1981), see Chapter 2. That is, once a randomly orientated grain has twinned, the resolved shear stress required to initiate the next twin in that grain will be low relative to that of a similarly orientated grain which had not been previously twinned. Because of this phenomenon larger grains will exhibit abnormally high twinning activity.

Additionally, with reference to the set of thin sections so far studied, those in proximity to the thrust might be expected to exhibit increased excessive twin activity for their larger grain size intervals, because they have been subjected to higher stress levels. These predictions are represented in Fig. 6.4 by the increased range of values for the larger grain size intervals.

6.3.4.3.2 TWINNING CUT OFF

As stated previously a twinning cut-off value (as defined by an It value of 10%), which defines the twinning field boundary would be represented by a range of the twinning activity values falling to zero at the critical grain size on the diagrams presented in Fig. 6.4, c.f. Fig. 6.6.

Inspection of Fig. 6.4 shows that the twinning activity from those specimens closest to the thrust do not show any perceptible indication of a twinning cut-off value (the distances below the thrust plane are shown on Fig. 6.7). On the other hand specimens with a lower bulk twinning activity, i.e. the specimens farthest away from the thrust, indicate that a twinning cut-off value may be present, Fig 6.e-i.

The actual data points for all of the best fit lines in Fig. 6.4 show a systematic relationship. For the lowest grain size interval, typically represented by a mean grain size of approximately 33μm, percentage volume twinned domain values are lower than that of the linear regressed line. This is a direct result of untwinned grains being included within that grain size interval and is indicative of there being a twinning cut-off value within this smallest class division. Hence a twinning cut-off value may be present but the general paucity of data, resulting from a general lack of grains of

less than critical size within this grain size interval, means that further quantification is difficult.

6.9.4.3.3 THE RELATIONSHIP BETWEEN THE TWINNING INCIDENCE, NUMBER OF TWINS AND PERCENTAGE VOLUME TWINNED DOMAIN

The twinning incidence parameter, number of twins and the percentage volume twinned domain parameter have been shown from the Portilla Limestone data to be logically related for those grain sizes where It values are below 100%, i.e. lowest grain size division, with the qualification that the twinning field boundary is poorly defined, c f. diagrams 6.4a-i.

Where the twinning incidence increases to 100% (note that this figure is based on a small data set, and that we are well into the twinning field which is usually defined by twinning incidence values of 10%) the corresponding percentage volume twinned domain values average 6%. An It value of 50% is represented by a percentage volume twinned domain value of between 1 and 2%, therefore the twinning field boundary represented by an It value of 10% is represented by percentage volume twinned domain values below at least 1%. Therefore it is possible to use these values of twinned domain to indicate where the approximate position of the twinning field boundary lies.

The number of twins/percentage volume twin domain ratio is approximately 1:1 for these specimens, however where the It parameter is high the higher stress levels indicated have resulted in ratios of 1:>1. This is because of individual twins coalescing, the result will be a lowering of the number of twins parameter relative to the percentage volume twin domain parameter.

However in this critical grain size interval there are very few data points. Hence the inclusion of any data points which have no twinned fraction will lower the percentage volume twinned domain for that grain size interval to a greater extent than in a larger data set. Additionally a technique where the twinning activity data is extrapolated to a critical grain size is prone to error as the exact relationship is not known. Although the conclusions I have been able to draw are logical.

6.9.4.3.4 PALAEOSTRESS DETERMINATION

When the It values (i.e. >50%) for the lowest grain size intervals (averaging 33μm) where compared with the It map for the experimental data presented in Fig. 4.51 the differential stress levels for all of the specimens is in excess of 400MPa. Additionally those specimens with It's of 100% indicate differential stress levels in excess of 500MPa.

Therefore the level of stress is very high across the profile examined. The range bars shown on Fig. 6.4 have been incorporated in 4.51and this gives a range of approximately ±31 MPa for the data sets discussed in this chapter. However the general paucity of data points within these grain size divisions suggests that errors may be large, although all of the data so far determined indicate logical trends.

6.9.5 TWINNING ACTIVITY ASSOCIATED WITH THRUSTING

6.9.5.1 INTRODUCTION AND DATA PRESENTATION

Figure 6.7 shows the variation in percentage volume twinned domain as a function of distance below the thrust contact for the set of thin sections analysed in the Portilla Limestone. The numbers represent individual thin sections with the preffix "84" removed for clarity, c.f. Figs. 6.4, 6.8 and Plates 6.6 and 6.7, for the corresponding data reductions and petrofabrics. The percentage volume twinned domain values have been normalised for a grain size of 125μm as this value corresponds to the mean for the whole data set.

6.9.5.2 INTERPRETATION AND DISCUSSION

Twinning activity generally increases with proximity to the thrust although this becomes complicated, with the highest percentage volume twinned domain values recorded at 1.9 metres below the contact, in the vicinity of the thrust.

Assuming that no "un-twinning" of previously twinned grains has occurred, the decrease in percentage volume twinned domain in the specimens adjacent to the thrust contact may result from :

1. An irregular thrust surface. A simple topographical high would produce a pressure shadow effect in the rocks of the corresponding

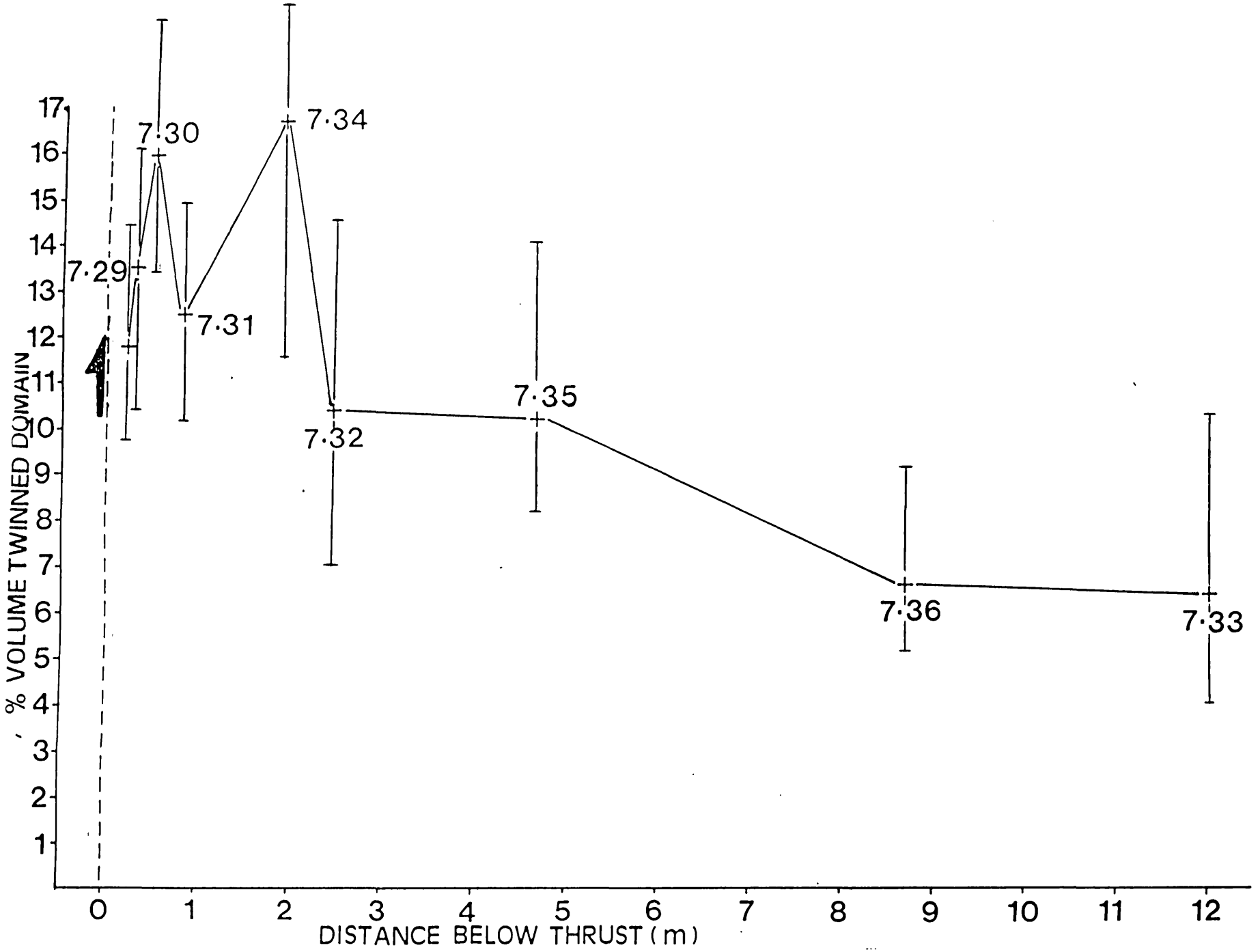


FIGURE 6.7 Diagram showing the percentage volume twin domain of the samples studied from the Cremenes-Corniero section of the Esla Nappe plotted against distance below the thrust contact. The range bars indicate the extrapolated range of the values from the relevant diagrams of Fig. 6.6.

PLATE 6.6 Representative photomicrographs of the Portilla limestone from the cremenes-Corniero section.

KEY : (a) - 7.28, (b) - 7.29, (c) - 7.30, (d) - 7.31, (e) - 7.34 and (f) - 7.32.

This series of photomicrographs show the subtle variation in twinning activity for the Portilla Limestone from the section studied. The scale bar in all of these photomicrographs is 1mm, but note that the scale bar varies between specimens.

The author realises that the subtlety of the twinning activity resulting from the textural analysis are not easily observed in the photomicrographs presented from the field work areas. This is the result of the high twinning incidence values, the thin, planar twins and the extreme birefringence of calcite, whilst trying to maintain continuity between specimens. The extreme birefringence in particular means that black and white photography of the materials presented in this Thesis results in very high contrast. Great time has been spent, both by the author and by Mr. N. Morton (to whom the author is indebted) of the Photographic Dept. at Imperial College in order to produce the best possible Plates for this Thesis, within the constraints available.

PLATE 6.6

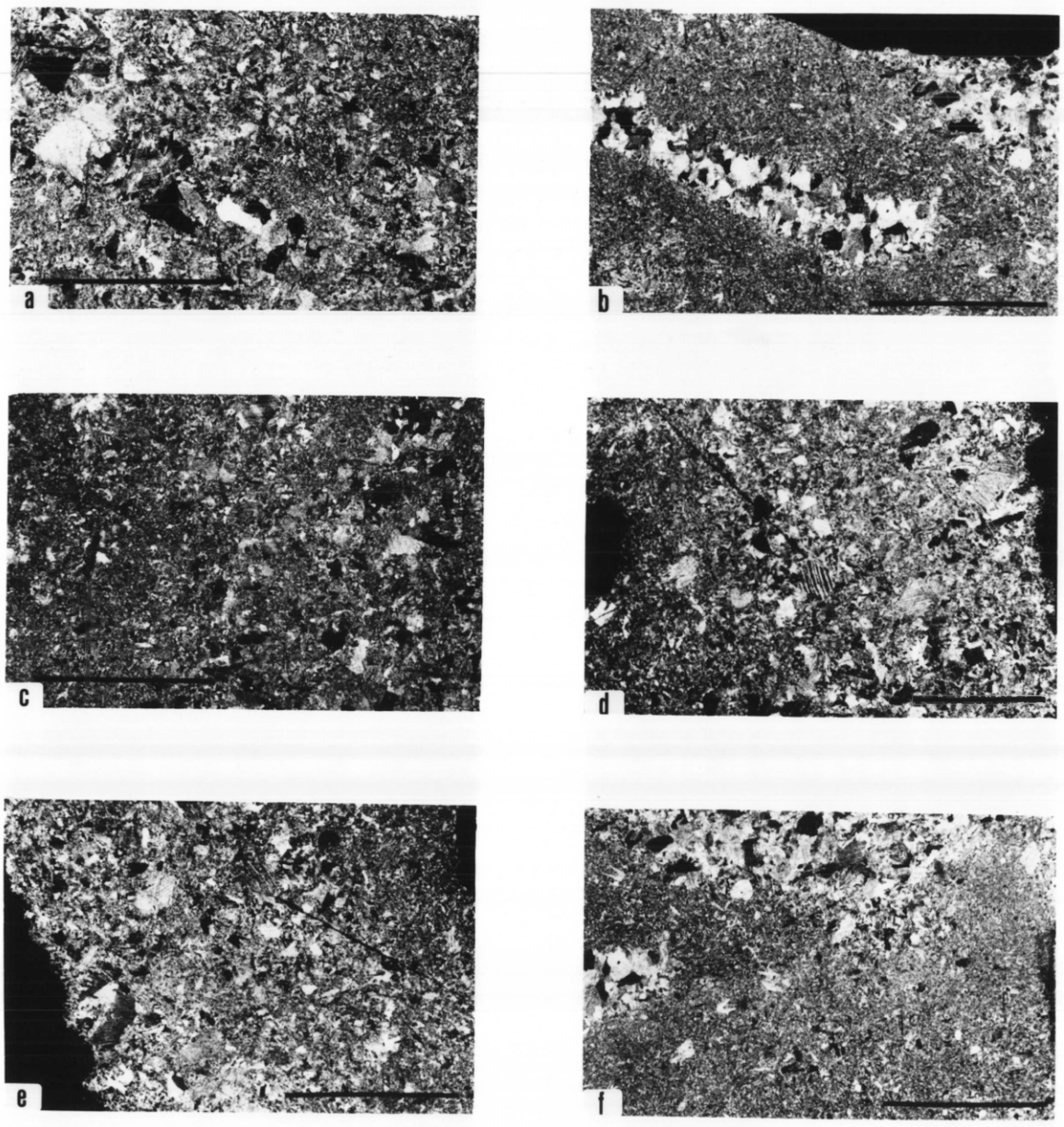


PLATE 6.7 Representative photomicrographs of the Portilla limestone from the Cremenes-Corniero section (cont.).

KEY : (a) - 7.35, (b) - 7.36 and (c) - 7.33.

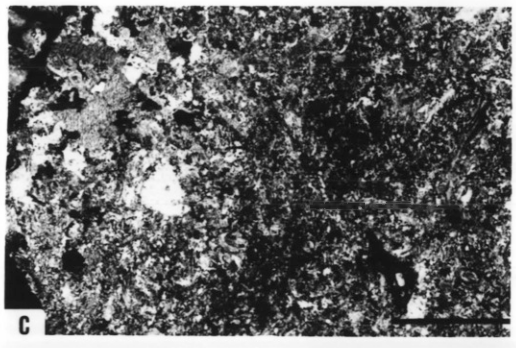
This series of photomicrographs show the subtle variation in twinning activity for the Portilla Limestone from the section studied. These three specimens are from the specimens farthest away from the thrust. The scale bar in all of these photomicrographs is 1mm, but note that the scale bar varies between specimens.

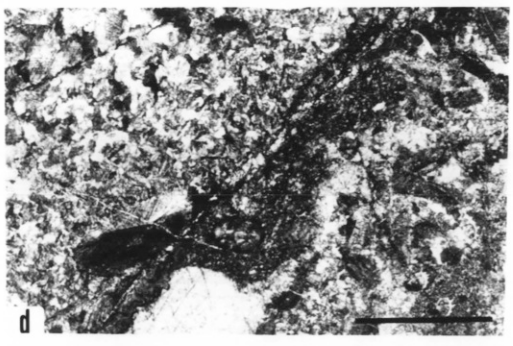
(d) and (e) - These photomicrographs show the development of cataclastic zones within the Portilla Limestone from the Cremenes-Corniero section. The former is from specimen 7.28, and the latter from 7.31.

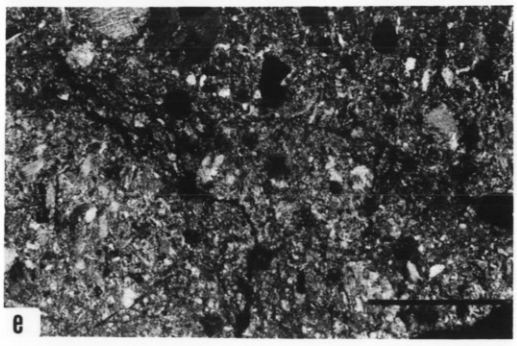
PLATE 6.7











hollow, while the more dominant overall high stress regime prevails below the contact zone.

However field observations show no evidence for thrust plane irregularities, although they would only need to be of metre scale to be effective.

2. As the tip of a thrust ramp propagates through a rock the region immediately adjacent to the thrust plane in the footwall will be subject to an extensional regime. Therefore it is possible that this local extensional regime would negate the general compressional regime associated with thrust emplacement and give the observed drop in twin activity.

The concentration of tensional axes in Fig. 6.9 and 6.10 also indicates an extensional regime. However this tends to prevail across the whole of the region sampled and is not restricted to the tip zone, although the fabric intensifies in the tip region.

3. When the thin sections adjacent to the thrust were thinned to approximately 10μm to facilitate petrofabric analysis, a series of irregularily orientated cataclastic zones were revealed, Plate 6.7d and e. These exhibit grain size reduction and it is thought that if strain is taken up by these zones then less accommodation is required by twin activity. Hence the observed drop in percentage volume twinned domain.

The presence of cataclastic zones in thin section 84:7.31 (Plate 6.7b), which also has a low percentage volume twinned domain value indicates that this may be the reason for the observed drop in percentage volume twinned domain associated with the emplacement of this thrust sheet, although a combination of the latter two factors appears to be the cause of this stress profile.

6.9.5.3 CONCLUSIONS

The critical grain size interval for further investigation of the calcite twinning activity in natural specimens from N. Spain is that of less than 100μm, in particular below 50μm.

As stated above, the level of differential stress obtained from the It parameter is consistently high across the profile examined. Additional data

from the critical grain size ranges is required to enable the twinning cut-off to be more accurately determined. At the present the general lack of data points in the critical grain size interval means that errors may be present. In addition an assessment of the accuracy of the data and the evaluation of any possible errors is difficult because there is no data available for comparison.

Further quantification of the relationship between percentage volume twinned domain and the twinning incidence parameter is required as this would provide a possible means to evaluate errors.

6.9.6 PETROFABRICS

6.9.6.1 INTRODUCTION

Petrofabrics are presented in Fig. 6.8. These represent individual thin sections from the footwall Portilla Limestone. The distance below the thrust for each specimen can be seen from Fig. 6.7, and the breakdown of the data is represented by the relevant graphs of Fig. 6.4. N.B. These diagrams should not be viewed in isolation.

6.9.6.2 DATA PRESENTATION

The petrofabrics in Fig. 6.8 represent e-twin poles and their host grain c axis orientation, the arrow pointing towards the e-twin pole.
These diagrams show the effects of the crystallographic preferred orientation developed through intracrystalline glide and e-twinning activity.

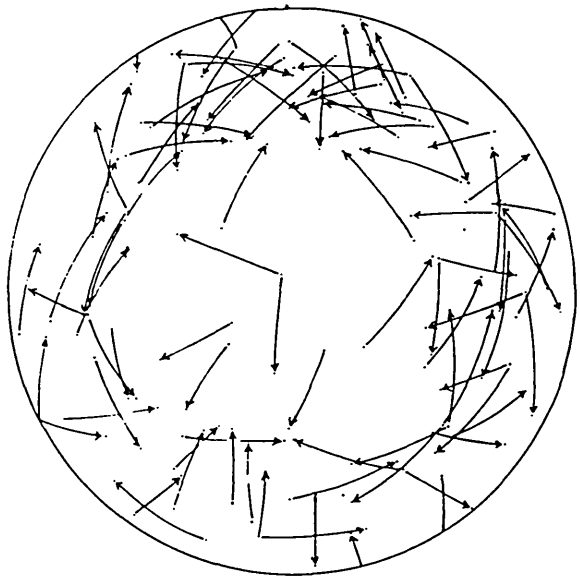
6.9.6.3 INTERPRETATION

6.9.6.3.1 THE EFFECT OF A PRE-DEFORMATIONAL FABRIC

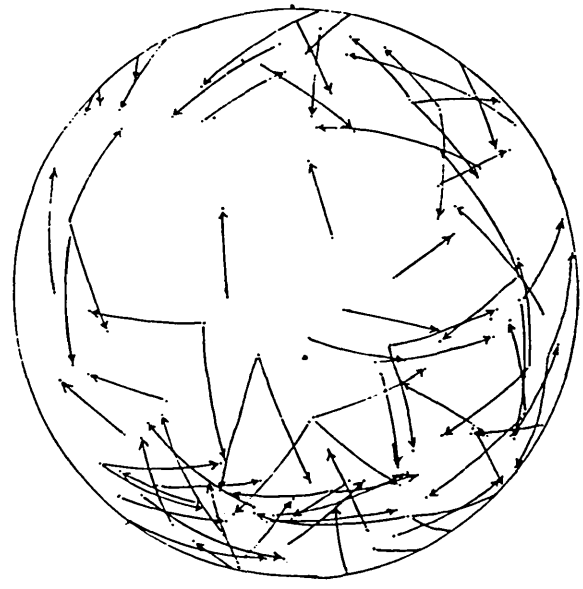
The petrofabric diagrams presented in Fig. 6.8 indicate that a peripheral equatorial girdle may exist, both in the orientation of the e-twin poles and the c axis. This intensifies as we approach the thrust contact, which is predicted as differential stress increases, c f. Fig. 6.8a and d.

The poles to e-twin lamellae represent the rotation of the lattice which forms the new crystallographic orientation of the crystallite. In experiments the e-twin lamellae form a girdle around the direction of

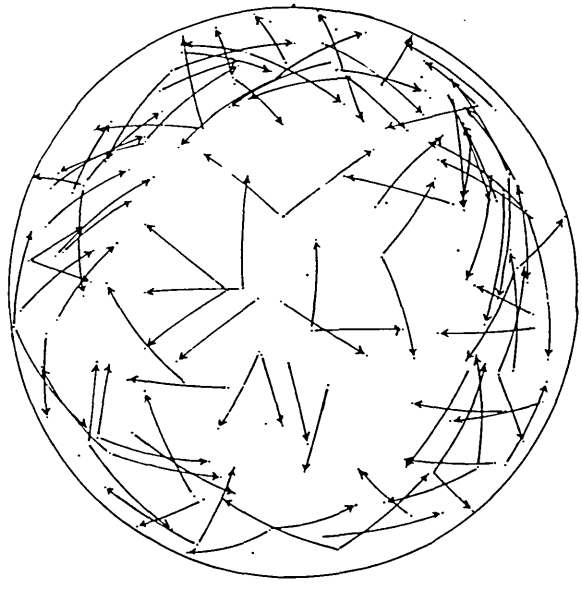
84:7·28



84:7·30



84:7·32



84:7·33

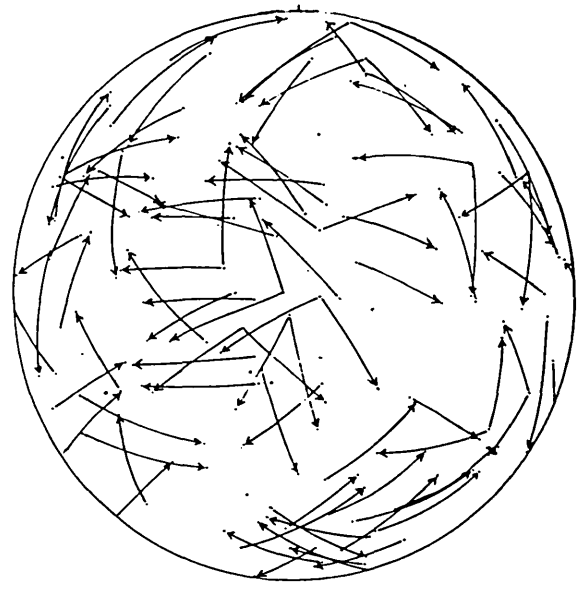


FIGURE 6.8 Selected petrofabrics showing the crystallographic reorientation resulting from twinning activity. These diagrams show the intensification of the fabric with proximity to the thrust, see Fig. 6.7 and text for discussion. The dots represent the original crystallite orientation of the untwinned grains in each of the samples.

maximum compressive stress. This is verified by experimental work (Turner and Weiss 1957).

The presence of a pre-deformational fabric will obviously control the orientation and magnitude of twinning activity when that material is deformed. Therefore any palaeostress estimates on such a rock would be misleading.

However a compressive stress of a given mean orientation acting upon a uniform starting texture will preferentially initiate twinning in relation to that direction, with a corresponding concentration of compressional and tensional axes (using the D. A. T. of Turner, 1954, see later). Therefore the development of a fabric as a result of twin activity is expected.

When those grains which have fractures (instead of twins) or are untwinned are plotted, their c axes give a more uniform initial crystallite orientation for the whole data set. Additionally, analysis of several thin sections orientated at right angles to the orientation depicted in Fig 6.1, i.e. perpendicular to the foliation, if present, and the movement direction, have shown that a preferred orientation of the original crystallites does not appear to be present.

Therefore an initial general uniform texture is present.

6.9.6.3.2 DYNAMIC ANAYSIS TECHNIQUE

The D. A. T. (Turner, 1954, see page 56) has been used to calculate the preferred compressional (C) and extensional (T) axes for the fabrics in Fig. 6.8. Two of these are presented in Fig. 6.9.

The C and T plots of Fig. 6.9 show a marked preferred orientation of tensional axes around the movement direction, implying stretching below the thrust plane. The preferred orientation intensifies as we approach the thrust presumably due to the increase of differential stress. The compressional axes exhibit a more uniform distribution, and some of the twin sets were activated with $\sigma 1$ vertical, i.e. due to the weight of the overlying thrust sheet.

Figure 6.10 shows the C and T axes only for the those grains which have more than ten discrete twin lamellae per grain for the whole of the data set. The effect of grain size has been ignored, although by

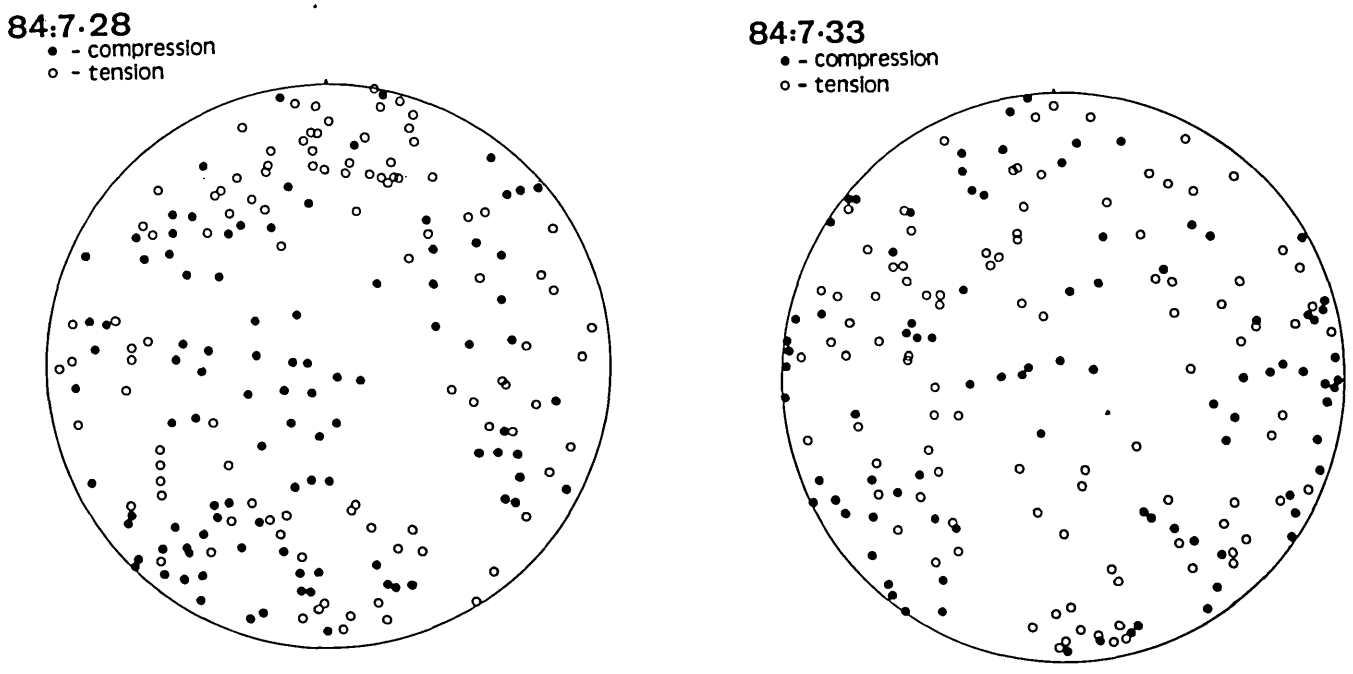


FIGURE 6.9 Selected Dynamic Analysis Technique petrofabrics showing the intensification of the preferred orientation of the tensional axes with proximity to the thrust, note that there is no general preferred orientation of the compressional axes. The location of these two samples is shown in relation to the thrust on Fig. 6.7.

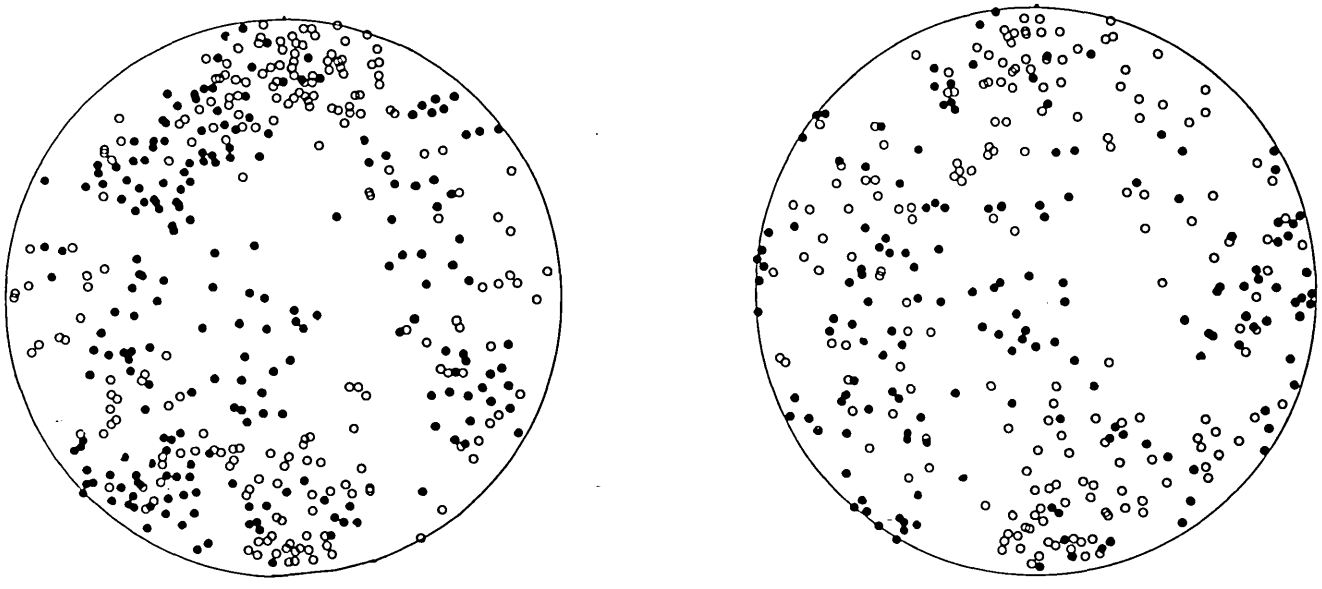


FIGURE 6.10 Two Dynamic Analysis Technique petrofabrics in which the C/T axes of those grains with ≥10 twin lamellae only are plotted. (a) represents the data from the five samples closest to the thrust, while (b) represents the four samples farthest from the thrust, see Fig. 6.7.

consideration of the relationship between grain size and both percentage volume twinned domain and twinning incidence outlined in the above discussion, those grains which have more than ten twin planes will tend towards the larger grain sizes. Fig. 6.10a represents the composite data for the five thin sections closest to the thrust, i.e. those with the higher bulk twin volumes, while Fig. 6.10b represents the composite data from the four thin sections farthest away from the thrust and correspondingly the lower bulk twin values relative to Fig. 6.10a.

It can be seen from Fig. 6.10 that the observed preferred orientation of tensional axes around the movement direction has become accentuated relative to Fig. 6.9. The compressional axes are more randomly orientated, as in Fig. 6.9, but there is an indication of a great circle gidle being present. The exact implication of this great circle girdle is not immediately obvious but may relate to changes in the applied stress field from;

a) one with $\sigma 1$ orientated approximately along the thrust plane at the time of initiation, to,

b) one with $\sigma 1$ orientated subnormal to the thrust plane.

These points are more fully discussed in the next section.

6.9.6.3.3 THE EFFECT OF A HETEROGENEOUS STRESS FIELD

The random pattern of compressional axes may result from variation in $\sigma 1$ during thrust sheet emplacement. Fig. 6.11 shows the predicted stress field around a Type II crack tip. It is clear that as a crack tip propagates through a rock the principal stress axes undergo rotation with respect to the thrust plane with fault propagation. In addition to this, in a natural system there may be other sources of heterogeneity in both stress magnitude and direction.

In the case of the Esla Nappe, which was principally chosen for its relative simplicity, there have been two later phases of folding which have rotated the rocks so that they are now subvertical and this may have involved sufficient strain to induce twinning of otherwise untwinned grains. Another modification may result from variation in the conditions along the thrust plane, e.g. variation in frictional resistance to movement with displacement, owing to thrust plane irregularities, variations in contrasting rock types and ramp/flat fault irregularities. In addition to this there will be a variation in the stress field due to variation in rates of propagation, i.e. as a dislocation moves along the thrust there is a variation both in the magnitude and the direction of differential stress, in time and space. Any (or any combination) of the above

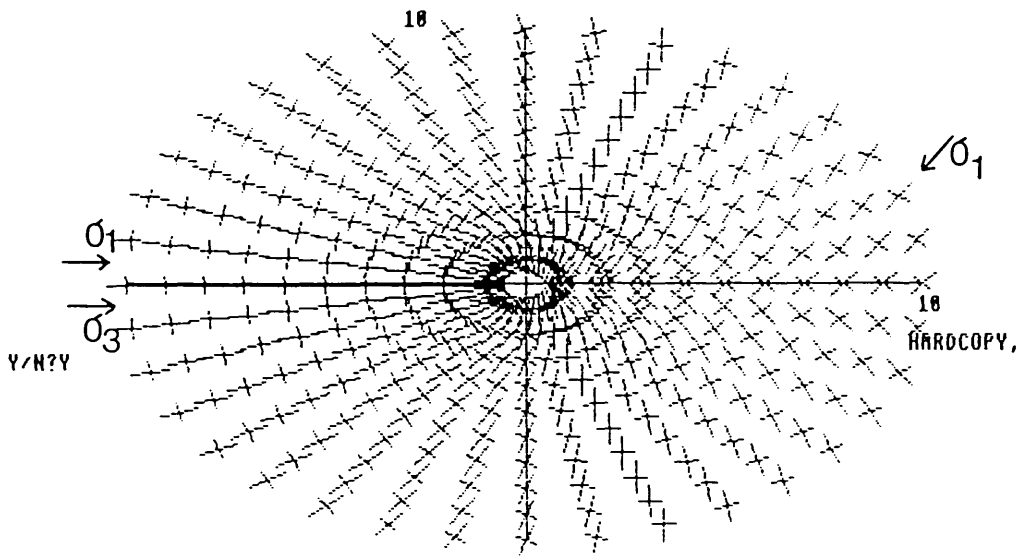


FIGURE 6.11 Diagram showing the stress field configuration around a Type II crack tip, see text for discussion. Diagram drawn by the computer program listed in Appendix 5.

factors will cause rotation of the principal stress axes, both in time and space. In the latter cases, however ,we would expect to see a corresponding variation in the orientation of the tensional axes, which is not observed.

6.9.6.4 CONCLUSIONS

The brief discussion outlined above shows that a natural system may be more complicated than an experimental one where the parameters are strictly controlled. Despite this, the preliminary results of the C and T axis work indicate that the rocks at this locality have been subjected to a relatively simple constrictional deformation, which has not been heavily obscured by extraneous complicating factors.

The above observations and conclusions are encouraging, but need to be compared and contrasted with other examples from other sample localities from the Esla Nappe.

CHAPTER 7 : FIELD AREA 2 : THE SOMIEDO NAPPE

7.1 INTRODUCTION

This chapter details the results of the field work carried out on the second of the field areas studied for this thesis, namely the Somiedo Nappe. After a series of introductory statements regarding location, relief, access, climate and drainage, this chapter details the results of a geometrical analysis of the thrust sheet, and then examines specimens from a number of different localities where there are important structural contacts. The orientation of the specimens and fabric diagrams presented are as described in section 6.4 of the preceding chapter, and the fault rock terminology is the same as that outlined in section 6.3 of the preceding chapter.

To avoid confusion the nomenclature used to describe the various sectors and structural units which constitute the Somiedo Nappe is the same as used by Bastida et al., (1987), which in turn was partially based on the previous work of Julivert et al., (1968), and Van der Bosch, (1969).

7.2 TECHNIQUES USED AND GENERAL AIMS OF THE STUDY

A geological map was prepared of the southern sector of the Somiedo Nappe, which is the area between San Emiliano, Puerta Ventana, Los Cuartos , at a scale of 1:50,000. This map is presented in the back enclosure and a structural map is shown in Fig. 7.1. Two restored sections were prepared along an west-east line which corresponds to the movement direction of the nappe, these are also presented in the back enclosure. Specimens were collected from a number of locations on the basal thrust and several smaller intraformational thrusts for textural analysis leading to the determination of palaeo-stresses.

The aim of this study is to compare the state of stress along several locations on the basal thrust with that which occured in some of the minor thrusts. To enable the correct positioning of the thrusts to be analysed at their time of formation the geometrical sections prepared were restored to their original positions.

7.3 LOCATION AND PHYSIOGEOGRAPHICAL FEATURES

The Somiedo Nappe is situated in the south-western sector of the fold and nappe province of the Cantabrians (Juilivert, 1971), see Fig. 5.2. Geographically it is situated in the Provinces of Leon and Asturias, and

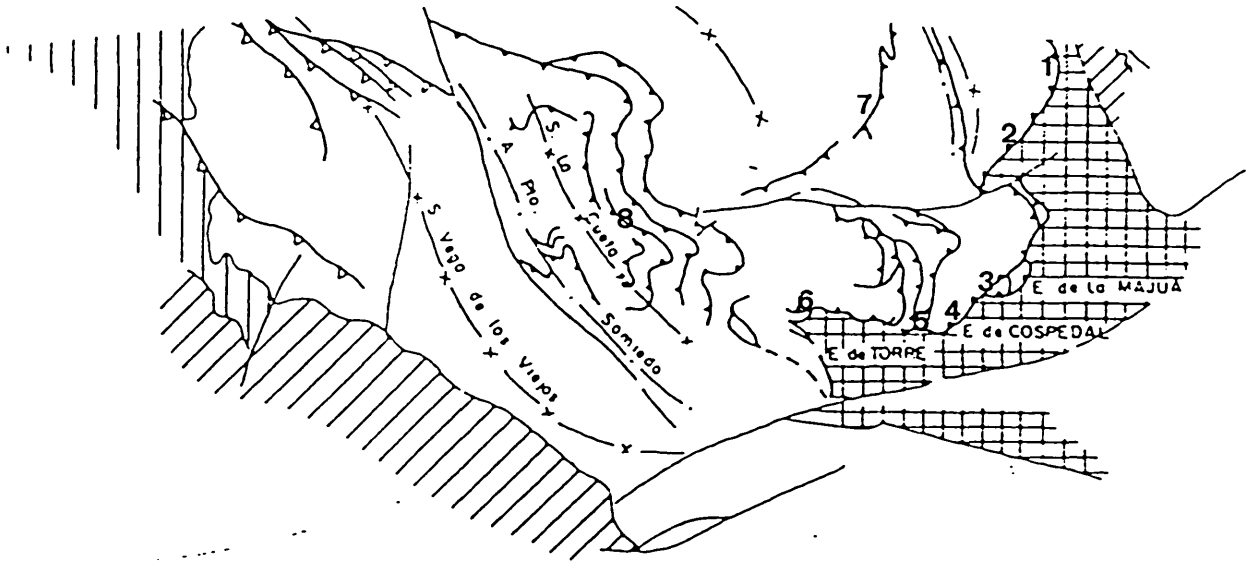


FIGURE 7.1 Structural map showing the key structural contacts of the Somiedo Nappe, for detail the reader is referred to the map and sections presented in the back enclosure of this Thesis.
The numbers represent sample localities :
KEY : 1 - Puerta Ventana, 2 - Torrestio road section, 3 - La Majua, 4 - Cospedal, 5 - Robledo, 6 - Torre de Babia, 7 - Santa Lucia Tectonic Wedge, 8 - Portilla Tectonic Wedge.

occupies the high ground that forms the border between these two Provinces. The relief varies from 1200 meters in the valley around Villasecino to 2100+ meters in the Picos Albos, see map in the enclosure at the back of this thesis.

The climate and therefore the vegetation and land use is dependent upon the physiogeographical location, the north facing slopes have a maritime climate, while the south facing slopes have a near continental climate. The majority of the land on the southern slopes is forested, while on the southern slopes the majority of the land is farmed. Drainage is by a number of rivers draining north and south, depending upon their location. Access was achieved via a series of tarmac roads and village/farm tracks. Exposure depends upon the vegetation cover, but is in general extremely good.

7.4 GENERAL GEOLOGICAL SETTING

The Somiedo Nappe is one of the major thrust sheets of the Cantabrians (see Fig. 5.2 and 5.4), and the stratigraphy is shown in Fig. 5.3. Like the Esla Nappe described in the preceding chapter it displays typical Appalachian style fold and thrust "thin skinned" tectonics. Because of the size of this unit, the results presented below are from the southern sector of the thrust sheet. For a detailed treatment of the Somiedo Nappe (a) as a whole, and (b) the north-west sector, the reader is referred to Gomez de Llarena, 1946; Gomez de Llarena and Rodriguez Arango, 1948; Garcia Fuente, 1959; Juilivert et al. (1968); Van der Bosch (1969); Truyols et al. (1982) and Bastida et al. (1987), and Heredia (1984), respectively.

The western margin of the Somiedo Nappe is marked by the mass of precambrian material which forms the Narcea Antiform. As a result of the décollement horizon being located in the Precambrian in this sector of the nappe the total thickness of the stratigraphic sequence is approximately 4,500 metres (Bastida et al., 1987).

The stratigraphic sequence shown in Fig. 5.3 consists of a series of alternating limestones, quartzites, sandstones, shales and ironstones, which enable the sequence as a whole to display a remarkable anisotropy, which at least in part controls the structure that develops. This is discussed later.

As is the case with all of the Cantabrian nappes internal strain features are restricted to the fault zones in the Somiedo Nappe, and the stratigraphy which constitutes the thrust sheet are strain free (c f. cataclastic damage

associated with folding of the more competent units, Blenkinsop, pers com.). Although cleavage is locally developed in certain areas, Plate 7.1.

7.5 STRUCTURE OF THE SOMIEDO NAPPE

The sequence of events is the same as described for the Esla Nappe, however the position of the Somiedo Nappe on the outer sector of the Asturian Arc means that the radial fold set is less well developed than for the Esla Nappe, see Chapter 6. The sequence of events is :

1. Initiation and emplacement of thrust sheets.
2. Development of reverse faults in the west of the nappe.
3. Development of the longitudinal fold set.
4. Development of the radial fold set.

From Bastida et al., 1987.

The Somiedo Thrust Sheet has a strong internal structure as a result of the presence of minor thrusts within the thrust sheet. These effectively compartmentalise the thrust sheet into many smaller thrust bound units which have undergone movement relative to each other.

7.5.1 THE BASAL THRUST

The general décollement, or basal thrust, is located near the base of the Lancara Limestone across most of this nappe. The basal thrust is easily recognised both as a result of the large stratigraphic jump it represents and the topographic feature which the overiding thrust sheet affects. The stratigraphic jump with the lower-middle Cambrian Lancara Formation resting upon the late Namurian and Westphalian sediments of the San Emiliano Formation is clearly visible along the eastern and southern margins of the nappe. The geometry of the hanging wall relative to the footwall along the east margin of the nappe implies that a footwall ramp is present, similarily the geometrical relationships between the villages of La Majua and Torre de Babia (Fig. 7.1) imply that an oblique ramp may be present, and that this forms the southern margin of the nappe.

It is only in the sector adjacent to the Narcea Antiform that the hanging wall flat geometery is disrupted, here the Lancara Limestone can be seen to rest comformably on the Precambrian represented by the Herreria Formation. Hence it has been inferred that the décollement level is at a lower stratigraphic level, i.e. situated in the Precambrian Herreria and Mora

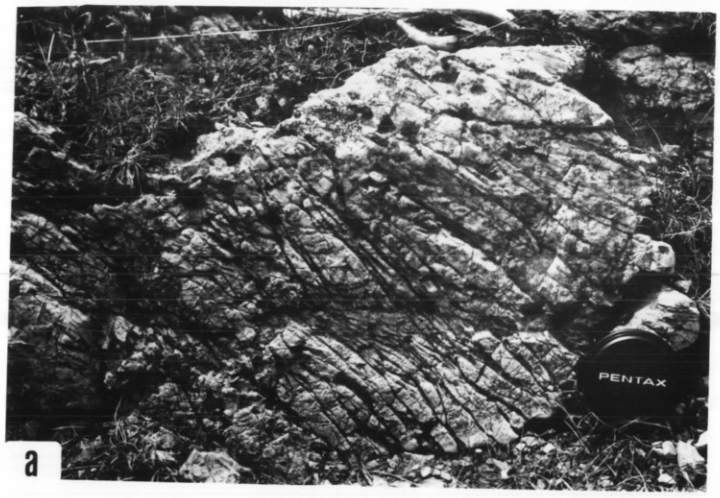
PLATE 7.1 Selected field photographs from the Somiedo Nappe, showing the characteristic microstructures.

(a) - Shows a typical example of the cataclasis that developes in some of the competent carbonate horizons. This specimen is from the Lancara Formation above the village of La Majua.

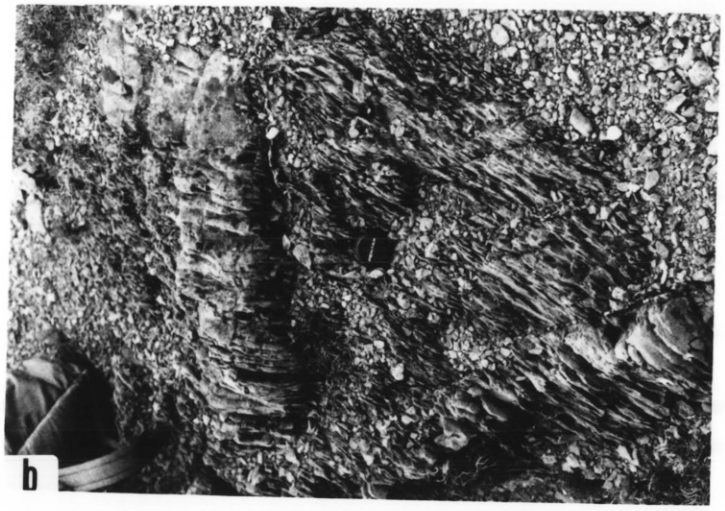
(b) - Shows the development of a fully pervasive axial planar cleavage in the La Vid3 Formation above the village of Torre de Babia.

(c) - Shows the development of non pervasive cleavage (orientated vertically in the photograph) in the La Vid2 Formation, approximately 1 Km to the north of the village of La Majua. Note the refraction of the cleavage from the dolomitic horizon to the shally bed at the top of the photograph.

PLATE 7.1



a



b



c

Formations (Heredia, 1984; Bastida, 1987), and hence a footwall ramp is implied.

The basal thrust will be described in more detail in the following section describing the textural analysis.

7.5.2 GEOMETERY OF THE THRUST SHEET

As discussed briefly above and shown in the restored sections in Fig. 7.2 the Somiedo thrust sheet has a complex internal geometery. These can be genetically grouped into the following, after Bastida et al. (1987).

1. Major internal thrust systems, defining individual thrust sheets.
2. Imbricate thrust systems.
3. Tectonic wedges.
4. Reverse faults.
5. Oblique ramps.

7.5.2.1 MAJOR INTERNAL THRUST SYSTEMS

So called because these [illegible] major thrust faults compartmentalise the interior of the thrust sheet. These systems are identical to the basal thrust from which they branch and possess a normal ramp and flat geometery, except that they have a smaller displacement. Only one such fault occurs in the area mapped, namely the Villar de Vildas thrust, although the Alto de la Mesa thrust may also be classed as a major internal thrust. The Belmonte thrust to the north of the Alto de la Mesa thrust does not outcrop in the area mapped but has been identified as a major internal fault which clearly branches onto the frontal basal thrust to the north of Puerta Ventana, see Bastida et al. (1987) Fig. 5.

The Villar de Vildas thrust is restricted in occurrence, in the area mapped, to the Santa Lucia Limestone, where it has the appearance of being a tectonic wedge (see later). However reconnaissance mapping and the maps of Heredia (1984), Fig. 3, and Bastida et al. (1987), Fig. 5, have shown that in the area to the north-west of the village of Villar de Vildas this thrust branches onto the basal thrust. The displacement on this fault has a maximun value of 3.5Km.

Therefore the presence of the thrust in the Santa Lucia Limestone to the east of The La Cueta syncline corresponds to the approximate position of the

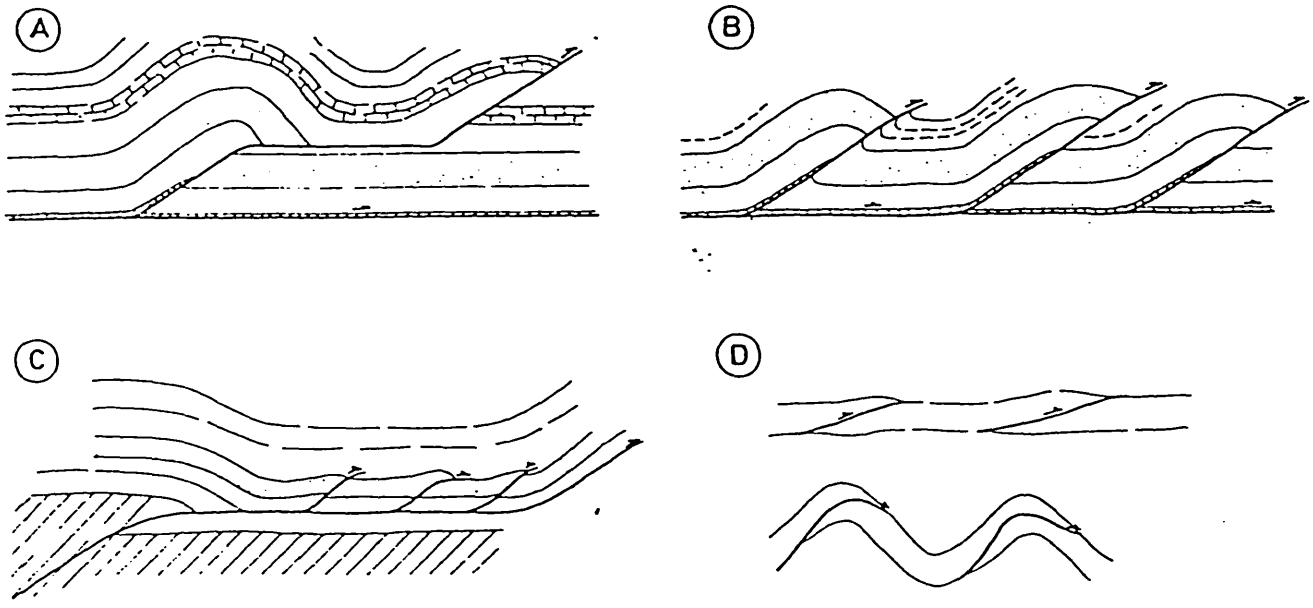


FIGURE 7.2 Sections showing the development of folds as a result of the ramp and flat configuration of a thrust sheet. After Bastida et al., 1987.

tip zone for this thrust, as here it appears as a tectonic wedge in terms of its displacement. This region is one of extreme complexity (Fig. 7.1), as a tectonic wedge is also present, and it appears that the tip zone and the wedge are interrelated. Possibly the wedge is the geometric consequence of the presence of the propagating tip zone. Plate 7.2a shows a smaller thrust which forms a tectonic wedge in the Santa Lucia above the tip zone in this area.

The La Cueta area (Plate 7.2d) has a number of monoclinal flexures, which because they are situated above the ramps of the Villar de Vildas thrust have been interpreted as being hanging wall folds Bastida et al. (1987).

7.5.2.2 IMBRICATE THRUSTS

These thrusts branch off the basal thrust and affect those formations up to the La Vid3 horizon, this is the incompetent shale upper member of the La Vid Formation, Fig. 5.3. These imbricates can be clearly seen along the southern margin of the nappe, between the villages of La Majua and Torre de Babia, Fig. 7.1, and have typically less than 1Km displacement. They can be clearly seen cutting up section in the field at a angle approximating to 30°, see Plate 7.2c.

The thrusts ramp up through the lower competent carbonate members of the La Vid Formation, but appear to flat and die out in the thick shale horizon the upper member of the La Vid Formation. There may be a roof thrust in this horizon, which would define a duplex, however there is no evidence of any displacement within this unit and it is concluded that the imbricates die out in this formation.

It can be seen from Fig. 7.1 that an east-west trending sinisteral strike slip fault cuts the sequence up to the level of the La Vid3 horizon, and also dies out in this thick shale horizon. The imbricates appear to be laterally branching into this fault, which then dies out within the La Vid3 horizon to the west. Associated with the termination of this fault is a region of tight folding, which is the "ductile bead" of this fault. The apparent propagation of this fault to the west, which is in the opposite sense to the propagation of the Somiedo Nappe, is explained by the fact that the fault dies out vertically in the La Vid3 horizon, which is exposed to the west of the lower stratigraphic formations.

There is a complex genetic interrelationship between the thrust systems and the strike slip fault, this is illustrated by comparing the two sections in

PLATE 7.2 Selected field photographs from the Somiedo Nappe, showing several types of structures that typify the Nappe.

(a) - Shows a Tectonic Wedge to the north-west of the village of Torre de Babia. The thrust flats in the La Vid3 Formation (LV3) and can be seen ramping up into the Santa Lucia Limestone (SLL). This photograph was taken looking to the north-east, and the ridge is approximately 2 Kms distant.

(b) - Shows the abrupt southern closure of the Lagos de Saliencia syncline, which was interpreted as the result of an oblique ramp at depth below this area. The photograph shows the contact between the La Vid3 (LV3) and Santa Lucia Limestone (SLL) Formation, which is folded to produce a spectacular mushroom fold. This photograph was taken looking to the north and the ridge is approximately 2.2 Km distant.

(c) - Shows the frontal hanging wall ramp (BQ) developed in one of the imbricate thrusts to the north west of the village of La Majua. The La Vid3 Formation (LV3) forms the footwall at this locality. Subsequent folding resulting from the stacking of thrusts below this thrust has resulted in the sequence now being locally inverted. The photograph was taken looking to the north-east, and the ridge is approximately 1.4 Km distant.

(d) - Shows the Tectonic Wedge to the east of the village of La Cueta, the specimens from which were used as the basis of one of the textural studies performed in this chapter. Subsequent folding has rotated the thrust so that it is now vertical. The photograph was taken looking to the south and the ridge is approximately 0.45 Km distant.

PLATE 7.2









the back enclosures. These are located to the south and north of the strike slip fault respectively, and demonstrate the variation in structure between the two sections below the La Vid3 stratigraphic horizon.

7.5.2.3 TECTONIC WEDGES

These are thrust faults which affect the competent Santa Lucia and Portilla Carbonate Formations, e.g. in the Picos Albos, to the west of the village of Torrestio and to the east of the village of La Cueta. They have small displacements, i.e. as little as tens of metres, and typically flat and die out in the incompetent shale and sandstones Formations above and below the carbonate formations, Plate 7.2a and d.

They are a manifestation of the mechanical property contrast between the different formations in the stratigraphic column.

7.5.2.4 REVERSE FAULTS

These faults are restricted in occurrence to the western sector of the nappe, Fig. 7.1. They cut the thrust faults and relate to the upwelling of the mass of Precambrian materials of the Narcea Antiform in the later stages of the Hercynian Orogeny. See also Heredia (1984), and Bastida et al. (1987).

7.5.2.5 OBLIQUE RAMPS

Bastida et al. (1987) have shown that the change in cartographic trace producing the abrupt southern termination of the Saliencia Lakes syncline (Fig. 7.1) is most satisfactorily explained if the presence of an oblique ramp is admitted. Therefore the flat corresponding to the Saliencea Lakes syncline is terminated by a south-west to north-east trending oblique ramp structure, which produces the north-west dips which characterise the north-eastern area mapped, Fig. 7.1. This closure is particularly spectacular in the Santa Lucia, Portilla and Caliza de Montana carbonate formations, Plate 7.2b. The Carboniferous materials which form the footwall (the Sobia-Bondon unit, see Fig. 5.2) are limited in their western extent in this sector. However in the area between San Emiliano and Torre de Babia (Fig. 7.1) the Carboniferous materials of the Sobia-Bondon unit clearly underlie the Somiedo Nappe. Therefore an oblique structure is postulated (Bastida et al., 1987).

The abrupt change in the cartographic trace of the basal thrust from north-south between Puerta Ventana and La Majua to east-west between La Majua

and Torre de Babia indicates that another major east-west oblique ramp structure is present in this region. This could also explain the imbricates which characterise this area, see section 7.5.2.2 and Fig. 7.1, as the back stresses produced by an oblique ramp would inhibit the westward propagation of the thrust sheet. Therefore the nappe propagates by a series of relatively minor footwall collapse thrusts, which are now preserved as imbricates.

7.5.3 DEVELOPMENT OF FOLDING

Bastida et al. (1987) have interpreted the longitudinal folds as the mechanical consequence of the emplacement of the nappe, although some tightening of the folds occurred after the nappes were emplaced. This may be related to the development of the reverse faults in the west of the area mapped, Fig. 7.1. The four situations which give rise to the formation of the folds are (from Bastida et al., 1987), and Fig. 7.2:

A. Minor thrusts with a flat/ramp trajectory, e.g. the Villar de Vildas thrust sheet.

B. Imricate thrusts producing hanging wall anticlines and footwall synclines, e.g. to the north-west of La Majua.

C. A flat zone which has its posterior margin monoclinally flexured by a wedge of Precambrian materials, e.g. the Vega de los Viejos syncline.

D. The tectonic wedges result in thickening of certain parts of the stratigraphy, which can then be tightened to give small scale folds, e.g. in the Santa Lucia to the west of La Cueta.

N.b. the letters correspond to the respective diagrams in Fig. 7.2.

As stated previously the radial fold set is restricted to minor flexuring in the Somiedo Nappe because this area is situated on the outer margin of the Asturian arc.

7.5.4 FACTORS WHICH DETERMINE THE ORIGIN AND EMPLACEMENT OF THE NAPPE

The absence of extensional features in the posterior part and the strong internal structuration of the Somiedo Nappe have led Bastida et al., (1987) to suggest that the nappe was not emplaced as a result of sliding on an inclined plane, i.e. the gravitational sliding model of Hubbert and Rubey (1959). The

major factor which initiated the development of Cantabrian nappes in general and the Somiedo Nappe in particular was the rising of the Hercynian mountain chain to the west, giving rise to eastward directed nappe structures in the Asturo-Leonese zone, e.g. the Mondendo Nappe, see Chapter 5. The emergence of this mass of material gave a posterior push to the Cantabrian nappes and produced a gravitational effect, Bastida et al. (1987). Therefore the model suggested to explain the initiation of the Somiedo Nappe is model (c) of Hubbert and Rubey (1959), i.e. a combination of posterior push and gravitational sliding, although the former is dominant and results in the latter, Bastida et al., (1987).

Bastida et al., (1987) state that according to the mechanical analysis of Hubbert and Ruby (1959) the maximum length for the five kilometre thick Somiedo Nappe would be approximately 18Kms. When the modifications suggested by Hsu (1969), Raleigh and Griggs (1963) and Forristall (1972) are applied, then the maximum predicted length of the hanging wall block is approximately 10Kms. The restored sections presented in the back enclosure indicate that the length of the Somiedo Nappe is approximately 35Kms. Hence some other factor needs to be considered.

The sediments of the Herreria Formation below the Lancara Formation would have potentially contained a lot of fluid which would have been unable to permeate the Lancara. Bastida et al. (1987) have calculated the pore pressure, indicated by the factor λ of Hubbert and Ruby (1959), as between 0.75 and 0.84 depending upon the cohesive strength of the material under consideration. The existence of high fluid pressures at the base of the nappe is further indicated by (Bastida et al., 1979) :

1. Abundant mineralisation (barite and cinnabar) associated with fractures along the basal thrust, and indicate a temperature of formation consistent with the overall conditions prevailing in the Cantabrians at this time, i.e. 150-230°C (Fernandez, 1974).

2. Irregular dolomitization of the Lancara Formation above the basal thrust.

Unlike the Esla Nappe discussed in the previous chapter the base of the Somiedo Nappe is not characterised by a well developed fault rock zone. Over most of the area mapped the base of the nappe appears to be characterised by a very thin layer of cataclasite and/or breccia, which is usually not exposed. There are some exceptions e.g. the Robledo-Cospedal zone, where the base of the

nappe is characterised by a wide zone of folding, accommodated by cataclasis. The axis of these folds is subparallel to the basal décollement plane and the extensional direction of these associated cataclastic fractures is subparallel to the movement direction of the nappe. Therefore this zone of deformation is interpretated as being the result of movement of the fault. Deformation in the hanging and footwall is restricted to a zone of pervasive fracturing intensifying as we approach the fault. The poor development of a fault rock zone may be explained by the fact that in the majority of the sections studied (see later) the Lancara is juxtaposed against the Caliza de Montana, or a carbonate unit in the San Emiliano Formation. Therefore there is little material to be incorporated into the fault zone, see discussion on fault rock development in Chapter 6.

The absence of a well defined layer of fault rock prohibits the possibility of the nappe sliding on a "viscous décollement", or "cataclastic decollement" horizon as suggested by Kehle (1970), and Brock and Engelder (1977), respectively (Bastida et al., 1987).

To conclude this section the Somiedo Nappe appears to have been emplaced as a result of a posterior push, with associated gravity sliding, on a layer with transient high pore fluid pressure.

7.5.5 TEXTURAL ANALYSIS

7.5.5.1 INTRODUCTION

The Somiedo Nappe is at first inspection ideal for the evaluation and application of the experimentally calibrated calcite twinning palaeopiezometric technique which was presented in Chapter 4 because :

(a) The major structural contacts are located in carbonate formations, e.g. the basal décollement horizon is the Lancara Limestone and the footwall rocks include prominent limestone ridges in the San Emiliano Formation. In addition the tectonic wedges described previously are located in carbonate formations, namely the Santa Lucia and Portilla Limestone, see Fig. 7.1 and 7.2, and Plate 7.2a and d.

(b) The position of the Somiedo Nappe on the outer margin of the Cantabrian Arc means that the influence of the radial folds (see Chapter 5) on the post-thrusting development of the nappe is much less than for the Esla Nappe, see Chapter 6.

7.5.5.2 SAMPLING PROGRAMME & ORIENTATION OF THE SPECIMENS

Samples were taken from several localities the exact position of which are shown on Fig. 7.1. These localities are known by the names of the nearest respective villages :

1. Puerta Ventana.
2. Torrestio road section.
3. La Majua.
4. Cospedal.
5. Robledo.
6. Torre de Babia.
7. Santa Lucia tectonic wedge to the west of Torrestio.
8. Portilla tectonic wedge to the east La Cueta.

The last two localities are from tectonic wedges, while the others are from the basal thrust and their imbricates.

Orientated samples were collected from each of these localities, and as for the sampling program reported in the previous chapter, the distance between specimens is such that there is a bias towards a lower sampling interval with proximity to the thrust, according to the constraints of exposure. As stated previously, the orientation of the thin sections and their respective fabric diagrams is shown in section 6.4 and Fig. 6.1.

However, when the thin sections were stained and examined in detail the Lancara Limestone forming the hanging wall was found to be strongly dolomitised and micritic. Additionally, when the carbonate lithologies in the San Emiliano Formation which form the footwall in the Puerta Ventana and La Majua localities (see Fig. 7.1) were studied in thin section the carbonate was micritic in character and contained a significant amount of sulphur. As a result the textural analysis of these materials is unsuitable for comparison with the experimental models presented in Chapter 4.

Therefore the last two localities only have been examined and the results of the textural analysis are presented below.

7.5.5.3 METHOD OF ANALYSIS AND DATA PRESENTATION

The method of analysis is the same as that used reported for the Portilla Limestone described in the previous chapter, i.e. for every thin section

examined 100 grains were analysed using the Universal Stage. The measurements of the twinning activity and grain size were obtained by the same techniques described in Chapter 1, and the data set was subdivided into groups according to mean grain size for the purpose outlined in Chapter 6, section 6.8.3.

Although the footwall has greatest potential for palaeostress analysis it was decided to analyse specimens from both the hanging wall and footwall blocks because :

1. The displacement associated with these tectonic wedges is minor compared with the basal decollement horizon and hence there is no deformation associated with the passage of the nappe over ramps and flats.

2. These minor thrust systems afford the opportunity to study the comparative effects of deformation between the hanging and footwall blocks.

7.5.5.4 THE SANTA LUCIA TECTONIC WEDGE, N-W OF TORRESTIO

7.5.5.4.1 INTRODUCTION

The location of this tectonic wedge is shown in Fig. 7.1 and the nature of these thrusts is described in section 7.5.2. The specimens were collected from a traverse situated in the centre of the carbonate unit so that the thickness of the hanging wall and footwall blocks is approximately equivalent.

Macroscopic deformation in the traverse analysed is restricted to the occurrence of minor fractures at high angle to the thrust plane, although at other localities along this thrust fracturing can be locally intense. Six specimens have been analysed, three from the hanging wall and three from the footwall, the exact position of each of these specimens in relation to the thrust is shown on Fig. 7.6. The results of the textural analysis is described below.

7.5.5.4.2 TWINNING ACTIVITY AS A FUNCTION OF GRAIN SIZE

Fig. 7.3 shows the twinning activity data plotted as a function of grain size for each of the six thin sections studied from this traverse. Representative photomicrographs of the thin sections studied are shown in Plate 7.3. As shown for the experimental data sets in Chapter 4 and the Esla Nappe data sets in Chapter 6 twinning activity decreases with decreasing grain

size. The linear regressed lines shown on these diagrams show a very close correlation and the correlation coefficients for the principal, or first, twin set are all above 93%, while the second twin set shows a more variable development. The number of data points represented by each division in these diagrams is shown in the histograms presented in Fig. 7.4., and representative photomicrographs of each of the samples analysed are presented in Plate 7.3.

7.5.5.4.3 TWINNING CUT OFF

Unlike the data sets presented from the Portilla Limestone of the Esla Nappe in the previous chapter, the It parameter (diagrams 7.3(1)a-f does indicate that a twinning cut-off is present in the lower grain size intervals. Correspondingly both the number of twins (diagrams 7.3(2)a-f) and the percentage volume twinned domain (diagrams 7.3(3)a-f) show a systematic relationship with grain size and indicate a twinning cut-off is present by decreasing to approximately zero in the lower grain size intervals.

The second twin set generally shows a more variable development than the first, with twinning activity increasing with increasing grain size but to a lesser extent than the principal twin set. However the systematic relationship of the second twin set to the principal twin set is very similar to that demonstrated by the the previous data reported in Chapter 4 and 6. Where the first twin set approaches It values of 100% the second twin set starts to show more pronounced development with increasing grain size, and the slope of the linear regressed line has a slope that approximates to that of the principal twin set, c.f. diagrams (1)d to f of Fig. 7.3. The interpretation of this is that once the principal twin set is active in all the grains in a data set the resolved shear stress acting on the second twin set increases and therefore the second twin set becomes increasingly more active.

7.5.5.4.4 THE RELATIONSHIP BETWEEN TWINNING INCIDENCE, NUMBER OF TWINS AND PERCENTAGE VOLUME TWIN DOMAIN

As is clear from comparison of the diagrams of Fig. 7.3 the three facets of twinning activity determined are a function of grain size and are therefore logically related. Whereas in the data reported from the Esla Nappe in the previous chapter the twinning field boundary (defined by an It value of 10%) was poorly defined, the data from these thin sections show a lower degree of twinning activity and a twinning cut-off is indicated in those specimens from the footwall.

FIGURE 7.3 Textural data from the Santa Lucia Tectonic Wedge, west of Torrestio.

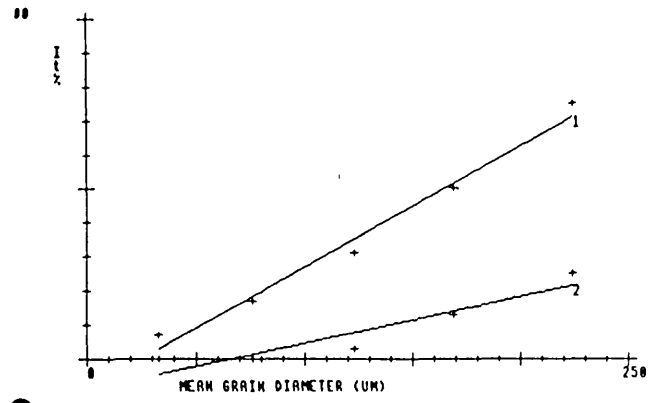
The series of diagrams (cont. on the following pages) in this figure present the twinning activity data determined for the samples analysed from the Santa Lucia Limestone at this locality, plotted as a function of grain size. There are three diagrams for each of the samples analysed from this locality, plotting It, number of twins, and percentage volume twin domain (1, 2 and 3 respectively).

For each sample two twin sets have been analysed, the primary, or principal, twin set, and then second twin set (1 and 2 respectively). The range bars for the appropriate parameters represent the full range of the values determined for each grain size interval.

The individual samples are identified by their respective headings.

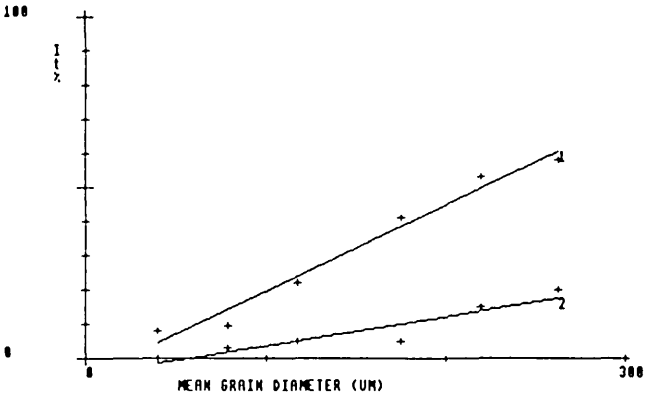
a1

THIN SECTION = 84:31.1: MEAN GRAIN DIAMETER/It%



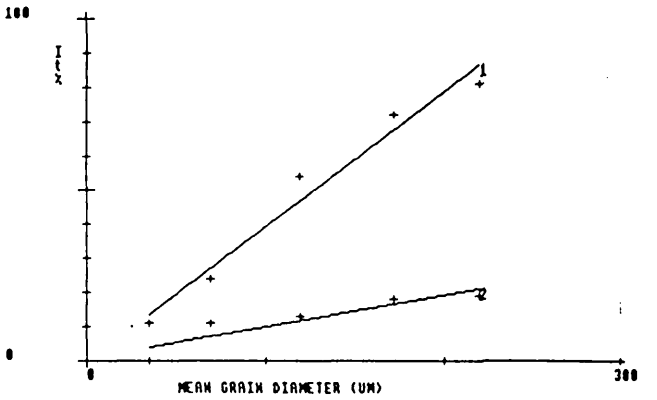
b

THIN SECTION = 84:31.2: MEAN GRAIN DIAMETER/It%



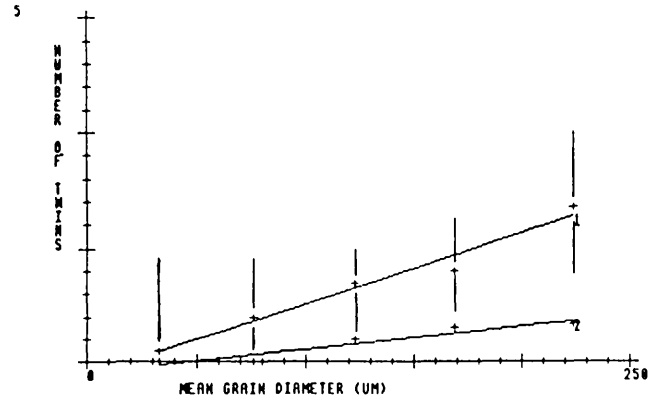
c

THIN SECTION = 84:31.3: MEAN GRAIN DIAMETER/It%

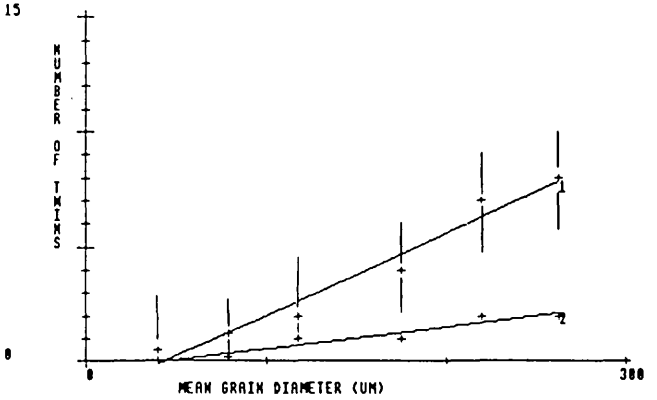


2

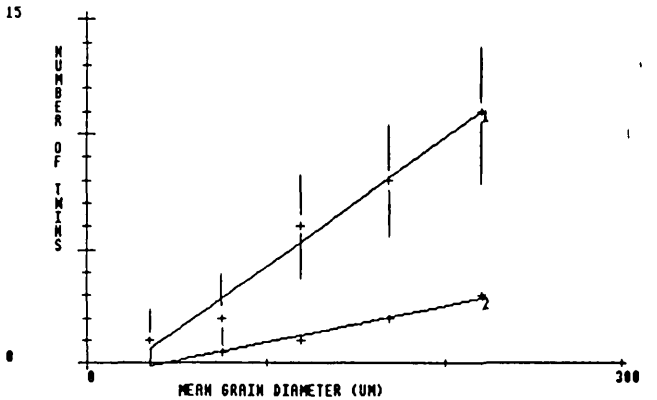
THIN SECTION = 84:31.1: MEAN GRAIN DIAMETER/NUMBER OF TWINS



THIN SECTION = 84:31.2: MEAN GRAIN DIAMETER/NUMBER OF TWINS

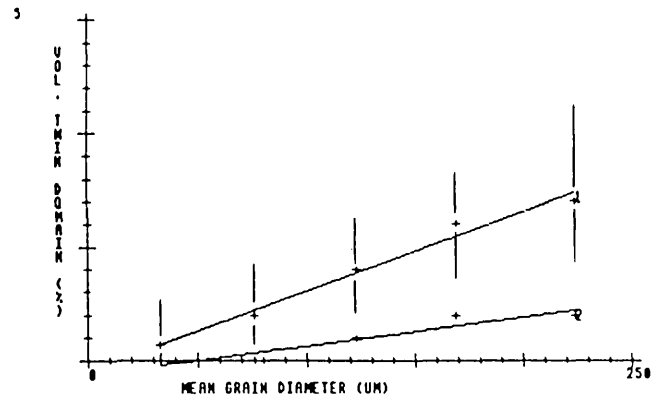


THIN SECTION = 84:31.3: MEAN GRAIN DIAMETER/NUMBER OF TWINS

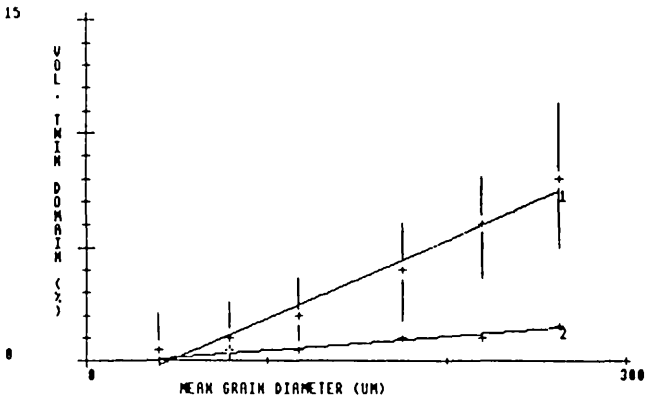


3

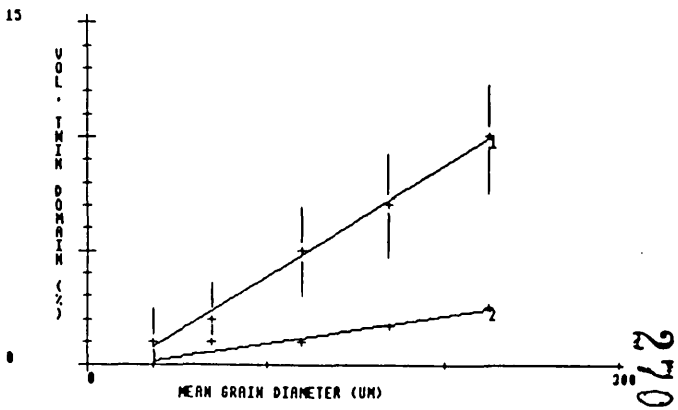
THIN SECTION = 84:31.1: MEAN GRAIN DIAMETER/%VOL. TWIN DOMAIN



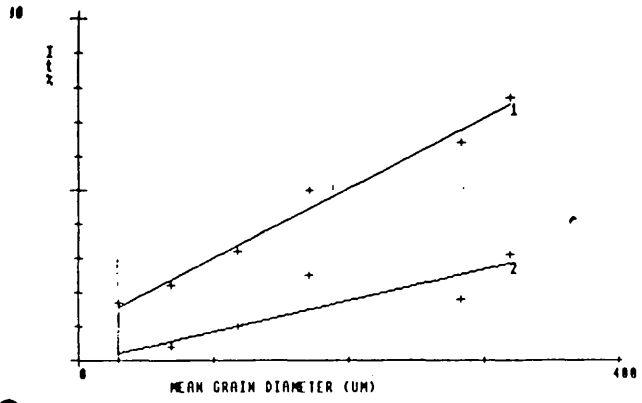
THIN SECTION = 84:31.2: MEAN GRAIN DIAMETER/%VOL. TWIN DOMAIN



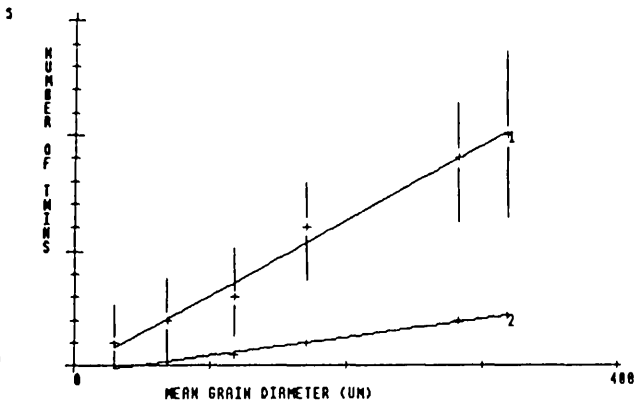
THIN SECTION = 84:31.3: MEAN GRAIN DIAMETER/%VOL. TWIN DOMAIN



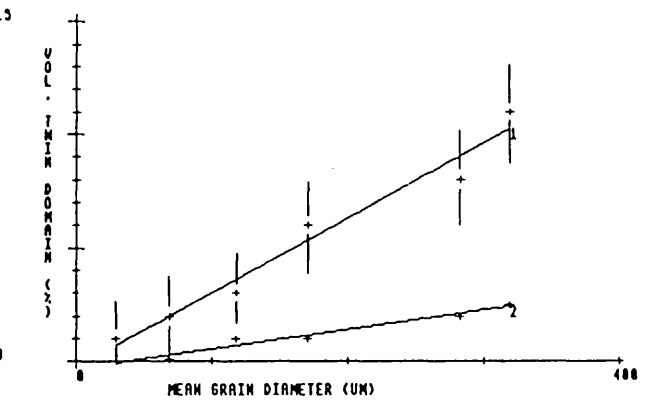
d 1 THIN SECTION = 84:31.4: MEAN GRAIN DIAMETER/It%



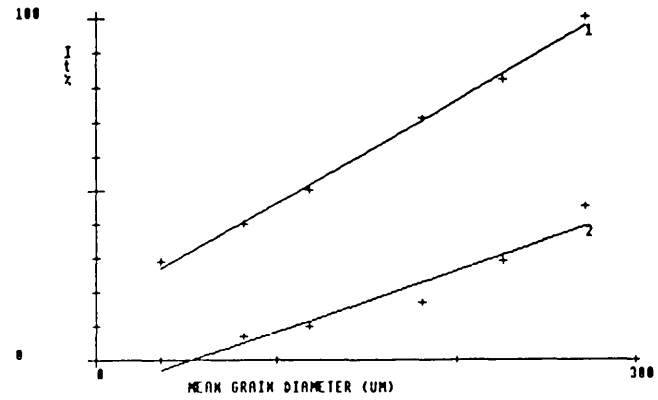
2 THIN SECTION = 84:31.4: MEAN GRAIN DIAMETER/NUMBER OF TWINS



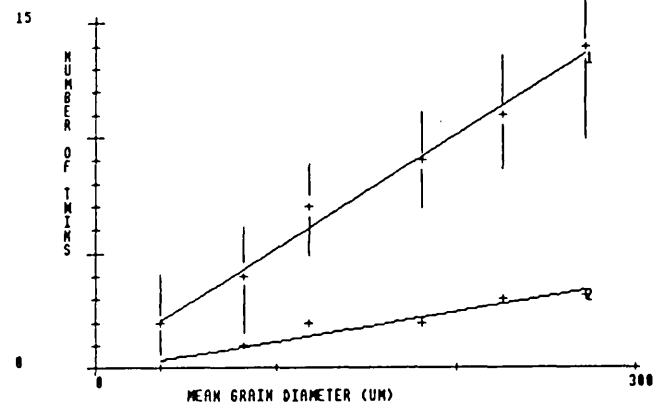
3 THIN SECTION = 84:31.4: MEAN GRAIN DIAMETER/%VOL. TWIN DOMAIN



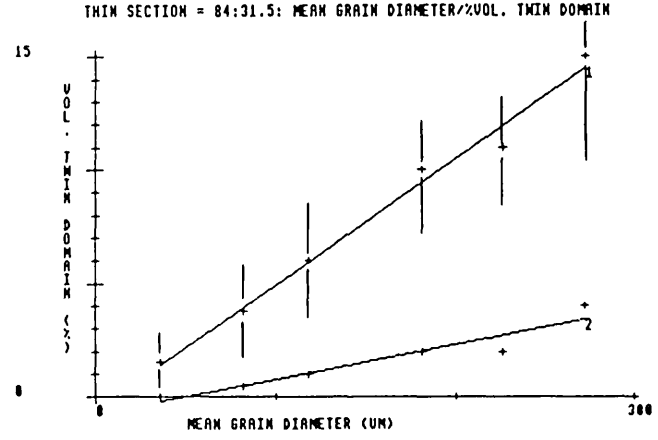
e THIN SECTION = 84:31.5: MEAN GRAIN DIAMETER/It%



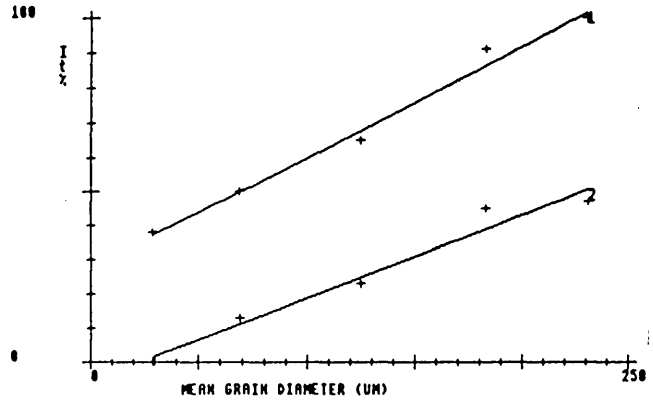
THIN SECTION = 84:31.5: MEAN GRAIN DIAMETER/NUMBER OF TWINS



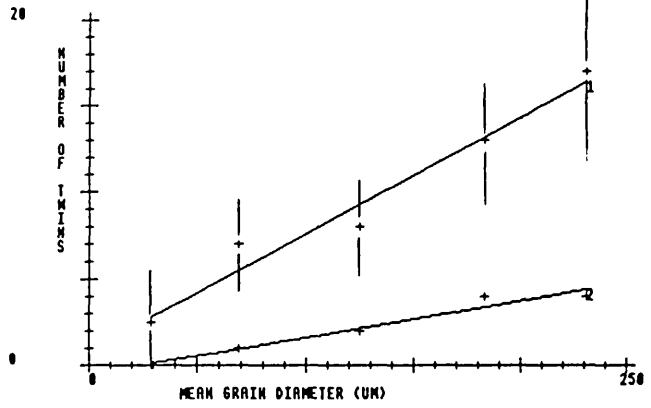
THIN SECTION = 84:31.5: MEAN GRAIN DIAMETER/%VOL. TWIN DOMAIN



f THIN SECTION = 84:31.6: MEAN GRAIN DIAMETER/It%



THIN SECTION = 84:31.6: MEAN GRAIN DIAMETER/NUMBER OF TWINS



THIN SECTION = 84:31.6: MEAN GRAIN DIAMETER/%VOL. TWIN DOMAIN

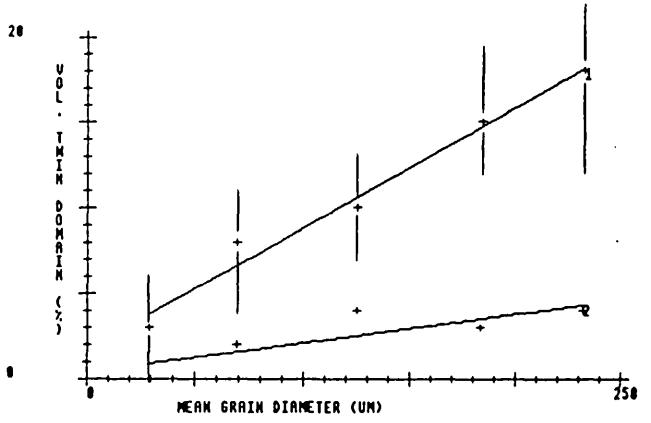
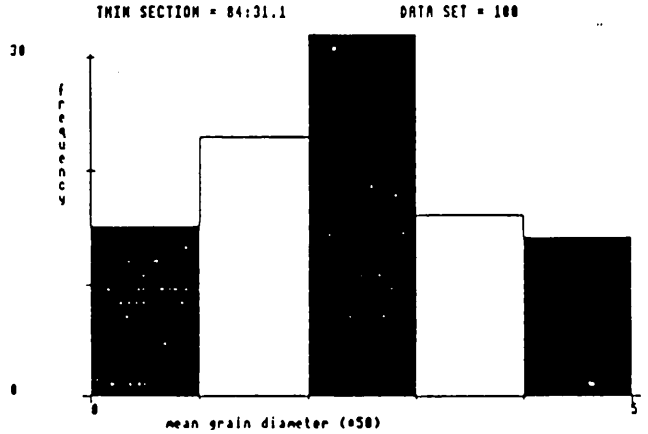
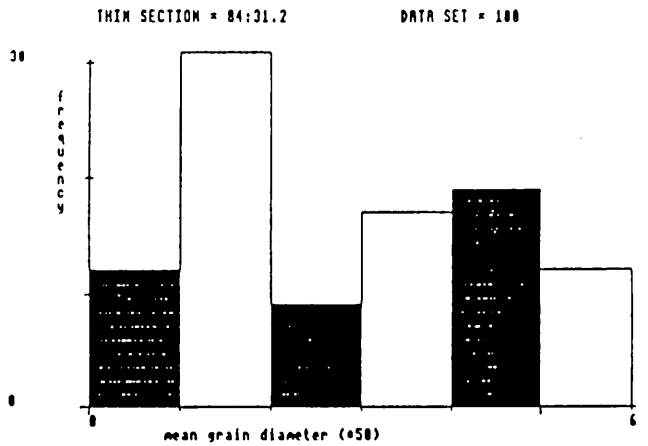
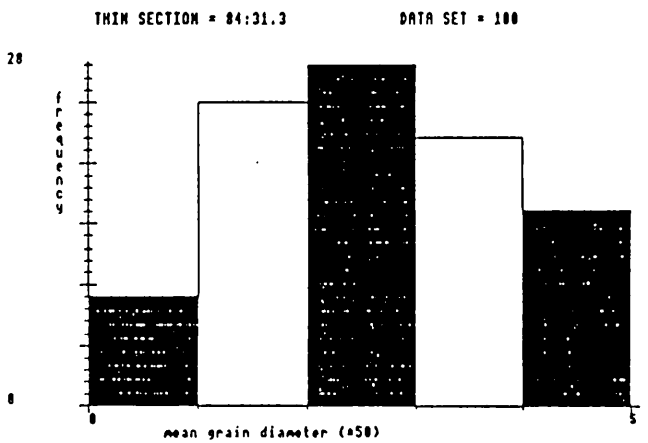
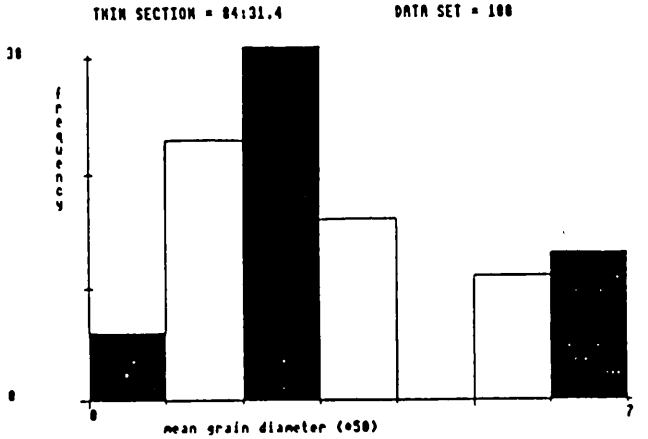


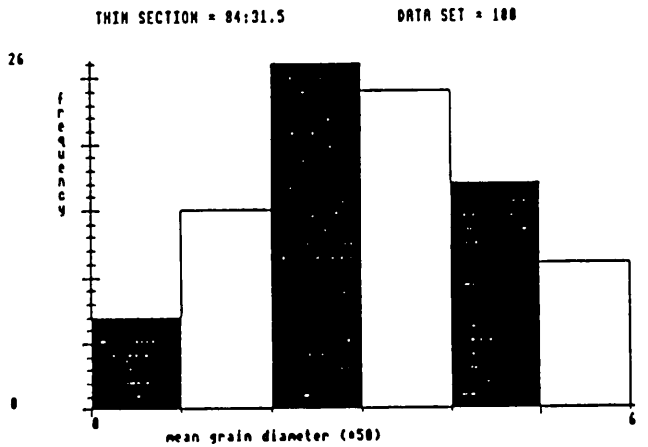
FIGURE 7.4 Histograms showing the number of data points (grains) in each of the grain size intervals for the diagrams in Fig. 7.3. The individual samples are identified by their respective headings.


THIN SECTION = 84:31.1
DATA SET = 100
30
0
frequency
0
5
mean grain diameter (*50)


THIN SECTION = 84:31.2
DATA SET = 100
30
0
frequency
0
6
mean grain diameter (*50)


THIN SECTION = 84:31.3
DATA SET = 100
28
0
frequency
0
5
mean grain diameter (*50)


THIN SECTION = 84:31.4
DATA SET = 100
30
0
frequency
0
7
mean grain diameter (*50)


THIN SECTION = 84:31.5
DATA SET = 100
26
0
frequency
0
6
mean grain diameter (*50)

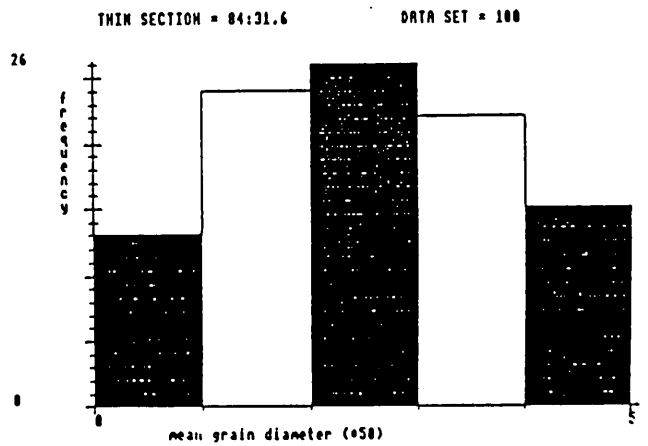

THIN SECTION = 84:31.6
DATA SET = 100
26
0
frequency
0
mean grain diameter (*50)

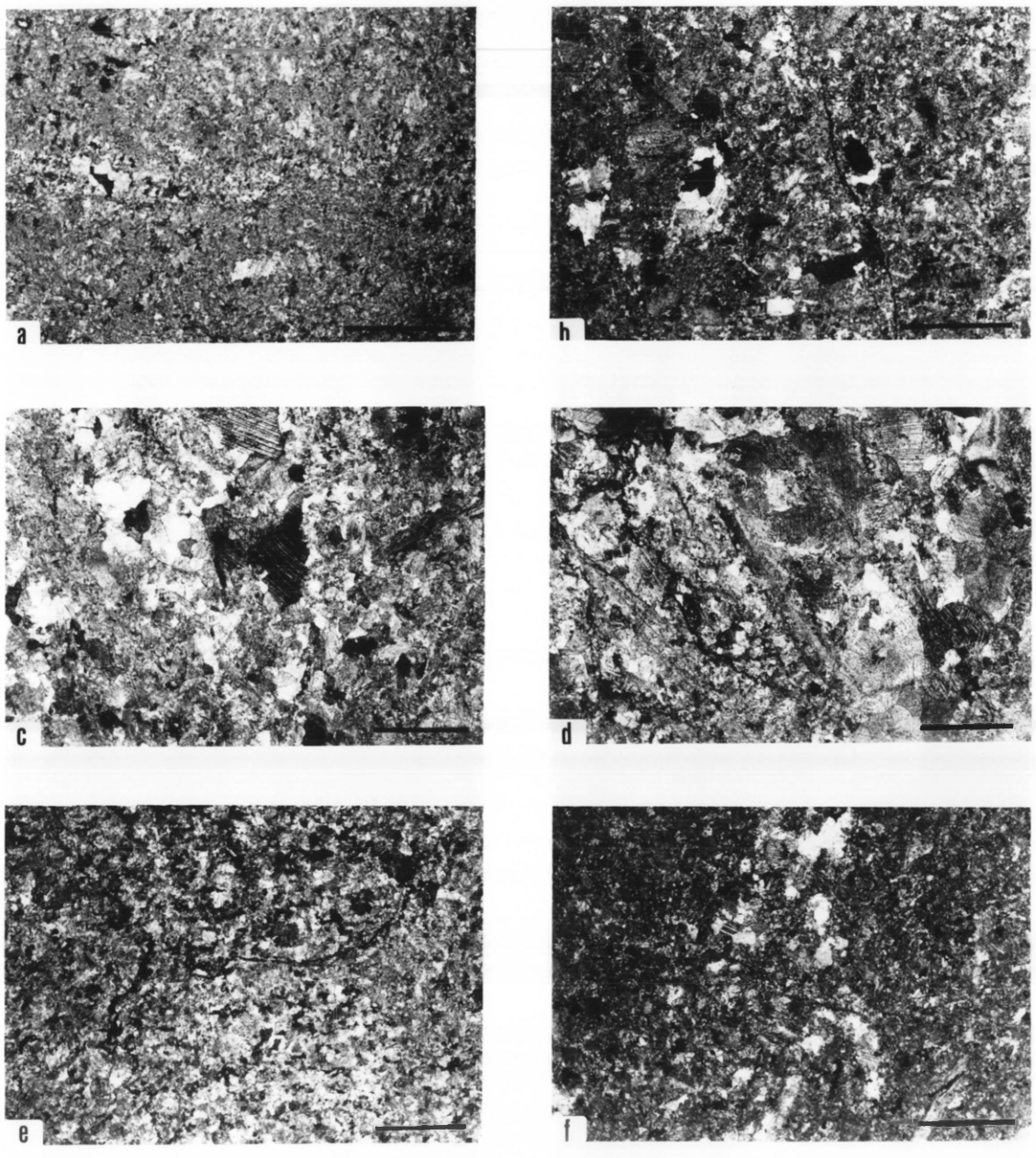
PLATE 7.3 Representative photomicrographs of the Santa Lucia Limestone from the Tectonic Wedge to the west of Torrestio (Somiedo Nappe).

KEY : (a) - 31.1, (b) - 31.2, (c) - 31.3, (d) 31.4, (e) - 31.5 and (f) - 31.6.

This series of photomicrographs show the subtle variation in twinning activity from the Santa Lucia Limestone of the Tectonic Wedge to the west of Torrestio. The scale bar in all of these photomicrographs is 1mm, but note that the scale bar may vary between specimens.

See text for discussion.

PLATE 7.3



The ratio of number of twins to percentage volume of twinned domain is approximately 1:1 in all of the specimens analysed, which is indicative of low temperature twin activity. The ratio of It:percentage volume twin domain (and therefore the number of twins) is approximately 10-20:1, increasing to approximately 30-50:2-3 (Fig. 7.15), which is in agreement with the data obtained from the Esla Nappe presented in Chapter 6. Note that these extrapolations are based principally upon the lower grain size intervals of the diagrams from Fig. 7.3 and hence the number of data points is low, see Fig. 7.4.

See discussion at the end of section 7.5.5.5.4.

7.5.5.4.5 PALAEOSTRESS DETERMINATION

As stated in the previous chapter the range of twinning activity data from a single specimen as shown in Fig. 7.3 represents a unique differential stress level. The results of the textural analysis described in the preceding sections have been superimposed on Fig 4.51 and the stress levels obtained are shown in Fig. 7.5. These stress levels are discussed in relation to the thrusting in the following section. The full range of It values were used in this comparison and the data shows an extremely good correlation with the range of It values obtained from the experimental analysis.

The stress levels obtained are all in excess than 200MPa and those in the hanging wall adjacent to the thrust are above 300MPa. The use of the whole data set in Fig. 7.5 allows the inclusion of range bars (representing the full range of the values measured) in the extrapolation, and hence the range bar is used to provide an upper and lower limit to the data from this natural system. When this method was used a maximum range of 22MPa was discernable, therefore an error of less than 10% has been evaluated, which is an extremely good and acceptable correlation. See discussion at the end of this chapter.

The close correlation of the twinning incidence parameters between the experimental data and the data determined from the Santa Lucia of this tectonic wedge suggests that this technique of extrapolating high temperature twins to low temperature twins is valid. This backs up one of the principal conclusions reached in Chapter 4, that the twinning incidence parameter is essentially insensitive to temperature.

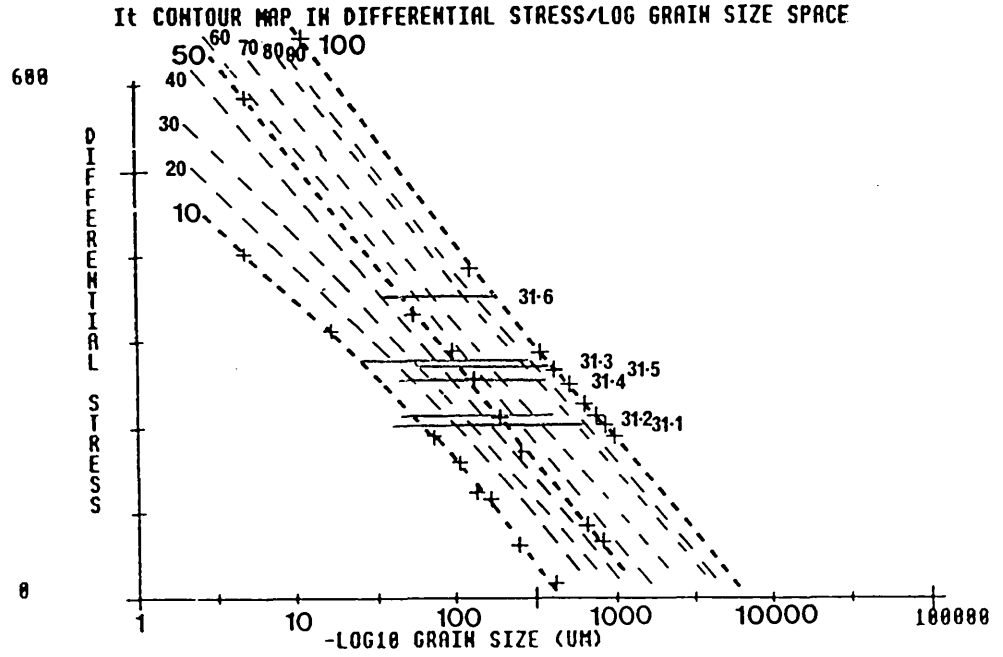


FIGURE 7.5 Fig. 4.51 plotting the experimental textural data presented in Chapter 4, with the textural data obtained from the Santa Lucia Tectonic Wedge superimposed (in red). The full range of the It parameter for each sample, shown in Fig. 7.3 is used, and the differential stress profile obtained is illustrated in Fig. 7.6.

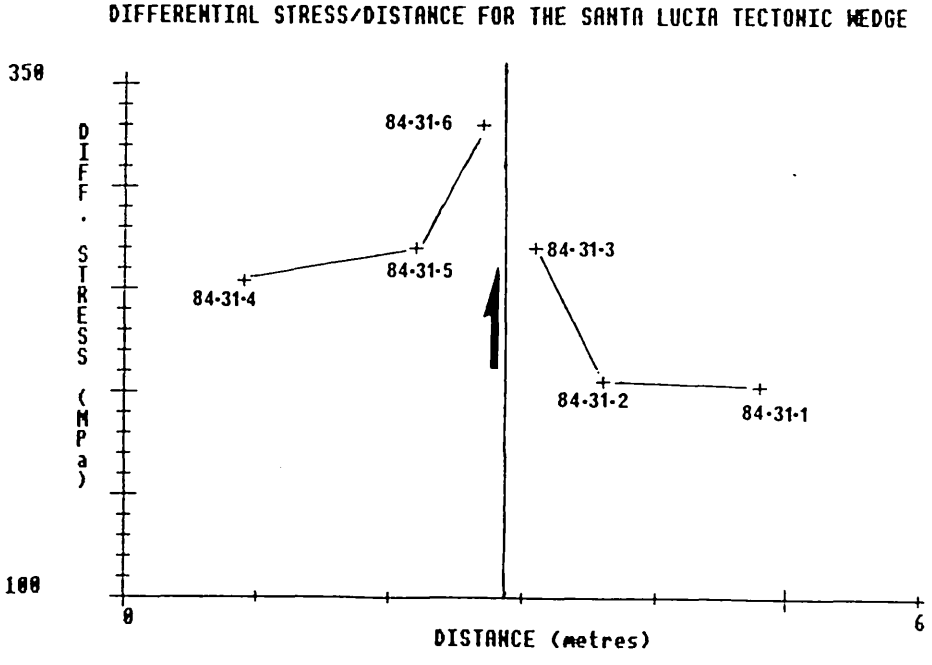


FIGURE 7.6 Diagram showing the levels of differential stress obtained by the calcite twinning palaeopiezometric technique presented in this Thesis, for the Santa Lucia Tectonic Wedge. The stress levels are obtained from Fig. 7.5, and the positions of the thrust and the samples are shown on this profile.

7.5.5.4.6 STRESS LEVELS ASSOCIATED WITH THRUSTING

The stress profile obtained from the extrapolation of the textural analysis to the experimental models, described above, is shown in relation to the thrust in Fig. 7.6.

Although the stress profile shows a general increase with proximity to the thrust, it is composed of two distinct segments, namely the footwall and hanging wall blocks. The footwall shows a marked increase in stress level as the thrust in approached, while the hanging wall shows a general higher level of stress which is distributed such that there is an approximately linear increase of stress as the thrust is approached. The implications of this stress profile are discussed in Chapter 8.

7.5.5.4.7 PETROFABRICS

Selected petrofabrics are presented in Fig. 7.7. These represent two thin sections one from the hanging wall and one from the footwall. The location of the specimens in relation to the thrust are shown in Fig. 7.6, and the method of presentation of the data is as given in the previous chapter, section 6.9.6.2.

The greater intensity of the crystallographic preferred orientation developed through e-twinning in the hanging wall is directly related to the higher It values, hence more twinned grains are included in the data set. Additionally the higher stress levels undergone by the hanging wall specimen may have resulted in a greater preferred orientation of the twin planes relative to the footwall specimen. The random initial fabric indicated by the petrofabrics in Fig. 7.7 have been backed up by the analysis of a section orientated at 90° to that shown in Fig. 6.1. Therefore an initial random crystallite orientation exists.

The D.A.T. of Turner (1954) has been used to calculate the orientation of the C and T axes, see section 6.9.6.3.2. Fig. 7.8 shows two diagrams for those grains whcih have more than ten discrete twin lamellae per grain, as presenting the data in this manner was shown in the previous chapter to accentuate any preferred orientation of the C and T axes. Fig. 7.8a represents the composite data for the three specimens from the footwall, and Fig. 7.8b represents the composite data for the three hanging wall specimens. As discussed in the previous chapter this method of representing the data has a bias towards the higher grain sizes as these will possess the higher twinning activity.

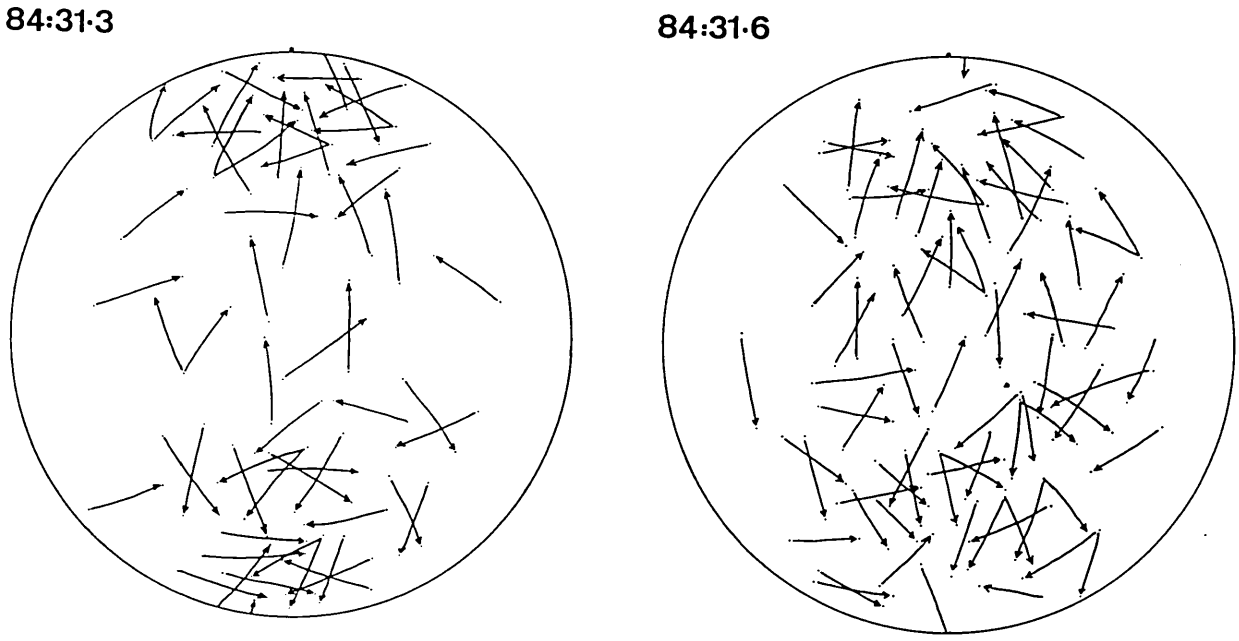


FIGURE 7.7 Selected petrofabrics from the Santa Lucia Tectonic Wedge to the west of the village of Torrestio. See Fig. 7.6 for the location of the two samples.

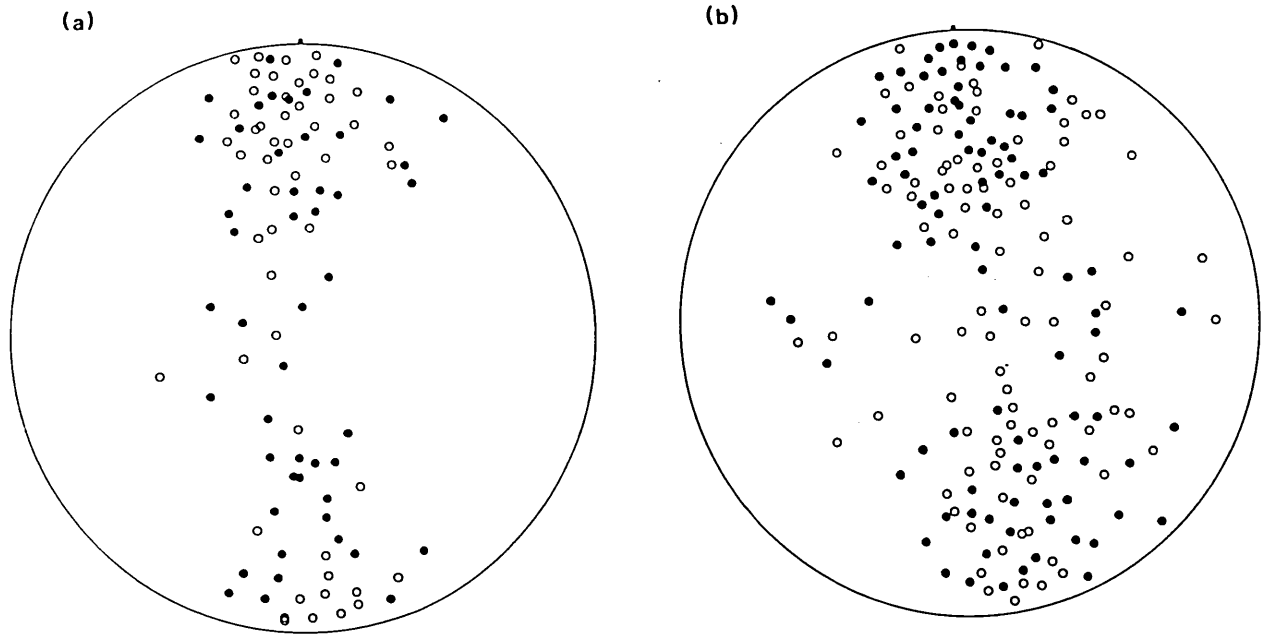


FIGURE 7.8 DAT petrofabrics for those grains with {10} twins: (a) footwall block, (b) hanging wall block.

Fig 7.8a demonstrates the preferred concentration of tensional axes around the movement direction, which is similar to that discussed for the Portilla Limestone in the previous chapter. Fig. 7.8b shows a more variable fabric, however the principal element of this fabric is a concentration of the compressional axes around the movement direction. This is predicted from the predicted orientation of the principal stress axes around a Type II crack and demonstrates the inherent variation of the fabric that develops is dependent upon position of the specimen in relation to the thrust plane.

7.5.5.5 THE PORTILLA TECTONIC WEDGE, EAST OF LA CUETA

7.5.5.5.1 INTRODUCTION

The location is shown on Fig. 7.1. As for the Santa Lucia tectonic wedge discussed in the previous section the specimens were collected from a traverse situated approximately in the greatest thickness of this carbonate unit from this locality. Therefore the thickness of the respective hanging wall and footwall blocks is approximately equivalent.

The fault plane was not observed and microscopic deformation is restricted to minor calcite veining, orientated at approximately 90° to the thrust plane and hence the bedding. Five specimens, three from the footwall and two from the hanging wall, have been analysed and their location in relation to each other and the thrust is shown in Fig. 7.12.

7.5.5.5.2 TWINNING ACTIVITY AS A FUNCTION OF GRAIN SIZE

Fig. 7.9 shows the textural data plotted as a function of grain size for each thin section studied in this traverse. Representative photomicrographs of each of the thin sections studied are shown in Plate 7.4. As was shown in the presentation of all the previous textural data, twinning activity decreases with decreasing grain size. The linear regression lines show an excellent correlation with the data points and the correlation coefficients for the principal twin set are above 92% and the second twin set shows a consistent but more variable trend than the principal twin set. This is consistent with the previous data discussed.

7.5.5.5.3 TWINNING CUT OFF

The It/grain size diagrams presented in Fig. 7.9(1)a-e clearly illustrate that a twinning cut-off is present for the lower grain size intervals. This is

FIGURE 7.9 Textural data from the Portilla Tectonic Wedge, east of La Cueta.

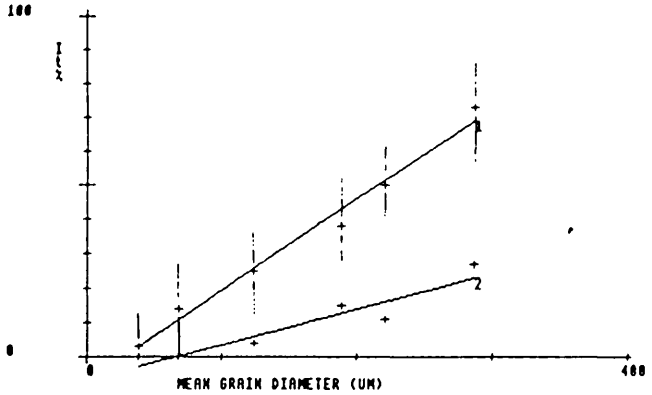
The series of diagrams (cont. on the following pages) in this figure present the twinning activity data determined for the samples analysed from the Portilla Limestone at this locality, plotted as a function of grain size. There are three diagrams for each of the samples analysed from this locality, plotting It, number of twins, and percentage volume twin domain (1, 2 and 3 respectively).

For each sample two twin sets have been analysed, the primary, or principal, twin set, and then second twin set (1 and 2 respectively). The range bars for the appropriate parameters represent the full range of the values determined for each grain size interval.

The individual samples are identified by their respective headings.

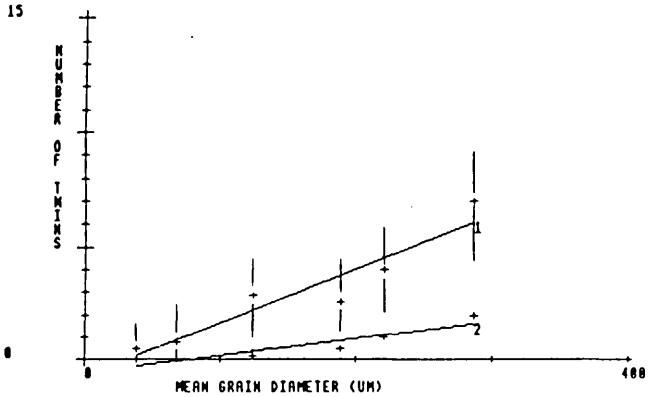
a 1

THIN SECTION = 84:36.1: MEAN GRAIN DIAMETER/It%



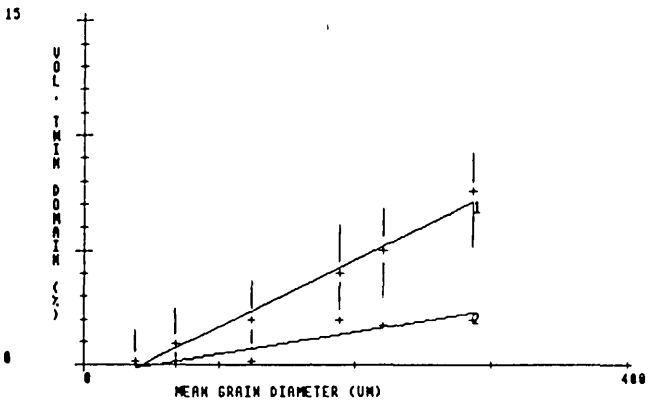
2

THIN SECTION = 84:36.1: MEAN GRAIN DIAMETER/NUMBER OF TWINS



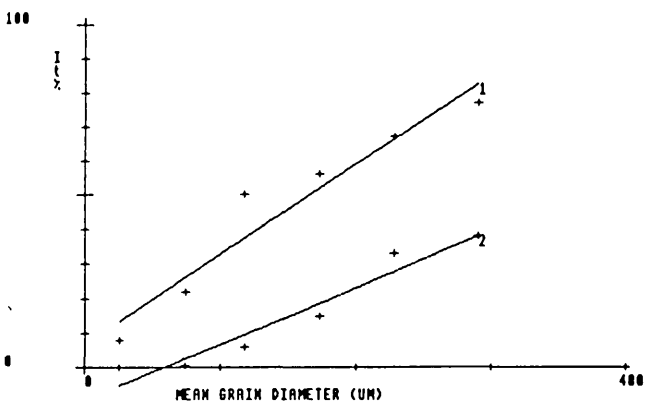
3

THIN SECTION = 84:36.1: MEAN GRAIN DIAMETER/%VOL. TWIN DOMAIN

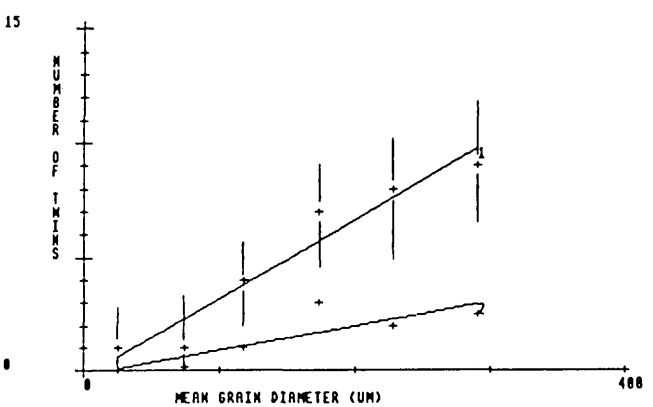


b

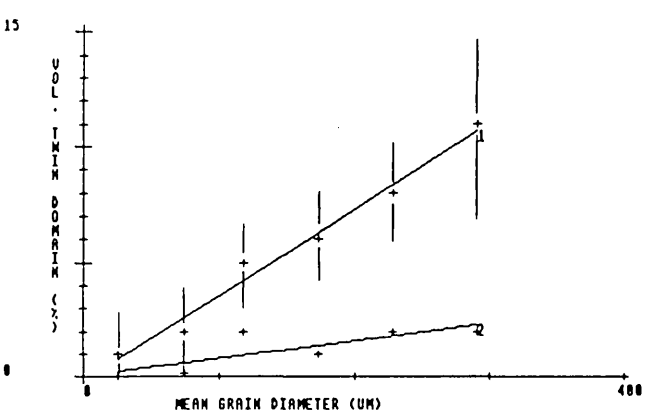
THIN SECTION = 84:36.2: MEAN GRAIN DIAMETER/It%



THIN SECTION = 84:36.2: MEAN GRAIN DIAMETER/NUMBER OF TWINS

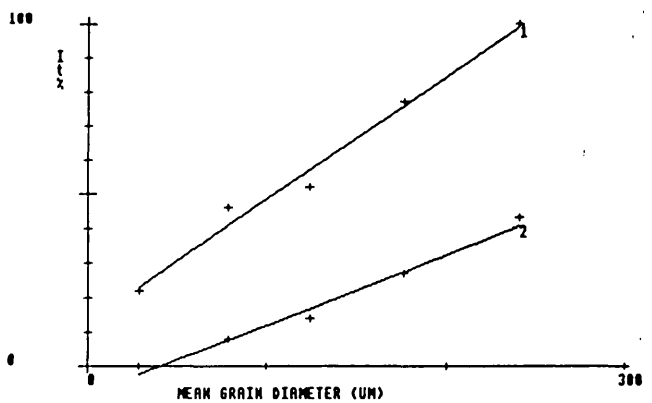


THIN SECTION = 84:36.2: MEAN GRAIN DIAMETER/%VOL. TWIN DOMAIN

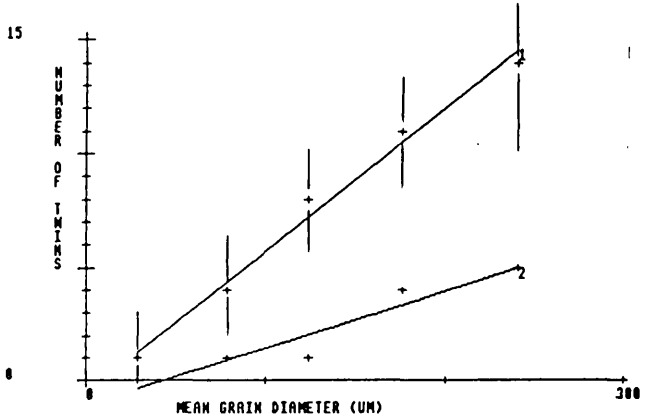


c

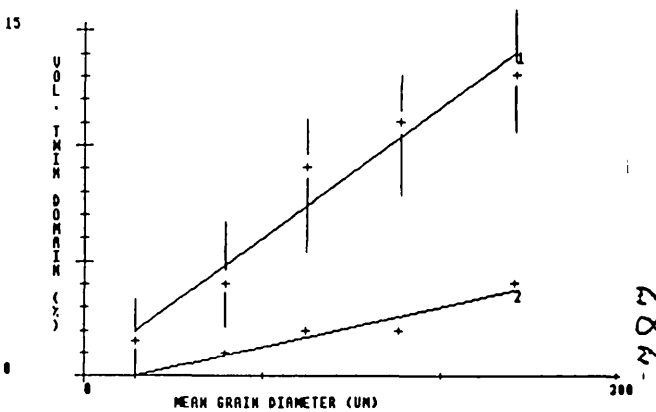
THIN SECTION = 84:36.3: MEAN GRAIN DIAMETER/It%



THIN SECTION = 84:36.3: MEAN GRAIN DIAMETER/NUMBER OF TWINS

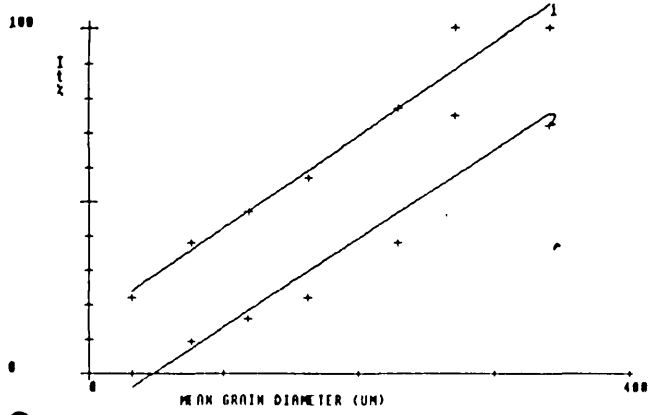


THIN SECTION = 84:36.3: MEAN GRAIN DIAMETER/%VOL. TWIN DOMAIN



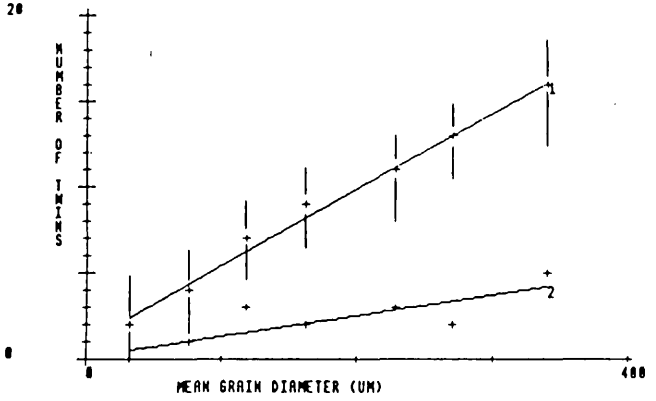
d **1**

THIN SECTION = 84:36.4: MEAN GRAIN DIAMETER/It%



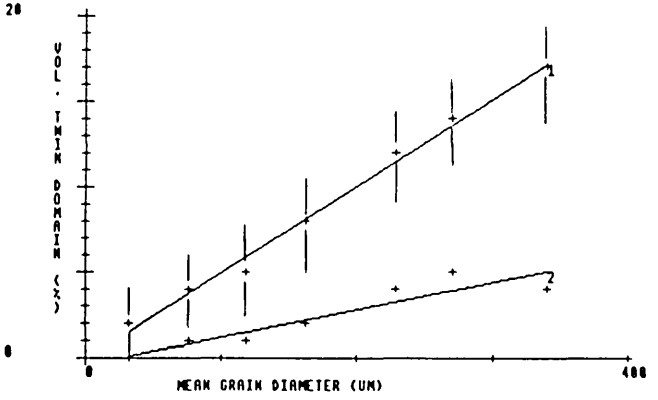
2

THIN SECTION = 84:36.4: MEAN GRAIN DIAMETER/NUMBER OF TWINS



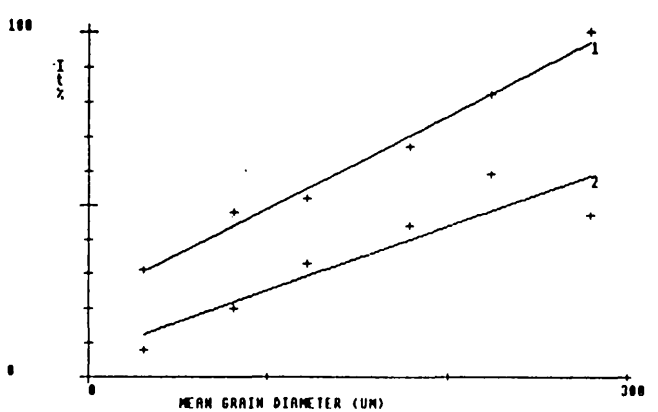
3

THIN SECTION = 84:36.4: MEAN GRAIN DIAMETER/%VOL. TWIN DOMAIN

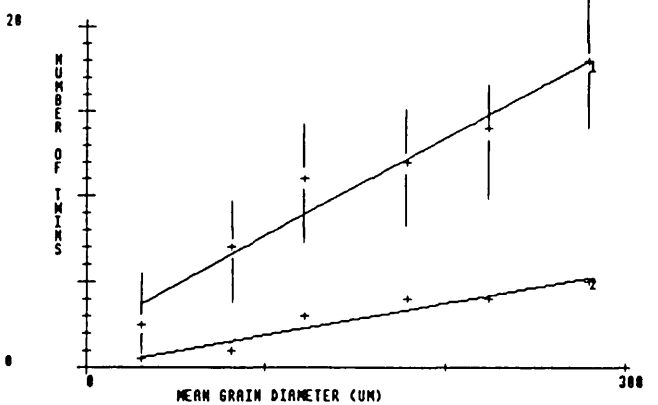


e

THIN SECTION = 84:36.5: MEAN GRAIN DIAMETER/It%



THIN SECTION = 84:36.5: MEAN GRAIN DIAMETER/NUMBER OF TWINS



THIN SECTION = 84:36.5: MEAN GRAIN DIAMETER/%VOL. TWIN DOMAIN

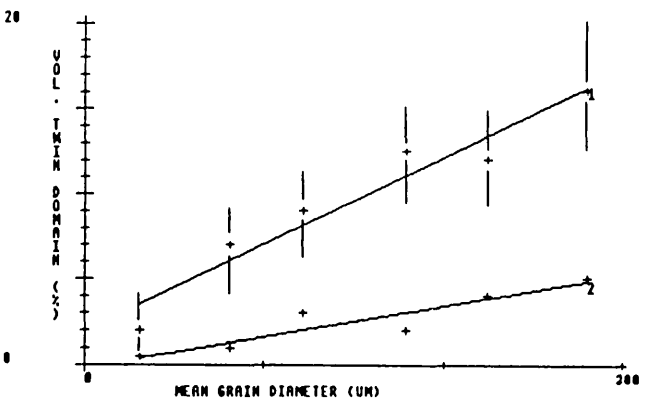
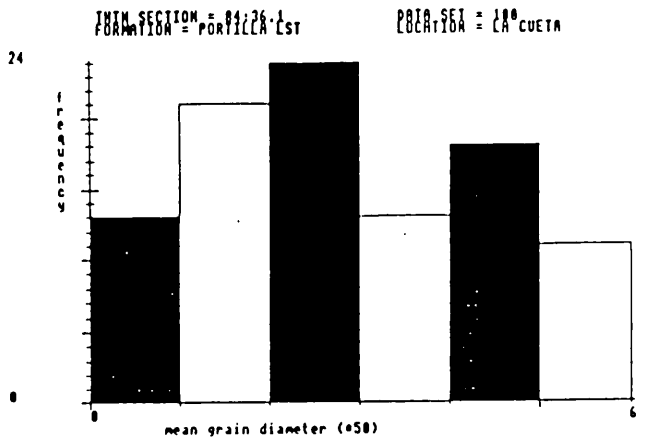
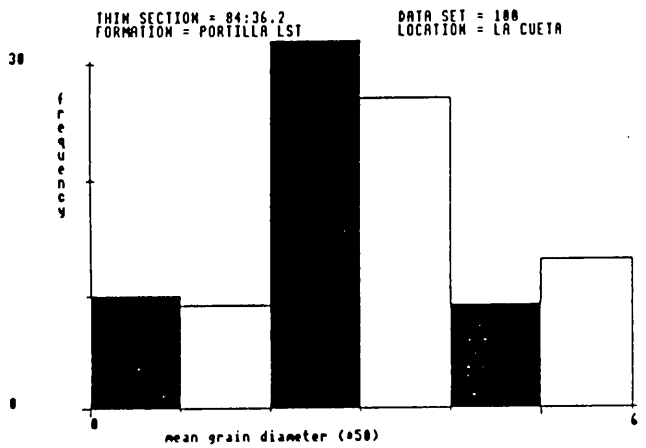
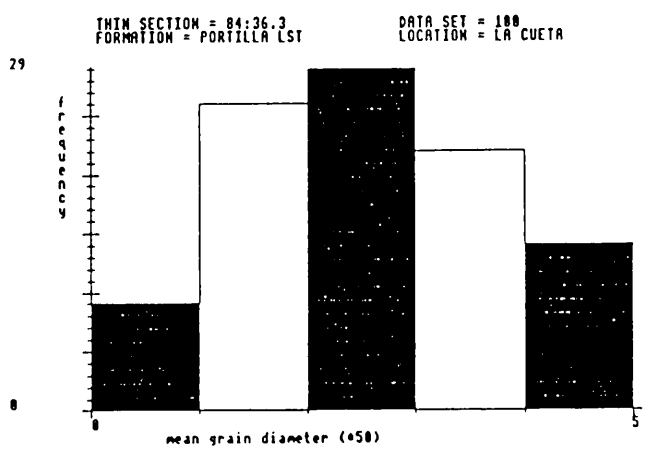
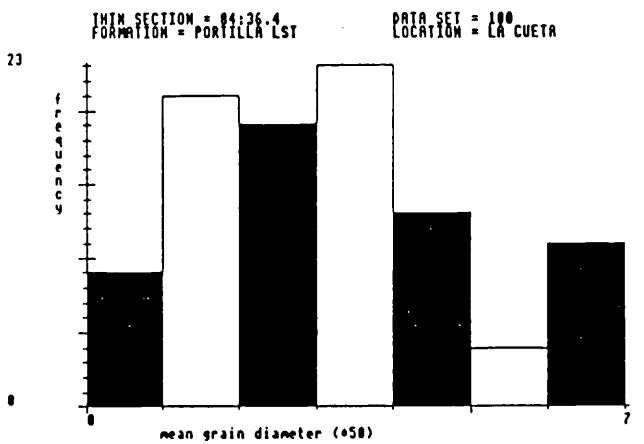


FIGURE 7.10 Histograms showing the number of data points (grains) in each of the grain size intervals for the diagrams in Fig. 7.9. The individual samples are identified by their respective headings.


THIN SECTION = 84:36.1
FORMATION = PORTILLA LST
DATA SET = 100
LOCATION = LA CUETA
24
0
frequency
0
6
mean grain diameter (*50)


THIN SECTION = 84:36.2
FORMATION = PORTILLA LST
DATA SET = 100
LOCATION = LA CUETA
30
0
frequency
0
6
mean grain diameter (*50)


THIN SECTION = 84:36.3
FORMATION = PORTILLA LST
DATA SET = 100
LOCATION = LA CUETA
29
0
frequency
0
5
mean grain diameter (*50)


THIN SECTION = 84:36.4
FORMATION = PORTILLA LST
DATA SET = 100
LOCATION = LA CUETA
23
0
frequency
0
7
mean grain diameter (*50)

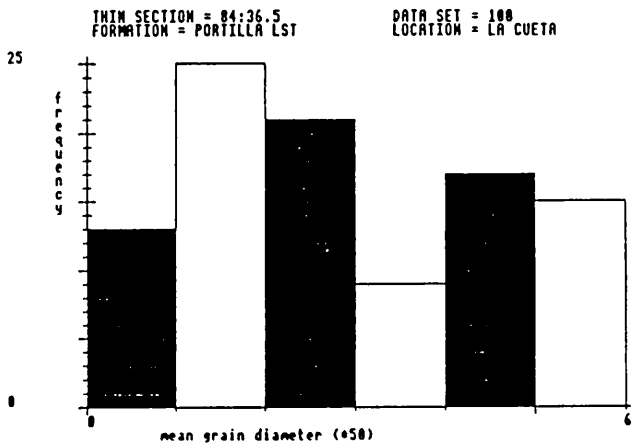

THIN SECTION = 84:36.5
FORMATION = PORTILLA LST
DATA SET = 100
LOCATION = LA CUETA
25
0
frequency
0
6
mean grain diameter (*50)

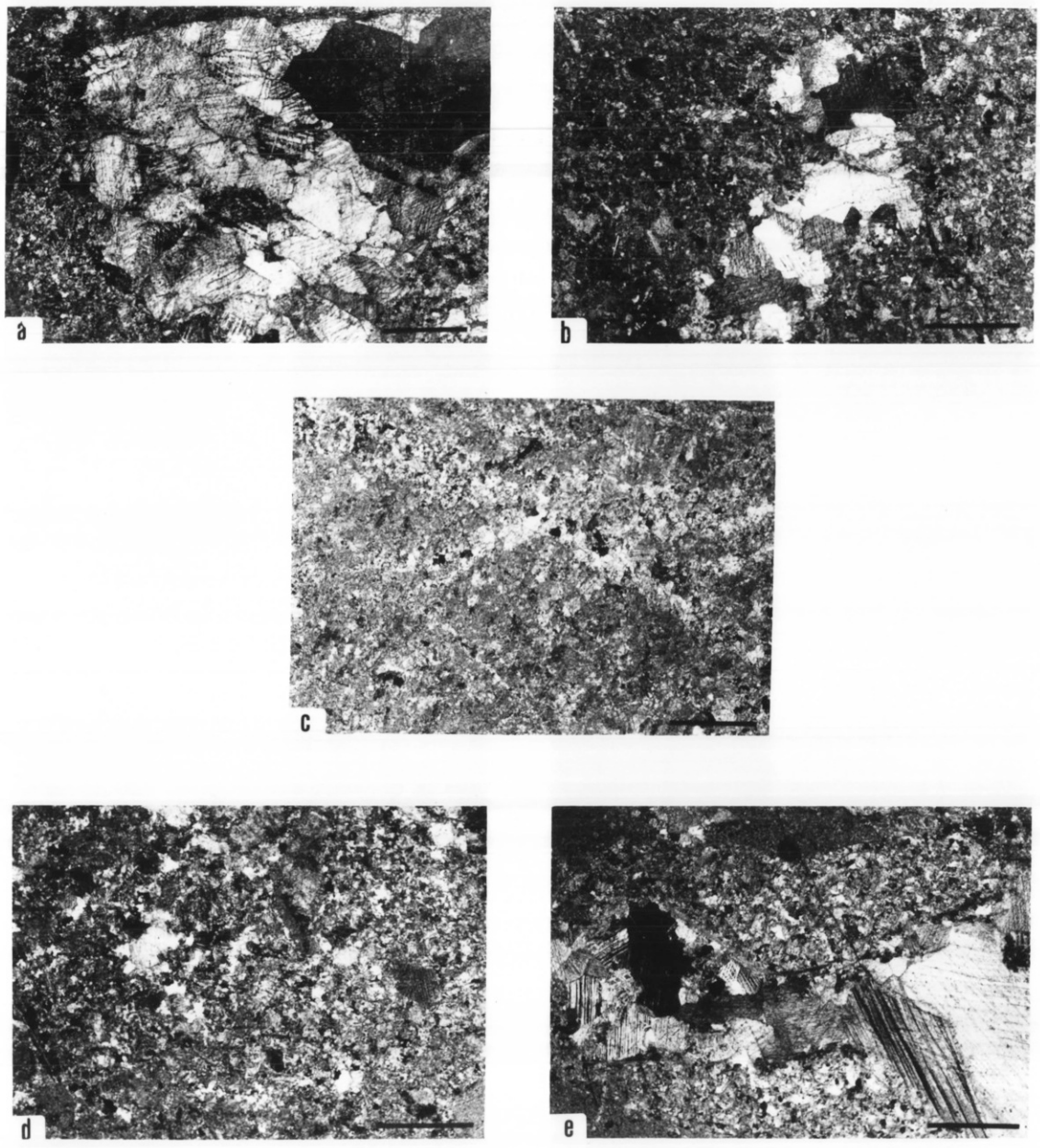
PLATE 7.4 Representative photomicrographs of the Portilla Limestone from the Tectonic Wedge to the east of La Cueta (Somiedo Nappe).

KEY : (a) - 36.1, (b) - 36.2, (c) - 36.3, (d) 36.4 and (e) - 36.5

This series of photomicrographs show the subtle variation in twinning activity from the Portilla Limestone of the Tectonic Wedge to the east of La Cueta. The scale bar in all of these photomicrographs is 1mm, but note that the scale bar may vary between specimens.

See text for discussion.

PLATE 7.4



verified by both the number of twins/grain size and percentage volume twin domain/grain size diagrams in Fig. 7.9(2) and (3)a-e respectively, c.f. Fig. 6.4 and 7.3. The second twin set shows the same systematic relationship relationship discussed insection 7.5.5.4.3 for the Santa Lucia tectonic wedge.

Palaeostress estimates based apon the twinning cut-off parameters shown in Fig. 7.9(1)a-e are discussed below.

7.5.5.5.4 THE RELATIONSHIP BETWEEN TWINNING INCIDENCE, NUMBER OF TWINS AND PERCENTAGE VOLUME TWIN DOMAIN

As was discussed for the data in the previous section, and can be seen from Fig. 7.9, the three facets of twinning activity determined are logically related.

The ratio of number of twins/percentage volume twin domain is approximatly 1:1 for all of the specimens studied. This is indicative of low temperature twin activity which typifies Upper Crustal deformation. The ratio of the It parameter to the other two facets of twin activity determined in this section is 10-20:1-2, increasing to approximately 50:3 and ultimately 100:>10 (Fig. 7.15). This is in full agreement with the data discussed previously and suggests that percentage volume twin domain can be used to at least indicate the position of the twinning field boundary if for some reason this boundary can not be located due to a lack of the critical grain size.

7.5.5.5.5 PALAEOSTRESS DETERMINATION

The twinning activity data have been superimposed upon the experimental model formulated in Chapter 4, and using the methods described in section 7.5.5.4.5 stress levels were obtained for this thrust system Fig. 7.11.

The stress levels derived are in excess of 170MPa and those from the hanging wall are a 100MPa higher. These are comparable to the stress levels obtained from the Santa Lucia tectonic wedge, except they are slightly lower. This may result from the higher stratigraphic position of this thrust system relative to the Santa Lucia system, see the sections in the back enclosure. The error evaluated for the stress levels determined from this analysis is 25MPa and was determined by the technique described in section 7.5.5.4.5.

See discussion at the end of this chapter.

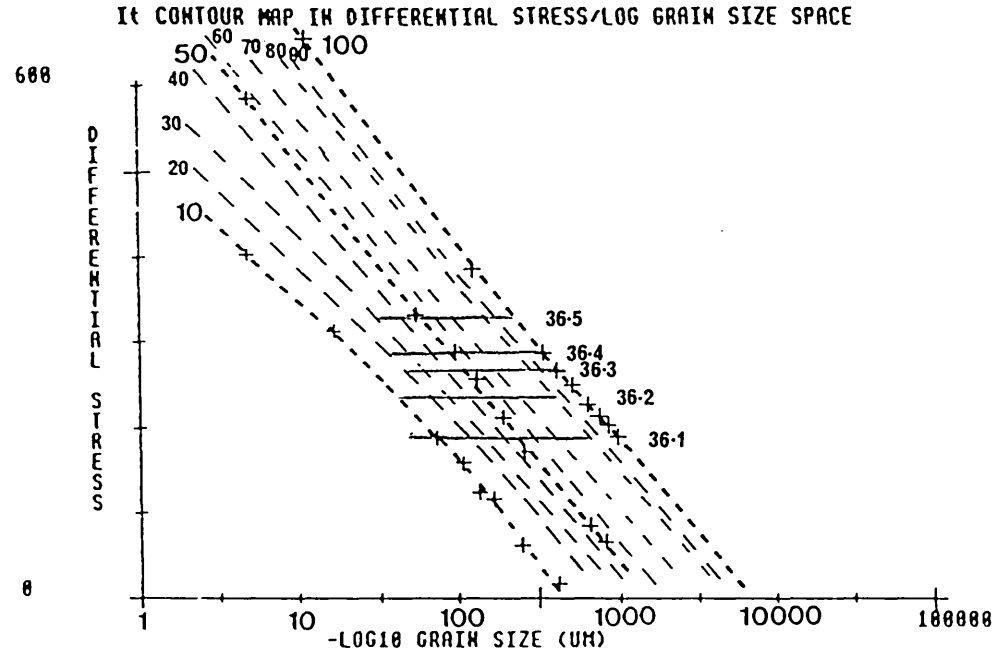


FIGURE 7.11 Fig. 4.51 plotting the experimental textural data presented in Chapter 4, with the textural data obtained from the Portilla Tectonic Wedge superimposed (in red). The full range of the It parameter for each sample, shown in Fig. 7.9 is used, and the differential stress profile obtained is presented in Fig. 7.12.

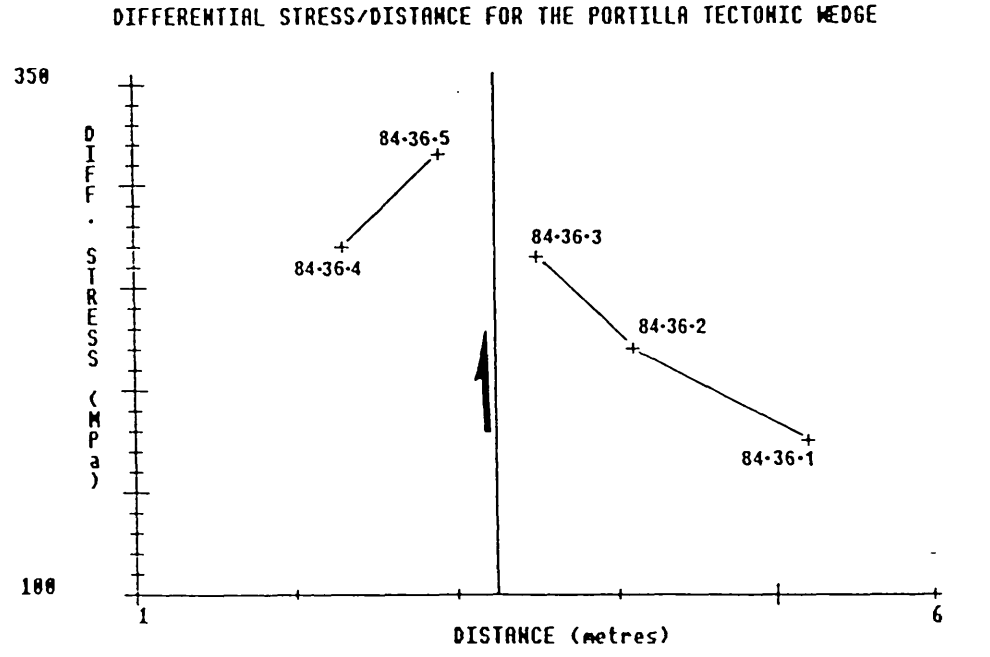


FIGURE 7.12 Diagram showing the levels of differential stress obtained by the calcite twinning palaepiezometric technique presented in this Thesis, for the Portilla Tectonic Wedge. The stress levels are obtained from Fig. 7.11, and the positions of the thrust and the samples are shown on this profile.

7.5.5.5.6 STRESS LEVELS ASSOCIATED WITH THE THRUST

The stress profile obtained from extrapolating the textural data presented in Fig. 7.9 to the experimental model, see Chapter 4, determined above is shown in relation to the thrust in Fig. 7.12. The profile is directly comparable with that determined for the Santa Lucia tectonic wedge presented previously in this chapter, Fig. 7.6.

There is a general increase in stress level as the thrust is approached, although the hanging wall shows significantly higher stress levels for the limited number of specimens studied. The implications of this stress profile are briefly discussed at the end of this chapter.

7.5.5.5.7 PETROFABRICS

To enable comparison with the textural data determined from the Santa Lucia tectonic wedge discussed in the previous section two petrofabrics, representing those specimens adjacent to the thrust from the footwall and hanging wall respectively are presented in Fig. 7.13. The exact position of these petrofabrics is shown on Fig. 7.12, and this method of presenting the data is described in section 6.9.6.2.

When Fig. 7.13 is compared with 7.7 a similar orientation of the textural data is observed. A stronger fabric is displayed by the hanging wall specimen (Fig. 7.13b), which is a result of it being subjected to higher stress levels than the footwall specimen (Fig. 7.13a). The cause of this increased intensity of the fabric is discussed in section 7.5.5.4.7. An initial starting fabric has been verified by the analysis of a thin section orientated at 90° to the orientation of the petrofabric discussed here.

Two petrofabrics have been determined using the D.A.T. of Turner (1954) and these are shown in Fig. 7.14 (see section 6.9.6.3.2). Fig. 7.14a and b represent the composite data for the footwall and hanging wall respectively fo those grains with more than ten twin lamellae, in the manner described in section 7.5.5.4.7.

Fig. 7.14a shows the characteristic footwall fabric with a concentration of the tensional axes sub-parallel to the movement direction, although the concentration is weaker, c.f. Fig. 6.9 and 6.10, and 7.8. Similarily Fig. 7.14b representing the hanging wall data is broadly comparable with that of Fig. 7.8b, although the concentration is weaker as a result of having one less thin

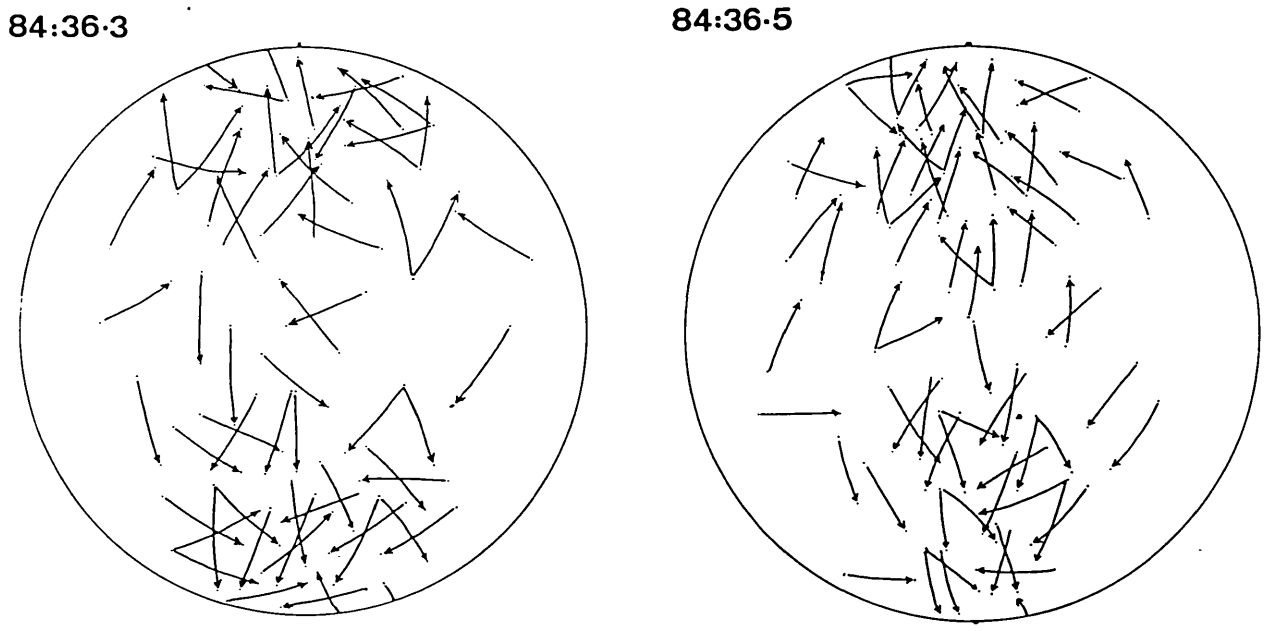


FIGURE 7.13 Selected petrofabrics from the Portilla Tectonic Wedge to the east of the village of La Cueta. The location of these two samples is shown on Fig. 7.12.

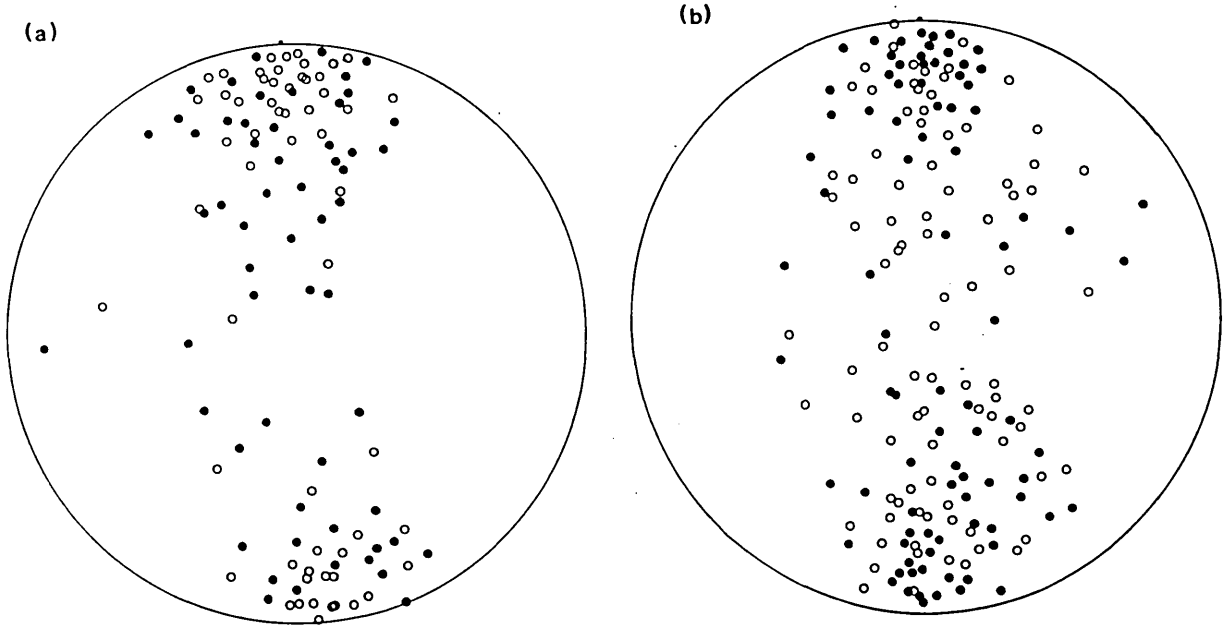


FIGURE 7.14 DAT petrofabrics for those grains with ≥10 twins: (a) footwall block, (b) hanging wall block.

section in this traverse relative to Fig. 7.8b. Therefore this data suggests that the inference regarding D.A.T. preferred orientation discussed in section 7.5.5.4.8 are valid.

7.5.6 CONCLUSION

The results of the textural analysis presented in this chapter demonstrate the application of the experimental calcite twinning palaeopiezometer formulated in Chapter 4. Although the stress levels appear to be a little high the twinning activity data determined suggests that the technique is extremely sound.

The general higher level of stress obtained from the hanging wall specimens is in accordence with this block being actively stressed during the emplacement of the hanging wall sequence, as opposed to the footwall which is passive and records the general level of stress.

The evaluation of errors is extremely important when applying an experimental model to a natural system, and the author realises the limitation of the technique where range bars are used to evaluate errors in the palaeopiezometer presented in this thesis. However until more data is avalable to test this model it is extremly difficult to evaluate any possible errors that may occur. Therefore at the present state of knowledge the errors, if present, appear to be less than 10%, which it is felt is a good indication of the reliability and potential of this palaeopiezometric technique.

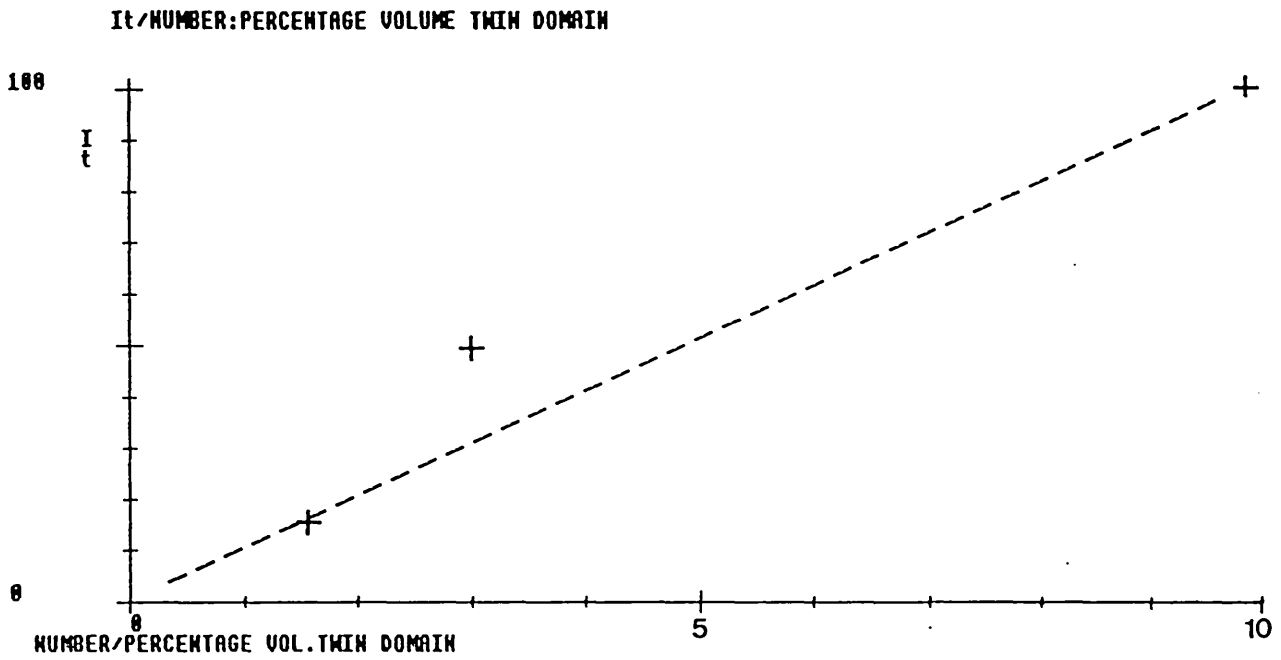


FIGURE 7.15 Diagram showing the relationship between the It parameter, and the number and percentage volume of twinning, assuming the number/volume ratio is approximately 1:1. Crosses represent real as opposed to extrapolated data.

CHAPTER 8 : CONCLUSIONS, GENERAL DISCUSSION AND SUGGESTIONS FOR FURTHER RESEARCH

8.1 INTRODUCTION

This chapter consists of a summary and general discussion of some of the results of the research reported in this thesis, including the general geological implications of the extrapolation of the experimental models to the Cantabrian fold and thrust belt. This chapter concludes with some suggestions for further research.

8.2 CONCLUSIONS AND GENERAL DISCUSSION

8.2.1 EXPERIMENTAL WORK

It has been shown in this thesis that the twinning activity in calcite rocks deformed in the work-hardening/recovery-creep field is a function of differential stress and grain size. Twinning is favoured at low temperatures, rapid strain rates and coarse grain sizes.

The twinning field boundary, defined by an It value of 10% was shown to be located at approximately 400Mpa for Solenhofen Limestone of 5μm grain size, at approximately 100MPa for Carrara Marble of 150μm grain size and at 10MPa for Taiwanese Marble of 380μm grain size. The It parameter increases to 50% at 580MPa, 208MPa and 76MPa, and to 100% at 740MPa, 392MPa and 196MPa for the respective grain sizes. Note that the It figure of 100% for Solenhofen Limestone is extrapolated as this level of differential stress is unattainable at the experimental conditions employed for this thesis. In addition to the twinning incidence parameter two other facets of the twinning activity were studied, namely the number of twins and the percentage volume twinned domain per grain. These were shown to be closely related to the twinning incidence parameter, i.e. all facets of twinning activity studied increase with increasing grain size for a given specimen. Additionally, as was discussed in Chapter 4, all of the data from previous experimental research for calcitic materials agrees extremely well with the data presented in this thesis. However, as a result of the thickness of the twins being a function of temperature (higher temperatures promoting twin boundary migration and therefore twin thickening, see Chapter 4), the volume of twin domain as a function of differential stress has to involve some appreciation of the temperature of formation for specimens deformed at elevated temperatures.

The decrease in twinning activity with grain size, or the hardening of twinning relative to r and f slip, as grain size decreases is probably a grain boundary effect, although the mechanism is not yet understood. Spiers (1981) suggests that impurities occurring in solid solution or as separate phases within the deforming material may effect the relative strengths of twinning and slip. However, the relative purity of all the materials used in this study suggest that if a compositional effect is present it is minor, and does not cause the observed difference in twinning activity between different experimental materials. However the observed behaviour of twinning activity as a function of grain size may be enhanced by variations in composition.

It was discussed in Chapter 2 that twins nucleate at stress concentrations and propagate by stress enhancement at the twin tips, i.e. behaviour analagous to crack propagation in metals (Mahajan and Williams, 1973). Therefore a true CRSS value for twinning does not exist and can only be approximated by taking into consideration the degree of stress enhancement which is characteristic of the material being analysed. Spiers (1981) suggests that this feature of twinning invalidates the assumption of rigid-plastic behaviour inherent in the Taylor-Bishop-Hill model of texture determination. An example is the negation of the stress enhancement factor at the twin tip by the back stress, with continued applied deformation the resolved shear stress acting on this twin system will vary, i.e. the state of stress in the bulk of the grain (assuming that the state of stress in the bulk of the grain remains constant) may depart from the assumed yield constraint hyperplane, Spiers (1981). See Chapter 2.

The effect of grain size upon twinning activity discussed in this chapter must be related to the fact that twinning is a highly heterogeneous mode of deformation resulting from the nucleation and propagation of twins according to the stress enhancement characteristics of the deforming material. When a twin nucleates the lattice disruption is of a finite width, obviously the smaller the grain size the more serious the compatibility problems within a grain will be, i.e. the back stresses generated in the grain as a result of the twin nucleation will be higher for a smaller grain size, relative to a larger one.

As a result the stress concentrations tending to nucleate twin initiation will be negated for the finer grain sizes, and the stress magnitude required to initiate twinning will have to increase in order to overcome the lateral constraints imposed by the grain boundaries. This leads to an increase in the effective CRSS required for twinning, relative to the finite CRSS of the slip systems, and hence lead eventually to slip system operation.

Therefore the decrease in twinning activity with grain size, or the hardening of twinning relative to r and f slip as grain size decreases, is probably a grain boundary effect, although the mechanism is not yet fully understood.

8.2.2 FIELD WORK

It has been shown that the twinning field boundary, as a function of differential stress decreases with increasing grain size, and has been shown to be essentially insensitive to temperature and strain rate. Therefore the experimental model formulated in this thesis can be readily extrapolated to sub experimental strain rates and temperatures, i.e. to natural systems.

As a result of the constant temperatures of formation of the natural specimens reported in Chapters 6 and 7 the percentage volume twinned domain values can be used to indicate the position of the twinning field boundary, or to verify its position, if there is a lack of the critical grain size to allow determination of the twinning field boundary. The constant temperature of formation of the natural twins examined in Chapters 6 and 7 is indicated by the ratio of number of twins/percentage volume of twinned domain, which is approximately 1:1 for all of the natural specimens studied, c f. Chapter 4.

The stress level obtained as a result of comparing the textural data obtained from the Portilla Limestone from the footwall of the Esla Nappe to that of the experimental model presented in Chapter 4, indicates that the level of stress across the whole profile analysed is in excess of 350MPa $\pm$25MPa, see Chapter 6. The specimens analysed from the Somiedo Nappe presented in Chapter 7 are from two tectonic wedges and not the basal thrust. However the stress levels obtained for the profiles are in excess of 200MPa, and for the specimens adjacent to the thrust from the hanging wall the stress levels are in excess of 300MPa. The level of stress obtained is marginally higher from the Santa Lucia tectonic wedge relative to the Portilla tectonic wedge, which is consistent with the former being at a lower stratigraphic level, and hence being subject to a higher confining pressure. Therefore the level of differential stress required to initiate the thrust in the former will be higher, and this is reflected in the twinning activity data for the two thrusts. The higher level of stress obtained for the basal thrust of the Esla Nappe relative to the thrusts studied from the Somiedo Nappe results from the same process, i.e. the lower stratigraphic position of the former requires a higher level of differential stress to initiate thrusting because of the greater confining pressure. The movement associated with the basal thrust of the Esla Nappe is greater than 15Km

(Allonso, 1987), and it is intuitively inferred that this amount of movement would actively stress the footwall rocks to a higher level, at least intermittently, than that associated with the tectonic wedges examined from the Somiedo Nappe. To conclude, the result of the higher stress levels inferred from the basal thrust of the Esla Nappe relative to the tectonic wedges from the Somiedo Nappe is probably a combination of the two factors briefly discussed above, although the following discussion suggests that the former is dominant for minor thrust systems.

The profiles in figs 7.6 and 7.12 from the Somiedo Nappe show that the level of stress associated with the hanging wall are significantly higher than those obtained for the footwall. Assuming that at the time of initiation of the thrusts, and ahead of the propagating tip after its initiation, the level of stress was equivalent in the hanging wall and footwall, the higher level of stress in the hanging wall must occur as a result of the continued build up of stress during the emplacement of the hanging wall block. This progressive, or active, stressing of the hanging wall relative to the footwall is consistent with the model of nappe emplacement where the hanging wall is active and continues to be positively stressed, while the footwall is passive and therefore records the level of stress at the time of initiation of the thrust.

The high levels of stress obtained from the thrusts studied in this thesis indicate that movement of the thrust would be difficult as the friction resistance along the thrust plane would be very high. However it must be remembered that the textural analysis presented in this thesis are from specimens in the respective hanging wall and footwall blocks, and <u>not</u> from the fault plane itself. Therefore the stress levels recorded are not indicative of the exact conditions which exist on the thrust plane itself at the time of deformation.

A thrust plane is a plane of easy movement once initiated and hence is weak relative to the surrounding materials. Therefore the thrust plane will have been subjected to a lower stress relative to the materials of the adjacent hanging wall and footwall blocks, as the fault plane accommodates stress by differential movement and the production of fault rocks. The materials of the respective hanging wall and footwall blocks are rigid blocks and therefore will be subjected to the maximum levels of differential stress that the respective system has been subjected to. The lower percentage volume twin domain values adjacent to the thrust in Fig. 6.7 from the basal thrust of the Esla Nappe indicate that twinning activity has a maximum value at approximately two metres from the thrust contact in the footwall. This verifies the above

argument that these thrust fault planes are subject to relativly low differential stress levels compared to their respective hanging wall and footwall blocks.

8.3 SUGGESTIONS FOR FURTHER RESEARCH

The research presented in this thesis has permitted the elucidation of several key areas for future research. These are :

1. A series of experiments and theoretical studies of e twin nucleation and propagation in calcite are required in order to quantify the operation of the system and the effect of grain size upon it. This work would enable the quantification of the compatibility constraints of twin development and the resultant back stresses acting upon a twin as a result of the proximity of the grain boundaries and the orientation of adjacent grains. A series of experiments upon both single crystal and monomodal grain size calcitic materials would allow the quantification of the stress enhancement characteristics of a given sample, and therefore permit the quantification of the effective CRSS for twinning.

2. Although the twinning activity data show a consistent and near linear relationship with grain size, this could be improved by taking into account the crystallographic orientation of the grains in the specimen to be examined with respect to the orientation of the principal stress axes of the imposed deformation. For example, after Spiers (1981), for grains with one twin set the volume fraction of twin to host (i.e. percentage volume twin domain) and shear accumulated by this twin system can be plotted against the Schmid factor for that grain. Spiers (1981) showed that by so doing the twinning activity data was found to be near statistically linear, Fig. 8.1. Therefore by plotting the data in this will quantify the relationship of twinning activity and crystal orientation.

3. Further experiments are required on a range of grain size calcitic materials, including single crystals, to enable the exact relationship between the various facets of twinning activity and their relationship to crystal orientation and grain size to be quantified.

4. The results of the palaeostress estimates presented in this thesis from the Cantabrian Zone of north-west Spain need to be compared and contrasted with other examples from a variety of structural configurations, both from the Cantabrians and from other locations.

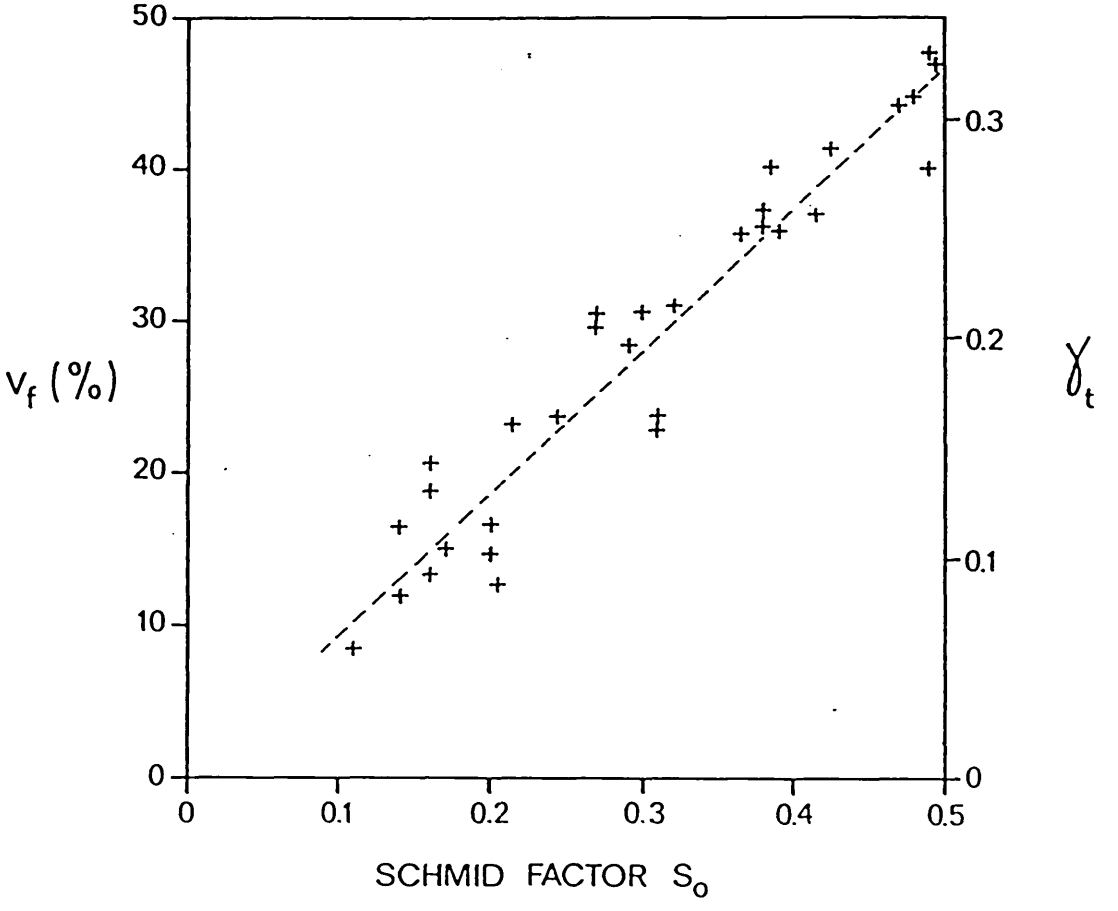


FIGURE 8.1 Diagram plotting twinning activity data (V_f, γ_t) for the e_3 twinning system plotted as a function of host grain Schmid factor S_o (calculated for the mid point orientation). N.B. V_f = twinned volume fraction (%); γ_t = shear strain due to twinning. After Spiers (1981).

5. It is hoped that the palaeostress estimates based upon calcite twinning will enable the formulation of some basic geological models concerning the evolution of the external part of the Hercynian orogenic belt in N. Spain.

Gravitational spreading occurred as a direct consequence of the Hercynian continental collision tectonism (Julivert 1967). The development of thrust faults is the most effective way of maintaining the mechanical equilibruim of the thickened wedge of continental crust. We can envisage the frontal zone of this continental wedge as a series of thrust faults, although only one or a combination may be active at any one time. The fault rocks we now see exposed at the surface in the Cantabrians can therefore be inferred to have progressively evolved as material was transported from the deeper levels of this wedge to the surface.

Figure 8.2 shows the transitions between modes of failure for Carrara Marble and Solenhofen Limestone and demonstrates how the deformation mechanisms are dependent upon confining pressure and temperature. A rock initially in the plastic regime which is then affected by gravitational spreading, accommodated by thrust faulting, undergoes a progressive decrease in confining pressure and temperature, assuming that friction on the thrust plane is constant. Hence it will cross the transition to the regime of cataclastic flow represented in Fig. 8.3.

If this process continues until the rock is exposed at the surface it will experience a continuous drop in confining pressure. Assuming that concurrently temperature has dropped to a constant value the rock follows a path similar to that depicted in Fig. 8.3. Therefore the rock will suffer a maximum level of differential stress along its deformation path. This can be quantified using the calcite twinning palaeopiezometer.

6. The distribuition of twinning activity as a function of grain size presented in this thesis appears to be scale invariant. It has long been recognised that a variety of processes in nature are scale invariant, and that "fractal analysis" provides a means by which such processes can be quantified, e.g. the renormalized group approach (RGA) of Wilson and Kogut (1964), see also Mandelbrot (1982) and Smalley et al. (1985). The following brief discussion should not be regarded as a comphrehensive account but merely an attempt to outline the general concept of fractal analysis and to investigate its potential use to analyse twinning activity.

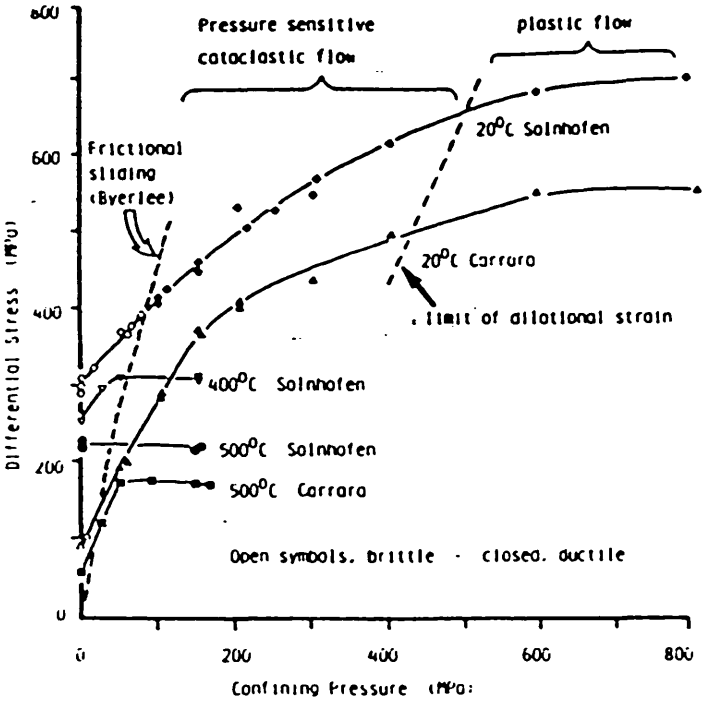


FIGURE 8.2 Diagram showing the transitions between modes fo failure for Carrara Marble and Solenhofen Limestone. After Rutter 1982 (NERC Report).

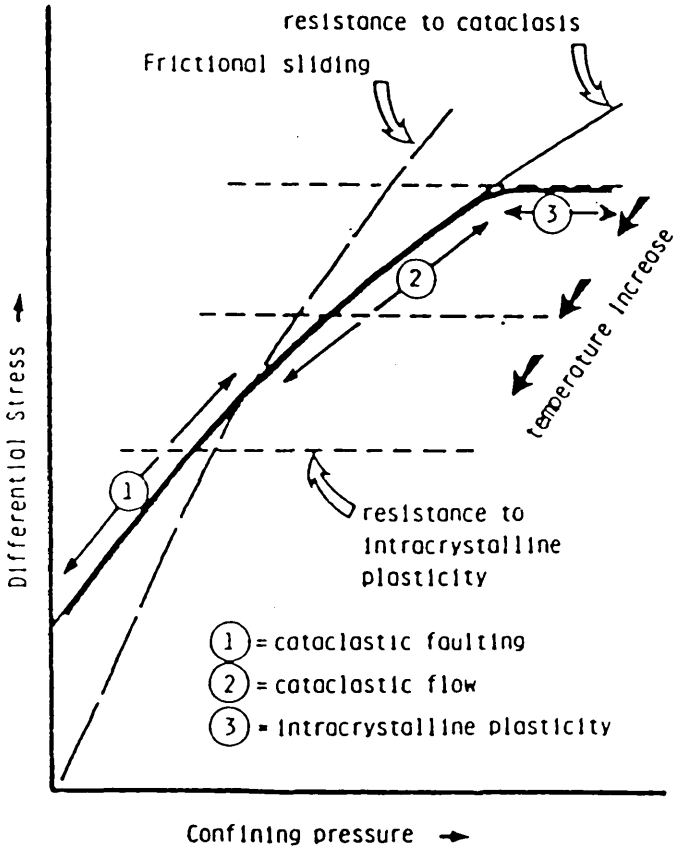


FIGURE 8.3 Diagram shows the theoretical PTt path for a rock, and demonstrates the transitions between modes of rock failure that the rock will undergo as it evolves. After Rutter 1982 (NERC Report).

The fractal dimension relates geometric behaviour at one scale to that of another. Turcotte (1986) presents a compilation of fractal dimensions for a variety of geological materials, Hyett (1987). The distribution of twinning activity data as a function of grain size shown in this thesis suggest that these parameters can be analysed using fractal analysis.

Note that the above suggestions for further research are not intended to be an exhaustive list, but merely are some suggestions as to key areas to enable further investigation of what is potentially a very powerful tool.

8.4 CONCLUDING STATEMENT

The textural analysis presented in Chapters 6 and 7 from the Cantabrian Zone and the results of their application to the experimentily calibrated calcite twinning palaeopiezometer presented in Chapter 4 are very encouraging. However further textural analyses from other Cantabrian thrust faults need to be determined in order to gain more information upon the state of stress and the rheological conditions associated with the emplacement of these and other nappes.

APPENDIX 1

COMPUTER PROGRAMS USED FOR DATA RECORDING, PROCESSING AND REDUCTION

Data is recorded, processed and reduced by a series of computer programmes written by Dr. E.H. Rutter and run on a Series B BBC microcomputer. There are three principal programs which are outlined below, and then described in more detail in the following sections, in addition to which there are several support programs which are used to store calibration data, e.g. NIMON1a, and to allow inspection and any necessary modification to a data file, e.g. EDDATA.

1. PREM2 : See Listing 1. This is a program modified from the pre-existing program PREMLOG by Dr. E.H. Rutter and enables data logging and control on the Nimonic Apparatus using an IEEE Interface. The data is logged into the raw data recording program RIGS.

2. PRFILES : See Listing 2. This is a program which creates a DATRED compatable file from the data logger file RIGS.

3. DATRED 7 : See Listing 3. This is a program which calculates the reduced experimental data from the raw data file created by the program PRFILES.

1. THE PROGRAM PREM2

This program obtains and stores in the RIGS file the raw milivolt output from the Niminic Apparatus. The program reads in a series of constants, which are of two types :

1. Calibration data, i.e. test invariant data.

2. Test data, i.e. data valid for the current test and entered by the operater prior to execution of the experiment. This includes the dimensions of the specimen, setting the clock, setting the sampling interval and entering the starting experimental parameters of the test.

After this data has been loaded into the raw data file RIGS the computer can start to recieve data from the Nimonic Apparatus. Data is read from five experimental variables each represented by a channel, these are :

1. Pore pressure (PH_20).

2. Temperature of the specimen (Tspec).

3. Confining pressure (σ_3).

4. Force gauge (FG).

5. Displacement (LVDT).

These channels are monitored in sequence using a programable digital voltimeter/scanner, and are converted into their milivolt analouges by an IEEE Interface to enable the computer to store the data by means of a random access filing system. These variables and their reduced derivatives can be viewed while the program and experiment are in operation by means of a online milivolt/time display, and a display of the reduced data as it is recorded.

2. THE PROGRAM PRFILES

After the test has been run this program allows the selection of data from the raw data file RIGS and creates a new file for the selected data which is data reduction compatable.

A channel is selected, usually Force Gauge, and the program plots the raw data corresponding to this channel against time on the screen in the form of x-y coordinates, where x is the record number and y is the milivolt. The operater then uses a cursor to select those records required and the computer then stores the information from all the channels corresponding to the selected records in a seperate file prior to data reduction.

3. THE PROGRAM DATRED7

This program accesses and reads the raw data contained in the file created by PRFILES and calculates and prints the reduced data in the form of PH_2O, Temperature, etc.

This program accesses all of the files created to date in order to obtain the following :

1. Calibration data from NIMON1a in the form of both the machine data and the calibration graphs gradients. This is printed out at the top of the reduced data file.

2. Specimen data is obtained from RIGS.

3. Raw data from the file created by PRFILES.

The graph plotting programs described and listed in Appendix 2 are then used to graphically represent the differential stress/strain data calculated and printed out by DATRED7. Examples of this form of graphical output are shown in Chapter 4.

Listing 1. The computer program PREP3.

```
10 REM Program PREP3.0, VERSION OF ANACONA WITHOUT PLOT FROM DISK ROUTINE, SP
ECIFICALLY FOR DATA LOGGING AND CONTROL (PREMA DVM AND IEEE VERSION)
 100MODE0
 20 MTCS=-1:ontime=-1:offtime=-1:PM%="N"
 30DEFcno%=13
 40DIM=0:I2=0:D1=0:D2=0:D3=0:D4=0:D5=0:D6=0:STARTT=0:GPAD=0
 50REG70=0:PM200=0:P0=0:T0=0:CS=0:DTIM0%=0:DIST0=0:DIST=0
 60T$=-NONAME":DA=0:DATIME=0:DADIST=0:DB=0:DBTIME=0:DBDIST=0
 70ON ERROR GOTO 80:ON CONT%=0:ON TMT%=0:ON NTX%=0:UPTO=0
 80APEA=1:DIA=1:STRC(NN)(CCCCCCCC)=-TTT=:TGX=0
 90CLOSE#0
 100*IEEE
 110PRINT#7,"A0"
 120PRINT#7,"R1"
 130PRINT#7,"L0"
 140PRINT#7,"T1"
 150 *DISC
 160REM SET ALL PORT OUTPUTS TO ZERO
 170PROCoff(1)
 180PROCoff(2)
 190PROCoff(3)
 200PROCoff(4)
 210PROCoff(5)
 220PROCoff(6)
 230PROCoff(7)
 240DIM X(2),Y(2),FF$(2),FIELDS$(2),FF%(2),W(2)
 250DIM CAL(4,2,3),G(3),APEA(3,3),EFCLIST(20)
 260PROCCLOSE
 270 PROCTOSET("0123456789")
 280 ONERROR GOTO 0:PRO
 290T$="OPENIN"+"11.PIGS"
 300PROCmachine
 310FOR FX=1TO3:GFX=3:NEXT FX
 320T1%=TIME/100
 330 T%%=100:MOTOR=0
 340T2%=T1%:Eflag=0
 350GAP=100000
 360 SX=0:LY=200:ST%=0:LY%=500:CN%=4
 370FOR FX=1TO-INC"+FX:nFX=FX:NEXT FX
 380 PROCtest_date
 390VDU14:FX4,0
 400 PREMX=1:SPX=-111=0
 410REPEAT
 420PROCrectangle
 430 PROCINLIST
 440PROCmenu
 450UNTILFALSE
 460END
 470:
 480DEFPROCINput
 490REPEAT
 500*FX21,0
 510 PROCshowtime
 520PROCcheck
 530PROCsendcheck
 540PROCprocess(Y(1),Y(2),Y(3),Y(4))
 550IF CONT=1 THEN PROCstressCheck
 560A$=INKEY$(1)
 570UNTILK$<>""
 580IFK$="G"THENEflag=1
 590IFK$="S"THENEflag=0
 600IFK$="M"THEN PROCflash
 610IFLEN(K$)="C" THEN CONX=1
 620IFK$="D" THEN CONX=0
 630IF TG%=1 THEN GOTO 610
 640IF TG%=0 THEN GOTO 660
 650IF K$="P" THEN TG%=1: GOTO 620
 660IF K$="F" THEN TG%=0: GOTO 630
 670ENDPROC
 680:
 690DEFPROCsendcheck
 700 IF MTC%<0 THEN PROCstress
 710T1%=TIME/100
 720IFABS(T1%-T2%)<GAP%*0 THEN GOTO 720 ELSE GOTO730
 730IFEflag=1THENGOTO740ELSEGOTO750
 740PROCsendata
 750PROCcheck
 760T2%=T1%
 770ENDPROC
 780:
 790DEF PROCcheckinkey
 800LPT$=INKEY$(2)
 810IFLPT$="M"THENPROCflash
 820IFLPT$="G"THEN Eflag=1
 830IFLPT$="S"THEN Eflag=0
 840REM CLEAR KEYBOARD BUFFER
 850*FX21,0
 860ENDPROC
 870:
 880DEFPROCcheck
 890T2%=TIME/100
 900 GOTO 860
 910IFABS(T2%-T1%)<STHENGOTO
 920:
 930PROCINLIST
 940PROCshowtime
 950T1%=T2%
 960 ENDPROC
 970:
 980DEFPROCmenu
 990CLS:CLG
1000MODE7
1010PROCshowtime
1020PRINTTAB(0,21,7);
1030PRINTTAB(10)CHR$(141)CHR$(131)"MAIN MENU"
1040PRINTTAB(20);"----------"
1050PRINT"(1) SET CLOCK"
1060PRINT"(2) SEND DATA TO DISK"
1070PRINT"(3) ENTER TEST PARAMETERS"
1080PRINT"(4) ON LINE AV GRAPH"
1090PRINT"(5) SELECT GRAPH PARAMETERS"
1100PRINT"(7) INSPECT DISK FILE"
1110PRINT"(8) STRESS CONTROL"
1120 PRINT"(M) CONST. STRAIN RATE MOTOR CONTROL"
1130 IF MTC% = TWO PRINT"(T) TEST MOTOR"
1140PRINT"(Y) STOP PROGRAM"
1150 PRINT
1160PRINT"(G) TO START SENDING DATA TO DISK, (S) TO STOP"
1170PRINT"(M) TO RETURN TO MENU, (C) TO CHANGE RECORDED DATA"
1180PRINT"(F) TO SWITCH ON STRESS CONTROL, (S) FOR OFF"
1190 PRINT"PRESS (L) UNTIL PLEASE TO ENTER TEST PARAMETERS"
1200VDU26
1210PROCINput
1220PROCstress
1230ENDPROC
1240:
1250IFVAL(K$)=1THENPROCsetclock
1260IFVAL(K$)=2THENPROCsend
1270IFVAL(K$)=3THENPROCparam
1280IFVAL(K$)=4THENPROCplotit
1290IFVAL(K$)=5THENPROCselgraf
1300IFVAL(K$)=7THENPROCfilechk
1310IFVAL(K$)=8THENPROCcalibrate
1320IF(K$)="A"THEN PROCsensitivity
1330IF(K$)="Y"THEN PROCend
1340IF(K$)="B" THEN PROCstresscontrol
1350 IF(K$)="M" THEN PROCconstrate
1360ENDPROC
1370:
1380DEFPROCplotit
1390CLSPROCshowtime
1400PROCgraf("TIME")
1410REPEAT
1420FOR J=1TO-LY
1430PROCshowtime
1440PROCcheck
1450PROCsendcheck
1460PROCINLIST
1470DTA=1:PROCPOINT(-J,Y(SPX+1))
1480PROCcheckinkey
1490PROCprocess(Y(1),Y(2),Y(3),Y(4))
1500 IF CONT=1 THEN PROCstresscheck
1510NEXT J
1520PROCInput
1530UNTILFALSE
1540ENDPROC
1550:
1560DEF PROCgraf(A$)
1570TST%=0
1580PROCSCALE
1590PROCAXES
1600PROCGRADUATE
1610PROCNUMBER
1620PROCNAMEY(A$)
1630PROCNAMEX("TIME(SECS)")
1640ENDPROC
1650:
1660DEFPROCsend
1670VDU7
1680FFcno%=0
1690VDU28,0,9,79,4
1700INPUT"Enter start record number "FFcno%
1710INPUT"Enter time between data sends (minutes) "GAP
1720IF GAP=VAL("E") THEN GOTO1720
1730PRINT"Enter 'G' to start sending, 'S' to stop"
1740PROCINput
1750*FX21,0
1760IFEflag=1THENPROCsendcheck
1770PROCcheckinkey
1780ENDPROC
1790:
1800DEFPROCsendata
1810PROCcheck
1820FFcno%=FFcno%+1
1830IFFLDS%=0:PRECIent=FFcno%
1840PTR#F#=PRECIent*FFcno%
1850A$=STR$(Y(1))
1860B$=STR$(Y(2))
1870C$=STR$(Y(3))
1880D$=STR$(Y(4))
1890E$=STR$(Y(5))
1900F$=time$
1910IFFX=1TOFIELDS%
1920FF$(FX)=LEFT$(A$+PAD$(FF%(FX)),10)
1930NEXT
1940IFFX=1TOFIELDS%
1950PRINT#F#,FF$(FX)
1960SOUND1,-10,255,4
1970NEXT
1980PROCcheck
1990PROCINPUT
2000:
2010DEFPROCgetdata(N)
2020IFLEN(PAD$+N$)>10THENN$=LEFT$(PAD$+N$,10):ELSEPAD$=LEFT$(PAD$+N$,N)
2030=PAD$
2040DEFPROCinput
2050byte%=0:IFOPEX=1TOFIELDS%
2060byte%=byte%+1
2070NEXT
2080:
2090DEF PROCfilecheck
2100GOTO 2120
2110ov1$="ov1"
2120*CLI-"LOAD "+ov1$+" "+STR$(TOP-2)
2130OPENOVERLAY
2140ENDPROC
2150:
2160DEFPROCGRAPH
2170PROCSCALE
2180PROCAXES
2190PROCGRADUATE
2200PROCNUMBER
2210FOR J=1TO-(1)
2220DTA=1:PROCPOINT(-J, Y(3))
2230IF J=1THENGOTO2250
2240MOVEFN CVX(X(-J-1)),FN-CVY(Y(-J-1)):DRAWFN-CVX(X(-J)),FN-CVY(Y(-J))
2250IF J<X(0)GOTO2300
2260MOVE5:PRINTTAB(FN CVX(X(-1))+2,FN CVY(Y(-1))+2);A$(N1):VDU4
2300NEXT J
2310ENDPROC
2320:
2330DEFPROCSCALE
2340PROCSCALE2(-SY,-LY):SY=-SY:LY=-LY
2350 STX=-ST: CRYX=-CRNX
2360PROCSCALE2(-ST,-LY):STX=-STX:LY=-LY
2370 STX=-ST: CRYX=-CRNX
2380 FX=1000/(-LY-SY): XAXIS=-LY*-SY
2390 CONVY=150/-STX*-Y : CONVY=1000/-STX*-Y
2400ENDPROC
2410:
2420:
2430DEFFN CVX(G)=X+G*CONVX
2440DEFFN CVY(G)=X+G*CONVY
2450:
2460DEFPROCSCALE2(L,H):BX=400/(H-L)
2470 LL=VAL(LEFT$(STR$(L),INSTR(STR$(L),"E")-1))
2480 LH=VAL(LEFT$(STR$(H),INSTR(STR$(H),"E")-1))
2490 PL=VAL(MID$(STR$(L),INSTR(STR$(L),"E")+1))
2500 LH=LH*10^VAL(MID$(STR$(H),INSTR(STR$(H),"E")+1))- PL)
2510 D=LH-LL
2520IF D<4THENREPEAT D=D*10 :PL=PL-1 :LL=LL*10 :LH=LH*10 :UNTIL D>=
2530IF D>50THENREPEAT D=D/10: PL=PL+1:LL=LL/10:LH=LH/10:UNTIL D<=
2540 LL=INT(LL+.1):LH=INT(LH+.5)
2550A=A*10: CRNY=SGN(LL)*(VAL(RIGHT$(STR$(LL),1))+1)
2560 SX=VAL(STR$(LL)+"E"+STR$(PL))
2570 LX=VAL(STR$(LH+"E"+STR$(PL))):ST=ABS(1-SX)/(LH-LL)
2580ENDPROC
2590:
2600DEFPROCAXES
2610 X0=0: Y0=0
2620IF SX<0THEN X0=SXELSEIF LX<0THEN X0=LX
2630IF SY<0THEN Y0=SYELSEIF LY<0THEN Y0=LY
2640MOVEFN CVX( SX),FN CVY( Y0):DRAWFN CVX( LX),FN CVY( Y0)
```

LISTING 1

```
2660ENDPROC
2670:
2680DEFPROCGRADUATE
2690FORX=-SXTO-LX+.1*STY STEP -STY
2700IF-CBX%MOD5=0THENDTA=1ELSEDTA=8
2710-CRX%=-CRX%+11PROCpoint(X,-YO)INEXT%
2720FORY=-SYTO-LY+.1*STY STEP -STY
2730IF-CBY%MOD5=0THENDTA=1ELSEDTA=8
2740-CBY%=-CBY%+11PROCpoint(-XO,Y)INEXTY
2750ENDPROC
2760:
2770DEFPROCNUMBERUNITS
2780MOVEFN-CVX(-LX)+4*LEN(STR$(-LY)),FN-CVY(-YO)-20:PRINT;-LX
2790MOVEFN-CVX(-XO)-150,FN-CVY(-LY)1PRINT;-LY
2800IF-LX<0AND-SX<0AND-LY<0AND-SY<0THENENDPROC
2810MOVEFN-CVX(-SX),FN-CVY(-YO)-20:PRINT;-SY
2820MOVEFN-CVX(-XO)-150,FN-CVY(-SY)+20:PRINT;-CY:UNI%
2830ENDPROC
2840:
2850DEFPROCPOINT(A,B)
2860UNI%
2870MOVEFN-CVX(A),FN-CVY(B-DTA)REMAEN-CVX(A)+DTA,FN-CVY(B)
2875 GOTO2910
2880IF TST%=2%% THEN GOTO 2900
2890IF Y(1) < SY<= LY+.5*DIM% THEN GOTO 2900 ELSE GOTO 2910
2895TST%=TST%+1:MOVEFN-CVX(A),FN-CVY(B+DTA)R,R,R,R,R,R:PRINT #C%;TT%:GOTO2
2900:
2910UNI%
2920ENDPROC
2930DEF PROC(A,B)
2940MOVEFN-CVX(A)-DTA,FN-CVY(B)REMAEN-CVX(A)+DTA,FN-CVY(B)
2950MOVEFN-CVX(A),FN-CVY(B-DTA)REMAEN-CVX(A),FN-CVY(B+DTA
2960ENDPROC
2970:
2980DEFPROCNAME(-WNME%)LOCAL
2990FOR A%=TOLEN-WNME%
3000MOVEFN-CVX(-XO-60),FN-CVY(-YO-A%*20):PRINTMID$(-WNME%,A%,1
3010NEXT A%UNI%
3020ENDPROC
3030:
3040DEFPROCNAME(-WNME%)
3050MOVEFN-CVX(-LX-LEN(-WNME%)*20),FN-CVY(-SY-60):PRINT-WNME%:UNI%
3060ENDPROC
3070:
3080DEFPROCTIMELIST
3090*IEEE
3100 IF PREM%=2 THEN GOTO 3210
3120IF TIME<0 THEN GOTO 3130 ELSE GOTO 3140
3130 REPEAT:UNTIL TIME>0
3140 INPUT#7,V%
3150 Y=SP%*1%-VAL(V%)*1000
3160 IF SP%=1 THEN SP%=-1
3170 SP%=SP%*1
3180 PRINT#7,"*"+STR$(SP%)
3190 K=TIME+110
3200 PREM%=2
3210 GOTO 3240
3220 IF TIME<K THEN GOTO 3230 ELSE GOTO 3240
3225 :
3230 REPEAT:UNTIL TIME>=K
3240 PRINT#7,"S1"
3245 K=TIME+25
3247 PREM%=1
3248 *FX15
3249 ENDPROC
3250:
3260DEFPROCCLOCK
3270:*****
3280DEFPROCOFF
3290PROCgetdatetime
3300CLS
3310PROCshowtime
3320GOTO3250
3330REPEATPROCshowtime
3340UNTILFALSE
3350ENDPROC
3360:
3370DEFPROCgetdatetime
3380CLS
3390PRINT"Give date,month,yr : "
3400REPEAT
3410PRINT"DAY ";
3420INPUTday
3430UNTILday<32ANDday>0
3440REPEAT
3450PRINT"Month ";
3460INPUTmonth
3470UNTILmonth<13ANDmonth>0
3480REPEAT
3490PRINT"Year ";
3500INPUTyear
3510UNTILyear>1799ANDyear<2500ORyear>99ANDyear<99
3520IFyear<99THENyear=year+1900
3530CLS
3540REPEAT
3550PRINT"Hours ";
3560INPUThour
3570UNTILhour<24ANDhour>-1
3580REPEAT
3590PRINT"Minutes ";
3600INPUTminute
3610UNTILminute<60ANDminute>-1
3620TIME=100*hour+minute*6000
3630T1%=TIME/100:T2%=T1%:FF%=1
3640ENDPROC
3650:
3660DEFPROCshowtime
3670VDU28,1,5,79,1
3680PRINT
3690PROCrectangle
3700IFTIME<0THENTIME=TIME+8640000
3710hour=TIMEDIV360000:REMHOUR
3720minute=TIMEDIV6000MOD60
3730second=TIMEDIV100MOD60
3740IF hour=0ANDminute=0ANDsecond=59THENPROCgetdate
3750IF minute=60THENminute=0
3760PRINTTAB(0,0);"Date = ";day;" ";
3770RESTORE3780
3780DATAJan,Feb,Mar,Apr,May,Jun,Jul,Aug,Sept,Oct,Nov,Dec
3790FORM=1TOmon%
3800READmon$
3810NEXT:
3820PRINTmon$;" ";CHR$157;CHR$132;" ";
3830PRINT"GMT = ";
3840IFhour<10THENPRINT" ";
3850PRINT;hour;":";
3860IFminute<10THENPRINT"0";
3870PRINT;minute;":";SPC(5);"FILE NAME = ";F$
3880T1%=T1%-hour*3600-minute*60-second:IFT1%<0THENT1%=T1%+86400
3890IFday<10THENT1%=T1%+T1%
3900IFmonth<10THENT2%=T2%+T2%
3910IFmonth<3THENT2%=T2%+T2%
3920IFmonth<4THENT2%=T2%+T2%
3930IFmonth<5THENT2%=T2%+T2%
3940IFmonth<6THENT2%=T2%+T2%
3950time%=STR$(month)+T1%+T2%+T2%+T2%
3960IF FFlag1=1 THENPRINTtime%;TAB(15);CHR$(34);"sending "+CHR$(137);TAB(2
1;"RECno "+RECno%;
3970IF FFlag1=0 THENPRINTtime%;TAB(15);"not sending";TAB(29);"RECno "+RECno%;
3980a%=2%%%
3990PRINTSPC(-2*Y(1)+SPC(2)Y(2)+SPC(2)Y(3)+SPC(2)Y(4)+SPC(2)Y(5)
4000a%=1%
4010UNI%
4020a%=2%%%
4030IF TG%=1 THEN PROCshowdata
4040a%=1%
4050UNI%
4060ENDPROC
4070:
4080DEFPROCOFF
4090UNI%:*FX10;0;
4100ENDPROC
4110:
4120DEFPROCinputdate
4130day=day+1
4140IFmonth=2ANDday>29THENday=1:month=3
4150IFmonth=2ANDday=29THENIFNOTFNLEAP(year)THENday=1:month=3
4160IFmonth=4ORmonth=6ORmonth=9ORmonth=11)ANDday=31)THENday=1:month=month
4170IF day>31THENday=1:month=month+1
4180IFmonth>12THENmonth=1:year=year+1
4190ENDPROC
4200:
4210DEFFNLEAP(Y)
4220IFYMOD4=0ANDYMOD100<>0 OR YMOD400=0)THEN=TRUEELSE=FALSE
4230:
4240DEF PROCselgra*
4245VDU7
4250CLS:CLG
4260VDU28,0,31,79,0
4270:
4280INPUT"BOTTOM Y "; SY
4290INPUT"TOP Y "; LY
4300INPUT"NUMBER * DIVISIONS "; LY
4310PRINT"SELECT CHANNELS TO PLOT "
4320INPUT"HOW MANY "CN%
4330FOR FX=1TOCN%
4340PRINT"CH. "FX;"=";
4350INPUTCH%(FX)
4360NEXT FX
4370UNI%
4380GOTO4140
4390ENDPROC
4400:
4410DEFPROCread_record
4420PTR#file=REC1en%*RECno%
4430FOR FX=1 TO FIELDS%
4440INPUT#file,F$(FX)
4450NEXT
4460ENDPROC
4470:
4480DEFPROCdisplay_record
4490PROCread_record
4500GOTO4520
4510IF ZZ=1 PROCprint_record:ENDPROC
4520REPEAT
4530CLS
4540VDU23;11,0;0;0;0 :REM CURSOR OFF
4550VDU14 :REM PAGE MODE ON
4560PROCpane1(1,1)
4570PRINT TAB(0,5)
4580FOR FX=1 TO FIELDS%
4590PRINT CHR$(129)FIELD$(FX)
4600PRINT TAB(1) F$(FX)
4610PROCline
4620NEXT
4630PROCpane1(1,0)
4640VDU15 :REM PAGE MODE OFF
4650:
4660*FNget_key
4670UNTIL F%=ASC"R"
4680ENDPROC
4690:
4700DEFPROCselect_record
4710REPEAT
4720PROCcheck
4730PROCsendcheck
4740PRINT" Enter record number "
4750A$=FNinput
4760IF VAL(A$)>0 AND ASC(A$)<48 THEN RECno%=-1 ELSE RECno%=VAL(A$)
4770UNTIL RECno%<1 AND RECno%=RECleng% EXT#file
4780ENDPROC
4790:
4800DEFPROCview_file
4810IFFIELDS%=13THENRECleng%=72:FILE$="11-PIGS"
4820IFFIELDS%=14THENRECleng%="TEMPERATURE":FIELD$(2)="FORCE":FIELD$(3)="CONFINING PRESSURE":F
IELD$(4)="PORE PRESSURE":FIELD$(5)="DISPLACEMENT":FIELD$(6)="TIME"
4830CLS
4840PROCselect_record
4850REPEAT
4860PROCcheck
4870PROCsendcheck
4880PROCcheckinkey
4890PROCdisplay_record
4900IF I=2% RECno%=RECno%-1
4910IF I=127 RECno%=RECno%+1
4920UNTIL RECno%<0 OR RECno%=RECleng%+EXT#file OR F%=820
4930ENDPROC
4940:
4950DEFPROCpane1(FLAG,FLAG2)
4960VDU28,0,4,79,0 :REM TEXT WINDOW
4970PRINT CHR$(131;CHR$157;CHR$172;"File Accessed :";FILE$
4980IF FLAG=1 PRINT CHR$(1;CHR$157;CHR$132;"Record number :";RECno%"
4990PRINT CHR$(131;CHR$157;CHR$132;
5000IF FLAG=1 PRINT"Page mode"CHR$(1"ON "ELSE PRINT"Page mode OFF"
5010UNI%,0,79,79,5
5020ENDPROC
5030:
5040DEFPROCline
5050PRINT CHR$(1); STRING$(79,CHR$172)
5060ENDPROC
5070:
5080DEF FNget_key
5090REPEAT
5100*FX4,1
5110:REM RELEASE EDIT KEYS
5120*FX21,1
5130:REM CLEAR KEYBOARD BUFFER
5140*FX21,0
5150*FX138,0,EY(1)
5160*FX7,1,0
5170:REM RESTORE EDIT KEYS
5180*FX4,0
5190PROCcheck
5200PROCsendcheck
5210PROCcheckinkey
5220UNTIL F%=820 OR F%=888
5230:
5240:
5250DEF FNinput
5260REPEAT
5270PROCcheck
5280PROCsendcheck
```

```
9290ef$21,0
9300INPUT"LINE #=
9310INTIL "<>"
9320ef$
9330:
9340DEF PROCtest
9350PROCrectangle
9360PROCcheck
9370PROCsendcheck
9380PROCcheckinkey
9390PROCshowdata
9400ENDPROC
9410:
9415VDU7
9275VDU7
9420:
9430DEF PROCdata
9440F=0
9450FOR I=1TO20
9460K=(K+ADVAL(CN%))
9470NEXT I
9480K=K/20
9490ENDPROC
9500:
9510DEFPROCrectangle
9520MOVE 0,913:DRAW 0,1023
9530MOVE 0,913 :DRAW 1279,913
9540MOVE 1279,1023 :DRAW 0,1023
9550MOVE 1279,1023 :DRAW 1279,913
9560ENDPROC
9570:
9575VDU7
9580:
9590DEF PROCdata
9600VDU7
9610CLS: 0,1
9620VDU7
9630VDU1;7,8,0,0,;
9640ef$=
9650ef$=
9660T=INKEY(100)
9670VDU1;7,7,0,0,;
9680GOTO 9600
9690ENDPROC
9700:
9800:
9870DEF PROCparam
9875VDU7
9880:CLS:G
9890:
9900:
9910INPUT"SPECIMEN LENGTH, L1,L2 "iL1,L2
9720PRINT"SPECIMEN DIAMETER, D1 THRU D6 "iD1,D2,D3,D4,D5,D6
9730PRINT"STARTING DISPLACEMENT, mm "; STARTT
9740PRINT"DISPLACEMENT RATE, mm/min "iGRAD
9750PRINT"FORCE GAUGE ZERO, mV "iFZ0
9760PRINT"PH200, P0, T0 "iPH200,P0,T0
9770INPUT"DATAFILE NAME "iT$
9780INPUT"ENTER LOAD-ON TIME"iLONTIME
9810INPUT"ENTER LOAD-ON PRESSURE, mV "iP0
9820INPUT"ENTER LOAD-ON TEMPERATURE, mV "T0
9830INPUT"ENTER LOAD-ON DISPLACEMENT, mV (CREEP TESTS ONLY) "iLVDT0
9840GOTO 7940
9850IF TRY$="Y" THEN GOTO 7960 ELSE GOTO 7940
7960INPUT"SPECIMEN LENGTH, L1,L2 "iL1,L2
7970INPUT"SPECIMEN DIAMETER, D1 THRU D6 "iD1,D2,D3,D4,D5,D6
7980D1=((D1+D2+D3+D4+D5+D6)/6):AVL=(L1+L2)/2:AREA=((DIA/2)^2)*PI
7990INPUT"STARTING DISPLACEMENT, mm "; STARTT
8000INPUT"DISPLACEMENT RATE, mm/min "iGRAD
8010INPUT"FORCE GAUGE ZERO, mV "iFZ0
8020INPUT"PH200, P0, T0 "iPH200,P0,T0
8030INPUT"DATAFILE NAME "iT$
8040DATIME=1:DRTIME=0:DADIST=0:DDDIST=0:DD=0:DA=GRAD/2^.4
8045 PROCsave_param
8050ENDPROC
8060:
8070:
8080:
8090DEF PROCend
8091VDU7
8095 PROCsave_param
8096CLOSE#0
8270PROCoff(0)
8280PROCoff(1)
8290PROCoff(2)
8300PROCoff(3)
8310PROCoff(4)
8320PROCoff(5)
8330PROCoff(6)
8340PROCoff(7)
8350END
8360:
8370DEFPROC(OFF,G$)
8380LOCAL I,S$
8390S$=""
8400FOR I=1 TO LEN(G$)
8410S$=S$+CHR$(ASC(MID$(G$,I,1))-32)
8420NEXT I
8430AFF&=&FF
8440ENDPROC
8450:
8460DEFPROCON(NN%)
8470IF NN%<0 OR NN%>7 THEN ENDPROC
8480NN%=2^NN%
8490AFF&=AFF&-NN%
8500ENDPROC
8510:
8520DEFPROCoff(NN%)
8530IF NN%<0 OR NN%>7 THEN ENDPROC
8540NN%=2^NN%
8550AFF&=AFF& AND (NOT NN%)
8560ENDPROC
8570:
8580DEFPROCstresscheck
8590REM HOLDS STRESS AT LEVEL SET BY STPCON
8600 IF (STPMPA*10)<STPCON THEN KNT%=KNT%+1 ELSE GOTO 8630
8610IF KNT%>=5 THEN GOTO 8620 ELSE GOTO 8640
8620 PROCoff(1)
8630 PROCON(0)
8640 KNT%=0
8650IF (STPMPA*10)>=STPCON THEN PROCoff(0)
8660 REM ACTION IF STRESS GOES OVER BY 100 BARS OR MORE
8670 IF(STPMPA*10)>(STPCON+100) GOTO 8720 ELSE GOTO8710
8680 PROCoff(0):PROCoff(1)
8690 SSS=INKEY(100)
8700 PROCON(1)
8710 GOTO8720
8720 PROCoff(1)
8730 REM DISPLACEMENT LIMIT
8740 IF ABS(DISPL)> THEN PROCoff(1)
8750 IF ABS(DISPL)>3 THEN PROCoff(1)
8760 ENDPROC
8770:
8780DEFPROCstressset(SP)
8790VDU7
8800REM SET REQUIRED STRESS LEVEL, STPCON
8790VDU28,1,5,79,1
8800CLS
8810PROCrectangle
8820PRINT" ** CONSTANT STRESS ROUTINE **"
8830INPUT"ENTER DESIRED STRESS LEVEL, (bars) "iSTPCON
8840CLS
8850PRINT"ENTER 'Y' TO START CONTROL ACTION, 'N' TO STOP IT"
8860SSS=INKEY$
8870ENDPROC
8880:
8890DEFPROCshowdata
8900REM TO DISPLAY REMOTE DATA
8910VDU28,58,11,79,5
8920@%=&20207
8930PRINT"STRESS (bars)="iSTEMPA*10
8940PRINT"DISPL (mm) ="iDISPL
8950PRINT" T ="; T
8960PRINT" P ="; P
8970PRINT"PH20(bar) ="iPH20*10
8980IF CON%=1 THEN PRINT"control ON "iSTPCON" b." ELSE PRINT"Press control
8990:
9000MOVE 960,640:DRAW 960,960
9010MOVE 1279,640:DRAW1279,640
9020MOVE1279,640:DRAW960,960
9030MOVE1279,960:DRAW1279,640
9040@%=10
9050ENDPROC
9060:
9070 DEFPROCprocess(Y(1),Y(2),Y(3),Y(4))
9080 T=Y(2):FG=Y(4):P=Y(3):PH20=Y(1)
9090LVDT=Y(5)
9100PH20=PH20+PH20+PH20+PH20
9110 ELTIME=VAL(time$)
9120 PROCCONV(ELTIME)
9130 ELTIME=ATIME
9140 PROCCONV(LONTIME)
9150 LONTIME=ATIME
9160 ETIME=ELTIME-LONTIME
9170PT=MP+PO+PZ:TT=MT+TO+TZ
9180 P=MP+P+PZ:T=MT+T+TZ
9190FG=FGZ0+(P-PT)+DFGZDP+(T-TT)+DFGZDT
9200FG=FG-FGZ
9210FG=MF+FG+(1+P+DMFDP-T+DMFDT)
9220DISPL=ETIME+GPAD/60
9230 SL$=INKEY$(1)
9240 IF SL$="L" GOTO9250 ELSE GOTO 9270
9250 LVDT=(Y(5)-TO+Y(2))*PO+Y(3)
9260 VDU7
9270 IF CON%=1 THEN DISPL=(LVDT-LVDT0)/2.75
9280LMD=.000014
9290MD=MO+(1-P+DMDDP+T+DMDDT)
9300IF FG<179 THEN CDISPL=DISPL-(LMD+FG+25.4) ELSE CDISPL=DISPL-(MD+(FG-179)
*25.4
9310STEMPA=FG/(AREA+LF)
9320PROCJACKT
9330REM CORRECTION FOR AREA IN SHEARED ZONE
9340STEMPA=(STEMPA/2)+(SIN(70+PI/180))/(1-(2+(CDISPL+STARTT)/(PI+DIA+25.4)))+
(.75+PI/180))
9350REM STRESS IS NOW SHEAR STRESS ALONG SAWCUT
9360ENDPROC
9370:
9380:
9390:
9400DEFPROCJACKT
9410BCU=-3.054E-2+T+25:BCU=-3.411325E-4+T+0.5:CCU=-.253675+T+200
9420IF(CDISPL+STARTT)<.025 THEN CJACK=BCU+(CDISPL+STARTT) ELSE CJACK=A*(CD
+STARTT)^BCU
9430IF T<550 AND (CDISPL+STARTT)>.25 THEN CJACK=5.29
9440STEMPA=STEMPA-CJACK
9450ENDPROC
9460:
9470DEFPROCmachine
9480a=OPENIN"MIMON1a"
9490INPUT#a,MF,MP0,MP,MT,MPH20,TZ,PZ,PH20Z
9500INPUT#a,DFGZDP,DFGZDT,DMFDP,DMFDT,DMDDP,DMDDT
9510CLOSE#a
9520ENDPROC
9530:
9540DEFPROCCONV(ATIME)
9550HOUR=ATIMEDIV(1000*3600)
9560DAYS=(ATIME-HOUR*1000*3600)DIV(1000*3600*24)
9570T=(ATIME-HOUR*1000*3600-DAYS*1000*3600*24)DIV(1000*3600)
9580MIN=(ATIME-HOUR*1000*3600-DAYS*1000*3600*24-T*1000*3600)DIV(1000*60)
9590SEC=(ATIME-HOUR*1000*3600-DAYS*1000*3600*24-T*1000*3600-MIN*1000*60)DIV1000
9600IF MON%=1 THEN MON=0
9610IF MON%=2 THEN MON=2678400
9620IF MON%=3 THEN MON=5097600
9630IF MON%=4 THEN MON=7776000
9640IF MON%=5 THEN MON=10454400
9650IF MON%=6 THEN MON=13046400
9660IF MON%=7 THEN MON=15724800
9670IF MON%=8 THEN MON=18316800
9680IF MON%=9 THEN MON=20995200
9690IF MON%=10 THEN MON=23587200
9700IF MON%=11 THEN MON=26265600
9710IF MON%=12 THEN MON=28857600
9720ATIME=SEC+60*MIN+3600*HOUR+24*3600*DAYS+MON
9730ENDPROC
9740:
9750:
9760DEF PROCconstant
```

```
LISTING 2 : The computer program CREATE.

 5 REM DATAFILE CREATOR PROGRAM PROFILES, MAKES A DATPED COMPATIBLE FILE FROM
ATA LOGGER FILE 'RIOS', MADE VIA PREMLOG FOR NIMBUS 1. SHORT VERSION
  10MODE0
  20 MTC$=--11ontlaem-lleftimem0ii$M8m"N"
  30PEnm#=13
  40LIneI=12m0IDI=mID2=0ID"=mID4=0ID5=mID6=mSTARTT=0ii(PAD=0
  50FG(0=0IDM200m0ii(P0=0ii"=m0ii"Sm0iDTIMi=mDISTOm0iDISTO
  60T$="NONAME":IDA=mDATIMEmmDAPISTmmDPOSTIMEmmDPDISTmm
  70PROFFSIGm0ii(ONE=0ii(ONTIMEm0ii(NT"=mmiVDTOm
  80APEA=1IDIA=11STPC(0=mmmm4e"TTT"=1TG(E0
  90CLOSE#0
 100DIMY(6),Y1=1,FF$(6),FIELD$(6),F$(6),NC$(6)
 200DIM CAL(4,2,3),Gd1,ADEF$,2,3,PFCLIST2000
 250 ONERROR GOTO 4990
 260t=lomOPENUP"I: RIOS"
 290PROCmachine
 295REM Ft=1TO1IG=FY1=INPUT F$
 297Y1=1TIME/100
 300 TS$=1DATM$TO$
 305T"=1:IFF1Flag=0
 310SAP=100000
 320 SV=0:IV=501 S1=0 I=FNCUR(Y" "
 350FOR F%=1TO%INC%:F%=BFYINF%TO
 375PROCtest_data
 380VDU14:Fd,0
 385REPEAT
 390PROCmenu
 400UNTILFALSE
 410END
 450
 470DEFPROCINput
 480REPEAT
 490F%=1,0
 495I$=INFY$(1)
 520UNTIL$=""
 530IF$="G"THENF1ag1=1
 540IF$="S"THENF1ag1=0
 550IF$="M"THEN PROCflash
 560IF$="F" THEN CON%=1
 570IF$="D" THEN CON%=0
 580IF TG%=1 THEN GOTO 610
 590IF TG%=0 THEN GOTO 600
 600IF K$="P" THEN TG%=1: GOTO 620
 610IF K$="P" THEN TG%=0: GOTO 620
 620ENDPROC
 630
 640DEFPROCmenu
 650CLS:CLG
 660VDU26
 670VDU28,0,31,79,0
 680PRINTTAB(10);"MAIN MENU - DATAFILE CREATOR PR
OGRAM, CR-FILE"
 690PRINTTAB(20);"----------"
 700PRINT"(S)  ENTER TEST PARAMETERS"
 710PRINT"(R)  PLOT FROM DISK FILE"
 720PRINT"(T) STOP PROGRAM"
 730 PRINT
 740VDU26
 750PROCInput
 760PROCselect
 770ENDPROC
 780
 790DEFPROCselect
 800IFVAL(K$)=3THENPROCparam
 810
 820IFVAL(K$)=RTHENPROCgraf(1):plot
 830IF(K$)="T"THEN PROCend
 840ENDPROC
 850
 860DEFPROCgraf(B%)
 870TST%=0
 880PROCSCALE
 890PROCAXES
 900PROCGRADUATE
 910PROCNUMBER
 920PROCNAMEX(B%)
 930PROCNAMEY("MILLIVOLTS")
 940ENDPROC
 950
 960DEFFNpad(PAD$,N)
 970IF LENPAD$<N PAD$=PAD$+STRING$(N-LENPAD$," "):ELSEPAD$=LEFT$(PAD$,N)
 980=PAD$
 990DEFPROCGRAPH
1000PROCSCALE
1010PROCAXES
1020PROCGRADUATE
1030PROCNUMBER
1040FOR J=1TOX(0)
1050DTA=0:PROCPOINT(X( J),Y( J))
1060IF J=1THENGOTO1250
1070MOVEFN CVX(X( J-1)),FN CVY(Y( J-1)):DRAWFN CVX(X( J)),FN CVY(Y( J))
1080IF J<X(0)GOTO1200
1090VDU4:PRINTTAB(FN CVX(X( J))+2,FN CVY(Y( J))-1);DA$:VDU5
1200VDU4:PRINTTAB(FN CVX(X( J))+2,FN CVY(Y( J))-1);DA$:VDU5
1210NEXT J
1220ENDPROC
1230
1240DEFPROCSCALE
1250PROCSCALE2(1,SY,LY,1,SY,1
1260 ST%=ST:CRYE=CENT
1270PROCSCALE2(2,SE,LE,1,SE,1
1280 ST%=ST:CRYE=CENT
1290 Y=10000/(LY-SY):I=SY:Y=0:X=0:Y1=-SY
1300 CONVE=Y:C=-SY:I=1:CONVE=Y:C=-SY
1310ENDPROC
1320
1330DEFFN CVY(G)=Y*G+CONV
1340DEFFN CVX(G)=X*G+CONV
1350
1360DEFPROCSCALE2(I,H,S,Z,O,U,C,A
1370 L=VAL(LEFT$(STR$(I),INSTR(STR$(I),"E")-1))
1380 H=VAL(LEFT$(STR$(H),INSTR(STR$(H),"E")-1))
1390 P=VAL(MID$(STR$(I),INSTR(STR$(I),"E")+1))
1400 IF H-(H=10^(VAL(MID$(STR$(H),INSTR(STR$(H),"E")+1)))-P
1410 D=H-L
1420 IF D="THENREPEAT D=.1*D:P=P-1:UNTIL D<>0
1430 IF D>50THENREPEAT D=D/10:P=P+1:UNTIL D<50
1440 L=INT(.1*L+.5):H=INT(.1*H+.5)
1450 A=INT(.1*D+.5):D=10^P:C=A*D:S=L*D:Z=H*D
1460 S=VAL(STR$(.1*S+.5)+"E"+STR$(P)):Z=VAL(STR$(.1*Z+.5)+"E"+STR$(P))
1470 C=VAL(STR$(.1*C+.5)+"E"+STR$(P+1)):A=C/5:O=S:U=Z
1480ENDPROC
1490
1500DEFPROCAXES
1510 X=640: Y=1023
1520 IF S<0 THEN O=INT(-S/(Z-S)*X):S=0:GOTO1540
1530 O=0
1540 IF Z>0 THEN U=INT((Z-S)/(Z-S)*X):Z=0:GOTO1560
1550 U=X
1560 MOVEFN CVX(S),FN CVY(0):DRAWFN CVX(Z),FN CVY(0)
1570 MOVEFN CVX(0),FN CVY(S):DRAWFN CVX(0),FN CVY(Y)
1580ENDPROC
1590
1600DEFPROCGRADUATE
1610FOR F%=STO(Z-.1)STEP  ST%
1620IF CRYE%MOD5=0THENDTA$=1:ELSEDTA$=
1630 CRYE%=CRYE+1:PROCpoint(F%, Y01)NEXT%
1640FOR Y=STO(Y-.1)STEP  ST%
1650IF CRYE%MOD5=0THENDTA$=1:ELSEDTA$=
```

```
1660 CRYE%=CRYE+1:PROCpoint(O,Y):NEXT%
1670ENDPROC
1680
1690DEFPROCNUMBER
1700FOR F%=STO(Z-.1)STEP  ST%
1710IF CRYE%MOD10=0THENDTA$=STR$(F%):ELSEDTA$=
1720 CRYE%=CRYE+1:PROCpoint(O,F%):NEXT%
1730ENDPROC
1740
1750DEFPROCNAMEX(B%)
1760IF B%=1THENDTA$="TIME(SECS)":ELSEDTA$="DISTANCE(FEET)"
1770VDU4:PRINTTAB(FN CVX(X/2)-LEN(DTA$)/2,FN CVY(0)+2)DTA$:VDU5
1780ENDPROC
1790
1800DEFPROCNAMEY(DTA$)
1810VDU4:PRINTTAB(FN CVX(0)-LEN(DTA$)-2,FN CVY(Y/2))DTA$:VDU5
1820ENDPROC
1830
1840DEFPROCPOINT(A,B)
1850VDU5
1860MOVEFN CVX(A),FN CVY(B):DRAWFN CVX(A),FN CVY(B)
1870IF TST%=2THEN GOTO 2910
1880IF TST%=1THENMOVEFN CVX(A),FN CVY(B):VDU8,8,8,8,8,8,8,8:PRINT MC$;TTT%;:GO
TO
1890VDU5
1900ENDPROC
1910DEF PROCpoint(A,B)
1920MOVEFN CVX(A)-DTA,FN CVY(B):DRAWFN CVX(A)+DTA,FN CVY(B)
1930MOVEFN CVX(A),FN CVY(B)-DTA:DRAWFN CVX(A),FN CVY(B)+DTA
1940ENDPROC
1950
1960DEFPROCNAMEY( UNAME$):VDU5
1970FOR G=1TOLEN( UNAME$)
1980MOVEFN CVX( 80)-8,FN CVY( 1Y)- 3*72+72 :PRINTMID$( UNAME$, G,1)
1990NEXT G:VDU4
2000ENDPROC
2010
2020DEFPROCNAMEX( HNAME$)
2030MOVEFN CVX('LX)-32+LEN( HNAME$)*4,FN CVY('Y0)-52 :VDU5:PRINT HNAME$:VDU4
2040ENDPROC
2050
2060DEFPROCrectangle
2070MOVE 0,913:DRAW 0,1023
2080MOVE 0,913 :DRAW 1279,913
2090MOVE 1279,1023 :DRAW 0,1023
2100MOVE 1279,1023 :DRAW 1279,913
2110ENDPROC
2120
2130DEFPROCplot
2140REM PLOTS GRAPH FROM DISK
2150REM SELECT PARAMETERS
2160INPUT"FILE",F$
2170VDU26,0,31,79,0
2180PRINT"TO PLOT A GRAPH FROM CURRENT DATA DISK FILE"
2190X=INFY(100)
2200PRINT"Enter bottom Y axis ";:INPUT SY
2210PRINT"Enter top Y axis ";:INPUT LY
2220PRINT"  Please enter start record number ";:INPUT SNT
2230PRINT"  Please enter finish record number ";:INPUT FNI
2240PRINT"  Sampling step = ";:INPUT STP%
2250PRINT"  How many channels? = ";:INPUT FN%
2260FOR I%=1 TO CN%
2270PRINT "Channel ";I%;" - ";
2280INPUT MC$(I%)
2290NEXT I%
2300 L%=FNX(1)%-SN%+SNT
2310VDU5:CLG
2320PROCrectangle
2330VDU25,1,5,79,1
2340PRINT"P" to record point, "G" start relaxation, FILENAME = ";T$
2350PRINT"10" to create datafile, "ESC" for menu"
2360PROCgraf("RECORD NUMBER")
2370X=X-STP%
2380REPEAT:X=X+STP%
2390REC%=SN%+X
2400RTEF(1)=e72+REC%
2410FOR F%=1 TO 2
2420INPUT#File,F$,F%
2430NEXT F%
2440FOR TT%=1 TO CN%
2450TT%=REC%
2460Y=FNCVY(PROCPOINT(X(TT%),VAL(F$)/NC%(TT%)))
2470NEXT TT%
2480UNTIL (X+STP%)>=L%
2490PROCcursor
2500ENDPROC
2510
2520PT%=PP%:OT%=00%
2530
2540DEF PROCflash
2550VDU7
2560COL 0,1
2570VDU26
2580VDU25,7,7,0,0,0
2590X=FX5,5
2600Y=FX5,5
2610TL=INFY(100)
2620VDU25,7,7,0,0,0
2630
2640ENDPROC
2650
2660DEF PROCcursor
2670OTT%=1:VDU5
2680REPEAT:TTT%=(TTT%+1)MOD(CN%+1):IF TTT%=0 THEN TTT%=1
2690MOVE FNCVX(X),FNCVY(Y):VDU5
2700IF TT%=1 THEN PRINT"    *** RESFILE EMPTY ***";CHR$(7):SS=INFY(100):IF SS=
00),A%:GCOL4,1:PRINT"    *** RESFILE EMPTY ***":GCOL 4,0
2710MOVE200,600
2720IF TT%<1 THEN PRINT"    *** LAST RECORD NUMBER = ";RECLIST%(TT%-1);" **
CHR$(7):MOVE200,A%:SS=INFY(100):GCOL4,1:PRINT"    *** LAST RECORD NUMBER =
RECLIST%(TT%-1);" ***":GCOL 4,0
2730MOVE200,A%:PRINT"EXTEND EXISTING RESFILE OR NEWFILE, E or N? ";T%=GET%
VE200,A%:GCOL4,1:PRINT"EXTEND EXISTING RESFILE OR NEWFILE, E or N? ";GCOL4,0
2740IF T%=ASC("N") THEN T%=0
2750IF T%=ASC("E") THENT%=RECLIST%(TT%-1)
2760VDU23,240,224,248,254,211,17%,4,2,1
2770VDU23,240,224,248,254,211,17%,4,2,1
2780CNT%=0
2790VDU5
2800PP%=100:OO%=100
2810FX4,1
2820PT%=100:OT%=100
2830REPEAT
2840SS=0
2850MOVE PP%,OO%
2860COL 4,0
2870VDU 240
2880CNT%=CNT%+1:SS=-1:GSLP=( X- SX)/(FN CVX(X)-FN CVX( SX))
2890REC%=(PP%-150)*GSLP+ SX
2900GCOL0,1:VDU4:VDU29,17,31,29,31
2910GCOL4,1:COLOUR 131:COLOUR 0:PRINTTAB(1,1);"RECORD ";REC%; :COLOUR 129:COLOUR 2
2920VDU5
2930SS=INFY(1):VDU4:FX4,0
2940IF SS=0 THEN GOTO 3020
2950IF CNT%<100 THEN GOTO 2770 ELSE GOTO 3000
2960GCOL0,1
2970GCOL4,0:FX4,1
2980IF CNT%<100 THEN CNT%=0: GOTO 2790
2990VDU5:SP%=4
3000FX4,1
3010IF SS=137 THEN PP%=PP%-SP%
3020IF SS=136 THEN PP%=PP%-SP%
3030IF SS=138 THEN OO%=OO%-SP%
3040IF SS=139 THEN OO%=OO%+SP%
3050IF SS=ASC("M") THEN PROCflash
3060IF SS=ASC("P") THEN PROCsquare
```

LISTING 2

```
*510MOVE PTX,OTX:GCOL 4,1:VDU24;
*520IF SS=ASC("O") THEN PROCset;file
*530IF SS=ASC("P") THEN PFLIST(TX%)=PEC%
*540IF SS=ASC("D") THEN PROFFSIG=PEC%:REM THIS IDENTIFIES RECORD NUMBER AT MOTOR
OFF
*550IF SS=ASC("Q") THEN VDU7
*560PTX=PPX:OTY=OOX
*570UNTIL FALSE
*580ENDPROC
*590DEFPROCsquare
*600MOVE PPX-8,OOX-5:DRAW PPX-8,OOX+5
*610MOVE PPX-8,OOX+5:DRAW PPX+8,OOX+5
*620MOVE PPX+8,OOX+5:DRAW PPX+8,OOX-5
*630MOVE PPX+8,OOX-5:DRAW PPX-8,OOX-5
*640ENDPROC
7%50ENDPROC
7%70DEF PROCparam
7%90CLS:CLG
7%95PRINT "****  TEST PARAMETER ENTRY  ****":PRINT
7%96PRINT"**  EXISTING VALUES  **":PRINT
7710PRINT"SPECIMEN LENGTH, L1,L2 ";L1,L2
7720PRINT"SPECIMEN DIAMETER, D1 THRU D5 ";D1,D2,D3,D4,D5,D6
7730PRINT"STARTING DISPLACEMENT, mm ";START
7740PRINT"DISPLACEMENT RATE, mm/min ";GRAD
7750PRINT"STRAIN GAUGE ZERO, mV ";EZERO
7760PRINT"PH200, P0, TO ";PH200,P0,T0:PRINT
7770PRINT"FILENAME = ";T$
7780INPUT"TO MODIFY, Y/N OR LOAD-ON TIME, ";TRY$
7790IF TRY$="" THEN GOTO 7990 ELSE GOTO 7840
7800INPUT"ENTER LOAD-ON TIME";LONTIME
7810INPUT"ENTER LOAD-ON PRESSURE, mV ";P0
7820INPUT"ENTER LOAD-ON TEMPERATURE, mV ";T0
7830INPUT"ENTER LOAD-ON DISPLACEMENT, mV (ZERO TESTS ONLY) ";DISTO
7840GOTO 7930
7850IF TRY$="Y" THEN GOTO 7860 ELSE GOTO 7910
7860INPUT"SPECIMEN LENGTH, L1,L2 ";L1,L2
7870INPUT"SPECIMEN DIAMETER, D1 THRU D6 ";D1,D2,D3,D4,D5,D6
7880DIA=(D1+D2+D3+D4+D5+D6)/6:AREA=.78539816*DIA*DIA
7890INPUT"STARTING DISPLACEMENT, mm ";START
7900INPUT"DISPLACEMENT RATE, mm/min ";GRAD
7910INPUT"ZERO GAUGE ZERO, mV ";EZERO
7920INPUT"PH200, P0, TO ";PH200,P0,T0
7930INPUT"DATAFILE NAME  = ";T$
7940DATIME=1:DRTIME=0:DADIST=0:DBDIST=0:DA=0:DB=0:DA=GRAD/2%.4
7945 PROCsave_param
7950ENDPROC
7960:
7970DEF PROCset;file
7980REM CREATES A DATRED COMPATIBLE DATAFILE FROM THE SELECTED DATA
7985DATIME=1:DRTIME=0:DADIST=0:DBDIST=0:DB=0:DA=GRAD/2%.4
7990A%=OPENOUT(T$)
8000PTR#A%=72*PFLIST(1)
8010 FOR FX%=1 TO PEC%:INPUT#A%,F$(FX%)
8020 IF FX%= THEN DTIME=VAL(F$(2))
8030 NEXT FX%
8040PRINT#A%,L1,L2,D1,D2,D3,D4,D5,D6,EZERO,START
8050PRINT#A%,DA,DATIME,DADIST,DB,DRTIME,DBDIST
8060PRINT#A%,DISTO,DTIME,EZERO,PH200,P0,T0
8070:
8080FOR FPEAT%=1 TO PEC%-1
8090PFEC=PFEC%(FPEAT%+1)-1
8100PTR#A%=72*PFLIST(1)
8110FOR FX%=1 TO PFEC
8120INPUT#A%,F$(FX%)
8130:
8140IF PFLIST(TTX%)=MOFFSIG THEN PH200=VAL(F$(1))
8170IF PFLIST(TTX%)=0 THEN GOTO 8200
8180PRINT#A%,VAL(F$(1)),DIST,VAL(F$(2)),VAL(F$(3)),VAL(F$(4)),VAL(F$(5))
8190GOTO 8210
8200PRINT#A%,0,0,0,0,0,0:GOTO 8210
8210UNTIL PFLIST(TTX%)=0
8220CLOSE#A%:A%=0
8230ENDPROC
8240:
8250DEF PROCend
8260CLOSE#0
8270END
8280DEFPROCsave_param
8290REM OPEN PARAMETER FILE
8300INPUT#A%,MF,MDX,MF,MT,MPX200,L2,D2,PH200
8310INPUT#A%,DEGZDP,DEGZD1,DMEDP,DMED1,EMPDV,DMPDT
8320CLOSE#A%
8330ENDPROC
8340:DEFPROCsave_param
8350REM SEND PARAMETERS TO DATA RECORD FILE
8360PTR#A%=72
8370PTR#A%=STR#(VDIST)
8380PTR#A%=STR#(START)
8390PTR#A%=STR#(AVL)
8400PTR#A%=STR#(DIA)
8410PTR#A%=STR#(GRAD)
8420:FX%=1:T$
8430PROCsendparam
8440PTR#A%=11*72
8450PTR#A%=STR#(EZERO)
8460PTR#A%=STR#(PH200)
8470PTR#A%=STR#(P0)
8480PTR#A%=STR#(T0)
8490PTR#A%=STR#(SIG(M))
8500PTR#A%=STR#(ONT)
8510PROCsendparam
8520PTR#A%=12*72
8530PTR#A%=STR#(PEC%-7)
8540PTR#A%=STR#(LONTIME)
8550PTR#A%=STR#(MOFFSIG)
8560PTR#A%=" "
8570PTR#A%=" "
8580PTR#A%=" "
8590PROCsendparam
```

```
11500:DEFPROCsendparam
11510 FORFX%=1TO
11520 FF$(FX)=STR$(ABS(FF$(FX),20)
11530 PRINT#A%,FF$(FX)
11540 NEXTFX
11550 ENDPROC
11560:
12000DEFPROCtest_data
12010PECcnt=10
12020PROCreader
12030VLVDT=VAL(F$(1))
12040START=VAL(F$(2))
12050AVL=VAL(F$(3))
12060DIA=VAL(F$(4))
12070GRAD=VAL(F$(5))
12080T$=F$(6)
12090PECno%=11
12100PROCreader
12110EZRO=VAL(F$(1))
12120PH200=VAL(F$(2))
12130P0=VAL(F$(3))
12140T0=VAL(F$(4))
12150STRCON=VAL(F$(5))
12160ONT=VAL(F$(6))
12170PECcnt=12
12180PROCreader
12190PECcnt=VAL(F$(1))
12200LONTIME=VAL(F$(2))
12210MOFFSIG=VAL(F$(3))
12220L1=AVL:L2=AVL
12230D1=DIA:D2=DIA:D3=DIA:D4=DIA:D5=DIA:D6=DIA
12240ENDPROC
12250:
12260DEFPROCreader
12270PTR#A%=PECno%*72
12280FOR FX%=1TO6
12290INPUT#A%,F$(FX%)
12300NEXTFX%
12310ENDPROC
12320:
12330:
```

```
'*  LISTING 3 : The computer program DATREDT.
 10 REM *PROGRAM DATREDT , THIS VERSION IS FOR STRESS/STRAIN AND RELAXATION DA
\ON AXISYMMETRIC SAMPLES*
 20 CLOSE*0
 30 INPUT"ENTER NAME OF RAW DATA FILE",T$
 40 INPUT"ENTER NAME OF REDUCED STRESS/STRAIN DATA FILE",S$
 50 INPUT"ENTER NAME OF REDUCED RELAXATION DATA FILE",P$
 60X=OPENIN"NIMONI"
 70INPUT£X,MF,MDO,MP
 80INPUT£X,MT,MPH2O,TZ
 90INPUT£X,PZ,PH2OZ
100PRINT"          MF=","         MD=","         MP="
110PRINTMF,MDO,MP
120PRINT
130PRINT"         MT=","      MPH2O="
140PRINTMT,MPH2O
150PRINT"         TZ=","         PZ=","     PH2OZ="
160PRINTTZ,PZ,PH2OZ
170INPUT£X,DFGZDP,DFGZDT,DMFDP
180INPUT£X,DMFDT,DMDDP,DMDDT
190PRINT"     DFGZDP=","     DFGZDT=","     DMFDP="
200PRINTDFGZDP,DFGZDT,DMFDP
210PRINT"      DMFDT=","      DMDDP=","      DMDDT="
220PRINT DMFDT,DMDDP,DMDDT
230CLOSE£X
240Y=OPENIN(T$)
250INPUTEY,L1,L2
260PRINT"SPECIMEN LENGTHS ";L1,L2
270INPUTEY,D1,D2,D3,D4,D5,D6
280PRINT"AV.SPEC.DIAM.= "¡(D1+D2+D3+D4+D5+D6)/6
290INPUTEY,CS,STARTT
300PRINT"CHARTSPEED= "¡CS¡" MM/MIN";SPC(5)¡"START DISPL MM= "¡STARTT
310INPUTEY,DA,DATIME,DADIST
320INPUTEY,DB,DBTIME,DBDIST
330PRINT"DIAL GAUGE A AND B ="
340PRINT" ","A",DA,DATIME,DADIST
350PRINT" ","B",DB,DBTIME,DBDIST
360INPUTEY,DISTO,DTIMOX,FGZO
370PRINT"START LOAD POINT= "¡DISTO,DTIMOX,FGZO
380PATIMEX=0 :ATIMEX=DTIMOX :PROCCONV :DTIMOX=ATIMEX
390 PRINT DTIMOX
400IF ABS(DADIST-DBDIST)>0 DTIME=ABS((DADIST-DBDIST))*(60/CS)
410IF ABS(DATIME-DBTIME)>0 DTIME=ABS(DATIME-DBTIME)*60
420REM  *GRAD IS MM/SEC*
430GRAD=(ABS((DA-DB)/DTIME))*25.4
440AVL=(L1+L2)/2
450AREA=(((D1+D2+D3+D4+D5+D6)/12)^2)*PI
460INPUTEY,PH200,PO,TO
470PRINT"      START","      START","      START"
480PRINT"     FGZO","  PRESSURE","TEMPERATURE"
490PRINTFGZO,PO,TO
500P=PO : T=TO : PH20=PH200
510PRINT
520REM  *READ VARIABLES FROM DATA FILE*
530PDISPL=0
540PETIMEX=0
550PATIMEX=0
560 MOFF=0
570Z=OPENOUT(S$)
580PRINT
590PRINT"   P(MPA) "¡TAB(11)¡" PH2O(MPA)";TAB(23)¡"  T DEG'C'";TAB(36)¡" STR.(
A)";TAB(51)¡"  % STRAIN";TAB(63)¡"  STR.RATE"
600REPEAT
610INPUTEY,FG,DIST,ATIMEX,P,PH2O,T
620 IF FG=0 GOTO 1000
630IF PH2O<0 THEN MOFF=1 ELSE MOFF=0
640 IF T<0 THEN CS=ABS(T)
650IF P>0 P=MP+P+PZ : ELSE P=MP+PO+PZ
660IF T>0 T=MT+T+TZ : ELSE T=MT+TO+TZ
670IF PH2O>0 PH2O=MPH2O+PH2O+PH2OZ : ELSE PH2O=MPH2O+PH2O0+PH2OZ
680 PT=MP+PO+PZ : TT=MT+TO+TZ
690FGZ=FGZO+(P-PT)*DFGZDP+(T-TT)*DFGZDT
700REM  *FG IS IN MV*
710FG=FG-FGZ
720 FG=MF*FG*(1+P*DMFDP-T*DMFDT)
730 IF FG=0 GOTO 970
740REM *CALC.ELAPSED MACHINE DISPL. AND ELAPSED TIME*
750IF ATIMEX>0 THEN PROCCONV
760 IF DTIMOX=0 AND DIST>0 AND ATIMEX>0  THEN DTIMOX=ATIMEX-INT((DIST-DISTO)*(
CS))
770ETIMEX=ATIMEX-DTIMOX
780IF ATIMEX>0 THEN ETIMEX=INT((DIST-DISTO)*60/CS))
790PDISPL=ETIMEX*GRAD
800 LMD=.000014
810 MD=MDO*(1-P*DMDDP+T*DMDDT)
820IF FG<179 THEN CDISPL=PDISPL-(LMD*FG*25.4) ELSE CDISPL=PDISPL-(MD*FG+.0025)*2

830DSTRAIN=(CDISPL-PDISPL)/(AVL*25.4)
840TSTRAIN=CDISPL/(AVL*25.4)
850IF ETIMEX=PETIMEX GOTO 880
860EDOT=DSTRAIN/(ETIMEX-PETIMEX)
870AREA=AREA*(DSTRAIN+1)
880STRPA=FG/AREA
890STRMPA=STRPA*1/147
900 PDISPL=CDISPL : PETIMEX=ETIMEX : PATIMEX=ATIMEX
910X=10203
920PRINT TAB(0);P;TAB(11);PH2O;TAB(23);T;TAB(36);STRMPA;TAB(51);TSTRAIN*100;TA
B(75);EDOT
930X=10
940 PRINT£X,P,PH2O,T,STRMPA,TSTRAIN,EDOT
950 IF MOFF=1 THEN PROCRELAX
960NEXT: EOFEY
970 CLOSE£0
980 END
990DEFPROCRELAX
1000PRINT"*STRESS RELAXATION STARTS*"
1010 RELDAT=OPENOUT(R$)
1020ETIMOX=ATIMEX :ETIMEX=0 :PETIMEX=0 : PATIMEX=0
1030 PRINT PTIMOX
1040DISPL=0 :PFG=FG :PFG2=FG
1050TDISPL=0 :LGN=AVL*(1-TSTRAIN)
1060 PEDOT=EDOT :TPSTRN=0 :PTPSTRN=0
1070STRMPA=STRMPA :STRMP2=STRMPA
1080PRINT"   P(MPA)";TAB(11);" PH2O(MPA)";TAB(23);"  T.'DEG'C'";TAB(36);" STR.(
A)";TAB(51);"   PSTRAIN";TAB(63);"    ETIME";TAB(75);"  STR.RATE"
1090REPEAT
1100INPUTEY,FG,DIST,ATIMEX,P,PH2O,T
1110 IF FG=0 GOTO 1470
1120IF PH2O<0 THEN MOFF=1 ELSE MOFF=0
1130IF T<0 THEN CS=ABS(T)
1140IF P>0 P=MP+P+PZ : ELSE P=MP+PO+PZ
1150IF T>0 T=MT+T+TZ : ELSE T=MT+TO+TZ
1160IF PH2O>0 PH2O=MPH2O+PH2O+PH2OZ : ELSE PH2O=MPH2O+PH2O0+PH2OZ
1170 PT=MP+PO+PZ : TT=MT+TO+TZ
1180FGZ=FGZO+(P-PT)*DFGZDP+(T-TT)*DFGZDT
1190REM  *FG IS IN MV*
1200FG=FG-FGZ
1210FG=MF*FG*(1+P*DMFDP-T*DMFDT)
1220IF ATIMEX>0 THEN ATIMEX=ATIMEX : PROCCONV : ATIMPX=ATIMEX : IF PATIMPX>ATIM
PEN ATIMPX=ATIMPX+31536000
1230 ETIMPX=ATIMPX-PTIMOX
1240IF ATIMEX=0 THEN ETIMEX=INT(DIST*60/CS))
1250FG=FG*10^6
1260MD=MDO*(1+P*DMDDP-T*DMDDT)
1270PDISPL=(FG-PFG)*(MD+AVL/(AREA*7))+PDISPL
1280RDISPL=(FG-PFG)*(LGN/(1-TRSTRN))
1290TRDISPL=TDISPL+RDISPL
1300TRSTRN=TRDISPL/(LGN*(1-TRSTRN))
1310DTIMRX=ETIMRX-PETIMRX
1320EDOT=DRSTRN/DTIMRX
1330 DEDOT=(PFG-FG)*(LOG(ABS(PEDOT))-LOG(ABS(EDOT)))/(PFG2-FG)+LOG(ABS(EDOT))
1340 OEDOT=10^DEDOT
1350PSTRMPA=PFG/(AREA*(1+PTRSTRN)*147)
1360STRMPA=FG/(AREA*(1+PTRSTRN)*147)
1370PRINTERELDAT,P,PH2O,T,PSTRMPA,PTPSTRN,PETIMRX,OEDOT
1380PRINT TAB(0);P;TAB(11);PH2O;TAB(23);T;TAB(36);PSTRMPA;TAB(51);PTRSTRN;TAB
3);PETIMRX;TAB(75);OEDOT
1390PFG2=PFG
1400PFG=FG : PETIMRX=ETIMRX : PRDISPL=RDISPL : PEDOT=EDOT
1410 PATIMRX=ATIMPX :PTPSTRN=TRSTRN
1420 UNTIL FG=0
1430 DEDOT=(FG-PFG)*(LOG(ABS(PEDOT))-LOG(ABS(EDOT)))/(PFG2-FG)+LOG(ABS(EDOT))
1440 OEDOT=10^DEDOT
1450PRINT TAB(0);P;TAB(11);PH2O;TAB(23);T;TAB(36);STRMPA;TAB(51);TRSTRN;TAB(6
;ETIMRX;TAB(75);OEDOT
1460PRINTEPELDAT,P,PH2O,T,STRMPA,TPSTRN,ETIMRX,OEDOT
1470 CLOSEEPELDAT
1480 ENDPROC
1490DEF PROCCONV
1500REM*TO CONVERT MONTH,DAY,HR,MIN,SEC TO SECONDS*
1510MONX=ATIMEX/10^10000000
1520DAYX=(ATIMEX-MOD(10000000000))/10000000
1530HRX=(ATIMEX-MOD(1000000))/100000
1540MINX=(ATIMEX-MOD(10000))/100
1550SECX=ATIMEX-MOD100
1560IF MONX=01 THEN MONX=0
1570IF MONX=02 THEN MONX=2678400
1580IF MONX=03 THEN MONX=5097600
1590IF MONX=04 THEN MONX=8548000
1600IF MONX=05 THEN MONX=10368000
1610IF MONX=06 THEN MONX=13046400
1620IF MONX=07 THEN MONX=15638400
1630IF MONX=08 THEN MONX=18316800
1640IF MONX=09 THEN MONX=20995200
1650IF MONX=10 THEN MONX=23587200
1660IF MONX=11 THEN MONX=26265600
1670IF MONX=12 THENMONX=28857600
1680REM*TOTAL ELAPSED SECONDS*
1690ATIMEX=SECX+60*MINX+3600*HRX+86400*DAYX+MONX
1700ENDPROC
```

LISTING 3

APPENDIX 2

COMPUTER PROGRAM USED TO DRAW X-Y GRAPHS - MULPLOT

This program is listed in Listing 4, and consists of a series of procedures which will scale and draw an X-Y graph from a series of data statements. This data is read into the program and used to set up the scale lengths and the plotting frame.

The procedures used are :

1. PROCSCALE : Sets up the scales, and the maximum and minimum values of the axes.

2. PROCAXES : This draws the axis and defines their common origin.

3. PROCGRADUATE : This marks off the axes into appropriate divisions, with every fifth bar being drawn larger.

4. PROCNUMBER : This numbers the divisions drawn by PROCGRADUATE with the appropriate values.

5. PROCNAMEX/Y : These label the axes.

6. PROCPOINT : This draws a cross at the points which are defined by the data statements.

6. PROCBSTLN : This calculates and draws the linear regression line for the data plotted by Procpoint.

```
   5 REM*PROGRAM GPLOT*
   10REM *READS AND PLOTS GROUPS OF DATA FROM DATA STATEMENTS*
   12 REM*NPY IS NO. OF SEPARATE STPT.LINE PLOTS; TERMINATE EACH DATA SET WITH X
Y=0,0*
   15 MODE0
   20DIM X(50),Y(50),M(10),C(10),CC(10)
   30REM*READ DATA TO FORCE SCALE LENGTHS AND SET UP PLOTTING FRAME*
   40*READ NP%,TITLE$,XLABEL$,YLABEL$,X(1),Y(1),X(2),Y(2)
   45 X(0)=0
   47PRINT "OUTPUT TO PRINTER, Y/N " ;SP%=GET
   48 CLS
   50PROCSCALE4
   55PROCSCALER
   60PROCAXES
   70PROCGRADUATE
   80PROCNUMBER
   90PROCNAMEX(XLABEL$)
   100PROCNAMEY(YLABEL$)
   110PRINT TAB(8,0);TITLE$
   150FOR I%=1 TO NP%
   160T%=0
   165*REPEAT
   170J%=J%+1
   176READ X(J%),Y(J%)
   175 UNTIL X(J%)=0 AND Y(J%)=0
   180T%(0)=J%-1
   190FOR J%=1 TO T%(0)
   200DTA=0 :PROCPOINT(X( J%),Y( J%))
   210NEXT J%
   220PROCPETLN
   230NEXT I%
   235 MOVE 0,1050
   240 KEY%=INKEY$GET
   250IF SP%=78 GOTO 280
   260VDU2
   270*SDUMP
   280MODE1 :CLS :PRINT"***BEST FIT STRAIGHT LINES"
   290PRINT"LINE","SLOPE","INTERCEPT","CORR.COEF."
   300FOR I%=1 TO NP%
   305PRINT TAB(2);I%;TAB(12);M(I%);TAB(20);C(I%);TAB(34);CC(I%)
   310NEXT I%
   315 VDU3
   320END
   9000DATA 2,KTH=1,STRESS,STRAIN,0,0,100,20
   9010DATA 1,1,3,2,4,3,0,0,2,2,4,4,5,5,0,0
   9000DEF PROCHP(X,Y,S$,AN,SC)
   9010LOCAL CO1,CO2,SI1,SI2,LX,LY,PX,PY,XX,YY
   9020CO1=COS(AN):SI1=-SIN(AN)
   9025 CO2=COS(PI/2-AN):SI2=SIN(AN+PI/2)
   9030*F=*F+1:IF*F=1 THEN DTA=8 ELSE *F=2
   9040A%=10:X%=M MOD256:Y%=M DIV256:?&70=ASC(S$):CALL(&FFF1)
   9050FOR XX=0 TO 7 :FOR YY=0TO7
   9060  IF ?(M+8-YY) AND 2^(7-XX) THEN PROCPIXEL
   9070  NEXT YY,XX
   9080ENDPROC
   9090DEF PROCPIXEL
   9100LX=XX-.5:PX=X+.5:LY=YY-.5:PY=YY+.5
   9110MOVE X+SC*(LX*CO1+LY*SI1),Y+SC*(LX*SI2+LX*CO2)
   9120MOVE X+SC*(PX*CO1+LY*SI1),Y+SC*(LY*SI2+PX*CO2)
   9130PLOT 85,Y+SC*(LX*CO1+PY*SI1),Y+SC*(PY*SI2+LX*CO2)
   9140PLOT 85,Y+SC*(PX*CO1+PY*SI1),Y+SC*(PY*SI2+PX*CO2)
   9150ENDPROC
   9180DEFPROCMESSAGE(I,Y,S$,AN,SC)
   9190LOCAL I,XP,YP
   9200AN=AN+PI/2
   9210FOR I=1 TO LEN(S$)
   9220  XP=SC*((COS(AN)*8*(I-1)))
   9230  YP=SC*(SIN(AN)*8*(I-1))
   9240  PROCCHP(Y+XP,Y+YP,MID$(S$,I,1),AN,SC)
   9250NEXT I
   9260ENDPROC
   9000DEF PROCGRAPH
   9100PROCSCALE
   9110PROCAXES
   9120PROCGRADUATE
   9130PROCNUMBER
   9500FOR I%=1TOT%(0)
   9510  DTA=8:PROCPOINT(X( I%),Y( I%))
   9520  NEXT I%
   9530ENDPROC
   9000DEF PROCSCALEA
   9010X%=X(1) :LX=-SX :SY=Y(1) :LY=-SY
   9020FOR I%=1 TO Y%(0)
   9030  IF X%>X(I%)THEN X%=X(I%)
   9040  IF LX<X(I%)THEN LX=X(I%)
   9050  IF Y%>Y(I%)THEN Y%=Y(I%)
   9060  IF LY<Y(I%)THEN LY=Y(I%)
   9070  NEXT
   9080ENDPROC
   9085*DEF PROCSCALER
   9090PROCSCALE2(-SX, LX) :SY=-5 :LY=5
   9100PROCSCALE2(-SY, LY) :SX=-5 :LX=5
   9110STX=ST :CRX%=CPNT
   9120PROCSCALE2(-SX, LX) :SY=-5 :LY=5
   9130STY=ST :CRY%=CPNT
   9140Y=1000/(LY-SY):X=800/(LX-SX)
   9150CONV%=150-SX*X :CONV=100-SY*Y
   9160ENDPROC
   9200
   9210DEF FN CVX(G) = X*G+CONVX
   9220DEF FN CVY(G) = Y*G+CONVY
   9230
   9240DEF PROCSCALE2(L,H) TAX=0:I%=0:H=A
   9250IF L<0 AND H>0 THEN L=0:I%=1 ELSE IF H<0 AND H-L/5 THEN H=0
   9260 IF L>0 THEN L=VAL(LEFT$(STR$(L),INSTR(STR$(L),"E")-1))
   9270 IF H<0 THEN H=VAL(LEFT$(STR$(H),INSTR(STR$(H),"E")-1))
   9280 PL=VAL(MID$(STR$(L),INSTR(STR$(L),"E")+1))
   9290 LH=LH*10^(VAL(MID$(STR$(H),INSTR(STR$(H),"E")+1))-PL)
   9300D=LH-LL
   9310IF D<XTHEN REPEAT D=D*10 :PL=PL-1 :LL=LL*10 :LH=LH*10 UNTIL D>X
   9320IF D>30THEN REPEAT D=D/10 :PL=PL+1 :LL=LL/10 :LH=LH/10 UNTIL D<3
   9330LL=INT(LL+.1) :LH=INT(LH+.5)
   9340X=410 :CONX=500-(LL)*(VAL(RIGHT$(STR$(LL),1)))+.1
   9350S=VAL(STR$(LL)+"E"+STR$(PL))
   9360 L=VAL(STR$(LH)+"E"+STR$(PL)) : ST=ABS(L-S)/(LH-LL)
   9370ENDPROC
   9380DEF PROCAXES
   9390IF Y0<0 :Y0=0
   9400IF SX>0 THEN X0=SX ELSE IF LX<0 THEN X0=LX
   9410IF SY>0 THEN Y0=SY ELSE IF LY<0 THEN Y0=LY
   9420MOVE FN CVX(SX),FN CVY(Y0) :DRAW FN CVX(LX),FN CVY(Y0)
   9430MOVE FN CVX(X0),FN CVY(SY) :DRAW FN CVX(X0),FN CVY(LY)
   9440ENDPROC
   9450DEF PROCGRADUATE
   9460FOR X=SX TO LX+.1*STX STEP STX
   9470  IF CRX%MOD5=0 THEN DTA=16 ELSE DTA=8
   9480  CRX%=CRX%+1 :PROCPOINT(X,Y0) :NEXT X
   9490FOR Y=SY TO LY+.1*STY STEP STY
   9500  IF CRY%MOD5=0 THEN DTA=16 ELSE DTA=8
   9510  CRY%=CRY%+1 :PROCPOINT(X0,Y) :NEXT Y
   9520ENDPROC
   9530DEF PROCNUMBER :VDU5
   9540MOVE FN CVX(LX)-4*LEN(STR$(LX)),FN CVY(Y0)-20 :PRINT;LX
   9550MOVEFN CVX(X0)-15,FN CVY(LY)+28:PRINT;LY
   9560IF LX>0AND SX<0AND LY>0AND SY<0THEN ENDPROC
   9570MOVE FN CVX(SX),FN CVY(Y0)-20:PRINT;SX
   9580MOVEFN CVX(X0)-150,FN CVY(SY)+30:PRINT;SY:VDU4
   9590ENDPROC
   9600DEF PROCPOINT(A,B)
   9610 MOVEFN CVX(A)-DTA,FN CVY(B):DRAWFN CVX(A)+DTA,FN CVY(B)
   9620MOVEFN CVX(A),FN CVY(B)-DTA :DRAWFN CVX(A),FN CVY(B)+DTA
   9630ENDPROC
   9640DEF PROCBSTLN
   9650LOCAL I,XX,YY,MEANX,MEANY,SUMX,SUMY,SUMXY,SUMYY,SUMXX,MINX,MAXX
   9660XY=0 : YY=0 :MEANX=0:MEANY=0:SUMX=0:SUMY=0:SUMXY=0:SUMYY=0:SUMXX=0:MINX=0
   MAXX=0:XY=0
   9670FOR I=1 TO X(0) :SUMX=SUMX+X(I) :SUMY=SUMY+Y(I)
   9680NEXT I
   9690MEANX=SUMX/X(0) :MEANY=SUMY/X(0)
   9700MINX=X(1):MAXX=MINX:SUMXY=0:SUMXY=0:SUMXY=0:XX=0:YY=0
   9710FOR I=1 TO X(0)
   9720SUMXY=SUMXY+X(I)*X(I) :SUMYY=SUMYY+Y(I)*Y(I)
   9730SUMXY=SUMXY+X(I)*Y(I)
   9740XX=XX+(X(I)-MEANX)^2 :YY=YY+(Y(I)-MEANY)^2 :XY=XY+(X(I)-MEANX)*(Y(I)-MEAN
   9750IF MINX>X(I) THEN MINX=X(I)
   9760IF MAXX<X(I) THEN MAXX=X(I)
   9770NEXT I
   9780M=(X*Y-X(0)*SUMXY-SUMX*SUMY)/(X(0)*SUMXX-SUMX*SUMX)
   9790C=(Y-M*SUMX-SUMY)/X(0)
   9800CC=XY/SQR(XX*YY)
   9810MAXX=MAXX+20:MINX=MINX-20
   9820PROCSCALEA
   9830MOVE FN CVX( SX),FN CVY(M*SX+C):DRAW FN CVX( LX),FN CVY(M*LX+C)
   9840A%=10
   9850VDU5: PRINT TAB(FN CVX( LX)+2,FN CVY(M*LX+ LY+C)/20+2);A%: VDU4
   9860ENDPROC
   9870DEF PROCNAMEY(VNAME$):VDU5
   9880FOR  A=1 TO LEN( VNAME$)
   9890   MOVE FN CVX( 0),-60+FN CVY( LY)+ A*32-32 :PRINTMID$( VNAME$, A,1)
   9900 NEXT :A%=0:VDU4
   9910ENDPROC
   9920DEF PROCNAMEX(HNAME$)
   9930MOVE FN CVX(LX)-32*LEN( HNAME$)-64,FN CVY(Y0)-52 :VDU5:PRINT HNAME$:VDU
   9940ENDPROC
```

LISTING 4

APPENDIX 3

COMPUTER PROGRAM USED TO DRAW HISTOGRAMS - HISTO

This program is listed in LISTING 5. The data is entered in the form of data statements, and the program calculates the plotting frame and the scale lengths in the same manner as for the program MULPLOT.

After the scale has been set, PROCHISTO draws the bars of a height equivalent to the maximum value held in the data staements. The bars are coloured alternately black and white.

LISTING 5 : The computer program HISTO.

```
 5 REM* THIS PROG. PLOTS ONE HISTOGRAM FROM DATA *
 10 DATA 8
 20 DATA 0,46,93,91,45,8,8,9
 30 DATA 45,8,8,9
 40 RESTORE :READ N
 50DIM X(N+1),Y(N+1)
 60:
 70Y(0)=N+1:Y(N+1)=0: IW=1
 80MODE0
 90FOR I=1 TO Y(0)-1
100  READ Y(I): X=X(I-1)+W: IW
110  NEXT I
120VDU19,0,4;0;
130VDU19,3,5;0;
140VDU19,2,7;0;
150VDU19,1,2;0;
160:
170PRINT TAB(10,0)"PROGRAMMER NAME = ";CHR$(34)TAB(45,0)"DATA SET = 5000"
180PROCscale
190PROChists
200GCOL0,2
210PROCaxes
220PROCgraduate
230PROCnumber
240PROCname("Mean grain diameter (x50um)")
250PROCname("Frequency")
255PROCdump
260DEF PROCdump
270VDU5:MOVE2000,2000
280 INPUT"DO YOU WANT TO SDUMP" S$
290 IF S$="Y" THEN300 ELSE310
300*SDUMP
310END
320:
330DEF PROCscale
340 SX=Y(1) : LX= SX : SY=Y(1) : LY= SY
350FOR I=1 TO Y(0)
360  IF SX>Y(I) THEN SX=Y(I)
370  IF LX<Y(I) THEN LX=Y(I)
380  IF SY>Y(I) THEN SY=Y(I)
390  IF LY<Y(I) THEN LY=Y(I)
400  NEXT
410PROCscale2(SX, LX) :SX= S : LX= S : SY= ST : LY= ST : CRY%= CRN%
420PROCscale2(SY, LY) : SX= S : LX= S : SY= ST : LY= ST : CRX%=CRN%
430X=1000/(LX- SX): Y=800/(LY- SY)
440 CRN%=(50- SX)* X : CRN%=100- SY* Y
450ENDPROC
460:
470DEF FN"CVX"(A)=(A- X)* CRN%
480DEF FN"CVY"(A)=(A- Y)* CRN%
490:
500DEF PROCscale2(L,H) :A%=A:B%=B:C%=C
510IF L<0 AND L<H/2 THEN L=0 ELSE IF H<0 AND H>L/2 THEN H=0
520T=LEN(LEFT$(STR$(L),INSTR(STR$(L),"E")-1))
530 L=VAL(LEFT$(STR$(L),T)+"E"+STR$(INSTR(STR$(L),"E")+1))
540T=LEN(LEFT$(STR$(H),INSTR(STR$(H),"E")-1))
550 H=VAL(LEFT$(STR$(H),T)+"E"+STR$(INSTR(STR$(H),"E")+1))
560 PL=VAL(MID$(STR$(L),INSTR(STR$(L),"E")+1))-(L<1)
570 LH=L+10^(VAL(MID$(STR$(H),INSTR(STR$(H),"E")+1))-PL)
580D=LH-L
590IF D<=5THEN REPEAT D=D*10 : PL=PL-1 : L=L*10 : LH=LH*10 UNTIL D>5
600IF D>50THEN REPEAT D=D/10 : PL=PL+1 : L=L/10 : LH=LH/10 UNTIL D<50
610 LL=INT(L+1) : LH=INT(LH+.5)
620X=X/10 : CRN%=SGN(LL)*(VAL(RIGHT$(STR$(LL),1))+1)
630 S=VAL(STR$(LL)+"E"+STR$(PL))
640 T=VAL(STR$(LH)+"E"+STR$(PL)) : ST=ABS(L-S)/(LH-LL)
650ENDPROC
660:
670DEF PROCbars(C)
680FOR A=1 TO Y(0)-1
690  YL=FN"CVY"(Y(A-1)) : YH=FN"CVY"(Y(A))
700  YB=FN"CVY"(0) : XL=FN"CVX"(X(A))
710  GCOL 0,C
720  MOVE XL, YB :MOVE XL, YH
730  PLOT 85, XP, YB :PLOT 85, XP, YH
740  GCOL 0,C-C
750  PLOT 85, XP+4, YB+32
760  PLOT 85, XP+4, YH+32
770  MOVE XP, YH
780  PLOT 85, XL+4, YH+32
790  PLOT 85, XL, YH
800  GCOL 0,3
810  MOVE XL, YH:DRAW XL+4, YH+32
820  DRAW XP+4, YH+32
830  DRAW XP, YH:DRAW XL, YH
840  DRAW XL, YB:DRAW XP, YB
850  DRAW XP, YH:DRAW XP+4, YH+32
860  DRAW XP+4, YB+32:DRAW XP, YB
870  NEXT A
880
890ENDPROC
900:
910DEF PROCaxes
920X=0 : Y=0
930IF SX>0 THEN X=SX ELSE IF LY<0 THEN X=LX
940IF SY>0 THEN Y=SY ELSE IF LY<0 THEN Y=LY
950MOVE FN"CVX"(SX),FN"CVY"(Y) :DRAW FN"CVX"(LX),FN"CVY"(Y)
960MOVE FN"CVY"(X),FN"CVY"(SY) :DRAW FN"CVY"(X),FN"CVY"(LY)
970ENDPROC
980:
990DEF PROCgraduate
1000FOR x=SX TO LX+.1*STX STEP STX
1010  IF "CRX%MOD5=0 THEN DTA=16 ELSE DTA=8
1020  "CRX%="CRX%+1 :PROCpoint(x,"Y0) :NEXT x
1030FOR y="SY TO "LY+.1*STY STEP "STY
1040  IF "CRY%MOD5=0 THEN DTA=16 ELSE DTA=8
1050  "CRY%="CRY%+1 :PROCpoint("X0,y) :NEXT y
1060ENDPROC
1070:
1080DEF PROCnumber :VDU5
1090MOVE FN"CVX("LX)-4*LEN(STR$("LX)),FN"CVY("Y0)-20:PRINT"LX
1100MOVE FN"CVX("X0)-150,FN"CVY("LY)+28:PRINT"LY
1110MOVE FN"CVX(SX),FN"CVY("Y0)-20:PRINT"SX
1120MOVE FN"CVX("X0)-150,FN"CVY(SY)+30:PRINT" SY:VDU4
1130ENDPROC
1140:
1150DEF PROCname$("Hname$)
1160MOVE FN"CVX("LX)-32*LEN("Hname$)-64,FN"CVY("Y0)-52:VDU5:PRINT"Hname$:VDU4
1170ENDPROC
1180:
1190DEF PROCname$("Vname$):VDU5
1200FOR "A=1 TO LEN("Vname$)
1210  :PRINTMID$("Vname$,"A,1)
1220  NEXT "A:VDU4
1230ENDPROC
1240:
1250DEF PROChists
1260FOR A=1 TO Y(0)-1
1270IF Y(A)<>Y(A+1) THEN C=C+1
1280 XL=FN"CVX(X("A)-"IW) : YB=FN"CVX(X("A))
1290 YH=FN"CVY(Y("A))
1300 YB=FN"CVY(0)
1310MOVE "XL,"YB :MOVE "XL, YH
1320PLOT 85, XP, YB :PLOT 85, XL, YH
1330PLOT 85, XP,"YB :PLOT 85, XP, YH
1340GCOL 0,3
1350MOVE "XL,"YH :DRAW "XP,"YB
1360DRAW "XP,"YH :DRAW "XL, YH :DRAW "XL,"YB
1370NEXT "A
1380ENDPROC
1390:
1400DEF PROCpoint(A,B)
1410MOVEFN"CVX(A)-DTA,FN"CVY(B):DRAWFN"CVX(A)+DTA,FN"CVY(B)
1420MOVEFN"CVX(A),FN"CVY(B)-DTA:DRAWFN"CVX(A),FN"CVY(B)+DTA
1430ENDPROC
1440 IF S$="Y" THEN 320 ELSE 330
```

LISTING 5

APPENDIX 4

THE COMPUTER PROGRAM USED TO STORE AND MANIPULATE TEXTURAL DATA - D.BASE

This program is listed in Listing 6. This program creates and stores on disc an array of data in the form of a sequential data file. The dimensions of the array have determined previously.

Any field in the file can be searched and the results are stored in memory, or can be saved on disc for future analysis or printed.

LISTING 6 : The computer program D.BASE.

```
10REM RAM BASED MULTIFILE SYSTEM
20*FX13,6
30ON ERROR GOTO 100
40 MODE7:ilen%=0:iflag=0:isafe=1000
50M$=STRING$(39," "):ibs=M$
60REPEAT
70 PRINTM$+d
80PROCmenu
90UNTIL SEL%=10
100CLS:END
110REM ERROR TRAP
120CLOSE#0
130 IF ERR<>17 REPORT:PRINT" at line ";ERL:PROCmessage("Operator error")
140GOTO60
150DEFPROCmenu
160REM RESTORE EDDIT KEYS
170*FX4,0
180VDU23;11,255;0;0;0;:REM CURSOR ON
190REPEAT:CLS
200 PROCfile
210VDU31,0,5
220PRINT"(1)  Create new file"
230PRINT"(2)  Load file"
240PRINT"(3)  Save file"
250PRINT"(4)  Display File"
260PRINT"(5)  Add records"
270PRINT"(6)  Modify record"
280PRINT"(7)  Sort by any field"
290PRINT"(8)  Create sub file (Search any field)"
300PRINT"(9)  Print file"
310PRINT"(10) Exit program"
320VDU31,0,22
330INPUT"Select option :"SEL%
340UNTIL SEL%>0 AND SEL%<11
350IF SEL%>2 AND len%=0 AND SEL%<10 PROCmessage("No file loaded"):RUN
360IF SEL%<3 AND flag=1 THEN PROCmessage("Killing file in 5 secs:ESCAPE to canc
el"):RUN
370CLS
380IF SEL%=1 PROCcreate
390IF SEL%=2 PROCload
400IF SEL%=3 PROCsave(len%)
410IF SEL%=4 PROCdisplay(len%)
420IF SEL%=5 PROCadd
430IF SEL%=6 PROCmodify
440IF SEL%=7 PROCsort(len%)
450IF SEL%=8 PROCsearchmenu(len%)
460IF SEL%=9 PROCprint(len%)
470ENDPROC
480DEF PROCcreate
490REPEAT:PRINT"File size (number of records)"
500INPUT FILESIZE%:UNTIL FILESIZE%>0:iFILESIZE%=FILESIZE%+1
510REPEAT:PRINT"Number of fields required (2-22)"
520INPUT FIELDS%:UNTIL FIELDS%>1 AND FIELDS%<23:iFIELDS%=FIELDS%-1
530flag=1
540DIM A$(FILESIZE%,FIELDS%),TYPE$(FIELDS%)
550FOR FX=0 TO FIELDS%:CLS
560PRINT"Field heading ";FX+1
570A$(0,FX)=FNinput
580REPEAT
590PRINT"Numeric field (Y/N)"
600K$=FNinput
610TYPE$(FX)=K$
620 UNTIL K$="Y" OR K$="N"
630NEXT
640PROCadd
650ENDPROC
660DEFPROCsave(LX)
670PROCgetname
680File=OPENOUT(FILE$)
690 PRINT#File,FILESIZE%,FIELDS%,LX
700FOR FX=0 TO FIELDS%
710PRINT#File,TYPE$(FX)
720NEXT
730FOR PX=0 TO LX
740FOR FX=0 TO FIELDS%
750PRINT#File,A$(PX,FX)
760NEXT:NEXT
770CLOSE#File
780ENDPROC
790DEFPROCload
800PROCgetname
810flag=1
820File=OPENIN(FILE$)
830INPUT#File,FILESIZE%,FIELDS%,len%
840DIM A$(FILESIZE%,FIELDS%),TYPE$(FIELDS%)
850FOR FX=0 TO FIELDS%
860INPUT#File,TYPE$(FX)
870NEXT
880FOR PX=0 TO len%
890FOR FX=0 TO FIELDS%
900INPUT#File,A$(PX,FX)
910NEXT:NEXT
920CLOSE#File
930ENDPROC
940DEFPROCgetname
950 REPEAT:PRINT"Enter file name (maximum of 7 characters)"
960FILE$=FNinput:UNTIL LEN(FILE$)<=7
970ENDPROC
980DEF FNinput
990REPEAT
1000INPUT LINE K$
1010UNTIL K$<>""
1020IF LEN(K$)>18 THEN K$=LEFT$(K$,18)
1030=K$
1040DEF FNwhichfield
1050REPEAT
1060FX=-1:FX=-1
1070PRINT"Enter field heading"
1080K$=FNinput
1090REPEAT:FX=FX+1
1100IF K$=LEFT$(A$(0,FX),LEN(K$)) THEN FX=FX
1110UNTIL K$=A$ OR FX=FIELDS%
1120IF FX=-1 PROCmessage("No such field field")
1130UNTIL FX>-1
1140=KX
1150DEF FNwhichrecord(FX)
1160REPEAT
1170PX=0:P%=0
1180PRINT"Give record entry under"CHR$129 A$(0,FX)
1190 K$=FNinput
1200REPEAT:P%=P%+1
1210IF K$=LEFT$(A$(P%,FX),LEN(K$)) THEN PX=P%
1220UNTIL K$=A$ OR P%=len%
1230IF P%=0 THEN PROCmessage("No such record")
1240UNTIL K$>0
1250=PX
1260DEFPROCadd
1270*FX14,6
1280REPEAT:CLS:len%=len%+1
1290PRINT"TYPE (EXIT) TO FINISH ENTRY OF RECORDS" '
1300DIM P%-1:mem=HIMEM-P%:PRINT CHR$130"Record number "ilen% TAB(19) CHR$134"By
tes free :"mem
1310FX=-1:PRINT
1320REPEAT:FX=FX+1
1330PRINT CHR$129 A$(0,FX) TAB(19) CHR$135;:A$(len%,FX)=FNinput
1340IF mem<safe A$(len%,FX)="EXIT"
1350 IF FX>0 THEN 1450
1360 INPUT"A,B"O,W
1370 O=O/O:O46457142B
1380 W=W/O:O46457142B
1390PRINT "GRAIN DIAMETER X = "TAB(21);O" UM"
1400PRINT "GRAIN DIAMETER Y = "TAB(21);W" UM"
1410PRINT"MEAN DIAMETER = "TAB(21);(O+W)/2
1420PRINT"GRAIN AREA = "TAB(21);O*W" UM2"
1440 PRINT "DIAMETRIC RATIO = "TAB(21)O/W
1450UNTIL A$(len%,FX)="EXIT" OR FX=FIELDS%
1460UNTIL A$(len%,FX)="EXIT" OR len%=FILESIZE%
1470IF len%=FILESIZE% OR mem<safe PROCmessage("REJECTED : File full")
1480len%=len%-1
1490*FX13,6
1500ENDPROC
1510DEFPROCdisplay(LX)
1520FX=1:top%=1
1530VDU23;11;0;0;0;0
1540REPEAT
1550CLS:PRINT CHR$132"Press space bar for menu"
1560 PROCline
1570PRINT CHR$129 A$(0,0) TAB(21) A$(0,FX)
1580PROCline
1590bottom%=top%+19
1600IF bottom%>LX THEN bottom%=LX
1610FOR PX=top% TO bottom%
1620PRINT CHR$130 A$(PX,0) TAB(20) CHR$131 A$(PX,FX)
1630NEXT
1640PROCgetkey
1650IF K=136 THEN FX=FX-1
1660IF K=137 THEN FX=FX+1
1670IF K=138 THEN top%=top%+20
1680IF K=139 THEN top%=top%-20
1690IF FX<1 THEN FX=FIELDS%
1700IF FX>FIELDS% THEN FX=1
1710IF top%<1 THEN top%=(INT(len%/20)*20)+1
1720IF top%>LX THEN top%=1
1730UNTIL K=32
1740ENDPROC
1750DEFPROCmodify
1760FX=FNwhichfield
1770PX=FNwhichrecord(FX)
1780REPEAT:CLS
1790PRINT CHR$134"Modify whole line with EDIT/COPY keys"
1800PRINT CHR$129"Type KILL to delete record"
1810PRINT CHR$130"Type EXIT for option page":PRINT
1820FOR FX=0 TO FIELDS%
1830PRINT A$(0,FX) TAB(21) A$(PX,FX)
1840NEXT
1850PRINT:PROCline:PRINT:PROCline
1860INPUT LINE TAB(0,VPOS-2) K$
1870IF LEN(K$)>39 THEN K$=LEFT$(K$,39)
1880FOR FX=0 TO FIELDS%
1890IF A$(0,FX)=LEFT$(K$,LEN(A$(0,FX))) THEN A$(PX,FX)=RIGHT$(K$,LEN(K$)-21)
1900NEXT FX
1910UNTIL K$="EXIT" OR K$="KILL"
1920IF K$="KILL" THEN REPEAT:FOR FX=0 TO FIELDS%:A$(PX,FX)=A$(PX+1,FX):NEXT:PX=
PX+1:UNTIL PX>len%:len%=len%-1
1930ENDPROC
1940DEFPROCsort(LX)
1950SFX=FNwhichfield
1960PRINT"Sorting by"CHR$129 A$(0,SFX)
1970IF TYPE$(SFX)="Y" THEN COMP$="VAL(A$(PX,SFX))<VAL(A$(PX-NX,SFX))" ELSE COM
P$="A$(PX,SFX)<A$(PX-NX,SFX)"
1980NX=1:REPEAT:NX=NX*2:UNTIL NX>LX
1990FOR DX=NX+1 TO NX+2
2000FOR EX=DX TO LX STEP NX
2010FOR PX=EX TO DX STEP -NX
2020IF EVAL COMP$="TRUE THEN FOR FX=0 TO FIELDS%:K$=A$(PX,SFX):A$(PX,SFX)=A$(PX
NX,SFX):A$(PX-NX,SFX)=K$:NEXT ELSE 2040
2030NEXT
2040NEXT FX:NEXT:UNTIL NX=1:ENDPROC
2050DEFPROCsearch(OP$,LX)
2060sublen%=0
2070SFX=FNwhichfield
2080PRINT"Search to operate on";CHR$129 A$(0,SFX)
2090IF SEL%=5 PRINT"Search for which character group"!A$=FNinput:L$="INSTR(A$(
%,SFX),A$)>0":IN$=L$
2100IF SEL%<5 PRINT"Operator "OP$:PRINT"Compare with"!A$=FNinput:IN$="VAL(A$(PX
SFX))"+OP$+"VAL(A$)":L$="A$(PX,SFX)"+OP$+"A$"
2110IF TYPE$(SFX)="Y" THEN COMP$=N$ ELSE COMP$=L$
2120FOR PX=1 TO LX
2130IF SEL%=5 AND LEN(A$)>LEN(A$(PX,SFX)) THEN 2150:REM BASIC I INSTR BUG
2140 IF EVAL(COMP$) sublen%=sublen%+1:FOR FX=0 TO FIELDS%:K$=A$(PX,FX):!A$(PX,F
)=A$(sublen%,FX):!A$(sublen%,FX)=K$:NEXT
2150NEXT
2160 IF sublen%=0 PROCmessage("Search is negative"):sublen%=LX
2170ENDPROC
2180DEFPROCgetkey
2190REPEAT
2200REM RELEASE EDIT KEYS
2210*FX4,1
2220REM CLEAR KEYBOARD BUFFER
2230*FX21,0
2240K=GET
2250 REM RESTORE EDIT KEYS
2260*FX4,0
2270UNTIL K=32 OR K=&88
2280ENDPROC
2290DEFPROCmessage(M$)
2300VDU23;11,0;0;0;0:REM CURSOR OFF
2310SOUND1,-15,255,5
2320PRINT CHR$129 M$
2330FINISH=TIME+500
2340REPEAT
2350UNTIL TIME>=FINISH
2360VDU23;11,255;0;0;0:REM CURSOR ON
2370ENDPROC
2380DEFPROCfile
2390CLS:PRINT
2400FOR N=1 TO 2
2410PRINT CHR$141;CHR$129;SPC(7)"RAM MULTIFILE SYSTEM"
2420NEXT
2430ENDPROC
2440DEFPROCline
2450PRINT STRING$(39," ")
2460ENDPROC
2470DEFPROCsearchmenu(sublen%)
2480VDU23;11,255;0;0;0:REM CURSOR ON
2490REPEAT
2500PROCfile:PRINT
2510PRINT"Shrink file (Non destructive)"
2520PRINT"Search any field for! "
2530VDU31,0,7
2540PRINT"(1) <> a"
2550PRINT"(2)  = a"
2560PRINT"(3) >= a"
2570PRINT"(4) <  a"
2580PRINT"(5) Substring"
2590PRINT:PRINT"Further options! ":PRINT
2600PRINT"(6) Save subfile"
2610PRINT"(7) View subfile"
2620PRINT"(8) Sort subfile by any field"
2630PRINT"(9) Print subfile"
2640PRINT"(10) Delete subfile from master file"
2650PRINT"(11) Return to main menu"
```

LISTING 6

APPENDIX 5

COMPUTER PROGRAM USED TO DRAW FIGURE 6.11

This program is listed in Listing 7, and was written by Dr. E.H. Rutter. It produces graphical output in the form of a series of crosses, which corresponds to the stress field configuration around a Type II crack tip.

Listing 7 :

```
>L.
   10CLS:CLG
    5PROCSCALE
    6PROCAXES
    7PROCNUMBER
   10FOR K=1 TO 36
   20FOR R = 1 TO 10
   30A=RAD(.01+(K-1)*10)
   40SX=2*(COS(A/2)*(1-(SIN(A/2)*SIN(3*A/2))))/(SIN(A/2)*COS(A/2)*COS(3*A/2.
   50OT=DEG(ATN(SX))/2
   55 B=(ATN(SX))/2+A
   60PROCgraf
   70NEXT R
   80NEXT K
   83 INPUT"HARDCOPY, Y/N";A$
   84 IF A$="Y" THEN GOTO 85 ELSE GOTO 90
   85 *SDUMP
   90END
  100 *GDUMP 0 0 1 1
  110DEFPROCgraf
  130X=R*COS(A)
  140Y=R*SIN(A)
  150PROCPOINT(X,Y)
  160ENDPROC
 2000DEF PROCCHR(X,Y,S$,AN,SC)
 2010LOCAL C01,C02,SI1,SI2,LX,LY,RX,XX,YY
 2020C01=COS(AN):SI1=-SIN(AN)
 2030C02=COS(PI/2-AN):SI2=SIN(AN+PI/2)
 2040`F=`F+1:IF`F=1 THEN DIM M 8 ELSE `F=2
 2050A%=10:X%=M MOD256:Y%=M DIV256:?M=ASC(S$):CALL(&FFF1)
 2060FOR XX=0 TO 7 :FOR YY=0TO7
 2070IF ?(M+8-YY) AND 2^(7-XX) THEN PROCPIXEL
 2080NEXT YY,XX
 2090ENDPROC
 2100DEF PROCPIXEL
 2110LX=XX-.5:RX=XX+.5:LY=YY-.5:RY=YY+.5
 2120MOVE X+SC*(LX*C01+LY*SI1),Y+SC*(LY*SI2+LX*C02)
 2130MOVE X+SC*(RX*C01+LY*SI1),Y+SC*(LY*SI2+RX*C02)
 2140PLOT 85,X+SC*(LX*C01+RY*SI1),Y+SC*(RY*SI2+LX*C02)
 2150PLOT 85,X+SC*(RX*C01+RY*SI1),Y+SC*(RY*SI2+RX*C02)
 2160ENDPROC
 2170DEFPROCMESSAGE(X,Y,S$,AN,SC)
```

APPENDIX 6

PREPARATION OF ULTRA THIN SECTIONS

The following acid-etch technique was used to prepare ultra fine thin sections from both the experimentally deformed specimens and the specimens presented in this thesis. After Spiers (1981).

1. The specimen was sawed in half along its long axis, or parallel to the movement direction for the field specimens.

2. The resultant surface was ground flat using 200, 380, 600 then 800 grade silicone carbide grinding paste and/or paper.

3. After cleaning the surface with alcohol it was given a polish with 5μm and then 2μm alumina powder.

4. The specimen was then cemented using epoxy resin onto the ground surface of a glass slide and left to dry.

5. After the resin had set, the excess specimen was sawn off to leave a thick specimen slab attached to the glass slide.

6. The thick section was ground down firstly using the automatic grinder situated in the Rock Cutting Department at Imperial College, and then by 200, 400 and 800 grade silicone carbide grinding paste in sequence until the section is approximately 20-30μm thick.

7. The thin section was then washed with de-ionised water and carefully dryed.

8. Using a small paint brush brush a drop of 2% dilute HCL over the specimen and observe until efferevescence stops.

9. Repeat steps 7 and 8 until a hole appears in the centre of the slide, or first order polarization colours are observed.

10. If necessary the acid is applied to relatively thick regions of the thin section in order to give as even a finish as possible.

11. The ultra thin section is now washed in de-ionised water and carefully

dryed, prior to staining for calcite and optical observation.

This method has the advantage over standard mechanical grinding and polishing techniques in that :

1. It is fast.
2. It allows observation of the thin section at all times.
3. It permits application of the acid, and hence preferential thinning of certain areas of the thin section if necessary.
4. The effect of the etch permits ease of observation of the textural features by preferential etching of twins and grain boundaries.
5. Destruction of the section is unlikely.

REFERENCES

Adams, F.D., and Nicholson, J.T. 1901. An experimental investigation into the flow of marble. Phil. Trans. Roy. Soc. Lond., A195, 363-401.

Anderson, T.F. 1969. Self diffusion of carbon and oxygen in calcite by isotope exchange with carbon dioxide. J. Geophys. Res., 74, 3918-3931.

Arboleya, M.L. 1978. Estudio estructural del Manto del Esla (Cordillera Cantabrica, Leon). Unpubl. Ph.D. Thesis, Univ. Autonoma de Barcelona, 227p.

Ashby, M.F., and Verrall, R.A. 1973. Diffusion accomodated flow and superplasticity. Acta Metall. 21, 149-163.

Ashby, M.F., and Verrall, R.A. 1978. Micromechanisms of flow and fracture and their relevance to the rheology of the upper mantle. Phil. Trans. R. Lond., A288, 59-95.

Ball, A., and Hutchinson, M.M. 1969. Superplasticity in the Aluminium-Zinc Eutectoid. Metal Science Journal, 3, 1-7.

Barber, D.J., and Wenk, H.R. 1973. The microstructure of experimentally deformed limestone. J. Mat. Sci., 8, 500-508.

Barber, D.J., and Wenk, H.R. 1979. On the geological significance of the microstructure of calcite. Tectonophysics,

Bastida, F., Marcos, A., Perez-Estaun, A., and Pulgar, J.A. 1987. Aproximacion a la mecanica de los cabalgamientos en el contexto general de la deformacion del N.W. de la Peninsula Iberica. Acta Geol. Hisp. Homenatge a Lluis Sole i Sabaris, 14, 135-142.

Bathurst, R.G.C. 1975. Pressure-solution. In : Developments in Sedimentology : Carbonate sediments and their diagenesis, 12, 2nd Edition. Elsevier, New York.

Bengus, V.Z. 1963. Dislocation interaction in calcite twinning. Sov. Phys. Cryst., 8, 322-326.

Bishop, J.F.W. 1953. A theoretical examination of the plastic deformation of crystals by glide. Phil. Mag., 44, 51-64.

Bishop, J.F.W. 1954. A theory of the tensile and compressive textures of face-centred cubic metals. J. Mech. Phys. Solid., 3, 130-142.

Bishop, J.F.W., and Hill, R. 1951a. A theory of the plastic distortion of a polycrystalline aggregate under combined stresses. Phil. Mag., 42, 414-427.

Bishop, J.F.W., and Hill, R. 1951b. A theoretical derivation of the plastic properties of a polycrystalline face-centred metal. Phi. Mag., 42., 1298-1307.

Boettcher, A.L., and Wyllie, P.J. 1967. Revision of the calcite-aragonite transition with the location of a triple point between calcite I, calcite II and aragonite. Nature, 213, 792-793.

Boettcher, A.L., and Wyllie, P.J. 1968. The calcite-aragonite transition measured in the system $CaO-CO_2-H_2O$. J. Geol., 76, 314-330.

de Boer, R.B. 1977. On the thermodynamics of pressure solution, interaction between chemical and mechanical forces. Geochemica et Cosmochemica Acta, 41, 249-256.

de Boer, R.B., Nagtegaal, P.J.C., and Duyvis, E.M. 1977. Pressure solution experiments on quartz sand. Geochemica et Cosmochemica Acta, 41, 257-264.

Borg, I., and Handin, J. 1967. Torsion of calcite single crystals. J. Geophys. Res., 72, 641-669.

Borg, I., and Turner, F.J. 1953. Deformation of Yule Marble. Part VI. Geol. Soc. Am. Bull., 64, 1343-1352.

Bowman, M.B.J. 1982. The stratigraphy of the San Emiliano formation and its relationship to other Namurian/Westphalian A sequences in the Cantabrian Mtns., N.W. Spain. Trab. Geol., Univ. Oviedo, 12, 23-35.

Boyer, S.E,, and Elliot, D. 1982. Thrust systems. Ass. Am. Pet. Geol. Bull., 66, 1196-1230.

Braillon, P., Mugnier, J., and Serughetti, J. 1972. Deformation plastique des cristaux de calcite en compression suivant [111]. C. R. Acad. Sci., Paris, 275B, 605-608.

Braillon, P., Mugnier, J., and Serughetti, J. 1974. Transmission electron microscopy observations of dislocations in calcite single crystals. Crystal Lattice Defects, 5, 73-78.

Briegal, U., and Goetzte, Y. 1975. Estimates of differential stress recorded in the dislocation structure of Lochseiten limestone (Switzerland). Tectonophysics, 48, 61-76.

Calnan, E.A., and Clews, C.J.B. 1950. Deformation textures in face-centred cubic metals. Phil. Mag., 41, 1085-1100.

Calnan, E.A., and Clews, C.J.B. 1951a. The development of deformation textures in metals. Part II: Body-centred cubic metals. Phil. Mag., 42, 616-635.

Calnan, E.A., and Clews, C.J.B. 1951b. The development of deformation textures in metals. Part III: Hexagonal structures. Phil. Mag., 42, 919-931.

Carslaw, H.S., and Jaegar, J.C. 1959. Conduction of heat in solids. Oxford : Clarendon Press.

Carter, N.L., and Raleigh, C.B. 1969. Principle stress directions from plastic flow in crystals. Geol. Soc. Am. Bull., 80, 1231-1264.

Casey, M., Rutter, E.H., Schmid, S.M., Siddans, A.W.B., and Whalley, J.S. 1978. Texture development in experimentally deformed calcite rocks. Proc. ICOTOM 5 (Aachen), 2, 231-240.

Christie, J.M., Ord, A., and Koch, P.S. 1980. Relationship between recrystallized grain size and flow stress in experimentally deformed quartzite (Abstr.). EOS, 61, 377.

Coble, R.L. 1963. A model for boundary diffusion controlled creep in polycrystalline materials. J. Appl. Phys., 34, 1679-1682.

Cuddy, L.J. 1970. Internal stresses and structures developed during creep. Met. Trans., 1, 395-401.

Dahlstrom, C.D.A. 1970. Balanced cross sections. Can. J. Earth Sci., 6, 743-757.

Dandekar, D.P. 1968. Variation in the elastic constaints of calcite with temperature. J. Appl. Phys., 39, 3694-3699.

De Sitter, L.U. 1959. The Rio Esla nappe in the zone of Leon of the Asturian Cantabric Mountain Chain. Not. Com. Inst. Geol. Min. Espana, 56, 3-24.

De Sitter, L.U. 1962. The structure of the southern slope of the Cantabrian Mountains. Leidse Geol. Meded., 26, 255-264.

Deer, W.A., Howie, R.A., and Zussman, J. 1963. Rock forming minerals. Longmans, London, 4 vols.

Dietrich, D., and Song, H. 1984. Calcite fabrics in a natural shear environment, the Helvetic nappes of western Switzerland. J. Struct. Geol., 6, 19-32.

Dorn, J.E. 1957. The spectrum of activation energies for creep. Creep and Recovery (Seminar) Am. Soc. for Metals, p 255.

Durney, D.W. 1972. Solution transfer, an important deformation mechanism. Nature, 235, 315-317.

Durney, D.W. 1976. Pressure-solution and crystallization deformation. Phil. Trans. R. Soc. Lond., A283, 229-240.

Edington, J.W., Melton, K.N., and Cutler, C.P. 1976. Superplasticity. Progr. Mater. Sci., 1, 61-158.

Edwards, G.H., Etheridge, M.A., and Hobbs, B.E. 1982. On the stress dependence of subgrain size. Text. and Microst., 5, 127-132.

Etheridge, M.A., and Wilkie, J.C. 1979. Grainsize reduction, grain boundary sliding and the flow strength of mylonites. Tectonophysics, 58, 159-178.

Fernandez, C.J. 1974. Las mineralizaciones de baritina de la Babia Baja (Leon). Unpubl. Tesis de Licenciatura Univ. de Oviedo.

Fernandez, C.J., and Soland Huguet, J. 1975. Estudio de las mineralizaciones de baritina de la Babia Baja (Leon). Brev. Geol. Asturica, XIX (4), 54-59.

Ferreira, M.P., and Turner, F.J. 1964. Microscopic structure and fabric of Yule Marble experimentally deformed at different strain rates. J. Geol., 72, 861-875.

Forristall, G.Z. 1972. Stress distributions and overthrust faulting: A critical

review. Geol. Soc. Am. Bull., 83, 3073-3081.

Friedman, M. 1964. Petrofabric techniques for the determination of principal stress directions in rocks. In: W.R. Judd (ed.), State of Stress in Earth's Crust, Elsevier, New York, 451-552.

Friedman, M., and Stearns, D.W. 1970. Relations between stresses derived from calcite twin lamellae and microfractures, Teton Anticline, Montana. Geol. Soc. Am. Abstr. Progs., 2, 555-556.

Friedman, M., and Higgs, N.C. 1981. Calcite fabrics in experimental shear zones. Geophysical Monograph, 24, 11-27.

Garcia Fuente, S. 1959. Mapa Geologico de Espana, Hoja no. 7, La Plaza (Teverga), Asturias. Inst. Geol. Min. Espana, 305H, 68p.

Goetze, C., and Kohlstedt, D.L. 1977. The dislocation structure of experimentally deformed marble. Contr. Min. Pet., 59, 293-306.

Goldsmith, J.R., and Newton, R.C. 1969. P-t-x relations in the system $CaCO_3$-$MgCO_3$ at high temperatures and pressures. Am. J. Sci., 267A, 160-190.

Gomez de Llarena, J. 1946. Nuevos yacimientos Cambricos en la Babia Baja (Leon) y Teverga (Asturias). Bol. Real Soc. Esp. Hist. Nat., 44, 101-111.

Gomez de Llarena, J., and Rodriguez Arango, C. 1948. Datos para el estudio geologico de la Babia Baja (Leon). Bol. Inst. Geol. Min. Espana., 61, 79-206.

Graf. D.L., and Lamar, J.E. 1955. Properties of calcium and magnesium carbonates and their bearing on some uses of carbonate rocks. Econ. Geol. 50th Anniv. vol., p 639.

Griggs, D.T. 1936. Deformation of rocks under high confining pressures. J. Geol., 44, 541-577.

Griggs, D.T. 1938. Deformation of single calcite crystals under high confining pressures. Am. Mineral., 23, 28-33.

Griggs, D.T. 1940. Experimental flow of rocks under conditions favoring recrystallization. Geol. Soc. Am. Bull., 51, 1001-1034.

Griggs, D.T., and Miller, W.B. 1951. Deformation of Yule Marble at 10,000 atmospheres confining pressure, room temperature. Geol. Soc. Am. Bull., 62, 853-862.

Griggs, D.T., Turner, F.J., and Borg, I 1953. Deformation of Yule Marble. Part IV: Effects at 300°C. Geol. Soc. Am. Bull., 64, 1327-1342.

Griggs, D.T., Turner, F.J., and Heard, H.C. 1960. Deformation of rocks at 500°C to 800°C. In: Griggs and Handin (ed.), Rock Deformation, Geol. Soc. Am. Mem., 79, 39-104.

Griggs, D.T., Paterson, M.S., Heard, H.C., and Turner, F.J. 1960. Annealing recrystallization in calcitic crystals and aggregates. Geol. Soc. Am. memoir, 79, 21-37.

Groshong, R.H. 1972. Strain calculated from twinning in calcite. Geol. Soc. Am. Bull., 83, 2025-2038.

Groshong, R.H. 1974. Experimental test of least-squares strain gage calculations using twinned calcite. Geol. Soc. Am. Bull., 85, 1855-1864.

Groves, G.W., and Kelly, A. 1963. Independent slip systems in crystals. Phil. Mag., 8, 877-887.

Groves, G.W., and Kelly, A. 1969. Change of shape due to dislocation climb. Phil. Mag., 19, 977-986.

Guillope, M., and Poirier, J.P. 1979. Dynamic recrystallization during creep of single-crystalline halite: an experimental study. J. Geophys. Res., 84, 5557-5567.

Hadizadeh, J. and Rutter, E.H., 1984. The low temperature Brittle-ductile Transition in a quartzite and the occurrence of cataclastic flow in nature. Geologische Rundschau, 72/2, (5).

Handin, J., Friedman, M., Logan, J.M., Pattison, L.J., and Swolfs, H.S. 1972. Experimental folding of rocks under confining pressure: Buckling of single layer rock beams. In: Flow and Fracture of Rocks, Am. Geophys. Union, 16, 1-28.

Handin, J.W., and Griggs, D.T. 1951. Deformation of Yule Marble. Part II:

Predicted fabric changes. Geol. Soc. Am. Bull., 62, 863-886.

Heard, H.C. 1963. Effects of large changes in strain rate in the experimental deformation of Yule Marble. J. Geol., 71, 162-195.

Heard, H.C., and Raleigh, C.B. 1972. Steady state flow in marble at 500°C to 800°C. Geol. Soc. Am. Bull., 83, 935-956.

Heinisch, H.L., Jr., Sines, G., Goodman, J.W., and Kirby, S.H. 1975. Elastic stresses and self-energies of dislocations of arbitrary orientation in anisotropic media: olivine, orthopyroxene, calcite and quartz. J. Geophys. Res., 80, 1885-1897.

Hirth, J.P., and Lothe, J. 1967. Theory of Dislocations. McGraw Hill, New York.

Hobbs, B.E. 1968. Recrystallization of quartz. Tectonophysics, 6, 353-401.

Hossack, J.R. 1979. The use of balanced cross sections in the calculation of orogenic contracrtion: A review. Jour. Geol. Soc., 136, 705-711.

Hsu, K.J. 1969. Role of cohesive strength in the mechanics of overthrust faulting and of landsliding. Geol. Soc. Am. Bull., 80, 927-952.

Hubbert, M.K., and Rubey, W.W. 1959. Role of fluid pressure in mechanics of overthrust faulting: 1. Mechanics of fluid-filled porous solids and its application to overthrust faulting. Geol. Soc. Am. Bull., 70, 115-166.

Hyett, A. 1987. Unpubl. M. Phil./Ph. D. Transfer Report, Univ. of Lond.

Irving, A.I., and Wyllie, P.J. 1973. Melting relationships in CaO-CO_2 and MgO-CO_2 to 36 kilobars with comments on CO_2 in the mantle. Earth Planet. Sci. Lett., 20, 220-225.

Jamieson, J.C. 1957. Introductory studies of high pressure polymorphism to 24,000 bars by x-ray diffraction with some comments on calcite II. J. Geol., 65, 334-343.

Jamieson, W.R., and Spang, J.H. 1976. Use of calcite twin lamellae to infer differential stress. Geol. Soc. Am. Bull., 87, 868-872.

Johannes, W., and Puhan, D. 1971. The calcite-aragonite transition,

reinvestigated. Contr. Min. Pet., 31, 29-38.

Julivert, M. 1971. Decollement tectonics in the Hercynian Cordillera of Northwest Spain. Am. Jour. Sci., 270, 1-29.

Julivert, M. 1978. Hercynian orogeny and Carboniferous paleogeography in northwestern Spain: a model of deformation-sedimentation relationships. Z. dt. Geol. Ges., 129 (2), 565-592.

Julivert, M., and Arboleya, M.L. 1984. A geometrical and kinematical approach to the nappe structure in an arcuate fold belt : the Cantabrian Nappes (Hercynian chain, N.W. Spain). J. Struct. Geol., 6, 499-519.

Julivert, M., and Marcos, A. 1973. Superimposed folding under flexural conditions in the Cantabrian zone (Hercynian Cordillera, Northwest Spain). Am. Jour. Sci., 273, 353-375.

Julivert, M., and Pello, J. 1967. Las dos etapas principales de deformacion herciniana en la Cordillera Cantabrica y el trazado de sus estructuras. Acta Geol. Hispanica, 4, 77-81.

Julivert, M., Pello, J., and Fernandez-Garcia, L. 1968. La estructura del Manto de Somiedo (Cordillera Cantabrica). Trab. Geol., 2, 1-44.

Kallend, J.S., and Davies, G.J. 1972. A simulation of texture development in FCC metals. Phil. Mag., 25 (2), 471-490.

Kamb, W.B. 1961. The thermodynamical theory of non-hydrostatically stressed solids. J. Geophys. Res., 66, 259-271.

Kehle, R.D. 1970. Analysis of gravity sliding and orogenic translation. Geol. Soc. Am. Bull., 81, 1641-1663.

Keith, R.E., and Gilman, J.J. 1960. Dislocation etch-pits and plastic deformation in calcite. Acta. Met., 1, 1-10.

Kern, H. 1971. Dreiaxiale Verformungen an Solnhofener Kalkstein in Temperaturbereich von 20°-650°C. Rontgenographische Gefugeuntersuchungen mit dem Texturgoniometer. Contr. Min. Pet., 31, 39-66.

Kern, H. 1977. Preferred orientation of experimentally deformed limestone,

marble, quartzite and rock salt at different temperatures and states of stress. Tectonophysics, 39, 103-120.

Kern, H., and Wenk, H.R. 1983. Calcite texture development in experimentally induced ductile shear zones. Contr. Min. Pet., 83, 231-236.

Kirby, S.H., and Raleigh, C.B. 1973. Mechanisms of high temperature, solid state flow in minerals and ceramics and their bearing on the creep behaviour of the mantle. Tectonophysics, 19, 165-194.

Klassen-Neklyudova, M.V. 1964. Mechanical twinning of crystals. New York: Consultants Bureau (Trans. J.E.S. Bradley).

Knopf, E.B. 1949. Fabric changes in Yule Marble after deformation in compression. Am. J. Sci., 247, 433-461, 537-569.

Kocks, U.F. 1970. The relation between polycrystal deformation and single-crystal deformation. Met. Trans., 1, 1121-1143.

Kohlstedt, D.L. 1980. Palaeostress levels in deeply eroded fault zones based on analysis of deformation-induced microstructures. In : Magnitude of deviatoric stresses in the Earth's crust and upper mantle. Open File Report, 80-265, 648-664, U.S. Geol. Surv., Menlo Park, California.

Kohlstedt, D.L., Goetze, C., and Durham, W.B. 1976. Experimental deformation of single crystal olivine with application to flow in the mantle. In : R.G.S. Strens (Ed.), Petrofabrics : The Physics and Chemistry of Minerals and Rocks. Wiley, New York, 35-49.

Kohlstedt, D.L., Cooper, R.F., Weathers, M.S., and Bird, J.M. 1979. Palaeostress analysis of defomation-induced microstructures : Moine Thrust zone and Ikertoq Shear zone. In : Analysis of actual fault zones in bedrock. Open File Report, 79-1239, 394-425, U.S. Geol. Surv., Menlo Park, California.

Kondo, S., Suito, K., and Matsushima, S. 1972. Ultrasonic observation of calcite I-II inversion to 700°C. J. Phys. Earth., 20, 245-250.

Lister, G.S. 1978. Texture transitions in plastically deformed calcite rocks. Proc. ICOTOM 5 (Aachen), 2, 199-210.

Lister, G.S., Paterson, M.S., and Hobbs, B.E. 1978. The simulation of fabric

development in plastic deformation and its application to quartzite: the model. Tectonophysics, 45, 107-158.

LLoyd, G.E. 1985. Review of the instruementation, techniques and applications of SEM in minerallogy. In : Applications of electron microscopy in the Earth Sciences (Ed. White, J.C.) MAC short course series II.

Mahajan, S., and Williams, D.F. 1973. Deformation twinning in metals and alloys. Int. Met. Reviews, 18, 43-60.

Maddock, R.H. 1986. Unpubl. Ph.D. Thesis, Univ. of Lond.

Mandelbrot, B.B. 1982. The Fractal Geometery of Nature. W.H. Freeman, San Fransico, Calif.

Marcos, A. 1968. La tectonica de la Unidad de la Sobia-Bodon. Trab. Geol. Univ. de Oviedo, 2, 59-87.

Marcos, A., and Pulgar, J.A. 1982. An approach to the tectonostratigraphic evolution of the Cantabrian Foreland thrust and fold belt, Hercynian Cordillera of N.W. Spain. N.Jb. Geol. Palaont. Abh., 163 (2), 256-260.

Mawer, C.K. 1985. Comment and reply on "Fault-related rocks ; suggestions for Terminology". Geology 13, 378-379.

Mercier, J.C.C., Anderson, D.A., and Carter, N.L. 1977. Stress in the lithosphere : inferences from steady state flow of rocks. Pure Appl. Geophys., 115, (1/2), 199-226.

Mirwald, P.W. 1976. A different thermal analysis study of the high-temperature polymorphism of calcite at high pressure. Contr. Min. Pet., 59, 33-40.

Motohashi, Y., Braillon, P., and Serughetti, J. 1976. Elastic energy, stress field of dislocations , and dislocation parameters in calcite crystals. Phys. Stat. Sol., 37, 263-281.

Nadai, A. 1963. Theory of Flow and Fracture of Solids. McGraw-Hill, New York.

Nicholas, A., and Poirier, J.P. 1976. Crystalline plasticity and solid state flow in metamorphic rocks. Wiley, New York, 444p.

Norton, M.G., and White, S.H. (in press). Microstructural equilibrium diagrams : application to the study of microstructural stabilities and palaeostress estimates in tectonites.

Nye, J.F. 1957. Physical properties of crystals. Oxford Univ. Press, 322p.

Olsson, W.A. 1974. Grain size dependence of yield stress in marble. J. Geophys. Res., 79, 4859-4862.

Owens, W., and Rutter, E.H. 1978. The development of magnetic susceptibility anisotropy through cyrstallographic preferred orientation in a calcite rock. Phys. Earth and Plan. Ints., 16, 215-222.

Paterson, M.S. 1969. The ductility of rocks. In: A.S. Argon (ed.), Physics of strength and plasticity. The Orowan 65th Anniversary Volume. M.I.T. Press, 377-392.

Paterson, M.S. 1973. Non-hydrostatic thermodynamics and its geologic applications. Rev. Geophys. Space Phys., 11, 355-389.

Paterson, M.S. 1976. Some current aspects of experimental rock deformation. Phil. Trans. R. Soc. of Lond. A, 283, 163-172.

Paterson, M.S. 1979. Deformation mechanisms in carbonate crystals. In: Borland, D.W., Clarebrough, L.M., and Moore, A.J.W. (eds.), Physics of Materials. CSIRO and Dept. Metallurgy, Univ. of Melbourne, 109-208.

Paterson, M.S., and Turner, F.J. 1970. Experimental deformation of constrained calcite in extension. In: P. Paulitsch (ed.), Experimental and Natural Rock Deformation. Springer, Heidelberg, 109-141.

Peach, C.J., Rutter, E.H., and Holloway, R.F. 1981. A new computer controlled facility for long duration rock testing at high pressures and temperatures. In : Progress in Experimental Petrology. Fifth progress report of research, N.E.R.C. Publication Series D No. 18.

Perez-Estaun, A. 1971. La ventana tectonica de Villabandin (Antiforme del Narcea, Leon). Brev. Geol. Asturica, XV (1), 7-13.

Piorier, J.P., and Nicolas, A. 1975. Deformation induced recrystallization due to progressive misorientation of subgrains, with special reference to mantle

peridotites. J. Geol., 83, 707-720.

Pontikis, V., and Poirier, J.P. 1975. Phenomenological and structural analysis of recovery controlled creep, with special reference to the creep of single crystal silver chloride. Phil. Mag., 32, 577-592.

Post, R.L. 1973. High temperature creep of Mt. Dunite dunite. Tectonophysics, 42, 75-110.

Raleigh, C.B. 1965. Glide mechanisms in experimentally deformed minerals. Science, 150, 739-741.

Raleigh, C.B., and Griggs, D.T. 1963. Effect of thetoe in the mechanics of overthrust faulting. Geol. Soc. Am. Bull., 74, 819-830.

Ramez, M.R.H., and Murrell, S.A.F. 1964. A petrofabric analysis of Carrara Marble. Int. J. Rock Mech. Mining, 1, 217-229.

Ramsey, J.G. 1967. Folding and fracturing of rocks. McGraw Hill, New York, 568p.

Reade, T.H. 1908. The mechanics of overthrust. Geol. Mag., 5, 518p.

Reches, Z. 1978. Analysis of faulting in a three dimensional strain field. Tectonophysics, 47, 109-129.

Reches, Z. 1983. Faulting of rocks in three dimensional strain fields II, Theoretical Analysis. Tectonophysics, 95, 133-156.

Ross, J.V., AveLallemant, H.G., and Carter, N.L. 1980. Stress dependence of recrystallized-grain and subgrain size in olivine. Tectonophysics, 70, 39-61.

Rutter, E.H. 1970. An experimental study of the factors affecting the rheological properties of rocks in simulated geological environments. Unpubl. Ph.D. Thesis, Univ. of London.

Rutter, E.H. 1972. The influence of interstitial water on the rheological behaviour of calcitic rocks. Tectonophysics, 14, 13-33.

Rutter, E.H. 1974. The influence of temperature, strain rate and interstitial water in the experimental deformation of calcitic rocks. Tectonophysics,

22, 311-334.

Rutter, E.H. 1976. The kinetics of rock deformation by pressure solution. Phil. Trans. R. Soc. Lond., A283, 203-219.

Rutter, E.H., and Rusbridge, M. 1977. The effect of non-coaxial strain paths on crystallographic preferred orientation development in the experimental deformation of a marble. Tectonophysics, 39, 73-86.

Rutter, E.H., and Schmid, S.M. 1975. Experimental study of unconfined flow of Solnhofen limestone at 500°-600°C. Geol. Soc. Am. Bull., 86, 145-152.

Sauvage, M., and Authier, A. 1965a. Etude des bandes de croissance et des dislocations de macle dans la calcite. Bull. Soc. Franc. Min. Crist., 88, 379-388.

Sauvage, M., and Authier, A. 1965. Observations topographiques de dislocations de macle dans la calcite. Phys. Stat. Sol., 13, 72-75.

Schmid, E. 1924. Proc. Int. Congress Appl. Mechanics (Delft), 342.

Schmid, E., and Boas, W. 1950. Plasticity of crystals. Translation from German of Kristallplastizitat. Hughes, London.

Schmid, S.M. 1975. The Glarus Overthrust : Field evidence and mechanical model. Eclogae Geol. Helv. 68, 247-280.

Schmid, S.M. 1976. Rheological evidence for changes in the deformation mechanism of Solnhofen limestone towards low stresses. Tectonophsics, 31, 21-28.

Schmid, S.M. 1982a. Laboratory experiments on rheology and deformation mechanisms in calcite rocks and their application to studies in the field. Habilitationsschrift E.T.H. Zurich. Mitt. geol. Inst. E.T.H. u. Univ. Zurich, N.F. 107.

Schmid, S.M. 1982b. Microfabric studies as indicators of deformation mechanisms and flow laws operative in mountain building. In: Hsu, K., (ed.) : Mountain Building Processes. Academic Press, London, 95-110.

Schmid, S.M., Boland, J.N., and Paterson, M.S. 1977. Superplastic flow in fine grained limestone. Tectonophysics, 43, 257-291.

Schmid, S.M., and Paterson, M.S. 1977. Strain analysis in an experimentally deformed oolitic limestone. In : Energitics of Geological Processes, Saxena, K., and Battacharji, S. (Ed.), Springer Verlag, New York, 67-93.

Schmid, S.M., Boland, J.N., and Paterson, M.S. 1980. High temperature flow and dynamic recrystallization in Carrara Marble. Tectonophysics, 65, 245-280.

Schmid, S.M., Casey, M, and Starkey, J. 1981. The microfabric of calcite tectonites from the Helvetic nappes (Swiss Alps). In: McClay, K.R., and Price, N.J. (eds.), Thrust and Nappe Tectonics. Geol. Soc. Spec. Publ. London, 9, 151-158.

Schmid, S.M., and Casey, M. 1986. Complete fabric anaysis of some commonly observed quartz c-axis patterns. Geophysical Monograph, A.G.U. 36, 263-286.

Schmid, S.M., Panozzo, R., and Bauer, S. 1986. Simple shear experiments on calcite rocks: rheology and microfabric. In press.

Serdengecti, S., and Boozer, G.D. 1961. Effects of strain rate and temperature on the behaviour of rocks subjected to triaxial compression. Symp. Rock Mech., 4th, Pennsylvania State Univ., 83-97.

Shaw, N.D. 1980. A comparison of experimental and natural calcitic microfabrics. Unpubl. Ph.D. Thesis, Univ. of London.

Sibson, R.H. 1977. Fault rocks and fault mechanisms. J. Geol. Soc. Lond., 133, 191-213.

Siemes, H. 1966. Rontgenographische Bestimmung der Texturen von unverformten und experimentell verformten Solnhofener Kalkstein. Proc. First Congress, ISRM (Lisbon), 3, 205-215.

Smalley, R.F., Turcotte, D.L., and Solla, S.A. 1985. A renormalization group approach to the stick-slip behaviour of faults. J. Geophys. Res., 90, 1894-1900.

Smolychowski, M.S. 1909. Some remarks on the mechanics of overthrust. Geol. Mag., 6, 204-205.

Spang, J.H. 1974. Numerical dynamic analysis of calcite twin lamellae in the Greenport Centre syncline. Am. J. Sci., 274, 1044-1058.

Spiers, C.J. 1979. Fabric development in calcite polycrystals deformed at 400°C. Bull. Soc. Franc. Min. Crist., 102, 282-289.

Spiers, C.J. 1981. The development of deformation textures in calcite rocks. Unpubl. Ph.D. Thesis, Univ. of London.

Taylor, G.I. 1938a. Analysis of plastic strain in a cubic crystal. In: Stephen Timoshenko 60th Anniversary Volume. MacMillan, New York, 218-224.

Taylor, G.I. 1938b. Plastic strain in metals. J. Inst. Met., 62, 307-324.

Thomas, J.M., and Renshaw, G.D. 1967. Influence of dislocations on the thermal decomposition of calcium carbonate. J. Chem. Soc. (A), 2058-2061.

Truyols, J., and others 1982. Mapa geologico de Espana E. 1:50,000, Hoja no. 77 (La Plaza). Inst. Geol. Min. Espana.

Tullis, T.E. 1980. The use of mechanical twinning in minerals as a measure of shear stress magnitudes. J. Geophys. Res., 85, 6263-6268.

Turcotte, D.L. 1986. Fractals and Fragmentation. J. Geophys. Res., 91, 1921-1926.

Turner, F.J. 1953. Nature and dynamic interpretation of deformation lamellae in calcite of three marbles. Am. J. Sci., 251, 276-298.

Turner, F.J., and Chi'h, C.S. 1951. Deformation of Yule Marble. Part III: Observed fabric changes due to deformation at 10,000 atmospheres confining pressure, room temperature, dry. Geol. Soc. Am. Bull., 62, 887-906.

Turner, F.J., Griggs, D.T., Clark, R.H., and Dixon, R.H. 1956. Deformation of Yule Marble. Part VII: Development of oriented fabrics at 300°-500°C. Geol. Soc. Am. Bull., 67, 1259-1294.

Turner, F.J., Griggs, D.T., and Heard, H.C. 1954. Experimental deformation of calcite crystals. Geol. Soc. Am. Bull., 65, 883-936.

Turner, F.J., and Orozco, M. 1976. Crystal bending in metamorphic calcite, and its relations to associated twinning. Contr. Min. Pet., 57, 83-97.

Turner, F.J., and Weiss, L.E. 1963. Structural analysis of metamorphic tectonites. McGraw-Hill, New York, 545p.

Twiss, R.J. 1977. Theory and applicability of a recrystallized grain size palaeopiezometer. In : Stress in the Earth, M. Wyss (Ed.), reprint from Pageoph., 115, in CCRG, 3, Birkhauser Verlag, Basel, 227-244.

Van Den Bosch, W.J. 1969. Geology of the Luna-Sil region. Cantabrian Mountains (N.W. Spain). Leidse Geol. Meded., 44, 137-225.

Vistelius, A.B. 1966. Structural Diagrams. Pergamon Press, Oxford, 178p.

von Mises, R. 1928. Mechanik der plastischen Formanderung von Kristallen. Z. angew. math. Mech., 8, 161-184.

Weathers, M.S., Cooper, R.F., Kohlstedt, D.L., and Bird, J.M. 1979. Differential stress determined from deformation-induced microstructures of the Moine Thrust zone. J. Geophys. Res., 84, 7495-7509.

Weertman, J. 1968. Dislocation climb theory of steady state creep. Trans. ASM, 61, 681-694.

Weiss, L.E., and Turner, F.J. 1972. Some observations on translation gliding and kinking in experimentally deformed calcite and dolomite. In: Flow and Fracture of Rocks, Am. Geophys. Union, 16, 95-108.

Wenk, H.R. 1978. Preferred orientation in minerals, review and outlook. Proc. ICOTOM 5 (Aachen), 2, 47-83.

Wenk, H.R., Venkitasubramanyan, C.S., and Baker, D.W. 1973. Preferred orientation in experimentally deformed limestone. Contr. Min. Pet., 38, 81-114.

Wever, F., and Schmid, W.E. 1930. Interpretation of deformation textures. Z. Metallkunde, 22, 133-141.

White, S.H. 1979a. Difficulties associated with palaeo-stress estimates. Bull. Mineral., 102, 210-215.

White, S.H. 1979b. Palaeo-stress estimates in the Moine Thrust zone, Eribol, Scotland. Nature, 280, 222-223.

White, S.H., Shaw, H.F., and Huggett, J.M. 1984. The use of back-scattered electron imagery for the petrofabric study of sandstones and shales. J. Sed. Pet., 54, 487-494.

Wilson, K.G., and Kogut, J. 1974. The renormalization group and the ϵ expansion. Phys. Rep., 12C, 75-200.

Wyllie, P.J., and Tuttle, O.F. 1960. The system $CaO-CO_2-H_2O$ and the origin of carbonatites. J. Pet., 1, 1-17.

STEPHANIAN
WESTPHALIAN
CALIZA DE MONTANA
girotte
DEVONIAN SUPERIOR
PORTILLA
HUERGAS
SANTA LUCIA
LA VID $_{1}{}^{2}{}^{3}$
SAN PEDRO
FORMIGOSO
BARRIOS
OVILLE
LANCARA
HERRERIA
MORA

B

A

LA CUETA

PTW

PICOS ALBOS

SLTW

TORESTIO

B'

A'

LA MAJUA

TORRE BABIA

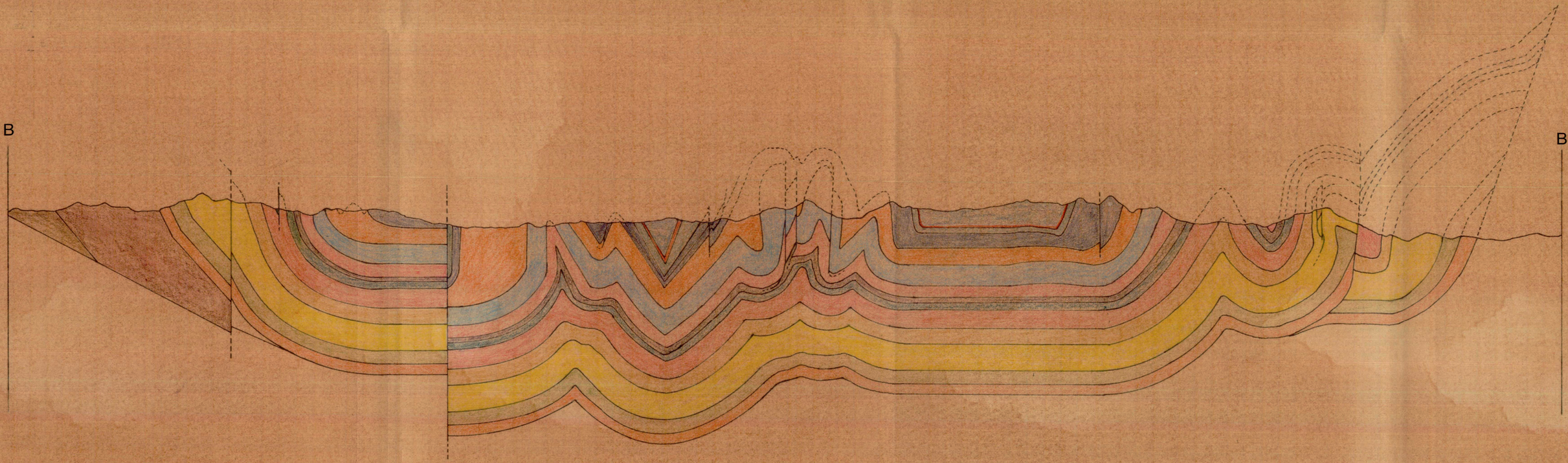
N

1km

Structural Legend

- Thrust Fault, tick on overthrust block.
- Normal Fault, tick on downthrown block.
- Anticlinal Fold.
- Synclinal Fold.
- Sedimentary contact.

Structural and stratigraphical map of the southern sector of the Somiedo Thrust sheet, the location of which is shown in red on Figure 5.2. The lines of two sections (A-A' and B-B') are shown.

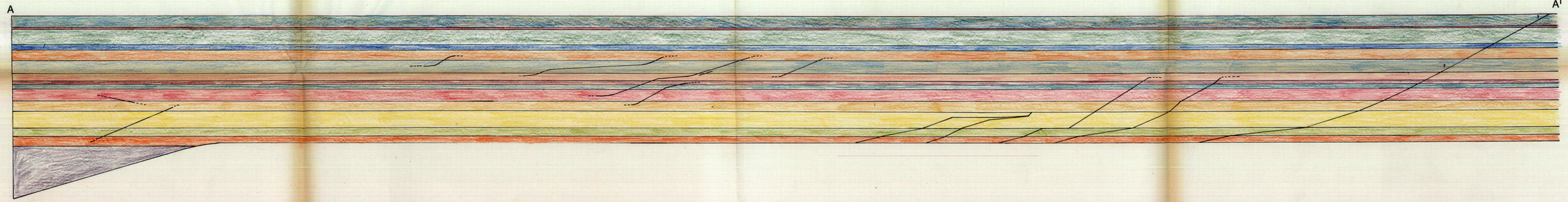


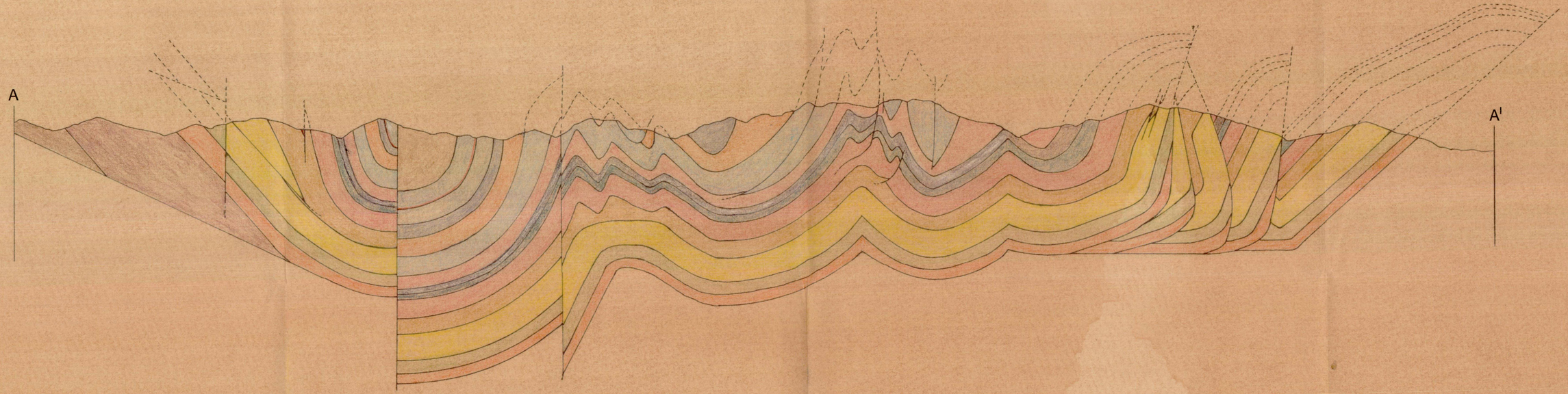
Section B-B'

Section along approximate direction of transport from the southern sector of the Somiedo thrust sheet. The line of section is shown on the accompanying map in the back enclosure of this Thesis.
Vertical scale equals horizontal scale. Stratigraphy as represented in the key shown on Map 1.
The corresponding restored section is presented in Section B-B'-Restored.

Section A-A'-Restored

Section along approximate direction of transport from the southern sector of the Somiedo thrust sheet. The line of section is shown on the accompanying map in the back enclosure of this Thesis.
Vertical scale equals horizontal scale. Stratigraphy as represented in the key shown on Map 1.
The corresponding section is presented in Section A-A'.





Section A-A'

Section along approximate direction of transport from the southern sector of the Somiedo thrust sheet. The line of section is shown on the accompanying map in the back enclosure of this Thesis.
Vertical scale equals horizontal scale. Stratigraphy as represented in the key shown on Map 1.
The corresponding restored section is presented in Section A-A'-Restored.

Section B-B'-Restored

Section along approximate direction of transport from the southern sector of the Somiedo thrust sheet. The line of section is shown on the accompanying map in the back enclosure of this Thesis.
Vertical scale equals horizontal scale. Stratigraphy as represented in the key shown on Map 1.
The corresponding section is presented in Section B-B'.

